

НАЦІОНАЛЬНА АКАДЕМІЯ НАУК УКРАЇНИ
ІНСТИТУТ ФІЗІОЛОГІЇ ім. О. О. БОГОМОЛЬЦЯ

*Кваліфікаційна наукова
праця на правах рукопису*

ГРИЩЕНКО ОЛЕКСІЙ ВАДИМОВИЧ

УДК 612.812:611.813.14

ДИСЕРТАЦІЯ
**ВПЛИВИ МУТАЦІЙ КАЛЬЦІЙЗВ'ЯЗУЮЧИХ БІЛКІВ ТА ЗМІН
ДЕПОЗАЛЕЖНОГО ВХОДУ ІОНІВ КАЛЬЦІЮ НА
ФУНКЦІОНУВАННЯ ЗБУДЛИВИХ ТА
НЕЗБУДЛИВИХ КЛІТИН**

03.00.13 – Фізіологія людини і тварин
Біологічні науки

Подається на здобуття наукового ступеня доктора біологічних наук

Дисертація містить результати власних досліджень. Використання ідей,
результатів і текстів інших авторів мають посилання на відповідне джерело

_____ О.В. Грищенко

Науковий консультант: Білан Павло Володимирович
доктор біологічних наук, професор

Київ – 2020

АНОТАЦІЯ

Грищенко О.В. Впливи мутацій кальційзв'язуючих білків та змін депозалежного входу іонів кальцію на функціонування збудливих та незбудливих клітин. – Кваліфікаційна наукова праця на правах рукопису за сукупністю наукових статей.

Дисертація на здобуття наукового ступеня доктора біологічних наук за спеціальністю 03.00.13 – фізіологія людини і тварин – Інститут фізіології ім. О.О. Богомольця НАН України, Київ, 2020.

У роботі представлені результати комплексного дослідження клітинних та молекулярних механізмів, залучених до кальцієвої регуляції в клітинах різних типів. У кардіоміоцитах як типових представниках електрозбудливих клітин, що здатні до скорочення, показана важлива роль кальційзв'язуючих білків у формуванні та регуляції змін внутрішньоклітинної концентрації іонів кальцію. Проаналізовано зміни електричних характеристик потенціалів дій та біофізичних параметрів скорочення кардіоміоцитів, викликаних мутаційними модифікаціями молекул тропоніну Т, що збільшують чутливість міофіламентів кардіоміоцитів до іонів кальцію. Показано, що з ростом чутливості міофіламентів пропорційно збільшується буферна кальцієва здатність клітин, і саме цим можуть бути пояснені зміни електричної та скорочувальної активності “мутантних” кардіоміоцитів. В електрично незбудливих клітинах одну з провідних ролей у підвищенні внутрішньоклітинної концентрації іонів кальцію відіграють кальцієві канали, що активуються вивільненням цих іонів із ендоплазматичного ретикулуму та його спустошенням. За допомогою методу “patch-clamp” вперше зареєстровані кальцієві струми в ацинарних клітинах, що виникають у відповідь на спустошення ретикулуму. Експериментально продемонстровано пряму кореляцію між спустошенням ендоплазматичного ретикулуму та активацією депозалежного струму. Доведено, що саме вхід іонів кальцію через депозалежні канали являє собою основний фактор, що призводить

до некрозу клітин при більшості патологій, котрі призводять до виникнення гострого панкреатиту. Із застосуванням конфокальної мікроскопії з'ясовані механізми кальцієвої регуляції в клітинах лобул екзокринної частини підшлункової залози, зокрема в нервових, зірчастих та імунних клітинах. Встановлено, що зірчасті клітини в звичайних умовах (за відсутності патологій) здатні генерувати кальцієві транзйєнти у відповідь на прикладання брадикініну; описані механізми виникнення і генерації цих кальцієвих транзйєнтів. В роботі вперше описані вірогідні механізми виникнення гострого панкреатиту, спричиненого дією аспарагінази і експериментально обґрунтовано можливий новий підхід у терапії гострого панкреатиту; в основі такого підходу лежить застосування галактози, що забезпечує адекватне регулювання необхідної концентрації АТФ в ацинарних клітинах підшлункової залози.

За допомогою флуоресцентних та електрофізіологічних методів дослідження вперше показано, що саме спонтанні коливання внутрішньоклітинної концентрації іонів кальцію, не пов'язані з генерацією трансмембранних струмів, призводять до скорочення кардіоміоцитів на ранніх стадіях розвитку останніх. Удосконалено методи оцінки кальцієвої буферної ємності кардіоміоцитів та їх внутрішньоклітинної перфузії у конфігурації "ціла клітина". Вперше виявлено пряму кореляцію між рівнем буферної ємності та шлуночковою аритмією при мутаціях тропоніну, що підвищують чутливість міофіламентів до іонів кальцію.

У роботі вперше зареєстровано кальцієвий струм через плазматичну мембрану ацинарних клітин підшлункової залози, що активується вивільненням Ca^{2+} з ендоплазматичного ретикулуму. Показано зв'язок між рівнем спустошення ендоплазматичного ретикулуму та активацією депозалежного кальцієвого трансмембранного струму. Отримані данні свідчать про те, що саме цей струм може бути одним із основних факторів, відповідальних за підвищення внутрішньоклітинної концентрації Ca^{2+} при розвитку гострого панкреатиту.

Вперше досліджена пряма дія жовчних кислот на механізми кальцієвої регуляції у клітинах підшлункової залози та запропоновано інтерпретацію

механізму виникнення гострого панкреатиту, пов'язаного зі збільшенням $[Ca^{2+}]_i$ та $[Na^+]_i$. Встановлено негативний вплив аспарагінази – реагента, який застосовують в клінічній практиці для лікування дитячого гострого лімфобластного лейкозу – на кальцієву сигналізацію ацинарних клітин підшлункової залози. Запропоновано використання галактози для запобігання зростання $[Ca^{2+}]_i$ та виникнення некрозу клітин підшлункової залози в моделі гострого панкреатиту, викликаного аспарагіназою.

Вперше в клітинах у структурі панкреатичних лобул були встановлені зміни кальцієвої сигналізації, що спричиняються брадикініном в концентраціях, які є типовими для панкреатиту. У зіркоподібних клітинах підшлункової залози вперше був виявлений двофазний кальцієвий сигнал у відповідь на активацію брадикінінових B_2 -рецепторів плазматичної мембрани та з'ясовані механізми генерації цього сигналу. Отримані нові дані, які підтверджують панкреопротективну дію блокаторів брадикінінового рецептору B_2 , та продемонстровано, що їх використання запобігає некрозу ацинарних клітин. Вперше визначені особливості кальцієвої регуляції при взаємодії клітин різних типів у екзокринній частці підшлункової залози в їх природному оточенні. Зокрема, вперше досліджена кальцієва сигналізація в нервових клітинах підшлункової залози у структурі панкреатичних лобул.

Результати дослідження є внеском у комплексне розуміння механізмів кальцієвої регуляції та сигналізації в електрозбудливих та незбудливих клітинах у нормі та патології.

Ключові слова: кардіоміоцити, кальційзв'язуючі білки, кальцієва буферна ємність клітини, клітини екзокринної частини підшлункової залози, кальцієвий депо-залежний струм.

SUMMARY

Gryshchenko O.V. Effect of calcium-binding protein mutations and changes in the store-operated calcium entry on the function of excitable and non-excitable cells. – Collection of scientific manuscripts.

Thesis for the Degree of Doctor of Biological Sciences in Human and Animal Physiology (03.00.13). – Bogomoletz Institute of Physiology, National Academy of Sciences of Ukraine. Kyiv, 2020.

The thesis is focused on the mechanisms of depo-dependent calcium entry and calcium-binding proteins in calcium handling in the cytosol of excitable and non-excitable cells.

To investigate this problem a fluorescence methods for detecting changes in intracellular calcium ion concentration, immunocytochemical, electrophysiological (patch-clamp) and statistical methods were used. The troponin complex represents a substantial portion of cytoplasmic Ca^{2+} buffering binding approximately 50% of Ca^{2+} released from the sarcoplasmic reticulum during a typical heartbeat. Using cardiomyocytes isolated from mice expressing troponin T mutants (TnT-I79N, TnT-F110I and TnT-R278C), we found that increasing myofilament Ca sensitivity produced a proportional increase in cytosolic Ca^{2+} binding. The underlying cause was an increase in the cytosolic Ca^{2+} binding affinity, whereas maximal Ca^{2+} binding capacity was unchanged. The effect was sufficiently large to alter Ca^{2+} handling in intact mouse hearts at physiological heart rates, resulting in increased end-diastolic $[\text{Ca}^{2+}]$ at fast pacing rates, and enhanced sarcoplasmic reticulum Ca^{2+} content and release after pauses. Accordingly, action potential (AP) regulation was altered, with post-pause AP prolongation, afterdepolarizations and triggered activity. Basing on the observation that early stage embryonic stem cells-derived cardiomyocytes continuously contracted in high extracellular potassium solution, we provide experimental evidence that the spontaneous activity of these cells is not generated by transmembrane ion currents, but by intracellular $[\text{Ca}^{2+}]_i$ oscillations. In cardiac muscle, Ca^{2+} release from sarcoplasmic

reticulum (SR) is reduced with successively shorter coupling intervals of premature stimuli, a phenomenon known as SR Ca^{2+} release refractoriness. Gene-targeted ablation of Casq2 (Casq2 KO) abolished SR Ca^{2+} release refractoriness in isolated mouse ventricular myocytes. Surprisingly, impaired Ca^{2+} -dependent inactivation of L-type Ca^{2+} current (I_{Ca}), which is responsible for triggering SR Ca^{2+} release, significantly contributed to the loss of Ca^{2+} release refractoriness in Casq2 KO myocytes. Recovery from Ca^{2+} -dependent inactivation of I_{Ca} was significantly accelerated in Casq2 KO compared to wild type (WT) myocytes.

Alcohol-related acute pancreatitis can be mediated by a combination of alcohol and fatty acids (fatty acid ethyl esters) and is initiated by a sustained elevation of the Ca^{2+} concentration inside pancreatic acinar cells ($[\text{Ca}^{2+}]_i$), due to excessive release of Ca^{2+} stored inside the cells followed by Ca^{2+} entry from the interstitial fluid. The sustained $[\text{Ca}^{2+}]_i$ elevation activates intracellular digestive proenzymes resulting in necrosis and inflammation. Electrophysiological data show that in the pancreatic acinar cells this store-operated inward current is relatively insensitive to removing external Na^+ , but sensitive to changes in the external Ca^{2+} concentration. It is therefore not a transient receptor potential (TRP) type nonselective cation current, but it is a Ca^{2+} -selective CRAC-type current consistent with the very marked current inhibition evoked by GSK-7975A. There is currently no specific treatment of pancreatitis, but the received data show that pharmacological CRAC blockade is highly effective against toxic $[\text{Ca}^{2+}]_i$ elevation, necrosis, and trypsin/protease activity and therefore has potential to effectively treat pancreatitis. Asparaginase, an essential element in the successful treatment of acute lymphoblastic leukaemia, the most common type of cancer affecting children, evoked intracellular Ca^{2+} release followed by Ca^{2+} entry and also substantially reduced Ca^{2+} extrusion because of decreased intracellular ATP levels. In isolated mouse pancreatic acinar cells or cell clusters, removal of extracellular glucose had little effect on this ATP loss, suggesting that glucose metabolism was severely inhibited under these conditions. Surprisingly, we show that replacing glucose with galactose prevented or markedly reduced the loss of ATP and any subsequent necrosis.

Ca^{2+} signalling in different cell types in exocrine pancreatic lobules was monitored simultaneously and signalling responses to various stimuli were directly compared. Normal pancreatic stellate cells (PSCs) are regarded as quiescent, only to become activated in chronic pancreatitis and pancreatic cancer. However, these cells in their normal microenvironment are far from quiescent, but are capable of generating substantial Ca^{2+} signals. We have compared Ca^{2+} signalling in PSCs and their better studied neighbouring acinar cells (PACs) and found complete separation of Ca^{2+} signalling in even closely neighbouring PACs and PSCs. Bradykinin (BK), at concentrations corresponding to the slightly elevated plasma BK levels that have been shown to occur in the auto-digestive disease acute pancreatitis in vivo, consistently elicited substantial Ca^{2+} signals in PSCs, but never in neighbouring PACs, whereas the physiological PAC stimulant cholecystokinin failed to evoke Ca^{2+} signals in PSCs. The BK-induced Ca^{2+} signals were mediated by B2 receptors and B2 receptor blockade protected against PAC necrosis evoked by agents causing acute pancreatitis. The initial Ca^{2+} rise in PSCs was due to inositol trisphosphate receptor-mediated release from internal stores, whereas the sustained phase depended on external Ca^{2+} entry through Ca^{2+} release-activated Ca^{2+} channels. We have, for the first time, recorded depolarization-evoked Ca^{2+} signals in pancreatic nerves and shown that, although acinar cells receive a functional cholinergic innervation, there is no evidence for functional innervation of the stellate cells. The stellate, like the acinar, cells are not electrically excitable as they do not generate Ca^{2+} signals in response to membrane depolarization. The principal agent evoking Ca^{2+} signals in the stellate cells is bradykinin, but in experimental alcohol-related acute pancreatitis, these cells become much less responsive to bradykinin.

Keywords: Ca^{2+} buffering, calcium release, capacitative Ca^{2+} entry, calcium signalling, L-type calcium channel, cardiomyocytes, exocrine pancreatic cells.

СПИСОК ОПУБЛІКОВАНИХ ПРАЦЬ ЗА ТЕМОЮ ДИСЕРТАЦІЇ

Основні наукові результати дисертації, опубліковані у фахових виданнях, віднесених до першого і другого квартилів (**Q1 і Q2**) відповідно до класифікації SCImago Journal and Country Rank або Journal Citation Reports:

1. **Gryshchenko O**, Lu ZJ, Fleischmann BK, Hescheler J. Outwards currents in embryonic stem cell-derived cardiomyocytes. *Pflugers Arch.* 2000 Apr; 439(6):798-807.
2. Igelmund P, Fleischmann BK, Fischer IR, Soest J, **Gryshchenko O**, Böhm-Pinger MM, Sauer H, Liu Q, Hescheler J. Action potential propagation failures in long-term recordings from embryonic stem cell-derived cardiomyocytes in tissue culture. *Pflugers Arch.* 1999 Apr; 437(5):669-79.
3. Viatchenko-Karpinski S, Fleischmann BK, Liu Q, Sauer H, **Gryshchenko O**, Ji GJ, Hescheler J. Intracellular Ca²⁺ oscillations drive spontaneous contractions in cardiomyocytes during early development. *Proc Natl Acad Sci U S A.* 1999 Jul 6; 96(14):8259-64.
4. **Gryshchenko O**, Fischer IR, Dittrich M, Viatchenko-Karpinski S, Soest J, Böhm-Pinger MM, Igelmund P, Fleischmann BK, Hescheler J. Role of ATP-dependent K(+) channels in the electrical excitability of early embryonic stem cell-derived cardiomyocytes. *J Cell Sci.* 1999 Sep; 112 (Pt 17):2903-12.
5. **Gryshchenko O**, Qu J, Nathan RD. Ischemia alters the electrical activity of pacemaker cells isolated from the rabbit sinoatrial node. *Am J Physiol Heart Circ Physiol.* 2002 Jun; 282(6):H2284-95.
6. Kruglikov I, **Gryshchenko O**, Shutov L, Kostyuk E, Kostyuk P, Voitenko N. Diabetes-induced abnormalities in ER calcium mobilization in primary and secondary nociceptive neurons. *Pflugers Arch.* 2004 Jul; 448(4):395-401.
7. Voronina SG, **Gryshchenko OV**, Gerasimenko OV, Green AK, Petersen OH, Tepikin AV. Bile acids induce a cationic current, depolarizing pancreatic acinar cells and increasing the intracellular Na⁺ concentration. *J Biol Chem.* 2005 Jan 21; 280(3):1764-70. Epub 2004 Nov 9.

8. Shutov L, Kruglikov I, **Gryshchenko O**, Khomula E, Viatchenko-Karpinski V, Belan P, Voitenko N. The effect of nimodipine on calcium homeostasis and pain sensitivity in diabetic rats. *Cell Mol Neurobiol*. 2006 Oct-Nov; 26(7-8):1541-57. Epub 2006 Jul 12. PubMed PMID: 16838100.
9. Schober T, Huke S, Venkataraman R, **Gryshchenko O**, Kryshstal D, Hwang HS, Baudenbacher FJ, Knollmann BC. Myofilament Ca sensitization increases cytosolic Ca binding affinity, alters intracellular Ca homeostasis, and causes pause-dependent Ca-triggered arrhythmia. *Circ Res*. 2012 Jul 6; 111(2):170-9.
10. Gerasimenko JV, **Gryshchenko O**, Ferdek PE, Stapleton E, Hébert TO, Bychkova S, Peng S, Begg M, Gerasimenko OV, Petersen OH. Ca²⁺ release-activated Ca²⁺ channel blockade as a potential tool in antipancreatitis therapy. *Proc Natl Acad Sci U S A*. 2013 Aug 6; 110(32):13186-91.
11. Kryshstal DO, **Gryshchenko O**, Gomez-Hurtado N, Knollmann BC. Impaired calcium-calmodulin-dependent inactivation of Cav1.2 contributes to loss of sarcoplasmic reticulum calcium release refractoriness in mice lacking calsequestrin 2. *J Mol Cell Cardiol*. 2015 May; 82:75-83.
12. **Gryshchenko O**, Gerasimenko JV, Gerasimenko OV, Petersen OH. Ca(2+) signals mediated by bradykinin type 2 receptors in normal pancreatic stellate cells can be inhibited by specific Ca(2+) channel blockade. *J Physiol*. 2016 Jan 15; 594(2):281-93.
13. **Gryshchenko O**, Gerasimenko JV, Gerasimenko OV, Petersen OH. Calcium signalling in pancreatic stellate cells: Mechanisms and potential roles. *Cell Calcium*. 2016 Mar; 59(2-3):140-4.
14. Peng S, Gerasimenko JV, Tsugorka T, **Gryshchenko O**, Samarasinghe S, Petersen OH, Gerasimenko OV. Calcium and adenosine triphosphate control of cellular pathology: asparaginase-induced pancreatitis elicited via protease-activated receptor 2. *Philos Trans R Soc Lond B Biol Sci*. 2016 Aug 5; 371(1700). pii: 20150423.

15. **Gryshchenko O**, Gerasimenko JV, Peng S, Gerasimenko OV, Petersen OH. Calcium signalling in the acinar environment of the exocrine pancreas: physiology and pathophysiology. *J Physiol*. 2018 Jul; 596(14):2663-2678.
16. Peng S, Gerasimenko JV, Tsugorka TM, **Gryshchenko O**, Samarasinghe S, Petersen OH, Gerasimenko OV. Galactose protects against cell damage in mouse models of acute pancreatitis. *J Clin Invest*. 2018 Aug 31; 128(9):3769-3778.

Наукові праці, які засвідчують апробацію матеріалів дисертації:

1. P Igelmund, IR Fischer, J Soest, **O Gryshchenko**, BK Fleischmann, J Hescheler. Nimodipine induces arrhythmia in cardiomyocyte clusters in three-dimensional cell culture. *PFLUGERS ARCHIV-EUROPEAN JOURNAL OF PHYSIOLOGY*, 1997, 433 (6), P293-P293.
2. **O Gryshchenko**, IR Fischer, J Soest, S Viatchenko-Karpinski, P Igelmund, Fleischmann BK, Hescheler J. Bursting behavior induced by ATP-sensitive K⁺ channels in embryonal stem cell derived cardiomyocytes. *PFLUGERS ARCHIV-EUROPEAN JOURNAL OF PHYSIOLOGY*, 1997, 433 (6), O131-O131.
3. **O Gryshchenko**, BK Fleischmann, J Hescheler. Outward rectifier K⁺ currents in early-and late stage cardiomyocytes derived from embryonic stem cells. *PFLUGERS ARCHIV-EUROPEAN JOURNAL OF PHYSIOLOGY*, 1997, 433 (6), P294-P294.
4. **O Gryshchenko**, RD Nathan. Simulated ischemia alters the electrical activity of pacemaker cells isolated from the rabbit sinoatrial node: Role of pH. *BIOPHYSICAL JOURNAL*, 2001, 80 (1), 641A-641A.
5. **O Gryshchenko**, JH Qu, RD Nathan. Ischemia alters calcium transients in SA node pacemaker cells. *BIOPHYSICAL JOURNAL*, 2002, 82 (1), 99A-99A.
6. YM Du, **O Gryshchenko**, H Attaya, RD Nathan. Ionic basis of ischemia-induced bradycardia in the rabbit sinoatrial node *FASEB JOURNAL*, 2005, 19 (5), A1633-A1633.

7. **O Gryshchenko**, S Huke, F Baudenbacher, JD Potter, BC Knollmann. Ca²⁺ sensitizing troponin T mutations linked to hypertrophic cardiomyopathy increase apparent cytosolic Ca²⁺ binding. *Biophysical Journal*, 2009, 96 (3), 513a.
8. HS Hwang, **O Gryshchenko**, SS Davies, BC Knollmann. Effects of γ -Ketoaldehydes on Ca²⁺ Current Induced SR Ca²⁺ Release in Ventricular Myocytes. *Biophysical Journal*, 2010, 98 (3), 548a.
9. **O Gryshchenko**, D Kryshchal, BC Knollmann. Refractoriness of Sarcoplasmic Reticulum Calcium Release in Cardiac Muscle Due to Calsequestrin. *Biophysical Journal*, 2010, 98 (3), 547a.
10. D Kryshchal, **O Gryshchenko**, BC Knollmann. Accelerated Recovery of L-Type Ca Current Contributes to the Loss of SR Ca Release Restitution in Mice Lacking Casq2. *Biophysical Journal*, 2012, 102 (3), 672a.
11. **Грищенко О**, Герасименко Ю, Герасименко О, Петерсен О. Депо-залежні струми в ацинарних клітинах підшлункової залози. Тези доповіді Українського Біофізичного Товариства (Луцьк, 2015).
12. **Gryshchenko O**, Gerasimenko JV, Gerasimenko OV, Petersen OH. The blockade of BK-induced Ca²⁺ signals in pancreatic stellate cells protected against PAC necrosis evoked by agents causing acute pancreatitis. 2016, Annual Meeting of European Academy, UK.
13. **Gryshchenko O**, Gerasimenko J, Gerasimenko O, Petersen O, Stellate cells. 2017, Annual Royal Society Meeting, London, UK.
14. **Gryshchenko O**, Gerasimenko J, Gerasimenko O, Petersen O. Calcium signalling in the acinar environment of the exocrine pancreas. 2019, 8th Annual Meeting of the Ukrainian Biophysical Society, Nov. 12-15 2019, Kyiv-Lutsk (Ukraine). Публікація тез, усна доповідь.

ЗМІСТ

АНОТАЦІЯ	2
СПИСОК ОПУБЛІКОВАНИХ ПРАЦЬ ЗА ТЕМОЮ ДИСЕРТАЦІЇ	8
ПЕРЕЛІК ОСНОВНИХ УМОВНИХ ПОЗНАЧЕНЬ	14
ВСТУП	16
РОЗДІЛ 1. ВНУТРІШНЬОКЛІТИННІ КОЛИВАННЯ Ca^{2+}	
ВИКЛИКАЮТЬ СПОНТАННІ СКОРОЧЕННЯ	
КАРДІОМІОЦИТІВ ПІД ЧАС РАННЬОГО	
РОЗВИТКУ.....	24
1.1 Вихідні іонні струми в ранішніх кардіоміоцитах, що походять від ембріональних стовбурових клітин.....	25
1.2 Роль K^+ каналів, що залежать від АТФ, в електричній збудливості ранішніх ембріональних кардіоміоцитів, отриманих від стовбурових клітин...	35
1.3 Внутрішньоклітинні коливання Ca^{2+} викликають спонтанні скорочення кардіоміоцитів під час ранішнього розвитку клітин.....	45
1.4 Порушення в розповсюдженні потенціалів дії в довготривалих записах активності в культурі кардіоміоцитів, отриманих з ембріональних стовбурових клітин.....	51
РОЗДІЛ 2. РОЛЬ КАЛЬЦІЙЗВ'ЯЗУЮЧИХ БІЛКІВ У ГЕНЕРАЦІЇ ЗМІН	
ВНУТРІШНЬОКЛІТИННОЇ КОНЦЕНТРАЦІЇ ІОНІВ	
КАЛЬЦІЮ.....	61
2.1. Мутації тропоніну Т, що зумовлюють збільшення чутливості міофіламентів до Ca^{2+} , підвищують цитозольне зв'язування Ca^{2+}	62
2.2. Роль кальсеквестрину2 (<i>Casq2</i>) у регуляції рефрактерності вивільнення Ca^{2+} із саркоплазматичного ретикулуму шлуночкових міоцитів.....	83
2.3 Ішемія змінює електричну активність кардіоміоцитів, виділених із синоатріального вузла.....	105
РОЗДІЛ 3. КАЛЬЦІЄВА СИГНАЛІЗАЦІЯ В ЕЛЕКТРИЧНО	
НЕЗБУДЛИВИХ КЛІТИНАХ.....	117

3.1. Депозалежні кальцієві трансмембранні струми в ацинарних клітинах підшлункової залози	118
3.2. Кальцієва сигналізація в зірчастих клітинах підшлункової залози	124
3.3. Катіонні трансмембранні струми, викликані прикладанням жовчних кислот	142
РОЗДІЛ 4. КАЛЬЦІЄВА СИГНАЛІЗАЦІЯ В РІЗНИХ ТИПАХ КЛІТИН	149
4.1. Кальцієва сигналізація в клітинах екзокринної частини підшлункової залози.....	149
4.2. Кальцій та аденозинтрифосфат контролюють клітинну патологію...	165
4.3. Галактоза захищає від пошкодження клітин при гострому панкреатиті.....	177
ВИСНОВКИ	189
ДОДАТОК 1. СПИСОК ПУБЛІКАЦІЙ ЗА ТЕМОЮ ДИСЕРТАЦІЇ	192

ПЕРЕЛІК ОСНОВНИХ УМОВНИХ ПОЗНАЧЕНЬ ТА СКОРОЧЕНЬ

Ca^{2+}	— іони кальцію
$[\text{Ca}^{2+}]_i$	— внутрішньоклітинна концентрація іонів кальцію
VDCC	— потенціал-залежні Ca^{2+} канали L-типу
CP	— саркоплазматичний ретикулум
RyR2	— ріанодинові рецептори другого типу
CICR	— кальцій-індуковане вивільнення кальцію
РГК	— родинна гіпертрофічна кардіоміопатія
TnT	— тропонін Т
SOCE	— депо-керований вхід Ca^{2+}
ЕТ	— ембріональні тільця
ПД	— потенціал дії
НКО	— натрій-кальцієвий обмінник
TnT-I79N	— Ca^{2+} сенсibiliзуючий мутант тропоніну Т
WT	— природний тип тропоніну
Kd	— константа дисоціації Ca^{2+} в цитозолі
Bmax	— загальна кількість місць зв'язування Ca^{2+} у цитозолі
Casq2	— кальсеквестрин2
Casq2 KO	— миші, нокаутовані по гену Casq2
CaM	— кальмодулін
NMDG ⁺	— Nметіл-D-глюкамін
CRAC	— Ca^{2+} канали активовані вивільненням Ca^{2+}
2-APB	— 2-аміноетоксидифеніл борату
POAEE	— етилові ефіри жирних кислот
ЗКПЗ	— зірчасті клітини підшлункової залози
БК	— брадикінін
ССК	— холецистокінін
WIN	— антагоніст БК рецепторів другого типу (B2) WIN64338
ЦПК	— циклопіазонова кислота

TLC-S	–	жовчна кислота tauroolithocholic acid 3-sulfate
АТФ	–	аденозинтрифосфат
ASNase	–	аспарагіназа

ВСТУП

Актуальність теми. Внутрішньоклітинні іони кальцію є одним з найбільш універсальних вторинних посередників. Вони задіяні у цілому ряді принципово важливих клітинних процесів, таких як клітинна збудливість, секреція, проліферація, синаптична передача, скорочення та інші (Avila et al., 2019). Іони кальцію (Ca^{2+}) беруть участь у передачі сигналів від структур плазматичної мембрани до внутрішньоклітинних структур, забезпечуючи таким чином реакцію клітини на зовнішній стимул (Petersen a. Verkhratsky, 2016). У процесі еволюції молекулярні механізми, що контролюють рівень внутрішньоклітинної концентрації іонів кальцію ($[\text{Ca}^{2+}]_i$), були сформовані дуже рано; вони необхідні для точного регулювання рівнів як вільного, так і зв'язаного кальцію у цитозолі, а також кількості кальцію, накопиченого у внутрішньоклітинних депо (Shahidul, 2020). Ці механізми є універсальними і по суті однакові і у прокаріот і еукаріот. Вони включають низьку проникність фосфоліпідних мембран для Ca^{2+} , високу внутрішньоклітинну буферну здатність та ефективну систему видалення Ca^{2+} за межі клітин (Case et al., 2007). Щоб зрозуміти на клітинному рівні загальні закономірності біологічних процесів, пов'язаних з кальцієм у організмі тварин і людини, кальцієву регуляцію вивчають на широкому колі різних модельних об'єктів, від дріжджів (*Saccharomyces cerevisiae*; Catterall et al., 2005) та нематод (*Caenorhabditis elegans*; Suzuki et al., 2010) до риб (*Danio rerio*; Kettunen, 2020) та мишей і щурів (Györke, 2017). Ці дослідження призвели до важливих фундаментальних відкриттів у царині механізмів контролю $[\text{Ca}^{2+}]_i$. Слід, проте, визнати, що деякі важливі аспекти кальцієвої регуляції все ще залишаються нез'ясованими.

Кальцієва сигналізація має велике значення для функціонування збудливих клітин. Саме іони кальцію відіграють основну роль у процесах спряження збудження і скорочення кардіоміоцитів. У кардіоміоцитах ссавців до скорочення призводить вхід іонів кальцію через потенціалкеровані Ca^{2+} канали L-типу (VDCC); ефект такого входу підсилюється вивільненням Ca^{2+} із саркоплазматичного ретикулуму (CP) через р'янодинові рецептори другого типу

(RyR2). Відповідний процес називається кальційіндуковане вивільнення кальцію (CICR; Ríos, 2018). Однак досі невідомо, як скорочення забезпечується в клітинах ранньої стадії кардіоміогенезу, коли експресія іонних каналів, включаючи VDCC, у цих клітинах є значно меншою, ніж у зрілих кардіоміоцитах. Отже, з'ясування кальційзалежних механізмів скорочення незрілих кардіоміоцитів є дуже важливим як в аспекті встановлення більш детальної картини сполучення між збудженням та скороченням, так і для лікування деяких захворювань серця, котрі ініціюються ще на стадії ембріогенезу.

Захворювання серцево-судинної системи посідають перші місця в переліку смертельних захворювань людини в усьому світі. Серед цих захворювань виділяється родинна гіпертрофічна кардіоміопатія (РГК) – одна з найпоширеніших причин раптової смерті (один випадок на 500 людей). РГК є етіологічно гетерогенною, але виникає значною мірою внаслідок аутосомно-домінантних мутацій у генах, що кодують скоротливі білки серцевих м'язів (Maron et al., 1995). Зокрема, заміна певної амінокислоти у білку тропоніну Т (TnT) підвищує чутливість міофіламентів до Ca^{2+} та може викликати шлуночкову аритмію. Механізм виникнення цього феномена досі залишається невідомим (Miller et al., 2001). Встановлення цього механізму є конче необхідним для лікування хворих на цю патологію, що становлять основну частку пацієнтів із захворюваннями серцево-судинної системи.

В електророзбудливих клітинах вхід іонів кальцію до цитозолу в основному відбувається через потенціалзалежні кальцієві канали. Активація цих каналів під час деполяризації мембрани призводить до виникнення транзйєнтів концентрації цитозольного Ca^{2+} , які ініціюють широкий спектр фізіологічних процесів, включаючи скорочення. На відміну від збудливих клітин, у незбудливих клітинах вхід Ca^{2+} опосередковується рецепторактивованими шляхами, які відіграють роль головного постачальника іонів кальцію всередину клітин. Напевно, найбільш поширеним рецепторкерованим механізмом входу Ca^{2+} є депо-керований вхід Ca^{2+} через канали плазматичної мембрани (SOCE), який

активується, коли концентрація Ca^{2+} у внутрішньоклітинних кальцієвих депо зменшується (Putney, 2005). Невдовзі після ідентифікації SOCE було виявлено високоселективний кальцієвий струм, що активується спустошенням внутрішньоклітинних Ca^{2+} депо, так званий I_{CRAC} (Hoth a. Penner, 1992). Екзокринні клітини не мають потенціал-залежних кальцієвих каналів, і тому зміни концентрації цитозольного Ca^{2+} , що регулюють секрецію ферментів травлення, генеруються завдяки складній взаємодії SOCE/ I_{CRAC} та вивільненням Ca^{2+} з внутрішньоклітинних депо (Petersen a. Terpink, 2008).

У ссавців секреція основної частини ферментів травлення здійснюється ацинарними клітинами підшлункової залози. Відомо, що синтез і секреція цих ферментів у нормі регулюються змінами концентрації вільного кальцію в цитоплазмі та ендоплазматичному ретикулумі цих клітин (Petersen, 2015). За патологічних умов стійке підвищення $[\text{Ca}^{2+}]_i$ активує внутрішньоклітинні проферменти травлення всередині клітин, що призводить до розвитку запалення та некрозу у підшлунковій залозі. Нажаль, відомості про функціонування механізмів залучених до кальцієвої регуляції як в ацинарних, так і в клітинах інших типів екзокринної частці підшлункової залози у нормальних та патологічних умовах, є дуже неповними. Зокрема, кальцієва регуляція при взаємодії клітин різних типів у екзокринній частці підшлункової залози в їх природному оточенні є майже недослідженою. Результати таких досліджень були б вкрай важливими як для детального встановлення ролі кальцієвої сигналізації у розвитку та підтриманні різних патологічних станів, так і для розробки новітніх підходів у лікуванні гострого та хронічного панкреатиту.

Таким чином, наше дослідження мало на меті встановити, яким чином механізми буферизації іонів кальцію у цитозолі та депозалежного входу Ca залучені у кальцієву регуляцію. У електрично збудливих та незбудливих клітинах в умовах норми та патології. Ця проблема розглянута на прикладі кардіоміоцитів та клітин екзокринної частки підшлункової залози.

Зв'язок роботи з науковими програмами, планами, темами.
Дисертаційна робота виконана відповідно до загального плану науково-дослідних

робіт відділу молекулярної біофізики Інституту фізіології ім. О. О. Богомольця НАН України в рамках науково-дослідних робіт «Ендогенна та фармакологічна регуляція внутрішньоклітинної та міжклітинної сигналізації в клітинах нервової системи в нормі та патології» (2011 - 2013; номер державної реєстрації – 0110U004750), «Клітинні сигнальні системи в нормі та патології» (2014 – 2018; номер державної реєстрації – 0113U007273) та «Сигналізація нейрональних кальцієвих сенсорних білків в нейронах ЦНС в нормі і патології» (2019 – 2013, номер державної реєстрації – 0115U003632).

Мета дослідження: встановити впливи мутацій кальційзв'язуючих білків та аномального депозалежного входу іонів кальцію на функціонування кардіоміоцитів та клітин підшлункової залози.

Завдання дослідження. Згідно з цією метою були поставлені наступні завдання:

1. З'ясувати кальційзалежні механізми виникнення спонтанних скорочень кардіоміоцитів на ранніх стадіях їх розвитку.
2. Встановити зміни кальцієвої регуляції в кардіоміоцитах, що експресують тропонін Т з мутацією I79N, яка викликає шлуночкову аритмію.
3. Визначити механізм порушення рефрактерності вивільнення Ca^{2+} із саркоплазматичного ретикулуму шлуночкових міоцитів мишей, зумовленого нокаутом гену калсеквестрину (*Casq2 KO*).
4. Зареєструвати трансмембранні струми, які активуються вивільненням іонів кальцію із внутрішньоклітинних депо панкреатичних ацинарних клітин та встановити зв'язок між спустошенням ендоплазматичного ретикулуму та активацією цих струмів.
5. Встановити можливу роль кальцієвого депозалежного струму у розвитку гострого панкреатиту.
6. Визначити вплив жовчних кислот на кальцієву проникність плазматичної мембрани ацинарних клітин підшлункової залози.

7. Встановити механізми кальцієвої регуляції зірчастих клітин підшлункової залози та з'ясувати ймовірну роль цих клітин у запобіганні виникнення некрозу ацинарних клітин.
8. Визначити особливості кальцієвої регуляції в клітинах різних типів у панкреатичних лобулах екзокринної частини підшлункової залози в нормі та патології.
9. Встановити роль порушень кальцієвої регуляції в ацинарних клітинах підшлункової залози у розвитку некрозу цих клітин, викликаного аспарагіназою.
10. З'ясувати вплив галактози на кальцієву регуляцію та функціональний стан ацинарних клітинах та на розвиток гострого аспарагіназаіндукованого панкреатиту.

Об'єкт дослідження – механізми регуляції внутрішньоклітинної концентрації іонів кальцію у клітинах підшлункової залози та кардіоміоцитах.

Предмет дослідження – впливи мутацій кальційзв'язуючих білків та змін депозалежного входу іонів кальцію на функціонування електрично збудливих та незбудливих клітин в нормальних та патологічних умовах.

Наукова новизна отриманих результатів. За допомогою флуоресцентних та електрофізіологічних методів дослідження вперше показано, що саме спонтанні коливання внутрішньоклітинної концентрації іонів кальцію, не пов'язані з генерацією трансмембранних струмів, призводять до скорочення кардіоміоцитів на ранніх стадіях розвитку останніх. Удосконалено методи оцінки кальцієвої буферної ємності кардіоміоцитів та їх внутрішньоклітинної перфузії у конфігурації “ціла клітина”. Вперше виявлено пряму кореляцію між рівнем буферної ємності та шлуночковою аритмією при мутаціях тропоніну, що підвищують чутливість міофіламентів до іонів кальцію.

У роботі вперше зареєстровано кальцієвий струм через плазматичну мембрану ацинарних клітин підшлункової залози, що активується вивільненням Ca^{2+} з ендоплазматичного ретикулуму. Показано зв'язок між рівнем спустошення ендоплазматичного ретикулуму та активацією депозалежного кальцієвого

трансмембранного струму. Отримані данні свідчать про те, що саме цей струм може бути одним із основних факторів, відповідальних за підвищення внутрішньоклітинної концентрації Ca^{2+} при розвитку гострого панкреатиту.

Вперше досліджена пряма дія жовчних кислот на механізми кальцієвої регуляції у клітинах підшлункової залози та запропоновано інтерпретацію механізму виникнення гострого панкреатиту, пов'язаного зі збільшенням $[\text{Ca}^{2+}]_i$ та $[\text{Na}^+]_i$. Встановлено негативний вплив аспарагінази – реагента, який застосовують в клінічній практиці для лікування дитячого гострого лімфобластного лейкозу – на кальцієву сигналізацію ацинарних клітин підшлункової залози. Запропоновано використання галактози для запобігання зростання $[\text{Ca}^{2+}]_i$ та виникнення некрозу клітин підшлункової залози в моделі гострого панкреатиту, викликаного аспарагіназою.

Вперше в клітинах у структурі панкреатичних лобул були встановлені зміни кальцієвої сигналізації, що спричиняються брадикініном в концентраціях, які є типовими для панкреатиту. У зіркоподібних клітинах підшлункової залози вперше був виявлений двофазний кальцієвий сигнал у відповідь на активацію брадикінінових V_2 -рецепторів плазматичної мембрани та з'ясовані механізми генерації цього сигналу. Отримані нові дані, які підтверджують панкреопротективну дію блокаторів брадикінінового рецептору V_2 , та продемонстровано, що їх використання запобігає некрозу ацинарних клітин. Вперше визначені особливості кальцієвої регуляції при взаємодії клітин різних типів у екзокринній частці підшлункової залози в їх природному оточенні. Зокрема, вперше досліджена кальцієва сигналізація в нервових клітинах підшлункової залози у структурі панкреатичних лобул.

Результати дослідження є внеском у комплексне розуміння механізмів кальцієвої регуляції та сигналізації в електробудливих та незбудливих клітинах у нормі та патології.

Теоретичне та практичне значення отриманих результатів. Результати дослідження, отримані в роботі, мають як фундаментальне, так і практичне значення. Порівняння роботи мембранних та внутрішньоклітинних

кальційрегулюючих структур в умовах виникнення патологій (мутації кальційзв'язуючих білків, гіперактивація депозалежного входу Ca^{2+} в клітину, індуковане різними чинниками виникнення некрозу ацинарних клітин та розвиток гострого панкреатиту підшлункової залози) істотно допомагають розумінню появи порушень регуляції внутрішньоклітинної концентрації Ca^{2+} і збагачують інформацію щодо патогенезу відповідних захворювань.

Практичне значення отриманих результатів полягає в тому, що вони дозволяють оцінити, які саме механізми регуляції внутрішньоклітинної концентрації іонів кальцію у клітинах різних типів (як електрозбудливих, так і незбудливих) ушкоджуються при розвитку низки патологій. Продемонстровано, що саме зміни цитозольної кальцієвої буферної ємності призводять до виникнення серцевих аритмій при Ca^{2+} -сенсibiliзуючих мутаціях тропоніну Т. Ці зміни у кальцієвій регуляції кардіоміоцитів можуть бути основою для модуляції серцевих скорочень у пацієнтів, що мають мутацію тропоніну TnT-I79N і в підсумку призводити до синдрому раптової зупинки серця. Досліджено ефект аспарагінази (речовини, яка застосовується в клінічній практиці для лікування дитячого гострого лімфобластного лейкозу) на панкреатичні клітини та запропоновано використання галактози для запобігання росту внутрішньоклітинної концентрації Ca^{2+} та виникненню некрозу клітин підшлункової залози. Крім того розширено наявні дані щодо механізму панкреопротектної дії блокаторів брадикінінового V2-рецептору, що запобігає некрозу ацинарних клітин та виникненню гострого панкреатиту.

Особистий внесок здобувача. Дисертаційна робота є особистою працею здобувача. Автор поставив задачу досліджень і самостійно розробив методики приготування кластерів підшлункової залози та візуалізації зіркоподібних клітин, вніс ряд удосконалень у методику оцінки кальцієвої буферної ємності ізольованих кардіоміоцитів, а також самостійно виконав основну частину експериментів, здійснював аналіз, статистичну обробку й узагальнення результатів. Деякі експерименти були проведені зі співавторами опублікованих робіт, зокрема співробітниками Інституту фізіології ім. О.О. Богомольця НАН

України к.б.н. С.В. Вятченко-Карпінським, Ю.В. Герасименко та Д.О. Кришталем. Дослідження молекулярних механізмів виникнення перших спонтанних скорочень кардіоміоцитів було проведено у співпраці з Інститутом нейрофізіології (Кьольн, Німеччина) (керівник проф. І. Хешлер). Експерименти з використанням клітин екзокринної частини підшлункової залози були проведені на базі Університету міста Кардіф (Кардіф, Велика Британія; керівник проф. О.Н. Петерсен). Дослідження кальційзв'язуючих білків кардіоміоцитів було проведено на базі Університету Вандербільта (Нешвіл, США; керівник проф. Б.С. Нолман). При плануванні, організації і проведенні досліджень по всіх розділах роботи частка особистої участі автора становила не менше 80%. Особисто проведено статистичний аналіз та інтерпретацію даних; відповідні результати опубліковано в наукових міжнародних виданнях. Автор не запозичав ідеї та розробки співавторів публікацій.

Матеріали, положення та висновки кандидатської дисертації здобувача не були використані при написанні докторської дисертації.

Апробація результатів дисертації. Усі матеріали дисертації докладалися на семінарах Інституту ім. О.О.Богомольця НАН України, а також на наступних міжнародних симпозіумах і з'їздах: Американського Біофізичного Товариства (Бостон, 2001, Сан Франциско, 2002, Бостон, 2009, Сан Франциско, 2010), Українського Біофізичного Товариства (Луцьк, 2015), конференції Європейської Академії (Кардіф, Велика Британія, 2016), зустрічі Королівського Наукового Товариства Великої Британії (Лондон, 2017), Українського Фізіологічного Товариства (Київ, 2019).

Результати дисертаційної роботи доповідалися також на наукових семінарах Інституту фізики НАН України та Українського Біофізичного Товариства.

Публікації. Результати дисертації викладено у 16 статтях (опублікованих у виданнях I та II квартиля реєстру Міністерства освіти та науки України) та 14 тезах міжнародних конференцій та з'їздів.

РОЗДІЛ 1
ВНУТРІШНЬОКЛІТИННІ КОЛИВАННЯ Ca^{2+} ВИКЛИКАЮТЬ
СПОНТАННІ СКОРОЧЕННЯ КАРДІОМІОЦИТІВ ПІД ЧАС РАННЬОГО
РОЗВИТКУ

1.1. Вихідні іонні струми в ранішніх кардіоміоцитах, що походять від ембріональних стовбурових клітин

Pflügers Arch – Eur J Physiol (2000) 439:798–807
Digital Object Identifier (DOI) 10.1007/s004249900196

ORIGINAL ARTICLE

O. Gryshchenko · Z.J. Lu · B.K. Fleischmann
J. Hescheler

Outwards currents in embryonic stem cell-derived cardiomyocytes

Received: 23 June 1999 / Received after revision: 6 October 1999 / Accepted: 15 October 1999 / Published online: 24 January 2000
© Springer-Verlag 2000

Abstract The aim of the present study was to investigate the expression and functional role of outwards currents during the early stages of cardiomyogenesis. The predominant repolarizing current in early-stage, embryonic stem (ES) cell-derived cardiomyocytes was a 4-aminopyridine (4-AP) sensitive [concentration for half-maximal inhibition (IC_{50}) 1.7 mM], transient outward current (I_{to}) with a current density of 10.3 ± 2.1 pA/pF ($n=72$). We observed two additional, rapidly activating, outwardly rectifying current components, $I_{K,sus}$ and I_{res} , in early- and late-stage cardiomyocytes. These currents were characterized by slow and no inactivation, respectively, during the depolarizing voltage step. $I_{K,sus}$ was detected in about 25% of cells investigated and displayed 4-AP hypersensitivity (IC_{50} 29 μ M), whereas I_{res} was found in all cells of both differentiation stages and was 4-AP insensitive. In contrast to early-stage cells, I_{res} formed the larger portion of the aggregate, whole-cell current in late-stage, ES cell-derived cardiomyocytes. The current densities of all three current components increased during development, however, the most prominent increase was observed for I_{res} from 3.6 ± 0.8 pA/pF ($n=72$) to 8 ± 1.1 pA/pF ($n=35$). In current-clamp recordings in early-stage, spontaneously contracting cardiomyocytes, 4-AP depolarized the cells, lengthened the action potential duration (APD) and increased the action potential frequency. In late-stage cells 4-AP had no effect on action potential frequency. We conclude that in early-stage cardiomyocytes I_{to} plays an important role in controlling electrical activity.

Key words ES cell-derived cardiomyocytes · Embryoid body · Early- and late-stage cardiomyocytes · Outward-rectifier currents · I_{to} · Membrane potential regulation

Introduction

In recent years, outwardly rectifying K^+ channels in cardiomyocytes have gained increasing attention because of their important role in determining action potential duration (APD [6]) and in their possible pro-arrhythmic role during the repolarization phase [35]. This is strengthened particularly by the observation that in ventricular cardiomyocytes obtained from patients suffering from end-stage heart failure [5, 23, 34] and in cardiomyocytes derived from hypertrophic ventricles of various animal models [4, 29, 40] the functional expression of outwardly rectifying K^+ currents is strongly reduced.

Two major components of outwardly rectifying K^+ channels have been described: a transient, rapidly activating and inactivating component (I_{to}) [8], presumably formed by Kv4.2 and Kv4.3 subunits, and a rapidly activating, slowly/non-inactivating current component composed of several subunits including Kv1.5 and Kv2.1 [2]. Recently, it was suggested that I_{to} is formed by different subunits during cardiac development: While in perinatal rat ventricular cardiomyocytes I_{to} appears to be encoded by the *Kv1.4* gene [17, 36], in adult myocytes this channel is composed presumably of Kv4.2/Kv4.3 subunits [12, 17, 26, 36, 39]. This is supported by the relatively faster recovery from inactivation, compared with Kv1.4, seen in adult rat ventricular cardiomyocytes [36] and the distribution pattern of mRNA in epicardial and pericardial ventricular cardiomyocytes [11]. Conclusive evidence has been provided by the generation of mice lacking the *Kv1.4* gene, in which I_{to} was expressed functionally in ventricular cardiomyocytes as in the cells of wild-type mice [20]. In addition, ventricular cardiomyocytes from the transgenic mouse carrying a dominant negative Kv4.2 mutant do not express I_{to} [3].

O. Gryshchenko and Z. J. Lu contributed equally to the manuscript

O. Gryshchenko · Z.J. Lu · B.K. Fleischmann · J. Hescheler (✉)
Zentrum Physiologie und Pathophysiologie
der Universität zu Köln, Institut für Neurophysiologie,
Robert-Koch-Strasse 39,
D-50931 Cologne, Germany
e-mail: jh@physiologie.uni-koeln.de
Tel.: +49-221-4786960, Fax: +49-221-4786965

Despite the notion that the heart is the first organ to form during embryogenesis, relatively little is known about the electrophysiological properties underlying the setting of the resting membrane potential (RMP), the control of APD and the spontaneous electrical activity in very early embryonic cardiomyocytes. Indeed, functional and molecular studies on the expression of ion channels at this early stage are limited because of the small size of the embryonic heart and the lack of permanent cell lines to model the earliest stages of cardiomyogenesis [18]. Our approach for the investigation of isolated, early-developmental-stage (EDS), murine cardiomyocytes is based on embryonic stem (ES) cells, which are pluripotent and therefore widely used for the generation of transgenic and knockout mice. ES cells can be differentiated in vitro as embryoid bodies (EBs), which produce, among other cells, embryonic cardiomyocytes. After longer cultivation of murine EBs (7–9 days), differentiated, late-developmental-stage (LDS) cardiomyocytes can be obtained, recapitulating the different cardiac phenotypes of the native murine heart [21].

The aim of the present study was to investigate the functional expression of outward currents during early stages of development and their role in controlling cardiac excitability. We provide evidence that during early stages of cardiomyogenesis I_{to} contributes the largest portion of the aggregate whole-cell current and plays an important role in setting RMP and action potential frequency. We also show that in LDS cardiomyocytes I_{res} forms the prominent fraction of the aggregate outward current and that 4-aminopyridine (4-AP)-sensitive K^+ currents play a less important role for cardiac excitability.

Materials and methods

In the present study, ES cells of the line D3 were used. The cells were cultivated and differentiated into spontaneously beating cardiomyocytes as previously described [37]. Briefly, ES cells were cultivated in hanging drops (about 400 cells per drop) for 2 days, then kept in suspension for 5 days and finally plated on gelatin-coated, single culture dishes for patch-clamp recordings. At 2–4 days after plating (i.e. 7+2–4 days), spontaneously contracting cell clusters could be observed within the EBs. EDS cardiomyocytes were obtained from 7+2- to 4-day- (preferably 3- to 4-day-) old EBs, whereas LDS cells were harvested from 7+9- to 15-day-old EBs.

The culture medium consisted of Dulbecco's modified Eagle's medium (DMEM) supplemented with 20% fetal calf serum, penicillin/streptomycin, glutamax, non-essential amino acids (all from GIBCO, Eggenstein, Germany) and β -mercaptoethanol (Serva, Heidelberg, Germany). For patch-clamp recordings, beating areas of 20–30 EBs were dissected and isolated by enzymatic dispersion using collagenase B (Boehringer Ingelheim, Ingelheim, Germany). The dissociated material was plated onto glass cover-slips, resuspended in culture medium and stored in the incubator. Within the first 12 h cells attached to the glass surface and spontaneously beating cardiomyocytes could be observed. For electrophysiological recordings, the glass cover-slips were transferred to a temperature-controlled recording chamber and perfused with extracellular solution. Only spontaneously beating cells were selected for experiments.

Voltage- and current-clamp recordings were made using the classic whole-cell or perforated-patch-clamp technique, respec-

tively. Since the recording of I_{to} required good voltage control, voltage-clamp experiments were performed only when series resistance was below 10 M Ω . Current-clamp data were obtained using the perforated-patch-clamp configuration. Currents and potentials were recorded using suitable amplifiers (Axopatch 200 A, Axon Instruments, Foster City, Calif., USA and EPC-9, Heka, Lambrecht, Germany) together with the ISO 2 (MFK, Niedermhausen, Germany) and Pulse (Heka) software packages, respectively. Data were sampled at 2 kHz, filtered at 1 kHz, stored on hard disk and analysed off-line using the ISO 2 or Pulse-Fit (Heka) analysis software. The effect of Ba^{2+} on action potential frequency was recorded continuously using a VR-3200 tape recorder (Bell and Howell, Friedberg/H., Germany). These data were downloaded from tape into SPIKE2 software at a digitization rate of 100 Hz and analysed as above. Averaged data are expressed as means \pm SEM. Statistical tests were performed using unpaired Student's *t*-test.

Unless otherwise indicated, outwards currents were elicited by 500-ms depolarizing voltage steps to test potentials ranging from -40 mV to 80 mV in 10-mV increments at a frequency of 0.1 Hz (holding potential, HP -80 mV). Unless otherwise stated, currents were leak subtracted using P/4 leak subtraction mode. Current density was estimated by measuring the peak current (I_{to} and $I_{K_{sus}}$) or the current at the end of the 500-ms step (I_{res}) at a test potential of +40 mV.

The functional expression of the rapidly activating, 4-AP hypersensitive component ($I_{K_{sus}}$) was investigated using a double-pulse protocol (no leak subtraction). A depolarizing prepulse (300 ms) to +40 mV (HP -20 mV) was applied, followed by a 20-ms repolarization to -20 mV and depolarizing voltage steps ranging from -10 to +80 mV in 10-mV increments at 0.6 Hz (see also [32]). Steady-state inactivation was evaluated by applying 1-s prepulses ranging from -90 to +30 mV in 10 mV increments, each followed by a 2-s depolarizing step to 40 mV at a frequency of 0.17 Hz (HP -80 mV, no leak subtraction). To investigate the characteristics of the inactivating current component, steady-state currents at the end of the 2-s depolarizing step were subtracted. The individual experiments were normalized and the dependence of peak current amplitude on prepulse potential analysed. An average of seven experiments was used for the Boltzman fit. To distinguish the different outwardly rectifying K^+ current components, 4-AP at different concentrations was used (see also Fig. 2). The 4-AP hypersensitive component (0.5 mM) was identified as $I_{K_{sus}}$, the 4-AP-resistant component at the end of the 500-ms pulse as I_{res} and the difference current upon application of 10 mM 4-AP as I_{to} (see Fig. 2). The recovery from inactivation was determined using 250-ms prepulses at different intervals to +30 mV. The plotting of peak currents as a function of prepulse to pulse interval yielded the time course for the estimate of recovery from inactivation. The data were fitted with the function, $y(t) = I_{\infty} \cdot \exp(-t/\tau)$, where I_{∞} is the steady-state current, t the time and τ the time constant. For an estimation of the inwardly rectifying K^+ current (I_{K1}) expression 200-ms hyperpolarizing currents to -100 mV were applied (HP -80 mV, no leak subtraction). Due to the spontaneous electrical activity and the diastolic depolarization APD was determined at 0 mV. The maximal diastolic potential was taken as an estimate of RMP in the spontaneously contracting cardiomyocytes.

For perforated-patch-clamp recordings, amphotericin B (Sigma, Deisenhofen, Germany) was dissolved in dimethylsulphoxide (DMSO) at 60 mg/ml, deep-frozen in aliquots and thawed prior to use. The tip of the pipette was filled with normal recording solution and the pipette then back-filled with the amphotericin B-containing solution, yielding a final concentration of 500 μ g/ml. The composition of the different solutions used was as follows (in mM): dissociation solution: NaCl 120, KCl 5.4, $MgSO_4$ 5, $CaCl_2$ 0.03, Na-pyruvate 5, glucose 20, taurine 20, 4-(2-hydroxyethyl)-1-piperazineethanesulphonic acid (HEPES) 10, collagenase B (Boehringer Mannheim, Mannheim, Germany) 0.5–1 mg/ml, pH 6.9 (NaOH). Pipette solution for current-clamp experiments: KCl 55, K_2SO_4 70, $MgCl_2$ 7, HEPES 10, pH 7.4 (KOH). External solution for current-clamp recordings (mM): NaCl 135, KCl 5.4, $MgCl_2$ 2, $CaCl_2$ 1.8, glucose 10, HEPES 10, pH 7.45 (NaOH). Pi-

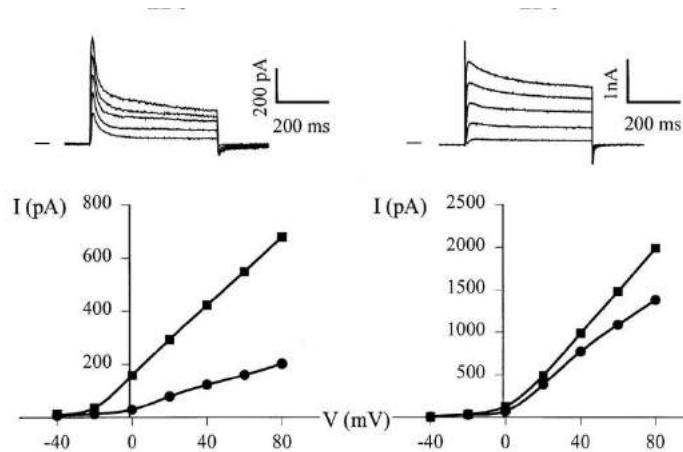


Fig. 1 Functional expression of outwardly rectifying currents in early- and late developmental-stage (EDS and LDS respectively) cardiomyocytes. Representative currents (upper panels) and current/voltage (I/V) curves (lower panels) recorded from an EDS (left) and an LDS (right) embryonic stem cell (ES)-derived cardiomyocyte in the whole-cell configuration mode (lines to the left of the current traces indicate zero current). Outward rectifier currents were evoked by 500-ms depolarizing voltage steps from a holding potential (HP) of -80 mV to step potentials ranging from -40 to 80 mV in 20 -mV increments. The squares indicate peak currents, the circles late currents measured at the end of the 500 -ms voltage steps. The original current traces are displayed for step potentials varying between 0 and 80 mV

ette solution for voltage clamp experiments: KCl 50 , K_2SO_4 80 , $MgCl_2$ 1 , ethyleneglycol-bis(3-aminoethylether)- N,N,N' -tetraacetic acid (EGTA) 10 , HEPES 10 , $CaCl_2$ 1 , adenosine $5'$ -triphosphate, magnesium salt (MgATP) 3 , pH 7.4 (KOH). External solution for voltage clamp experiments: choline chloride 140 , $CaCl_2$ 1.8 , $MgCl_2$ 1 , $CdCl_2$ 0.1 , KCl 5.4 , HEPES 10 , glucose 10 , pH 7.45 (KOH). I_{K1} recording solutions: pipette solution: KCl 50 , K-aspartate 80 , $MgCl_2$ 1 , MgATP 3 , EGTA 10 , HEPES 10 , pH 7.4 (KOH). External solution: NaCl 140 , KCl 5.4 , $CaCl_2$ 3.6 , $MgCl_2$ 1 , HEPES 10 , glucose 10 pH 7.4 (NaOH). All experiments were performed at 35 ± 1 °C. The conditions chosen allowed stable recordings in both the current- and voltage-clamp mode from spontaneously contracting, ES cell-derived cardiomyocytes. Pipettes were made by a DMZ Universal Puller (DMZ, Munich, Germany) from 1.5 mm borosilicate glass capillaries (Clark Electromedical Instruments, UK). 4-AP was obtained from Sigma, margatoxin and charybdotoxin from Peptide Institute (Herts., UK). A stock solution of 4-AP was made by dissolving it in extracellular solution. The pH was corrected, the solution divided into aliquots and deep-frozen. Prior to the experiments aliquots were thawed and diluted to the desired concentration.

Results

Undifferentiated ES cells exhibited no spontaneous electrical activity, nor did depolarizing current injections elicit action potentials ($n=30$, data not shown). This was further corroborated by voltage-clamp experiments in which only small-amplitude and linear current/voltage (I/V) relationships were detected ($n=30$, data not shown). These data indicated that voltage-dependent ion channels are not expressed at the ES cell stage.

In contrast, ES cell-derived cardiomyocytes, beginning 2 days after plating ($7+2$ days), generated action potentials of different shape, depending on the developmental stage and the cell type, as reported before [21]. The average APD in spontaneously beating EDS ($7+2-4$ days) and LDS ($7+9-15$ days) cardiomyocytes was 169 ± 31.6 ms ($n=21$) and 82 ± 11.7 ms ($n=15$), respectively. EDS cells had a RMP of -48 ± 7 mV and action potential frequency of 1.32 ± 0.41 Hz ($n=21$) whereas LDS cells displayed a RMP of -54 ± 5.2 mV and an action potential frequency of 1.58 ± 0.23 Hz ($n=15$).

To investigate the currents involved in determining APD, RMP and spontaneous electrical activity, we investigated the expression of outwardly rectifying channels at various differentiation stages. The contamination of these outwards currents by the activation of voltage-dependent Ca^{2+} currents and the Ca^{2+} -activated, transient, outward current [8, 19, 27, 41] or the activation of Na^+ currents was excluded by addition of Cd^{2+} and replacement of Na^+ in the extracellular solution. The known interference of Cd^{2+} with the biophysical characteristics of I_{to} [1, 34] and of Na^+ [13] replacement with I_{to} density was not considered critical for the investigations performed in the present study.

Figure 1 shows current traces representative of the functional expression of outwardly rectifying currents in EDS (left) and LDS (right) ES cell-derived, spontaneously contracting cardiomyocytes. As can be seen, 500 -ms depolarizing voltage steps ranging from test potentials of 0 mV (I/V , -40 mV) to $+80$ mV in 20 -mV increments (holding potential -80 mV) elicited outwardly rectifying currents in both EDS and LDS cardiomyocytes. The current densities of the transient and sustained current components increased during development (see also below). Whereas in EDS cells the amplitude of the transient component was larger than the sustained component at the end of the 500 -ms depolarizing voltage step, the latter represented the larger fraction of the aggregate, whole-cell current in LDS cardiomyocytes. This can be clearly seen in the I/V relationship (Fig. 1, lower panels). The threshold of activation for both current components at either differentiation stage was between -30 and

Fig. 2 Pharmacological dissection of the outwardly rectifying currents expressed in a LDS cardiomyocyte using different concentrations of the K^+ channel blocker 4-aminopyridine (4-AP). The upper panels show original currents under control conditions (left, 1) and after application of 0.5 (middle, 2) or 10 (right, 3) mM 4-AP. The difference current 1–2 is the rapidly activating, slowly inactivating $I_{K,sus}$ (left-hand side, middle panel). The difference current 2–3 is the characteristic rapidly activating and inactivating current component I_{to} . The remaining, 4-AP-resistant component (upper right panel) is I_{res} . The pulse protocol was identical to the one used in Fig. 1, current traces and I/V curves show step potentials ranging from -20 to 80 mV

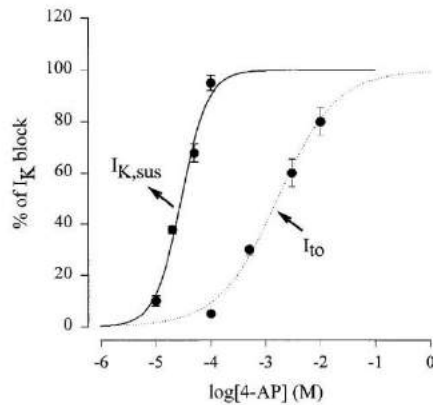
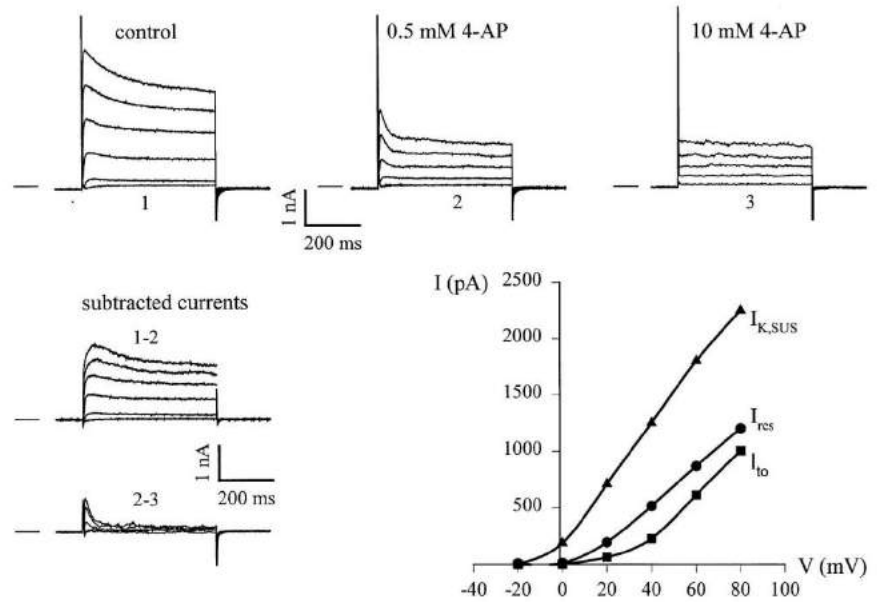


Fig. 3 Dose/response curve for the inhibition of the outwardly rectifying K^+ currents I_{to} and $I_{K,sus}$ by 4-AP in EDS and LDS cardiomyocytes in the voltage-clamp mode. The lines show the fit with Langmuir's isotherm ($n=19$)

-20 mV, similar to that for neonatal rat ventricular cardiomyocytes [30]. In addition, the voltage dependence of activation was almost identical for the transient and plateau phases of the current at both differentiation stages.

To distinguish between the main components of rapidly activating outwardly rectifying currents in ES cell-derived cardiomyocytes we used 4-AP, a known blocker of K^+ channels [22]. Figure 2 shows the blocking effect of different concentrations of 4-AP on outwardly rectifying currents recorded from a LDS cardiomyocyte. Three different components of rapidly activating outwardly rectifying currents can be distinguished on the basis of their inactivation characteristics and their sensitivity towards 4-AP: a 4-AP-hypersensitive, slowly inactivating component ($I_{K,sus}$), a 4-AP-sensitive, rapidly inactivating component (I_{to}) and a 4-AP-resistant current component

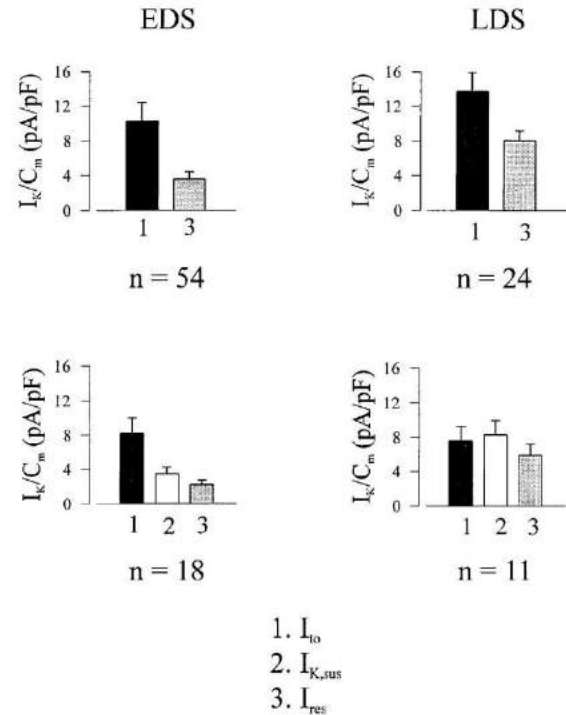


Fig. 4 Current densities of the different outwardly rectifying K^+ current components in EDS (left) and LDS (right), ES cell-derived cardiomyocytes. Most of the cells expressed only the I_{to} and $I_{K,sus}$ components (upper panels), but about 25% of both EDS and LDS cardiomyocytes also expressed $I_{K,sus}$ (lower panels)

with no inactivation during the depolarizing voltage step (I_{res}). The biophysical characteristics with regard to activation and inactivation are shown more clearly in the difference currents and in the corresponding I/V curves

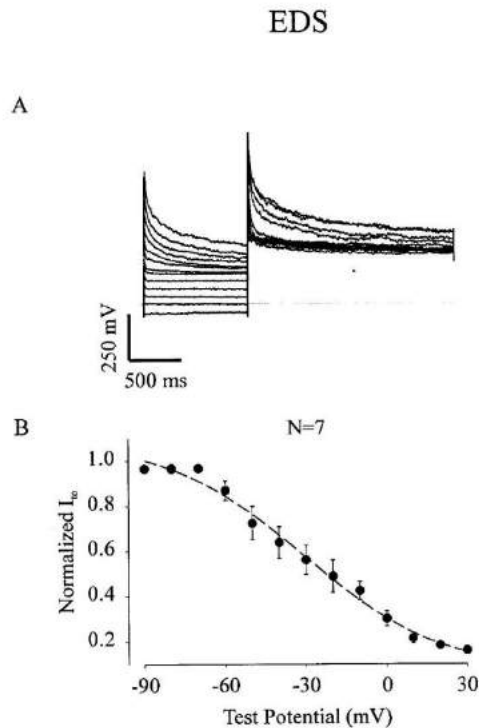


Fig. 5A,B Steady-state inactivation characteristics of I_{to} in EDS cells tested by applying 1-s prepulses from -90 to $+30$ mV in 10 mV increments followed by a 2-s depolarizing step to $+40$ mV (HP -80 mV). **A** Pronounced inactivation of the rapidly inactivating current component. However, even at positive prepulse potentials a small inactivating component was present (dotted line indicates zero current). **B** Mean data from seven EDS cardiomyocytes as shown in **A**. The line shows the fit of a Boltzmann function

of Fig. 2. A quantitative estimate of the sensitivity of $I_{K,sus}$ and I_{to} to 4-AP was obtained by constructing concentration-response curves for EDS and LDS cardiomyocytes ($n=19$). I_{to} was equally sensitive towards 4-AP at both stages. As depicted in Fig. 3, 4-AP depressed I_{to} with a half-maximal inhibitory concentration (IC_{50}) of 1.7 mM and $I_{K,sus}$ with an IC_{50} of 29 μ M.

The functional expression and current density of the three outwardly rectifying current components was investigated, using their sensitivity to 4-AP as the distinguishing characteristic, in a large number of EDS and LDS cells (see also Fig. 2). In 75% of EDS cells ($n=72$), two components of outwardly rectifying currents were found: I_{to} (current density 10.3 ± 2.1 pA/pF) and I_{res} (current density 3.6 ± 0.8 pA/pF). $I_{K,sus}$, the slowly inactivating, 4-AP-hypersensitive current (complete block by 0.2 mM 4-AP) was observed with a current density of 3.5 ± 0.9 pA/pF in only 25% of these cells (Fig. 4). In 69% of LDS cardiomyocytes ($n=35$) I_{to} (current density 13.7 ± 2.2 pA/pF) and I_{res} (8 ± 1.1 pA/pF) were detected. $I_{K,sus}$ could also be detected (current density 8.3 ± 1.1 pA/pF) in 31% of cells tested (Fig. 4).

Since I_{to} was the predominant K^+ outward current component in EDS cells, the steady-state inactivation of I_{to}

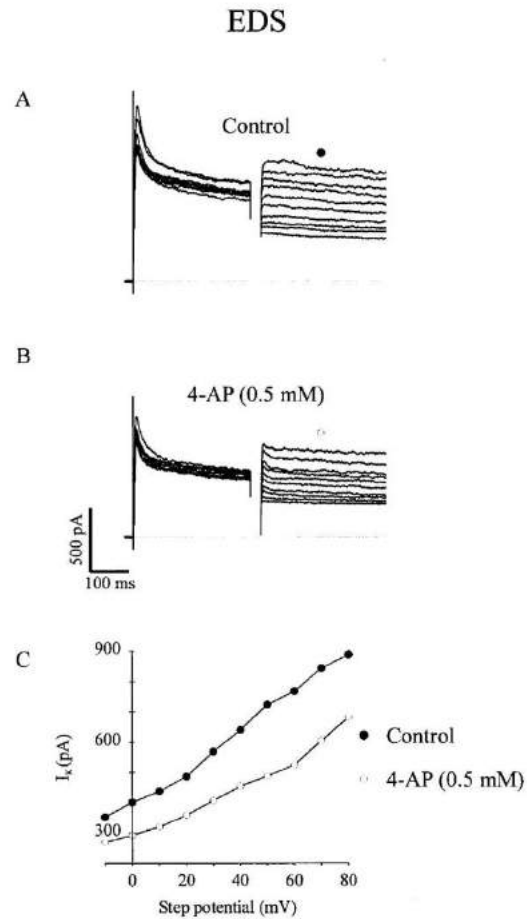


Fig. 6A–C ES cell-derived cardiomyocytes express an outwardly rectifying current ($I_{K,sus}$) characterized by 4-AP hypersensitivity. $I_{K,sus}$ was separated from I_{to} in an EDS cardiomyocyte by applying a 300-ms depolarizing prepulse (from HP) of -20 to $+40$ mV, followed by a 20-ms repolarization to HP and a subsequent 300-ms step from -10 to $+80$ mV in 10-mV increments. **A** Representative experiment showing the rapidly activating, slowly inactivating current. **B** Inhibition of a fraction of the cumulative, inactivation-resistant current by 0.5 mM 4-AP (dotted line indicates zero current). **C** I/V relation for peak I_K in absence (**A**) and presence (**B**) of 4-AP

was characterized at this developmental stage [32] (Fig. 5A). The voltage-dependent inactivation of I_{to} was less pronounced than in atrial human cardiomyocytes. Fitting a Boltzmann function to the steady-state inactivation curve obtained from seven representative EDS cells yielded a mid-point of -31 ± 4 mV and a slope factor K of 25.9 ± 5.7 mV (Fig. 5B). Because I_{to} is subject to pronounced, use-dependent inactivation, recovery from inactivation was estimated by applying prepulses at varying intervals to a test potential of $+40$ mV from a HP of -80 mV ($n=3$). A single-exponential fit of these data yielded a τ of 2.7 s (data not shown), close to the value estimated for Kv1.4 [25].

The presence of a 4-AP-hypersensitive current component ($I_{K,sus}$) was further confirmed by applying double-pulse protocols leading to inactivation of I_{to} [32]. As de-

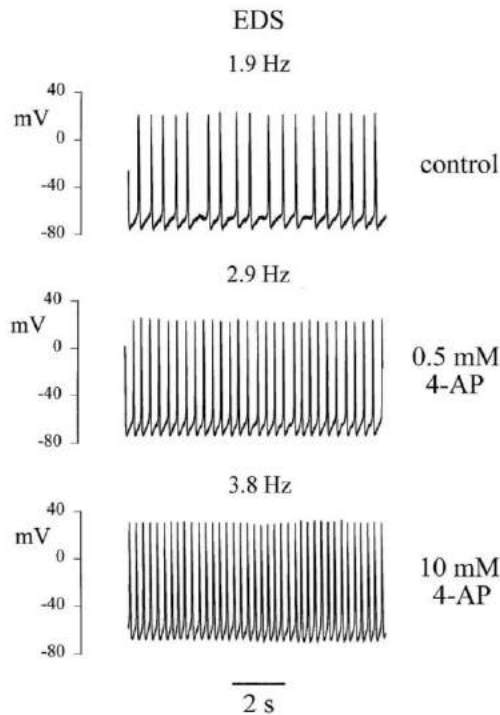


Fig. 7 Effect of 4-AP on action potential frequency and resting membrane potential (RMP) in a representative EDS cardiomyocyte in the current-clamp mode using the perforated-patch-clamp technique

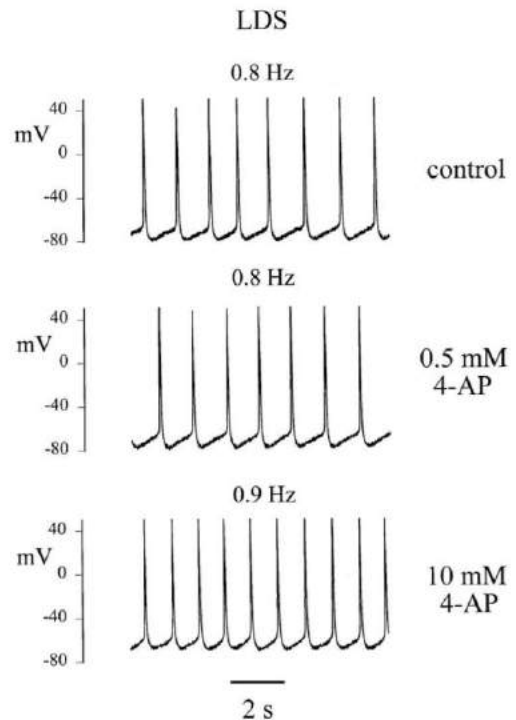


Fig. 8 Effect of 4-AP on action potential frequency and RMP in a representative LDS cardiomyocyte in the current-clamp mode using the perforated-patch-clamp technique

picted in Fig. 6A and C, an outwardly rectifying current component was identified upon applying depolarizing pre-pulses from a HP of -20 mV. In addition, application of $500 \mu\text{M}$ 4-AP resulted in a partial block of peak outwards currents ($28 \pm 8\%$ at 0 mV, $32 \pm 12\%$ at $+50$ mV, $n=3$) at all potentials tested (Fig. 6B and C). In contrast to 4-AP, application of charybdotoxin (CHTX, 25 – 200 nM), a blocker of $\text{Kv}1.2$, $\text{Kv}1.3$ [15] and large-conductance, Ca^{2+} -activated K^+ (K_{Ca}) channels [7], did not block outwards currents at either differentiation stage ($n=4$, data not shown). Similarly, application of margatoxin (5 – 20 nM, $n=2$, data not shown), a blocker of $\text{Kv}1.2$, $\text{Kv}1.3$ and $\text{Kv}1.6$ channels [15], also failed to block outwards currents.

Because of the prominent expression of I_{to} and the low current density of I_{K1} [16] at the EDS cell stage we investigated whether this K^+ current plays a role in setting RMP and determining APD. For this purpose the influence of different concentrations of 4-AP on action potential frequency, APD and RMP of spontaneously beating cells was examined in the current-clamp mode. In EDS cells the spontaneous electrical activity proved to be dose-dependently sensitive to 4-AP (Fig. 7). Indeed, the application of 10 mM 4-AP almost doubled AP frequency (Fig. 7, lower panel, increase by $83 \pm 8.8\%$, $n=7$); with 0.5 mM 4-AP a positive chronotropic effect was noted. In contrast, in LDS cells even 10 mM 4-AP did not change the action potentials significantly (increase of frequency by $10 \pm 3\%$, $n=9$, Fig. 8). The action of 4-AP

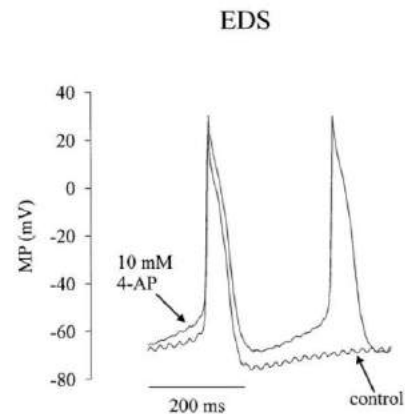


Fig. 9 Effect of 4-AP (10 mM) on spontaneous electrical activity and action potential duration in an EDS cardiomyocyte in the current-clamp mode using the perforated-patch-clamp technique

was fully reversible by washout. In both differentiation stages high concentrations of 4-AP (3 – 10 mM) slightly depolarized the RMP by 6 ± 1.2 mV ($n=14$) (Figs. 6 and 7, lower panels). Moreover, in EDS cells 4-AP induced a dose-dependent increase in the rate of the diastolic depolarization (Fig. 9). At 10 mM, 4-AP changed the latter from 53.28 ± 5.49 to 92.09 ± 14.62 mV/s ($n=3$). Whereas 10 mM 4-AP did not alter the APD of terminally differ-

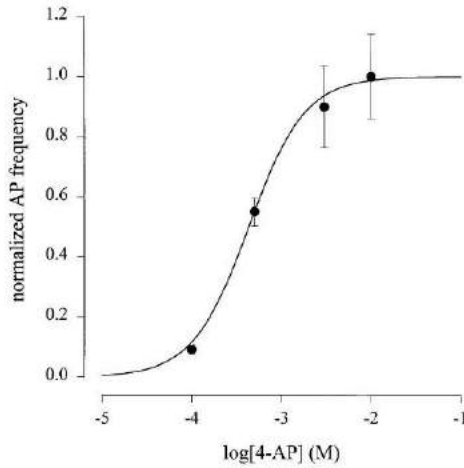


Fig. 10 Dose/response relation for the effect of 4-AP on action potential frequency, tested in the current clamp mode ($n=7$). The frequency in the presence of 10 mM 4-AP was taken as 1. The continuous line is the fit of Langmuir's isotherm

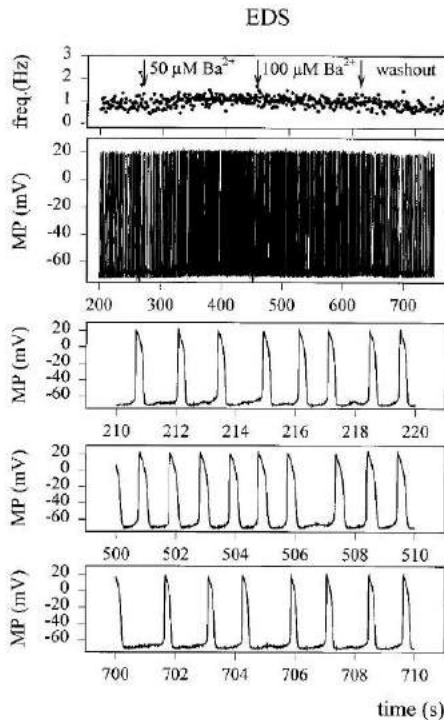


Fig. 11 The inwardly rectifying K^+ current I_{K1} is not involved in the control of the spontaneous electrical activity in EDS cardiomyocytes. Long-term current-clamp recordings, using the perforated-patch-clamp technique, of the spontaneous electrical activity (second panel from top) of an EDS cardiomyocyte upon addition of 50 or 100 μM Ba^{2+} . Top panel: Action potential frequency. The lower three panels show action potentials recorded in the absence (third panel from top) or presence of Ba^{2+} (100 μM , fourth panel) and after washout (last panel). Note the extended time scale in these three panels. For clarity, the display of the experiment (second panel from top) was only started 200 s after initiation of the recordings

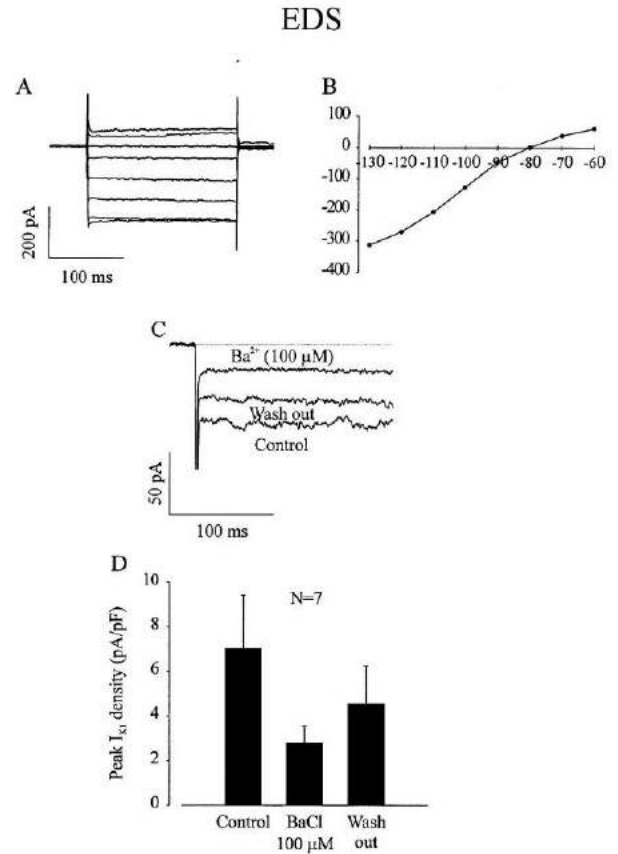


Fig. 12A–D Sensitivity of I_{K1} in EDS cells to low extracellular $[Ba^{2+}]$. **A** I_{K1} recorded by applying voltage steps to test potentials ranging from -130 to -60 mV (HP -80 mV). **B** The I/V relationship showing a reversal potential close to the K^+ equilibrium potential and pronounced inward rectification. **C** Inhibition of I_{K1} by extracellular Ba^{2+} (100 μM) and its partial reversal by wash out (test potential -100 mV, HP -80 mV, dotted lines indicate zero current). **D** Effect of Ba^{2+} (100 μM) on I_{K1} density at a test potential of -100 mV (HP -80 mV)

entiated cells (data not shown), it prolonged the latter in EDS cardiomyocytes by $11 \pm 0.8\%$ ($n=5$, Fig. 9). CHTX (10–300 nM) altered neither APD nor RMP significantly in either differentiation stage ($n=7$, data not shown).

We next examined the role of $I_{K_{sus}}$ in determining RMP and action potential frequency at both differentiation stages. For this purpose the action of 4-AP (100 μM) on APD and RMP was tested in cells in which the $I_{K_{sus}}$ contributed 30–50% of the aggregate, whole-cell current. In these cells the 4-AP-induced block of $I_{K_{sus}}$ markedly prolonged APD by $42 \pm 7.6\%$ ($n=3$) but had no significant effect on the spontaneous action potential frequency (data not shown). The quantitative changes of action potential frequency upon addition of increasing concentrations of 4-AP was investigated in EDS cardiomyocytes (Fig. 10). The maximal frequency obtained after application of 10 mM 4-AP was taken as reference value for the normalization of frequencies recorded under control conditions and under increasing

concentrations of 4-AP. This analysis yielded a half-maximal excitatory concentration (EC_{50}) for 4-AP of 0.45 mM (Fig. 10).

Since I_{K1} plays an important role in determining the RMP and APD in terminally differentiated cardiomyocytes [38], we investigated next whether this current is involved in setting the RMP in EDS cardiomyocytes. As depicted in Fig. 11 application of Ba^{2+} (50–100 μ M), a known blocker of I_{K1} , prolonged APD by approximately 10%, ($n=3$) but had no relevant effect on frequency. This is further corroborated by the aforementioned observation, that I_{K1} density is low in EDS cardiomyocytes [16] compared with LDS cells [21]. Voltage-clamp experiments were performed to demonstrate further that the chosen $[Ba^{2+}]$ blocked a substantial fraction of I_{K1} . As seen in Fig. 12, EDS cells functionally express I_{K1} (Fig. 12A, B) and application of 100 μ M Ba^{2+} depressed this current (Fig. 12C). At a test potential of -100 mV I_{K1} was blocked by $56 \pm 5\%$ ($n=7$) (Fig. 12D) and even at -40 mV, a potential positive to the K^+ reversal potential, I_{K1} was blocked by $62 \pm 7\%$ ($n=7$, data not shown).

Discussion

Three components of outwardly rectifying currents could be identified in ES cell-derived cardiomyocytes during early and late stages of development: a rapidly activating and inactivating, I_{to} -like, 4-AP sensitive (IC_{50} 1.7 mM) component, a rapidly activating, slowly inactivating, 4-AP-hypersensitive (IC_{50} 29 μ M) component ($I_{K,sus}$) as well as a rapidly activating, 4-AP-insensitive component (I_{res}) that displayed no inactivation during depolarizing voltage steps. Although the nature of I_{res} was not investigated in detail its activation kinetics, threshold of activation and outward rectification indicate it as a possible K^+ current. Indeed, in embryonic day E11–E13 murine atrial and ventricular cardiomyocytes three distinct outwardly rectifying K^+ channels with characteristics similar to those in ES cell-derived cardiomyocytes are detected [10]. Whereas I_{to} is the major portion of the aggregate, whole-cell current in our EDS cardiomyocytes I_{res} becomes the predominant component in LDS ES cell-derived cardiomyocytes. An increase in current density of outwardly rectifying currents during postnatal development has been reported previously for mouse [31] and rat [36, 39] cardiomyocytes. In the present study we investigated their expression during early embryonic development. These early stages are particularly interesting since cardiac development is already finalized around E15. At the early developmental stage I_{to} is the predominant K^+ conductance, in particular because I_{K1} expression is still low. The biophysical characteristics of I_{to} appeared similar to those in adult cardiomyocytes, however even at strongly depolarized prepulse potentials a small inactivating component was observed and the midpoint of the steady-state inactivation was shifted to more depolarized potentials. This may be due to different biophysical characteristics of I_{to} during early stages of cardiomyogenesis,

the presence of a small component of $I_{K,sus}$, which does not display use-dependent inactivation and extracellular Cd^{2+} , which is known to alter the biophysical characteristics of I_{to} [13]. The functional expression of $I_{K,sus}$, which has been reported in human atrial cardiomyocytes [32] and murine embryonic [10] and adult ventricular cardiomyocytes [14] was confirmed by pharmacological dissection of the 4-AP-sensitive current components and examination of their biophysical characteristics using a double-pulse protocol. Thus, the 4-AP-hypersensitive current component was similar to that in adult mice (14.5 μ M) [14] and human atrial cardiomyocytes (49 μ M) [32] and indicates that the encoding gene is *Kv1.5*. As reported for E17–E20 murine ventricular cardiomyocytes [10], $I_{K,sus}$ could not be identified in most LDS cells, possibly pointing towards pronounced up-regulation after birth. Since CHTX and MTX blocked neither outwards currents nor electrical activity, *Kv1.2*, *Kv1.3* and *Kv1.6* subunits do not appear to be expressed functionally at this embryonic stage. Similar observations have been made in rat ventricular cardiomyocytes, in which a pronounced increase in *Kv1.2* channels starting 10 days after birth is observed [39]. Interestingly, in the same study a postnatal decrease of *Kv2.1* channels was reported. It remains unclear whether *Kv2.1* (a non-inactivating, but 4-AP-sensitive current) or another K^+ channel subunit may encode the prominent, 4-AP-insensitive plateau phase in the LDS cells. Its postnatal down-regulation may explain the APD prolongation observed in adult murine ventricular cardiomyocytes with 4-AP [14].

The observed changes in ion channel expression during development were accompanied by changes in the spontaneous electrical activity. The increase in current density, in particular for I_{res} and I_{K1} [21], most likely underlies the pronounced reduction of the APD and the more negative RMP in terminally differentiated cardiomyocytes. In EDS cells 4-AP induced a concentration-dependent increase (EC_{50} 0.45 mM) of the spontaneous action potential frequency, APD and depolarization of the RMP. This EC_{50} does not differ greatly from our IC_{50} for I_{to} (1.7 mM) measured under voltage-clamp conditions. The discrepancy may be related to the fact that a fraction of I_{to} is already inactivated due to the relatively depolarized RMP in EDS cardiomyocytes. These data suggest unequivocally that I_{to} is an important determinant of electrical activity during early cardiomyogenesis. Future studies should be aimed at elucidating the precise mechanism of how I_{to} affects these parameters. Due to the known short time constants of deactivation, the main action of I_{to} probably occurs during the plateau phase. In contrast to the effect of 4-AP on EDS cells, ES cell-derived ventricular-like cardiomyocytes [21] and adult, murine ventricular cardiomyocytes [14], in our LDS cells 4-AP did not result in a pronounced increase of APD. This may be due to several reasons including, (i) differences in the cell population studied, since the present study investigated exclusively spontaneously beating cardiomyocytes, and (ii), the prominent expression of the 4-AP-insensitive component I_{res} (see also above) and of

I_{K1} [16, 21]. The present findings are consistent with a recent report on fetal rat ventricular cardiomyocytes, in which I_{K1} expression is low [38]. An important role for outwardly rectifying K^+ currents in the control of RMP is presumably related to the more depolarized RMP, during which channel open probability is higher. Besides I_{to} , the adenosine 5'-triphosphate (ATP)-sensitive, inwardly rectifying K^+ current ($I_{K,ATP}$) is believed to be involved in the regulation of spontaneous electrical activity in both fetal rat ventricular cardiomyocytes [38] and early-stage ES cell-derived cardiomyocytes [16]. This is particularly important in the light of the observation that hypoxic conditions depress I_{to} [24, 28].

The low expression of RMP-stabilizing currents in EDS cardiomyocytes [10, 18, 21, 38] may underlie their vulnerability towards different pharmacological agents. Indeed, substances that block K^+ channels, such as class III antiarrhythmic agents [33] or other ion channel blockers such as antiepileptic drugs [9], have a pronounced teratogenic potential at the embryonic stage. The critical time window is E9–E15 of embryonic development, when, as pointed out above, early cardiomyogenesis occurs. Changes of the cardiac output due to bradycardia, negative inotropy and low-output failure may result in hypoxia leading to haemorrhage and ultimately to a variety of severe malformations.

Our data further support the importance of the investigation of membrane proteins involved in the establishment and regulation of the electrical activity in heart during embryonic development. Our studies may therefore, provide a better understanding of the cellular defects governing disorders such as cardiomyopathies and cardiac failure, since early ontogenetic stages are probably recapitulated under pathological conditions.

Acknowledgements We thank Dr. Anna Wobus for supplying us with the D3 ES cell line, Marianne Faulhaber and Birgit Hops for culturing ES cells and preparing EBs.

References

- Agus ZS, Dukes ID, Morad M (1991) Divalent cations modulate the transient outward current in rat ventricular myocytes. *Am J Physiol* 261:C310–C318
- Barry DM, Nerbonne JM (1996) Myocardial potassium channels: electrophysiological and molecular diversity. *Annu Rev Physiol* 58:363–394
- Barry DM, Xu H, Schuessler RB, Nerbonne JM (1998) Functional knockout of the transient outward current, long-QT syndrome, and cardiac remodeling in mice expressing a dominant-negative $Kv4$ α subunit. *Circ Res* 83:560–567
- Benitah JP, Gomez AM, Bailly P, Da Ponte JP, Berson G, Delgado C, Lorente P (1993) Heterogeneity of the early outward current in ventricular cells isolated from normal and hypertrophied rat hearts. *J Physiol (Lond)* 469:111–138
- Beuckelmann DJ, Nabauer M, Erdmann E (1993) Alterations of K^+ currents in isolated human ventricular myocytes from patients with terminal heart failure. *Circ Res* 73:379–385
- Carmeliet E (1993) Mechanisms and control of repolarization. *Eur Heart J* 14 (Suppl H):3–13
- Chicchi GG, Gimenez-Gallego G, Ber E, Garcia ML, Winquist R, Cascieri MA (1988) Purification and characterization of a unique, potent inhibitor of apamin binding from *Leiurus quinquestriatus hebraeus* venom. *J Biol Chem* 263:10192–10197
- Coraboeuf E, Carmeliet E (1982) Existence of two transient outward currents in sheep cardiac Purkinje fibers. *Pflügers Arch* 392:352–359
- Danielsson BR, Azarbayjani F, Skold AC, Webster WS (1997) Initiation of phenytoin teratogenesis: pharmacologically induced embryonic bradycardia and arrhythmia resulting in hypoxia and possible free radical damage at reoxygenation. *Teratology* 56:271–281
- Davies MP, An RH, Doevendans P, Kubalak S, Chien KR, Kass RS (1996) Developmental changes in ionic channel activity in the embryonic murine heart. *Circ Res* 78:15–25
- Dixon JE, McKinnon D (1994) Quantitative analysis of potassium channel mRNA expression in atrial and ventricular muscle of rats. *Circ Res* 75:252–260
- Dixon JE, Shi W, Wang HS, McDonald C, Yu H, Wymore RS, Cohen IS, McKinnon D (1996) Role of the $Kv4.3$ K^+ channel in ventricular muscle. A molecular correlate for the transient outward current. *Circ Res* 79:659–668
- Dukes ID, Morad M (1991) The transient K^+ current in rat ventricular myocytes: evaluation of its Ca^{2+} and Na^+ dependence. *J Physiol (Lond)* 435:395–420
- Fiset C, Clark RB, Larsen TS, Giles WR (1997) A rapidly activating sustained K^+ current modulates repolarization and excitation-contraction coupling in adult mouse ventricle. *J Physiol (Lond)* 504:557–563
- Grismer S, Nguyen AN, Aiyar J, Hanson DC, Mather RJ, Gutman GA, Karmilowicz MJ, Auperin DD, Chandy KG (1994) Pharmacological characterization of five cloned voltage-gated K^+ channels, types $Kv1.1$, 1.2 , 1.3 , 1.5 , and 3.1 , stably expressed in mammalian cell lines. *Mol Pharmacol* 45:1227–1234
- Gryshchenko O, Fischer IR, Dittich M, Viatchenko-Karpinski S, Soest J, Boehm-Pinger M, Igelmund P, Fleischmann BK, Hescheler J (1999) Role of ATP-dependent K^+ channels in the electrical excitability of early embryonic stem cell-derived cardiomyocytes. *J Cell Sci* 112:2903–2912
- Guo W, Kamiya K, Hojo M, Kodama I, Toyama J (1998) Regulation of $Kv4.2$ and $Kv1.4K^+$ channel expression by myocardial hypertrophic factors in cultured newborn rat ventricular cells. *J Mol Cell Cardiol* 30:1449–1455
- Hescheler J, Fleischmann BK, Lentini S, Maltsev VA, Rohwedel J, Wobus AM, Addicks K (1997) Embryonic stem cells: a model to study structural and functional properties in cardiomyogenesis. *Cardiovasc Res* 36:149–162
- Hiraoka M, Kawano S (1989) Calcium-sensitive and insensitive transient outward current in rabbit ventricular myocytes. *J Physiol (Lond)* 410:187–212
- London B, Wang D, Hill JA, Bennett P (1998) The transient outward current in mice lacking the potassium channel gene $Kv1.4$. *J Physiol (Lond)* 509:171–182
- Maltsev VA, Wobus AM, Rohwedel J, Bader M, Hescheler J (1994) Cardiomyocytes differentiated in vitro from embryonic stem cells developmentally express cardiac-specific genes and ionic currents. *Circ Res* 75:233–244
- Muraki K, Imaizumi Y, Watanabe M, Habuchi Y, Giles WR (1995) Delayed rectifier K^+ current in rabbit atrial myocytes. *Am J Physiol* 269:H524–H532
- Nabauer M, Beuckelmann DJ, Erdmann E (1993) Characteristics of transient outward current in human ventricular myocytes from patients with terminal heart failure. *Circ Res* 73:386–394
- Pike GK, Bretag AH, Roberts ML (1993) Modification of the transient outward current of rat atrial myocytes by metabolic inhibition and oxidant stress. *J Physiol (Lond)* 470:365–382
- Po S, Roberds S, Snyders DJ, Tamkun MM, Bennett PB (1993) Heteromultimeric assembly of human potassium channels. Molecular basis of a transient outward current? *Circ Res* 72:1326–1336
- Shimoni Y, Fiset C, Clark RB, Dixon JE, McKinnon D, Giles WR (1997) Thyroid hormone regulates postnatal expression of

- transient K^+ channel isoforms in rat ventricle. *J Physiol (Lond)* 500:65–73
27. Sipido KR, Callewaert G, Carmeliet E (1993) $[Ca^{2+}]_i$ transients and $[Ca^{2+}]_i$ -dependent chloride current in single Purkinje cells from rabbit heart. *J Physiol (Lond)* 468:641–667
 28. Thierfelder S, Hirche H, Benndorf K (1994) Anoxia decreases the transient K^+ outward current in isolated ventricular heart cells of the mouse. *Pflügers Arch* 427:547–549
 29. Tomita F, Bassett AL, Myerburg RJ, Kimura S (1994) Diminished transient outward currents in rat hypertrophied ventricular myocytes. *Circ Res* 75:296–303
 30. Wahler GM, Dollinger SJ, Smith JM, Flemal KL (1994) Time course of postnatal changes in rat heart action potential and in transient outward current is different. *Am J Physiol* 267:H1157–H1166
 31. Wang L, Duff HJ (1997) Developmental changes in transient outward current in mouse ventricle. *Circ Res* 81:120–127
 32. Wang Z, Fermini B, Nattel S (1993) Delayed rectifier outward current and repolarization in human atrial myocytes. *Circ Res* 73:276–285
 33. Webster WS, Brown-Woodman PD, Snow MD, Danielsson BR (1996) Teratogenic potential of almokalant, dofetilide, and D-sotalol: drugs with potassium channel blocking activity. *Teratology* 53:168–175
 34. Wettwer E, Amos GJ, Posival H, Ravens U (1994) Transient outward current in human ventricular myocytes of subepicardial and subendocardial origin. *Circ Res* 75:473–482
 35. Wickenden AD, Kaprielian R, Kassiri Z, Tsoporis JN, Tsushima R, Fishman GI, Backx PH (1998) The role of action potential prolongation and altered intracellular calcium handling in the pathogenesis of heart failure. *Cardiovasc Res* 37:312–323
 36. Wickenden AD, Kaprielian R, Parker TG, Jones OT, Backx PH (1997) Effects of development and thyroid hormone on K^+ currents and K^+ channel gene expression in rat ventricle. *J Physiol (Lond)* 504:271–286
 37. Wobus AM, Wallukat G, Hescheler J (1991) Pluripotent mouse embryonic stem cells are able to differentiate into cardiomyocytes expressing chronotropic responses to adrenergic and cholinergic agents and Ca^{2+} channel blockers. *Differentiation* 48:173–182
 38. Xie LH, Takano M, Noma A (1997) Development of inwardly rectifying K^+ channel family in rat ventricular myocytes. *Am J Physiol* 272:H1741–H1750
 39. Xu H, Dixon JE, Barry DM, Trimmer JS, Merlie JP, McKinnon D, Nerbonne JM (1996) Developmental analysis reveals mismatches in the expression of K^+ channel alpha subunits and voltage-gated K^+ channel currents in rat ventricular myocytes. *J Gen Physiol* 108:405–419
 40. Xu XP, Best PM (1991) Decreased transient outward K^+ current in ventricular myocytes from acromegalic rats. *Am J Physiol* 260:H935–H942
 41. Zygmunt AC, Gibbons WR (1992) Properties of the calcium-activated chloride current in heart. *J Gen Physiol* 99:391–414

1.2. Роль K^+ каналів, що залежать від АТФ, в електричній збудливості ранішніх ембріональних кардіоміоцитів, отриманих від стовбурових клітин

Journal of Cell Science 112, 2903–2912 (1999)
Printed in Great Britain © The Company of Biologists Limited 1999
JCS0520

Role of ATP-dependent K^+ channels in the electrical excitability of early embryonic stem cell-derived cardiomyocytes

O. Gryshchenko*, I. R. Fischer*, M. Dittrich, S. Viatchenko-Karpinski, J. Soest, M. M. Böhm-Pinger, P. Igelmund, B. K. Fleischmann and J. Hescheler

Zentrum Physiologie und Pathophysiologie der Universität zu Köln, Institut für Neurophysiologie, Robert-Koch-Str. 39, D-50931 Köln, Germany

*These two authors contributed equally to this manuscript
Author for correspondence (e-mail: jh@physiologie.uni-koeln.de)

Accepted 26 June 1999; published on WWW 12 August 1999

SUMMARY

Single, murine embryonic stem cell-derived early stage cardiomyocytes dissociated from embryoid bodies expressed two inward rectifier K^+ channels, I_{K1} and the ATP dependent K^+ current. I_{K1} exhibited low density in early stage cardiomyocytes, but increased significantly in late stage cells. In contrast, the ATP dependent K^+ current was expressed at similar densities in early and late stage cardiomyocytes. This current was found to be involved in the determination of the membrane potential, since glibenclamide depolarized early cardiomyocytes and exerted a positive chronotropic effect. Some cardiomyocytes displayed a bursting behavior of action potentials, characterized by alternating periods with and without action potentials. During the phases without action potentials, the membrane potential was hyperpolarized, indicating the involvement of K^+ channels in the generation of this bursting behavior. Extracellular recording techniques were applied to spontaneously contracting areas of whole embryoid bodies. In 20% of these bursting behavior similar to that seen in the single cells was

observed. In regularly beating embryoid bodies, bursting could be induced by reduction of substrates from the extracellular medium as well as by superfusion with the positive chronotropic agents Bay K 8644 or isoproterenol. Perfusion with substrate-reduced medium induced bursting behavior after a short latency, isoproterenol and Bay K 8644 resulted in a positive chronotropic response followed by bursting behavior with longer latencies. The spontaneous bursting was blocked by glibenclamide. These experimental results suggest that intermittent activation of ATP dependent K^+ channels underlies the bursting behavior observed in single cardiomyocytes and in the whole embryoid body. Conditions of metabolic stress lead to the rhythmic suppression of action potential generation. Our data indicate that ATP dependent K^+ channels play a prominent role in the cellular excitability of early cardiomyocytes.

Key words: Embryonic stem cell-derived cardiomyocyte, $I_{K,ATP}$, Bursting

INTRODUCTION

ATP-dependent inwardly rectifying K^+ channels ($I_{K,ATP}$) which were first detected in the heart (Noma, 1983; Trube and Hescheler, 1984) consist of two subunits, the inward rectifier channel (KIR 6.2; Babenko et al., 1998b) and the sulphonylurea receptor (SUR) (Inagaki et al., 1995). Although the function of this channel became evident in pancreatic β -cells coupling the metabolic state with cellular excitability (Meissner and Preissler, 1979; Henquin et al., 1982; Ashcroft et al., 1984), there is still discussion whether such a link is also of relevance for the heart. It has not been demonstrated conclusively, that under physiological conditions, the ATP concentration in the vicinity of K^+ channels can drop down to a low enough level to activate $I_{K,ATP}$. This is different under hypoxic conditions where evidence for an upregulation of $I_{K,ATP}$ was reported (Noma, 1983; Weiss and Lamp, 1989; Benndorf et al., 1992; Nichols et al., 1991; Geschwind et al.,

1989). In a report by O'Rourke et al. (1994) $I_{K,ATP}$ was suggested to underlie the cyclic changes of action potentials (APs) observed in guinea pig ventricular cardiomyocytes. The changes of $I_{K,ATP}$ activity were linked to a primary glycolytic oscillator as already described in skeletal (Tornheim and Lowenstein, 1975) and cardiac muscle (Frenkel, 1966).

We here investigate whether ATP-sensitive K^+ channels (i) are already expressed in early stages of cardiac development and (ii) have a functional role in these early cardiomyocytes. The expression and the biophysical properties of $I_{K,ATP}$ during development have been recently reported in rat cardiomyocytes (Xie et al., 1997). Our examinations are based on murine pluripotent embryonic stem (ES) cells, widely used for the generation of transgenic and knockout mice (Bradley et al., 1984). ES-cells can also be differentiated in vitro as embryoid bodies (EBs), which produce among others murine embryonic cardiomyocytes (Doetschman et al., 1985; Wobus et al., 1991). Since cardiomyocytes of early stages (E8.5–E10.5) cannot be

obtained *in vivo* (Davies et al., 1996), EBs provide a unique model for the investigation of early stage cardiomyocytes (7+2-4 days of cultivation) (Maltsev et al., 1993, 1994). The validity of the model (Mueller-Klieser, 1997) has been demonstrated by several groups using electrophysiological (Wobus et al., 1991), histological (Hescheler et al., 1997), ultrastructural (Westfall et al., 1997) as well as molecular biological techniques (Miller Hance et al., 1993). After longer cultivation of the EBs, differentiated late stage cardiomyocytes (7+>9 days of cultivation) can be obtained recapitulating the different cardiac phenotypes of the native heart (Maltsev et al., 1994).

We here report that ATP-dependent K^+ channels are expressed in early stage cardiomyocytes. We demonstrate the functional involvement of these channels in the generation of rhythmic bursts of actions potentials and by this in the early setting of cellular excitability.

MATERIALS AND METHODS

Production of EBs

ES cells of the line D3 were cultivated and differentiated into spontaneously beating cardiomyocytes as previously described (Maltsev et al., 1994). Briefly, cells were cultivated in hanging drops (ca. 400 cells per drop) for 2 days, afterwards kept in suspension for 5 days and finally plated on gelatinized, single culture dishes and multiwell culture plates for extracellular and patch-clamp recordings, respectively. Two (7+2d) to four days (7+4d) after plating, spontaneously contracting cell clusters could be observed. The culture medium consisted of DMEM supplemented with 20% fetal calf serum, penicillin/streptomycin, glutamax (a glutamate analogue), MEM (all from Gibco, Eggenstein, FRG), and β -mercaptoethanol (Serva, Heidelberg, FRG).

Extracellular recordings

For long-term field potential recordings from cardiomyocyte clusters, EBs were plated on 30 mm culture dishes (Nunc, Roskilde, DK) with 2-3 EBs per dish. Extracellular electrodes were permanently placed onto the tissue after the appearance of spontaneously contracting areas. The electrodes were prepared from Teflon-insulated 125 μ m thick silver wire (A-M Systems, Everett, WA, USA). The different electrode was insulated except for the blunt tip whereas the indifferent electrode was free of insulation on a length of about 10 mm. The dish was placed into an incubator at 37°C, 5% CO_2 , 100% humidity. The culture medium was renewed every 2 days and with each washout of a test substance.

For application of test substances, 2-20 ml of a stock solution were pipetted into the medium, and the culture dish was gently swirled for approximately 5 seconds. Applications of substances were preceded by control swirls without application. For washout of test substances, the medium was replaced three times. For the experiments with substrate reduction, the culture medium was replaced by the following solution (denoted as substrate deprived saline, in mmol/l): NaCl 135, KCl 5, $MgCl_2$ 2, $CaCl_2$ 2, glucose 10, Hepes 5, pH 7.4 (NaOH). In some experiments the possible involvement of Cl^- channels was tested by using the following solutions (in mmol/l): NaCl 110 (reduced to 40), Na-glutamate 0 (elevated to 70) $NaHCO_3$ 45, KCl 5, $MgCl_2$ 2, $CaCl_2$ 2, glucose 10, NaH_2PO_4 1, pH 7.4 (NaOH).

All recordings were performed with the EBs inside the incubator. The signals were amplified with Grass P511K amplifiers (Grass, Quincy, MA, USA), digitized with a CED1401 interface (Cambridge Electronic Design (CED), Cambridge, UK) and continuously stored on computer disk using SPIKE2 software (CED). The analog signals were band-pass filtered from 1 Hz to 30 Hz and digitized at a sample rate of 100 Hz. Simultaneously, the signals were fed to threshold

discriminators which delivered a single event for each spike to the computer.

Patch-clamp recordings

For patch-clamp recordings, beating areas of 20-30 EBs were dissected and isolated by enzymatic dispersion, using collagenase B (Boehringer, Ingelheim, FRG), as described in more detail by Maltsev et al. (1994). The solution used for the dissociation of the dissected areas was the following (in mmol/l): NaCl 120, KCl 5.4, $MgSO_4$ 5, $CaCl_2$ 0.03, Na pyruvate 5, glucose 20, taurine 20, Hepes 10, collagenase B 0.5-1 mg/ml, pH 6.9 (NaOH). The dissociated material was plated onto glass coverslips and stored in the incubator. Within the first 12 hours, cells attached to the glass surface and spontaneously beating cardiomyocytes could be observed. For electrophysiological recordings, glass coverslips were transferred to a temperature-controlled recording chamber and superfused with extracellular solution. Only spontaneously beating cells were selected for the experiments. The electrical activity of the cells was recorded using the perforated (amphotericin B) patch-clamp configuration (Korn and Horn, 1989) and standard whole cell recording techniques (Hamill et al., 1981). Ionic currents were recorded using an Axopatch 200A amplifier (Axon Instruments, Foster City, USA). Data were acquired using the Iso2 software package (MFK, Niederrhausen, FRG). Data were sampled at 2 kHz and stored on hard disk.

All patch-clamp experiments were performed at 35°C. Pipettes were made on a DMZ Universal Puller (DMZ, München, FRG) from 1.5 mm borosilicate glass capillaries (Clark Electromedical Instruments, Reading, UK).

The composition of the different recording solutions used was the following (in mmol/l): Pipette solution for voltage- and current-clamp recordings: KCl 55, $MgCl_2$ 7, K_2SO_4 70, Hepes 10, pH 7.4 (KOH). Extracellular solution for current-clamp recordings: NaCl 135, KCl 5.4, $MgCl_2$ 2, $CaCl_2$ 1.8, glucose 10, Hepes 10, pH 7.4 (NaOH). Extracellular solution for voltage-clamp recordings: KCl 140, NaCl 5, $MgCl_2$ 2, $CaCl_2$ 1.8, glucose 5, Hepes 5, pH 7.4 (KOH). Amphotericin B (Sigma, Deisenhofen, FRG) was dissolved in DMSO at a concentration of 60 mg/ml, frozen in aliquots and thawed prior to use. The tip of the pipette was filled with normal recording solution and then backfilled with the amphotericin B containing solution, yielding a final amphotericin B concentration of 500 μ g/ml.

Test substances

Glibenclamide (Sigma, Deisenhofen, FRG), cromakalim (Sigma) Bay K 8644 (Bayer, Wuppertal, FRG) and thapsigargin (Molecular Probes, Leiden, Netherlands) were dissolved in 100% DMSO, diluted in extracellular solution or culture medium to the final concentration for superfusion of the recording chamber (patch-clamp) or added to the bath/culture dish by a pipette (patch-clamp, extracellular recordings). The final concentration of the solvent was below 0.05%. Isoproterenol (Sigma), charybdotoxin (Scientific Marketing Associates, Herts, UK) and 2,4-dinitrophenol (Sigma) were prepared in extracellular solution or culture medium as stock solution. Stock solutions were frozen, defrosted and diluted to the desired concentration prior to the experiments. Averaged data are expressed as mean \pm S.E.M.

RESULTS

First, the electrical activity of spontaneously beating, ES cell-derived cardiomyocytes was monitored by recording extracellular field potentials. In 20% of EBs ($n=153$) a bursting behavior of the spontaneous electrical activity was observed as exemplified in Fig. 1A. The bursting behavior proved stable up to several days and was characterized by intervals with action potentials (APs) intercalated by silent intervals without APs.

The mean duration period amounted to 49 ± 9 seconds ($n=14$) and was composed of a burst duration of 28 ± 5 seconds and an interburst interval of 21 ± 6 seconds (Fig. 1B). Thus, the relative burst duration amounted to $58 \pm 4\%$ of the period duration. At the beginning of the bursts, the instantaneous AP frequency (reciprocal of the interval length) rapidly increased to a maximal level of 2.4 ± 1.4 Hz within $27 \pm 5\%$ of the entire burst duration (data from Fig. 1B, mean values not shown). Then, the AP frequency slowly declined until a sudden stop of the spontaneous electrical activity occurred (Fig. 1A).

A similar pattern of electrical activity has previously been described for pancreatic β -cells and correlated with $I_{K,ATP}$ activity (Henquin and Meissner, 1984; Ashcroft et al., 1984; Corkey et al., 1988; Jonas et al., 1998). Therefore, the nature of the spontaneous bursting behavior in early cardiomyocytes was further investigated by blocking $I_{K,ATP}$ with glibenclamide or by increasing $I_{K,ATP}$ by the agonist cromakalim. As shown in Fig. 2A, addition of glibenclamide (1 mmol/l final concentration) to an EB resulted in suppression of the bursting behavior for more than 20 minutes (Fig. 2A,B). During this time, the EB displayed regular APs at a frequency of 4-5 Hz, thereafter the bursting behavior slowly reappeared presumably due to a binding of glibenclamide to extracellular proteins (Coppack et al., 1990). Repetitive glibenclamide application yielded reproducible effects as observed in all EBs tested ($n=37$). An increase of the glibenclamide concentration led to a prolongation of the suppression of the bursting behavior (data

not shown). High concentrations of glibenclamide (100 mmol/l, $n=5$), which presumably blocked $I_{K,ATP}$ completely, suppressed bursting for about 20 minutes and then led to a complete breakdown of the spiking activity (Fig. 2C) probably due to membrane depolarization and Ca^{2+} overload. Glibenclamide (2 or 10 μ mol/l) evoked in regularly beating (non-bursting) EBs a strong positive chronotropic response ($n=2$, data not shown). To exclude the known action of glibenclamide on Cl^- channels we tested their possible involvement on steady-state spontaneous electrical activity of EBs by partial replacement of Cl^- by glutamate. In bursting as well as non-bursting EBs no effect was observed (data not shown, $n=9$).

Application of cromakalim (100 μ mol/l, $n=13$), a known opener of ATP sensitive K^+ channels, to spontaneously bursting EBs resulted in a reduction of the bursting duration from 47 ± 7 seconds to 24 ± 1 seconds and a lengthening of the interval from 24 ± 6 seconds to 44 ± 3 seconds ($n=6$). The response to cromakalim varied between cells. In two experiments the period duration increased and the spontaneous activity stopped completely (Fig. 3), in two the period duration remained unaltered whereas it increased in the other two. Therefore it is unclear whether the oscillator itself was influenced by increased $I_{K,ATP}$ activity. The abrupt halt of beating in the two experiments was probably due to membrane hyperpolarization (see Fig. 8B). The effect of cromakalim was reversible upon washout.

Since $I_{K,ATP}$ is closely linked to the metabolic state of the cell, the next set of experiments was designed to obtain more information about the mechanisms inducing the bursting behavior in EBs. Fig. 4 demonstrates that bursting could be induced by reduction of fueling substrates from the extracellular medium (see Materials and Methods). After addition of the substrate deprived saline a stable bursting behavior was evoked after approximately 5 minutes ($n=3$, Fig. 4A). The bursting behavior could also be induced by increasing the energy consumption. Isoproterenol and Bay K 8644 are well known for their positive inotropic and chronotropic effects which will raise the fueling substrate demand of cardiomyocytes. Isoproterenol (5-10 μ mol/l) caused an immediate increase in the beating frequency by $112 \pm 20\%$ ($n=32$). In 5 out of 23 investigated EBs, bursting behavior appeared within 5-20 minutes. The effect of isoproterenol was fully reversible upon washout (data not shown). Application of 1-10 μ mol/l Bay K 8644 induced an increase of the AP frequency by $100 \pm 14\%$ ($n=20$). During transition to bursting, irregular oscillations of the AP frequency occurred (Fig. 4B,C) in 5 out of these 20 experiments, which developed over time into the typical bursting behavior (Fig. 4B). The effect of Bay K 8644 was fully reversible after washout.

In order to investigate the spontaneous electrical activity and the functional expression of $I_{K,ATP}$ and other inward rectifier K^+ currents in single ES-cell derived cardiomyocytes, perforated patch clamp recordings were performed. In current clamp recordings a bursting behavior identical to that observed in the whole EB was detected (Fig. 5A). This behavior was seen in about 5% of the single cells investigated. The bursting was characterized by intervals of APs lasting for 26 ± 6 seconds interrupted by 21 ± 5 second long intervals without APs ($n=12$ periods) which is similar to the findings in extracellular

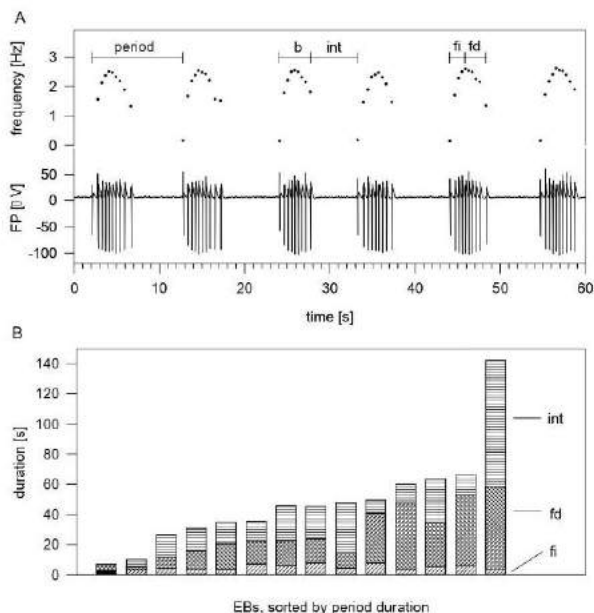


Fig. 1. Spontaneous bursting behavior recorded with extracellular electrodes in beating areas of whole EBs. (A) Typical recording of the field potential (FP) and instantaneous frequency, illustrating the different phases of the bursting behavior: The behavior was characterized by alternating bursts (b) and electrically silent intervals (int). The bursts consisted of an initial phase with increasing action potential frequency (fi) followed by a phase with decreasing frequency (fd). (B) Relationship between burst (= fi + fd) and interval duration in 14 EBs. Each column represents a single EB, showing mean values calculated from 10-15 successive burst periods.

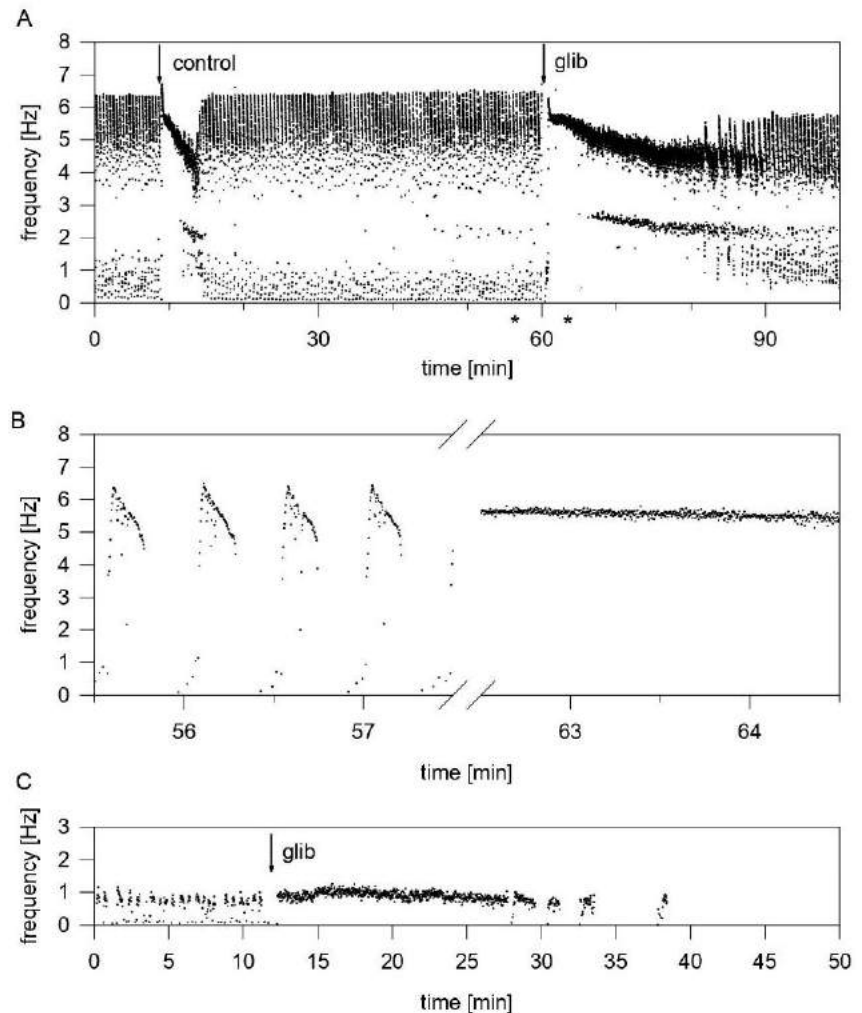


Fig. 2. Effect of glibenclamide (glib) on spontaneous bursting activity in whole EBs, recorded with extracellular electrodes. Since the substance was applied by pipetting to the culture medium and swirling of the culture dish, each experiment was preceded by a control swirling as shown in A. Typically, swirling alone induced a short, reproducible interruption of the bursting behavior and recovery of regular beating. (A) Application of 1 mmol/l glibenclamide suppressed bursting and induced regular beating for 20 minutes. Afterwards bursting slowly reappeared. (B) Segments of A (asterisks in A indicate the time points used for B) at an extended time scale. (C) Application of 100 mmol/l glibenclamide in another EB suppressed bursting and finally led to complete breakdown of the spiking activity.

recordings in EBs. During the bursting, a steady hyperpolarization and decline of the AP frequency occurred (Fig. 5D). A more detailed analysis of this experiment showed that during a single burst the frequency diminished steadily from a maximal frequency of about 3 Hz to about 1.5 Hz; the rate of the frequency decline was 0.05 ± 0.006 Hz/second ($n=10$ periods). The action potential duration (APD) did not change significantly between the beginning (134 ± 1 milliseconds) and the end of a burst (136 ± 4 milliseconds, $n=12$ periods) (Fig. 5D). To rule out a possible involvement of cyclic changes of the intracellular free Ca^{2+} concentration $[\text{Ca}^{2+}]_i$ and the possible activation of large-conductance Ca^{2+} -activated K^+ current ($\text{I}_{\text{K}_{\text{Ca}}}$), we tested whether the bursting behavior could be altered by application of thapsigargin (Tg), a selective inhibitor of the sarcoplasmic Ca^{2+} -ATPase. In Ca^{2+} imaging experiments we previously have found that application of Tg leads to a fast rise in $[\text{Ca}^{2+}]_i$ (Kolossoy et al., 1998). As shown in Fig. 6, Tg ($0.5 \mu\text{mol/l}$) did not significantly alter the bursting behavior (27 ± 5 second long bursts, 21 ± 3 second without APs., $n=12$ periods after Tg application). Moreover, charybdotoxin ($100 \mu\text{mol/l}$), a blocker of $\text{I}_{\text{K}_{\text{Ca}}}$ did not block outward currents

in voltage-clamp recordings ($n=4$, data not shown). Therefore, in agreement with the extracellular recordings it was assumed that $\text{I}_{\text{K}_{\text{ATP}}}$ is preferentially involved in the generation of the bursting behavior.

The functional expression of inward rectifier K^+ channels was investigated with voltage clamp recordings on spontaneously beating early (7+2-4d) and late stage (7+9-12d) ES cell-derived cardiomyocytes. Symmetrical high K^+ containing solutions were used to increase the amplitude of the inward rectifier K^+ currents. Currents were evoked by 150 millisecond lasting voltage steps, applied from a holding potential (HP) of 0 mV to potentials ranging from -160 mV to $+40$ mV in 40 mV increments. This pulse protocol revealed the inward rectifier current ($\text{I}_{\text{K}1}$) in late stage cells (Fig. 7A,C), which was blocked by extracellular Ba^{2+} (2 mmol/l , Fig. 7B). $\text{I}_{\text{K}1}$ displayed fast inactivation at step potentials negative to -40 mV (Fig. 1A). The Ba^{2+} resistant current component (Fig. 7B) was identified as the hyperpolarization activated non selective cation current (I_h) based on I/V-curve, Cs^+ sensitivity and slow activation kinetics (data not shown). In order to evoke $\text{I}_{\text{K}_{\text{ATP}}}$, the metabolic uncoupler 2,4-

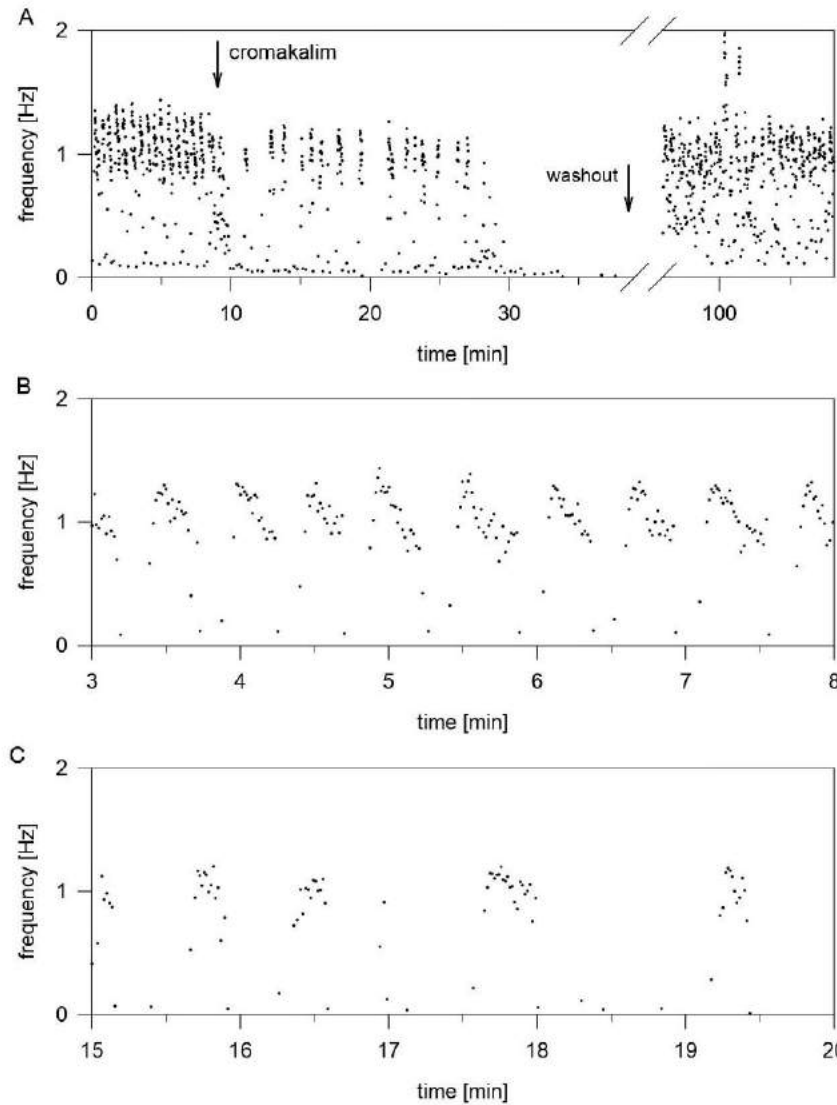


Fig. 3. Effect of cromakalim (100 μ mol/l) on spontaneous bursting activity, recorded with an extracellular electrode. Cromakalim decreased the burst duration and the maximal frequency within the bursts and increased the interburst interval. Finally, the activity was completely blocked. The right part of A shows the activity of the EB 1 hour after washout demonstrating the reversibility of the cromakalim effect. (B and C) Segments of the control and application phase, respectively, at a more extended time scale.

dinitrophenol (DNP), a known activator of $I_{K,ATP}$ (Wilde et al., 1990) was applied at a concentration of 1 mmol/l. After superfusion with DNP, a pronounced increase of the inward current at negative potentials was noted (Fig. 7D). The DNP effect occurred within 1–5 minutes of application ($n=15$). The DNP-activated current was blocked by glibenclamide. In order to obtain an instantaneous block of $I_{K,ATP}$ a relatively high concentration of glibenclamide (100 μ mol/l, $n=4$) was chosen (Fig. 7E). In the presence of glibenclamide, the sustained component of the inward current was reduced (Fig. 7C,E), suggesting that $I_{K,ATP}$ was open at rest. For the isolation of the DNP-evoked current, traces in the presence of glibenclamide and DNP (Fig. 7E) were subtracted from the current traces in the presence of DNP alone (Fig. 7D). The difference currents were inward currents at negative potentials with fast activation kinetics, time-dependent inactivation at the most negative step potential of -160 mV

and non-inactivating currents at more positive potentials (Fig. 7F). The current-voltage (I/V) relationship of the difference currents displayed inward rectification, with a reversal potential close to 0 mV as expected for a K^+ -selective conductance in symmetrical K^+ solutions (Fig. 7G). Thus, several lines of evidence indicated that the DNP-induced K^+ currents shown in Fig. 7 were $I_{K,ATP}$: (i) as it showed fast activation kinetics, (ii) displayed inwardly rectifying I/V-behavior, (iii) was evoked by DNP, and (iv) was blocked by glibenclamide.

I_{K1} density increased significantly during development with a current density of 45.1 ± 0.2 pA/pF ($n=21$) in early stage cardiomyocytes and of 90.9 ± 5.3 pA/pF ($n=21$) in late stage cardiomyocytes. In contrast, there was no significant difference in $I_{K,ATP}$ density between early and late stage cardiomyocytes. As shown in Fig. 7H $I_{K,ATP}$ density at both differentiation stages was around 50 pA/pF. This suggests that $I_{K,ATP}$ is a

functionally relevant current which is already expressed early during cardiomyogenesis.

The possible role of $I_{K,ATP}$ in the regulation of the resting membrane potential and in the spontaneous electrical activity of ES cell-derived cardiomyocytes was investigated in the current clamp mode. Application of glibenclamide to a spontaneously beating, early stage cardiomyocyte depolarized the membrane potential and led to an increase in the beating frequency (Fig. 8A) similar as seen in the extracellular recordings of whole EBs. Furthermore, superfusion of DNP (1 mmol/l) caused a sudden decline of the action potential (AP) frequency shortly after drug application (4 out of 4 cells tested). The spontaneous APs stopped completely and a hyperpolarization of the membrane potential was observed (4.1 ± 1 mV, $n=4$, Fig. 8B). After DNP washout, the spontaneous electrical activity reappeared and the membrane

potential returned to control values (Fig. 8B). These results suggest that $I_{K,ATP}$ is involved in the control of the membrane potential and that further activation by DNP leads to hyperpolarization of the membrane potential and block of AP generation, as observed during bursting.

DISCUSSION

We demonstrate the pivotal role of ATP-sensitive K^+ -channels in the control and metabolic modulation of cellular excitability in early stage cardiomyocytes. In extracellular recordings from beating EBs as well as in patch-clamp studies we show a prominent bursting of action potentials in murine, ES cell-derived cardiomyocytes. Our hypothesis that $I_{K,ATP}$ underlies the bursting behavior is supported by several lines of evidence:

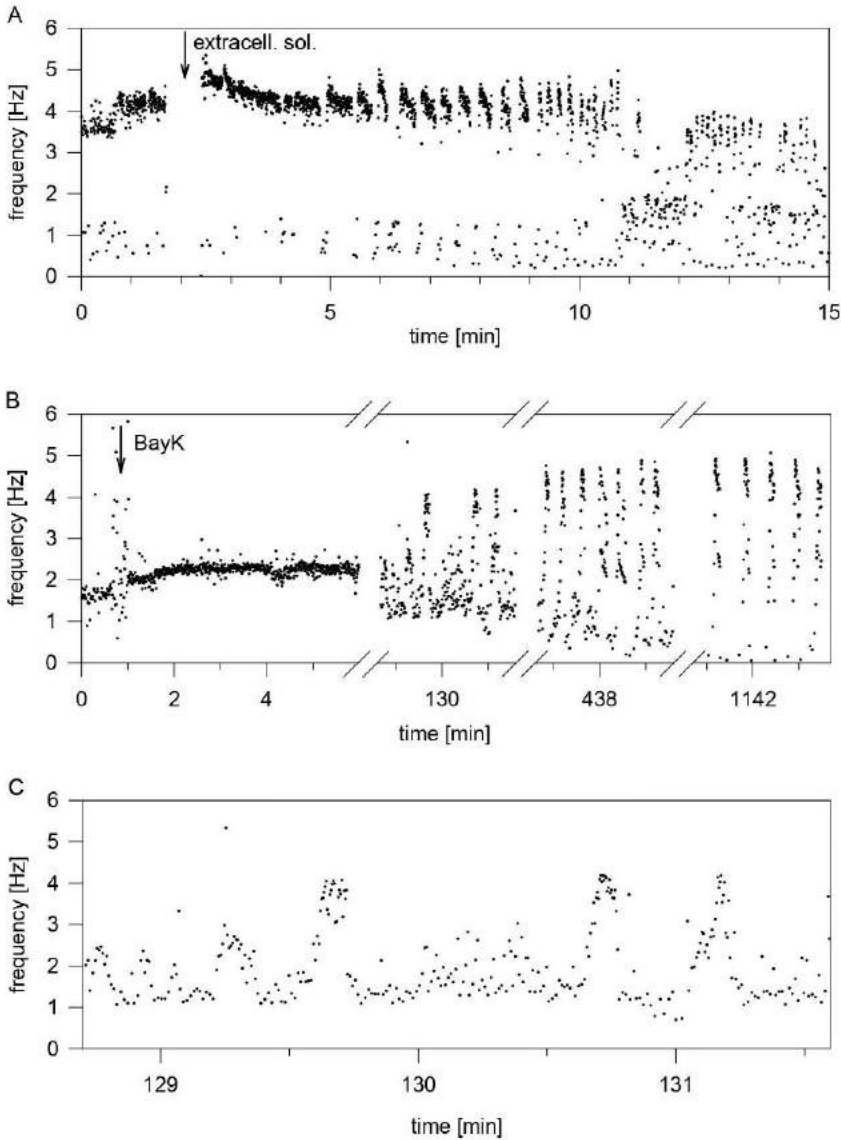


Fig. 4. Effect of extracellular solution (A) and Bay K 8644 (B,C) on regularly beating EBs. Replacement of the culture medium by extracellular solution induced bursting behavior with a short latency. Addition of Bay K 8644 (1 μ mol/l) first induced an increase in the beating frequency, followed by slowly developing bursting behavior. With time, maximal frequency and interval duration increased (B). The transition phase was characterized by irregular oscillations of the AP frequency without longer intervals (C).

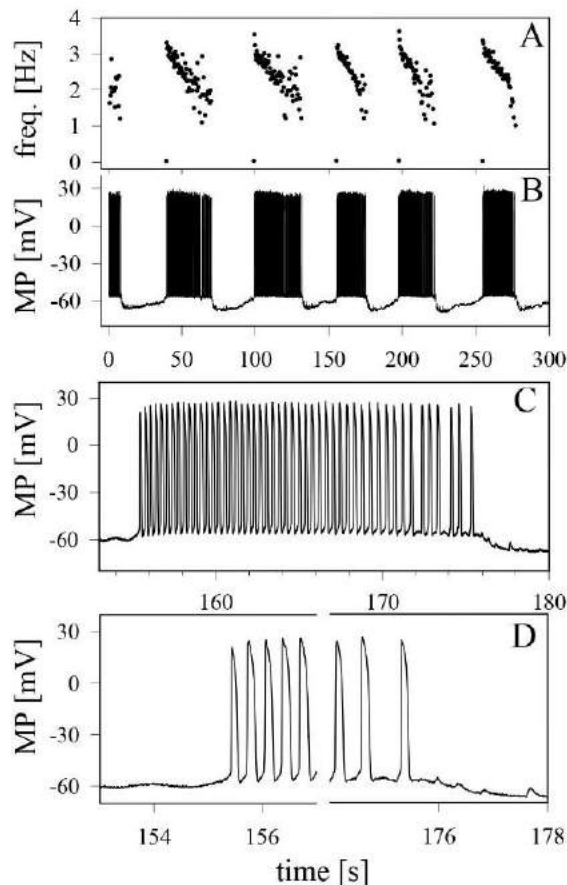


Fig. 5. Spontaneous bursting behavior in an ES cell-derived early stage cardiomyocyte (7+3 d) recorded with the perforated patch-clamp technique in the current-clamp mode. (A) Instantaneous AP frequency (A) and membrane potential (B-D). This cell displayed APs at decreasing frequency interrupted by intervals without APs. The transition from a period with APs to a silent period was sudden and accompanied by a prominent membrane potential hyperpolarization. (C,D) Segments of B displayed in a more extended time course.

(i) Application of the $I_{K,ATP}$ blocker glibenclamide ($1 \mu\text{mol/l}$) converted bursting into regular beating. In single cells it depolarized the membrane potential. (ii) The $I_{K,ATP}$ agonist cromakalim resulted in a decrease of the bursting duration and an increase of the bursting interval. (iii) Reduction of metabolic substrates in the culture medium induced bursting behavior. In parallel, a metabolic uncoupler, DNP, hyperpolarized the membrane potential and decreased AP frequency in single cells. (iv) Increased demand of fueling substrates by the positive inotropic and chronotropic agonists, isoproterenol and Bay K 8644 also evoked bursting. These substances are known to raise the cellular energy demand by increasing $[\text{Ca}^{2+}]_i$ and consequently the rate of membrane pumps and exchangers. Isoproterenol had an immediate positive chronotropic effect and bursting occurred shortly after application. The positive chronotropic response of Bay K 8644 had a longer latency and therefore bursting appeared later. (v) In single cell experiments, the interburst interval showed hyperpolarization suggesting the

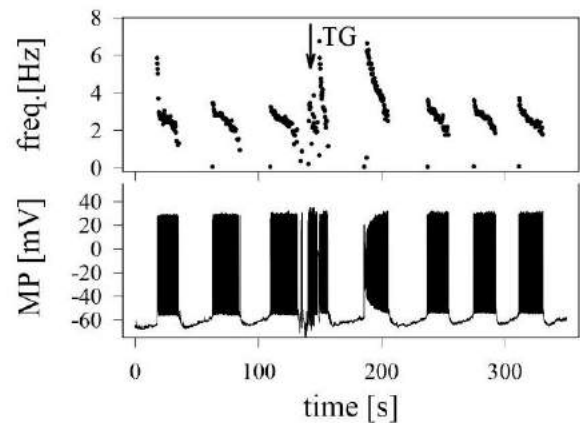


Fig. 6. Application of $0.5 \mu\text{mol/l}$ thapsigargin (Tg), a known inhibitor of the sarcoplasmic Ca^{2+} -ATPase, did not alter the bursting behavior (same cell as in Fig. 5). The instantaneous frequency is shown in the upper panel, the membrane potential in the lower panel.

activation of K^+ channels. Finally, (vi) ATP-dependent K^+ channels were expressed at a higher density as compared to I_{K1} in early stage cardiomyocytes. The primary involvement of other channels in the bursting behavior can be excluded since Cl^- replacement experiments did not alter the steady state membrane excitability, Na^+ channels are not functionally involved in the APs of these early stage cardiomyocytes (Maltsev et al., 1994) and $I_{K,Ca}$ was excluded in experiments using Tg and charybdotoxin.

Oscillatory changes but not a bursting behavior of membrane excitability have been previously shown in guinea pig ventricular cardiomyocytes (O'Rourke et al., 1994). In this study cyclic changes of ATP and NADPH activities altered membrane excitability by influencing $I_{K,ATP}$. It is also known that the activity of $I_{K,ATP}$ is critically dependent on ADP. Recent experiments have shown that the ADP binding site is located on SUR and that ADP binding interferes with the ATP block, which may occur directly at the KIR 6.2 channel (Shyng et al., 1998a; Shyng and Nichols, 1998b; Ueda et al., 1997, 1999). It has been suggested that ATP-requiring processes at the cardiomyocyte membrane are preferentially supported by ATP produced via glycolysis (McDonald and MacLeod, 1973; Bricknell and Opie, 1978; Weiss and Hiltbrand, 1985). Moreover, a close link between ATP-generating glycolytic enzymes and ATP-sensitive K^+ channels has been suggested (Weiss and Lamp, 1987, 1989). The different latencies of burst induction between isoproterenol and Bay K 8644 may be related to their different mechanisms of action and thus energy consumption. The direct or indirect involvement of mitochondrial oscillations (Aon et al., 1991) cannot be ruled out completely for our system but appears unlikely since bursting occurred spontaneously and could be induced in the presence of extracellular glutamate and pyruvate, substrates which can be used by the mitochondria for the oxidative metabolism.

Similar to the findings of O'Rourke et al. (1994), an oscillatory behavior of membrane excitability prior to bursting was observed in experiments using Bay K 8644. Differences in

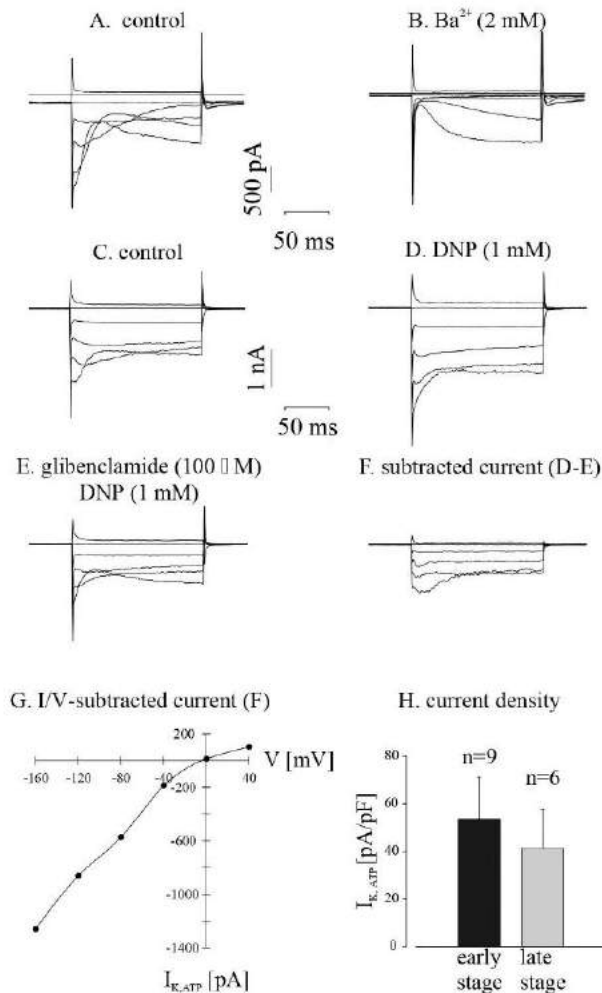


Fig. 7. Perforated patch-clamp recordings in the voltage-clamp mode from ES cell-derived, spontaneously beating, late stage cardiomyocytes (7+9 d) in equimolar K^+ solution. (A) Inward rectifier currents (I_{K1}): 150 milliseconds lasting voltage steps were applied from a holding potential of 0 mV to step potentials ranging from -160 mV to +40 mV in 40 mV intervals. I_{K1} displayed a time dependent fast inactivation at negative step potentials. (B) I_{K1} was blocked by application of extracellular Ba^{2+} at a concentration of 2 mmol/l. The Ba^{2+} insensitive inward current detected at negative step potentials was I_r . (C) ATP sensitive K^+ current ($I_{K,ATP}$) expression in ES-cell derived cardiomyocytes: Similarly to the cardiomyocyte in A, time-dependent inactivating I_{K1} were observed at negative step potentials (same voltage protocol as in A). (D) Application of 1 mmol/l 2,4-dinitrophenol (DNP) induced with a short delay an increase of currents displaying less time-dependent inactivation at negative potentials. (E) Application of 100 μ mol/l glibenclamide blocked DNP-evoked currents. Note the reduction of the I_{K1} amplitude. (F) The subtraction of the currents in presence of glibenclamide from the currents in presence of DNP yielded inward rectifier non inactivating currents with fast activation kinetics. (G) I/V relationship of peak $I_{K,ATP}$ obtained from D. (H) $I_{K,ATP}$ density in early (7+2-4 d) and late (7+9-12 d) stage cells. The current densities were similar at both stages.

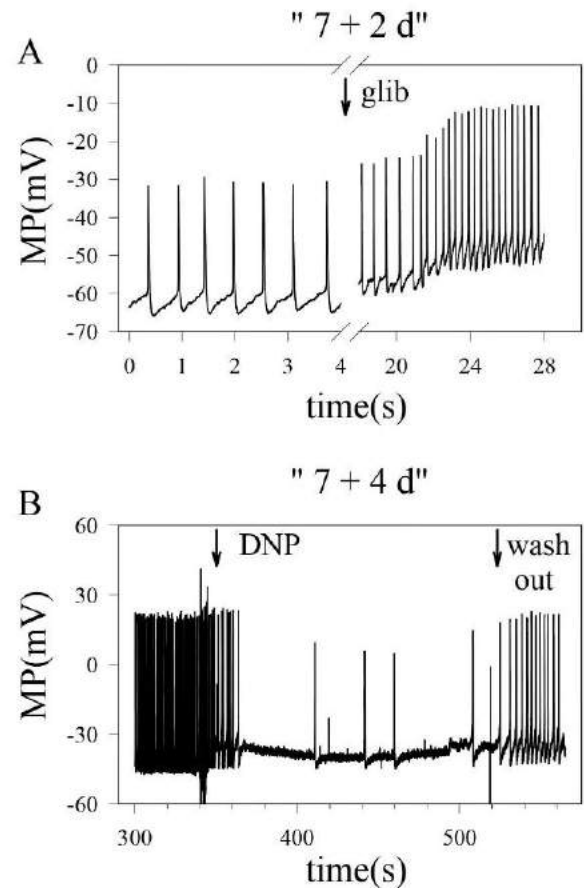


Fig. 8. Effect of glibenclamide (glib) and DNP on resting membrane potential and chronotropy of spontaneously beating, early stage ES cell-derived cardiomyocytes (7+2d, 7+4 d) recorded with the perforated patch-clamp technique. Note the relatively depolarized membrane potential, characteristic for early stage ES cell-derived cardiomyocytes. (A) Application of 100 μ mol/l glibenclamide induced depolarization of the membrane potential and positive chronotropy. (B) Application of 1 mmol/l DNP caused hyperpolarization of the membrane potential and negative chronotropy. The APs halted nearly completely, three APs of smaller amplitude were still observed during the hyperpolarized period. Washout of DNP induced a recovery of the spontaneous electrical activity.

energy balance and supply may explain the individual spontaneous electrical behavior of EBs in culture medium and of EBs exposed to extracellular solution or positive chronotropic substances. In single cell recordings, however, the bursting behavior was only rarely observed (5% of cells) and was not induced upon application of DNP or withdrawal of metabolic substrates. Thus, the conditions required for the entrainment of the primary oscillatory rhythm generator, which in case of the glycolytic pathway is critically dependent on substrate influx (Boiteux et al., 1975; Markus et al., 1984), may be difficult to maintain with patch-clamp recordings in single cells.

$I_{K,ATP}$ probably plays an important role during the initial period of ischemia and hypoxia in the adult heart (Thierfelder et al., 1994a). It is not yet clear though, if $I_{K,ATP}$ has a

cardioprotective (reduction of contractile work) (Cole et al., 1991; Grover et al., 1989; Gross and Auchampach, 1992) or proarrhythmic effects (shortening of the action potential duration) (Janse and Wit, 1989; O'Rourke et al., 1994) under conditions of metabolic stress. I_{K1} displays a partial run-down under hypoxic conditions, which makes the role of $I_{K,ATP}$ in the control of the resting membrane potential (Noma and Shibasaki, 1985; Trube and Hescheler, 1984; Xie et al., 1997) even more important. Moreover, the low I_{K1} densities in ES cell-derived cardiomyocytes detected in the present study favors prominent changes of the membrane potential upon further closing or opening of ATP-sensitive K^+ channels, as the current clamp experiments with glibenclamide or DNP demonstrate. This is in line with findings in fetal ventricular cardiomyocytes of the rat, where higher densities for $I_{K,ATP}$ than for I_{K1} were reported (Xie et al., 1997). Furthermore, a prominent expression of $I_{K,ATP}$ was also detected in embryonal murine cardiomyocytes (Davies et al., 1996). The relevant role of $I_{K,ATP}$ in the control of resting membrane potential in particular under conditions of metabolic stress is further underlined by the observation that at this early stage the transient outward rectifier potassium current I_{to} plays an important role in regulating the membrane potential (O. Gryshchenko and B. K. Fleischmann, unpublished results) and that this current is depressed by hypoxia (Thierfelder et al., 1994b).

In a recent report mice deficient of the KIR 6.2 gene (Miki et al., 1998), known to encode among others the ATP sensitive channel in heart muscle (Babenko et al., 1998a,b), are not suffering of a major pancreatic and/or cardiac defects. This indicates either that $I_{K,ATP}$ is not initially important role during embryonic cardiogenesis or that compensatory mechanisms may arise due to the general nature of the knock out.

We conclude that $I_{K,ATP}$ is in contrast to the adult heart a major determinant for cellular excitability during early cardiomyogenesis. Due to this important role metabolic oscillations can directly be translated into bursting of APs. These cyclic changes of electrical activity may reduce the workload and increase Ca^{2+} extrusion through the forward mode of the Na^+-Ca^{2+} exchanger. Thus, bursting behavior may serve as a cardioprotective mechanism under conditions of low O_2 saturation in the embryo.

We thank Dr A. M. Wobus for supplying us with the O_3 ES cell line. We thank Marianne Faulhaber, Birgit Hops and Claudia Maychrzak for cell culture work and Dr Susanne Ullrich for critically reading the manuscript. We acknowledge the electronic and mechanic workshop of the institute for their skillful technical support. Bay K 8644 was a gift from Bayer (Wuppertal, Germany).

REFERENCES

- Aon, M. A., Cortassa, S., Westerhoff, H. V., Berden, J. A., Van Spronsen, E. and Van Dam, K. (1991). Dynamic regulation of yeast glycolytic oscillations by mitochondrial functions. *J. Cell Sci.* **99**, 325-334.
- Ashcroft, F. M., Harrison, D. E. and Ashcroft, S. J. (1984). Glucose induces closure of single potassium channels in isolated rat pancreatic beta-cells. *Nature* **312**, 446-448.
- Babenko, A. P., Aguilar-Bryan, L. and Bryan, J. (1998a). A view of $sur/KIR6.X$, KATP channels. *Annu. Rev. Physiol.* **60**, 667-687.
- Babenko, A. P., Gonzalez, G., Aguilar-Bryan, L. and Bryan, J. (1998b). Reconstituted human cardiac KATP channels: functional identity with the native channels from the sarcolemma of human ventricular cells. *Circ. Res.* **83**, 1132-1143.
- Benndorf, K., Bollmann, G., Friedrich, M. and Hirsch, H. (1992). Anoxia induces time-independent K^+ current through KATP channels in isolated heart cells of the guinea-pig. *J. Physiol. Lond.* **454**, 339-357.
- Boiteux, A., Goldbeter, A. and Hess, B. (1975). Control of oscillating glycolysis of yeast by stochastic, periodic, and steady source of substrate: a model and experimental study. *Proc. Nat. Acad. Sci. USA* **72**, 3829-3833.
- Bradley, A., Evans, M., Kaufman, M. H. and Robertson, E. (1984). Formation of germ-line chimaeras from embryo-derived teratocarcinoma cell lines. *Nature* **309**, 255-256.
- Bricknell, O. L. and Opie, L. H. (1978). Effects of substrates on tissue metabolic changes in the isolated rat heart during underperfusion and on release of lactate dehydrogenase and arrhythmias during reperfusion. *Circ. Res.* **43**, 102-115.
- Cole, W. C., McPherson, C. D. and Sontag, D. (1991). ATP-regulated K^+ channels protect the myocardium against ischemia/reperfusion damage. *Circ. Res.* **69**, 571-581.
- Coppack, S. W., Lant, A. E., McIntosh, C. S. and Rodgers, A. V. (1990). Pharmacokinetic and pharmacodynamic studies of glibenclamide in non-insulin dependent diabetes mellitus. *Br. J. Clin. Pharmacol.* **29**, 673-684.
- Corkey, B. E., Tornheim, K., Deeney, J. T., Glennon, M. C., Parker, J. C., Matschinsky, F. M., Ruderman, N. B. and Prentki, M. (1988). Linked oscillations of free Ca^{2+} and the ATP/ADP ratio in permeabilized RINm5F insulinoma cells supplemented with a glycolyzing cell-free muscle extract. *J. Biol. Chem.* **263**, 4254-4258.
- Davies, M. P., An, R. H., Doevendans, P., Kubalak, S., Chien, K. R. and Kass, R. S. (1996). Developmental changes in ionic channel activity in the embryonic murine heart. *Circ. Res.* **78**, 15-25.
- Doetschman, T. C., Eistetter, H., Katz, M., Schmidt, W. and Kemler, R. (1985). The in vitro development of blastocyst-derived embryonic stem cell lines: formation of visceral yolk sac, blood islands and myocardium. *J. Embryol. Exp. Morphol.* **87**, 27-45.
- Frenkel, R. (1966). Reduced diphosphopyridine nucleotide oscillations in cell-free extracts from beef heart. *Arch. Biochem. Biophys.* **115**, 112-121.
- Geschwind, J. F., Hiriart, M., Glennon, M. C., Najafi, H., Corkey, B. E., Matschinsky, F. M. and Prentki, M. (1989). Selective activation of Ca^{2+} influx by extracellular ATP in a pancreatic beta-cell line (HIT). *Biochim. Biophys. Acta* **1012**, 107-115.
- Gross, G. J. and Auchampach, J. A. (1992). Role of ATP dependent potassium channels in myocardial ischaemia. *Cardiovasc. Res.* **26**, 1011-1016.
- Grover, G. J., McCullough, J. R., Henry, D. E., Conder, M. L. and Sleph, P. G. (1989). Anti-ischemic effects of the potassium channel activators pinacidil and cromakalim and the reversal of these effects with the potassium channel blocker glyburide. *J. Pharmacol. Exp. Ther.* **251**, 98-104.
- Hamill, O. P., Marty, A., Neher, E., Sakmann, B. and Sigworth, F. J. (1981). Improved patch-clamp techniques for high-resolution current recording from cells and cell-free membrane patches. *Pflügers Arch.* **391**, 85-100.
- Henquin, J. C., Meissner, H. P. and Schmeer, W. (1982). Cyclic variations of glucose-induced electrical activity in pancreatic B cells. *Pflügers Arch.* **393**, 322-327.
- Henquin, J. C. and Meissner, H. P. (1984). Significance of ionic fluxes and changes in membrane potential for stimulus-secretion coupling in pancreatic B-cells. *Experientia* **40**, 1043-1052.
- Hescheler, J., Fleischmann, B. K., Lentini, S., Maltsev V. A., Rohwedel J., Wobus A. M. and Addicks K. Embryonic stem cells: a model to study structural and functional properties in cardiomyogenesis (1997). *Cardiovasc. Res.* **36**, 149-162.
- Inagaki, N., Gonoi, T., Clement, J. P. 4., Namba, N., Inazawa, J., Gonzalez, G., Aguilar-Bryan, L., Seino, S. and Bryan, J. (1995). Reconstitution of IKATP: an inward rectifier subunit plus the sulfonylurea receptor. *Science* **270**, 1166-1170.
- Janse, M. J. and Wit, A. L. (1989). Electrophysiological mechanisms of ventricular arrhythmias resulting from myocardial ischemia and infarction. *Physiol. Rev.* **69**, 1049-1169.
- Jonas, J. C., Gilon, P. and Henquin, J. C. (1998). Temporal and quantitative correlations between insulin secretion and stably elevated or oscillatory cytoplasmic Ca^{2+} in mouse pancreatic beta-cells. *Diabetes* **47**, 1266-1273.
- Kolossov, E., Fleischmann, B. K., Liu, Q., Bloch, W., Viatchesko-Karpinski, S., Manzke, O., Ji, G. J., Bohlen, H., Addicks, K. and Hescheler, J. (1998). Functional characteristics of ES cell-derived cardiac precursor cells identified by tissue specific expression of the Green Fluorescent Protein. *J. Cell Biol.* **143**, 2045-2056.

- Korn, S. J. and Horn, R. (1989). Influence of sodium-calcium exchange on calcium current rundown and the duration of calcium-dependent chloride currents in pituitary cells, studied with whole cell and perforated patch recording. *J. Gen. Physiol.* **94**, 789-812.
- Maltsev, V. A., Rohwedel, J., Hescheler, J. and Wobus, A. M. (1993). Embryonic stem cells differentiate in vitro into cardiomyocytes representing sinusnodal, atrial and ventricular cell types. *Mech. Dev.* **44**, 41-50.
- Maltsev, V. A., Wobus, A. M., Rohwedel, J., Bader, M. and Hescheler, J. (1994). Cardiomyocytes differentiated in vitro from embryonic stem cells developmentally express cardiac-specific genes and ionic currents. *Circ. Res.* **75**, 233-244.
- Markus, M., Kuschmitz, D. and Hess, B. (1984). Chaotic dynamics in yeast glycolysis under periodic substrate input flux. *FEBS Lett.* **172**, 235-238.
- McDonald, T. F. and MacLeod, D. P. (1973). Metabolism and the electrical activity of anoxic ventricular muscle. *J. Physiol. Lond.* **229**, 559-582.
- Meissner, H. P. and Preissler, M. (1979). Glucose-induced changes of the membrane potential of pancreatic B-cells: their significance for the regulation of insulin release. *Advan. Exp. Med. Biol.* **119**, 97-107.
- Miki, T., Nagashima, K., Tashiro, E., Kotake, K., Yoshitomi, H., Tamamoto, A., Gono, T., Iwanaga, T., Miyazaki, J. and Seino, S. (1998). Defective insulin secretion and enhanced insulin action in KATP channel-deficient mice. *Proc. Nat. Acad. Sci. USA* **95**, 10402-10406.
- Miller Hance, W. C., LaCorbiere, M., Fuller, S. J., Evans, S. M., Lyons, G., Schmidt, C., Robbins, J. and Chien, K. R. (1993). In vitro chamber specification during embryonic stem cell cardiogenesis. Expression of the ventricular myosin light chain-2 gene is independent of heart tube formation. *J. Biol. Chem.* **268**, 25244-25252.
- Mueller-Klieser, W. (1997). Three-dimensional cell cultures: from molecular mechanisms to clinical applications. *Am. J. Physiol.* **273**, C1109-1123.
- Nichols, C. G., Ripoll, C. and Lederer, W. J. (1991). ATP-sensitive potassium channel modulation of the guinea pig ventricular action potential and contraction. *Circ. Res.* **68**, 280-287.
- Noma, A. (1983). ATP-regulated K⁺ channels in cardiac muscle. *Nature* **305**, 147-148.
- Noma, A. and Shibasaki, T. (1985). Membrane current through adenosine-triphosphate-regulated potassium channels in guinea-pig ventricular cells. *J. Physiol. Lond.* **363**, 463-480.
- O'Rourke, B., Ramza, B. M. and Marban, E. (1994). Oscillations of membrane current and excitability driven by metabolic oscillations in heart cells. *Science* **265**, 962-966.
- Shyng, S. L., Ferrigni, T., Shepard, J. B., Nestorowicz, A., Glaser, B., Permutt, M. A. and Nichols, C. G. (1998a). Functional analyses of novel mutations in the sulfonylurea receptor 1 associated with persistent hyperinsulinemic hypoglycemia of infancy. *Diabetes* **47**, 1145-1151.
- Shyng, S. L. and Nichols, C. G. (1998b). Membrane phospholipid control of nucleotide sensitivity of KATP channels. *Science* **282**, 1138-1141.
- Thierfelder, S., Doepner, B., Gebhardt, C., Hirc, H. and Benndorf, K. (1994a). ATP-sensitive K⁺ channels in heart muscle cells first open and subsequently close at maintained anoxia. *FEBS Lett.* **351**, 365-369.
- Thierfelder, S., Hirc, H. and Benndorf, K. (1994b). Anoxia decreases the transient K⁺ outward current in isolated ventricular heart cells of the mouse. *Pflugers Arch.* **427**, 547-549.
- Tornheim, K. and Lowenstein, J. M. (1975). The purine nucleotide cycle. Control of phosphofructokinase and glycolytic oscillations in muscle extracts. *J. Biol. Chem.* **250**, 6304-6314.
- Trube, G. and Hescheler, J. (1984). Inward-rectifying channels in isolated patches of the heart cell membrane: ATP-dependence and comparison with cell-attached patches. *Pflugers Arch.* **401**, 178-184.
- Ueda, K., Inagaki, N. and Seino, S. (1997). MgADP antagonism to Mg²⁺-independent ATP binding of the sulfonylurea receptor SUR1. *J. Biol. Chem.* **272**, 22983-22986.
- Ueda, K., Komine, J., Matsuo, M., Seino, S. and Amachi, T. (1999). Cooperative binding of ATP and MgADP in the sulfonylurea receptor is modulated by glibenclamide. *Proc. Nat. Acad. Sci. USA* **96**, 1268-1272.
- Weiss, J. and Hiltbrand, B. (1985). Functional compartmentation of glycolytic versus oxidative metabolism in isolated rabbit heart. *J. Clin. Invest.* **75**, 436-447.
- Weiss, J. N. and Lamp, S. T. (1987). Glycolysis preferentially inhibits ATP-sensitive K⁺ channels in isolated guinea pig cardiac myocytes. *Science* **238**, 67-69.
- Weiss, J. N. and Lamp, S. T. (1989). Cardiac ATP-sensitive K⁺ channels. Evidence for preferential regulation by glycolysis. *J. Gen. Physiol.* **94**, 911-935.
- Westfall, M. V., Pasyk, K. A., Yule, D. I., Samuelson, L. C. and Metzger, J. M. (1997). Ultrastructure and cell-cell coupling of cardiac myocytes differentiating in embryonic stem cell cultures. *Cell Motil. Cytoskel.* **36**, 43-54.
- Wilde, A. A., Escande, D., Schumacher, C. A., Thuringer, D., Mestre, M., Fiolet, J. W. and Janse, M. J. (1990). Potassium accumulation in the globally ischemic mammalian heart. A role for the ATP-sensitive potassium channel. *Circ. Res.* **67**, 835-843.
- Wobus, A. M., Wallukat, G. and Hescheler, J. (1991). Pluripotent mouse embryonic stem cells are able to differentiate into cardiomyocytes expressing chronotropic responses to adrenergic and cholinergic agents and Ca²⁺ channel blockers. *Differentiation* **48**, 173-182.
- Xie, L. H., Takano, M. and Noma, A. (1997). Development of inwardly rectifying K⁺ channel family in rat ventricular myocytes. *Am. J. Physiol.* **272**, H1741-50.

1.3. Внутрішньоклітинні коливання Ca^{2+} викликають спонтанні скорочення кардіоміоцитів під час ранішнього розвитку клітин

Proc. Natl. Acad. Sci. USA
Vol. 96, pp. 8259–8264, July 1999
Physiology

Intracellular Ca^{2+} oscillations drive spontaneous contractions in cardiomyocytes during early development

S. VIATCHENKO-KARPINSKI*, B. K. FLEISCHMANN*, Q. LIU, H. SAUER, O. GRYSHCHENKO, G. J. JI, AND J. HESCHELER†

Institute of Neurophysiology, University of Cologne, Robert-Koch-Strasse 39, 50931 Köln, Germany

Communicated by Robert E. Forster, University of Pennsylvania School of Medicine, Philadelphia, PA, April 19, 1999 (received for review December 21, 1998)

ABSTRACT Activity of cardiac pacemaker cells is caused by a balanced interplay of ion channels. However, it is not known how the rhythmic beating is initiated during early stages of cardiomyogenesis, when the expression of ion channels is still incomplete. Based on the observation that early-stage embryonic stem cell-derived cardiomyocytes continuously contracted in high extracellular K^+ solution, here we provide experimental evidence that the spontaneous activity of these cells is not generated by transmembrane ion currents, but by intracellular $[\text{Ca}^{2+}]_i$ oscillations. This early activity was clearly independent of voltage dependent L-type Ca^{2+} channels and the interplay between these and ryanodine sensitive Ca^{2+} stores. We also show that intracellular Ca^{2+} oscillations evoke small membrane depolarizations and that these can trigger L-type Ca^{2+} channel driven action potentials.

It is postulated that the heart is contracting because of the electromechanical coupling. First, an action potential (AP) is evoked leading to the opening of voltage-dependent L-type Ca^{2+} channels (VDCCs). Second, the Ca^{2+} entering into the cardiomyocyte through VDCC triggers the release of Ca^{2+} from the ryanodine-sensitive Ca^{2+} stores [Ca^{2+} -induced Ca^{2+} release (CICR)], leading to a marked increase of the free cytosolic Ca^{2+} concentration ($[\text{Ca}^{2+}]_i$) (1–4). This mechanism raises $[\text{Ca}^{2+}]_i$ high enough to initiate the interaction of the contractile filaments and subsequent contractions. Additional confirmation of this hypothesis has been provided by the finding of Ca^{2+} sparks (5).

In the sinus node and the cells of the conduction system, VDCCs are rhythmically activated by diastolic depolarizations and related APs (6–9). The hyperpolarization activated non-selective cation current (I_h) underlying these spontaneous diastolic depolarizations (10) has recently been cloned (11–13).

The rhythmic APs, CICR, and contractions require the functional expression of a variety of membrane ion channels and intracellular Ca^{2+} release sites (14), as well as Ca^{2+} extrusion mechanisms (15). Previous studies showed, however, that murine embryonic cardiomyocytes do not express the full ensemble of ion channels and that some channels are expressed at lower densities (16, 17, 18). Therefore, we wondered whether these cells displayed already spontaneous electrical activity and CICR.

Cardiomyocytes before day embryonic day 11 post coitum, cannot be obtained from the embryo because the heart is too small to be subjected to single cell preparations (17). Recent work has established the embryoid body (EB) cell system as a tool for the investigation of early cardiomyogenesis (18–20). Ultrastructural (18), molecular biological (21), and electro-

physiological (16, 22) studies have demonstrated that, within the EB, the various stages of cardiomyogenesis parallel the murine heart development.

Here, we provide evidence that spontaneous contractions of early cardiomyocytes differentiated within EBs do not require CICR but are triggered by $[\text{Ca}^{2+}]_i$ oscillations. We further show that these $[\text{Ca}^{2+}]_i$ oscillations, rather than CICR, induce the earliest APs in these cardiomyocytes.

MATERIALS AND METHODS

Cell Preparation. Cardiomyocytes were derived from the pluripotent embryonic stem (ES) cell line D3 (19, 20). The differentiation protocol was similar, as described before (16, 20). In brief, undifferentiated ES cells were cultivated on feeder layers and, for passaging, were dispersed with trypsin. Embryoid bodies (EBs) were generated by cultivating the ES cells first for 2 days in hanging drops (400 cells/20 μl), then for 5 days in suspension, and finally by plating for 1–15 days on gelatin-coated glass coverslips. About 12–24 hours after plating, spontaneously contracting cell clusters appeared. For the preparation of isolated stage-1 (differentiated for 9 days), stage-2 (differentiated for 10–11 days), and stage-4 (differentiated for 17–22 days) cardiomyocytes, beating areas of 20–30 EBs were dissected and isolated by enzymatic dispersion by using collagenase B (Boehringer Ingelheim), as described in more detail by Maltsev *et al.* (16). The solution used for dissociation of the dissected areas contained (in mM): NaCl 120, KCl 5.4, MgSO_4 5, CaCl_2 0.03, Na pyruvate 5, glucose 20, taurine 20, Hepes 10, collagenase B 0.5–1 mg/ml, pH 6.9 (NaOH). The dissociated material was plated onto glass coverslips and was stored in the incubator. Within the first 12 hours, cells attached to the glass surface.

Electrophysiology. For electrophysiological recordings, the glass coverslips were transferred to a temperature-controlled recording chamber and were superfused with extracellular solution. Only spontaneously beating cells were selected for the experiments. Cellular electrical activity was recorded in the current-clamp and voltage-clamp mode (23) by using the perforated patch-clamp configuration (24). Ionic currents were recorded by using an Axopatch 200 A (Axon Instruments, Foster City, CA) or an EPC-9 amplifier (HEKA Electronics, Lambrecht/Pfalz, Germany). Data were acquired by using the ISO 2 (MFK, Niedernhausen, Germany) or the PULSE (HEKA Electronics) software package. Data were digitized at 10 kHz and were filtered at 1 kHz.

Pipettes (3–4 megaohms) were prepared on a DMZ Universal Puller (DMZ, München, Germany) from 1.5-mm bo-

Abbreviations: AP, action potential; VDCC, voltage-dependent L-type Ca^{2+} channels; CICR, Ca^{2+} -induced Ca^{2+} release; EB, embryonic body; ES cell, embryonic stem cell; CLSM, confocal laser scanning microscopy.

*S.V.-K. and B.K.F. contributed equally to the manuscript.

†To whom reprint requests should be addressed. e-mail: JH@physiologie.uni-koeln.de.

The publication costs of this article were defrayed in part by page charge payment. This article must therefore be hereby marked "advertisement" in accordance with 18 U.S.C. §1734 solely to indicate this fact.

PNAS is available online at www.pnas.org.

rosilicate glass capillaries (Clark Electromedical Instruments, Reading, U.K.). The composition of the different recording solutions used was the following (in mM): Extracellular solutions: NaCl 140, KCl 5, CaCl₂ 2, MgCl₂ 2, Hepes 5, and glucose 10; high K⁺ solution: NaCl 5, KCl 140, CaCl₂ 2, MgCl₂ 2, Hepes 5, and glucose 10; low Na⁺ solution: NaCl 15, KCl 5, CholineCl 120, CaCl₂ 2, MgCl₂ 2, Hepes 5, and glucose 10; low Na⁺, high K⁺ solution: NaCl 15, KCl 140, MgCl₂ 2, Hepes 5, and glucose 10, pH 7.4 (NaOH); intracellular solution: KCl 55, K₂SO₄ 70, MgCl₂ 7, and Hepes 10, pH 7.4 (KOH). Amphotericin B (Sigma) was dissolved (7.5 mg) as stock solution in 125 μ l of DMSO. The pipette was backfilled with amphotericin containing intracellular solution, and the pipette tip was shortly put into amphotericin free intracellular solution. The final concentration of amphotericin B in the pipette solution was 1 mg/ml. The series resistance reached a steady-state level of 10–20 megaohms within 5–15 min after obtaining a gigaohm seal. All experiments were carried out at 35–37°C. Data are given as means \pm SEM.

[Ca²⁺]_i Measurements with the Photomultiplier Tube. Cells were loaded for 12–15 min in DMEM with the cell-permeable dye fura-2AM (1 μ M, Molecular Probes) at 37°C. Then, coverslips were transferred to a temperature-controlled recording chamber and were perfused for 10 min with extracellular solution before the start of the experiments. Superfusion was performed by gravity at a rate of 1 ml/min. A 90% volume exchange was achieved within \approx 10 sec. Monochromatic excitation light (340, 380 nm) was generated by a monochromator at a frequency of 50 Hz (TILL Photonics, Planegg, Germany). The monochromator was coupled to the epifluorescence attachment of an inverted microscope (Zeiss, 135M) through a small quartz light guide. The excitation light was directed to the objective (40 \times , Zeiss) via a dichroic mirror (TILL Photonics). The emitted fluorescence from the fura-2 loaded cells was monitored through a 470-nm interference filter by using a photomultiplier attached to the anterior port of the microscope. Spontaneously beating cardiomyocytes were investigated. The cell of interest was identified before the experiment, and other cells were excluded from the visual field with an iris mounted on the epifluorescence attachment. Fluorescence intensities were stored on a videotape by using a pulse-code modulator (VR 100, Instrutech, Mineola, NY). Background fluorescence was determined at the end of the experiments by removing the cell of interest from the visual field and determining the remaining fluorescence. The fluorescence of unloaded cardiomyocytes was negligible. For analysis, data were downloaded from the videotape via pulse-code modulator into an Axon software program (Axon Instruments) at a sampling rate of 250 Hz and were filtered at 100 Hz. Files in ASCII format were imported into a spreadsheet program (SIGMA PLOT, Jandel Scientific, Erkrath, Germany), and background intensities were subtracted at both wavelengths individually. The data are displayed as 340/380 ratios.

Confocal Laser Scanning Microscopy (CLSM). [Ca²⁺]_i was monitored in whole EBs as well as in single cardiac cells by using the fluorescent dye fluo-3, AM (Molecular Probes). Cells were loaded for 15 min in DMEM with 10 μ M fluo-3, AM and were dissolved in dimethyl sulfoxide (final concentration 0.1%) and pluronic F-127 (Molecular Probes, final concentration $<0.025\%$). Then, the coverslips were rinsed in the standard extracellular solution and were transferred to the recording chamber. Fluo-3 fluorescence was monitored by an inverted CLSM (LSM 410, Zeiss) using a 25 \times objective numerical aperture 0.80 (Neofluar, Zeiss). For fluorescence excitation, the 488-nm band of an argon laser was used. Emission was recorded by using a longpass LP 515 filter set. Pixel images (265 \times 265 and 128 \times 100 images) were acquired every 0.36 and 0.15 sec, respectively. To determine contractions of cardiomyocytes, transmission images and fluorescence images were recorded simultaneously by using the overlay

option of the confocal setup. Contractions of cardiomyocytes caused changes in light diffraction in the transmission image and were monitored as deviations from the basal gray level. Processing of images was carried out by using the time-software facilities of the confocal setup. Images were acquired and stored to 16-megabyte video memory of the confocal setup at the selected time intervals indicated. Each series of images was scaled between pixel intensity 0 (background fluorescence) and 255 (maximum fluorescence in that series). The pixel values in a region of interest (selected by using an overlay mask) were analyzed by using SIGMA PLOT. The fluorescence changes occurring within single cells during the time course of the experiment were individually recorded, and the data were presented in arbitrary units as percentage of fluorescence variation F with respect to the resting level F_0 .

Test Substances. Bay K 8644 and nisoldipine (kindly provided by Bayer AG, Leverkusen, Germany) were dissolved in ethanol (final concentration $<0.1\%$) and thapsigargin (Molecular Probes) was dissolved in DMSO (final concentration $<0.1\%$). All remaining substances used were purchased from Sigma, were dissolved to the final concentration in extracellular solution, and were applied by gravitational flow. Caffeine was applied through a puffer pipette (General Valve, Fairfield, NJ).

RESULTS

Pluripotent, murine ES cells of the cell line D3 were differentiated as EBs to investigate stage-1 (differentiated for 8–9 days) and stage-2 (differentiated for 10–11 days) cardiomyocytes corresponding to a stage before embryonic day 11 post coitum of the murine embryonic heart. Terminally differentiated (stage 4) cardiomyocytes (differentiated for 16–22 days) resembled the different cardiac cell phenotypes of murine neonates (16, 19, 20).

Our study was initiated by the observation that stage-1 and -2 cardiomyocytes stably contracted for hours under conditions in which the membrane potential was depolarized by superfusion with 140 mM K⁺. A similar contraction frequency of \approx 1 Hz occurred in the presence of physiological saline solution and high K⁺. This feature was not observed in stage-4 ES cell-derived cardiomyocytes, which, similarly to adult cardiomyocytes, showed hypercontraction and cell death within seconds of exposure to high K⁺.

Because omission of extracellular Ca²⁺ did not stop contractions immediately, we examined whether rhythmic changes of [Ca²⁺]_i generated these contractions in stage-1 and -2 cardiomyocytes. By using CLSM as well as photometry, [Ca²⁺]_i was measured under physiological conditions, in the presence of 140 mM K⁺, and after pharmacological intervention. As seen in Fig. 1A, [Ca²⁺]_i oscillations were observed with the cells in normal extracellular solution. Application of high K⁺ led to a transient rise of [Ca²⁺]_i, presumably because of the activation of VDCC. During the declining phase rhythmic, large-amplitude [Ca²⁺]_i oscillations occurred. These were time-locked with the spontaneous contractile activity ($n = 3$), indicating that they were driven by the [Ca²⁺]_i oscillations. Spontaneously contracting fura-2 loaded stage-1 and -2 cardiomyocytes displayed deflections of 340/380-nm signals in opposite directions. This excluded that the observed changes of [Ca²⁺]_i were evoked by movement artifacts. To further confirm that [Ca²⁺]_i oscillations are unrelated to membrane channels, different pharmacological agents were tested in regard to their efficacy in interrupting the oscillations (Fig. 1B–D). The persistence of [Ca²⁺]_i oscillations and contractions under high K⁺ made the involvement of VDCC unlikely. This was corroborated by the observation that [Ca²⁺]_i oscillations continued in the presence of the selective VDCC blocker nisoldipine (2 μ M) (Fig. 1B, $n = 5$). The significantly faster decline of the 340/380 ratio in normal extracellular solution as

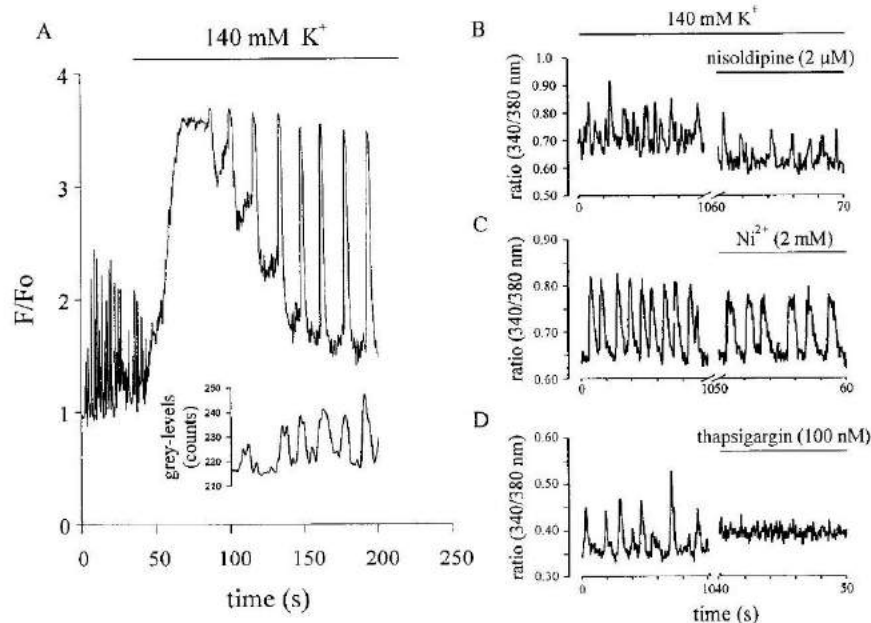


FIG. 1. (A) Effect of high K^+ on $[Ca^{2+}]_i$ oscillations and contractions observed with CLSM in a single stage-2 cardiomyocyte. Depolarization resulted in a transient rise of $[Ca^{2+}]_i$, presumably because of the activation of VDCC channels and in an alteration of the amplitude and frequency of oscillations. The inset shows cell contractions time-locked with $[Ca^{2+}]_i$ oscillations during superfusion with high K^+ . Cell membrane depolarization resulted in an initial discontinuation of contractions, which resumed with the decline of $[Ca^{2+}]_i$. F/F_0 indicates the ratio between the actual and the initial intensity of the fluorescent dye. Grey-levels represent the intensity of the transmitted light, which varied with cell contraction. (B–D) Effect of different pharmacological agents on 340/380 ratios in fura-2AM-loaded spontaneously beating stage-2 cells. (B) The VDCC blocker nisoldipine (2 μ M) did not impair $[Ca^{2+}]_i$ oscillations but lead to a lowering of steady-state $[Ca^{2+}]_i$ levels. (C) Similarly, Ni^{2+} (2 mM), known to block the Na^+-Ca^{2+} exchanger, did not interrupt $[Ca^{2+}]_i$ oscillations. (D) The Ca^{2+} -ATPase inhibitor thapsigargin (100 nM) led to an abrupt halt of the $[Ca^{2+}]_i$ oscillations and a concomitant increase of the resting $[Ca^{2+}]_i$.

compared with high K^+ solution indicated the functional expression of the Na^+-Ca^{2+} exchanger in stage-1 and -2 cardiomyocytes ($n = 11$) (25, 26). However, it is unlikely that the Na^+-Ca^{2+} exchanger evoked the $[Ca^{2+}]_i$ oscillations through its backward mode (27) or its reduced activity in high K^+ (28) because these persisted even after addition of 2 mM Ni^{2+} , a known blocker of the Na^+-Ca^{2+} exchanger (Fig. 1C; note the slowing of the decline of the 340/380 ratio, $n = 2$) or Ni^{2+} plus nisoldipine ($n = 3$, data not shown). In contrast, thapsigargin, a sarcoplasmic Ca^{2+} -ATPase inhibitor, led to a rise in $[Ca^{2+}]_i$ and an abrupt halt of $[Ca^{2+}]_i$ oscillations (Fig. 1D, $n = 7$), showing that these intracellular $[Ca^{2+}]_i$ oscillations drive spontaneous contractions in stage-1 and -2 cardiomyocytes.

To examine whether the $[Ca^{2+}]_i$ oscillations translated into changes of the membrane potential, current clamp experiments were performed. Stage-1 cells were characterized by a depolarized resting potential (minimal diastolic potential, -56 ± 14 mV, $n = 14$) and APs of small amplitude (≤ 30 mV, Fig. 2A). Most of the stage-2 cells also showed depolarized resting potentials (-62 ± 10 mV, $n = 9$) but already displayed APs of larger amplitude (≥ 30 mV, Fig. 2B and C). Stage-1 and most of the stage-2 cardiomyocytes were characterized by small fluctuations of the membrane potential intercalated between the APs (Fig. 2A–C). These fluctuations occurred at a frequency of 1.3 ± 0.5 Hz ($n = 18$), were associated with spontaneous contractions of the cells, and proved to depend on the resting potential. In cardiomyocytes with resting potentials negative to -40 mV, the average amplitude amounted to 17 ± 1 mV ($n = 19$), and, in those with resting potentials positive to -40 mV, the amplitude was 9 ± 2 mV ($n = 8$). Stage-4 sinusodal-like cardiomyocytes displayed diastolic depolarizations (Fig. 2D). These cells are known to express I_f and $I_{K, ACh}$ (16). In contrast to stage 1 and 2, stage-4 cardiomyocytes did

not display the small fluctuations (see Fig. 2D), suggesting a correlation between the $[Ca^{2+}]_i$ oscillations and the membrane potential fluctuations. Therefore, the origin of these was further investigated by pharmacological tools. Superfusion with 140 mM K^+ depolarized the resting potential of stage-1 and -2 cells close to 0 mV and interrupted both APs and membrane potential fluctuations (Fig. 3A, $n = 4$). However, the cardiomyocytes continued to display spontaneous contractions (microscopic observation). Addition of the VDCC blocker nisoldipine (50 nM, $n = 4$) interrupted the generation of APs but not the membrane potential fluctuations and the accompanying contractions (Fig. 3B). APs and membrane potential fluctuations as well as contractions were completely blocked by addition of thapsigargin (Fig. 3C, 100 nM, $n = 3$). These data indicate that (i) the membrane potential fluctuations do not trigger the $[Ca^{2+}]_i$ oscillations, (ii) the fluctuations depend on the filling state of intracellular Ca^{2+} stores, (iii) the fluctuations are independent of the opening of VDCC, and (iv) the APs are triggered by the fluctuations. Hence, Ca^{2+} imaging and patch-clamp experiments in the current clamp mode demonstrate that spontaneous contractions of cardiomyocytes during early development depend neither on the membrane potential nor on the transmembrane L-type Ca^{2+} current but are governed by $[Ca^{2+}]_i$ oscillations.

Because early APs are not required for the generation of contractions, they must serve another function in the early embryonic heart. It is known that ES cell-derived cardiomyocytes express connexin, forming functional gap-junctions very early during development (29). Hence, we wondered whether the early APs are required to provide synchronization of contractions between cardiomyocytes. Therefore, isolated clusters of cardiomyocytes were loaded with the cell permeable dye fluo3-AM. CLSM revealed Ca^{2+} waves propagating with a velocity of 300 ± 64 μ m/sec ($n = 3$). Waves synchronous with

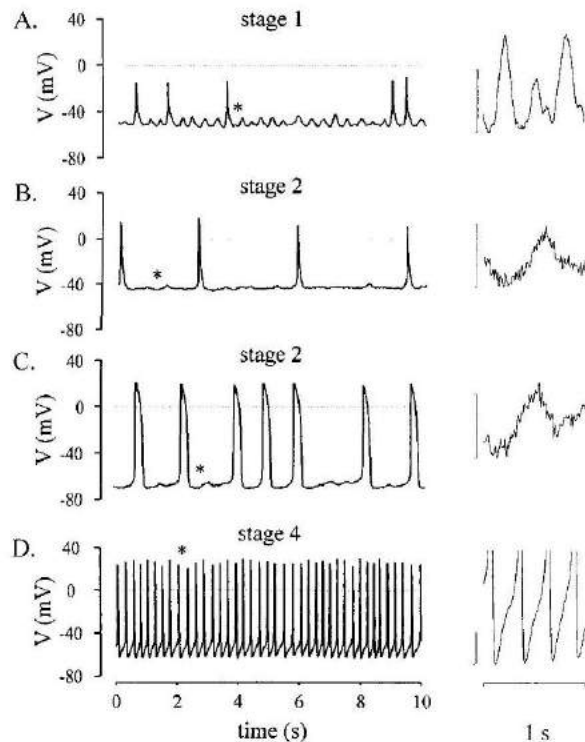


FIG. 2. Electrical activity recorded in spontaneously beating ES cell-derived cardiomyocytes in the current clamp mode. (A) Typical recording from a stage-1 cell with depolarized resting potential and APs of small amplitude. Membrane potential fluctuations (marked by an asterisk) shown at extended scales (vertical calibration bar represents 10 mV) on the right were intercalated between APs. (B) Stage-2 cells displayed typically depolarized resting potentials but larger APs than stage-1 cells. The membrane potential fluctuations were still observed. (C) Transitional stage (stage 2) cell, which displayed a more negative resting potential and small diastolic depolarizations before the generation of APs. Membrane potential fluctuations were still present. (D) Stage-4 pacemaker-like cells were characterized by an unstable resting potential and the typical diastolic depolarization.

cell contractions were observed in single cells as well as in beating foci in plated EBs, excluding Ca^{2+} overload caused by cell damage by enzymatic dissociation as the underlying mechanism. Fig. 4 shows recordings of $[\text{Ca}^{2+}]_i$ in normal extracellular solution (Fig. 4A) as well as on superfusion with high K^+ -solution (Fig. 4B). Under control conditions, the Ca^{2+} wave spread in a coordinated manner, indicating an electrical coupling between the cardiomyocytes through gap junctions. The initiation site and the direction of propagation of the waves remained unaltered during the course of the experiment. In high K^+ -solution, the $[\text{Ca}^{2+}]_i$ oscillations persisted but occurred in a desynchronized manner. No initiation site or direction of propagation could be identified. Further, the frequency and amplitude of the $[\text{Ca}^{2+}]_i$ oscillations differed markedly between individual cells (Fig. 4B).

DISCUSSION

The heart is the first organ to form during embryonic development. The autonomic rhythm can be observed as early as in embryonic day 9.5 of murine embryonic development (30). The major finding of our study is that contractions of the heart during early development are not evoked by transmembrane ion currents resulting in APs but by intracellular $[\text{Ca}^{2+}]_i$ oscillations. Further, CICR is not required for functioning of the early embryonic heart because ES cell-derived stage-1 and

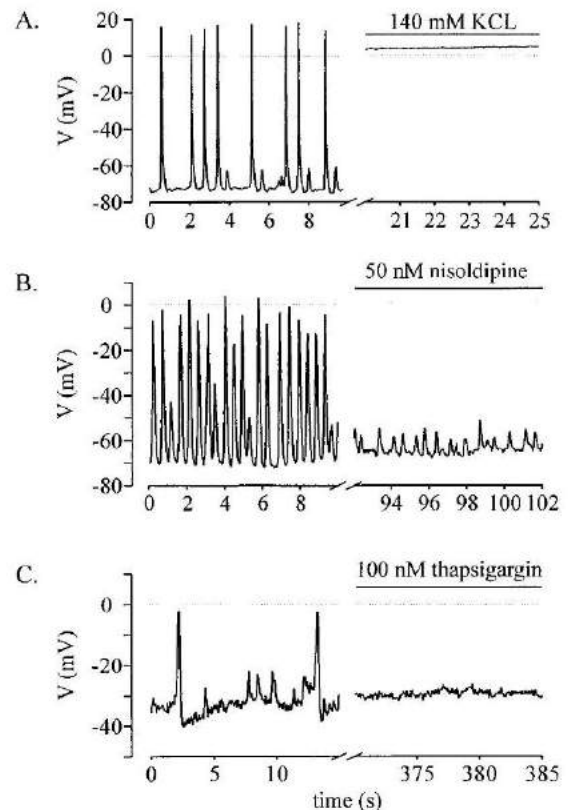


FIG. 3. Pharmacological characterization of the APs and membrane potential fluctuations in spontaneously beating stage-1 and -2 cells measured under current clamp. (A) Superfusion of 140 mM K^+ led to depolarization of the resting potential close to 0 mV and halted both APs and small membrane potential fluctuations. (B) Superfusion of the VDCC blocker nisoldipine (50 nM) interrupted the APs but not the small membrane potential fluctuations. (C) Application of the sarcoplasmic ATPase inhibitor thapsigargin (100 nM) to a stage-1 cell blocked both APs and membrane potential fluctuations and led to a depolarization of the resting potential.

-2 cardiomyocytes continued to contract under high K^+ when the membrane potential was depolarized. These findings differ from those suggesting that electromechanical coupling in the fetal heart depends largely on trans-sarcolemmal Ca^{2+} influx rather than Ca^{2+} released from the sarcoplasmic reticulum (31–34). However, these studies were performed at late embryonic stages whereas the work presented here investigates early embryonic cardiomyocytes. Membrane potential-independent contractions are in complete contrast to the functioning of the adult heart, where incubation of heart tissue in high extracellular K^+ solution (cardioplegic solution) is used as standard procedure to prevent contractions.

Thus, the present findings envision intracellular Ca^{2+} stores as the primary rhythm generator in murine cardiomyocytes early during development whereas VDCC may serve primarily for store refilling (35). The increase of $[\text{Ca}^{2+}]_i$ leads to activation of a Ca^{2+} -activated conductance (nonselective cation current and/or Na^+ - Ca^{2+} exchanger), resulting in the small depolarization of the resting potential and the occasional generation of APs via activation of VDCC, similar to observations made on cultured cardiac cells (36). Preliminary experimental results on the nature of this Ca^{2+} activated conductance under a $[\text{Ca}^{2+}]_i$ increase induced by caffeine point toward a nonselective cation current because the reversal potential of this current was close to 0 mV and shifted to more negative potentials on replacement of extracellular Na^+ by

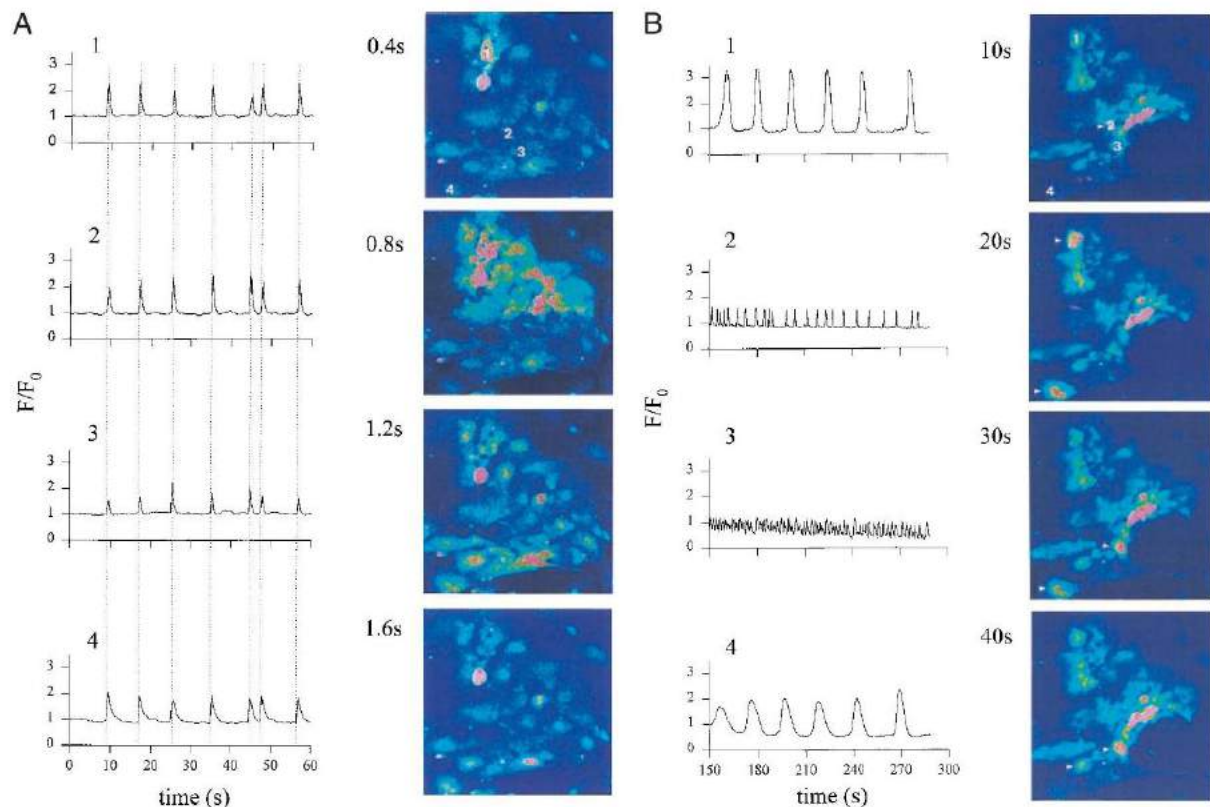


FIG. 4. CLSM images of $[Ca^{2+}]_i$ oscillations in a spontaneously contracting area of cardiomyocytes isolated from a stage-2 EB. (A) Control conditions. A $[Ca^{2+}]_i$ wave spread with a velocity of $\sim 400 \mu m \cdot sec^{-1}$ from the initiation site (cell 1) to the termination site (cell 4). The tracings of $[Ca^{2+}]_i$ changes in different cells (cell 1–4) demonstrate the synchronization of the $[Ca^{2+}]_i$ signal, indicating electrical coupling between adjacent cells. (B) $[Ca^{2+}]_i$ oscillations recorded in the same area of cardiomyocytes after superfusion with high K^+ . The images were recorded after decline toward resting $[Ca^{2+}]_i$ of the initial transient $[Ca^{2+}]_i$ rise after switching to high K^+ . The initial $[Ca^{2+}]_i$ increase was caused by the activation of VDCC. Note that, under high K^+ $[Ca^{2+}]_i$ oscillations in cells 1–4 are desynchronized and differ in amplitude and frequency.

choline. This behavior is clearly different from the characteristics of the Na^+-Ca^{2+} exchanger-mediated current (25, 26, 37, 38). In contrast to early-stage cardiomyocytes, terminally differentiated pacemaker cells were characterized by membrane driven events. In these cells, interplay between different ion channels, in particular VDCC, K^+ channels, and I_f , allows the generation of spontaneous activity, governing the heart beat (6, 8, 9, 39).

Because we clearly demonstrated that APs do not translate into CICR, we investigated whether they serve to synchronize the heart beat. In multicellular preparations, the cardiomyocytes were electrically coupled by gap junctions, even at this early developmental stage (29). The pacemaker cell with the highest frequency of $[Ca^{2+}]_i$ oscillations (internal oscillator) determined the contractile activity of the whole cardiomyocyte cluster. Application of high extracellular K^+ caused the cardiomyocytes to electrically uncouple and contract again under control of their internal oscillator (40). It is tempting to speculate that this very early motif is even found in cardiomyocytes before the onset of spontaneous APs. Indeed, an oscillatory behavior of the resting potential at this very early stage was observed by using membrane potential-sensitive dyes in combination with photodiode arrays (41). Subsequently, APs coupled with contractions were observed in the embryonic rat heart at embryonic day 9.5 (42).

There is evidence that mechanisms important during early embryonic development may remain dormant in terminally differentiated cells but may assume *de novo* significance in the case of pathological cell transformation. It can be speculated that, in certain pathological conditions, the internal oscillator

(40) again becomes predominant and induces cardiac arrhythmias, as suggested for ouabain intoxication or extended β -adrenergic stimulation. The resemblance between embryonic and pathologically transformed cells may be related to the functional expression of Ca^{2+} activated conductances (36, 43–45). Thus, Ca^{2+} overload associated with spontaneous Ca^{2+} release from intracellular Ca^{2+} stores (46, 47) may result in the generation of arrhythmias: i.e., delayed after depolarizations (44, 48).

We thank Dr. A. M. Wobus for providing ES cells of the cell line D3, M. Faulhaber and B. Hops for assistance in cell culture work, Dr. M. Morad (Georgetown University), Dr. Ganitkevich, and Dr. S. Herzig (University of Cologne) for reading an earlier version of the manuscript and helpful discussions. We further thank Dr. N. Smyth (University of Cologne) for critically reading the final version of the manuscript. The support of the machine and electronic shop is greatly acknowledged.

1. Fabiato, A. (1985) *J. Gen. Physiol.* **85**, 247–289.
2. du Bell, W. H. & Houser, S. R. (1987) *Cell Calcium* **8**, 259–268.
3. Barceñas-Ruiz, L. & Wier, W. G. (1987) *Circ. Res.* **61**, 148–154.
4. Nabauer, M., Callewaert, G., Cleemann, L. & Morad, M. (1989) *Science* **244**, 800–803.
5. Cheng, H., Lederer, W. J. & Cannell, M. B. (1993) *Science* **262**, 740–744.
6. Noble, D. (1983) *Symp. Soc. Exp. Biol.* **37**, 1–28.
7. Brown, H. F., Kimura, J., Noble, D., Noble, S. J. & Taupignon, A. (1984) *Proc. R. Soc. London Ser. B* **222**, 329–347.
8. Denyer, J. C. & Brown, H. F. (1990) *J. Physiol. (London)* **428**, 405–424.

9. Irisawa, H., Brown, H. F. & Giles, W. (1993) *Physiol. Rev.* **73**, 197–227.
10. DiFrancesco, D. (1993) *Annu. Rev. Physiol.* **55**, 455–472.
11. Ludwig, A., Zong, X., Jeglitsch, M., Hofmann, F. & Biel, M. (1998) *Nature (London)* **393**, 587–591.
12. Gauss, R., Seifert, R. & Kaupp, U. B. (1998) *Nature (London)* **393**, 583–587.
13. Santoro, B., Liu, D. T., Yao, H., Bartsch, D., Kandel, E. R., Siegelbaum, S. A. & Tibbs, G. R. (1998) *Cell* **93**, 717–729.
14. Bers, D. M. (1997) *Circ. Res.* **81**, 636–638.
15. Bers, D. M. (1997) *Basic Res. Cardiol.* **92**, Suppl. 1, 1–10.
16. Maltsev, V. A., Wobus, A. M., Rohwedel, J., Bader, M. & Hescheler, J. (1994) *Circ. Res.* **75**, 233–244.
17. Davies, M. P., An, R. H., Doevendans, P., Kubalak, S., Chien, K. R. & Kass, R. S. (1996) *Circ. Res.* **78**, 15–25.
18. Hescheler, J., Fleischmann, B. K., Lentini, S., Maltsev, V. A., Rohwedel, J., Wobus, A. M. & Addicks, K. (1997) *Cardiovasc. Res.* **36**, 149–162.
19. Doetschman, T. C., Eistetter, H., Katz, M., Schmidt, W. & Kemler, R. (1985) *J. Embryol. Exp. Morphol.* **87**, 27–45.
20. Wobus, A. M., Wallukat, G. & Hescheler, J. (1991) *Differentiation (Berlin)* **48**, 173–182.
21. Miller-Hance, W. C., La Corbiere, M., Fuller, S. J., Evans, S. M., Lyons, G., Schmidt, C., Robbins, J. & Chien, K. R. (1993) *J. Biol. Chem.* **268**, 25244–25252.
22. Ji, G. J., Fleischmann, B. K., Bloch, W., Feelisch, M., Andressen, C., Addicks, K. & Hescheler, J. (1999) *FASEB J.* **13**, 313–324.
23. Hamill, O. P., Marty, A., Neher, E., Sakmann, B. & Sigworth, F. J. (1981) *Pflugers Arch.* **391**, 85–100.
24. Korn, S. J. & Horn, R. (1989) *J. Gen. Physiol.* **94**, 789–812.
25. Kimura, J., Noma, A. & Irisawa, H. (1986) *Nature (London)* **319**, 596–597.
26. Mechmann, S. & Pott, L. (1986) *Nature (London)* **319**, 597–599.
27. Barcenas-Ruiz, L., Beuckelmann, D. J. & Wier, W. G. (1987) *Science* **238**, 1720–1722.
28. Orchard, C. H., Eisner, D. A. & Allen, D. G. (1983) *Nature (London)* **304**, 735–738.
29. Saitoh, M., Oyamada, M., Oyamada, Y., Kaku, T. & Mori, M. (1997) *Carcinogenesis* **18**, 1319–1328.
30. Fishman, M. C. & Chien, K. R. (1997) *Development (Cambridge, U.K.)* **124**, 2099–2117.
31. Nayler, W. G. & Fassold, E. (1977) *Cardiovasc. Res.* **11**, 231–237.
32. Mahony, L. & Jones, L. R. (1986) *J. Biol. Chem.* **261**, 15257–15265.
33. Klitzner, T. S. & Friedman, W. F. (1989) *Pediatr. Res.* **26**, 98–101.
34. Chin, T. K., Friedman, W. F. & Klitzner, T. S. (1990) *Circ. Res.* **67**, 574–579.
35. Kolossov, E., Fleischmann, B. K., Liu, Q., Bloch, W., Viatchenko-Karpinski, S., Manzke, O., Ji, G. J., Bohlen, H., Addicks, K. & Hescheler, J. (1998) *J. Cell Biol.* **143**, 2045–2056.
36. Clusin, W. T. (1983) *Nature (London)* **301**, 248–250.
37. Clusin, W. T., Fischmeister, R. & De Haan, R. L. (1983) *Am. J. Physiol.* **245**, H528–H532.
38. Lipp, P. & Pott, L. (1988) *J. Physiol. (London)* **403**, 355–366.
39. DiFrancesco, D. & Noble, D. (1985) *Philos. Trans. R. Soc. London Ser. B* **307**, 353–398.
40. Tsien, R. W., Kass, R. S. & Weingart, R. (1979) *J. Exp. Biol.* **81**, 205–215.
41. Kamino, K. (1991) *Physiol. Rev.* **71**, 53–91.
42. Bers, D. M. & MacLeod, K. T. (1986) *Circ. Res.* **58**, 769–782.
43. Hordof, A. J., Spotnitz, A., Mary Rabine, L., Edie, R. N. & Rosen, M. R. (1978) *Circulation* **57**, 223–229.
44. Kass, R. S., Tsien, R. W. & Weingart, R. (1978) *J. Physiol. (London)* **281**, 209–226.
45. Clusin, W. T., Bristow, M. R., Karagueuzian, H. S., Katzung, B. G. & Schroeder, J. S. (1982) *Am. J. Cardiol.* **49**, 606–612.
46. Clusin, W. T., Buchbinder, M. & Harrison, D. C. (1983) *Lancet* **i**, 272–274.
47. Clusin, W. T. (1983) *Proc. Natl. Acad. Sci. USA* **80**, 3865–3869.
48. Kass, R. S., Lederer, W. J., Tsien, R. W. & Weingart, R. (1978) *J. Physiol. (London)* **281**, 187–208.

1.4. **Порушення в розповсюдженні потенціалів дії в довготривалих записах активності в культурі кардіоміоцитів, отриманих з ембріональних стовбурових клітин**

Pflügers Arch – Eur J Physiol (1999) 437:669–679

© Springer-Verlag 1999

ORIGINAL ARTICLE

Peter Igelmund · Bernd K. Fleischmann
Ivo R. Fischer · Julia Soest · Oleksii Gryshchenko
Michaela M. Böhm-Pinger · Heinrich Sauer
Qinghua Liu · Jürgen Hescheler

Action potential propagation failures in long-term recordings from embryonic stem cell-derived cardiomyocytes in tissue culture

Received: 5 August 1998 / Received after revision: 30 October 1998 / Accepted: 27 November 1998

Abstract Three-dimensional cell aggregates (embryoid bodies, EBs) containing clusters of spontaneously beating cardiomyocytes were derived from permanent mouse embryonic stem (ES) cells. Extracellular recordings of the population action potentials of cardiomyocyte clusters were made using permanently mounted silver wire electrodes and microelectrode arrays integrated into the bottom of the culture dish. These techniques allowed long-term recordings (for up to several weeks) from individual EBs under cell culture conditions. The normal electrical activity consisted of regular spiking with a frequency of 0.5–5 Hz. However, most EBs (87%) spontaneously developed temporary or persistent complex activity patterns because of intermittent block of action potential propagation at narrow pathways connecting larger beating areas. Similar propagation blocks could also be reversibly induced in regularly spiking EBs by nimodipine (NDP). In addition to a slowing of pacemaker activity, NDP (20–200 nM) induced a stepwise decrease of the action potential frequency at the recording site. Perforated patch-clamp recordings from enzymatically isolated ES-cell-derived cardiomyocytes showed that similar activity patterns do not occur at the single-cell level. We suggest that this novel approach may provide a useful tool for in vitro studies of chronotropy and phenomena of propagation failure similar to AV block.

Key words Calcium current · Cardiomyocytes · Conduction block · Discontinuous conduction · Embryonic stem cells · Embryoid body · Microelectrode array · Nimodipine

Introduction

Although the generation of arrhythmias in the native heart has been investigated widely, only a few in vitro models are currently available for studying the underlying mechanisms. For instance, Rohr and coworkers [21] introduced two-dimensional patterned growth cultures of neonatal rat ventricular myocytes. Using optical recording techniques and geometrically defined cultures, they could quantitatively demonstrate the dependence of action potential propagation on the architecture of the excitable tissue (e.g. [4, 20, 22]). De Haan and coworkers investigated the role of electrical coupling in action potential propagation and synchronization using pairs of spherical aggregates of chick embryonic heart cells [1, 30]. Electrical coupling between cardiac cells can be further investigated using preparations such as pairs of isolated ventricular [9, 24, 26] or sinoatrial nodal cells [25].

These and other in vitro cardiac models [11, 13, 18, 27] are based on only one phenotype of cardiomyocyte, mostly ventricular cells. In the present study, we introduce a different approach using extracellular recordings of the spontaneous electrical activity of cardiomyocytes within three-dimensional cell aggregates (embryoid bodies, EBs) derived from murine embryonic stem (ES) cells [2, 7, 14, 15, 28]. In contrast to the other cardiac cell models, beating EBs appear to be organized into areas of primary pacemaking cells as well as areas containing ventricular myocytes [7]. Up to now, cardiomyocytes in this model have been electrophysiologically investigated only with patch-clamp recordings from isolated cells [14, 15, 28, 29]. Here, we characterize the electrical population behavior of these multicellular aggregates by recording extracellular field potentials from spontaneously beating cardiomyocyte clusters in EBs. Extracellular silver electrodes as well as microelectrode arrays (MEAs) allow long-term (several weeks) electrocardiogram-like recordings from populations of cells, providing information about the activity of single pacemaker cells, action potential propagation, and interactions between different pacemakers.

P. Igelmund · B.K. Fleischmann · I.R. Fischer · J. Soest
O. Gryshchenko · M.M. Böhm-Pinger · H. Sauer · Q. Liu
J. Hescheler (✉)
Zentrum Physiologie und
Pathophysiologie der Universität zu Köln,
Institut für Neurophysiologie, Robert-Koch-Str. 39,
D-50931 Cologne, Germany
e-mail: jh@physiologie.uni-koeln.de
Tel.: +49-221-4786960; Fax: +49-221-4786965

With extracellular and patch-clamp recordings, respectively, we investigated the spontaneous electrical activity of cardiomyocyte clusters in EBs, of small groups of cells, and of single cardiomyocytes, and we tested the effect of the L-type Ca^{2+} channel antagonist nimodipine (NDP). Our results provide evidence for spontaneously occurring arrhythmias caused by action potential propagation failures at structural discontinuities in multicellular cardiomyocyte clusters. Applying NDP to regularly beating EBs induced similar propagation failures that could cause beating arrest even before the frequency of the pacemaker was affected. We suggest that this new approach may be useful for investigating the arrhythmogenic potential of drugs.

Materials and methods

Production of embryoid bodies

Embryonic stem cells of the line D3 [2] were cultivated on a layer of murine fibroblasts (feeder layer) and differentiated into spontaneously beating cardiomyocytes as previously described [14, 15, 28]. Briefly, the ES cells (without feeder layer cells) were cultivated in hanging drops (approx. 400 cells per 20 μl) for 2 days, then they were kept in suspension for 5 days and finally they were plated on gelatinated single culture dishes and microelectrode arrays (MEAs) for extracellular recordings, on multiwell culture plates for patch-clamp recordings, and on glass coverslips for confocal microscopy (Fig. 1). Spontaneously contracting cell clusters could be observed 2–4 days after plating (7+2d to 7+4d).

The culture medium consisted of Dulbecco's Modified Eagle's Medium (DMEM) supplemented with 20% fetal calf serum, 1% Minimal Essential Medium (MEM), 2 mM Glutamax, 50 units/ml penicillin and streptomycin (all from Gibco, Eggenstein, Germany), and 5×10^{-5} M β -mercaptoethanol (Serva, Heidelberg, Germany).

Extracellular recordings

For long-term field potential recordings from cardiomyocytes, EBs were plated on 30-mm culture dishes (Nunc, Roskilde, Denmark) with two to three EBs per dish. Extracellular electrodes were permanently placed onto the tissue after the appearance of spontaneously contracting areas. The electrodes were prepared from Teflon-insulated 125- μm -thick silver wire (A-M Systems, Everett, Wash., USA). The different electrode was insulated except for the blunt tip, whereas the indifferent electrode was free of insulation for a length of about 10 mm. Both electrode wires were mounted to a glass plate (40 mm \times 10 mm), previously formed according to Fig. 1, with a tip distance of 5–10 mm, and sterilized with ethanol. With the aid of the microscope, the glass plate was glued to the culture dish with the different electrode placed next (<100 μm) to a contracting area. The whole assembly was enclosed in a larger culture dish for sterility, only the two silver wires protruding under the cover, and the whole system was placed into an incubator (UniIncu 150, UniEquip, Martinsried, Germany) at 37°C, 5% CO_2 , 100% humidity. The medium was renewed every 2–4 days and with each washout of nimodipine (NDP).

In some experiments, single EBs were plated on MEAs for multiple recording from several locations of individual EBs (Fig. 1). The electrode matrix of the MEAs consisted of 60 TiN-coated gold electrodes with a diameter of 10 or 30 μm , arranged in eight columns and eight rows with a distance of 100 or 200 μm between adjacent electrodes (see Figs. 4, 5). Stable recordings without degradation were possible for up to 8 days. The MEAs were provided

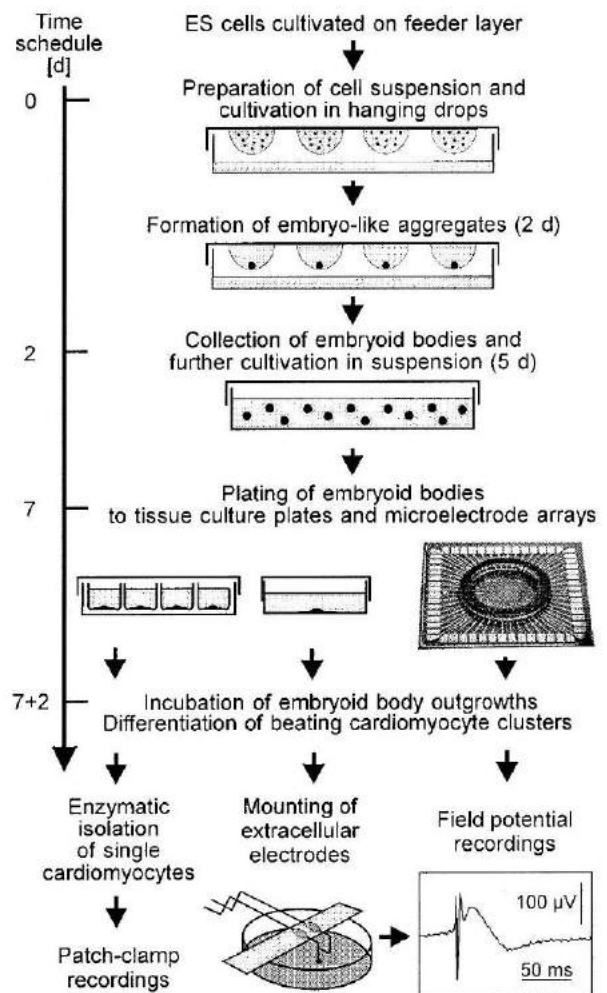


Fig. 1 Procedure of formation and electrophysiological investigation of embryoid bodies (EBs) containing spontaneously beating cardiomyocytes (see text); example of extracellularly recorded action potential (filter 1 Hz to 1 kHz, sample rate 5 kHz)

by Dr. H. Hämmerle (Naturwissenschaftlich-Medizinisches Institut (NMI) at the Universität Tübingen, Reutlingen, Germany; see also [17]).

To apply nimodipine (NDP) (Bayer, Wuppertal, Germany), the incubator was shortly opened, and 2–20 μl of a stock solution [20 μM NDP in 10% dimethylsulfoxide (DMSO)/90% culture medium] was pipetted into the medium, and the culture dish was gently swirled for approximately 5 s. Since swirling alone transiently increased the beating frequency of the EBs, applications of NDP were preceded by control swirls without application. For washout of NDP, the culture dish was taken out of the incubator, and on a sterile bench the medium was replaced three times. Application and washout procedures disturbed the recordings for about 10–20 s and 2–4 min, respectively. For most experiments a final NDP concentration of 50 nM was applied. In some EBs, depending on the reaction to the first NDP application, a subsequent application was carried out, using a higher concentration.

All recordings were performed with the EBs inside the incubator. The signals were amplified with Grass P511K amplifiers (Grass, Quincy, Mass., USA) and fed to threshold discriminators which delivered a single event for each spike. Both continuous

and event data were continuously stored on computer disk using a CED1401 interface [Cambridge Electronic Design (CED), Cambridge, UK] with the SPIKE2 software (CED). To limit the size of the data files, the analog signals were band-pass filtered from 1 Hz to 30 Hz and digitized with a sample rate of 100 Hz, if not otherwise indicated. The strong low-pass filtering largely depressed the fast component of the population action potentials but the slow component was only little affected (see Figs. 2, 5, 9). In some experiments, the sample rate and the low-pass filter setting were temporarily elevated in order to visualize the fast spike components (see Figs. 1, 7). To correlate the electrical and mechanical activity, field potential recordings were stored on video tape (HiFi audio channels) together with the video signal from the microscope. For on-line control, the analog field potential data as well as the frequency of instantaneous beats, based on the triggered events, were continuously displayed. For off-line analysis, data were semi-automatically processed in SPIKE2 using self-written macro scripts. To analyze arrhythmias, it was essential to rid the data of trigger errors. Therefore, new event channels were created off-line on the base of the respective waveform data, taking the minimum or maximum of a spike as the event time. To compensate for the low sample rate, the event time was interpolated by fitting a parabola to the peak and the two adjacent points of the waveform data. Although the calculated event times do not represent the time of activation of the cells, they are an exact baseline for calculating the interval lengths. All relevant recordings were controlled by comparing the event channels with the analog data at an highly extended time scale on the computer screen. Remaining trigger errors were corrected manually with the SPIKE2 program.

Patch-clamp recordings

For patch-clamp recordings, beating areas of 20–30 EBs were dissected and isolated by enzymatic dissociation, using collagenase B (Boehringer, Ingelheim, Germany). The dissociation solution contained (in mM): NaCl 120, KCl 5.4, MgSO₄ 5, CaCl₂ 0.03, Na pyruvate 5, glucose 20, taurine 20, HEPES 10, collagenase B 0.5–1 mg/ml, pH 6.9 (NaOH).

The dissociated material was plated onto glass coverslips and resuspended in culture medium and stored in the incubator. Within the first 12 h, cells attached to the glass surface and spontaneously beating cardiomyocytes could be observed. For electrophysiological recordings, the glass coverslips were transferred to a temperature-controlled recording chamber and perfused with extracellular solution. All patch-clamp experiments were performed at 35°C. Only spontaneously beating cells were selected for the experiments. The electrical activity of the cells was recorded using the amphotericin B technique of the classic whole-cell configuration [6, 12]. Ionic currents were recorded using an Axopatch 200A amplifier (Axon Instruments, Foster City, Calif., USA). Data were acquired using the Iso 2 software package (MFK, Niedernhausen, Germany). Data were sampled at 2 kHz and recorded on-line onto a VR-3200 tape (Bell and Howell, Friedberg/H., Germany); some of the data were stored directly to the computer hard disk. Data were downloaded from tape into SPIKE2 software at a digitization rate of 100 Hz and analyzed as mentioned above. Averaged data are expressed as mean \pm SEM.

Pipettes were made using a DMZ Universal Puller (DMZ, Munich, Germany) from 1.5 mm borosilicate glass capillaries (Clark Electromedical Instruments, Reading, UK). Amphotericin B (Sigma, Deisenhofen, Germany) was dissolved in DMSO at a concentration of 60 mg/ml, frozen in aliquots and defrosted prior to use. The tip of the pipette was filled with normal recording solution and then backfilled with the amphotericin-B-containing solution, yielding a final amphotericin B concentration of 500 μ g/ml. The compositions of the different solutions used were as follows (mM) – pipette solution: KCl 55, MgCl₂ 7, K₂SO₄ 70, HEPES 10, pH 7.4 (KOH); for recording Ca²⁺ currents (*I*_{Ca}), the same solution was used, but K⁺ was replaced by Cs⁺; external solution for current-clamp recordings: NaCl 135, KCl 5.4, MgCl₂ 2, CaCl₂ 1.8,

glucose 10, HEPES 10, pH 7.45 (NaOH); for voltage-clamp experiments: MgCl₂ 1, CaCl₂ 1.8, choline chloride 140, glucose 10, HEPES 10, pH 7.45 (KOH).

Confocal microscopy

To visualize ventricular myocytes, EBs were grown from ES cells that were stably transfected with the pGNA/MLC-2.1 reporter construct [5], containing the *lacZ* gene under the control of a 2.1-kb fragment from the ventricular myosin light chain-2 (MLC-2v) promoter and the neomycin-resistance gene under control of the Rous sarcoma virus long terminal repeat (RSV-LTR) [29]. Reporter gene activity was evaluated using the ImaGene Red C₁₂RG *lacZ* gene expression kit (Molecular Probes, Eugene, Ore., USA). This kit permits the detection of *lacZ* expression in single living cells by imaging the highly fluorescent product 2-dodecylresorufin which arises from dodecylresorufin β -D-galactopyranoside (C₁₂RG) by enzymatic hydrolysis. In brief, EBs outgrown on glass coverslips were washed three times in DMEM. To inhibit endogenous β -D-galactosidase, they were subsequently incubated for 1 h at 37°C in DMEM supplemented with 300 μ M chloroquine. The chloroquine-containing DMEM was removed and DMEM containing 33 μ M C₁₂RG was added. After a 2-h incubation with the β -galactosidase substrate, EBs were washed twice and subsequently inspected using a confocal laser scanning microscope (LSM 410, Carl Zeiss, Jena, Germany) supplemented with a 25 \times , N.A. 0.83 objective (Plan Neofluar, Zeiss). Image acquisition was performed by simultaneously recording fluorescence and transmission using the overlay option of the confocal setup. For excitation, the 543-nm band of a helium/neon laser of the confocal setup was used. Emission was recorded using a long-pass LP590-nm filter set. Transmitted light was recorded using the transmission light photomultiplier tube of the confocal setup.

Results

Extracellular recordings

Spontaneously contracting areas developed 2–4 days after plating the EBs (7+2d–7+4d). A single EB usually contained one to three contracting areas with diameters of 100–500 μ m, beating with individual rhythms or synchronized. During further development, beating areas elongated (>1 mm) and often formed clusters of cells connected by narrow strands of contracting cells (see Figs. 3, 4, 5F). With extracellular electrodes placed close to or inside a contracting area, the activity of the cells very near the electrode (<100 μ m) could be recorded. Recordings from approximately 120 individual EBs lasted up to 42 days. In the different EBs, population action potentials occurred with frequencies of 0.5–5 Hz. Simultaneous observation through the microscope and of video recordings confirmed that the population action potentials are time-locked with the contractions. The population action potentials consist of a fast component lasting approximately 5 ms and a slow component lasting 50–300 ms (Fig. 1). The amplitude of the population action potentials ranged between 20 μ V and 2 mV. The fast component could be blocked by 10 μ M tetrodotoxin (not shown), indicating that this component is caused by the opening of Na⁺ channels.

Examples of the spontaneous electrical activity of different EBs are demonstrated in Fig. 2. The most com-

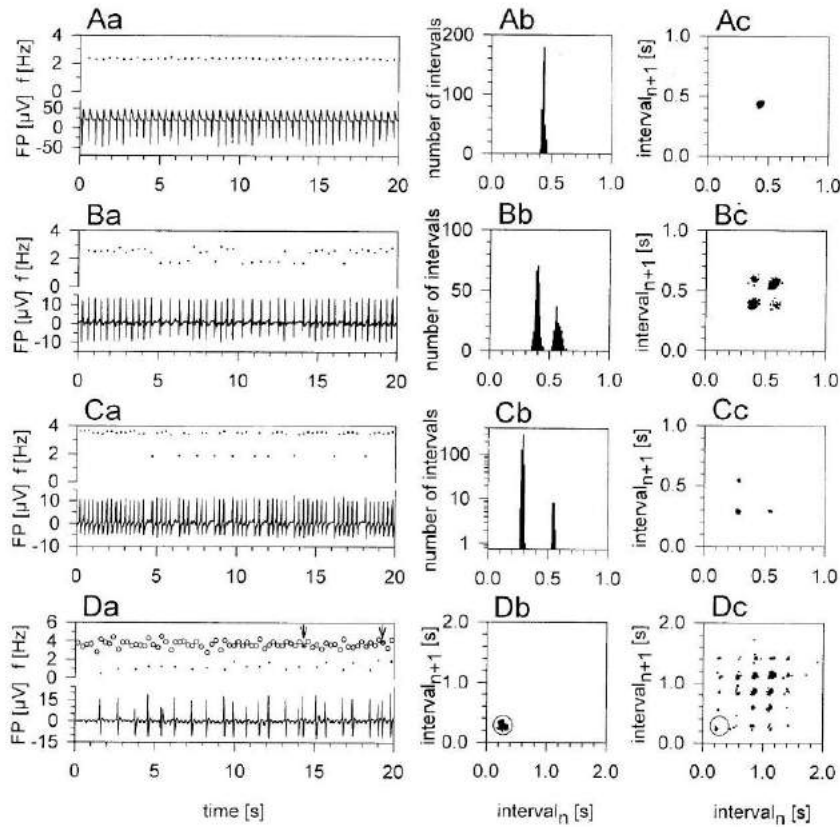


Fig. 2A–D Recordings from various EBs showing different rhythm patterns. **A–C** **a** Field potential (*FP*) and instantaneous spike frequency (*f*; calculated as the reciprocal of the interval between two population action potentials) shown for a time window of 20 s. **b** Distribution of interval durations for 500 successive intervals. **c** Phase plane histograms depicting the spike interval *n* versus interval *n*+1, thus displaying interrelations between successive intervals. Same data as in **b**. **A** Rhythm with regular spike intervals. **B** Rhythm with two different interval lengths presumably produced by two pacemakers. **C** Rhythm with two different interval lengths presumably produced by activity of a single pacemaker and sporadic single propagation failures. **D** Rhythm with multiple propagation failures. **a** Field potential and instantaneous frequency of large spikes (*dots*) and small waves (*circles*). The spikes are closely phase-locked to the waves, with one spike occurring mostly after two to four waves. The irregular spike intervals are produced by action potential propagation failures between the pacemaker area and the recording site. The waves are interpreted to represent the ongoing pacemaker rhythm. The *arrows* indicate time points when spike intervals were as short as wave intervals, i.e., two successive action potentials were conducted without propagation failure. **b**, **c** Phase plane histograms of the intervals between waves (**b**) and between spikes (**c**). The area containing the wave intervals is marked by a *circle* in **b** and **c**. The variability of the spike amplitude within one recording is an artifact caused by the low sampling rate (50 Hz in **A**, **D**, 100 Hz in **B**, **C**). Age of EBs: 7+11d (**A**), 7+12d (**B**), 7+17d (**C**), 7+30d (**D**)

mon firing pattern, which appears in virtually every EB at least for some of its lifetime, is homogeneous spiking with a single frequency (Fig. 2A). In 21 out of 25 EBs (84%) analyzed, we observed periods of irregular activity lasting for several hours or days, characterized by two

or more preferred frequencies (Fig. 2B–D). Microscopy observation and combined video and field potential recording reveal that this irregularity is based on intermittent propagation failure: regular contractions were observed distant from the recording site while the contractions were irregular close to the recording site. The irregular activity was phase-locked to the distant regular beating but showed contraction failures. The irregular contractions were tightly coupled to the recorded action potentials. Activity with sporadic 2:1 propagation block has two preferred interval lengths and appears with three spots of high density in the phase plane histograms, as shown in Fig. 2C. Variable sequences of 2:1 to 5:1 propagation failures result in a higher number of preferred interval lengths between the action potentials and more complex patterns in the phase plane histograms, as shown in the example of Fig. 2D. In this recording (Fig. 2Da), the pacemaker rhythm is visible through the electrotonically propagated small waves appearing in the pauses between the large spikes (see also Figs. 5A, 9). It should be noted that the small waves may be generated by cardiac tissue driven by the pacemaker rather than by the pacemaker itself.

As previously reported (e.g. [4, 19, 20, 22]), propagation failures may be related to discontinuities in the architecture of the conducting structures. In order to visualize the clustering of cardiac phenotypes within the beating area of EBs, we used confocal laser scanning microscopy in combination with vital β -galactosidase stain-

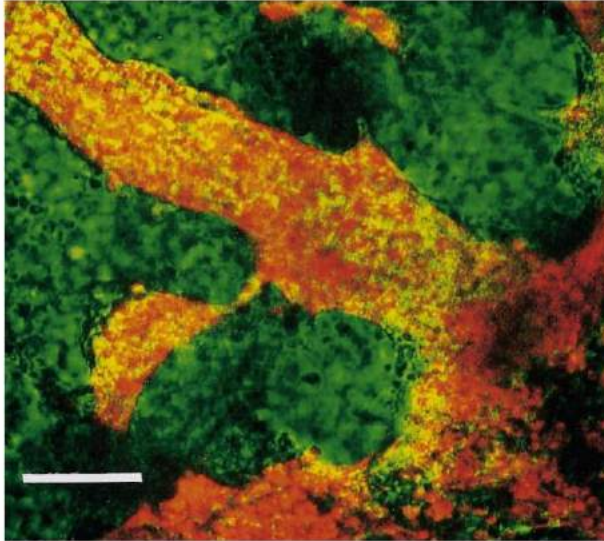
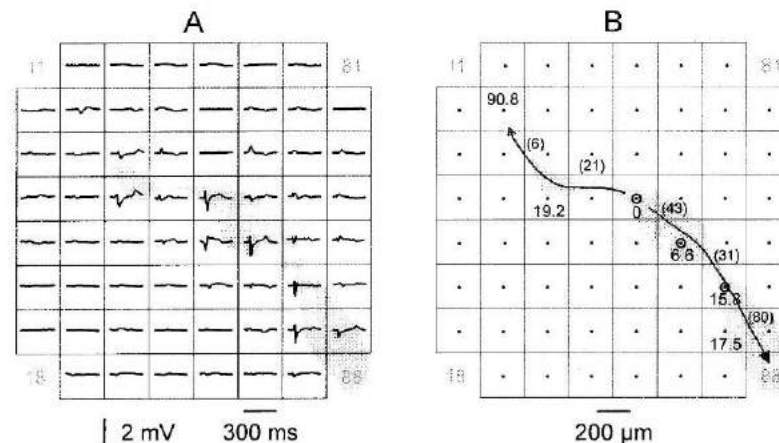


Fig. 3 Localization of ventricular cardiomyocytes in an EB (7+4d), visualized by a β -galactosidase reporter gene assay. The false-color image shows an overlay of 2-dodecylresorufin fluorescence (red) and transmission (green). Note the clustering of ventricular cardiomyocytes and the formation of a thin connecting strand between larger areas. The bar represents 100 μ m

Fig. 4A, B Spatial characterization of the activity of an EB (7+7d) grown on a microelectrode array (MEA). The 60 electrodes were arranged as indicated by the dots in **B** and 17 numbered according to the gray numbers in the corners. The gray areas indicate the spatial distribution of spontaneous contracting tissue as revealed by video microscopy. **A** Examples of the field potential recordings at the different electrodes (filter 1 Hz–100 Hz, sample rate 500 Hz). **B** Latency of the population action potentials relative to the origin [(ms), numbers without brackets] and propagation velocity in the different regions [(mm/s), numbers in brackets]. Action potentials usually originated near electrode E54 and propagated in two directions. The propagation velocity varied between 6 and 80 mm/s in the different regions, presumably depending on the extent of the conducting tissue. Recordings from electrodes E54, E65, and E76 (marked by circles in **B**) are further analyzed in Fig. 7



ing [16]. Experiments were performed on EBs derived from a transgenic ES cell line, where *lacZ* gene expression was under control of the ventricular-specific myosin light chain (MLC-2v) promoter [29]. The staining clearly showed that ventricular cardiomyocytes within the EBs are not distributed at random but are aggregated in clusters (Fig. 3). Apart from the positively stained beating clusters, beating was also observed in unstained areas presumably representing non-ventricular cardiomyocytes, including pacemaker cells.

In order to correlate the architecture of beating areas with the electrical activity, we used MEAs for multiple recordings from individual EBs. In eight EBs, spontaneous activity was recorded for up to 8 days. As revealed with combined video and field potential recording, the electrical activity was tightly restricted to contracting areas (Fig. 4A). The conduction velocity, extrapolated from the latency between two electrodes, correlated with the width of the contracting tissue (Fig. 4B) and was least (approximately 6 mm/s) in regions containing narrow strands of contracting tissue. However, the precise site of the decrease in conduction velocity could not be resolved because of the relatively large interelectrode distance. It is most likely that the propagation failures occurred in EBs where the tissue contained a narrow strand between two larger contracting areas. Such a situation is shown in Fig. 5. Here, recordings from two separate electrodes directly demonstrate propagation failures similar to the behavior shown in Fig. 2D.

A statistical evaluation of the complex beating patterns recorded with extracellular electrodes is shown in Fig. 6A,B for 28 recordings (21 EBs) which contained two or more clearly distinguishable frequencies. In order to quantitatively characterize the propagation blocks, the respective frequencies (f_n) were normalized to the highest frequency (f_1). As depicted in Fig. 6A, the relative frequencies (f_n/f_1) varied between 0.14 and 0.8. The distribution histogram (Fig. 6B) indicates a clear maximum at the bin $f_n/f_1 = 0.5$ –0.55,¹ suggesting that the recorded

¹ In most of these cases, f_n/f_1 is slightly greater than 0.5. The deviation is presumably caused by faster action potential propagation after longer intervals (compare Fig. 9D).

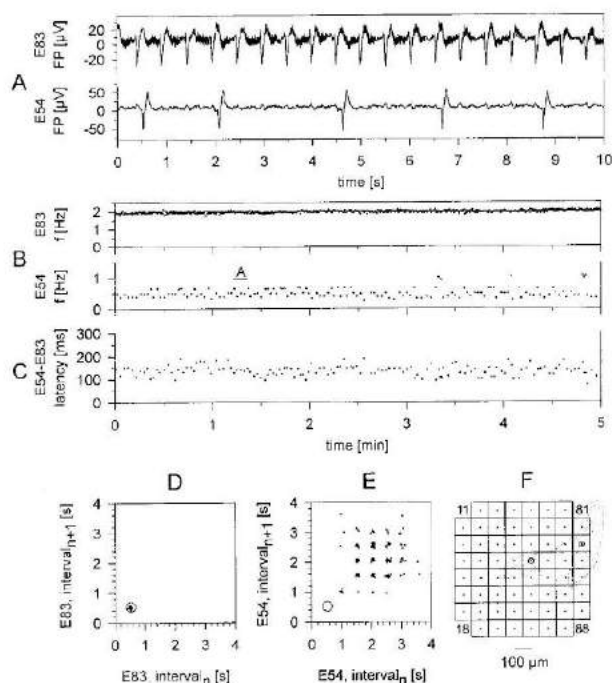


Fig. 5A–F Action potential propagation block, shown by double recording from an EB (7+8d) grown on a microelectrode array (MEA). **A** Simultaneous recordings from two electrodes (E54 and E83). **B**, **C** Instantaneous action potential frequency at the two electrodes (**B**) and latency between the action potentials at E83 and E54 (**C**) over a 5-min period. The horizontal bar in **B** indicates the section shown in **A**. **D**, **E** Phase plane histograms of the data shown in **B** for E83 (582 intervals) and E54 (138 intervals), respectively. The circle in **D** and **E** marks the position of the activity at E83. **F** Location of the contracting tissue (gray area, truncated at the upper end) and the recording electrodes in the MEA (numbered according to the numbers in the corners). Data were recorded from E83 and E54 as marked by circles (distance 316 μm). Action potentials at E83 appeared with a regular frequency of 2 Hz while the frequency at E54 was lower and rather variable. Action potentials at E54 were strongly coupled to action potentials at E83 with a latency of 100–200 ms. In the phase plane histogram (**E**), the intervals at E54 consistently appeared as multiples of the interval at E83, a situation which is similar to that shown in Fig. 2D.

activity results from a single pacemaker, with a 2:1 propagation block or sporadic single propagation failures (this type of activity is shown in Fig. 2C). Higher degrees of propagation blocks, i.e. 3:1, 4:1, 5:1, and 6:1 blocks (as shown in Figs. 2D, 5E) produce complex patterns with relative frequencies f_n/f_1 of 0.33, 0.25, 0.20, and 0.17, respectively (Fig. 6A).

In 17 out of the 28 recordings containing 2 or more preferred frequencies, f_2/f_1 was clearly higher than 0.5 (Fig. 6A; an example is shown in Fig. 2B). Microscopic observation revealed that, in these cases, different beating intervals are associated with different origins and propagation directions of the contraction wave, which can only be explained by the existence of at least two pacemakers. With the MEA technique, the activity of various pacemakers can be directly demonstrated. As

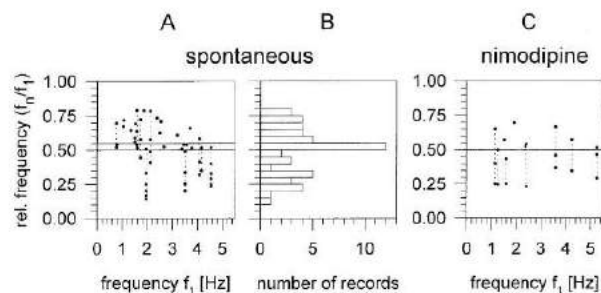


Fig. 6 Statistical evaluation of complex beating rhythms occurring spontaneously (**A**, **B**) and induced by nimodipine (NDP) application (**C**). The various frequencies (f_n) recorded simultaneously (within some minutes) from a beating area were related to the highest frequency (f_1) measured in this area in the same time window. **A**, **C** The relative frequencies (f_n/f_1) as a function of f_1 . Recordings with two preferred frequencies are depicted by a single dot representing f_2/f_1 , recordings with multiple frequencies are depicted by multiple dots (f_n/f_1) connected by a vertical dashed line. **B** The distribution of the values included in **A**. **A**, **B** Twenty-eight records from 21 EBs (7+4d–7+30d). **C** Ten experiments from 4 EBs (7+3d–7+16d) where the NDP-induced stepwise decrease could be quantified without major distortion by the effect on pacemaker activity.

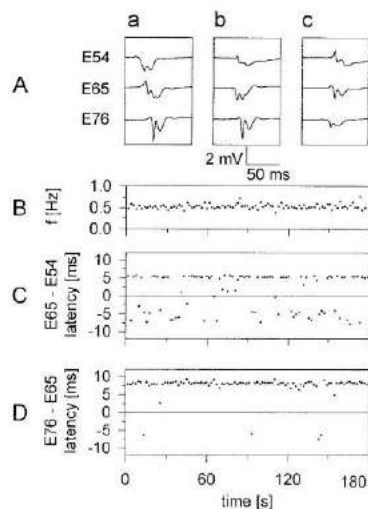


Fig. 7 **A** Synchronous recordings from electrodes E54, E65, and E76 of the MEA preparation shown in Fig. 4, 1 day later (age 7+8d). Distance E54–E65=E65–E76=283 μm . Filter 1 Hz–300 Hz, sample rate 1 kHz. **B** Instantaneous frequency (f), **C** latency between E54 and E65, and **D** latency between E65 and E76. The variability of the latencies between different electrodes reveals that the origin of the action potentials varied between several defined sites. In general, the action potentials at electrode E54 preceded those at E65 by 5 ms (**Aa**, **C**). Sometimes, however, the action potentials originated near E65 and propagated to E54 and E76 (Fig. 6Ab, C, D). Finally, the action potentials could sporadically originate near E76, leading to a reversal of the latency between E65 and E76 (**Ac**, **D**).

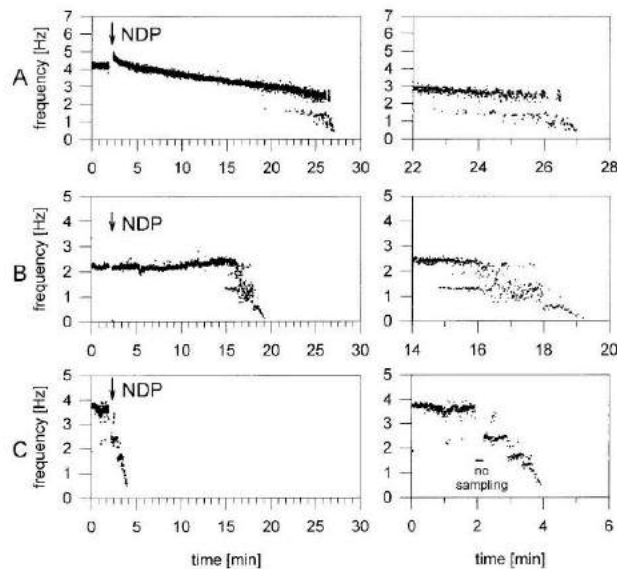


Fig. 8 Discontinuous depression of spiking activity by 50 nM nimodipine (NDP) in three different EBs (A–C). Overview (left) of the instantaneous beating frequency and detailed view of the final reaction with extended time scale (right). NDP was added to the medium with a pipette, and the culture dish was slightly swirled. During this time, data collection was shortly interrupted. In **A**, NDP first induced a slow decline of the frequency. After 20 min, a second frequency band appeared which also declined continuously until beating stopped completely. The relative frequency (f_2/f_1) of this band was 0.57–0.52. We interpret this pattern as a superposition of slowing down of pacemaker activity and a block of action potential propagation. In **B**, 12 min passed before any depressive effect of NDP was obvious. Then, a second frequency band with $f_2/f_1=0.54$ appeared, overlapping in time with the presence of the primary frequency. After a further stepwise drop ($f_2/f_1=0.24$), the frequency declined continuously to zero. In **C**, rapid stepwise decline to $f_2/f_1=0.66$, 0.45, and 0.36 occurred immediately after NDP application. In both examples, **B** and **C**, failures of action potential propagation appeared before slowing down of the pacemaker activity was observed. Age of the EBs: **A** 7+16d, **B** 7+4d, **C** 7+9d

shown in Fig. 7, the origin of the action potentials can vary between different sites even in regularly beating EBs.

Effect of NDP on beating areas in EBs

During extracellular recordings of the beating activity, NDP (20–200 nM) was applied in 38 experiments (14 EBs). In all cases, NDP reversibly reduced the beating frequency and finally blocked beating. Complete arrest was achieved after variable latencies of 2–30 min. There was no correlation between the latency of the block and the NDP concentration, nor between the latency of the block and the age of the EBs (7+4d–7+42d). In 14 out of 29 quantitatively analyzed experiments,² the spiking frequency was continuously reduced by NDP until a sudden stop occurred. In the other 15 cases, however, the fre-

² Nine of 38 experiments were not analyzed in this report because of large-frequency scatter.

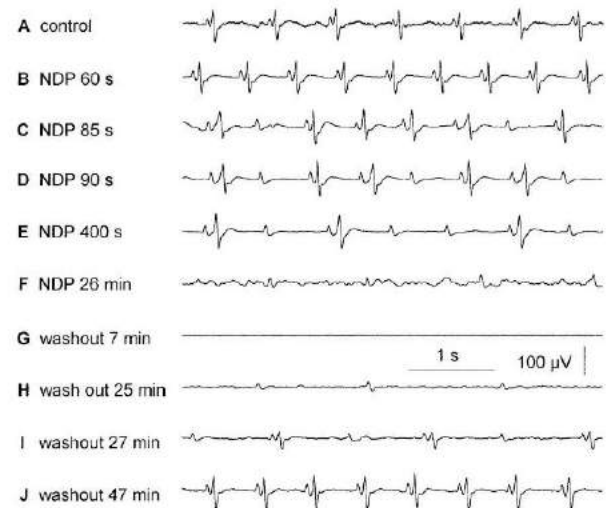


Fig. 9 Effect of nimodipine (NDP) on pacemaker activity and action potential propagation. Five-second periods of the field potential recorded from an EB (7+10d) before (**A**) and during application (**B–F**) and after washout (**G–J**) of 25 nM NDP. A quantitative analysis of the data is shown in Fig. 10. Under control conditions, this EB produced population action potentials which were comparable to the P wave and the QRS complex of electrocardiograms (**A**), i.e., the population action potential consisted of a small (P-like) spike followed by a larger (R-like) spike. The latency between the P- and R-like spike was constant (**A**, Fig. 10C), indicating that the P-like spike represents the activity of the primary pacemaker and the R-like spike the activity of a driven area. With application of NDP, the frequency of both the P-like and the R-like spikes at first increased due to the unspecific effect of swirling the culture dish (**B**, Fig. 10A, B). Then the frequency of the P-like spikes returned to the control level and was relatively stable for about 20 min (**B–E**, Fig. 10A) before declining to zero (**G**). The R-like spikes, in contrast, were immediately affected by NDP. The first sign of NDP's action was an increase of the latency between the P-like and the R-like spikes from about 60 to 75 ms (**B**, Fig. 10C). Then propagation failures occurred with increasing number (**C–E**, Fig. 10B) developing into a stable 2:1 block (Fig. 10A, B). During this transition time, Wenckebach-like periods appeared, as known from second-order AV propagation failures in the native heart, i.e., the latency between P-like and R-like spikes increased in successive beats and recovered after a single failure of the R-like spike (**C**, **D**).³ In the further course, the latency increased to about 130 ms (Fig. 10C), and finally the R-like spikes were completely blocked after 26 min while the P-like spike activity continued for several minutes (**F**). After washout of NDP, the activity was resumed in the reverse order (**G–J**)

quency of the recorded signals decreased in a stepwise manner, caused by intermittent block of action potential propagation which occurred at the same time as or even before the slowing of the pacemaker (Fig. 8). These different effects of NDP on pacemaker activity and action potential propagation are directly demonstrated in Figs. 9 and 10. The propagation block was preceded by a decrease in the conduction velocity (Fig. 10C). Figure 6C shows the statistical evaluation of the NDP-induced stepwise reductions of frequency. Relative frequencies of

³ Because of the unknown phenotype of the cells, these data do not imply identical mechanisms to those involved in AV nodal dysfunction in the heart.

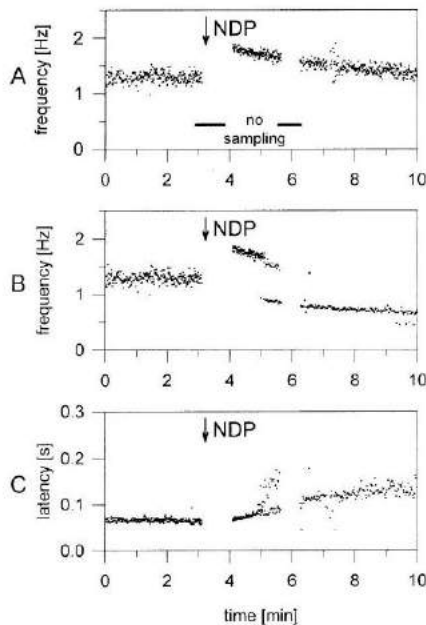


Fig. 10A–C Quantitative analysis of the data shown in Fig. 9. Time course of the instantaneous frequency of the small P-like spikes (A) and the large R-like spikes (B), and of the latency (measured at the negative peak) between the P-like and the R-like spikes (C). The time of addition of NDP to the culture dish is indicated by arrows. During the times marked by horizontal bars, the recording was interrupted by artifacts due to substance application and cable connection problems. For further explanation, see legend to Fig. 9

$f_2/f_1 \gg 0.5$ in Figs. 6C and 8C reveal the existence of secondary pacemakers, which in the absence of propagation blocks were overdriven by the first pacemaker, similar to the data in Figs. 2B, 6A.

Patch-clamp recordings

In order to compare the effects of NDP on the population activity of whole beating areas with the effects on small conglomerates of cardiomyocytes and single cells, patch-

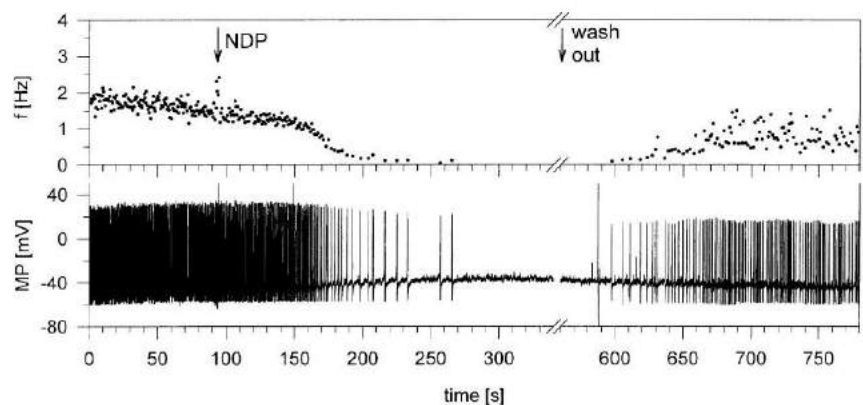
clamp experiments were performed on spontaneously contracting cells obtained by enzymatic dissociation from EBs. The effect of NDP on action potentials and I_{Ca} was investigated using current- and voltage-clamp recordings.

The conglomerates consisted of three to ten cells, which, in current-clamp mode, displayed regularly shaped action potentials with a frequency of 2–4 Hz (not shown). Stable action potentials could be recorded for up to 1 h; the minimal diastolic potential remained stable during the recordings and was between -65 and -55 mV, with the peak of the depolarization around $+30$ mV. The action potential duration (APD_{90%}) amounted to 41.4 ± 5.3 ms ($n=11$). In contrast to the action potential frequency of conglomerates of cells, that of single cells varied more during the experiment. Moreover, the minimal diastolic potential was quite depolarized in some cells, probably caused by the somewhat varying cell quality, as a result of the enzymatic isolation procedure. For this reason, only cells with a minimal diastolic potential more negative than -40 mV (-52.8 ± 3.9 mV, $n=6$) and a stable action potential frequency (1.8 ± 0.3 Hz, $n=6$) were chosen.

In the experiments with groups of cells, bath application of 30–40 nM NDP caused a depression and complete stop of spontaneous electrical activity (not shown). Usually, a decrease in the action potential frequency and intermittent irregular beating could be observed within the first 100 s of drug application. Complete arrest occurred after a latency of 200–800 s ($n=11$), which is within the range of the latencies measured with extracellular electrodes in intact EBs. Concomitant with these changes, a depolarization of the minimal diastolic membrane potential by 2.3 ± 0.8 mV occurred. There was no indication of a propagation block as seen in the multicellular field potential recordings. Spontaneous electrical activity could be recovered upon washout of NDP with action potential frequencies close to control values. Similar to the experiments with intact EBs, there was no correlation between the sensitivity of the cells to NDP and their age ($n=4$ cell groups of age 7+2d–7+4d, $n=7$ cell groups of age 7+9d–7+12d).

In four out of six single-cell recordings, 10 nM NDP stopped the beating of the spontaneously contracting car-

Fig. 11 Effect of nimodipine (NDP) on the electrical activity of a single cardiomyocyte (7+9d). Addition of 10 nM NDP (arrow) resulted in a decline of the action potential frequency (f) until complete arrest. After washout, there was a slow recovery of the spontaneous activity. (MP Membrane potential)



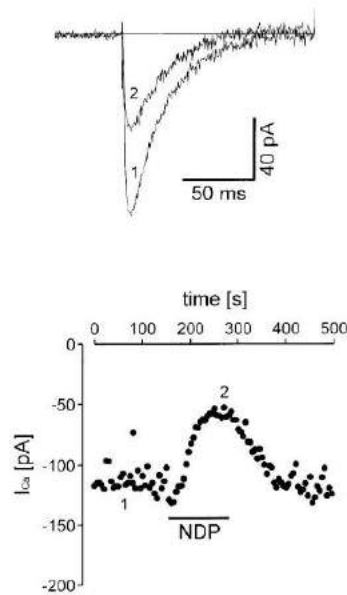


Fig. 12 Effect of nimodipine (NDP) on L-type Ca^{2+} currents in a single cardiomyocyte (7+4d). Currents were evoked by 150 ms depolarizing voltage steps from a holding potential of -50 mV to a test potential of $+10$ mV (frequency: 0.2 Hz). The lower panel displays the Ca^{2+} currents (I_{Ca}). Every single point represents the peak current amplitude evoked by a depolarizing voltage pulse. This demonstrates a fast but incomplete block of I_{Ca} by 10 nM NDP and the reversibility during washout

diomyocytes. The time lag between drug administration and the cessation of beating varied from 200 to 500 s ($n=4$). Approximately 60 s after bath application of NDP, a decrease in the frequency and/or the amplitude of the action potentials could be observed. Moreover, with the onset of the drug effect a depolarization of the membrane potential by 5 ± 2 mV could be seen in three cells. In five out of six cells, the NDP effect was reversible upon washout. However, the frequency of the beating prior to the drug application did not fully recover (Fig. 11).

In order to demonstrate the effect of NDP on L-type Ca^{2+} channels, voltage-clamp experiments were performed on single cardiomyocytes. As for current-clamp recordings from single cells, the low concentration of 10 nM NDP was chosen. The average peak current evoked by depolarizing voltage steps from a holding potential of -50 mV to a step potential of $+10$ mV was 128 ± 24 pA ($n=6$, Fig. 12). Application of 10 nM NDP reduced the peak amplitude by $62.4 \pm 6.7\%$ ($n=6$). In most of the cells, the depression of the current started about 20 s after addition of the drug to the bath, and achieved maximal values about 1 min after NDP application. The effect of NDP was reversible upon washout. I_{Ca} recovered to the full amplitude after perfusion with normal extracellular solution.

Discussion

In the present paper, we introduce a novel technique allowing the long-term recording of the electrical field potential generated by synchronously beating cardiomyocyte clusters in murine ES cell-derived EBs. This in vitro model is unique since it contains all the different cardiac phenotypes [7, 14, 15]. In line with ultrastructural studies [7] we demonstrate, using vital staining of ventricular myocytes [5, 29] and confocal microscopy, that ventricular myocytes are tightly clustered within the beating areas. This and the MEA-recordings suggests also clusters of the other cardiac phenotypes, e.g. sinusoidal-like and atrial-like cells. Future development of cardiac phenotype-specific reporter genes will provide detailed information on the spatial distribution of cardiac phenotypes.

By recording population action potentials from the beating areas, we obtained insight into the electrical interaction between cardiomyocytes. As well as the regular beating activity, most EBs intermittently produced more complex rhythms with two or more preferred interval lengths. Our data show that this is due to propagation failures between the primary pacemaker and the recording site. In many EBs, these propagation failures resulted in a temporary takeover of the spontaneous action potential generation by a secondary pacemaker.

At least four different mechanisms may account for propagation failures: (1) impedance mismatch at structural discontinuities in the cardiac tissue, (2) changes in cell-to-cell coupling, (3) changes in the steepness of the diastolic depolarization, and (4) Ca^{2+} channel blockade in situations of impedance mismatch or during a reduction of the fast Na^+ inward current. MEA recordings combined with microscopic and video observation suggest that, in our experiments, spontaneous propagation failures are mainly due to the first alternative, i.e., structural discontinuities. They occur in structures where a pacemaker area is connected to the area of recording via a narrow pathway. Our results are in line with the well-known fact that structural discontinuities can play an important role in the generation of cardiac arrhythmias (e.g., [8]). The relationship between the tissue architecture and action potential propagation in cardiac tissue has been investigated by Rohr and colleagues in elegant experiments with patterned growth cultures (e.g., [4, 20, 21]). Ventricular cardiomyocytes were grown on a culture substrate which contained regions that either prevent or support attachment of cells, conditioning the geometry of the resulting tissue. By investigating this model with multiple-site optical recording of transmembrane voltage, it was quantitatively demonstrated that expansions of the excitable tissue (i.e., transitions from narrow strands to larger areas) cause propagation delay and unidirectional propagation block [4, 20]. Unidirectional propagation block has similarly been demonstrated in asymmetrical pairs of isolated ventricular cells [9]. In both situations, a small current source is connected to a large current load, resulting in a current-to-load mismatch.

Effects of NDP

In addition to the known negative chronotropic effect of dihydropyridines [14, 28], about 50% of our experiments revealed action potential propagation failures in response to NDP application. In many EBs, this developed prior to the negative chronotropic effect. Patch-clamp recordings excluded the possibility that complex rhythm patterns induced by NDP are generated at the single-cell level. Therefore, these arrhythmias in the EBs cannot be explained by a simple drug effect on the L-type Ca^{2+} channel (I_{Ca}) of the primary pacemaker cell, but by the effect on the properties of excitable cells between the rhythm-generating cell and the recording electrode. This is in line with the findings that I_{Ca} is of crucial importance for action potential propagation at abrupt structural discontinuities in patterned growth cultures [19] and in asymmetrical pairs of cardiac cells [10]. In addition, experiments with cell pairs [10, 24] as well as computer simulations of ionic mechanisms of propagation in cardiac tissue [23] revealed a major role for I_{Ca} in sustaining conduction in situations of reduced intercellular coupling. Although we do not know the exact location of the block in our experiments, these studies as well as our MEA recordings of spontaneous propagation failures support the interpretation that NDP-induced propagation block occurred at transitions from narrow pathways to larger areas of cardiomyocytes.

In conclusion, our results suggest that field potential recordings from clusters of ES cell-derived cardiomyocytes within EBs provide a useful tool for studying in vitro chronotropy and action potential propagation, and thus phenomena of propagation failure similar to AV block. Although at present several features may appear disadvantageous (e.g., the unpredictable geometry of the beating clusters, undefined coupling characteristics) we see upon further investigation clear advantages as compared to the already established cardiac cell culture models: (1) in contrast to other multicellular preparations, EBs are composed of all different phenotypes of cardiomyocytes; (2) the model allows long-term recordings in combination with histological analysis; and (3), most importantly, it allows investigation of genetically altered ES cell-derived cardiomyocytes. This is particularly interesting for knock-outs resulting in lethal mutations. The differentiation of genetically altered ES cells into EBs allows the functional investigation of cardiomyocytes containing lethal mutations, for example β_1 integrin deficiency [3].

Acknowledgements We thank Marianne Faulhaber and Birgit Hops for culturing ES cells and preparing EBs, Drs. Alexei Pereverzev and Anna Wobus for help with the cell culture, and Drs. Stefan Dhein, Alexei Pereverzev and Michael Dittrich for valuable discussions and helpful suggestions. We are grateful to Drs. Wolfgang-Michael Franz and Anna M. Wobus for supplying us with the MLC-2v ES cell clone. The skillful technical support by the institute's electronics shop and mechanics shop (Jürgen Staszewski and Harald Metzner and their teams) is gratefully acknowledged. Nimodipine was a gift of Bayer (Wuppertal, Germany).

References

1. Clapham DE, Shrier A, De Haan RI (1980) Junctional resistance and action potential delay between embryonic heart cell aggregates. *J Gen Physiol* 75:633–654
2. Doetschman TC, Eistetter HR, Katz M, Schmidt W, Kemler R (1985) The in vitro development of blastocyst-derived embryonic stem cell lines: formation of visceral yolk sac, blood islands and myocardium. *J Embryol Exp Morphol* 87:27–45
3. Fässler R, Rohwedel J, Maltsev V, Bloch W, Lentini S, Guan K, Gullberg D, Hescheler J, Addicks K, Wobus AM (1996) Differentiation and integrity of cardiac muscle cells are impaired in the absence of β_1 integrin. *J Cell Sci* 109:2989–2999
4. Fast VG, Kléber AG (1995) Cardiac tissue geometry as a determinant of unidirectional conduction block: assessment of microscopic excitation spread by optical mapping in patterned cell cultures and in a computer model. *Cardiovasc Res* 29:697–707
5. Franz WM, Breves D, Klingel K, Brem G, Hofschneider PH, Kandolf R (1993) Heart-specific targeting of firefly luciferase by the myosin light chain-2 promoter and developmental regulation in transgenic mice. *Circ Res* 73:629–638
6. Hamill OP, Marty A, Neher E, Sakmann B, Sigworth FJ (1981) Improved patch-clamp techniques for high-resolution current recording from cells and cell-free patches. *Pflügers Arch* 391:85–100
7. Hescheler J, Fleischmann BK, Lentini S, Maltsev VA, Rohwedel J, Wobus AM, Addicks K (1997) Embryonic stem cells: a model to study structural and functional properties in cardiomyogenesis. *Cardiovasc Res* 36:149–162
8. Janse MJ, Wit AL (1989) Electrophysiological mechanisms of ventricular arrhythmias resulting from myocardial ischemia and infarction. *Physiol Rev* 69:1049–1169
9. Joyner RW, Sugiura H, Tan RC (1991) Unidirectional block between isolated rabbit ventricular cells coupled by a variable resistance. *Biophys J* 60:1038–1045
10. Joyner RW, Kumar R, Wilders R, Jongsma JJ, Verheijck EE, Golod DA, van Ginneken AC, Wagner MB, Goolsby WN (1996) Modulating L-type calcium current affects discontinuous cardiac action potential conduction. *Biophys J* 71:237–245
11. Kessler-Isackson G, Schlesinger H, Djaldetti M, Brodie C, Sampson SR, Bergman M (1996) Cardiomyocytes in culture – a model to study the cellular actions of amiodarone. *Isr J Med Sci* 32:1212–1216
12. Korn SJ, Horn R (1989) Influence of sodium-calcium exchange on calcium current rundown and the duration of calcium dependent chloride currents in pituitary cells, studied with whole cell and perforated patch recordings. *J Gen Physiol* 94:789–812
13. Kruppenbacher JP, May T, Eggers HJ, Piper HM (1993) Cardiomyocytes of adult mice in long-term culture. *Naturwissenschaften* 80:132–134
14. Maltsev VA, Rohwedel J, Hescheler J, Wobus AM (1993) Embryonic stem cells differentiate in vitro into cardiomyocytes representing sinusnodal, atrial and ventricular cell types. *Mech Dev* 44:41–50
15. Maltsev VA, Wobus AM, Rohwedel J, Bader M, Hescheler J (1994) Cardiomyocytes differentiated in vitro from embryonic stem cells developmentally express cardiac-specific genes and ionic currents. *Circ Res* 75:233–244
16. Metzger JM, Lin WI, Samuelson LC (1996) Vital staining of cardiac myocytes during embryonic stem cell cardiogenesis in vitro. *Circ Res* 78:547–552
17. Nisch W, Böck J, Hämmerle H, Mohr A (1994) A thin film microelectrode array for monitoring extracellular neuronal activity in vitro. *Biosens Bioelectron* 9:737–741
18. Rabkin SW (1992) Effect of antiarrhythmic drugs on choline uptake in cardiac cells in culture. *Cardiovasc Res* 26:67–71
19. Rohr S, Kucera JP (1997) Involvement of the calcium inward current in cardiac impulse propagation: induction of unidirectional conduction block by nifedipine and reversal by Bay K 8644. *Biophys J* 72:754–766

20. Rohr S, Salzberg BM (1994) Characterization of impulse propagation at the microscopic level across geometrically defined expansions of excitable tissue: multiple site optical recording of transmembrane voltage (MSORTV) in patterned growth heart cell cultures. *J Gen Physiol* 104:287–309
21. Rohr S, Schölly DM, Kléber AG (1991) Patterned growth of neonatal rat heart cells in culture. Morphological and electrophysiological characterization. *Circ Res* 68:114–130
22. Rohr S, Kucera JP, Kléber AG (1997) Form and function: impulse propagation in designer cultures of cardiomyocytes. *News Physiol Sci* 12:171–177
23. Shaw RM, Rudy Y (1997) Ionic mechanisms of propagation in cardiac tissue. Roles of the sodium and L-type calcium currents during reduced excitability and decreased gap junction coupling. *Circ Res* 81:727–741
24. Sugiura H, Joyner RW (1992) Action potential conduction between guinea pig ventricular cells can be modulated by calcium current. *Am J Physiol* 263:H1591–H1604
25. Verheijck EE, Wilders R, Joyner RW, Golod DA, Kumar R, Jongsma HJ, Bouman LN, van Ginneken AC (1998) Pacemaker synchronization of electrically coupled rabbit sinoatrial node cells. *J Gen Physiol* 111:95–112
26. Weingart R, Maurer P (1988) Action potential transfer in cell pairs isolated from adult rat and guinea pig ventricles. *Circ Res* 63:72–80
27. Weisensee D, Bereiter-Hahn J, Schoeppe W, Low-Friedrich I (1993) Effects of cytokines on the contractility of cultured cardiac myocytes. *Int J Immunopharmacol* 15:581–587
28. Wobus AM, Wallukat G, Hescheler J (1991) Pluripotent mouse embryonic stem cells are able to differentiate into cardiomyocytes expressing chronotropic responses to adrenergic and cholinergic agents and Ca^{2+} channel blockers. *Differentiation* 48:173–182
29. Wobus AM, Kaomei G, Shan J, Wellner MC, Rohwedel J, Ji G, Fleischmann B, Katus HA, Hescheler J, Franz WM (1997) Retinoic acid accelerates embryonic stem cell-derived cardiac differentiation and enhances development of ventricular cardiomyocytes. *J Mol Cell Cardiol* 29:1525–1539
30. Ypey DL, Clapham DE, De Haan RL (1979) Development of electrical coupling and action potential synchrony between paired aggregates of embryonic heart cells. *J Membr Biol* 51:75–96

РОЗДІЛ 2

РОЛЬ КАЛЬЦІЙЗВ'ЯЗУЮЧИХ БІЛКІВ У ГЕНЕРАЦІЇ ЗМІН ВНУТРІШНЬОКЛІТИННОЇ КОНЦЕНТРАЦІЇ ІОНІВ КАЛЬЦІЮ

2.1. Мутації тропоніну Т, що зумовлюють збільшення чутливості міофіламентів до Ca^{2+} , підвищують цитозольне зв'язування Ca^{2+}



NIH Public Access

Author Manuscript

Circ Res. Author manuscript; available in PMC 2013 July 06.

Published in final edited form as:

Circ Res. 2012 July 6; 111(2): 170–179. doi:10.1161/CIRCRESAHA.112.270041.

Myofilament Ca sensitization increases cytosolic Ca binding affinity, alters intracellular Ca homeostasis and causes pause-dependent Ca triggered arrhythmia

Tilmann Schober^{1,*}, Sabine Huke^{1,*}, Raghav Venkataraman^{2,*}, Oleksiy Gryshchenko¹, Dmytro Kryshchal¹, Hyun-Seok Hwang¹, Franz J. Baudenbacher², and Björn C. Knollmann¹

¹Division of Clinical Pharmacology, Department of Medicine, Vanderbilt University Medical School, Nashville, TN, USA

²Biomedical Engineering and Physics, Vanderbilt University, Nashville, TN, USA

Abstract

Rationale—Ca binding to the troponin complex represents a major portion of cytosolic Ca buffering. Troponin mutations that increase myofilament Ca sensitivity are associated with familial hypertrophic cardiomyopathy and confer a high risk for sudden death. In mice, Ca sensitization causes ventricular arrhythmias, but the underlying mechanisms remain unclear.

Objective—To test the hypothesis that myofilament Ca sensitization increases cytosolic Ca buffering, and to determine the resulting arrhythmogenic changes in Ca homeostasis in the intact mouse heart.

Methods and Results—Using cardiomyocytes isolated from mice expressing troponin T (TnT) mutants (TnT-I79N, TnT-F110I, TnT-R278C), we found that increasing myofilament Ca sensitivity produced a proportional increase in cytosolic Ca binding. The underlying cause was an increase in the cytosolic Ca binding affinity, whereas maximal Ca binding capacity was unchanged. The effect was sufficiently large to alter Ca handling in intact mouse hearts at physiological heart rates, resulting in increased end-diastolic [Ca] at fast pacing rates, and enhanced sarcoplasmic reticulum Ca content and release after pauses. Accordingly, action potential (AP) regulation was altered, with post-pause AP prolongation, afterdepolarizations and triggered activity. Acute Ca sensitization with EMD 57033 mimicked the effects of Ca sensitizing TnT mutants and produced pause-dependent ventricular ectopy and sustained ventricular tachycardia after acute myocardial infarction.

Conclusions—Myofilament Ca sensitization increases cytosolic Ca binding affinity. A major proarrhythmic consequence is a pause-dependent potentiation of Ca release, AP prolongation and triggered activity. Increased cytosolic Ca binding represents a novel mechanism of pause-dependent arrhythmia that may be relevant for inherited and acquired cardiomyopathies.

Corresponding author: Björn C. Knollmann, MD, PhD, Professor of Medicine and Pharmacology, Division of Clinical Pharmacology, Oates Institute for Experimental Therapeutics, Vanderbilt University School of Medicine, Medical Research Building IV, Rm. 1265, 2215B Garland Ave, Nashville, TN 37232-0575, Phone: (615) 343-6493, bjorn.knollmann@vanderbilt.edu.
*these authors contributed equally

³current address: Pediatric Hematology/Oncology and Cardiology, Children's Hospital II/III, Johann Wolfgang Goethe University, Frankfurt, Germany

DISCLOSURES

NONE

Keywords

myofilament Ca sensitivity; familial hypertrophic cardiomyopathy; Ca buffering; early afterdepolarizations; arrhythmia

INTRODUCTION

Familial Hypertrophic Cardiomyopathy (FHC) is a heterogeneous disease resulting from autosomal-dominant mutations in genes encoding cardiac contractile proteins.¹ Sudden cardiac death (SCD) is the main culprit for the mortality in FHC patients,² with ventricular tachycardia (VT) and/or ventricular fibrillation as the underlying mechanism for the SCD.³ Even though, in general, the degree of cardiac hypertrophy is an important risk factor for SCD,⁴ certain mutations in thin filament proteins confer a high risk of SCD even in the absence of marked cardiac hypertrophy.⁵ In particular, mutations in troponin T (TnT) are responsible for approximately 7% of FHC cases,⁶ but represent a major proportion of those referred for tertiary care.⁵⁻⁷ For these mutations, the risk of SCD seems to be less dependent on structural remodelling like hypertrophy and fibrosis,^{8,9} suggesting that other mechanisms importantly contribute to arrhythmia susceptibility. In vitro, FHC-linked TnT mutations frequently increase myofilament Ca sensitivity of force development.¹⁰ We previously demonstrated that myofilament Ca sensitization increases the susceptibility for ventricular arrhythmias, and found a direct correlation between the degree of Ca sensitization and the risk for ventricular arrhythmias in TnT mutant mice.¹¹ However, the underlying mechanisms remain unknown.¹²

The troponin complex represents a substantial portion of cytoplasmic Ca buffering, binding approximately 50% of Ca released from the sarcoplasmic reticulum (SR) during a typical heart beat.¹³ The effect of a TnT mutation on myofilament Ca sensitivity is likely due to an indirect action of TnT on Ca binding by troponin C (TnC), which is possible because TnT, TnC and troponin I (TnI) form a trimeric protein complex.¹⁴ Hence, we hypothesize that increased myofilament Ca sensitivity alters cytoplasmic Ca buffering. Based on experiments that introduced exogenous Ca buffers into myocytes,¹⁵ increased cytosolic Ca buffering should lead to reduced systolic Ca transient with a slow rate of decay and increased cytosolic [Ca] at the end of diastole.¹⁶ As the heart rate increases further, Ca may stay partly bound even at the end of diastole. On the other hand, when heart rate slows, or during a pause, the excessive Ca bound to the myofilaments during the preceding rapid beats may get mobilized and taken up into the sarcoplasmic reticulum (SR). Thus, we further hypothesize that as a consequence of increased cytosolic Ca buffering, Ca release after a pause will be increased. Increased Ca release after a brief pause is a phenomenon also observed in normal myocardium (the resulting increased contraction is often referred to as post-rest potentiation), but this process may be abnormally enhanced in the setting of increased cytosolic Ca buffering. Intracellular Ca regulates membrane currents and directly alters the membrane potential via the electrogenic Na/Ca exchanger (NCX).⁹ Hence, an increased post-rest potentiation of Ca-sensitized hearts may cause pause-dependent action potential (AP) prolongation, afterdepolarizations and triggered activity.

To test these hypotheses, we examined the effect of both acutely and chronically increasing myofilament Ca sensitivity on myocyte Ca buffering, Ca cycling and action potential (AP). As chronic model we used transgenic mice expressing the Ca sensitizing human TnT mutant TnT-I79N. In FHC patients, this mutation is associated with a high rate of SCD at young age.¹⁷ This group was compared to mice expressing either the human wild-type TnT (WT) or the TnT-R278C mutant. TnT-R278C does not increase myofilament Ca sensitivity¹⁸ and is associated with a better prognosis.^{7,19} We also used a FHC-linked TnT mutation that

causes intermediate Ca sensitization (TnT-F110I).¹¹ As an acute model, we used the Ca sensitizer EMD57033, which has relatively specific myofilament Ca sensitizing properties.^{20, 21}

As hypothesized, we find that Ca sensitizing TnT mutations increase cytosolic Ca binding and alter myocyte Ca handling with increased end-diastolic [Ca] at fast pacing rates and enhanced SR Ca content and release after pauses. AP regulation is altered with post-pause AP prolongation, afterdepolarizations and triggered activity. Acute Ca sensitization of non-transgenic hearts with EMD mimics the effects of Ca sensitizing TnT mutants and produces pause-dependent ventricular ectopy and sustained VT in mouse hearts with acute myocardial infarction (MI). Our findings suggest a novel mechanism of pause-dependent arrhythmia that could be relevant for inherited and acquired human cardiomyopathies with increased myofilament Ca sensitivity.

METHODS

A detailed methods section describing the mouse models, intracellular Ca, AP and ECG measurements, and data analysis is available online.

RESULTS

Myofilament Ca sensitization increases cytosolic Ca binding by altering its apparent K_d

To test the hypothesis that increased myofilament Ca sensitivity changes cytosolic Ca binding, we quantified cytosolic Ca buffering in ventricular myocytes from transgenic mice with varying levels of myofilament Ca sensitivity.^{11, 18, 22} To measure cytosolic Ca buffering, caffeine was rapidly applied to release Ca from the SR (Figure 1A, upper trace). Integration of the NCX current (Figure 1A, lower trace) yielded the total amount of Ca released from the SR.²³ We did not block cytosolic Ca removal via mitochondrial Ca uptake or sarcolemmal Ca-ATPase and therefore somewhat underestimate $[Ca]_{total}$. Importantly though, the rates of non-NCX mediated Ca removal were not different between the mutations (Online Figure I) and are not expected to bias the result. SR Ca content was reduced by pretreatment with a low concentration of caffeine²⁴ to achieve caffeine transients that match the amplitude of the Ca transient during a typical myocyte contraction.²⁵ The rise in free cytosolic Ca was significantly smaller in myocytes expressing the Ca sensitizing TnT-I79N mutant compared to WT, even though the total amount of Ca released from the SR was the same (Figure 1A). On average, the ratio between the total amount of Ca released from the SR and the resulting peak change in $[Ca]_{free}$ ($=\Delta[Ca]_{total}/\Delta[Ca]_{free}$) was significantly higher in TnT-I79N myocytes (Figure 1B–D), indicating that significantly more Ca was bound in TnT-I79N compared to WT myocytes and myocytes expressing the non-sensitizing TnT-R278C mutant. Myocytes expressing the TnT-F110I mutant that has intermediate Ca sensitizing effects¹¹ exhibited also an intermediate effect on cytosolic Ca binding (Figure 1D). At the same time, the concentrations of key Ca binding proteins SERCA, calsequestrin, phospholamban, NCX and calmodulin were not significantly different among the groups (Online Figure II).

We also used an independent method to confirm the effect of the TnT-I79N mutation on cytosolic Ca buffering (Online Figure III).²⁶ Compared to non-transgenic myocytes (NTG), Ca-sensitized TnT-I79N myocytes exhibited much smaller rises in $[Ca]_{free}$ in response to approximately the same amount of total Ca influx into the cytosol, which was calculated by integrating the Ca current (Online Figure IIIA, middle trace). As before, we calculated the ratio between the increase in $[Ca]_{total}$ and the resulting change in $[Ca]_{free}$ for each myocyte. On average, cytosolic Ca binding capacity was significantly higher in TnT-I79N compared to NTG myocytes (Online Figure IIIB).

We next examined how sensitizing TnT mutants increase cytosolic Ca binding by calculating cytosolic K_d and B_{max} for each myocyte using the protocol by Trafford et al.²³ as illustrated in Figure 2A. Both the Ca sensitizing TnT-I79N and TnT-F110I mutants significantly lowered average K_d (Figure 2B), but did not change maximal cytosolic buffering capacity (B_{max}). The K_d of the non-sensitizing TnT-R278C mutant was not significantly different from that of WT myocytes. Taken together, these data demonstrate that Ca sensitizing TnT mutants increase Ca buffering by lowering the apparent K_d for cytosolic Ca binding (presumably to TnC).

A potential limitation is that cytosolic Ca buffering could be measured experimentally only at resting diastolic $[Ca]_{free}$, which was on average $0.13 \pm 0.08 \mu M$, and not significantly different between the four groups of myocytes. To examine the effect of the TnT mutations on cytosolic buffering at different diastolic $[Ca]_{free}$, we first modeled full buffering curves for all groups (Figure 2D) based on the average K_d and B_{max} obtained experimentally (Figure 2B & C). Note that initially, the buffering curves of Ca-sensitized myocytes are much steeper compared to those of WT and R278C myocytes. Hence, more Ca can be buffered when end-diastolic $[Ca]_{free}$ is low. However, since the total number of Ca binding sites (B_{max}) is unchanged, Ca binding will saturate more rapidly in Ca-sensitized compared to non-sensitized myocytes. As a result, the amount of Ca that can be bound by sensitized myofilaments is expected to diminish more rapidly than that of non-sensitized myofilaments as steady-state end-diastolic $[Ca]_{free}$ rises. To quantify this phenomenon, we next calculated for each genotype their capacity to buffer systolic Ca transients during a myocyte twitch as a function of end-diastolic $[Ca]_{free}$ (Figure 2E). Consistent with the experimental results of Figure 1D, cytosolic Ca buffering is increased in I79N and F110I myocytes at resting diastolic $[Ca]_{free}$ values (Figure 2E, points a & b). However, as steady-state end-diastolic $[Ca]_{free}$ rises (i.e., during rapid stimulation), the difference in buffering power between the groups is progressively reduced and may even reverse at high end-diastolic $[Ca]_{free}$ (Figure 2E). Taken together, the modeling results suggest that the net effect of changes in myofilament Ca binding affinity (K_d) on the Ca transient amplitude during a twitch will depend on the level of end-diastolic $[Ca]_{free}$.

To test whether acute myofilament Ca sensitization can reproduce the effects of Ca sensitizing TnT mutants, we used the Ca sensitizer EMD57033 (Online Figure IVA). Measurements of the intracellular Ca buffering using the Trafford method²³ yielded results that were comparable to TnT-I79N: significantly more Ca was bound in myocytes treated with EMD compared to vehicle-treated myocytes (Online Figure IVB). The increased buffering capacity can be attributed to an increased cytosolic Ca binding affinity (K_d), whereas maximal Ca binding capacity (B_{max}) was unchanged (Online Figure IVB).

Ca sensitization prolongs Ca transients, increases end-diastolic [Ca] and potentiates post-pause SR Ca content and release

Increased cytosolic Ca buffering can be predicted to change intracellular Ca cycling during a twitch.¹⁶ We first studied the effect of Ca sensitization in field-stimulated intact myocytes. Consistent with their increased cytosolic Ca buffering (Figures 1 & 2), TnT-I79N myocytes exhibit depressed systolic Ca transients with slowed decay rates when paced at 1 Hz (Figure 3A,C,D). End-diastolic $[Ca]_{free}$ was modestly but significantly increased (Figure 3A,E). Ca transients of myocytes expressing the non-sensitizing TnT-R278C were not different from WT myocytes. At a faster pacing of 5 Hz, decay kinetics of TnT-I79N myocytes remain slower and end-diastolic $[Ca]$ further increased compared to both WT and TnT-R278C (Figure 3B,D,E). Ca transient amplitude remained the same in TnT-WT and TnT-R278C, but increased significantly in the TnT-I79N group. As a result, I79N Ca transient amplitude was only modestly lower compared to the non-sensitized myocytes at 5 Hz, a difference that was no longer statistically significant (Figure 3B,C). The latter result is consistent with

modelling predictions that the effect of the TnT-I79N mutation on cytosolic buffering is reduced when end-diastolic $[Ca]_{free}$ is increased (Figure 2E, points a and c).

We next determined the effect of increased Ca binding affinity on intracellular Ca cycling in the intact heart at physiological heart rates. Hearts were subjected to pacing trains at cycle lengths ranging from 150 to 80 ms, which correspond to physiological heart rates of mice *in vivo*. To test the effect of a sudden change in heart rate, we introduced a 1000 ms pause followed by an extrastimulus (S2) and recorded Ca fluorescence (Figure 4A). Similar to the results in isolated myocytes, Ca removal from the cytosol is slowed and end-diastolic $[Ca]_{free}$ during the pacing train are significantly increased in TnT-I79N compared to WT and TnT-R278C hearts (Figure 4B,C). The systolic Ca transients during the pacing train (S1) were not statistically different among the groups (Figure 4D), but TnT-I79N hearts showed significantly increased S2 Ca transient amplitudes after the pause (Figure 4E). This post-pause potentiation of SR Ca release is even more evident when plotting the ratio of S1 and S2 (Figure 4F). Importantly, pretreatment of hearts with the myosin inhibitor blebbistatin, which both de-sensitizes and uncouples myofilaments,¹¹ prevented the altered Ca handling in TnT-I79N hearts (Online Figure V).

L-type Ca currents that are responsible for triggering SR Ca release are not significantly different in TnT-I79N compared to TnT-WT myocytes.⁹ Hence, we hypothesized that increased SR Ca content may be the underlying cause for the pause-induced large Ca transient in the Ca-sensitized hearts. To test this hypothesis, voltage-clamped myocytes were stimulated from a holding potential of -70 mV with brief membrane depolarizations to 0 mV at 0.5 s cycle length (2 Hz). To measure *steady-state* SR Ca content during the pacing train, caffeine was applied 0.5 s (= pacing cycle length, [PCL]) after the last pacing stimulus (Figure 5A). To measure *post-pause* SR Ca content, caffeine was applied 4 s after the last stimulus (Figure 5A). SR Ca content was determined by measuring the NCX current integral in response to the caffeine application (Figure 5B). End-diastolic SR Ca content was not statistically different between TnT-I79N and TnT-WT myocytes during steady-state pacing (Figure 5C). After the pause, SR Ca content was significantly larger in TnT-I79N myocytes compared to TnT-WT myocytes (Figure 5C).

Taken together, these data demonstrate that the main consequences of increased myofilament Ca binding affinity during physiological heart rates are an increased end-diastolic $[Ca]_{free}$ and a pause-dependent increase of SR Ca release.

Increasing Ca sensitivity causes action potential prolongation, early afterdepolarizations (EADs) and triggered activity after pauses

Since the myocyte membrane potential is closely linked to intracellular $[Ca]_{free}$ via the electrogenic NCX, we next examined the effect of enhanced post-rest potentiation of SR Ca release on the cardiac AP in the intact heart at physiological heart rates. Monophasic action potentials (MAP) were recorded using a pacing protocol analogous to the Ca transient measurements presented in Figure 4. TnT-I79N hearts were susceptible to induction of VT, which can be triggered after a pause (Figure 6A). Figure 6B shows representative examples of MAP recordings. Consistent with previous studies,^{9, 11} the S1 AP during steady-state pacing had a triangular shape in TnT-I79N hearts, but the overall action potential duration (measured as the duration at 90% repolarization, APD90) was not different among the groups (summary data not shown). On the other hand, the post-pause beat (S2) had a trend towards longer APD90 in TnT-I79N at normal pacing rates with a PCL of 150 ms. At fast pacing rates, the AP prolongation was more pronounced and reached statistical significance (Figure 6C). This post-pause AP prolongation became even more apparent when comparing the relative APD changes after every pause (Fig 6D), i.e. the relationship between the S1

and the S2 beat. Similarly, an acute increase in Ca sensitivity with EMD also resulted in a striking post-pause AP prolongation compared to both WT and TnT-R278C (Figure 6E,F).

Prolonged APs can cause EADs and triggered arrhythmias.²⁷ Thus, we investigated whether the post-pause AP prolongation in Ca-sensitized hearts increases the rate of EADs. Figure 7A shows a typical example of an EAD. Chronically increased Ca sensitivity in TnT-I79N resulted in an increased occurrence of EADs at fast pacing rates (Figure 7B). The mean takeoff potential of the EADs was around 80% repolarisation level ($81\% \pm 2\%$, $n=17$). There was no difference in the incidence of EADs between TnT-R278C and WT. Application of EMD caused a significant increase in post-pause EADs already at normal heart rates with a PCL of 150 ms, at faster pacing rates this increase was even more dramatic (Figure 7C).

EADs were frequently followed by triggered activity (Figure 7A). Hence, we examined the occurrence of triggered beats following the post-pause beat. Triggered beats occurred more frequently in TnT-I79N at fast pacing rates (PCL 100 ms), while TnT-R278C was not statistically different from control (Figure 7D). Likewise, EMD significantly increased the incidence of triggered beats (Figure 7E) compared to baseline and washout recordings. Taken together, these results demonstrate that myofilament Ca sensitization increases the rate of EADs and triggered beats after pauses.

Increasing Ca sensitivity renders hearts with acute MI susceptible to pause-dependent ventricular ectopy and sustained VT

To explore the relevance of myofilament Ca sensitization as an arrhythmogenic mechanism in acquired heart disease, we next tested the effect of EMD in isolated hearts after inducing an acute MI by coronary ligation (Figure 8). Ca transients were recorded from the non-ischemic area at the base of the left ventricle. Analogous to the effects of Ca sensitizing TnT-mutants (Figure 4), EMD treatment slowed cytosolic Ca removal and caused an increase in end-diastolic $[Ca]_{free}$ (Figure 8A–C). Post-pause Ca transients were significantly larger in EMD-treated compared to vehicle-treated MI hearts. The large S2 Ca transient in EMD-treated hearts was frequently followed by either a single triggered premature beat or sustained VT (Figure 8A, lower panels). Compared to non-ischemic NTG control hearts, all MI hearts exhibit an increased incidence of ectopic beats during steady-state pacing (Figure 8D). Interestingly, EMD had no effect on the rate of ventricular ectopy during steady-state pacing (Figure 8D). Rather, we find that EMD selectively increased the incidence of post-pause ventricular ectopy (Figure 8E) and caused sustained VT in 5 out of 7 MI hearts examined (Figure 8F).

DISCUSSION

We report three major findings: (1) Both chronic and acute increases in myofilament Ca sensitivity (caused by TnT mutations or the drug EMD57033, respectively), produce a proportional increase in cytosolic Ca binding affinity (Figures 1 & 2, Online Figure IV). (2) The increased myofilament Ca binding results in increased end-diastolic $[Ca]_{free}$ during steady-state pacing and potentiates SR Ca release after brief pauses (Figures 3–5). (3) Ca-sensitized hearts exhibit altered AP regulation characterized by post-pause AP prolongation, afterdepolarizations and triggered activity (Figures 6–7), likely as a result of excessive post-rest potentiation of Ca release generated by cytosolic Ca accumulation during physiologic heart rates. Taken together, these observations suggest a novel mechanism for triggering ventricular ectopy that occurs as a direct consequence of increased myofilament Ca sensitivity. If a substrate able to support reentrant excitation is present, i.e., induced by rapid pacing (as reported previously¹¹) or in the setting of an acute MI (Figure 8), the triggered beats can initiate sustained VT. Hence, our results are likely relevant for the pathogenesis of

ventricular arrhythmia in inherited and acquired cardiomyopathies associated with increased myofilament Ca sensitivity.

Mechanism of increased cytosolic Ca buffering caused by myofilament Ca-sensitization

Since TnT by itself does not bind Ca in amounts sufficient to alter Ca buffering, finding increased Ca buffering in myocytes expressing TnT mutants may seem surprising. However, protein conformation changes in TnT can change Ca binding to TnC.²⁸ Given the polymeric nature of the thin filament, even mutations in other thin filament proteins²⁹ or changes in cross-bridge activity²⁰ alter myofilament Ca sensitivity and likely change the Ca binding affinity ($=K_d$) of TnC in intact fibers. Given the fixed cytoplasmic volume of intact myocytes and the fact that TnC binds close to 50% of Ca released during a typical heart beat,¹³ even a small change in the K_d of TnC should result in a significant change in cytosolic $[Ca]_{free}$ during a physiological Ca release in the beating heart. On the other hand, the total number of Ca binding sites in the cytosol (=maximal buffering capacity, B_{max}) did not change (Figure 2). This result is consistent with the finding that protein expression levels of TnT, TnC or TnI are not affected by the investigated TnT mutations.^{18, 30} The hypothesis that myofilament Ca sensitization can increase myofilament Ca binding is further supported by our experiments with EMD57033 (Online Figure IV). EMD binds to the C-lobe of TnC in a region that interacts with TnI as well as TnT with a K_d of approximately 8 μM .²¹ Previous reports did not show significantly increased TnC Ca binding in response to EMD,²⁰ but differences in the experimental approach (e.g. equilibrium vs. dynamic) as well as the possibility that EMD only increases Ca binding at physiological $[Ca]_{free}$ may explain the different results.

Increased myofilament Ca buffering alters myocyte Ca homeostasis

In the intact myocytes, $[Ca]_{free}$ is determined at any given time point by the rate of sarcolemmal and SR Ca fluxes and the Ca buffering properties of the cytosol.³¹ As long as the net rate of Ca flux into the cytosol remains unchanged, systolic $[Ca]_{free}$ will be decreased in the context of increased Ca buffering. Other groups have shown that increasing maximal Ca binding capacity (B_{max}) by Ca chelators can reduce Ca transient amplitude.¹⁶ Here we directly demonstrate that increasing cytosolic Ca binding affinity (= lower K_d) without changing B_{max} , was similarly able to reduce Ca transient amplitude. The increased net Ca buffering is sufficient to lower systolic $[Ca]_{free}$ (Figure 1) and likely contributes to the decreased Ca transient amplitude in TnT-I79N cardiomyocytes at slow pacing rates (Figure 3A). Assuming that the increased myofilament Ca sensitivity affect TnC Ca “on” rates as well as “off” rates, the other consequence is slower Ca dissociation from the sensitized myofilaments during diastole. Consistent with this theory, we observed slow Ca transient decay rates in Ca-sensitized hearts, both in isolated cells and in whole hearts (Figures 3 and 5). Next, slow Ca decay rates can be predicted to lead to increased diastolic $[Ca]_{free}$, once the diastolic interval is not sufficiently long to allow for complete cytosolic Ca removal. Again, our observations agree with this notion. Diastolic $[Ca]_{free}$ is increased both in isolated myocytes and in intact heart at physiological heart rates. A possible limitation is that the Ca indicators used to measure $[Ca]_{free}$ introduce exogenous cytosolic buffering that will further slow the Ca decay kinetics and will exacerbate the rate-dependent increase in end-diastolic $[Ca]_{free}$. However, we previously reported that rapid pacing causes an excessive increase in end-diastolic pressure in indicator-free TnT mutant hearts,³² suggesting that the presence of Ca indicators was not responsible for this phenomenon.

A surprising finding was that increased myofilament buffering did not reduce Ca transient amplitude at physiological heart rates (Figure 3B and 4D). While we cannot exclude that other factor such as differences in sarcomere length¹³ or RyR2 SR Ca release channel activity³³ are contributory, our modeling studies provide a plausible explanation:

Myofilament Ca sensitization only changes K_d but not B_{max} (Figure 2). Modeling the effect of an altered K_d predicts that the differences in cytosolic buffering are progressively reduced and may even reverse as end-diastolic $[Ca]_{free}$ rises (Figure 2E). Since end-diastolic $[Ca]_{free}$ is increased in Ca-sensitized muscle during steady-state pacing, finding unchanged Ca transient amplitudes suggests that the extra cytosolic Ca buffering provided by myofilament sensitization is largely saturated at physiological heart rates. This situation is illustrated in Figure 2E by the points a and c. On the other hand, the increased myofilament Ca accumulated during steady-state pacing is likely responsible for the exaggerated post-rest potentiation of Ca release (Figure 4).

Post-rest potentiation is a physiological phenomenon observed in mammalian cardiac muscle that describes a larger contraction upon restimulation of isolated myocardium after short periods of rest.³⁴ The major underlying mechanisms are a shift of Ca from the cytosol into the SR resulting in larger SR load and also a more complete recovery of L-type Ca current and RyR2 refractoriness, together leading to enhanced Ca release after a pause.³³ Post-rest potentiation is enhanced with faster pacing rates³⁵ and can be abolished by pretreatment with ryanodine.³⁶ Our findings support the hypothesis that an increased SR load was responsible for the enhanced post-rest potentiation of Ca-sensitized hearts: While SR load was the same during steady state, the SR load was significantly increased after a pause in Ca-sensitized TnT-179N compared to WT myocytes (Figure 5). We interpret this result as follows: In a situation where cytosolic Ca affinity (i.e., K_d) is increased by myofilament sensitization, the extra Ca accumulated in the cytosol during the pacing train and bound to the myofilaments can be mobilized during a pause, of which a large fraction will be pumped into the SR.³³ In addition, the increased end-diastolic $[Ca]_{free}$ found in Ca-sensitized cardiac muscle (Figures 5 & 8) will further increase post-rest potentiation.

Myofilament sensitization as a cause of pause-dependent EADs and triggered arrhythmia

In mouse models expressing human TnT mutations associated with hypertrophic cardiomyopathy, the degree of Ca sensitization correlates with the risk for VT.^{9, 11} We reported previously reentrant activation pattern, likely produced as the result of increased CV dispersion and AP alternans.¹¹ However, an additional triggering mechanism is still required to initiate VT. Here, we find that Ca-sensitized hearts exhibit pause-dependent AP prolongation, EADs and triggered activity (Figures 6–7). Cardiac AP repolarization is highly interconnected with intracellular $[Ca]_{free}$.^{25, 37} Hence, the large post-pause S2 Ca transients found in Ca-sensitized hearts (Figure 4) presumably activate inward NCX current,³⁸ thereby causing the striking AP prolongation shown in Figure 6. Prolonged AP durations and elevated intracellular $[Ca]$ are also well-recognized mechanism for late EADs.²⁵

Another form of pause-dependent arrhythmia is torsades de pointes that occurs in patients with the long QT syndrome (LQTS).³⁹ A brief pause or slowing of the heart rate in the setting of baseline APD prolongation leads to an increased incidence of EADs and possibly torsades if the substrate is sufficiently primed.^{40–42} In LQTS, the physiologic post-pause APD prolongation in the setting of already prolonged APs causes triggered activity. In the case of increased myofilament Ca sensitivity, APD and QT are normal during steady-state pacing¹¹ or in vivo.^{9, 22} Rather, as we show here, the APD prolongation after a pause is abnormally enhanced, leading to post-pause EADs and potentially VT. As increased myofilament Ca sensitivity is frequently found in hypertrophic cardiomyopathy,¹⁰ such a triggering mechanism could be life-threatening when paired with structural remodelling of the heart.

Potential implications

In this study, we present a new mechanism of how increased myofilament Ca sensitivity can render hearts susceptible to ventricular arrhythmia: increased cytosolic Ca buffering leads to pause-dependent increased SR Ca load and triggered activity. In addition to inherited cardiac diseases such as TnT-linked FHC, our findings have implications for more common acquired human cardiomyopathies. Increased myofilament Ca sensitivity is also found in animals post-myocardial infarction⁴³ and in humans with heart failure;⁴⁴ which are heart diseases with a high incidence of ventricular arrhythmias and sudden death.⁴⁵ In both cases, the pathophysiology is extremely complex, but altered myocyte Ca regulation with increased end-diastolic [Ca] is one of the central findings.

Supplementary Material

Refer to Web version on PubMed Central for supplementary material.

Acknowledgments

SOURCES OF FUNDING

Funding support by NIH grants R01HL71670 (BCK, FCB), R01HL88635 (BCK), American Heart Association Established Investigator Award 0840071N (BCK) and Scientist Development Grant 10SDG2640109 (SH).

Non-standard abbreviations and acronyms

AP	Action Potential
APD	Action Potential Duration
CV	Conduction Velocity (CV)
EAD	Early Afterdepolarization
FHC	Familial Hypertrophic Cardiomyopathy
MAP	Monophasic Action Potential
MI	Myocardial Infarction
NCX	Na Ca exchanger
NTG	Non-transgenic
PCL	Pacing Cycle Length
SCD	Sudden Cardiac Death
SR	Sarcoplasmatic Reticulum
TnC	Troponin C
TnI	Troponin I
TnT	Troponin T
VT	Ventricular Tachycardia
WT	Wild-type

References

1. Marian AJ, Roberts R. The molecular genetic basis for hypertrophic cardiomyopathy. *J Mol Cell Cardiol.* 2001; 33(4):655–670. [PubMed: 11273720]

2. Maron BJ, Olivetto I, Spirito P, Casey SA, Bellone P, Gohman TE, Graham KJ, Burton DA, Cecchi F. Epidemiology of hypertrophic cardiomyopathy-related death: revisited in a large non-referral-based patient population. *Circulation*. 2000; 102(8):858–864. [PubMed: 10952953]
3. Maron BJ, Shen WK, Link MS, Epstein AE, Almquist AK, Daubert JP, Bardy GH, Favale S, Rea RF, Boriani G, Estes NA 3rd, Spirito P. Efficacy of implantable cardioverter-defibrillators for the prevention of sudden death in patients with hypertrophic cardiomyopathy [see comments]. *N Engl J Med*. 2000; 342(6):365–373. [PubMed: 10666426]
4. Spirito P, Bellone P, Harris KM, Bernabo P, Bruzzi P, Maron BJ. Magnitude of left ventricular hypertrophy and risk of sudden death in hypertrophic cardiomyopathy. *N Engl J Med*. 2000; 342(24):1778–1785. [PubMed: 10853000]
5. Varnava AM, Elliott PM, Baboonian C, Davison F, Davies MJ, McKenna WJ. Hypertrophic cardiomyopathy: histopathological features of sudden death in cardiac troponin T disease. *Circulation*. 2001; 104(12):1380–1384. [PubMed: 11560853]
6. Richard P, Charron P, Carrier L, Ledeuil C, Cheav T, Pichereau C, Benaiche A, Isnard R, Dubourg O, Burban M, Gueffet JP, Millaire A, Desnos M, Schwartz K, Hainque B, Komajda M. Hypertrophic cardiomyopathy: distribution of disease genes, spectrum of mutations, and implications for a molecular diagnosis strategy. *Circulation*. 2003; 107(17):2227–2232. [PubMed: 12707239]
7. Van Driest SL, Ellsworth EG, Ommen SR, Tajik AJ, Gersh BJ, Ackerman MJ. Prevalence and spectrum of thin filament mutations in an outpatient referral population with hypertrophic cardiomyopathy. *Circulation*. 2003; 108(4):445–451. [PubMed: 12860912]
8. Maass AH, Ikeda K, Oberdorf-Maass S, Maier SK, Leinwand LA. Hypertrophy, fibrosis, and sudden cardiac death in response to pathological stimuli in mice with mutations in cardiac troponin T. *Circulation*. 2004; 110(15):2102–2109. [PubMed: 15466629]
9. Knollmann BC, Kirchhof P, Sirenko SG, Degen H, Greene AE, Schober T, Mackow JC, Fabritz L, Potter JD, Morad M. Familial hypertrophic cardiomyopathy-linked mutant troponin T causes stress-induced ventricular tachycardia and Ca²⁺-dependent action potential remodeling. *Circ Res*. 2003; 92(4):428–436. [PubMed: 12600890]
10. Knollmann BC, Potter JD. Altered regulation of cardiac muscle contraction by troponin T mutations that cause familial hypertrophic cardiomyopathy. *Trends Cardiovasc Med*. 2001; 11(5):206–212. [PubMed: 11597833]
11. Baudenbacher F, Schober T, Pinto JR, Sidorov VY, Hilliard F, Solaro RJ, Potter JD, Knollmann BC. Myofilament Ca²⁺ sensitization causes susceptibility to cardiac arrhythmia in mice. *J Clin Invest*. 2008; 118(12):3893–3903. [PubMed: 19033660]
12. Huke S, Knollmann BC. Increased myofilament Ca(2+)-sensitivity and arrhythmia susceptibility. *J Mol Cell Cardiol*. 2010
13. Bers, DM. Excitation and Contraction Coupling and Cardiac Contractile Force. 2. Dordrecht/Boston/London: Kluwer Academic Publishers; 2001. Calcium Sources and Sinks; p. 39–56.
14. Solaro RJ. Troponin C - troponin I interactions and molecular signalling in cardiac myofilaments. *Adv Exp Med Biol*. 1995; 382:109–115. [PubMed: 8540387]
15. Diaz ME, Trafford AW, Eisner DA. The effects of exogenous calcium buffers on the systolic calcium transient in rat ventricular myocytes. *Biophys J*. 2001; 80(4):1915–1925. [PubMed: 11259304]
16. Ter Keurs HE, Boyden PA. Calcium and arrhythmogenesis. *Physiol Rev*. 2007; 87(2):457–506. [PubMed: 17429038]
17. Watkins H, McKenna WJ, Thierfelder L, Suk HJ, Anan R, O'Donoghue A, Spirito P, Matsumori A, Moravec CS, Seidman JG, Seidman CE. Mutations in the genes for cardiac troponin T and alpha-tropomyosin in hypertrophic cardiomyopathy. *N Engl J Med*. 1995; 332(16):1058–1064. [PubMed: 7898523]
18. Hernandez O, Szczesna-Cordary D, Knollmann BC, Miller T, Bell M, Zhao J, Sirenko SG, Diaz Z, Guzman G, Xu Y, Wang Y, Kerrick WG, Potter JD. F110I and R278C troponin T mutations that cause familial hypertrophic cardiomyopathy affect muscle contraction in transgenic mice and reconstituted human cardiac fibers. *J Biol Chem*. 2005; 280(44):37183–37194. [PubMed: 16115869]

19. Theopistou A, Anastasakis A, Miliou A, Rigopoulos A, Toutouzas P, Stefanadis C. Clinical features of hypertrophic cardiomyopathy caused by an Arg278Cys missense mutation in the cardiac troponin T gene. *Am J Cardiol.* 2004; 94(2):246–249. [PubMed: 15246915]
20. Solaro RJ, Gambassi G, Warshaw DM, Keller MR, Spurgeon HA, Beier N, Lakatta EG. Stereoselective actions of thiadiazinones on canine cardiac myocytes and myofilaments. *Circ Res.* 1993; 73(6):981–990. [PubMed: 8222092]
21. Wang X, Li MX, Spyropoulos L, Beier N, Chandra M, Solaro RJ, Sykes BD. Structure of the C-domain of human cardiac troponin C in complex with the Ca²⁺ sensitizing drug EMD 57033. *J Biol Chem.* 2001; 276(27):25456–25466. [PubMed: 11320096]
22. Knollmann BC, Blatt SA, Horton K, de Freitas F, Miller T, Bell M, Housmans PR, Weissman NJ, Morad M, Potter JD. Inotropic stimulation induces cardiac dysfunction in transgenic mice expressing a troponin T (I79N) mutation linked to familial hypertrophic cardiomyopathy. *J Biol Chem.* 2001; 276(13):10039–10048. [PubMed: 11113119]
23. Trafford AW, Diaz ME, Eisner DA. A novel, rapid and reversible method to measure Ca buffering and time-course of total sarcoplasmic reticulum Ca content in cardiac ventricular myocytes. *Pflügers Arch.* 1999; 437(3):501–503. [PubMed: 9914410]
24. Trafford AW, Sibbring GC, Diaz ME, Eisner DA. The effects of low concentrations of caffeine on spontaneous Ca release in isolated rat ventricular myocytes. *Cell Calcium.* 2000; 28(4):269–276. [PubMed: 11032782]
25. Bers DM. Calcium and cardiac rhythms: physiological and pathophysiological. *Circ Res.* 2002; 90(1):14–17. [PubMed: 11786512]
26. Berlin JR, Bassani JW, Bers DM. Intrinsic cytosolic calcium buffering properties of single rat cardiac myocytes. *Biophys J.* 1994; 67(4):1775–1787. [PubMed: 7819510]
27. January CT, Moscucci A. Cellular mechanisms of early afterdepolarizations. *Ann N Y Acad Sci.* 1992; 644:23–32. [PubMed: 1562117]
28. Gomes AV, Venkatraman G, Davis JP, Tikunova SB, Engel P, Solaro RJ, Potter JD. Cardiac troponin T isoforms affect the Ca(2+) sensitivity of force development in the presence of slow skeletal troponin I: insights into the role of troponin T isoforms in the fetal heart. *J Biol Chem.* 2004; 279(48):49579–49587. [PubMed: 15358779]
29. Bottinelli R, Coviello DA, Redwood CS, Pellegrino MA, Maron BJ, Spirito P, Watkins H, Reggiani C. A mutant tropomyosin that causes hypertrophic cardiomyopathy is expressed in vivo and associated with an increased calcium sensitivity [see comments]. *Circ Res.* 1998; 82(1):106–115. [PubMed: 9440709]
30. Miller T, Szczesna D, Housmans PR, Zhao J, de Freitas F, Gomes AV, Culbreath L, McCue J, Wang Y, Xu Y, Kerrick WG, Potter JD. Abnormal contractile function in transgenic mice expressing a familial hypertrophic cardiomyopathy-linked troponin T (I79N) mutation. *J Biol Chem.* 2001; 276(6):3743–3755. [PubMed: 11060294]
31. Bers DM. Calcium fluxes involved in control of cardiac myocyte contraction. *Circ Res.* 2000; 87(4):275–281. [PubMed: 10948060]
32. Sirenko SG, Potter JD, Knollmann BC. Differential effect of troponin T mutations on the inotropic responsiveness of mouse hearts—role of myofilament Ca²⁺ sensitivity increase. *J Physiol.* 2006; 575(Pt 1):201–213. [PubMed: 16777946]
33. Bers, DM. *Excitation and Contraction Coupling and Cardiac Contractile Force.* 2. Dordrecht/Boston/London: Kluwer Academic Publishers; 2001. Sarcoplasmic Reticulum; p. 161-202.
34. Koch-Weser J, Blinks JR. The Influence of the Interval between Beats on Myocardial Contractility. *Pharmacol Rev.* 1963; 15:601–652. [PubMed: 14064358]
35. Allen DG, Jewell BR, Wood EH. Studies of the contractility of mammalian myocardium at low rates of stimulation. *J Physiol.* 1976; 254(1):1–17. [PubMed: 1249717]
36. Banijamali HS, Gao WD, MacIntosh BR, ter Keurs HE. Force-interval relations of twitches and cold contractures in rat cardiac trabeculae. Effect of ryanodine. *Circ Res.* 1991; 69(4):937–948. [PubMed: 1718623]
37. Carmeliet E. Intracellular Ca(2+) concentration and rate adaptation of the cardiac action potential. *Cell Calcium.* 2004; 35(6):557–573. [PubMed: 15110146]

38. Knollmann BC, Schober T, Petersen AO, Sirenko SG, Franz MR. Action potential characterization in intact mouse heart: steady-state cycle length dependence and electrical restitution. *Am J Physiol Heart Circ Physiol*. 2007; 292(1):H614–621. [PubMed: 16963611]
39. Viskin S, Fish R, Zeltser D, Belhassen B, Heller K, Brosh D, Laniado S, Barron HV. Arrhythmias in the congenital long QT syndrome: how often is torsade de pointes pause dependent? *Heart*. 2000; 83(6):661–666. [PubMed: 10814624]
40. Vos MA, Gorenck B, Verduyn SC, van der Hulst FF, Leunissen JD, Dohmen I, Wellens HJ. Observations on the onset of torsade de pointes arrhythmias in the acquired long QT syndrome. *Cardiovasc Res*. 2000; 48(3):421–429. [PubMed: 11090837]
41. Roden DM, Anderson ME. The pause that refreshes, or does it? Mechanisms in torsades de pointes. *Heart*. 2000; 84(3):235–237. [PubMed: 10956280]
42. Liu J, Laurita KR. The mechanism of pause-induced torsade de pointes in long QT syndrome. *J Cardiovasc Electrophysiol*. 2005; 16(9):981–987. [PubMed: 16174020]
43. de Waard M, van der Velden J, Bito V, Ozdemir S, Biesmans L, Boontje N, Dekkers D, Schoonderwoerd K, Schuurbiers H, de Crom R, Stienen G, Sipido K, Lamers J, Duncker D. Early exercise training normalizes myofilament function and attenuates left ventricular pump dysfunction in mice with a large myocardial infarction. *Circ Res*. 2007; 100(7):1079–1088. [PubMed: 17347478]
44. van der Velden J, Papp Z, Zaremba R, Boontje NM, de Jong JW, Owen VJ, Burton PB, Goldmann P, Jaquet K, Stienen GJ. Increased Ca²⁺-sensitivity of the contractile apparatus in end-stage human heart failure results from altered phosphorylation of contractile proteins. *Cardiovasc Res*. 2003; 57(1):37–47. [PubMed: 12504812]
45. Tomaselli GF, Zipes DP. What causes sudden death in heart failure? *Circ Res*. 2004; 95(8):754–763. [PubMed: 15486322]

Novelty and Significance

What Is Known?

- Familial hypertrophic cardiomyopathy (FHC) is an inherited disease caused by mutations in sarcomeric proteins that is associated with a high risk for ventricular arrhythmia and sudden death.
- FHC-linked mutations often increase myofilament Ca sensitivity, which has been linked to increased arrhythmia susceptibility.
- Myofilaments are the dominant cytosolic Ca buffer, binding about 50% of Ca entering the cytosol during a normal heart beat.

What New Information Does This Article Contribute?

- Ca sensitizing FHC-mutants increase the cytosolic Ca binding affinity (K_d), and cause excess cytosolic Ca accumulation during physiological heart rates, which shifts into the sarcoplasmic reticulum (SR) during longer diastolic intervals.
- The pause-dependent excessive SR Ca uptake and subsequent release causes action potential prolongation, early afterdepolarizations and triggered beats that can be prevented by myofilament Ca desensitization.
- Acute Ca sensitization with EMD 57033 mimics the effects of Ca sensitizing FHC-mutants and produces pause-dependent ventricular arrhythmia after acute myocardial infarction (MI).

Increased myofilament Ca sensitivity is commonly caused by FHC mutations, but has also been described after MI. Both diseases are associated with a high risk for ventricular arrhythmia and sudden death. We previously found that increasing myofilament Ca sensitivity renders mouse hearts susceptible to ventricular tachycardia. However, the underlying cellular mechanisms remain unclear. Here, we report a novel arrhythmia triggering mechanism that is based on myofilament Ca sensitization. The initiating event is the increased cytosolic Ca binding affinity that leads to Ca accumulation in the cytosol during physiological heart rates. The accumulated Ca is mobilized and taken up by the SR during longer diastolic intervals or skipped heart beats (=pauses). The resulting post-pause excessive Ca release causes action potential prolongation, afterdepolarizations and triggered ventricular beats. Triggered beats lead to ventricular tachycardia in structurally abnormal hearts, e.g. after MI. To our knowledge, our findings provide the first direct evidence of the mechanism responsible for triggering ventricular arrhythmia in Ca sensitized hearts, which may contribute to sudden death risk in FHC and ischemic cardiomyopathy. We propose that increased cytosolic Ca binding affinity represents a heretofore unrecognized pause-dependent arrhythmia mechanism that could manifest itself in patients with normal QT duration during regular sinus rhythm.

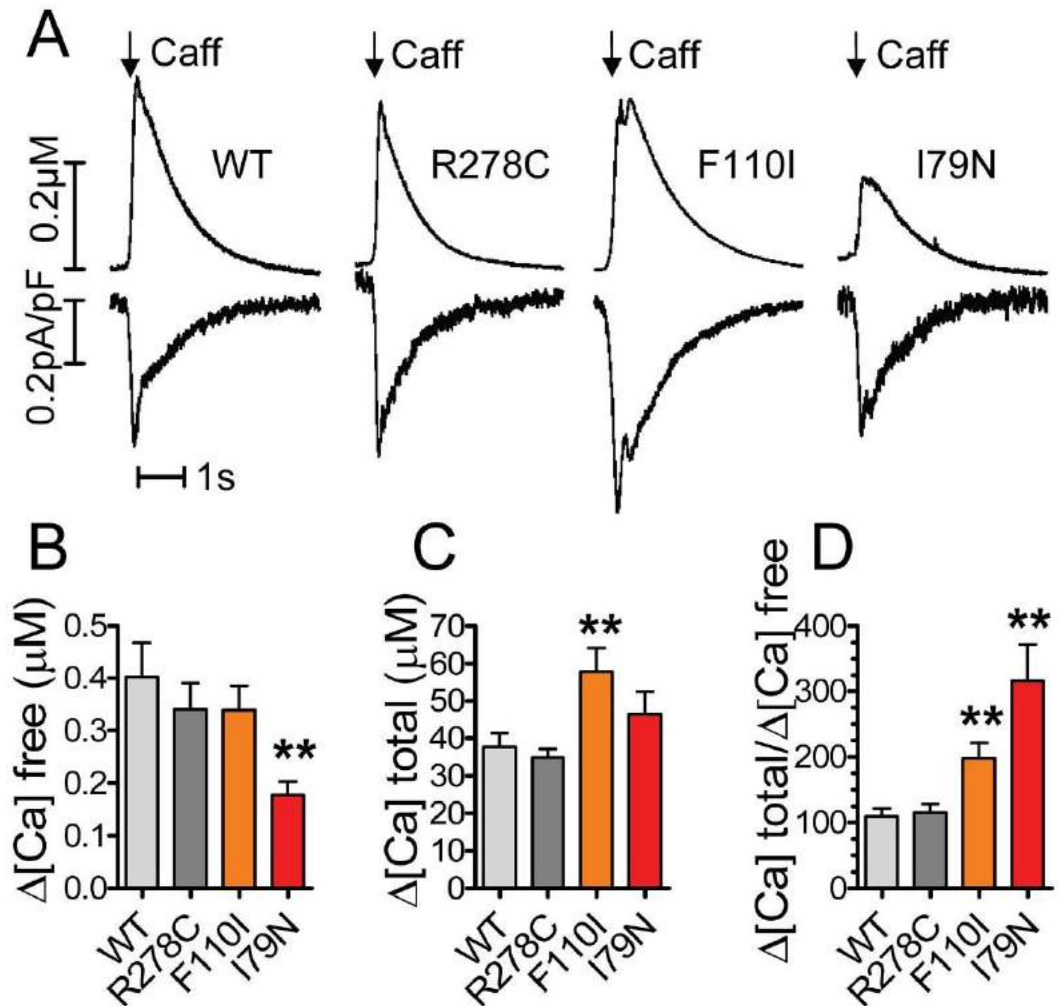


Figure 1. Ca^{2+} sensitizing troponin T (TnT) mutants increase apparent cytosolic Ca^{2+} binding
Cytosolic Ca^{2+} fluorescence was recorded from voltage-clamped myocytes loaded with the fluorescent indicator Fluo-4 (25 μM). **A**, Representative examples of mice expressing either human wild-type cardiac TnT (WT) or mutant TnT (TnT-R278C, TnT-F110I, TnT-I79N). Myofilament Ca^{2+} sensitivity was altered in the following order: TnT-R278C \leq TnT-WT $<$ TnT-F110I $<$ TnT-I79N. **Upper trace**: Rapidly applied caffeine was used to release Ca^{2+} from the sarcoplasmic reticulum (SR). **Lower trace**: Integration of the $\text{Na}^{+} \text{Ca}^{2+}$ exchanger current yielded the total amount of Ca^{2+} released from the SR. **B–D**, Myocytes expressing the Ca^{2+} sensitizing TnT mutants show a higher net cytosolic Ca^{2+} binding calculated by a smaller rise in $[\text{Ca}^{2+}]_{\text{free}}$ and an higher $\Delta[\text{Ca}^{2+}]_{\text{total}}$. $n=11$ –13 myocytes per group. ** $p<0.01$ vs WT and TnT-R278C

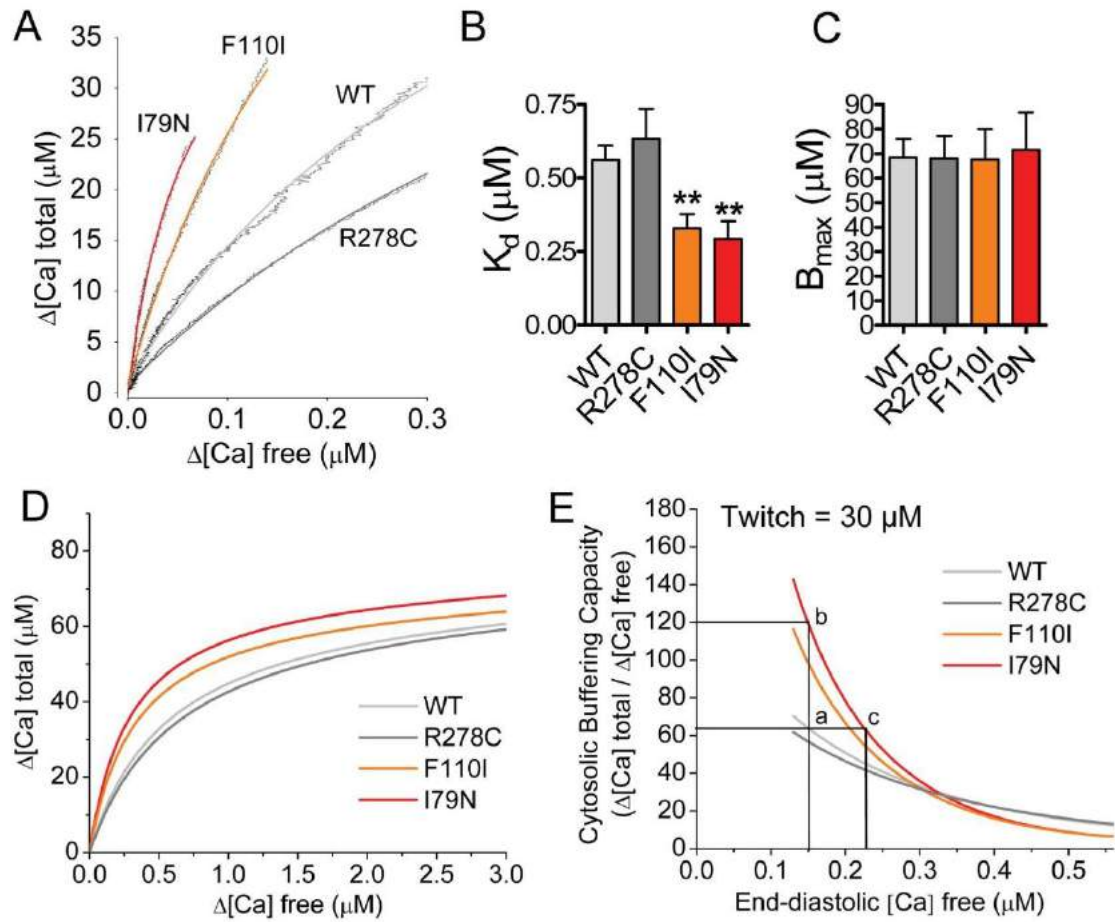


Figure 2. Ca^{2+} sensitizing TnT mutants alter the apparent K_d of cytosolic Ca^{2+} buffering
Cytosolic buffering parameters (K_d and B_{max}) were determined using the Ca^{2+} binding data presented in Figure 1. $\Delta[\text{Ca}^{2+}]_{total}$ was plotted as a function of $\Delta[\text{Ca}^{2+}]_{free}$, fitted to a modified Michaelis-Menten equation and B_{max} and K_d calculated for each myocyte. **A**, Representative buffering plots. **B–C**, Ca^{2+} sensitizing TnT-I79N and TnT-F110I mutants show significantly lowered average K_d , but did not change maximal cytosolic buffering capacity (B_{max}). The non-sensitizing TnT-R278C mutant was not different from wild-type (WT) myocytes. $n=9-10$ myocytes per group. $**p<0.01$ vs TnT-R278C and WT. **D**, Cytosolic buffering curves calculated from experimental K_d and B_{max} obtained in **B** and **C**. **E**, Predicted cytosolic buffering capacity as a function of steady-state end-diastolic $[\text{Ca}^{2+}]_{free}$. A simulated twitch Ca^{2+} increase of $30 \mu\text{M}$ ($= \Delta[\text{Ca}^{2+}]_{total}$) was used to compare buffering capacity in the four groups based on the buffering curves from **D**. The cytosolic buffering capacity decreases as end-diastolic $[\text{Ca}^{2+}]_{free}$ increases. Note that at the same low diastolic Ca^{2+} this results in increased buffering capacity in the TnT-I79N (a vs. b) and therefore expected decreased systolic Ca^{2+} . But buffering capacity can be the same in I79N and WT when diastolic $[\text{Ca}^{2+}]$ is different (a vs. c).

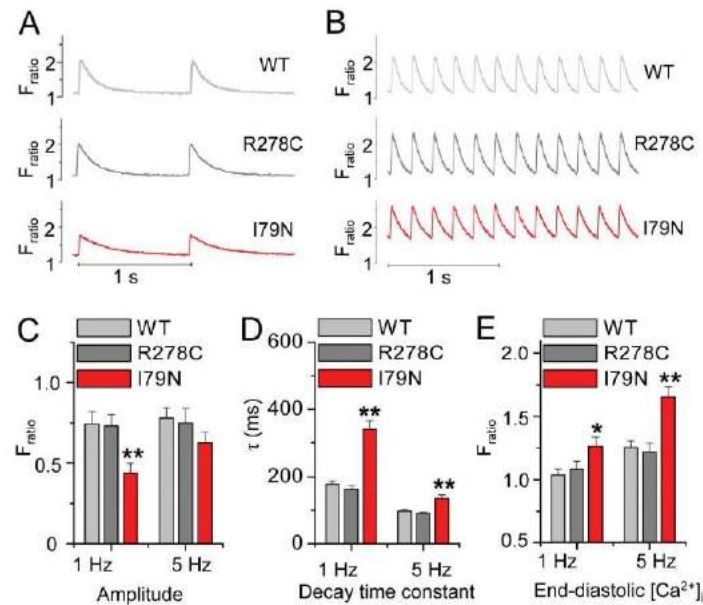


Figure 3. Ca²⁺ sensitized TnT-I79N myocytes exhibit prolonged Ca²⁺ transients and increased end-diastolic Ca²⁺ concentrations

Ca²⁺ transients were measured in field-stimulated ventricular myocytes, loaded with fura-2AM. **A–B**, Representative traces from three myocytes stimulated at 1 Hz (**A**) and 5 Hz (**B**). **C–E**, Average data. At 1 Hz, Ca²⁺ transients from the Ca²⁺ sensitized TnT-I79N myocytes have smaller amplitudes, slow decay kinetics and increased end-diastolic [Ca²⁺]. At a faster pacing rate of 5 Hz, the amplitude is nearly normalized, but decay kinetics remain significantly longer and end-diastolic [Ca²⁺] is further increased compared to both TnT-WT and TnT-R278C. *p<0.05, **p<0.01 compared to WT and R278C, n = 39–63 myocytes from 6–7 mice per group. Except for WT and R278C amplitude, all other parameter means measured at 5 Hz were significantly different from those measured at 1 Hz for each genotype (p<0.01, not indicated in the figure).

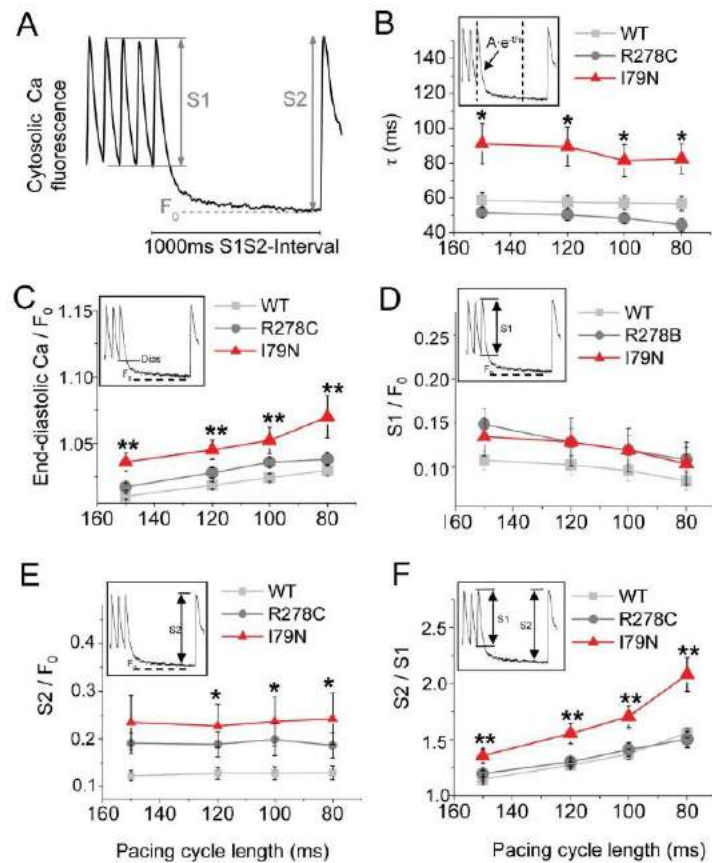


Figure 4. TnT-I79N hearts have increased Ca²⁺ transients in response to an extrastimulus after a pause

Ca²⁺ transients were measured from intact hearts using ratios of rhod-2 fluorescence. Hearts were subjected to rapid pacing at different pacing cycle length (S1), followed by a 1 second pause and an extrastimulus (S2 pulse). **A**, Representative trace demonstrating the pacing protocol, pacing cycle length 100 ms. **B–F**, Average data. Ca²⁺ removal from the cytosol is slowed (**B**) and end-diastolic Ca²⁺ concentrations are significantly increased in TnT-I79N (**C**). Ca²⁺ transients of TnT-I79N hearts have unchanged amplitude at steady state pacing (**D**), but show a significantly enhanced Ca²⁺ release after a pause (**E, F**). n=8–10 mice per group. *p<0.05, **p<0.01 TnT-I79N vs wild-type (WT).

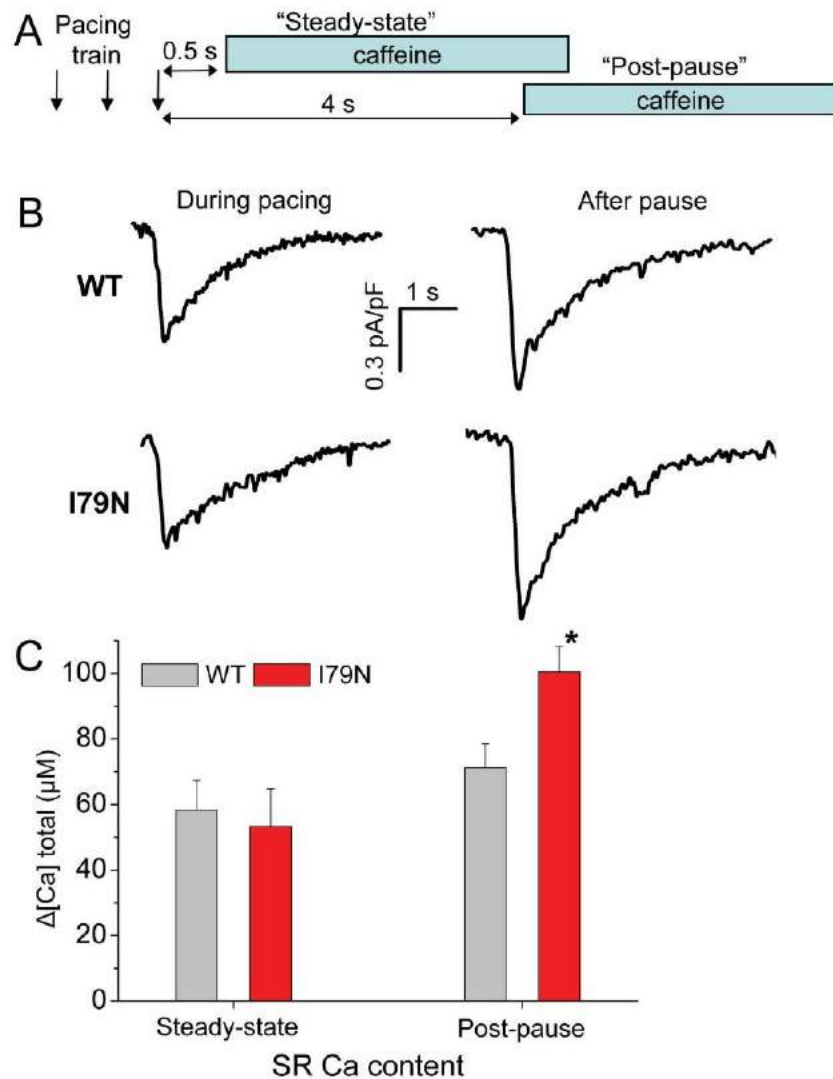


Figure 5. SR Ca^{2+} content is increased in TnT-I79N myocytes after a pause

A, Experimental protocol. Voltage-clamped myocytes were stimulated with a pacing train (2 Hz, 20 s) of brief membrane depolarizations (0 mV, 50 ms) from a holding potential of -70 mV. To measure end-diastolic SR Ca^{2+} content during steady-state pacing and after a pause, caffeine (10 mM) was applied either 0.5 s (= pacing cycle length) or 4 s following the last pacing stimulus. **B**, Representative NCX current records elicited by caffeine application. SR content was calculated from the NCX current integral. **C**, SR Ca^{2+} content is significantly increased in TnT-I79N vs TnT-WT myocytes only after a pause. $N = 8-12$ myocytes from 3-4 animals per genotype, * $p < 0.05$.

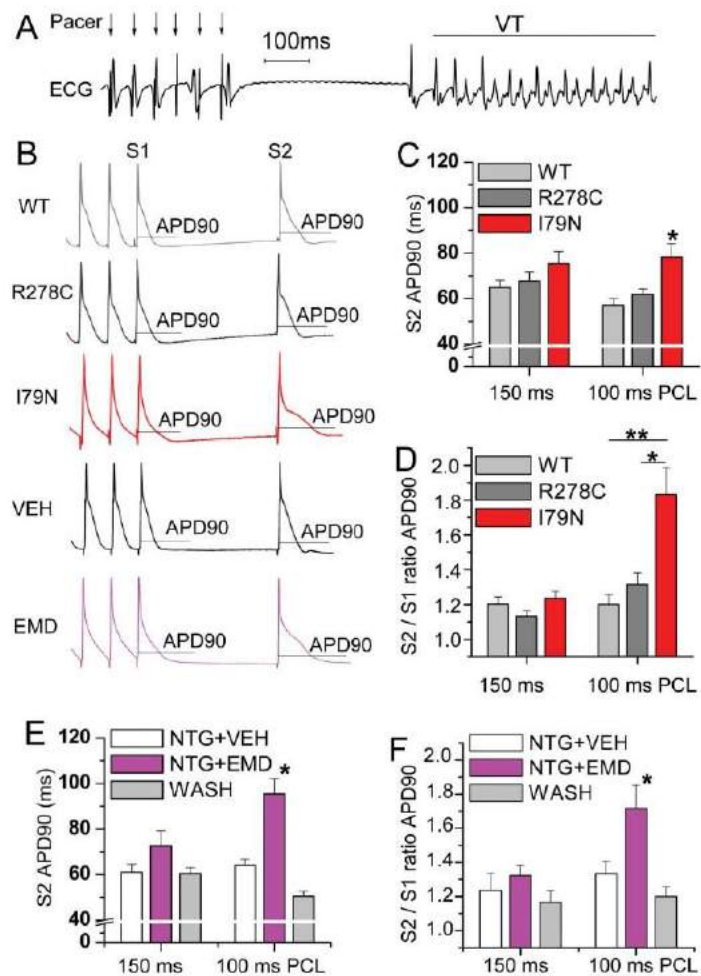


Figure 6. Increasing Ca^{2+} sensitivity causes post-pause action potential prolongation
 Hearts were subjected to rapid pacing (S1) at different pacing cycle length (PCL), followed by a 500 ms pause and an extrastimulus (S2). **A**, Example of spontaneous ventricular tachycardia (VT) in a TnT-I79N mouse after a pause following fast pacing. **B**, Representative examples of monophasic action potentials recorded during the stimulation protocol, PCL 100 ms. **C and D**, Ca^{2+} sensitized TnT-I79N hearts show rate-dependent AP prolongation after the pause. Panel **D** shows the relative post-pause APD90 (S2) compared to pre-pause APD90 (S1). $N=5-8$ mice per group. **E and F**, Acutely increased Ca^{2+} sensitivity with EMD ($3 \mu\text{M}$) also causes rate-dependent AP prolongation after pauses. $n=4-11$ mice per group. * $p<0.05$, ** $p<0.01$.

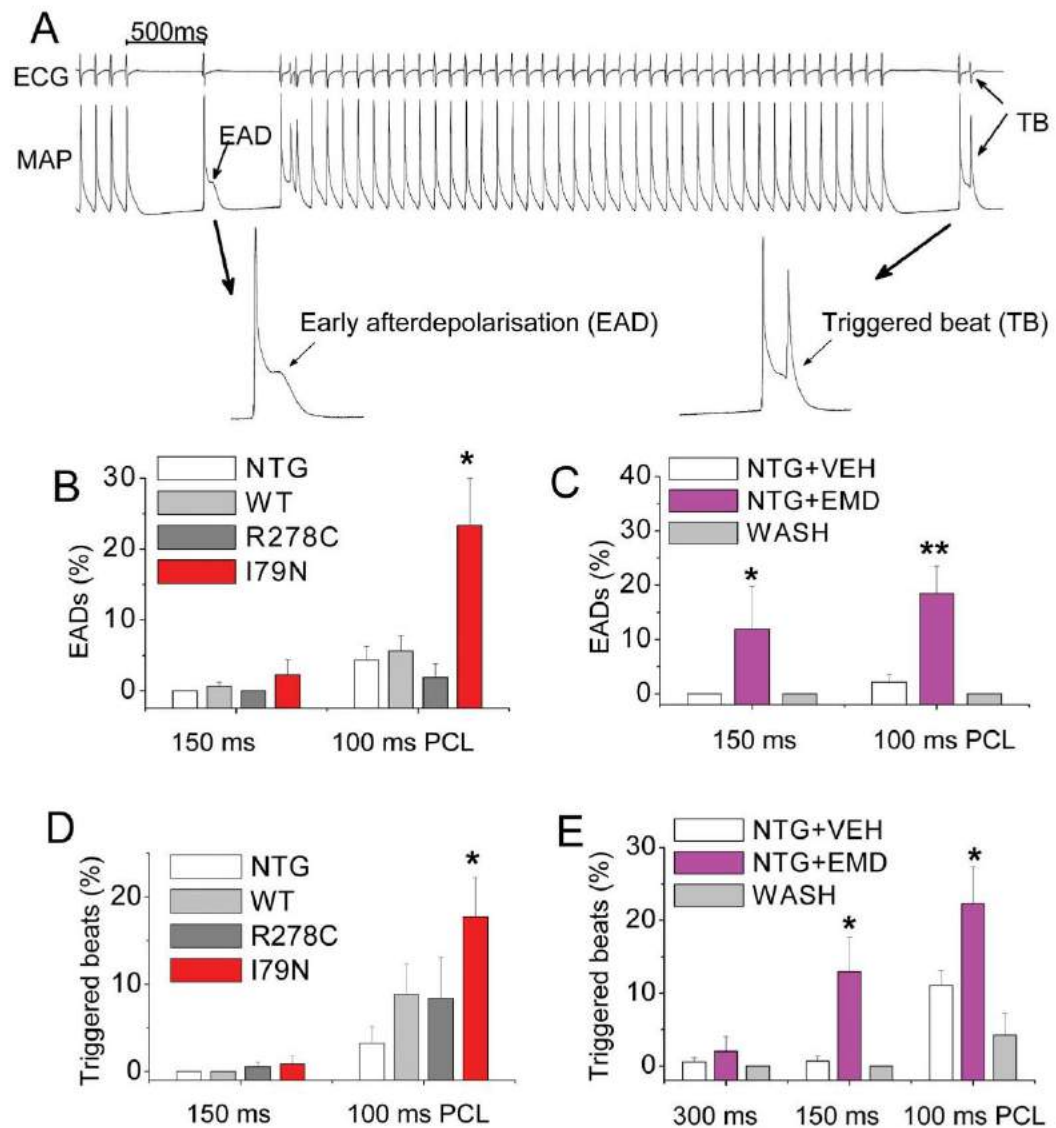


Figure 7. Ca^{2+} sensitization causes early afterdepolarizations (EADs) and triggers premature beats after pauses

A, Pacing train with an extra stimulus (S2) after a 500 ms pause. Example record from a NTG heart treated with EMD ($3 \mu\text{M}$) shows an EAD followed by a triggered beat. Pacing cycle length (PCL) 100ms. **B**, At fast pacing rates, the incidence of EADs is increased in the Ca^{2+} sensitized TnT-I79N hearts. $n = 4-11$ mice per group. **C**, NTG hearts treated with EMD exhibit an increased rate of EADs compared to vehicle (VEH) treated NTG hearts and recordings after washout (WASH). $n = 7-10$ mice. **D**, In TnT-I79N hearts, the S2 beat frequently triggers premature beats. $n = 4-11$ mice per group. **E**, The incidence of triggered beats is increased by acute Ca^{2+} sensitization with EMD. $n = 11-14$ mice. * $p < 0.05$, ** $p < 0.01$.

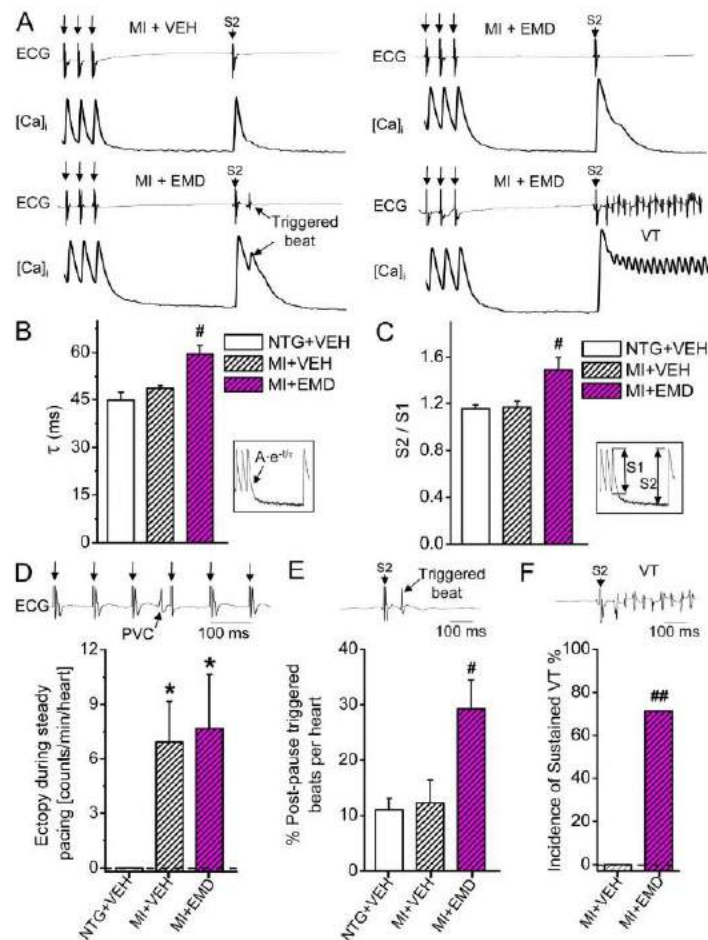


Figure 8. In hearts with acute MI, Ca^{2+} sensitization with EMD 57033 enhances post-pause Ca^{2+} transients and triggers sustained VT

A, upper panels: Representative examples of simultaneously recorded ECG and Ca^{2+} fluorescence traces in the presence of EMD ($3 \mu\text{M}$) or vehicle (VEH). **Lower panels:** Pause-dependent triggered beats and sustained VT in EMD-treated MI hearts. **B–C,** EMD slowed cytosolic Ca^{2+} removal and increased post-pause Ca^{2+} release. **D,** Compared to non-ischemic hearts (NTG), MI hearts exhibit an increased incidence of ectopic beats during steady state pacing, which is not affected by EMD. **E,** Acute MI by itself does not increase the occurrence of post-pause ectopic beats compared to NTG; MI hearts treated with EMD exhibit a 3-fold increase in post-pause triggered beats. **F,** EMD causes pause-triggered sustained VT in MI hearts. Black arrows: pacing stimuli. * $p < 0.05$ compared to NTG+VEH, # $p < 0.05$ and ## $p < 0.01$ compared to both MI+VEH and NTG+VEH, $n = 7$ –9 hearts per group.

2.2. Роль кальсеквестрину2 (*Casq2*) у регуляції рефрактерності вивільнення Ca^{2+} із саркоплазматичного ретикулу міоцитів



HHS Public Access

Author manuscript

J Mol Cell Cardiol. Author manuscript; available in PMC 2016 May 01.

Published in final edited form as:

J Mol Cell Cardiol. 2015 May ; 82: 75–83. doi:10.1016/j.yjmcc.2015.02.027.

Impaired calcium-calmodulin-dependent inactivation of $\text{Ca}_v1.2$ contributes to loss of sarcoplasmic reticulum calcium release refractoriness in mice lacking calsequestrin 2

Dmytro O. Kryshchal¹, Oleksiy Gryshchenko^{1,2}, Nieves Gomez-Hurtado¹, and Bjorn C. Knollmann¹

¹Department of Medicine, Vanderbilt University, Nashville, TN, USA

²Department of General Physiology of Nervous System, Bogomoletz Institute of Physiology, Kyiv, Ukraine

Abstract

Aims—In cardiac muscle, Ca^{2+} release from sarcoplasmic reticulum (SR) is reduced with successively shorter coupling intervals of premature stimuli, a phenomenon known as SR Ca^{2+} release refractoriness. We recently reported that the SR luminal Ca^{2+} binding protein calsequestrin 2 (*Casq2*) contributes to release refractoriness in intact mouse hearts, but the underlying mechanisms remain unclear. Here, we further investigate the mechanisms responsible for physiological release refractoriness.

Methods and Results—Gene-targeted ablation of *Casq2* (*Casq2* KO) abolished SR Ca^{2+} release refractoriness in isolated mouse ventricular myocytes. Surprisingly, impaired Ca^{2+} -dependent inactivation of L-type Ca^{2+} current (I_{Ca}), which is responsible for triggering SR Ca^{2+} release, significantly contributed to loss of Ca^{2+} release refractoriness in *Casq2* KO myocytes. Recovery from Ca^{2+} -dependent inactivation of I_{Ca} was significantly accelerated in *Casq2* KO compared to wild-type (WT) myocytes. In contrast, voltage-dependent inactivation measured by using Ba^{2+} as charge carrier was not significantly different between WT and *Casq2* KO myocytes. Ca^{2+} -dependent inactivation of I_{Ca} was normalized by intracellular dialysis of excess apo-CaM (20 μM), which also partially restored physiological Ca^{2+} release refractoriness in *Casq2* KO myocytes.

Conclusions—Our findings reveal that the intra-SR protein *Casq2* is largely responsible for the phenomenon of SR Ca^{2+} release refractoriness in murine ventricular myocytes. We also report a novel mechanism of impaired Ca^{2+} -CaM-dependent inactivation of $\text{Ca}_v1.2$, which contributes to

© 2015 Published by Elsevier Ltd.

Correspondence: Björn C. Knollmann, MD, PhD, Professor of Medicine and Pharmacology, Division of Clinical Pharmacology, Vanderbilt University School of Medicine, Medical Research Building IV, Rm. 1265, 2215B Garland Ave, Nashville, TN 37232-0575, Phone: (615) 343-6493, bjorn.knollmann@vanderbilt.edu.

Conflict of Interest

The authors declare no conflict of interest.

Publisher's Disclaimer: This is a PDF file of an unedited manuscript that has been accepted for publication. As a service to our customers we are providing this early version of the manuscript. The manuscript will undergo copyediting, typesetting, and review of the resulting proof before it is published in its final citable form. Please note that during the production process errors may be discovered which could affect the content, and all legal disclaimers that apply to the journal pertain.

Author Manuscript

Author Manuscript

Author Manuscript

Author Manuscript

the loss of SR Ca^{2+} release refractoriness in the Casq2 KO mouse model and, therefore, may further increase risk for ventricular arrhythmia *in vivo*.

Keywords

Calsequestrin; calmodulin; calcium release restitution; L-type calcium channel; sarcoplasmic reticulum

1. Introduction

Precise control of the release of Ca^{2+} from intracellular stores of sarcoplasmic reticulum (SR) in cardiac myocytes is important for normal contractility and functioning of cardiac muscle [2]. On the other hand, spontaneous Ca^{2+} release from ryanodine receptor (RyR2) SR Ca^{2+} release channels is thought to be one of the underlying mechanisms responsible for ventricular arrhythmia and sudden cardiac death. Both acquired (such as acute myocardial infarction and heart failure) and inherited (e.g. catecholaminergic polymorphic ventricular tachycardia) arrhythmia syndromes are accompanied by abnormalities in Ca^{2+} handling in cardiac myocytes [2]. Published reports suggest that spontaneous Ca^{2+} release from the SR, particularly due to alterations in RyR2 activity, may serve as a trigger for ventricular arrhythmia in heart failure [3–6]. Moreover, interventions that decrease sudden cardiac death and increase survival in patients with heart failure also normalize cardiac Ca^{2+} handling [7, 8]. In aggregate, these data suggest that altered myocyte Ca^{2+} release and ventricular arrhythmias are closely linked.

Calsequestrin 2 (Casq2) is a high-capacity Ca^{2+} -binding protein located in the junctional sarcoplasmic reticulum (jSR) of cardiac muscle [9–11]. Casq2 binds to the RyR2, either directly or via two other jSR proteins, junctin and triadin [12, 13] which together form the SR Ca^{2+} release unit (CRU) [14]. This protein complex is responsible for Ca^{2+} release from the SR, triggered by increase in cytosolic Ca^{2+} concentration due to activation of L-type Ca^{2+} channels ($\text{Ca}_v1.2$), also known as Ca^{2+} -induced Ca^{2+} release (CICR) [15, 16]. In this way, CRUs are responsible for the precise control of Ca^{2+} release during excitation-contraction coupling in cardiac tissue [17]. Functionally, Ca^{2+} entering through $\text{Ca}_v1.2$ during an action potential triggers Ca^{2+} release from the SR [15]. In case of two consecutive stimuli, the amplitude of the resulting Ca^{2+} transient depends on the diastolic interval that preceded the second stimulus – a phenomenon known as Ca^{2+} release refractoriness [18].

Casq2, the major intra-SR Ca^{2+} buffering protein [18], has been suggested to modulate activity of RyR2 Ca^{2+} -release channels [19, 20] regulating its sensitivity to intra-SR luminal Ca^{2+} . We recently found that Casq2, acting both as intra-SR Ca^{2+} buffer and as a regulator of sensitivity of RyR2 to luminal Ca^{2+} , importantly governs Ca^{2+} transient restitution in intact mouse hearts [1]. Here, we further investigate the role of Casq2 in regulating SR Ca^{2+} release refractoriness in isolated ventricular myocytes under experimental condition that allow control of the physiological trigger of Ca^{2+} release, the $\text{Ca}_v1.2$ current.

2. Methods

2.1. Ethics

All experiments were approved by the institutional animal care and use committees at Animal Care and Use Committees of Vanderbilt University and performed in accordance with NIH guidelines. Mouse heart harvest was performed under general anesthesia (inhalation of 3% isoflurane vapor) and animals euthanized by exsanguination.

2.2. Restitution protocols

Restitution curves were obtained by introducing an additional stimulation pulse (S2) at different time intervals (S1–S2 coupling intervals) with respect to the regular pacing pulses (S1) as shown in Fig. 2A. The same experimental protocol was used in all the experiments studying refractoriness of either cytosolic Ca^{2+} transients or $\text{Ca}_v1.2$ currents. To analyze the kinetics of the recovery of cytosolic Ca^{2+} transients, recovery ratios were calculated from the amplitudes of S2 (extrasystolic) and S1 (regular baseline pacing) beat. To plot restitution curves, we expressed either the S2 Ca^{2+} release transient or the amplitude of $\text{Ca}_v1.2$ currents during S2 stimulus as a function of the S1–S2 coupling interval, using the following formula:

$$1 - \frac{\text{S1}-\text{S2}}{\text{S1}} \times 100\%$$

Our approach for analyzing SR Ca^{2+} restitution is different from the one that was used in our previous reports [1]. To better reflect that Ca^{2+} reuptake is not complete and hence the SR is still depleted during the very premature S2 beats, we use the value of the peak of the S2 transient rather than the S2 transient amplitude (see Fig. 1 for details). This approach takes into account the Ca^{2+} in the cytosol that is not yet taken up when the premature S2 stimulus is delivered and obviously cannot be released. We posit that this is a more accurate approach for measuring RyR2 release refractoriness in the intact myocyte.

2.3. Myocyte isolation and cytosolic Ca^{2+} transient measurements

Ventricular myocytes from 12 to 16 weeks old male and female Casq2 KO or wild-type (WT) mice from the same C57BL/6 strain were isolated using a modified collagenase/ protease method as previously described [21]. All experiments on field-stimulated myocytes were conducted in Tyrode's solution (TS) containing (in mM): NaCl 134, KCl 5.4, MgCl_2 1, CaCl_2 2, glucose 10, HEPES 10, adjusted to pH 7.4 with NaOH. After isolation, myocytes were loaded with Fura-2 acetoxymethyl ester, Fura-2 AM as described previously [22]. Briefly, myocytes were incubated with 2 μM Fura 2 AM for 6 minutes at room temperature to load the indicator in the cytosol. Myocytes were then washed twice for 10 minutes with TS containing 250 μM probenecid to retain the indicator in the cytosol. A minimum of 30 min was allowed for de-esterification before imaging the cells.

Fura-2-loaded healthy rod-shaped isolated ventricular myocytes were placed into the experimental chamber, field stimulated, and superfused with TS. Intracellular Ca^{2+} transients were measured using a dual-beam excitation fluorescence photometry setup

(IonOptix Corp.) utilizing the protocol shown in Fig. 2A. After that, myocytes were exposed for 4 seconds to TS containing 10 mmol/l caffeine using a rapid concentration-clamp system. The amplitude of the caffeine-induced Ca^{2+} transient was used as an estimate of total SR Ca^{2+} content [18]. All experiments were conducted at room temperature ($\sim 23^\circ\text{C}$). Ca^{2+} transients were analyzed using specialized data analysis software (IonWizard, IonOptixCorp.). Excitation wavelengths of 360 and 380 nm were used to monitor the fluorescence signals of Ca^{2+} -bound and Ca^{2+} -free fura-2, and $[\text{Ca}^{2+}]_i$ measurements are reported as fluorescence ratios (F_{ratio}).

For the measurements of cytosolic Ca^{2+} transients in voltage-clamp mode, cells were loaded with fluo-4 pentapotassium salt (final concentration 100 μM), added into pipette solution from stock. Pipette solution contained (in mM): CsCl 125, MgATP 5, MgCl_2 1, glutathione (GSH) 5, cAMP 0.05, HEPES 20, adjusted to pH 7.25 with CsOH. External K-free solution contained (in mM): NaCl 134, CsCl 5, MgCl_2 1, CaCl_2 2, glucose 10, HEPES 10, adjusted to pH 7.4 with NaOH. The same S1–S2 stimulation protocol, only applied in voltage-clamp mode, was used. Fig. 3A demonstrates representative examples of membrane currents and corresponding $[\text{Ca}^{2+}]_i$ transients from the cytosol in response to S1 and S2 voltage stimuli. Again, in the end of experiment each cell was exposed to TS containing 10 mmol/l caffeine to estimate total SR Ca^{2+} content. All chemicals, unless otherwise specified, were obtained from Sigma (St. Louis, MO).

2.4. Measurements of $\text{Ca}_v1.2$ current

For measurements of $\text{Ca}_v1.2$ current, freshly isolated murine ventricular myocytes were whole-cell patched in Tyrode's solution and then solution was changed to K^+ -free solution (described above) containing either 2 mM CaCl_2 or 2mM BaCl_2 . In all experiments, myocytes were pre-incubated for 30 min in 50 μM Ryanodine + 10 μM Thapsigargin + 30 μM TTX to eliminate SR Ca^{2+} release and block sodium currents. The pipette solution contained (in mM): CsCl 110, MgCl_2 1, MgATP 5, cAMP 0.2; EGTA 14; Fluo-4 0.1, Hepes 20; pH=7.25 (CsOH). For experiments testing effect of calmodulin (CaM) on inactivation of I_{Ca} , CaM purified from bovine testes (Sigma) was added into pipette solution for a final concentration of 20 μM . All experiments were carried out at room temperature.

2.5. Western Blot

Ventricular cardiomyocytes obtained from wild-type and *Casq2* KO mice were homogenized and centrifuged at 100 g for 1 min at 4°C to eliminate the cellular debris. The supernatants were used for immunoblotting. The extracted proteins were separated on SDS-PAGE gels and transferred to polyvinylidene difluoride membranes. The membranes were blocked with 5% milk and incubated overnight with primary antibodies: Calmodulin (Cell signaling antibodies) and GAPDH (Ambion). Specific bands were detected using Pierce ECL protein detection system. Western blot analyses were performed using ImageJ software (NIH).

2.6. Statistical analysis

Differences between groups were assessed using a one-way analysis of variance (ANOVA). If statistically significant differences were found, individual groups were compared with

Student's two-sided *t* test. Results were considered statistically significant if the *P* value was <0.05. Unless otherwise indicated, results are expressed as arithmetic means \pm SE.

3. Results

3.1. Refractoriness of SR Ca^{2+} release is eliminated in ventricular myocytes lacking Casq2

Previous studies have shown that ventricular myocytes isolated from Casq2 KO mice exhibit elevated rates of premature spontaneous Ca^{2+} releases, delayed after depolarizations and triggered beats, and catecholamine-induced ventricular arrhythmias *in vivo* [21, 22]. We hypothesized that the arrhythmogenic potential of loss of Casq2 may be related to how quickly a secondary Ca^{2+} release can be elicited in cardiac myocyte. To investigate this hypothesis, we compared refractoriness of SR Ca^{2+} release in intact ventricular myocytes from WT and Casq2 KO mice using a field stimulation protocol (Fig. 2A). Under these conditions, myocytes from WT mice exhibit robust time-dependent refractoriness of Ca^{2+} release from the SR, i.e., the cytosolic Ca^{2+} transients in response to premature S2 stimuli were significantly smaller compared to the transients elicited during regular S1 pacing, especially at the shortest S1–S2 interval (Fig. 2B). Unlike WT, myocytes from Casq2 KO animals exhibited near complete absence of SR Ca^{2+} release refractoriness, even at very short S1–S2 coupling intervals (Fig. 2C).

Average restitution curves were plotted for each group (Fig. 2D), demonstrating an almost complete lack of SR Ca^{2+} release refractoriness in Casq2 KO myocytes. At the same time, SR Ca^{2+} content, estimated by the amplitude of Ca^{2+} transient as response to rapid application of caffeine (10 mM/L), was similar for both models (Fig. 2E). Our results indicate that Casq2 protein is responsible for SR Ca^{2+} refractoriness observed in isolated ventricular myocytes. Our data are in agreement with our previous report, where dramatic acceleration of Ca^{2+} release recovery was found at the whole heart level [1].

3.2. Accelerated recovery of $\text{Ca}_v1.2$ current contributes to the loss of SR Ca^{2+} release refractoriness in Casq2 KO myocytes

There are several factors that may contribute to the refractoriness of SR Ca^{2+} release in cardiac muscle. Since $\text{Ca}_v1.2$ current serves as the trigger for Ca^{2+} release from the SR during the cardiac action potential, refractoriness of $\text{Ca}_v1.2$ channels can be one of potential contributors to SR Ca^{2+} release refractoriness. To test this hypothesis, we next used an experimental protocol in which voltage clamp was used instead of field stimulation (Fig. 3A). $\text{Ca}_v1.2$ tail currents were used to activate Ca^{2+} release from the SR. This approach allows maintaining the Ca^{2+} current trigger essentially constant and hence eliminating possible refractoriness of $\text{Ca}_v1.2$ channels. Fig. 3B and C demonstrate representative recordings from voltage-clamped WT and Casq2 KO myocytes in response to the S1–S2 protocol shown above. Comparison of respective Ca^{2+} transient records from two approaches (field stimulation vs. voltage clamp) demonstrates the importance of $\text{Ca}_v1.2$ refractoriness for SR Ca^{2+} release, because refractoriness of SR Ca^{2+} release was accelerated substantially in voltage-clamped compared to field-stimulated cells for both WT and Casq2 KO myocytes.

Next, we compared the restitution kinetics of $\text{Ca}_v1.2$ currents in WT vs Casq2 KO myocytes (Fig. 4 A). Myocytes were pre-incubated with ryanodine (50 μM) and thapsigargin (10 μM) for 30 min to eliminate SR Ca^{2+} release. 200 μM cAMP was present in the pipette solution to fully phosphorylate the channels and to model conditions of adrenergic stimulation under which CPVT-related arrhythmias usually occur. Both groups had decreased I_{Ca} at short S1–S2 intervals, but surprisingly, I_{Ca} recovered significantly faster in Casq2 KO vs WT myocytes. At the same time, current-voltage relationships were not significantly different between the two groups (Fig. 4 B). Thus, recovery of $\text{Ca}_v1.2$ in mice lacking Casq2 is accelerated and could contribute to loss of SR Ca^{2+} release refractoriness in this model.

3.3. Ca^{2+} -dependent inactivation of $\text{Ca}_v1.2$ to cytosolic Ca^{2+} is suppressed in Casq2 KO myocytes

$\text{Ca}_v1.2$ channels exhibit both voltage- and Ca^{2+} -dependent inactivation [23, 24]. A plausible explanation for the accelerated recovery of I_{Ca} in Casq2 KO myocytes is that $\text{Ca}_v1.2$ channel inactivation is impaired. Therefore, we next investigated the rate of decay of I_{Ca} using a longer depolarizing step of 200 ms. The declining phase of I_{Ca} (=inactivation) was well fitted by a single-exponential function. The rate of inactivation was substantially slower in Casq2 KO myocytes ($\tau=93\pm11$ ms, $n=10$) compared to WT ($\tau=45\pm4$ ms, $n=10$, $p<0.005$), as shown in Fig. 5A. To distinguish between voltage- and Ca^{2+} -dependent inactivation, we next replaced Ca^{2+} in the external solution with equimolar Ba^{2+} . Ba^{2+} currents are nearly insensitive to Ba^{2+} -dependent inactivation of $\text{Ca}_v1.2$ channels [25]. Consequently, inactivation of I_{Ba} was much slower than that of I_{Ca} (compare Fig. 5A and 5B). Importantly, the difference in τ between WT and Casq2 KO myocytes was eliminated (WT: $\tau=145\pm19$ ms, Casq2 KO: $\tau=145\pm20$ ms, $n=10$ for each group). Moreover, substituting Ba^{2+} for Ca^{2+} also abolished the differences in the $\text{Ca}_v1.2$ current restitution curves in Casq2 KO and WT myocytes (Fig. 5C). Taken together, these results indicate that Ca^{2+} -dependent inactivation of $\text{Ca}_v1.2$ is defective in Casq2 KO myocytes, which is responsible for the difference between $\text{Ca}_v1.2$ current restitution curves of WT and Casq2 KO myocytes.

3.4. Apo-Calmodulin rescues the inactivation defect of $\text{Ca}_v1.2$ current and partially recovers refractoriness of SR Ca^{2+} release in Casq2 KO myocytes

The Ca^{2+} -free form of CaM (apo-CaM) is tightly bound to the C-terminus of $\text{Ca}_v1.2$ channels and serves as Ca^{2+} sensor for Ca^{2+} -dependent inactivation [26, 27]. To test if CaM-dependent regulation of $\text{Ca}_v1.2$ channels was altered, we added apo-CaM (20 μM) to the pipette solution and repeated the I_{Ca} measurements. Apo-CaM significantly accelerated inactivation of I_{Ca} in Casq2 KO myocytes (Fig. 6A), rendering the I_{Ca} inactivation kinetics almost identical to that of WT myocytes (Casq2 KO + CaM: $\tau=46\pm3$ ms, $n=7$, vs. WT: $\tau=45\pm4$ ms for WT, $n=10$, $p=0.8$). In contrast, adding CaM had no significant effect on the rate of I_{Ca} inactivation in WT myocytes (Fig. 6B). Fig. 6C and Table 1 compare tau values for all the experiments. Addition of CaM also normalized the I_{Ca} restitution curve of Casq2 KO (Fig. 6D). At the same time, the total amount of CaM protein was not different between WT and Casq2 KO myocytes (Supplemental Fig. 1).

Finally, we studied the effect of apo-CaM on refractoriness of SR Ca^{2+} release in Casq2 KO and WT myocytes. For these experiments, we used the S1–S2 protocol in voltage-clamp

mode, similar to that used in Fig. 3, but L-type Ca^{2+} currents were elicited by 30-ms depolarizing step to 0mV from holding potential of -70 mV rather than using tail currents to activate SR Ca^{2+} release (to allow physiological Ca^{2+} -induced inactivation of L-type Ca^{2+} channels). AIP ($1\ \mu\text{M}$) was added to intracellular solution to prevent CaMKII activation by CaM, because activated CaMKII will phosphorylate RyR2 and could accelerate SR Ca^{2+} release refractoriness [28]. Under these conditions, addition of CaM resulted in a partial restoration of SR Ca^{2+} release refractoriness in Casq2 KO myocytes (Fig. 7). Ca^{2+} transient decay during the S1 beat was significantly slower in Casq2 KO compared to WT myocytes, which was completely normalized by adding CaM in Casq2KO myocytes (WT + CaM: $\tau=226\pm 25$ ms; Casq2 KO + CaM: $\tau=201\pm 11$ ms; Casq2 KO: $\tau=425\pm 78$ ms, $p<0.05$ vs. both CaM groups; $n=9-14$ cells per group). This result suggests that impaired CaM-dependent $\text{Ca}_v1.2$ inactivation contributes to excess Ca^{2+} influx in Casq2 KO myocytes. Furthermore, because CaM addition completely normalizes LTCC Ca^{2+} refractoriness in Casq2 KO myocytes but has no effect on WT myocytes (Fig. 6), the results of Fig. 7D also indicate that the $\text{Ca}_v1.2$ inactivation defect is responsible for approximately 50% of the loss of Ca^{2+} release refractoriness found in Casq2 KO myocytes.

4. Discussion

4.1. Casq2 – a critical determinant for physiological SR Ca^{2+} release refractoriness

Structurally, the CRU of cardiac myocyte includes $\text{Ca}_v1.2$ channels located in the sarcolemma and juxtaposed RyR2 SR Ca^{2+} release channels in the junctional SR. RyR2 channels are associated with other SR proteins like triadin and junctin, and through them also with Casq2. During action potential, Ca^{2+} influx via $\text{Ca}_v1.2$ causes much bigger amount of Ca^{2+} being released from the SR. The amplitude of the resulting cytosolic Ca^{2+} transient depends on the diastolic interval between two stimuli (normally, the amplitude of the second Ca^{2+} release is lower when the diastolic interval is short – Fig. 2 and 3), a phenomenon described as Ca^{2+} release restitution. Release restitution is regulated and affected by number of different voltage-, time- and Ca^{2+} -dependent processes such as refractoriness (recovery from inactivation) of $\text{Ca}_v1.2$ channels, recovery of RyR2 channels and SR Ca^{2+} uptake kinetics [29]. Two previous studies have reported that accelerated restitution of SR Ca^{2+} release is associated with human arrhythmia diseases: Our earlier report demonstrating accelerated Ca^{2+} transient recovery in intact Casq2 KO hearts [1], which are a model of a rare genetic form of catecholaminergic polymorphic ventricular tachycardia (CPVT, discussed in more detail below), and a study in the canine model of post-myocardial infarction ventricular fibrillation [30]. The later study by Belevych et al. demonstrated that acceleration of Ca^{2+} release restitution of post-MI myocytes was attributable to RyR2 phosphorylation and oxidation. In current study, we investigate in more detail the role that Casq2 plays in Ca^{2+} release restitution in isolated ventricular myocytes, and also test $\text{Ca}_v1.2$ as one of potential contributors to the restitution of SR Ca^{2+} release. We show that not only is Casq2 a critical determinant for the restitution of Ca^{2+} release from the SR but also recovery of I_{Ca} is accelerated in mice lacking Casq2 and this, along with loss of intra-SR Ca^{2+} buffering and altered sensitivity of RyR2 to luminal Ca^{2+} [1], contributes to the loss of SR Ca^{2+} release restitution in Casq2 KO mice. We further demonstrate that accelerated recovery from inactivation of I_{Ca} in Casq2 KO model is due to impaired sensitivity of

Ca_v1.2 channel to intracellular Ca²⁺ and this altered Ca²⁺ sensitivity can be recovered by application of excess apo-CaM.

4.2. SR Ca²⁺ release refractoriness and ventricular arrhythmia

CPVT is a highly lethal form of inherited arrhythmogenic disease characterized by adrenergically mediated polymorphic ventricular tachycardia caused by mutations in genes that encode CRU-composing proteins [31, 32]. The most common form is caused by mutations in RyR2 [31, 33]. Much less common, CPVT can be caused by mutations in Casq2 [32, 34], triadin or calmodulin [35]. Unlike CPVT caused by RyR2 mutations, CPVT linked to Casq2 mutations is usually autosomal recessive, with complete absence of Casq2 predicted for patients homozygous for Casq2 nonsense mutations. Despite this fact, they display surprisingly normal cardiac contractile function [34]. *Ex vivo*, isolated ventricular myocytes from Casq2 KO mice display normal SR Ca²⁺ release and contractile function under basal conditions, but exposure to catecholamines causes increased diastolic SR Ca²⁺ leak, resulting in premature spontaneous SR Ca²⁺ releases and triggered beats [21], which are considered major hallmarks of CPVT phenotype and a culprit for arrhythmia onset *in vivo*. Even modest reduction in Casq2 is able to increase diastolic SR Ca²⁺ leak and cause spontaneous SR Ca²⁺ release [22]. Unlike Casq2 KO [21], heterozygous Casq2 +/- mice have normal level of all the other CRU-composing SR proteins (namely, triadin-1 and junctin), which makes Casq2 the prime candidate responsible for arrhythmogenic phenotype in this model. On the other hand, triadin is crucially important for maintaining the structural and functional integrity of the cardiac CRU, and its ablation reduces SR Ca²⁺ release and impairs negative feedback of SR Ca²⁺ release on Ca_v1.2 currents [36]. Recently, junctin itself, without (or in addition to) involvement of Casq2, was reported as one of important modulators of RyR2 sensitivity to luminal Ca²⁺ [37].

Studies have shown that altered Ca²⁺ handling and, in particular, premature spontaneous Ca²⁺ releases from the SR serve as a culprit for CPVT [38]. Our data demonstrate that in Casq2 KO murine ventricular myocytes refractoriness of Ca²⁺ release from the SR is accelerated compared to myocytes from WT animals, and this acceleration is not accompanied by alterations in SR Ca²⁺ content (Fig. 2 E). These results confirm on a cellular level the accelerated recovery of Ca²⁺ transients previously reported from the same mouse model on a whole-heart level [1]. Unchanged SR Ca²⁺ content despite dramatic loss of SR Ca²⁺ buffering might be explained by substantial increase in SR volume of Casq2 KO myocytes, which effectively compensates for the absence of Casq2 [21].

4.3. Accelerated Ca_v1.2 recovery from inactivation importantly contributes to loss of Ca²⁺ release refractoriness in Casq2 KO myocytes

Our study shows that, surprisingly, recovery from inactivation of Ca_v1.2 current is accelerated in Casq2 KO mouse model (Fig. 4A), providing enhanced triggering for CICR during premature stimulation. Along with faster rise in free intra-SR Ca²⁺ [1], this creates a potential for much more massive, compared to WT, SR Ca²⁺ release at very short S1–S2 intervals. What are the possible mechanisms for the accelerated recovery of Ca_v1.2 currents produced by ablation of Casq2? We found no difference in Ca_v1.2 current density (Fig. 4B), hence, it is unlikely that the difference in recovery from inactivation is due to changes in

$\text{Ca}_v1.2$ expression level. On the other hand, substituting Ca^{2+} with Ba^{2+} as charge carrier abolished the differences in $\text{Ca}_v1.2$ current inactivation and restitution (Fig. 5), suggesting that difference in Ca^{2+} -dependent inactivation (CDI) of the channel is the most likely culprit.

We reported previously that inactivation of $\text{Ca}_v1.2$ is also impaired in ventricular myocytes lacking triadin [36]. Since expression of triadin is decreased in Casq2 KO mice [21], one could suggest that loss of triadin contributed to the accelerated recovery of $\text{Ca}_v1.2$ from inactivation. However, in triadin null myocytes, the difference in inactivation rate of $\text{Ca}_v1.2$ current was abolished by blocking RyR2 Ca^{2+} release with ryanodine [36]. Since all our $\text{Ca}_v1.2$ measurements in Casq2 KO myocytes were done in presence of ryanodine and thapsigargin, it seems unlikely that decrease in triadin can explain the accelerated recovery from inactivation of $\text{Ca}_v1.2$ in Casq2 KO myocytes.

4.4. Defective regulation by CaM mediates accelerated recovery of $\text{Ca}_v1.2$ in Casq2 KO myocytes

Studies have shown that Ca^{2+} binding to CaM is responsible for CDI [26, 27]. Acute overexpression of engineered, Ca^{2+} -insensitive mutant CaM in rat ventricular myocytes can efficiently displace endogenous CaM on native $\text{Ca}_v1.2$ channels, resulting in strong inhibition of CDI without perturbation of other gating functions, such as voltage-dependent inactivation [27]. Since apo-CaM, the Ca^{2+} -free form of CaM pre-associates with target molecules [39] such as L-type Ca^{2+} channels, whose function is subsequently modulated when an elevation of Ca^{2+} calcifies the associated CaM [26, 40, 41], any reduced availability of apo-CaM could contribute to impaired CDI, as has been shown experimentally for $\text{Ca}_v1.3$, where lack of pre-associated apo-CaM rendered $\text{Ca}_v1.3$ channels incapable of CDI while still being able to open normally [42]. Since there is extensive competition for CaM in the intracellular milieu (only one out of 100 is free), it seems possible that due to the increased SR Ca^{2+} leak and elevated diastolic Ca^{2+} in Casq2 KO myocytes [21, 22] available apo-CaM is reduced. Moreover, in *Xenopus* oocytes, injection of excess purified CaM protein was able to reduce dramatically the inhibitory effect of mutant, Ca^{2+} -insensitive CaM_{1234} on CDI of $\text{Ca}_v1.2$ channels [43]. This effect presumably is based on the competition for the same binding site located in the proximal C terminus of the α_{1C} subunit of $\text{Ca}_v1.2$ that both “normal” CaM and mutant CaM_{1234} share. In brain, there is another Ca^{2+} sensor protein known to have overlapping binding sites with CaM in pCT of $\text{Ca}_v1.2$ – Ca-binding protein 1 (CaBP1) [43]. CaBP1 is structurally related to CaM but its effect on $\text{Ca}_v1.2$ is opposite to that of CaM: Addition of CaBP1 slows down CDI [44] and CaBP1 competes with CaM for aforementioned binding sites in $\text{Ca}_v1.2$ [43]. However, CaBP1 is not expressed in the heart [45], hence its involvement in attenuation of CDI in Casq2 KO ventricular myocytes seems doubtful. Another possibility would be that CaM protein expression is reduced in Casq2 KO myocytes. But our experiments show no difference in CaM protein between Casq2 KO and WT myocytes (suppl. Fig. 1).

4.5. Implication of defective $\text{Ca}_v1.2$ regulation by CaM for arrhythmogenesis

How could the impaired Ca^{2+} -dependent inactivation of $\text{Ca}_v1.2$ and faster recovery of Ca^{2+} current contribute to the arrhythmogenesis in Casq2 KO mice? The impaired Ca/CaM-

dependent inactivation of $\text{Ca}_v1.2$ will result in greater Ca^{2+} influx during each beat, leading to further Ca^{2+} loading of the myocytes especially during catecholaminergic stimulation, which, in turn, increases the probability of spontaneous diastolic Ca^{2+} releases. Premature spontaneous Ca^{2+} release from the SR is generally accepted as the culprit for CPVT [38, 48]. Interestingly, it was reported that Ca^{2+} channel blocker verapamil provides added benefit in CPVT patients when administered along with β -blockers [46, 47], a finding that is consistent with our hypothesis that enhanced Ca^{2+} influx via $\text{Ca}_v1.2$ contributes to excess myocyte Ca loading and arrhythmogenesis in Casq2 KO myocytes. Analogous to CPVT, increased SR Ca^{2+} leak and DADs have also been observed in animal models of heart failure [48, 49]. It is intriguing to speculate that impaired CaM dependent $\text{Ca}_v1.2$ may also contribute to arrhythmogenesis in heart failure and other heart diseases associated with increased SR Ca^{2+} leak, a hypothesis that should be tested in future studies.

One could argue that excess CaM used in our voltage clamp experiments can also inhibit RyR2 and in this way restore refractoriness of SR Ca^{2+} release. While CaM is a physiological inhibitor of RyR2, it binds with high affinity to RyR2 and the CaM inhibitory action on RyR2 is saturated at physiological free concentrations of 100nM. As such, excess CaM will not further inhibit RyR2 channels and hence is not expected to contribute to the normalization of Ca^{2+} release refractoriness.

5. Summary and Conclusions

In the presented study we investigated mechanisms responsible for SR Ca^{2+} release refractoriness in cardiac muscle. We find that gene-targeted ablation of Casq2 results in complete loss of SR Ca^{2+} release refractoriness (Fig. 2&3). Surprisingly, accelerated recovery of I_{Ca} (Fig. 4) also contributed to the loss of SR Ca^{2+} release restitution in mice lacking Casq2. We found that the faster recovery of I_{Ca} in Casq2 KO mice is due to impaired Ca^{2+} -dependent inactivation of $\text{Ca}_v1.2$ (Fig. 5), which could be reversed by excess apo-CaM (Fig. 6). Because excess CaM also partially restored release refractoriness in Casq2 KO myocytes (Fig. 7), these results suggest that impaired Ca^{2+} -CaM-dependent inactivation of $\text{Ca}_v1.2$ independently contributes to loss of SR Ca^{2+} release refractoriness in Casq2 KO mice. We conclude that impaired CaM-dependent $\text{Ca}_v1.2$ regulation may independently contribute to arrhythmogenesis in CPVT, a new concept that could also be relevant in other heart diseases (e.g. heart failure) associated with increased SR Ca^{2+} leak.

Supplementary Material

Refer to Web version on PubMed Central for supplementary material.

Acknowledgments

Funding

This work was partly supported by the United States National Institutes of Health [HL88635, HL71670 & HL108173 to B.C.K.]; by the American Heart Association [13IRG13680003 to B.C.K., 12POST12080080 to D.K.], and by the Australian National Health & Medical Research Council [APP1005974 to B.C.K.].

References

1. Korniyev D, Petrosky AD, Zepeda B, Ferreira M, Knollmann B, Escobar AL. Calsequestrin 2 deletion shortens the refractoriness of Ca^{2+} release and reduces rate-dependent Ca^{2+} -alternans in intact mouse hearts. *J Mol Cell Cardiol.* 2012; 52:21–31. [PubMed: 21983287]
2. Bers DM. Cardiac excitation-contraction coupling. *Nature.* 2002; 415:198–205. [PubMed: 11805843]
3. Belevych A, Kubalova Z, Terentyev D, Hamlin RL, Carnes CA, Gyorke S. Enhanced ryanodine receptor-mediated calcium leak determines reduced sarcoplasmic reticulum calcium content in chronic canine heart failure. *Biophys J.* 2007; 93:4083–4092. [PubMed: 17827226]
4. Kubalova Z, Terentyev D, Viatchenko-Karpinski S, Nishijima Y, Gyorke I, Terentyeva R, da Cunha DN, Sridhar A, Feldman DS, Hamlin RL, Carnes CA, Gyorke S. Abnormal intrastore calcium signaling in chronic heart failure. *Proc Natl Acad Sci U S A.* 2005; 102:14104–14109. [PubMed: 16172392]
5. Marx SO, Reiken S, Hisamatsu Y, Jayaraman T, Burkhardt D, Roseblat N, Marks AR. PKA phosphorylation dissociates FKBP12.6 from the calcium release channel (ryanodine receptor): defective regulation in failing hearts. *Cell.* 2000; 101:365–376. [PubMed: 10830164]
6. Wehrens XH, Lehman SE, Reiken S, Vest JA, Wronski A, Marks AR. Ryanodine receptor/calcium release channel PKA phosphorylation: a critical mediator of heart failure progression. *Proc Natl Acad Sci U S A.* 2006; 103:511–518. [PubMed: 16407108]
7. Plank DM, Yatani A, Ritsch H, Witt S, Glascock B, Lalli MJ, Periasamy M, Fiset C, Benkusky N, Valdivia HH, Sussman MA. Calcium dynamics in the failing heart: restoration by beta-adrenergic receptor blockade. *Am J Physiol Heart Circ Physiol.* 2003; 285:H305–315. [PubMed: 12649072]
8. Terracciano CM, Hardy J, Birks EJ, Khaghani A, Banner NR, Yacoub MH. Clinical recovery from end-stage heart failure using left-ventricular assist device and pharmacological therapy correlates with increased sarcoplasmic reticulum calcium content but not with regression of cellular hypertrophy. *Circulation.* 2004; 109:2263–2265. [PubMed: 15136495]
9. Jones LR, Cala SE. Biochemical evidence for functional heterogeneity of cardiac sarcoplasmic reticulum vesicles. *J Biol Chem.* 1981; 256:11809–11818. [PubMed: 6271762]
10. Cala SE, Jones LR. Rapid purification of calsequestrin from cardiac and skeletal muscle sarcoplasmic reticulum vesicles by Ca^{2+} -dependent elution from phenyl-sepharose. *J Biol Chem.* 1983; 258:11932–11936. [PubMed: 6619149]
11. Campbell KP, MacLennan DH, Jorgensen AO, Mintzer MC. Purification and characterization of calsequestrin from canine cardiac sarcoplasmic reticulum and identification of the 53,000 dalton glycoprotein. *J Biol Chem.* 1983; 258:1197–1204. [PubMed: 6337133]
12. Kobayashi YM, Jones LR. Identification of triadin 1 as the predominant triadin isoform expressed in mammalian myocardium. *J Biol Chem.* 1999; 274:28660–28668. [PubMed: 10497235]
13. Jones LR, Zhang L, Sanborn K, Jorgensen AO, Kelley J. Purification, primary structure, and immunological characterization of the 26-kDa calsequestrin binding protein (junctin) from cardiac junctional sarcoplasmic reticulum. *J Biol Chem.* 1995; 270:30787–30796. [PubMed: 8530521]
14. Zhang L, Kelley J, Schmeisser G, Kobayashi YM, Jones LR. Complex formation between junctin, triadin, calsequestrin, and the ryanodine receptor. Proteins of the cardiac junctional sarcoplasmic reticulum membrane. *J Biol Chem.* 1997; 272:23389–23397. [PubMed: 9287354]
15. Endo M, Tanaka M, Ogawa Y. Calcium induced release of calcium from the sarcoplasmic reticulum of skinned skeletal muscle fibres. *Nature.* 1970; 228:34–36. [PubMed: 5456208]
16. Fabiato A, Fabiato F. Contractions induced by a calcium-triggered release of calcium from the sarcoplasmic reticulum of single skinned cardiac cells. *J Physiol.* 1975; 249:469–495. [PubMed: 809571]
17. Flucher BE, Franzini-Armstrong C. Formation of junctions involved in excitation-contraction coupling in skeletal and cardiac muscle. *Proc Natl Acad Sci U S A.* 1996; 93:8101–8106. [PubMed: 8755610]
18. Bers, DM. Excitation-contraction coupling and cardiac contractile force. Dordrecht; Boston: Kluwer Academic Publishers; 2001.

19. Ikemoto N, Ronjat M, Meszaros LG, Koshita M. Postulated role of calsequestrin in the regulation of calcium release from sarcoplasmic reticulum. *Biochemistry*. 1989; 28:6764–6771. [PubMed: 2790030]
20. Gyorke I, Hester N, Jones LR, Gyorke S. The role of calsequestrin, triadin, and junctin in conferring cardiac ryanodine receptor responsiveness to luminal calcium. *Biophys J*. 2004; 86:2121–2128. [PubMed: 15041652]
21. Knollmann BC, Chopra N, Hlaing T, Akin B, Yang T, Ettensohn K, Knollmann BE, Horton KD, Weissman NJ, Holinstat I, Zhang W, Roden DM, Jones LR, Franzini-Armstrong C, Pfeifer K. Casq2 deletion causes sarcoplasmic reticulum volume increase, premature Ca²⁺ release, and catecholaminergic polymorphic ventricular tachycardia. *J Clin Invest*. 2006; 116:2510–2520. [PubMed: 16932808]
22. Chopra N, Kannankeril PJ, Yang T, Hlaing T, Holinstat I, Ettensohn K, Pfeifer K, Akin B, Jones LR, Franzini-Armstrong C, Knollmann BC. Modest reductions of cardiac calsequestrin increase sarcoplasmic reticulum Ca²⁺ leak independent of luminal Ca²⁺ and trigger ventricular arrhythmias in mice. *Circ Res*. 2007; 101:617–626. [PubMed: 17656677]
23. Kass RS, Sanguinetti MC. Inactivation of calcium channel current in the calf cardiac Purkinje fiber. Evidence for voltage- and calcium-mediated mechanisms. *J Gen Physiol*. 1984; 84:705–726. [PubMed: 6096480]
24. Lee KS, Marban E, Tsien RW. Inactivation of calcium channels in mammalian heart cells: joint dependence on membrane potential and intracellular calcium. *J Physiol*. 1985; 364:395–411. [PubMed: 2411919]
25. Ferreira G, Yi J, Rios E, Shirokov R. Ion-dependent inactivation of barium current through L-type calcium channels. *J Gen Physiol*. 1997; 109:449–461. [PubMed: 9101404]
26. Peterson BZ, DeMaria CD, Adelman JP, Yue DT. Calmodulin is the Ca²⁺ sensor for Ca²⁺-dependent inactivation of L-type calcium channels. *Neuron*. 1999; 22:549–558. [PubMed: 10197534]
27. Alseikhan BA, DeMaria CD, Colecraft HM, Yue DT. Engineered calmodulins reveal the unexpected eminence of Ca²⁺ channel inactivation in controlling heart excitation. *Proc Natl Acad Sci U S A*. 2002; 99:17185–17190. [PubMed: 12486220]
28. Polakova E, Illaste A, Niggli E, Sobie EA. Maximal acceleration of Ca²⁺ release refractoriness by beta-adrenergic stimulation requires dual activation of kinases PKA and CaMKII in mouse ventricular myocytes. *J Physiol*. 2014
29. Liu OZ, Lederer WJ, Sobie EA. Does the Goldilocks Principle apply to calcium release restitution in heart cells? *J Mol Cell Cardiol*. 52:3–6. [PubMed: 22056316]
30. Belevych AE, Terentyev D, Terentyeva R, Ito HT, Gyorke I, Bonilla IM, Carnes CA, Billman GE, Gyorke S. Shortened Ca²⁺ signaling refractoriness underlies cellular arrhythmogenesis in a postinfarction model of sudden cardiac death. *Circ Res*. 2012; 110:569–577. [PubMed: 22223353]
31. Priori SG, Napolitano C, Tiso N, Memmi M, Vignati G, Bloise R, Sorrentino V, Danieli GA. Mutations in the cardiac ryanodine receptor gene (hRyR2) underlie catecholaminergic polymorphic ventricular tachycardia. *Circulation*. 2001; 103:196–200. [PubMed: 11208676]
32. Lahat H, Pras E, Olender T, Avidan N, Ben-Asher E, Man O, Levy-Nissenbaum E, Khoury A, Lorber A, Goldman B, Lancet D, Eldar M. A missense mutation in a highly conserved region of CASQ2 is associated with autosomal recessive catecholamine-induced polymorphic ventricular tachycardia in Bedouin families from Israel. *Am J Hum Genet*. 2001; 69:1378–1384. [PubMed: 11704930]
33. Priori SG, Napolitano C, Memmi M, Colombi B, Drago F, Gasparini M, DeSimone L, Coltorti F, Bloise R, Keegan R, Cruz Filho FE, Vignati G, Benatar A, DeLogu A. Clinical and molecular characterization of patients with catecholaminergic polymorphic ventricular tachycardia. *Circulation*. 2002; 106:69–74. [PubMed: 12093772]
34. Postma AV, Denjoy I, Hoomtje TM, Lupoglazoff JM, Da Costa A, Sebillon P, Mannens MM, Wilde AA, Guicheney P. Absence of calsequestrin 2 causes severe forms of catecholaminergic polymorphic ventricular tachycardia. *Circ Res*. 2002; 91:e21–26. [PubMed: 12386154]
35. Nyegaard M, Overgaard MT, Sondergaard MT, Vranas M, Behr ER, Hildebrandt LL, Lund J, Hedley PL, Camm AJ, Wettrell G, Fosdal I, Christiansen M, Borglum AD. Mutations in

- calmodulin cause ventricular tachycardia and sudden cardiac death. *Am J Hum Genet.* 2012; 91:703–712. [PubMed: 23040497]
36. Chopra N, Yang T, Asghari P, Moore ED, Huke S, Akin B, Cattolica RA, Perez CF, Hlaing T, Knollmann-Ritschel BE, Jones LR, Pessah IN, Allen PD, Franzini-Armstrong C, Knollmann BC. Ablation of triadin causes loss of cardiac Ca²⁺ release units, impaired excitation-contraction coupling, and cardiac arrhythmias. *Proc Natl Acad Sci U S A.* 2009; 106:7636–7641. [PubMed: 19383796]
 37. Altschaffl BA, Arvanitis DA, Fuentes O, Yuan Q, Kranias EG, Valdivia HH. Dual role of junctin in the regulation of ryanodine receptors and calcium release in cardiac ventricular myocytes. *J Physiol.* 589:6063–6080. [PubMed: 22025663]
 38. Watanabe H, Knollmann BC. Mechanism underlying catecholaminergic polymorphic ventricular tachycardia and approaches to therapy. *J Electrocardiol.* 44:650–655. [PubMed: 21872879]
 39. Jurado LA, Chockalingam PS, Jarrett HW. Apocalmodulin. *Physiol Rev.* 1999; 79:661–682. [PubMed: 10390515]
 40. Erickson MG, Alseikhan BA, Peterson BZ, Yue DT. Preassociation of calmodulin with voltage-gated Ca(2+) channels revealed by FRET in single living cells. *Neuron.* 2001; 31:973–985. [PubMed: 11580897]
 41. Zuhlke RD, Pitt GS, Deisseroth K, Tsien RW, Reuter H. Calmodulin supports both inactivation and facilitation of L-type calcium channels. *Nature.* 1999; 399:159–162. [PubMed: 10335846]
 42. Ben Johny M, Yang PS, Bazzazi H, Yue DT. Dynamic switching of calmodulin interactions underlies Ca²⁺ regulation of CaV1.3 channels. *Nat Commun.* 4:1717. [PubMed: 23591884]
 43. Oz S, Benmocha A, Sasson Y, Sachyani D, Almagor L, Lee A, Hirsch JA, Dascal N. Competitive and non-competitive regulation of calcium-dependent inactivation in CaV1.2 L-type Ca²⁺ channels by calmodulin and Ca²⁺-binding protein 1. *J Biol Chem.* 288:12680–12691. [PubMed: 23530039]
 44. Zhou H, Yu K, McCoy KL, Lee A. Molecular mechanism for divergent regulation of Cav1.2 Ca²⁺ channels by calmodulin and Ca²⁺-binding protein-1. *J Biol Chem.* 2005; 280:29612–29619. [PubMed: 15980432]
 45. Haeseleer F, Sokal I, Verlinde CL, Erdjument-Bromage H, Tempst P, Pronin AN, Benovic JL, Fariss RN, Palczewski K. Five members of a novel Ca(2+)-binding protein (CABP) subfamily with similarity to calmodulin. *J Biol Chem.* 2000; 275:1247–1260. [PubMed: 10625670]
 46. Swan H, Laitinen P, Kontula K, Toivonen L. Calcium channel antagonism reduces exercise-induced ventricular arrhythmias in catecholaminergic polymorphic ventricular tachycardia patients with RyR2 mutations. *J Cardiovasc Electrophysiol.* 2005; 16:162–166. [PubMed: 15720454]
 47. Rosso R, Kalman JM, Rogowski O, Diamant S, Birger A, Biner S, Belhassen B, Viskin S. Calcium channel blockers and beta-blockers versus beta-blockers alone for preventing exercise-induced arrhythmias in catecholaminergic polymorphic ventricular tachycardia. *Heart Rhythm.* 2007; 4:1149–1154. [PubMed: 17765612]
 48. Ai X, Curran JW, Shannon TR, Bers DM, Pogwizd SM. Ca²⁺/calmodulin-dependent protein kinase modulates cardiac ryanodine receptor phosphorylation and sarcoplasmic reticulum Ca²⁺ leak in heart failure. *Circ Res.* 2005; 97:1314–1322. [PubMed: 16269653]
 49. van Oort RJ, McCauley MD, Dixit SS, Pereira L, Yang Y, Respress JL, Wang Q, De Almeida AC, Skapura DG, Anderson ME, Bers DM, Wehrens XH. Ryanodine receptor phosphorylation by calcium/calmodulin-dependent protein kinase II promotes life-threatening ventricular arrhythmias in mice with heart failure. *Circulation.* 2010; 122:2669–2679. [PubMed: 21098440]

Highlights

- Ablation of Casq2 results in complete loss of SR Ca^{2+} release restitution.
- Accelerated recovery of I_{Ca} contributes to this phenomenon in Casq2 KO mice.
- I_{Ca} recovers faster in Casq2 KO cells due to impaired Ca^{2+} -dependent inactivation of $\text{Ca}_v1.2$.
- Accelerated recovery of I_{Ca} in Casq2 KO mice can be reversed by excess apo-CaM.
- Excess apo-CaM partially restores SR Ca^{2+} release restitution in Casq2 KO myocytes.

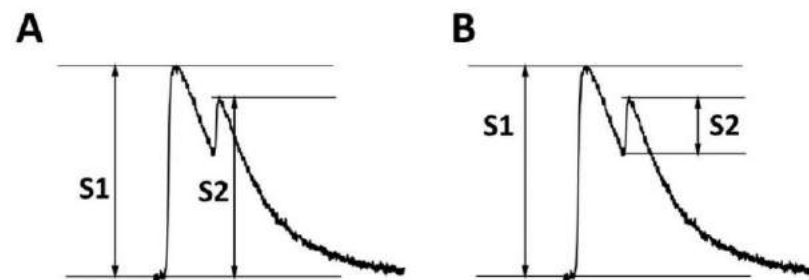


Fig. 1. Calculation of S2 amplitude

To calculate the restitution curve of Ca^{2+} release, we included the Ca^{2+} that still remains in the cytosol for measuring the amplitude of the premature S2 beat (**A**), because that Ca^{2+} has not been taken up into the SR and hence cannot be released. Previous approaches [1] measured S2 as the height of the premature S2 (**B**), which results in a restitution curve that mostly reflects the rate of SR Ca^{2+} uptake, and not the intrinsic refractoriness of the RyR2 Ca^{2+} release channel complex.

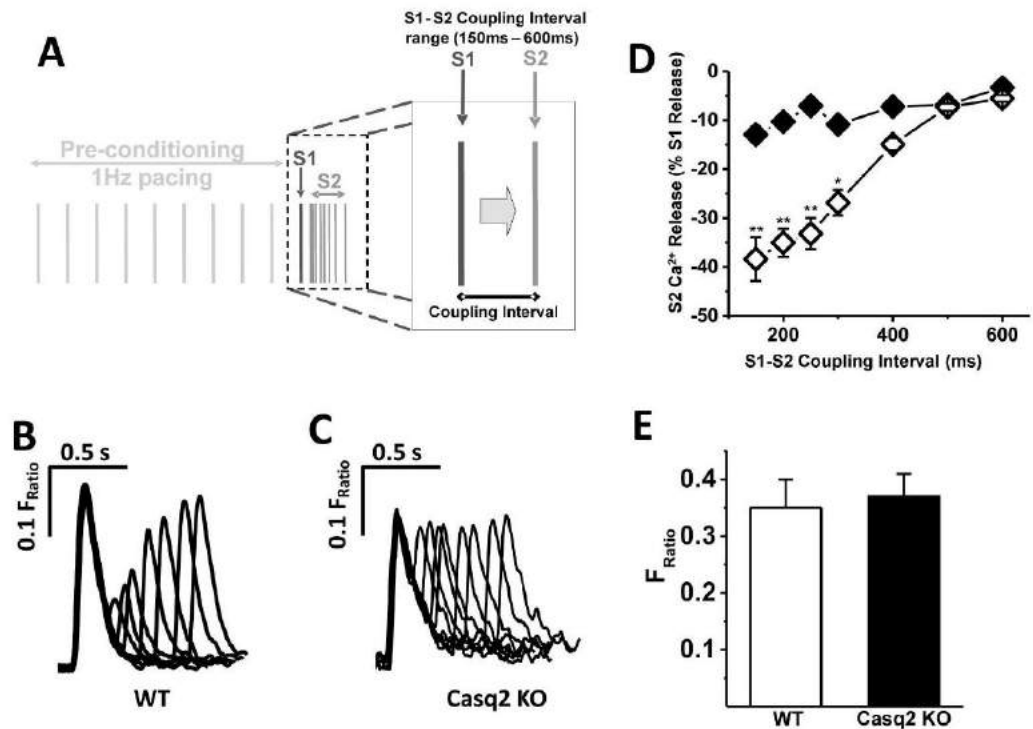


Fig. 2. Refractoriness of SR Ca^{2+} release in field-stimulated myocytes

A - Experimental protocol used to assess refractoriness of SR Ca^{2+} release in a cytosol of murine LV myocytes using electric field stimulation. Premature extra stimuli (S2) were applied at successively shorter S1-S2 coupling intervals following a 1 Hz conditioning train (S1 stimuli). **B** and **C** - representative examples of Ca^{2+} transient recorded in WT and Casq2 KO myocytes, respectively in response to the S1-S2 protocol shown in **A**. Note the complete loss of Ca^{2+} release refractoriness in the Casq2 KO myocyte. **D** - Average S2 Ca^{2+} release fraction plotted as a function of varying the S1-S2 coupling interval (n=7 for WT, open diamonds; n=6 for Casq2 KO, black diamonds; ** $P < 0.005$, * $P < 0.05$). **E** - SR Ca^{2+} content measured by rapid caffeine application (n = 5–6 myocytes per group).

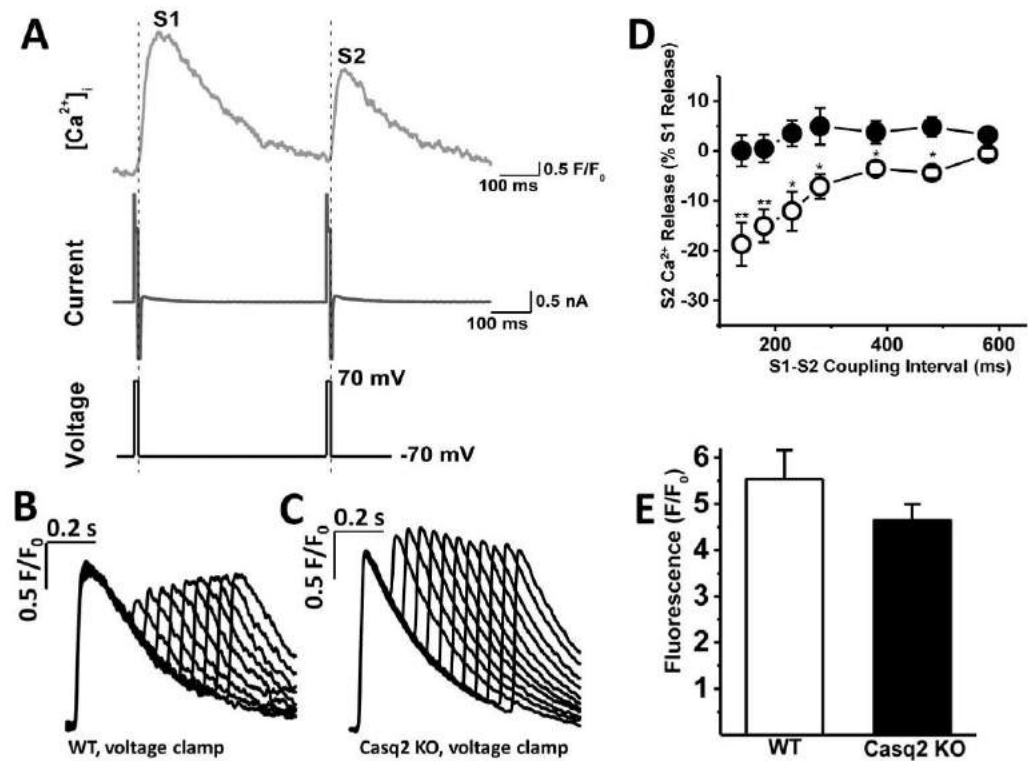


Fig. 3. Refractoriness of SR Ca²⁺ release in voltage-clamped myocytes

A –voltage clamp protocol (bottom trace), corresponding membrane currents (middle trace) and $[Ca^{2+}]_i$ (top trace) during an S1 and S2 stimuli used to assess Ca²⁺ release refractoriness in voltage-clamped myocytes. To maintain constant Ca²⁺ trigger, SR Ca²⁺ release was activated with I_{Ca} tail currents that elicited maximal Ca²⁺ release during the S1 train. **B** and **C** - representative examples of Ca²⁺ transients recorded in WT and Casq2 KO myocytes, respectively, in response to the S1–S2 voltage clamp protocol shown in **A**. **D** - S2 Ca²⁺ release fraction changes as a result of varying the S1–S2 coupling interval (n=12 for WT, open circles and Casq2 KO, black circles; ** $P < 0.005$, * $P < 0.05$). **E** – SR Ca²⁺ content measured by rapid caffeine application (n = 8 myocytes per group).

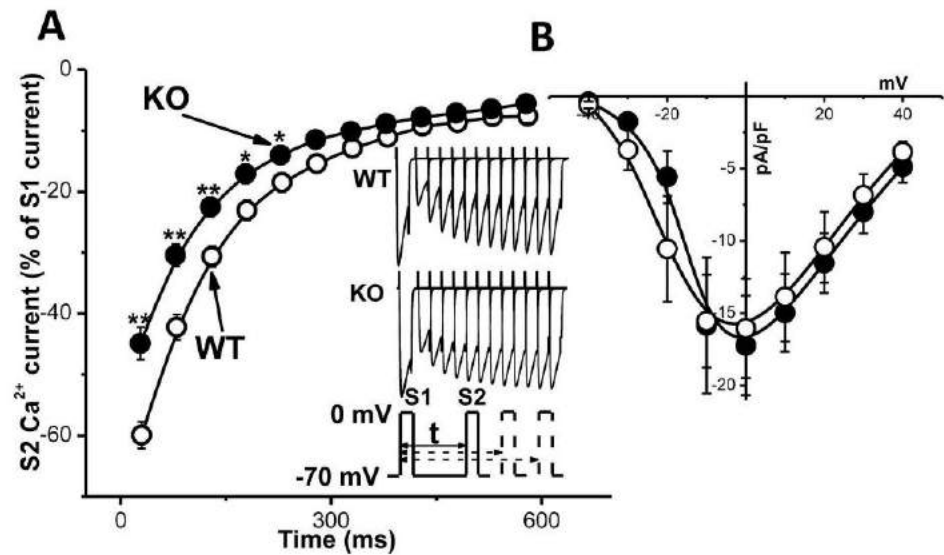


Fig. 4. Restitution of $\text{Ca}_v1.2$ current is accelerated in Casq2 KO myocytes

A – Average $\text{Ca}_v1.2$ current restitution curve for WT (white circles, $n=12$) and Casq2 KO (black circles, $n=12$) myocytes. Inset shows representative examples of $\text{Ca}_v1.2$ current records for each group and the voltage protocol. $\text{Ca}_v1.2$ currents were elicited by a 50-ms depolarizing steps to 0 mV from holding potential -70 mV. Myocytes were pre-incubated in 50 μM Ryanodine + 10 μM Thapsigargin + 30 μM TTX for 30 min to deplete the SR and eliminate I_{Na} . $^{***}P < 0.005$, $^{*}P < 0.05$. **B** – current-voltage relationships of $\text{Ca}_v1.2$ peak currents of WT (white circles, $n=6$) and Casq2 KO (black circles, $n=6$). There was no significant difference in voltage dependence or $\text{Ca}_v1.2$ current density between the two mouse models.

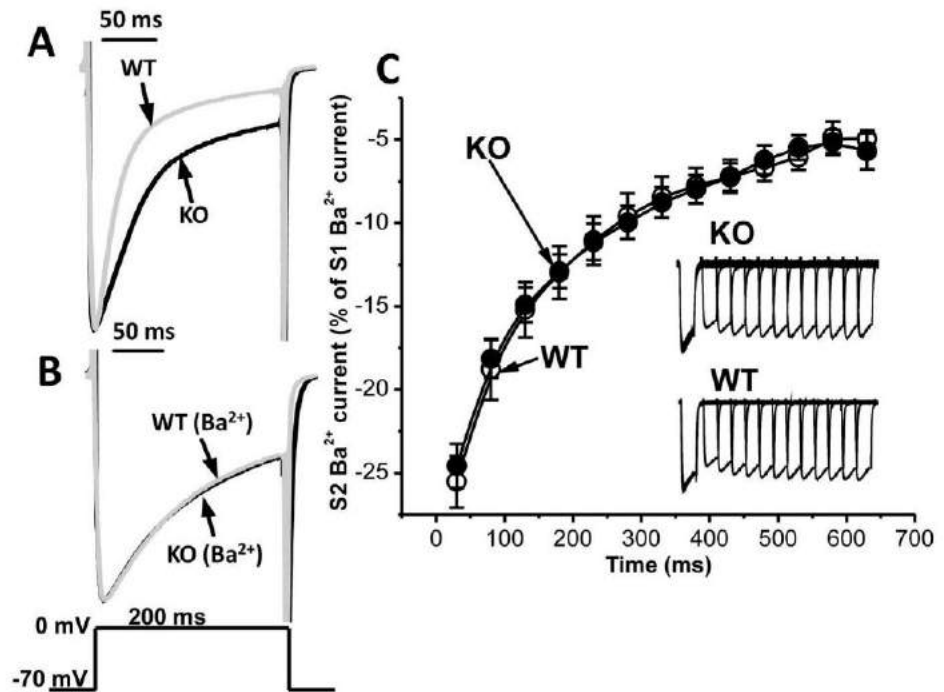


Fig. 5. Ca^{2+} -dependent inactivation of $\text{Ca}_v1.2$ current is defective in Casq2 KO myocytes
A – Representative $\text{Ca}_v1.2$ current for WT (light gray) and Casq2 KO (black) myocytes elicited by 200-ms depolarizing step to 0 mV from holding potential -70 mV in bath solution containing 2 mM Ca^{2+} . To illustrate the difference in $\text{Ca}_v1.2$ current inactivation, current traces were normalized to peak amplitude value for each myocyte. **B** – $\text{Ca}_v1.2$ currents recorded in bath solution containing 2 mM Ba^{2+} . Note that substituting Ca^{2+} with Ba^{2+} completely abolished the difference in $\text{Ca}_v1.2$ current inactivation. **C** – Average restitution curves and representative records (inset) of Ba^{2+} current for WT (white circles, n=13) and Casq2 KO (black circles, n=13) myocytes. The same experimental conditions and voltage protocol as in Fig. 4 were used.

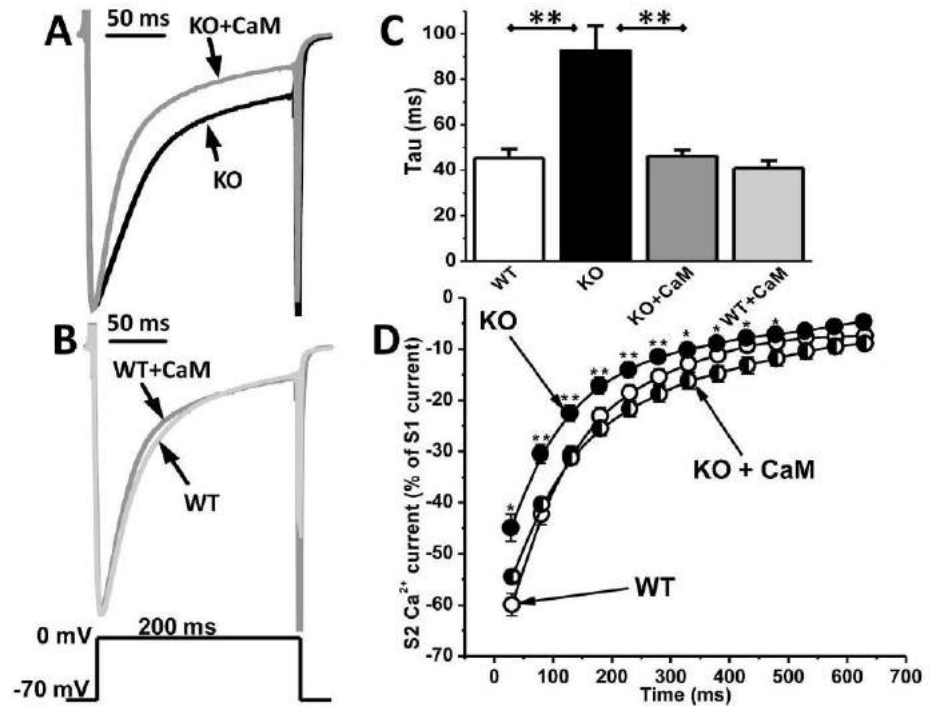


Fig. 6. Apo-CaM accelerates inactivation kinetics of Ca_v1.2 current only in Casq2 KO myocytes
A– Addition of apo-calmodulin (CaM, 20 μ M) to the intracellular dialysis solution accelerated inactivation of Ca_v1.2 Ca²⁺ currents in Casq2 KO myocytes. **B** – Addition of CaM had no effect on inactivation kinetics of Ca_v1.2 in WT myocytes. Voltage protocol is shown below. The declining phase of Ca_v1.2 current was well fitted by a single exponential function. **C** – Average inactivation time constant (τ) for all 4 groups ($n=7-10$ cells per group, $**P<0.005$). **D** – Average restitution curves of Ca_v1.2 currents for WT (white circles, $n=12$) and Casq2 KO myocytes in the presence (black/white circles, $n=6$) and absence (black circles, $n=12$) of CaM (20 μ M) in the pipette solution. Myocytes were pre-incubated in 50 μ M Ryanodine + 10 μ M Thapsigargin + 30 μ M TTX for 30 min. $**P<0.005$, $*P<0.05$ for Casq2 KO compared to Casq2 KO + CaM.

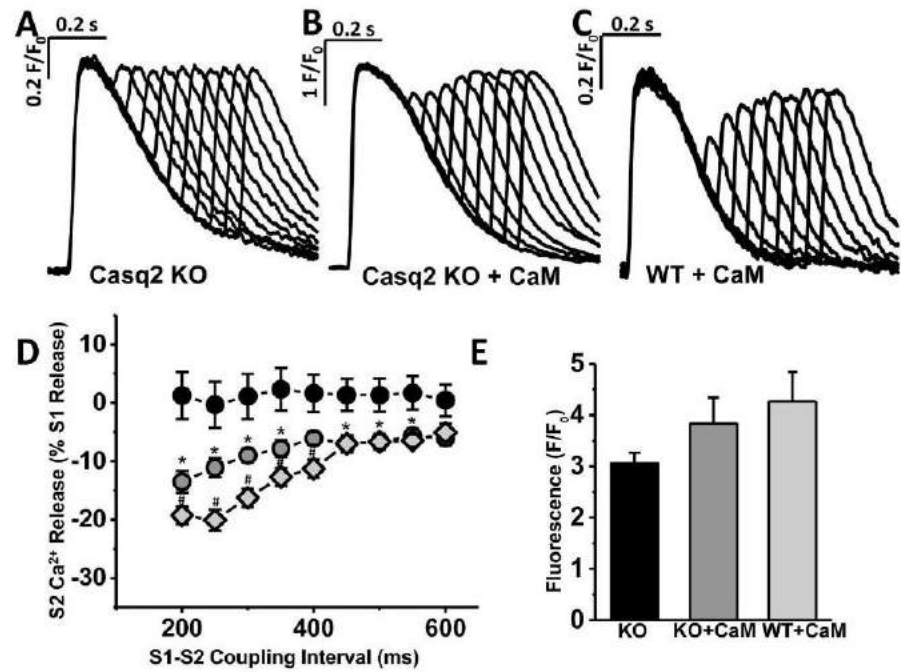


Fig. 7. Apo-CaM partly restores SR Ca^{2+} release refractoriness in *Casq2* KO myocytes
 Representative examples of Ca^{2+} transient restitution in *Casq2* KO myocytes in the absence (A) and in the presence of CaM (20 μM) in the pipette solution (B), as well as in WT myocytes in the presence of CaM (C). **D** - S2 Ca^{2+} release fraction plotted as a function of the S1-S2 coupling interval ($n=8-10$; *Casq2* KO w/o CaM - black circles; *Casq2* KO+CaM - grey circles, $*P < 0.05$ (vs. *Casq2* KO w/o CaM); WT+CaM - light-grey diamonds, $\#P < 0.05$ (vs. *Casq2* KO+CaM)). **E** - No significant difference in SR Ca^{2+} content was detected between three experimental groups.

Table 1

Tau values for I_{Ca} and I_{Ba} inactivation.

	N	Current density (pA/pF)	Tau (ms)	P-value (for tau vs WT)
WT	10	15.8	45	
Casq2 KO	10	14.8	93	0.002 (vs. WT)
Casq2 KO + CaM	7	17.9	46	0.002 (vs. Casq2 KO) 0.8 (vs. WT)
WT + CaM	7	15.4	41	0.4 (vs. WT)
WT (Ba^{2+})	10	11.2	145	
Casq2 KO (Ba^{2+})	10	9.2	145	0.99 (vs. WT (Ba^{2+}))

2.3. Ішемія змінює електричну активність кардіоміоцитів, виділених із синоатріального вузла

O. Gryshchenko, J. Qu and R. D. Nathan

Am J Physiol Heart Circ Physiol 282:2284-2295, 2002. First published Feb 7, 2002;
doi:10.1152/ajpheart.00833.2001

You might find this additional information useful...

This article cites 33 articles, 14 of which you can access free at:

<http://ajpheart.physiology.org/cgi/content/full/282/6/H2284#BIBL>

This article has been cited by 3 other HighWire hosted articles:

Simulated ischemia enhances L-type calcium current in pacemaker cells isolated from the rabbit sinoatrial node

Y.-M. Du and R. D. Nathan

Am J Physiol Heart Circ Physiol, November 1, 2007; 293 (5): H2986-H2994.

[\[Abstract\]](#) [\[Full Text\]](#) [\[PDF\]](#)

The Effect of Bupivacaine on Myocardial Tissue Hypoxia and Acidosis During Ventricular Fibrillation

G. Weinberg, C. Paisanthasan, D. Feinstein and W. Hoffman

Anesth. Analg., March 1, 2004; 98 (3): 790-795.

[\[Abstract\]](#) [\[Full Text\]](#) [\[PDF\]](#)

Early effects of metabolic inhibition on intracellular Ca²⁺ in toad pacemaker cells: involvement of Ca²⁺ stores

Y.-K. Ju and D. G. Allen

Am J Physiol Heart Circ Physiol, April 1, 2003; 284 (4): H1087-H1094.

[\[Abstract\]](#) [\[Full Text\]](#) [\[PDF\]](#)

Updated information and services including high-resolution figures, can be found at:

<http://ajpheart.physiology.org/cgi/content/full/282/6/H2284>

Additional material and information about *AJP - Heart and Circulatory Physiology* can be found at:

<http://www.the-aps.org/publications/ajpheart>

This information is current as of January 24, 2008 .

Ischemia alters the electrical activity of pacemaker cells isolated from the rabbit sinoatrial node

O. GRYSHCENKO, J. QU, AND R. D. NATHAN

Department of Physiology, Texas Tech University Health Sciences Center, Lubbock, Texas 79430

Received 24 September 2001; accepted in final form 5 February 2002

Gryshchenko, O., J. Qu, and R. D. Nathan. Ischemia alters the electrical activity of pacemaker cells isolated from the rabbit sinoatrial node. *Am J Physiol Heart Circ Physiol* 282: H2284–H2295, 2002. First published February 7, 2002; 10.1152/ajpheart.00833.2001.—The purpose of this study was to investigate the mechanisms responsible for ischemia-induced changes in spontaneous electrical activity. An ischemic-like Tyrode solution (pH 6.6) reversibly depolarized the maximum diastolic potential (MDP) and reduced the action potential (AP) overshoot (OS). We used SNARF-1, which is an indicator of intracellular pH (pH_i), and perforated-patch techniques to test the hypothesis that acidosis caused these effects. Acidic but otherwise normal Tyrode solution (pH 6.8) produced similar effects. Basic Tyrode solution (pH 8.5) hyperpolarized the MDP, shortened the AP, and slowed the firing rate. In the presence of “ischemic” Tyrode solution, hyperpolarizing current restored the MDP and OS to control values. HOE-642, an inhibitor of Na/H exchange, did not alter pH_i or electrical activity and did not prevent the effects of ischemic Tyrode solution or recovery after washout. Time-independent net inward current but not hyperpolarization-activated inward current was enhanced by ischemic Tyrode solution or by 30 μ M BaCl₂, a selective blocker of inward-rectifying K currents at this concentration. The results suggest that 1) acidosis was responsible for the ischemia-induced effects but Na/H exchange was not involved, 2) the OS was reduced because of depolarization-induced inactivation of inward currents that generate the AP upstroke, and 3) reduction of an inward-rectifying outward K current contributed to the depolarization.

electrophysiology; Na/H exchange; perforated-patch techniques; SNARF-1 fluorescence; HOE-642

AN ESTIMATED 70–80% of all electronic pacemakers (~500,000 in the US as of 1999) are implanted in patients 65 years of age and older (16). Abnormalities of sinoatrial (SA) node impulse generation as well as conduction disturbances are common in these patients and constitute much of the need for permanent pacemakers. For example, disruption of the blood supply of the SA node (ischemia) is responsible for some arrhythmias that occur shortly after orthotopic heart transplants and inferior wall acute myocardial infarctions (1, 35). Several multicellular models have been used to investigate the mechanisms responsible for ischemia-induced arrhythmias in the SA node. For example,

occlusion of the SA node artery markedly slowed the firing rate of blood-perfused canine right atrial preparations (20). Similar effects were seen in rat hearts just after Langendorff perfusion was interrupted (2). In rabbit right atrial preparations, exposure to hypoxia reduced the concentrations of ATP and creatine phosphate (45), depolarized the maximum diastolic potential (MDP), and decreased the action potential (AP) overshoot (OS) and upstroke velocity as well as the slope of diastolic depolarization (25, 31, 45). Removal of glucose from the bathing solution potentiated these effects (31), and metabolic inhibitors such as cyanide and 2,4-dinitrophenol produced similar but more rapid effects (25).

In comparison with right atrial preparations, isolated SA node pacemaker cells have both advantages and disadvantages. One advantage is that electrophysiological and fluorescence techniques can be employed simultaneously to correlate changes in electrical activity with the loss or gain of intracellular ions such as Ca²⁺ and H⁺. Another advantage is that whole-cell patch-clamp techniques can be used to investigate the changes in ionic currents that underlie ischemia-induced alterations of spontaneous electrical activity. On the other hand, the disadvantages include the absence of a restricted extracellular space surrounding the cells where metabolites can accumulate and the absence of other cell types such as neutrophils, which release oxygen radicals. Despite these disadvantages, Han and coworkers (18) observed marked reductions of the amplitude, duration, and frequency of spontaneous APs when rabbit isolated SA node cells were exposed to cyanide or 2,4-dinitrophenol for 5–10 min. Even these brief exposures activated ATP- and glibenclamide-sensitive K channels (K_{ATP}) (19) and reduced L-type Ca currents ($I_{Ca,L}$), delayed-rectifier K currents (I_K), and hyperpolarization-activated inward current (I_f) (18).

During acute myocardial ischemia, the extracellular environment is characterized by hypoxia, acidosis, and increased levels of K⁺ (for reviews, see Refs. 9 and 10). In preliminary experiments, we observed a gradual depolarization of the membrane potential and slowing of the firing rate when rabbit isolated SA node pace-

Address for reprint requests and other correspondence: R. D. Nathan, Dept. of Physiology, Texas Tech Univ. Health Sciences Center, 3601 Fourth St., Lubbock, TX 79430 (E-mail: Richard.Nathan@ttuhsc.edu).

The costs of publication of this article were defrayed in part by the payment of page charges. The article must therefore be hereby marked “advertisement” in accordance with 18 U.S.C. Section 1734 solely to indicate this fact.

maker cells were exposed to a glucose-free hypoxic Tyrode solution (34). Because these effects were accelerated by the reduction of extracellular pH (pH_o) to 6.8, and because a pH_o of 6.5 had altered the electrical activity of rabbit right atrial preparations in a similar fashion (37), we decided to test the hypothesis that acidosis was responsible for the "ischemia"-induced alterations we had observed previously. In the present study, we exposed SA node pacemaker cells to a glucose-free bathing solution that was titrated to pH 6.6 and bubbled with 100% N_2 . A pH of 6.6 was chosen because Yan and Kleber (44) measured a pH of 6.6 in the perfusate of rabbit papillary muscle after no-flow ischemia. Intracellular pH (pH_i) is also important because it influences the rate of anaerobic glycolysis, the development of active tension, and the functions of ion channels and exchangers (9, 44). Therefore, we used SNARF-1, a fluorescent indicator of pH_i (3, 8), and perforated-patch recordings of spontaneous electrical activity to test our hypothesis.

MATERIALS AND METHODS

Isolation of SA node pacemaker cells. As approved by this institution's Animal Care and Use Committee, male New Zealand White rabbits (body wt 1.0–1.5 kg) were stunned by a blow to the junction of the head and neck, and the heart was rapidly removed. A small hole was cut in the right atrium and infused with a HEPES-buffered salt solution (HBSS), which contained 20 mM 2,3-butanedione monoxime (BDM; Sigma-Aldrich Chemicals) to remove blood from the right atrium and eliminate its contraction (24, 39). After its excision, the right atrium was pinned to the bottom of a Sylgard-coated petri dish and immersed in fresh HBSS with BDM. The entire SA node was removed, trimmed of pericardium and fat, and cut into several pieces. Single cells were isolated as described previously (30) but with the following modifications. The pieces were digested at 37°C during 4–6 exposures (5–10 min each) to the solutions as follows: 1) 5 ml of a nominally Ca- and Mg-free buffer containing protease (P-8038, 2.8 U/ml; Sigma) and 0.1% BSA (A-2153, Sigma); 2) same as solution 1, but the enzyme buffer contained 20 μ M $CaCl_2$ and was stirred at 200 rpm; 3) same as solution 2, but the enzyme buffer contained 30 μ M $CaCl_2$ and the protease was replaced by type II collagenase (122–243 U/ml; Worthington Biochemicals); 4) same as solution 3, but with 50 μ M $CaCl_2$; 5) and 6) same as step 4 if necessary. BDM (20 mM) was included sometimes with one or both of the enzymes to prevent contracture of the isolated pacemaker cells (24, 39). Its effects on contraction and spontaneous electrical activity were reversed completely after washout and by the time the cells were studied. After each of steps 3–6, freed cells were transferred to a centrifuge tube containing either HBSS and 1.0% BSA at room temperature or a cold modified Kraft-Brühe (KB) solution. Both solutions also contained a mixture of protease inhibitors (P-2714; Sigma). After centrifugation (180 $\times g$ for 10 min at room temperature), the cells were resuspended in culture medium or maintained in cold KB solution for 45 min and then plated on small pieces of no. 0 glass ($\sim 3 \times 3$ mm and coated with laminin; L-2020; Sigma) in 35-mm plastic petri dishes. "Freshly isolated" cells were kept in KB at 4°C for up to 24 h, and "cultured" cells were maintained in an incubator (95% air-5% CO_2) at 37°C for up to 4 days.

Electrophysiology. A perforated-patch technique (22) was employed to record spontaneous electrical activity or ionic currents in freshly isolated or cultured pacemaker cells. The patch pipette contained (in mM) 75 K_2SO_4 , 55 KCl, 7 $MgCl_2$, and 10 HEPES; and 300 μ g/ml nystatin. pH was adjusted to 7.2 with KOH. A small amount of this solution without nystatin was drawn into the tip of the pipette just before a gigaohm seal was made with the cell membrane. Even though monovalent cations and anions are permeable through nystatin-induced channels, divalent ions are not; therefore, K_2SO_4 was included in the pipette solution to minimize the development of a Donnan potential due to impermeant anions in the cytoplasm (22). Because this technique prevents washout of important molecules such as cAMP, "rundown" of spontaneous electrical activity in rabbit SA node pacemaker cells can be avoided (30). This was verified in the present study because the changes in electrical activity were completely reversible after washout of the ischemic Tyrode solutions. The pipette resistance was ~ 5 M Ω , and electronic compensation was used to minimize the series resistance that remained after membrane perforation was complete. We included whole cell currents only if the membrane potential was well controlled during their acquisition. Pacemaker cells were superfused with normal Tyrode solution containing 10 mM HEPES (Table 1). HEPES, rather than $NaHCO_3/CO_2$, was better able to hold the pH constant over the course of each experiment. Experiments were performed at $35 \pm 1.0^\circ C$ (model TC-1 temperature controller; Cell MicroControls, Virginia Beach, VA). In most experiments, membrane potentials were corrected by -2.7 mV for the calculated pipette-to-bath liquid-junction potential. After obtaining a pipette-to-membrane seal, we waited 10–20 min for patch perforation before recording the spontaneous electrical activity. Complete exchange of superfusion solutions required 1–2 min.

Measurements of pH_i . A xenon arc lamp and a Zeiss inverted microscope provided 485-nm excitation, and a filter-based photometer system (Photon Technology International) allowed simultaneous acquisition of SNARF-1 fluorescence at 580 nm (F_{580}) and 640 nm (F_{640}). A shutter limited the duration of illumination to 1 s, thereby minimizing photobleaching of the dye and damage to the cells (3). Light collected by the photomultipliers was restricted by an adjustable mask to an area the size of the cell. Pacemaker cells were incubated with the acetoxymethyl ester (AM) form of SNARF-1 (2.5 μ M) at room temperature for only 15 min to minimize its entry into cytoplasmic compartments (5). The cells were then superfused with normal Tyrode solution for 15–30 min to eliminate extracellular dye. Background F_{580} and F_{640} , which were collected from a cell-free area the same size as the cell, were $<1\%$ of the SNARF-1 fluorescence;

Table 1. Experimental solutions

Tyrode Solution	Glucose, mM	Bubbled with 100% Air or N_2 *	pH
Normal†	5.5	Air	7.4
pH 6.8	5.5	Air	6.8
pH 8.5	5.5	Air	8.5
pH 7.4 ischemic	0	N_2	7.4
pH 6.6 ischemic	0	N_2	6.6

* When solutions were bubbled with 100% N_2 , PO_2 measured in cell chamber averaged only 8% below ambient level. † Normal Tyrode solution contained (in mM) 130 NaCl, 5.4 KCl, 1.8 $CaCl_2$, 0.6 $MgCl_2$, 0.6 $NaHPO_4$, 1.0 or 0 $NaHCO_3$, 5.5 glucose, and 10 HEPES; pH was titrated to 7.4 with NaOH.

therefore, they were neglected in calculations of the F_{580}/F_{640} ratio. Compared with SNARF-1-loaded cells, the autofluorescence of unloaded cells was $\sim 1\%$ of F_{580} and $<1\%$ of F_{640} ; therefore, it too was neglected in calculations of the F_{580}/F_{640} ratio.

In situ calibration of SNARF-1 fluorescence. Cells were loaded with $2.5 \mu\text{M}$ SNARF-1 at room temperature for 15 min and then rinsed in Tyrode solution for at least 15 min. After the F_{580}/F_{640} ratio had stabilized in normal Tyrode solution, the cells were exposed to several high-K concentration ([K]) buffers at 35°C . Each buffer contained (in mM) 125 KCl, 5 NaCl, 1.1 MgCl_2 , 2.7 CaCl_2 , 5.0 EGTA, 10 MES [acidic dissociation constant (pK_a) = 6.1 at 25°C], 10 HEPES (pK_a = 7.5), and 10 *N,N*-bis(2-hydroxyethyl)glycine (bicine, pK_a = 8.3); pH was titrated with 6 M KOH. Nigericin ($9.6 \mu\text{M}$) and valinomycin ($6.4 \mu\text{M}$) were also included to collapse the ionic gradients for K^+ and H^+ (5, 28). They were dissolved in 100% EtOH, prepared as 33.5 and 22.5 mM stock solutions, respectively, and then aliquoted and frozen until the day of the experiment. The final concentration of EtOH in each high- K^+ buffer was 0.6%. We were careful to rinse the cell chamber and tubing with EtOH and water after each experiment to remove any remaining trace levels of nigericin or valinomycin (4). Several pacemaker cells were exposed consecutively to seven high- K^+ buffers with pH ranging from 5.86 to 8.75 (Fig. 1A). At the end of this procedure, a repeat measurement of the F_{580}/F_{640} ratio at pH 6.82 was quite similar to the one obtained 1 h earlier, which confirms the stability of the cells. The mean values \pm SE for eight cells were plotted versus pH and fit by Eq. 1 (Fig. 1B). The in situ pK value for SNARF-1 was calculated using Eq. 2 (3, 5)

$$R = (R_{\min} \cdot 10^{(\text{pH} - \text{pK}_{\text{app}})} + R_{\max}) / (1 + 10^{(\text{pH} - \text{pK}_{\text{app}})}) \quad (1)$$

$$\text{pK} = \text{pK}_{\text{app}} + \log_{10} \beta \quad (2)$$

where $R = F_{580}/F_{640}$, pK_{app} is the apparent pK , and $\beta = F_{640(\text{max})}/F_{640(\text{min})}$. The following are the best-fit parameters for Eq. 1: $R_{\max} = 6.96 \pm 0.10$, $R_{\min} = 1.04 \pm 0.12$, and $\text{pK}_{\text{app}} = 7.46 \pm 0.04$. Using pK_{app} , the average β ($1.31 \pm$

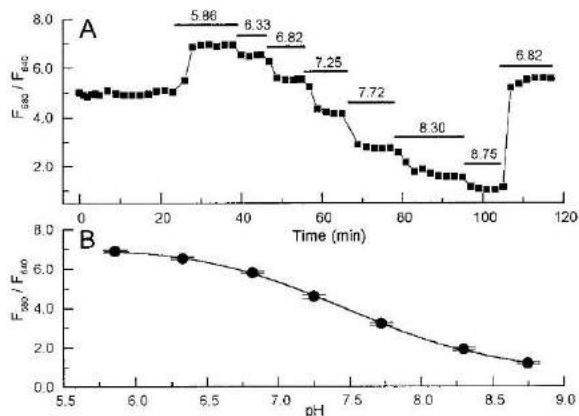


Fig. 1. In situ calibration of SNARF-1 fluorescence at 35°C . A: after a control period in normal Tyrode solution, a 3-day cultured pacemaker cell was exposed consecutively to high K-concentration buffers with pH ranging from 5.86 to 8.75. B: means \pm SE for ratios of SNARF-1 fluorescence at 580 nm (F_{580}) and 640 nm (F_{640}). F_{580}/F_{640} values are plotted vs. pH; note that all the error bars are within the solid circles. Measurements were made from eight pacemaker cells except at pH 8.75, where only five cells were employed. Equation 1 (see text) was used to obtain a best fit of the mean values.

0.16), and Eq. 2, we obtained a pK of 7.58 ± 0.04 . This value is consistent with other SNARF-1 pK values measured in situ: 7.4–7.6 for lens epithelial cells (3), 7.6–7.8 for carotid body type 1 cells (8), and 7.6 for rat cardiac myocytes (5). Values for the F_{580}/F_{640} ratio and the best-fit parameters above were employed in Eq. 3 to calculate the pH in each of the experiments described in the RESULTS

$$\text{pH} = \text{pK}_{\text{app}} + \log_{10}[(R_{\max} - R)/(R - R_{\min})] \quad (3)$$

Solutions. The compositions of the cell-isolation solutions, culture medium, and HBSS have been described (30). The modified KB solution contained (in mM) 70 L-glutamic acid, 25 KCl, 10 KH_2PO_4 , 3 MgCl_2 , 20 taurine, 10 dextrose, 0.3 EGTA, and 10 HEPES, and the pH was titrated to 7.4 with KOH. SNARF-1-AM ($50 \mu\text{g}$; Molecular Probes) was dissolved in $10 \mu\text{l}$ of anhydrous dimethylsulfoxide (DMSO; Sigma), $10 \mu\text{l}$ of Pluronic F-127 (25% wt/wt in anhydrous DMSO), and 17.6 ml of normal Tyrode solution (see Table 1). Aliquots (0.5 ml) of this solution were frozen at -80°C , thawed just before use, and added to 0.5 ml of Tyrode solution to yield a final concentration of $2.5 \mu\text{M}$ SNARF-1-AM. Table 1 lists the solutions used in the various experiments. HOE-642 (cariporide) was a gift of Aventis Pharma in Frankfurt, Germany.

Data analysis. Analog data were digitized at 12- or 16-bit resolution using Labmaster DMA boards, which were controlled by FeliX (Photon Technology International) and pClamp 8.0 (Axon Instruments) software. For measurements of pH, FeliX was employed to acquire SNARF-1 at F_{580} and F_{640} at a rate of 200 points/s and to average the raw data over 1-s periods. Periods of 10–20 s were used by pClamp to acquire spontaneous electrical activity. The MDP, OS, duration (Dur) at -20 mV , and frequency of APs (beat rate, BR) were measured from several APs and averaged. These parameters are presented as means \pm SE for those cells exposed to a particular condition. Two-tailed paired Student's *t*-tests were used for statistical analyses. Differences between means were considered significant if $P < 0.05$.

RESULTS

We use the terms ischemic, ischemia, and reperfusion to denote experimental conditions that simulate ischemia and reperfusion in vivo (Table 1). In our preliminary studies (34), the MDP depolarized significantly in seven pacemaker cells exposed to ischemic conditions for 5–10 min; however, during reperfusion, the MDP did not recover to control levels in some of these cells. To rule out the possibility that this depolarization resulted from increased leakage current or rundown of ionic currents during the perforated-patch recordings, we limited exposures in the present study to 3–5 min and included in the averaged results (Table 2) only cells in which the MDP recovered to within 5 mV of the control value during washout of the “test” solution. The averaged difference between control and washout MDPs was $1.4 \pm 0.2 \text{ mV}$ ($n = 40$). The results for freshly isolated and cultured pacemaker cells were combined because their electrophysiological properties did not differ significantly. For example, under control conditions, the MDP values were $-66 \pm 1 \text{ mV}$ for cultured cells ($n = 26$) and $-63 \pm 1 \text{ mV}$ for freshly isolated cells ($n = 12$); and the pH_i values were 7.26 ± 0.02 for cultured cells ($n = 86$) and 7.23 ± 0.06 for freshly isolated cells ($n = 9$). At the end of each perforated-patch recording, the presence of I_f was used to

Table 2. Alterations of pacemaker cell electrical activity

Condition	MDP,* mV	OS,* mV	Dur, ms	Beat Rate, beats/ min
Control (n = 12)	-65 ± 1	24 ± 2	243 ± 25	59 ± 6
pH 6.6 ischemic Tyrode solution	-53 ± 2‡	20 ± 2†	258 ± 18	58 ± 6
Control (n = 10)	-67 ± 2	20 ± 3	230 ± 21	65 ± 3
pH 7.4 ischemic Tyrode solution	-66 ± 2	20 ± 3	224 ± 29	60 ± 3
Control (n = 10)	-63 ± 2	32 ± 2	305 ± 43	61 ± 4
pH 6.8 Tyrode solution	-52 ± 3‡	27 ± 3†	336 ± 38	61 ± 6
Control (n = 7)	-64 ± 2	25 ± 1	188 ± 16	81 ± 3
pH 8.5 Tyrode solution	-69 ± 2‡	25 ± 1	177 ± 16†	78 ± 3‡
Control (n = 7)	-70 ± 3	25 ± 2	190 ± 18	68 ± 6
5–10 mM NH ₄ Cl	-65 ± 3‡	25 ± 2	202 ± 19	67 ± 6
Control (n = 8)	-63 ± 2	26 ± 2	209 ± 11	71 ± 6
pH 6.6 ischemic Tyrode solution + HOE-642	-54 ± 2‡	24 ± 2†	227 ± 14	67 ± 5
Control (n = 4)	-65 ± 4	28 ± 5	197 ± 15	59 ± 8
Normal Tyrode solution + 30 μM HOE-642	-64 ± 4	29 ± 5	206 ± 20	63 ± 4
Control (n = 7)	-62 ± 1	26 ± 2	211 ± 18	66 ± 5
pH 6.6 ischemic Tyrode solution	-52 ± 1‡	22 ± 2†	212 ± 20	73 ± 7
pH 6.6 ischemic Tyrode solution + injection of hyperpolarizing current	-61 ± 1	27 ± 1	213 ± 16	44 ± 5†

Values are means ± SE; n, no. of freshly isolated and/or cultured pacemaker cells. *Membrane potentials were corrected by -2.7 mV to account for calculated liquid-junction potential between patch pipette and bath. MDP, maximum diastolic potential; OS, action potential overshoot; Dur, action potential duration measured at -20 mV. A two-tailed Student's *t*-test for paired variants was used to determine whether differences in mean values were statistically significant (*P* < 0.05); †*P* < 0.05, ‡*P* < 0.001.

confirm the identity of pacemaker cells. Although data were collected from pacemaker cells that had been in culture for 1–4 days, 2- and 3-day cells were employed most often because these cells provided the most consistent results. Nevertheless, there were no significant differences among the results obtained from 1-, 2-, 3-, and 4-day cells. For example, the pH_i values among 2-day cells (7.24 ± 0.03, *n* = 37), 3-day cells (7.26 ± 0.04, *n* = 35), and 4-day cells (7.33 ± 0.07, *n* = 14) did not differ significantly.

pH 6.6 ischemic Tyrode solution. The purpose of these experiments was to simulate ischemic conditions in vivo. Nevertheless, even though myocardial ischemia is characterized by increased levels of K⁺ (9, 10), we decided not to include elevated [K] in the pH 6.6 ischemic Tyrode solution (see Table 1), because the strong K depolarization of the MDP would mask the unknown effects of the remaining components (reduced pH, hypoxia, and the absence of glucose). For example, normal Tyrode solution that contained 10–13 mM KCl depolarized the MDP by 17 ± 4 mV (range = 11–24 mV, *n* = 4). Figure 2A illustrates the effects of pH 6.6 ischemic Tyrode solution on spontaneous electrical activity. After only 3 min, the MDP had depolarized by 14 mV, the OS had fallen by 3 mV, and the Dur had shortened by 9 ms; there was no change in BR. As shown in Fig. 2B, there was essentially complete recovery during washout. Of the twelve pacemaker cells exposed to pH 6.6 ischemic Tyrode solution for up to 4 min, twelve exhibited depolarization of the MDP and nine exhibited reduction of the OS. On average, the MDP depolarized from -65 ± 1 to -53 ± 2 mV (*P* < 0.00001), and the OS declined from 24 ± 2 to 20 ± 2 mV (*P* < 0.05). The Dur and BR were not altered significantly (Table 2), and both the MDP and OS recovered completely during washout of pH 6.6 ischemic Tyrode solution (data not shown). In the cell shown

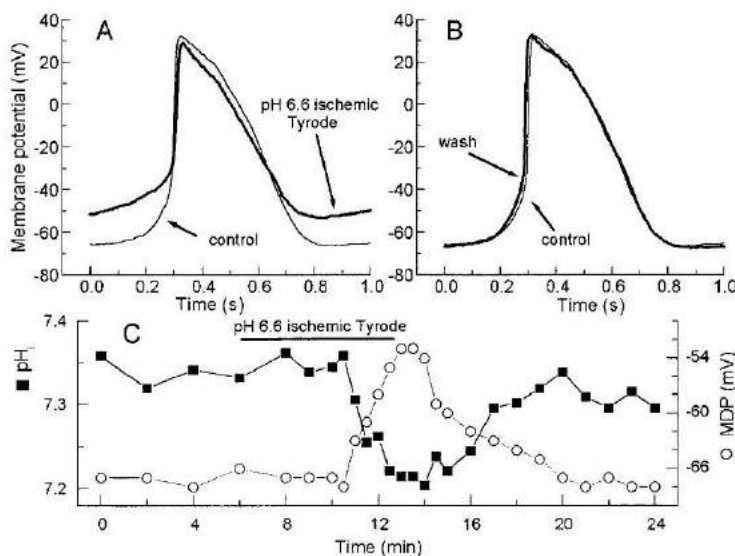


Fig. 2. pH 6.6 ischemic Tyrode solution alters intracellular pH (pH_i) and spontaneous electrical activity. A: a 2-day pacemaker cell was exposed to pH 6.6 ischemic Tyrode solution for only 3 min. B: recovery of electrical activity was complete 9 min after washout of ischemic Tyrode solution. C: in another 2-day cell, the maximum diastolic potential (MDP) depolarized and repolarized concomitant with the fall and partial recovery of pH_i. In this and subsequent figures, horizontal line indicates the period when the cell was exposed to a test solution. Complete exchange of bathing solutions required 1–2 min.

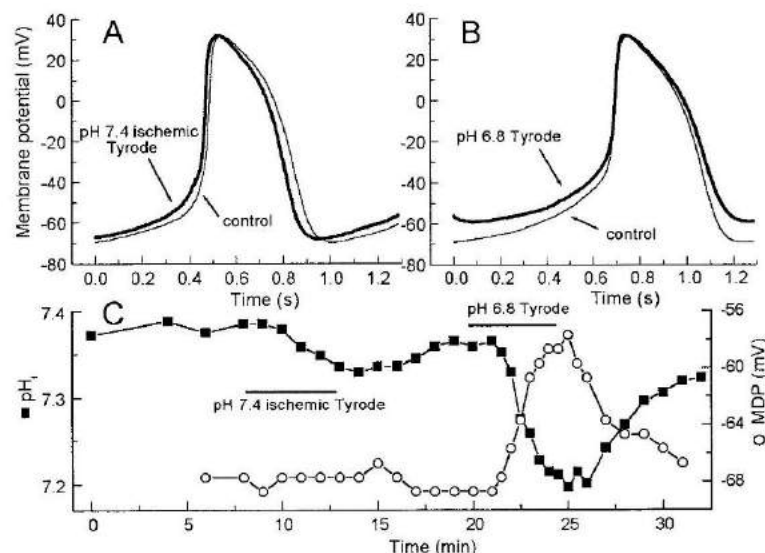
in Fig. 2C, pH_i began to fall ~4 min after normal Tyrode solution was replaced by pH 6.6 ischemic Tyrode solution. Complete exchange of solutions was achieved in 1–2 min. A reduction of pH_i was confirmed in another 7 pacemaker cells.

Role of pH. To explore the mechanisms responsible for ischemia-induced reductions of the MDP and OS, we tested the components of pH 6.6 ischemic Tyrode solution (see Table 1). "Hypoxic" Tyrode solution, which contained glucose (5.5 mM) but was bubbled with 100% N_2 , reduced pH_i very little and had no significant effect on the MDP, OS, Dur, or BR of 4 freshly isolated pacemaker cells (data not shown). This lack of effect was probably because the PO_2 of hypoxic Tyrode solution flowing through the cell chamber was only 8% below the ambient level. Figure 3A illustrates the effects of ischemic Tyrode solution with normal pH_i (7.4). Although the Dur decreased from 336 to 313 ms and the MDP depolarized by 2 mV in this cell, the changes in Dur, MDP, OS, and BR for 10 pacemaker cells were not significant (Table 2). As indicated in Fig. 3C, the pH_i fell slightly in 4 of 7 cells, but it did not change in the other 3. Unlike pH 7.4 ischemic Tyrode solution, the reduction of pH of normal Tyrode solution from 7.4 to 6.8 did depolarize the MDP and attenuate the OS significantly. Of 10 pacemaker cells, 10 exhibited depolarization of the MDP and 8 exhibited reduction of the OS. On average, the MDP depolarized from -63 ± 2 to -52 ± 3 mV ($P < 0.00001$), and the OS declined from 32 ± 2 to 27 ± 3 mV ($P < 0.05$). In the example illustrated in Fig. 3B, the MDP depolarized from -69 to -60 mV, but there was no change in OS. An increase in Dur, which was only 9% in this experiment, was observed in 8 of 10 pacemaker cells. Nevertheless, on average the Dur values for normal Tyrode solution (305 ± 43 ms) and pH 6.8 Tyrode solution (336 ± 38 ms) were not significantly different. In 8 cells

exposed to pH 6.6 Tyrode solution, however, the increase in Dur (from 248 ± 24 to 284 ± 34 ms) was significant ($P < 0.05$). Figure 3C illustrates the relationship between the MDP and pH_i . When this pacemaker cell was exposed to pH 7.4 ischemic Tyrode solution, pH_i decreased little (from 7.38 to 7.34) and there was no significant change in the MDP. In contrast, when the same cell was exposed to normal Tyrode solution titrated to pH 6.8, the MDP depolarized 11 mV in parallel with a decline in pH_i from 7.36 to 7.20. Similar reductions of pH_i were seen in another 4 cells. Taken together, these results suggest that the significant depolarization of the MDP and decline of the OS induced by pH 6.6 ischemic Tyrode solution (Table 2) resulted from the acidic pH of the solution and not from hypoxia or the absence of glucose.

To further explore the role of pH, we exposed pacemaker cells to otherwise normal Tyrode solution but with the pH titrated to 8.5. In the example illustrated in Fig. 4A, the MDP hyperpolarized (from -68 to -71 mV), the Dur was shortened by 5%, and the BR was slowed by 5%; there was no change in the OS. Recovery was essentially complete after washout of pH 8.5 Tyrode solution (Fig. 4B). Of the 7 pacemaker cells exposed to pH 8.5 Tyrode solution, 7 exhibited hyperpolarization of the MDP, 6 exhibited shortening of the Dur, and 5 exhibited slowing of the BR. On average, the MDP hyperpolarized from -64 ± 2 to -69 ± 2 mV ($P < 0.0001$), the Dur decreased from 188 ± 16 to 177 ± 16 ms ($P < 0.05$), and the BR slowed from 81 ± 3 to 78 ± 3 beats/min ($P < 0.05$); there was no change in the OS (Table 2). The slower BR could have been due to the longer time to reach threshold from a hyperpolarized MDP. An increase in pH_i after extracellular alkalosis (Fig. 4C) was confirmed in another 6 pacemaker cells. These results and those obtained with pH 6.8 Tyrode

Fig. 3. Role of pH in the changes produced by pH 6.6 ischemic Tyrode solution. A: a 2-day pacemaker cell was exposed to pH 7.4 ischemic Tyrode solution for 10 min. B: a 3-day pacemaker cell was exposed to otherwise normal Tyrode solution but with pH titrated to 6.8 for 4 min. C: in the same cell, the MDP depolarized and repolarized almost in parallel with the fall and partial recovery of pH_i .



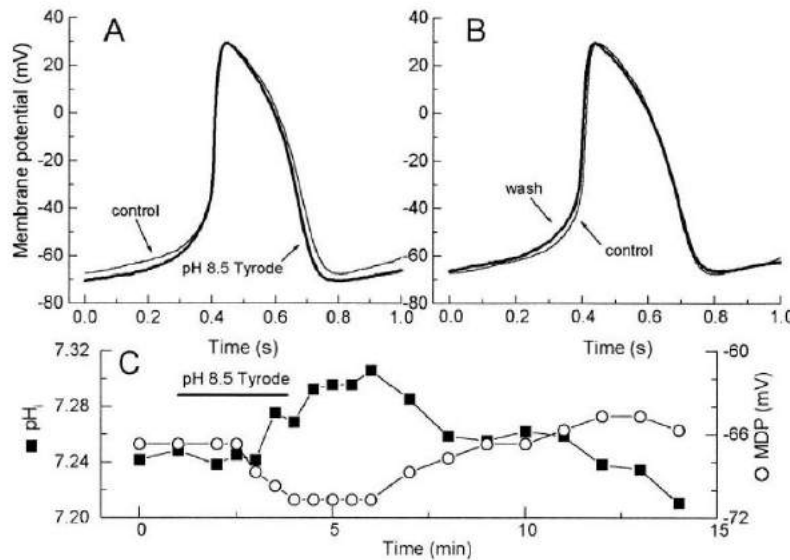


Fig. 4. pH 8.5 Tyrode solution alters pH_i and spontaneous electrical activity. A: a 3-day pacemaker cell was exposed to pH 8.5 Tyrode solution for 4 min. B: recovery of electrical activity was essentially complete 3 min after washout of pH 8.5 Tyrode solution. C: in the same cell, the MDP hyperpolarized and then returned to control values concomitant with the increase and recovery of pH_i .

solution support the hypothesis that pH alone can modulate spontaneous electrical activity.

To investigate the role of pH_i with pH_o fixed at 7.4, we briefly (2–4 min) exposed pacemaker cells to NH_4Cl . This common protocol first increases pH_i as NH_3 enters the cells and then decreases pH_i during washout of NH_4Cl as long as NH_4^+ remains in the cytoplasm (6). The results of these experiments were unexpected: the MDP depolarized not while pH_i was falling but when pH_i was rising. In the example illustrated in Fig. 5A, during alkalosis the MDP depolarized from -76 to -66 mV, the OS increased from 28 to 29 mV, the Dur increased by 8%, and the BR increased

by 7%. Recovery was almost complete after washout of NH_4Cl (Fig. 5B). On average, during alkalosis the MDP depolarized from -70 ± 3 to -65 ± 3 mV ($n = 7$; $P < 0.001$). In contrast, there was no significant change in OS, Dur, or BR (Table 2). In 3 simultaneous recordings of SNARF-1 fluorescence and electrical activity, the MDP depolarized in parallel with alkalosis; however, in another 3 cells, the depolarization preceded the increase in pH_i as in Fig. 5C. Recovery of the MDP occurred during acidosis in 3 of the cells (Fig. 5C), but the MDP did not recover in the other 3. In contrast, all 7 of the cells reported in Table 2 exhibited recovery of the MDP after washout of NH_4Cl . A mechanism for

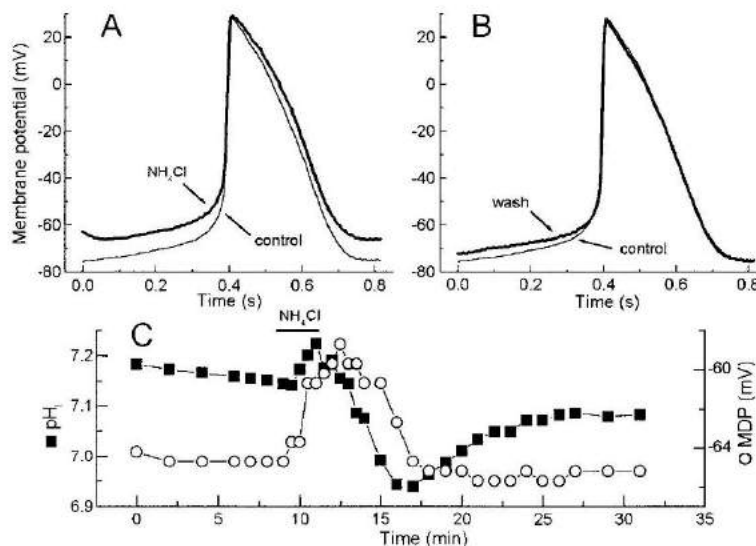


Fig. 5. NH_4Cl alters pH_i and spontaneous electrical activity. A: a 2-day pacemaker cell was exposed to 10 mM NH_4Cl in normal Tyrode solution (pH 7.4) for 4 min. B: recovery of electrical activity was almost complete 4 min after washout of NH_4Cl . C: a 3-day pacemaker cell was exposed to 5 mM NH_4Cl ; the MDP began to depolarize just before the rise in pH_i and began to recover after the initial fall in pH_i .

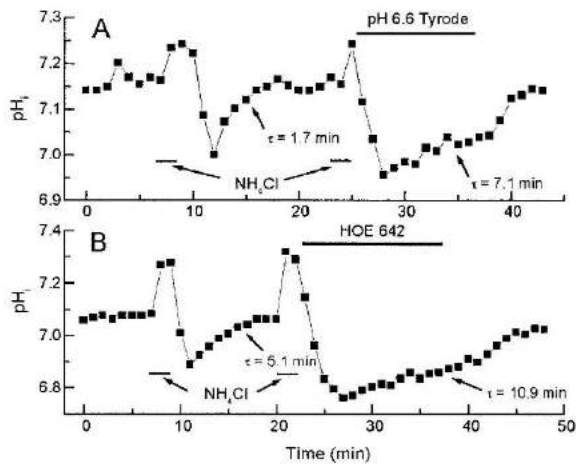


Fig. 6. Both pH 6.6 Tyrode solution and HOE-642 (cariporide) slow the recovery of pH_i from acidosis. A: a 1-day pacemaker cell was exposed in 2-min periods to 5 mM NH_4Cl in normal Tyrode solution (pH 7.4). During its second recovery from acidosis, the cell was exposed to pH 6.6 Tyrode solution; this increased the time constant for recovery (τ) from 1.7 to 7.1 min. B: in another pacemaker cell, exposure to 10 μM HOE-642 in normal Tyrode solution increased τ from 5.1 to 10.9 min. Origin software (OriginLab) was used to fit the time course of recovery by a single exponential.

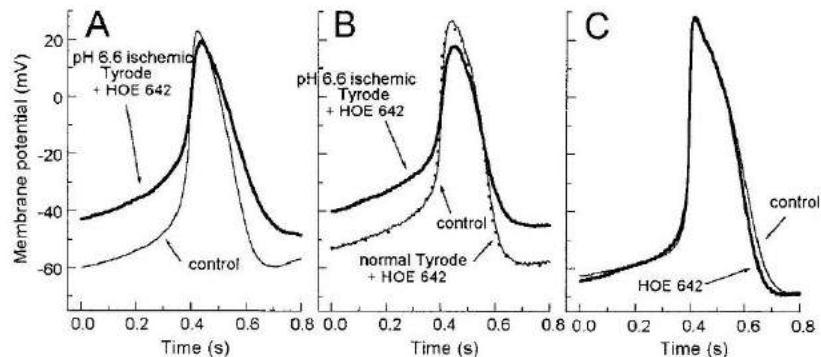
NH_4Cl -induced changes in the MDP is described in the DISCUSSION.

Role of Na/H exchange. It has been suggested that ischemia-induced intracellular acidification activates Na/H exchange and leads to increased intracellular Na (Na_i) and then to intracellular Ca (Ca_i) overload as a result of reduced Na/Ca exchange (38). More recent studies, however, have come to a different conclusion (36). Because pH was an important factor in the ischemia-induced changes in electrical activity described here, we tested the hypothesis that Na/H exchange also played a role. Previous studies have shown that extracellular acidosis attenuates Na/H exchange, thereby resulting in a reduction of pH_i . For example, Vaughan-Jones and co-workers (41) found that when pH_o was reduced from 7.5 to 6.5, net acid efflux during recovery from acidosis [calculated as buffering power $\times d(pH_i)/$

dt] was reduced by 65%. We observed qualitatively similar effects in SA node pacemaker cells. For example, the recovery of pH_i after NH_4Cl -induced acidosis was slowed markedly when a cell was exposed to pH 6.6 Tyrode solution: the time constant for recovery increased from 1.7 to 7.1 min (Fig. 6A). On average, the time constant for recovery increased from 3.2 ± 0.7 to 8.2 ± 1.6 min ($n = 8$; $P < 0.005$). To complement these experiments, we used HOE-642, a potent and selective inhibitor of the Na/H exchanger isoform 1 (NHE-1; see Ref. 36), to test the hypothesis that the reduction of pH_i and concomitant depolarization of the MDP induced by pH 6.6 ischemic Tyrode solution were due to inhibition of Na/H exchange. At a concentration of 30 μM , HOE-642 blocked the recovery of pH_i in 2 cells after NH_4Cl -induced acidosis, which confirms that, like amiloride (7), HOE-642 can block Na/H exchange in rabbit SA node pacemaker cells. At a concentration of 10 μM , HOE-642 blocked the recovery of 1 cell and slowed the recovery of 5 others. For example, the time constant for recovery from acidosis was increased from 5.1 to 10.9 min when HOE-642 was present (Fig. 6B). On average, 10 μM HOE-642 increased this time constant from 3.2 ± 0.6 to 6.9 ± 2.0 min ($n = 5$; $P < 0.05$). However, compared with pH 6.6 ischemic Tyrode solution and pH 6.8 Tyrode solution (see Figs. 2 and 3), HOE-642 had a smaller effect on normal pH_i . In the presence of pH 7.4 Tyrode solution, 30 μM HOE-642 reduced pH_i by <0.05 pH unit in 4 cells and had no measurable effect in 4 others. Taken together, these results suggest that the reduction of pH_i by pH 6.6 ischemic Tyrode solution (see Fig. 2) cannot be explained by blockade of Na/H exchange.

Although blockade of Na/H exchange was not responsible for the reduction of pH_i , did this intracellular acidosis stimulate Na/H exchange? Such stimulation would have increased Na_i and then Ca_i via Na/Ca exchange. Could this enhancement of Na_i and Ca_i have depolarized the MDP and reduced the OS? If these ideas are correct, blockade of Na/H exchange would have prevented the changes in MDP and OS. Nevertheless, addition of HOE-642 to pH 6.6 ischemic Tyrode solution did not prevent depolarization of the MDP and reduction of the OS (Fig. 7A). In fact, the MDP changed

Fig. 7. HOE-642 does not modify spontaneous electrical activity or prevent the effects of pH 6.6 ischemic Tyrode solution or its recovery. A: a 2-day pacemaker cell was exposed for 4 min to pH 6.6 ischemic Tyrode solution containing 25 μM HOE-642. B: a 4-day pacemaker cell was exposed for 5 min to pH 6.6 ischemic Tyrode solution containing 20 μM HOE-642. Replacement of this solution by normal Tyrode solution containing 30 μM HOE-642 did not prevent recovery of the electrical activity after 4 min (compare with control). C: a 3-day pacemaker cell was exposed for 8 min to normal Tyrode solution containing 30 μM HOE-642.



from -63 ± 2 to -54 ± 2 mV ($P < 0.00001$), and the OS changed from 26 ± 2 to 24 ± 2 mV ($P < 0.05$) in 8 pacemaker cells. These effects were not significantly different from those produced by pH 6.6 ischemic Tyrode solution or pH 6.8 Tyrode solution (Table 2). Again, neither the DR nor BR was changed significantly. Even though HOE-642 slowed the recovery of pH_i from acidosis (see Fig. 6B), the drug had no effect on recovery of the MDP and OS when pH 6.6 ischemic Tyrode solution was replaced by normal Tyrode solution containing HOE-642 (Fig. 7B). Similar results were obtained in 6 of 8 pacemaker cells. Finally, HOE-642 itself had no effect on electrical activity. As illustrated in Fig. 7C, the MDP and OS were unchanged during an 8-min exposure to 30 μ M HOE-642, a concentration 30-fold greater than that used to block NHE-1 in isolated rat ventricular myocytes (36). On average, the MDP changed from -65 ± 4 to -64 ± 4 mV ($P > 0.05$) and the OS changed from 28 ± 5 to 29 ± 5 mV ($P > 0.05$) when 4 pacemaker cells were exposed to 30 μ M HOE-642 (Table 2). Taken together, these results suggest that although pH 6.6 ischemic Tyrode solution reduced pH_i, Na/H exchange played no role in the concomitant depolarization of the MDP and reduction of the OS.

Role of ion channels. In contrast to a direct effect of acidosis, reduction of the OS when pacemaker cells were exposed to pH 6.6 ischemic Tyrode solution or pH 6.8 Tyrode solution (Table 2) could have resulted indirectly from depolarization-induced inactivation of inward currents that generate the upstroke of the AP. To test this hypothesis, we injected hyperpolarizing current after pacemaker cells had been depolarized by pH 6.6 ischemic Tyrode solution. As illustrated in Fig. 8, when the MDP was forced back to the control level, the BR slowed and the OS recovered completely in 5 of 7 pacemaker cells. On average, when these cells were exposed to pH 6.6 ischemic Tyrode solution, the MDP depolarized from -62 ± 1 to -52 ± 1 mV ($P < 0.001$) and the OS decreased from 26 ± 2 to 22 ± 2 mV ($P < 0.05$; Table 2). While cells were exposed to pH 6.6 ischemic Tyrode solution, injection of hyperpolarizing current repolarized the MDP to -61 ± 1 and increased the OS to 27 ± 1 mV, both of which are consistent with the control values. Hyperpolarizing current also slowed

the BR significantly, from 66 ± 5 to 44 ± 5 beats/min ($P < 0.05$). We observed similar changes in 2 pacemaker cells exposed to pH 6.6 Tyrode solution.

These results support the idea that reductions of the OS, when cells were exposed to pH 6.6 ischemic Tyrode solution, were due to acidosis-induced depolarization of the membrane potential. But what caused this depolarization? One possibility is enhancement of an inward current. A small hyperpolarization-activated inward current (I_f) has been observed at the MDP of some cultured (27) and freshly isolated SA node pacemaker cells (46); therefore, we tested the hypothesis that I_f was enhanced by our ischemic conditions. Nevertheless, with I_f defined as the time-dependent inward current during hyperpolarizing voltage steps, we found no significant increase in its amplitude when cells were exposed to pH 6.6 ischemic Tyrode solution (Fig. 9, A–C). In fact, there was little difference in the current-voltage (I - V) relationships for I_f (Fig. 9D). For example, mean values of I_f in 9 pacemaker cells exposed to normal Tyrode solution (-16.6 ± 4.7 pA) and then exposed to pH 6.6 ischemic Tyrode solution (-17.1 ± 3.8 pA) did not differ significantly at -70 mV, a potential reached by some of the pacemaker cells. In contrast, the initial (time-independent) net inward current (I_{initial}), which preceded the onset of I_f , did increase in 7 of these cells (Fig. 9B). On average, I_{initial} increased significantly at -70 mV from -24 ± 12 to -40 ± 12 pA ($P < 0.05$). This increase was not due to a gradual increase in leakage current, because I_{initial} decreased during washout and after 5 min its mean (-25 ± 16 pA) did not differ from the control. To investigate I_{initial} further, we used additional test potentials to cover the diastolic range between -60 and -40 mV. As illustrated in Fig. 9E, pH 6.6 ischemic Tyrode solution reversibly increased I_{initial} by 2–5 pA at those potentials. Similar results were obtained in another 5 pacemaker cells.

Finally, we exposed pacemaker cells to normal Tyrode solution containing 30 μ M BaCl₂ to investigate the nature of I_{initial} . Like pH 6.6 ischemic Tyrode solution, this concentration increased I_{initial} by 2–5 pA in 4 pacemaker cells. Again, like pH 6.6 ischemic Tyrode solution, normal Tyrode solution containing 20–50 μ M

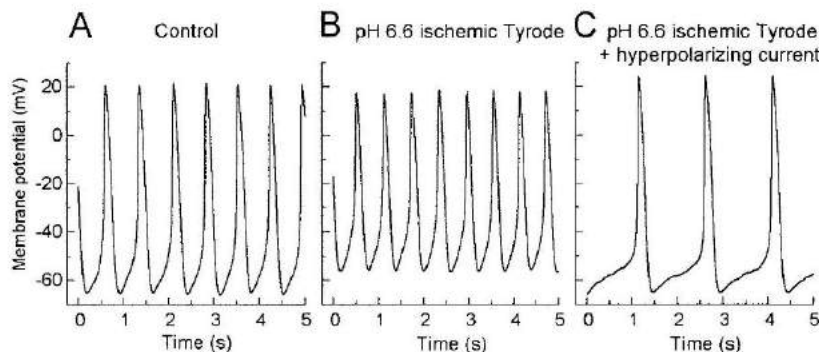
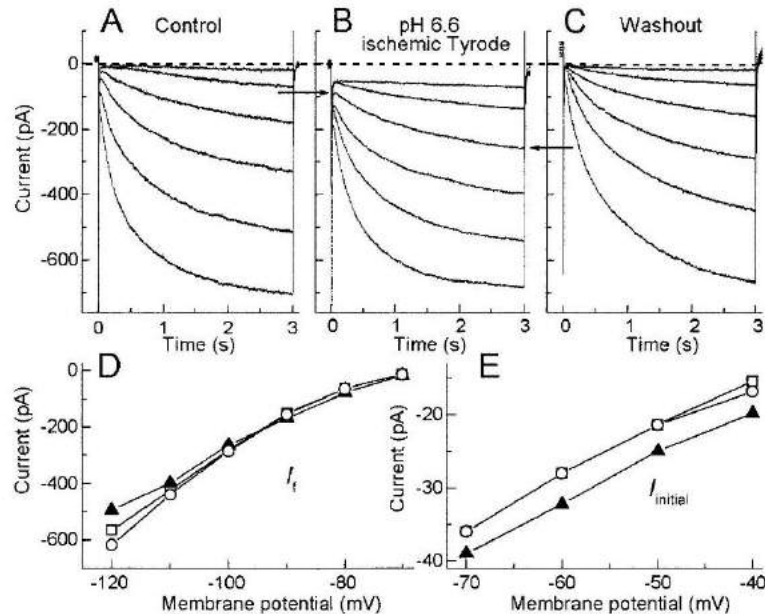


Fig. 8. Injection of hyperpolarizing current repolarizes the MDP and reverses the reduction of overshoot (OS) produced by a pH 6.6 ischemic Tyrode solution. A: a control recording was obtained from a 1-day pacemaker cell. B: same cell was exposed to pH 6.6 ischemic Tyrode solution for 3 min. C: while the cell was exposed to pH 6.6 ischemic Tyrode solution, injection of hyperpolarizing current through the recording pipette slowed the firing rate of the cell from 100 to 40 beats/min, repolarized the MDP to the control level, and increased the OS above the control level.

Fig. 9. pH 6.6 ischemic Tyrode solution increases the initial (time-independent) net inward current (I_{initial}) but not the hyperpolarization-activated inward current (I_f). A: voltage steps (3 s) from -70 to -120 mV were applied from a holding potential of -50 mV while a 1-day pacemaker cell was exposed to normal Tyrode solution. B: same cell after 5 min in pH 6.6 ischemic Tyrode solution. C: same cell after 5 min in normal Tyrode solution. D: current-voltage (I - V) relationships for I_f , which was defined as the difference between the end and beginning of time-dependent inward current (see arrows in B). In D and E, there were no corrections for the pipette-to-bath liquid-junction potential, and the conditions were as follows: normal Tyrode solution (\square), 5 min in pH 6.6 ischemic Tyrode solution (\blacktriangle), and 5 min after washout of pH 6.6 ischemic Tyrode solution (\circ).



BaCl₂ reversibly depolarized the MDP by 11 ± 2 mV ($n = 7$; $P < 0.001$).

DISCUSSION

The purpose of this study was to investigate, in isolated SA node pacemaker cells, the mechanisms responsible for ischemia-induced changes in spontaneous electrical activity. The most important findings are 1) pH 6.6 ischemic Tyrode solution reversibly decreased the OS and depolarized the MDP; 2) similar changes were produced by normal Tyrode solution if the pH was titrated to ≤ 6.8 ; 3) increasing pH_o to 8.5 hyperpolarized the MDP, shortened the Dur, and slowed the BR; 4) although HOE-642 slowed or blocked the recovery of pH_i after NH₄Cl-induced acidosis, this inhibitor of Na/H exchange did not prevent the changes induced by pH 6.6 ischemic Tyrode solution or the recovery during washout; 5) in the presence of pH 6.6 ischemic Tyrode solution, injection of hyperpolarizing current restored the MDP and OS to original values; 6) pH 6.6 ischemic Tyrode solution increased time-independent, net inward current (I_{initial}) but not I_f in the pacemaker range of potentials; and 7) BaCl₂ (20–50 μ M) in normal Tyrode solution reversibly increased I_{initial} and depolarized the MDP.

Ischemia-induced changes in pH. The reduction of pH_o during ischemia is partially due to hampered removal of extracellular CO₂ and lactate when blood flow is diminished (10). For example, after 10 min of global ischemia, pH_o was reduced to 6.54–6.66 (12) in the isolated, perfused rabbit interventricular septum and to 6.86 in blood-perfused rabbit papillary muscle (44). In the present study, we titrated the pH of ischemic Tyrode solution to 6.6 to approximate global ischemia

in situ. The sources of intracellular acidosis during ischemia are controversial but most likely are due to the retention of H⁺ from glycolytic ATP turnover, CO₂ accumulation, and eventually, net ATP breakdown (14). Furthermore, extracellular acidosis inhibits Na/H exchange (41), thereby hampering the removal of excess H⁺ in the cytoplasm. Because of these multiple factors, the extent of acidosis is quite variable. For example, pH_i fell from 7.0 to 6.6 after only 4 min of global ischemia in rabbit hearts (29), but to only 6.89 after 12 min of global ischemia in perfused rabbit papillary muscles (44). By comparison, pH_i fell from 7.2 to 6.5 in isolated rat ventricular myocytes exposed to simulated ischemia for 30 min (glucose-free anoxic Tyrode solution with pH titrated to 6.4) (26). To insure complete recovery of the electrophysiological properties, we exposed isolated pacemaker cells to pH 6.6 ischemic Tyrode solution for only 4–5 min. During this period, pH_i fell by only 0.06–0.15 unit. Still, this brief treatment was sufficient to depolarize the MDP by 12 mV. The following are two possible explanations: 1) pH_o , not pH_i , was responsible for the depolarization; and 2) the changes in pH_i were actually much greater at the sarcolemma, where they could influence ion channels; however, we could not detect them by observing whole cell-averaged SNARF-1 fluorescence. This problem could have been particularly severe in our experiments with NH₄Cl, when pH_i was constantly changing and therefore even more likely to be nonuniform.

Ischemia-induced changes in SA node electrical activity. In the rabbit right atrium, which contains the SA node, hypoxia (Tyrode solution was bubbled with 95% N₂-5% CO₂) depolarized the MDP and reduced the

OS, AP upstroke velocity, and slope of diastolic depolarization (25, 31, 45); removal of glucose potentiated these effects (31). Metabolic inhibition with cyanide or 2,4-dinitrophenol (25) produced similar but more rapid effects.

In freshly isolated rabbit SA node pacemaker cells, 5- to 10-min exposures to cyanide or 2,4-dinitrophenol markedly reduced the amplitude, duration, and frequency of spontaneous APs and attenuated $I_{Ca,L}$, I_K , and I_f (18). Han and co-workers (19) have also shown that cyanide activates K_{ATP} channels in these cells. In contrast, we did not observe shortening of the AP when pacemaker cells were exposed to pH 6.6 ischemic Tyrode solution. Such a shortening would be expected if $I_{K(ATP)}$ were activated. This discrepancy might be due in part to the much shorter duration (4–5 min) and therefore less metabolic blockade produced by pH 6.6 ischemic Tyrode solution in our experiments compared with the 60-min exposures to cyanide employed in the previous study. Another difference between our study and previous ones is that pH 6.6 ischemic Tyrode solution did not slow pacemaker activity, possibly because this treatment was too brief to activate $I_{K(ATP)}$. In comparison, Posner and co-workers (33) found that the mean BR of isolated right atria was slowed significantly from 173 to 129 beats/min when rabbits were raised in a hypoxic environment ($PO_2 = 65$ mmHg) for 3 wk. They also showed that acidosis alone could slow BR dramatically (on average, from 173 to 18 beats/min). Nevertheless, an important difference between their experiments and ours is that they exposed the atria to pH 6.5 Tyrode solution for 1 h, whereas we exposed SA node pacemaker cells to pH 6.6 or 6.8 Tyrode solution for an average of only 4.1 ± 0.2 min ($n = 18$).

pH-induced changes in SA node electrical activity. There is little information about pH-induced changes in SA node electrical activity and the underlying mechanisms. In small pieces of rabbit SA node tissue, reduction of pH_o to 6.5 depolarized the MDP, slowed the BR, and reduced the OS and maximum upstroke velocity, but had no effect on Dur (37). Opposite effects were seen when pH_o was increased to 8.5. Some of the present results are similar: exposure of pacemaker cells to pH 6.8 Tyrode solution for 4 min produced an 11-mV depolarization of the MDP and a 5-mV reduction of the OS, but no significant effect on Dur; exposure to pH 8.5 Tyrode solution hyperpolarized the MDP by 5 mV. In contrast to the previous study, increasing pH_o to 8.5 shortened the Dur and had no effect on the OS. In SA node tissue, the BR was slowed (by 6.6%) 10 min after pH_o was reduced to 6.5 and BR was accelerated (by 10.1%) 10 min after pH_o was increased to 8.5. In contrast, we observed no change in BR 4 min after pH_o was reduced to 6.8 and a significant slowing of BR (by 3.7%) 4 min after pH_o was increased to 8.5. Unfortunately, Satoh and Seyama (37) did not mention whether any of the changes they observed were statistically significant. Although some of the results of the two studies differ, this is not surprising because the extracellular environments of isolated pacemaker cells

and pacemaker cells within SA node tissue are so different.

Role of Na/H exchange. Na/H exchange contributes to the maintenance of H^+ homeostasis in rabbit SA node cells (7), and extracellular acidosis attenuates Na/H exchange in sheep Purkinje fibers (41). Therefore, we tested the hypothesis that pH 6.6 ischemic Tyrode solution inhibits Na/H exchange, thereby reducing pH_i in SA node pacemaker cells. We found that the time constant for recovery of pH_i from NH_4Cl -induced acidosis was increased significantly (from 3.2 to 8.2 min) by pH 6.6 Tyrode solution, which suggests that acidic pH_o does indeed attenuate Na/H exchange. Nevertheless, in the presence of pH 7.4 Tyrode solution, 30 μM HOE-642, a potent inhibitor of NHE-1 (36), which also significantly increased the time constant for recovery of pH_i from NH_4Cl -induced acidosis (from 3.2 to 6.9 min), reduced pH_i by <0.05 pH unit in 4 cells and had no measurable effect in 4 others. These results suggest that Na/H exchange plays no role in the reduction of pH_i in response to extracellular acidosis. Furthermore, HOE-642 did not alter spontaneous electrical activity, did not prevent the changes in electrical activity induced by pH 6.6 ischemic Tyrode, and did not prevent recovery of electrical activity after washout of pH 6.6 ischemic Tyrode solution. Thus we conclude that Na/H exchange does not contribute to these changes nor does it facilitate recovery from such effects.

Ionic mechanisms. The results of previous investigations can suggest which currents might have been altered to produce the observed changes in spontaneous electrical activity. For example, reducing pH_o to 6.5 decreased the rapid component of I_K ($I_{K,r}$), whereas increasing pH_o to 8.5 enhanced $I_{K,r}$ in rabbit ventricular myocytes (42). In SA node pacemaker cells, I_K was reduced by cyanide (18) or by acidosis ($pH_o = 6.5$) (37), and partial blockade of $I_{K,r}$ by E-4031 depolarized the MDP and reduced the OS (43). These results suggest that in the present study, depolarization of the MDP by pH 6.6 ischemic Tyrode solution or by pH 6.8 Tyrode solution, and hyperpolarization of the MDP by pH 8.5 Tyrode solution could have been due to reduction and enhancement of $I_{K,r}$, respectively. Cyanide (18) and acidosis ($pH_o = 6.5$; Ref. 37) also reduced $I_{Ca,L}$ in SA node pacemaker cells, and such a reduction could have attenuated I_K and thereby depolarized the MDP if the peak of the AP were reduced sufficiently. Although we cannot rule out a direct effect of acidosis on the L-type Ca single-channel conductance, inactivation of $I_{Ca,L}$ by a depolarized membrane potential is sufficient to explain the reduction of OS in the present study, because even in the presence of pH 6.6 ischemic Tyrode solution, injection of hyperpolarizing current and the consequent recovery of MDP to a more negative potential returned the OS to its original level. On the other hand, the OS did not increase when pacemaker cells were exposed to pH 8.5 Tyrode solution and the MDP hyperpolarized. Nevertheless, this result might be explained by the fact that the original MDP (-64 ± 2 mV) was already sufficiently negative to remove any

inactivation of $I_{Ca,L}$ (15). Hyperpolarization of the MDP when pacemaker cells were exposed to pH 8.5 Tyrode suggested that we would see a similar effect when NH_4Cl increased pH_i ; however, the MDP depolarized significantly during this period. Such a depolarization, which has been observed previously under similar conditions (6, 41), has been attributed to the reduced electrochemical gradient for I_K when NH_4Cl -containing Tyrode solution is first introduced because NH_4^+ is permeable through K channels (6).

Finally, our voltage-clamp recordings suggest that even though ischemic conditions have no significant effect on I_f , they do enhance time-independent $I_{initial}$ in the pacemaker range of potentials (-70 to -40 mV). This increase is more likely to result from reduction of an outward current than from enhancement of an inward current, because acidic pH reduces the single-channel conductance and open probability of most ion channels (9). Therefore, acidosis-induced enhancement of sustained inward current (17) or TTX-sensitive "window" current (30) is unlikely. Because $30 \mu M$ $BaCl_2$ in normal Tyrode solution increased $I_{initial}$ in 4 pacemaker cells and because concentrations $\leq 50 \mu M$ are selective blockers of inward-rectifying K currents in ventricular myocytes (21) and cardiac Purkinje fibers (11, 40), we speculate that $BaCl_2$ blocked an inward-rectifying K current in our experiments. Although we have no information on the identity of this current, we speculate that it might be ACh-activated K current ($I_{K,ACh}$), because this current is activated in rabbit SA node pacemaker cells even in the absence of ACh (23), whereas I_{K1} is rarely found in these cells (32). Nevertheless, the actual identity of the ischemia-sensitive current is unknown. Therefore, additional voltage-clamp measurements of time-dependent and -independent currents, fluorescence measurements of Ca_i , and models of isolated SA node pacemaker cells (e.g., Ref. 13) will be necessary to fully understand the mechanisms responsible for the ischemia-induced changes.

The authors thank Radmila Terentjeva for assistance in isolating SA node pacemaker cells and Dr. Raul Martinez-Zaguilan for helpful suggestions and comments on the manuscript.

This study was supported by American Heart Association Grant 9950645N.

Present address of J. Qu: Dept. of Pharmacology, Columbia University, College of Physicians and Surgeons, New York, NY 10032.

REFERENCES

- Alboni P, Baggioni GF, Scarfo S, Cappato R, Percoco GF, Paparella N, and Antonioli GE. Role of sinus node artery disease in sick sinus syndrome in inferior wall acute myocardial infarction. *Am J Cardiol* 67: 1180–1184, 1991.
- Baba N, Leighton RF, and Weissler AM. Experimental cardiac ischemia: observation of the sinoatrial and atrioventricular nodes. *Lab Invest* 23: 168–178, 1970.
- Bassnett S, Reinisch L, and Beebe DC. Intracellular pH measurement using single excitation-dual emission fluorescence ratios. *Am J Physiol Cell Physiol* 258: C171–C178, 1990.
- Bevensee MO, Bashi E, and Boron WF. Effect of trace levels of nigericin on intracellular pH and acid-base transport in rat renal mesangial cells. *J Membr Biol* 169: 131–139, 1999.
- Blank PS, Silverman HS, Chung OY, Hogue BA, Stern MD, Hansford RG, Lakatta EG, and Capogrossi MC. Cytosolic pH measurements in single cardiac myocytes using carboxy-seminaphthorhodafuor-1. *Am J Physiol Heart Circ Physiol* 263: H276–H284, 1992.
- Boron WF and DeWeer P. Intracellular pH transients in squid giant axons caused by CO_2 , NH_3 , and metabolic inhibitors. *J Gen Physiol* 67: 91–112, 1976.
- Buckler KJ, Denyer JC, Vaughan-Jones RD, and Brown HF. Intracellular pH regulation in rabbit isolated sino-atrial node cells (Abstract). *J Physiol (Lond)* 426: 22P, 1990.
- Buckler KJ and Vaughan-Jones RD. Application of a new pH-sensitive fluoroprobe (carboxy-SNARF-1) for intracellular pH measurement in small, isolated cells. *Pflügers Arch* 417: 234–239, 1990.
- Carmeliet E. Cardiac ionic currents and acute ischemia: from channels to arrhythmias. *Physiol Rev* 79: 917–1017, 1999.
- Ch'en FFT, Vaughan-Jones RD, Clarke K, and Noble D. Modeling myocardial ischaemia and reperfusion. *Prog Biophys Mol Biol* 69: 515–538, 1998.
- Cohen IS, Falk RT, and Mulrine NK. Actions of barium and rubidium on membrane currents in canine Purkinje fibres. *J Physiol (Lond)* 338: 589–612, 1983.
- Couper GS, Weiss J, Hiltbrand B, and Shine KI. Extracellular pH and tension during ischemia in the isolated rabbit ventricle. *Am J Physiol Heart Circ Physiol* 247: H916–H927, 1984.
- Demir SS, Clark JW, Murphey CR, and Giles WR. A mathematical model of a rabbit sinoatrial node cell. *Am J Physiol Cell Physiol* 266: C832–C852, 1994.
- Dennis SC, Gevers W, and Opie LH. Protons in ischemia: where do they come from; where do they go to? *J Mol Cell Cardiol* 23: 1077–1086, 1991.
- Fermi B and Nathan RD. Removal of sialic acid alters both T- and L-type calcium currents in cardiac myocytes. *Am J Physiol Heart Circ Physiol* 260: H735–H743, 1991.
- Gregoratos G. Permanent pacemakers in older persons. *J Am Geriatr Soc* 47: 1125–1135, 1999.
- Guo J, Ono K, and Noma A. A sustained inward current activated at the diastolic potential range in rabbit sino-atrial node cells. *J Physiol (Lond)* 483: 1–13, 1995.
- Han X, Habuchi Y, and Giles WR. Effects of metabolic inhibition on action potentials and ionic currents in cardiac pacemaker cells (Abstract). *Circ* 90, Suppl 1: 582, 1994.
- Han X, Light PE, Giles WR, and French RJ. Identification and properties of an ATP-sensitive K^+ current in rabbit sino-atrial node pacemaker cells. *J Physiol (Lond)* 490: 337–350, 1996.
- Himori N, Walls AP, and Burkman AM. Ischaemically induced alterations in electrical activity and mechanical performance of isolated blood perfused canine myocardial preparations. *Cardiovasc Res* 24: 786–792, 1990.
- Hirano Y and Hiraoka M. Barium-induced automatic activity in isolated ventricular myocytes from guinea-pig hearts. *J Physiol (Lond)* 395: 455–472, 1988.
- Horn R and Marty A. Muscarinic activation of ionic currents measured by a new whole-cell recording method. *J Gen Physiol* 92: 145–159, 1988.
- Ito H, Ono K, and Noma A. Background conductance attributable to spontaneous opening of muscarinic K^+ channels in rabbit sino-atrial node cells. *J Physiol (Lond)* 476: 55–68, 1994.
- Kivisto T, Makiranta M, Oikarinen EL, Karhu S, Weckström M, and Sellin LC. 2,3-butanedione monoxime (BDM) increases initial yields and improves long-term survival of isolated cardiac myocytes. *Jpn J Physiol* 45: 203–210, 1995.
- Kohlhardt M, Mnich Z, and Maier G. Alterations of the excitation process of the sinoatrial pacemaker cell in the presence of anoxia and metabolic inhibitors. *J Mol Cell Cardiol* 9: 477–488, 1977.
- Ladilov YV, Siegmund B, Balser C, and Piper HM. Simulated ischemia increases the susceptibility of rat cardiomyocytes to hypercontracture. *Circ Res* 80: 69–75, 1997.
- Liu ZW, Zou AR, Demir SS, Clark JW, and Nathan RD. Characterization of a hyperpolarization-activated inward current in cultured pacemaker cells from the sinoatrial node. *J Mol Cell Cardiol* 28: 2523–2535, 1996.

28. Martínez-Zaguilán R, Gurulé MW, and Lynch RM. Simultaneous measurement of intracellular pH and Ca^{2+} in insulin-secreting cells by spectral imaging microscopy. *Am J Physiol Cell Physiol* 270: C1438–C1446, 1996.
29. Mohabir R, Lee HC, Kurz RW, and Clusin WT. Effects of ischemia and hypercarbic acidosis on myocyte calcium transients, contraction, and pH_i in perfused rabbit hearts. *Circ Res* 69: 1525–1537, 1991.
30. Muramatsu H, Zou AR, Berkowitz GA, and Nathan RD. Characterization of a TTX-sensitive Na^+ current in pacemaker cells isolated from rabbit sinoatrial node. *Am J Physiol Heart Circ Physiol* 270: H2108–H2119, 1996.
31. Nishi K, Yoshikawa Y, Sugahara K, and Morioka T. Changes in electrical activity and ultrastructure of sinoatrial nodal cells of the rabbit's heart exposed to hypoxic solution. *Circ Res* 46: 201–213, 1980.
32. Noma A, Nakayama T, Kurachi Y, and Irisawa H. Resting K^+ conductances in pacemaker and non-pacemaker heart cells of the rabbit. *Jpn J Physiol* 34: 245–254, 1984.
33. Posner P, Baker SP, Epstein ML, MacIntosh BR, and Buss DD. Effects of chronic hypoxia during maturation on the negative chronotropic effect of $[\text{H}^+]$ on the rabbit sino-atrial node. *Biol Neonate* 59: 109–113, 1991.
34. Qu J, Bell CL, and Nathan RD. Ischemia-induced changes in electrical activity and cytoplasmic Ca^{2+} in single cells isolated from the rabbit SA node (Abstract). *J Mol Cell Cardiol* 30: A252, 1998.
35. Rothman SA, Jeevanandam V, Combs WG, Furukawa S, Hsia HH, Eisen HJ, Buxton AE, and Miller JM. Eliminating bradyarrhythmias after orthotopic heart transplantation. *Circ* 94, Suppl II: 278–282, 1996.
36. Russ U, Balser C, Scholz W, Albus U, Lang HJ, Weichert A, Scholkens BA, and Goergelein H. Effects of the Na^+/H^+ -exchange inhibitor Hoe 642 on intracellular pH, calcium and sodium in isolated rat ventricular myocytes. *Pflügers Arch* 433: 26–34, 1996.
37. Satoh S and Seyama I. On the mechanism by which changes in extracellular pH affect the electrical activity of the rabbit sinoatrial node. *J Physiol (Lond)* 381: 181–191, 1986.
38. Scholz W and Albus U. Na^+/H^+ exchange and its inhibition in cardiac ischemia and reperfusion. *Basic Res Cardiol* 88: 443–455, 1993.
39. Sellin LC and McArdle JJ. Multiple effects of 2,3-butanedione monoxime. *Pharmacol Toxicol* 74: 305–313, 1994.
40. Vassalle M, Kotake H, and Lin CI. Pacemaker current, membrane resistance, and K^+ in sheep cardiac Purkinje fibres. *Cardiovasc Res* 26: 383–391, 1992.
41. Vaughan-Jones RD, Wu ML, and Bountra C. Sodium-hydrogen exchange and its role in controlling contractility during acidosis in cardiac muscle. *Mol Cell Biochem* 89: 157–162, 1989.
42. Vereecke J and Carmeliet E. The effect of external pH on the delayed rectifying K^+ current in cardiac ventricular myocytes. *Pflügers Arch* 439: 739–751, 2000.
43. Verheijck EE, van Ginneken ACG, Bourrier J, and Bouman LN. Effects of delayed rectifier current blockade by E-4031 on impulse generation in single sinoatrial nodal myocytes of the rabbit. *Circ Res* 76: 607–615, 1995.
44. Yan GX and Kleber AG. Changes in extracellular and intracellular pH in ischemic rabbit papillary muscle. *Circ Res* 71: 460–470, 1992.
45. Yoshikawa Y, Kano T, Higuchi M, and Nishi K. Effects of coenzyme Q_{10} on recovery of hypoxia-induced changes in ATP and creatine phosphate contents of sinoatrial nodal cells of the rabbit's heart after reoxygenation. *Arch Int Pharmacodyn Ther* 287: 96–108, 1987.
46. Zaza A, Micheletti M, Briosechi A, and Rocchetti M. Ionic currents during sustained pacemaker activity in rabbit sinoatrial myocytes. *J Physiol (Lond)* 505: 677–688, 1997.



РОЗДІЛ 3

КАЛЬЦІЄВА СИГНАЛІЗАЦІЯ В ЕЛЕКТРИЧНО НЕЗБУДЛИВИХ КЛІТИНАХ

3.1. Депозалежні кальцієві трансмембранні струми в ацинарних клітинах підшлункової залози

Ca²⁺ release-activated Ca²⁺ channel blockade as a potential tool in antipancreatitis therapy

Julia V. Gerasimenko^{a,1}, Oleksiy Gryshchenko^{b,1}, Pawel E. Ferdek^{a,1,2}, Eloise Stapleton^a, Tania O. G. Hébert^a, Solomiia Bychkova^c, Shuang Peng^{a,d}, Malcolm Begg^e, Oleg V. Gerasimenko^{a,2}, and Ole H. Petersen^{a,2}

^aMedical Research Council Group, Cardiff School of Biosciences, Cardiff University, Cardiff CF10 3AX Wales, United Kingdom; ^bBogomoletz Institute of Physiology, Kiev 01024, Ukraine; ^cIvan Franko National University of Lviv, Lviv 79000, Ukraine; ^dDepartment of Physiology, Medical College, Jinan University, Guangzhou 510632, China; and ^eRespiratory Therapy Area Unit, Medicines Research Centre, GlaxoSmithKline, Stevenage SG1 2NY, England, United Kingdom

Edited* by Tullio Pozzan, Foundation for Advanced Biomedical Research, Padua, Italy, and approved June 28, 2013 (received for review January 16, 2013)

Alcohol-related acute pancreatitis can be mediated by a combination of alcohol and fatty acids (fatty acid ethyl esters) and is initiated by a sustained elevation of the Ca²⁺ concentration inside pancreatic acinar cells ([Ca²⁺]_i), due to excessive release of Ca²⁺ stored inside the cells followed by Ca²⁺ entry from the interstitial fluid. The sustained [Ca²⁺]_i elevation activates intracellular digestive proenzymes resulting in necrosis and inflammation. We tested the hypothesis that pharmacological blockade of store-operated or Ca²⁺ release-activated Ca²⁺ channels (CRAC) would prevent sustained elevation of [Ca²⁺]_i and therefore protease activation and necrosis. In isolated mouse pancreatic acinar cells, CRAC channels were activated by blocking Ca²⁺ ATPase pumps in the endoplasmic reticulum with thapsigargin in the absence of external Ca²⁺. Ca²⁺ entry then occurred upon admission of Ca²⁺ to the extracellular solution. The CRAC channel blocker developed by GlaxoSmithKline, GSK-7975A, inhibited store-operated Ca²⁺ entry in a concentration-dependent manner within the range of 1 to 50 μM (IC₅₀ = 3.4 μM), but had little or no effect on the physiological Ca²⁺ spiking evoked by acetylcholine or cholecystokinin. Palmitoleic acid ethyl ester (100 μM), an important mediator of alcohol-related pancreatitis, evoked a sustained elevation of [Ca²⁺]_i, which was markedly reduced by CRAC blockade. Importantly, the palmitoleic acid ethyl ester-induced trypsin and protease activity as well as necrosis were almost abolished by blocking CRAC channels. There is currently no specific treatment of pancreatitis, but our data show that pharmacological CRAC blockade is highly effective against toxic [Ca²⁺]_i elevation, necrosis, and trypsin/protease activity and therefore has potential to effectively treat pancreatitis.

capacitative Ca²⁺ entry | alcohol metabolite | pancreas | hepatocyte Ca²⁺ entry | AR42J

Acute pancreatitis is a human disease mostly caused by alcohol abuse or complications from biliary disease. In this disease, against which there is currently no effective therapy, digestive proenzymes are prematurely activated inside the acinar cells leading to autodigestion and necrosis (1–3). Intracellular Ca²⁺ plays a critical role in the initiation of this disease process (2–4), but intracellular Ca²⁺ also plays a critical role in the physiological regulation of the normal exocytotic secretion of the digestive proenzymes (5).

The pancreatic acinar cells are capable of generating multiple patterns of cytosolic Ca²⁺ signals depending on the type and concentration of the stimulating agent (5). The physiological Ca²⁺ signals regulating secretion—evoked by the neurotransmitter acetylcholine (ACh) or the hormone cholecystokinin (CCK)—consist of repetitive short-lasting rises in the cytosolic Ca²⁺ concentration ([Ca²⁺]_i). These are mostly confined to the apical area, in which the secretory (zymogen) granules (ZGs) are concentrated, by a belt of perigranular mitochondria operating as a firewall against the globalization of the Ca²⁺ signals (6). Rapid Ca²⁺ uptake into the perigranular mitochondria following local cytosolic Ca²⁺ signals also plays a crucial role in activating local mitochondrial ATP production, which is essential for the

exocytotic secretion process (5–9). At supraphysiological concentrations of ACh or CCK, or in response to various types of pathological stimulants, sustained global elevations of [Ca²⁺]_i occur (2, 4). Such signals initiate trypsinogen activation in the apical region of the pancreatic acinar cells as well as vacuole formation (10, 11). Both the trypsinogen activation and the intracellular vacuolization can be prevented by intracellular Ca²⁺ chelation or simply by removal of extracellular Ca²⁺ (10).

Unlike nerve and endocrine as well as muscle cells, exocrine cells do not possess voltage-gated Ca²⁺ channels and the cytosolic Ca²⁺ signals governing pancreatic acinar secretion are primarily generated by release of Ca²⁺ from intracellular stores, principally the endoplasmic reticulum (ER) (5, 12, 13). However, the intracellular Ca²⁺ stores are by definition finite. Ca²⁺ ATPase pumps in the plasma membrane are activated to increase extrusion of Ca²⁺ whenever [Ca²⁺]_i increases and therefore pancreatic acinar cells would run out of Ca²⁺ in the ER if there were not a mechanism of compensatory Ca²⁺ uptake from the external solution (5). This uptake mechanism is known as store-operated or Ca²⁺ release-activated Ca²⁺ entry (CRAC) and CRAC channels in the plasma membrane have generally been well characterized (14). The molecular nature of these channels (Orai1) is now also known (15) and the link between Ca²⁺ depletion of the ER and opening of the CRAC channels has been established: A reduction in the Ca²⁺ concentration in the ER ([Ca²⁺]_{ER}) causes translocation of a Ca²⁺-sensing protein, called STIM1, widely distributed in the ER membrane to so-called puncta in the ER close to the plasma membrane, where it can interact with and open Orai1 channels (16–18). This mechanism also operates in the pancreatic acinar cells, because stimulant-elicited release of Ca²⁺ from the ER results in translocation of STIM1 to puncta close to the basolateral plasma membrane, specifically at locations where the ER is devoid of ribosomes and where interaction between STIM1 and Orai1 therefore occurs (19). Despite this, electrophysiological investigations of the currents evoked by Ca²⁺ store depletion have so far failed to provide evidence for the existence in pancreatic acinar cells of Ca²⁺-selective currents of the CRAC type (20–22) originally discovered in mast cells (23), although activation of nonselective currents were shown (21, 22). Therefore, although the linkage between agonist-evoked Ca²⁺ release from the ER and store-operated Ca²⁺ entry, through STIM1

Author contributions: J.V.G., O.G., P.E.F., M.B., O.V.G., and O.H.P. designed research; J.V.G., O.G., P.E.F., E.S., T.O.G.H., S.B., and S.P. performed research; M.B. contributed new reagents/analytic tools; J.V.G., O.G., P.E.F., E.S., and O.V.G. analyzed data; and J.V.G., O.V.G., and O.H.P. wrote the paper.

The authors declare no conflict of interest.

*This Direct Submission article had a prearranged editor.

Freely available online through the PNAS open access option.

¹J.V.G., O.G., and P.E.F. contributed equally to this work.

²To whom correspondence may be addressed. E-mail: PetersenOH@cardiff.ac.uk, FerdekPE@cardiff.ac.uk, or GerasimenkoOV@cardiff.ac.uk.

This article contains supporting information online at www.pnas.org/lookup/suppl/doi:10.1073/pnas.1300910110/-DCSupplemental.

and Orai1, is established for the pancreatic acinar cells (19), there is uncertainty about the biophysical nature of the principal Ca^{2+} entry channels. Endocytic Ca^{2+} uptake (24) could also be important and does occur in pancreatic acinar cells (25). It is also the case that there are important intracellular Ca^{2+} stores (acid) outside the ER (4, 26–29). Ca^{2+} release from acid stores—located in ZGs, endosomes, and lysosomes—plays a crucial role in intracellular trypsinogen activation elicited by alcohol and fatty acid ethyl esters in experiments on permeabilized pancreatic acinar cells (28, 29), and trypsinogen activation induced by hyperstimulation occurs in postexocytotic endocytic (and acid) structures (25). In view of the complexities of pancreatic acinar cell Ca^{2+} signaling in physiology and pathology and, in particular, the uncertainty about the nature of the Ca^{2+} entry pathways, it is unknown whether blockade of Ca^{2+} -selective CRAC channels could in principle be effective as therapy against acute pancreatitis. With the availability of relatively specific CRAC channel blockers (30–34) there is now an opportunity to test the hypothesis that one type of Ca^{2+} entry channel is so important that pharmacological blockade could afford effective protection against toxic Ca^{2+} signal generation and its consequences in intact pancreatic acinar cells. Given the current absence of any specific therapy against pancreatitis, a demonstration that pharmacological blockade of CRAC channels could prevent the dangerous necrosis evoked by agents known to initiate pancreatitis, would be a proof of principle that a specific therapy could be developed. In this study we have therefore tested the effect of the CRAC channel blocker developed by GlaxoSmithKline, GSK-7975A (33, 34) on store-operated Ca^{2+} entry, induced by inhibiting specifically the Ca^{2+} -ATPase pumps in the ER, as well as on Ca^{2+} signal generation elicited by palmitoleic acid ethyl ester (POAEE), one of the mediators of alcohol-related pancreatitis (26, 35–38). As part of this investigation we also provide a characterization of Ca^{2+} -selective CRAC currents in pancreatic acinar cells. We show that pharmacological CRAC channel blockade prevents the sustained toxic elevation of $[\text{Ca}^{2+}]_i$, which is induced by severe depletion of intracellular Ca^{2+} stores or by POAEE. In contrast, such a blockade has little effect on the physiological Ca^{2+} spiking (oscillations) evoked by ACh or CCK and has only minor or no effects on Ca^{2+} entry in hepatocytes and the pancreatic acinar cell line AR42J. Importantly, the CRAC blocker is also effective against the intracellular protease activation and necrosis induced by POAEE. We conclude that pharmacological CRAC blockade has potential for effective treatment of acute pancreatitis.

Results

GSK-7975A Blocks Store-Operated Ca^{2+} Entry in Normal Pancreatic Acinar Cells. Our standard protocol for store-operated Ca^{2+} entry investigations consisted of first emptying the ER store of Ca^{2+} by applying the specific ER Ca^{2+} pump blocker thapsigargin (TG) in the absence of external Ca^{2+} . This caused a transient rise in $[\text{Ca}^{2+}]_i$ (Fig. 1A). After $[\text{Ca}^{2+}]_i$ had returned to near its normal resting level, Ca^{2+} was admitted to the external solution and this resulted in a substantial rise in $[\text{Ca}^{2+}]_i$, which was sustained as long as Ca^{2+} was present outside the cell (Fig. 1A). When the CRAC blocker GSK-7975A was applied before the admission of Ca^{2+} to the external solution, the subsequent rise in $[\text{Ca}^{2+}]_i$ was markedly reduced (Fig. 1B–D). As seen in Fig. 1D, the effect of GSK-7975A was maintained after washout of the compound at least for the first 10–15 min. As summarized in Fig. 1E, the inhibitory effect was already marked 5 min after start of exposure to GSK-7975A and after 10 min exposure there was very little Ca^{2+} entry. Ten minutes after the start of washout of GSK-7975A, there was still no recovery of Ca^{2+} entry (Fig. 1E). Importantly, GSK-7975A had no influence on the thapsigargin-evoked Ca^{2+} mobilization from the ER store (Fig. 1D). GSK-7975A also had little or no effect on the Ca^{2+} spiking responses

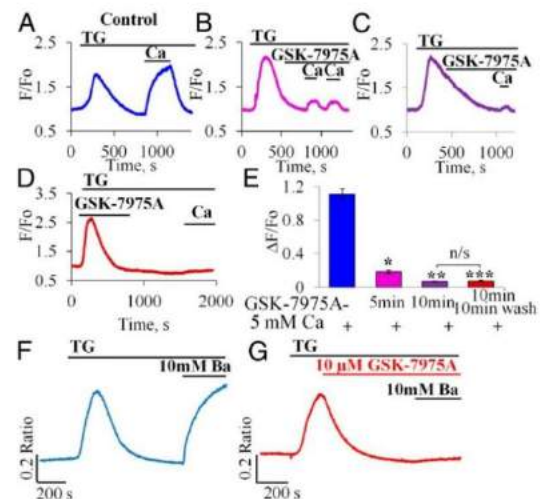


Fig. 1. CRAC channel blocker inhibits Ca^{2+} and Ba^{2+} influx. (A–C) Effects of different periods of incubation [5 min, $n = 5$ (B) and 10 min, $n = 14$ (C)] of pancreatic acinar cells with GSK-7975A (10 μM) compared with control (A, $n = 5$) (15 min incubation did not significantly further increase the degree of blockade, $n = 3$). (D) Washout of GSK-7975A did not result in recovery of the Ca^{2+} signal within ~ 10 min. (E) Summary of results shown in A–D. Mean $[\text{Ca}^{2+}]_i$ amplitude change ($\Delta F/F_0$) due to Ca^{2+} influx ($n = 5$, example trace in A) was dramatically reduced after 5 min with GSK-7975A ($n = 14$, $*P < 10^{-6}$, example trace in B) and reduced further after 10 min with GSK-7975A ($n = 14$, $**P < 10^{-11}$, example trace in C). Inhibition was effectively irreversible (after washing out for 10 min) as amplitude remained very low ($n = 7$, $***P < 10^{-8}$, example trace in D). As seen in E, there was no significant difference in averaged amplitudes from experiments of the type shown in C and D ($P > 0.69$); whereas the averaged amplitudes from the type of experiments shown in B and C are significantly different ($P < 10^{-6}$). Data presented as mean \pm SEM (F and G) GSK-7975A inhibits Ba^{2+} influx in pancreatic acinar cells. Representative traces of changes in $[\text{Ba}^{2+}]_i$ (using Fura-2) due to Ba^{2+} influx in cells exposed to GSK-7975A (10 μM) for 10 min (G) compared with control untreated cells (F).

to low (physiological) concentrations of the normal stimulants of pancreatic secretion, namely ACh (50 and 100 nM) or CCK (5 μM) (Fig. S1 A–F) but reduced the late elevated $[\text{Ca}^{2+}]_i$ plateau phase following stimulation with a high concentration of ACh (1 μM) (Fig. S1 G and H).

Inhibition of Unidirectional Ba^{2+} Influx. Net Ca^{2+} transport across the plasma membrane depends not only on Ca^{2+} influx, but also on Ca^{2+} extrusion and in the pancreatic acinar cells, extrusion is mediated exclusively by the plasma membrane Ca^{2+} pump, activated by a rise in $[\text{Ca}^{2+}]_i$ (39). To assess changes in unidirectional Ca^{2+} influx, we used measurements of $[\text{Ba}^{2+}]_i$, because Ba^{2+} can easily pass through CRAC channels (40), but cannot be extruded by the plasma membrane Ca^{2+} pump (39, 40). As seen in Fig. 1 F and G, preincubation with GSK-7975A for 10 min markedly reduced store-operated Ba^{2+} entry into the pancreatic acinar cells. Our data on the inhibition of Ba^{2+} entry by the CRAC blocker are summarized in Fig. S1 I–K.

Concentration Dependence of the Acute Effects of GSK-7975A on Ca^{2+} Entry. We also investigated the acute effect of the CRAC blocking agent. As seen in Fig. 2A, application of 10 μM GSK-7975A soon after admission of Ca^{2+} to the external solution resulted, after a delay of a few minutes, in a sharp reduction of $[\text{Ca}^{2+}]_i$, which, in the continued presence of external Ca^{2+} , fell to

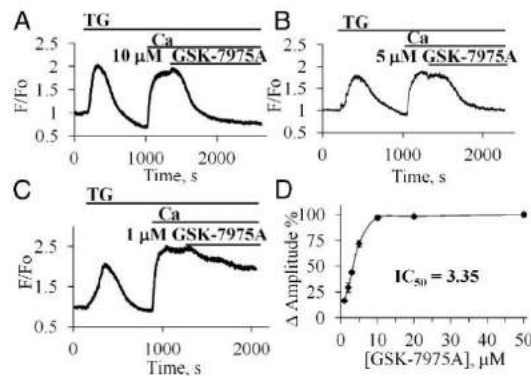


Fig. 2. Concentration dependence of the inhibitory effect of GSK-7975A on the elevated $[Ca^{2+}]_i$ following readmission of external Ca^{2+} after thapsigargin treatment. (A–C) Effects of acute application of GSK-7975A in different concentrations [10 μ M (A), 5 μ M (B), 1 μ M (C)] on the elevated $[Ca^{2+}]_i$ plateau in the presence of 5 mM $CaCl_2$. (D) Summary of the results of the experiments on the concentration dependence of the inhibitory effect of GSK-7975A normalized to the inhibitory effect of 50 μ M (100%).

near the normal resting level within 5–10 min. The relatively slow time course of the GSK-7975A-induced reduction in $[Ca^{2+}]_i$ is not necessarily a reflection of a slow action of the CRAC blocker, but may reflect the time it takes for the plasma membrane Ca^{2+} pump to extrude the excess of Ca^{2+} in the cytosol. We also tested the effects of different CRAC blocker concentrations. As seen in Fig. 2A and B, the effects of 5 and 10 μ M GSK-7975A were very similar, indicating that the maximal effect had already been attained at 5 μ M. A small reduction in $[Ca^{2+}]_i$ was seen at 1 μ M (Fig. 2C). Fig. 2D shows the relationship between CRAC blocker concentration and the degree of reduction in $[Ca^{2+}]_i$. IC_{50} was calculated to be 3.4 μ M. The estimated $t_{1/2}$ was 292.8 ± 88.3 s. Even the highest concentration of GSK-7975A tested (50 μ M) did not abolish Ca^{2+} entry into pancreatic acinar cells, at the external $[Ca^{2+}]_o$ of 5 mM, but dramatically inhibited it by $87.6 \pm 1.9\%$ ($n = 10$).

Inhibition of Store-Operated Ca^{2+} Current. Application of 2 μ M TG activated a slowly developing inward membrane current (Fig. 3A, i) with a maximal amplitude of 8.4 ± 0.6 pA ($n = 35$, or 0.349 pA/pF; $C_m = 22.3 \pm 1.7$ pF) at a membrane potential of -50 mV and $[Ca^{2+}]_o = 10$ mM. Replacement of extracellular Na^+ by N-methyl-D-glucamine (NMDG $^+$) had little or no effect on the current (Fig. 3A, i, $n = 8$), whereas a reduction in $[Ca^{2+}]_o$ from 10 to 1 mM caused a marked decrease in the maximally developed inward current ($n = 7$) (Fig. 3A, ii). The store-operated inward current was blocked by 100 μ M 2-Aminoethoxydiphenyl borate (2-APB) ($n = 7$) (Fig. 3A, i), a well-known (but not specific) blocker of CRAC channels (14). The current–voltage relationship showed clear inward rectification (Fig. 3B). We recorded the store-operated Ca^{2+} current in experiments in which we also monitored changes in the Ca^{2+} concentration inside the stores (41). The TG-induced inward current developed with a delay after the reduction in the store Ca^{2+} concentration (Fig. 3C) ($n = 9$). GSK-7975 (10 μ M) evoked a marked reduction (by $83.0 \pm 4.1\%$) in the TG-induced inward current in each of the six experiments carried out (Fig. 3D).

The Effect of Blocking CRAC Channels on $[Ca^{2+}]_i$ Changes Evoked by Palmitoleic Acid Ethyl Ester. Elevation of $[Ca^{2+}]_i$ in pancreatic acinar cells can be induced by either alcohol or fatty acids (42, 43), but in combination—as fatty acid ethyl esters—they are

much more powerful Ca^{2+} releasers (37) and are recognized as important mediators of alcohol-induced pancreatitis (35–38, 42). We therefore tested the effects of blocking CRAC channels on the changes in $[Ca^{2+}]_i$ induced by palmitoleic acid ethyl ester (POAEE). As previously shown, POAEE evokes substantial and sustained elevations of $[Ca^{2+}]_i$ in normal isolated pancreatic acinar cells, initiated by release of Ca^{2+} from the ER (37, 42) as well as acid stores (28). Fig. 4A shows the substantial and sustained rise in $[Ca^{2+}]_i$ elicited by 100 μ M POAEE as well as the much diminished cytosolic Ca^{2+} signal evoked by the same concentration of POAEE in the presence of GSK-7975A. Fig. 4B shows the mean values of all of the data from this series of experiments. It is clear that GSK-7975A very markedly inhibits the $[Ca^{2+}]_i$ elevation normally evoked by 100 μ M POAEE.

Inhibition of CRAC Channels Protects Against POAEE-Induced Trypsin and Protease Activation. It has been shown previously that hyperstimulation-induced trypsinogen activation and vacuolization can be prevented by intracellular Ca^{2+} chelation or simply by removal of extracellular Ca^{2+} (10). Preincubation (1 h) of pancreatic acinar cells with POAEE (100 μ M) induced a substantial increase of protease activity (from $6.8 \pm 1.3\%$ of cells in control to $31.2 \pm 1.6\%$ of cells, Fig. 4C). Pretreatment of cells with 10 μ M GSK-7975A for 10 min before POAEE application reduced protease activity to levels relatively close to control (Fig. 4C). Similar levels of inhibition by GSK-7975A were observed in experiments assessing trypsin activity, using the specific trypsin substrate BZIPAR (10, 28, 29). Preincubation of pancreatic acinar cells with POAEE (100 μ M for 1 h) induced substantial increase of trypsin activity (from $3.4 \pm 0.5\%$ of cells in control to

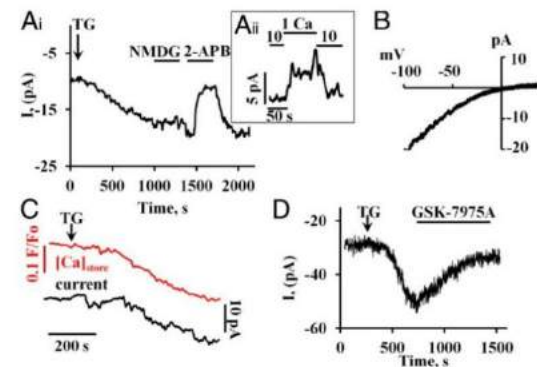


Fig. 3. Store-operated ionic currents, developing after thapsigargin treatment, recorded with the whole cell patch clamp configuration. The individual traces shown were all recorded at a holding potential of -50 mV and with an external $[Ca^{2+}]_o$ of 10 mM. To prevent activation of the large Ca^{2+} -dependent ion currents in acinar cells (13), patch clamp pipettes were filled with a solution containing a mixture of 10 mM BAPTA and 2 mM Ca^{2+} . (A, i) Inward current induced by bath application of 2 μ M TG to empty the ER Ca^{2+} content. Replacing Na^+ with NMDG $^+$ had little effect on the inward current, but 100 μ M of 2-APB practically abolished the current. This effect was rapidly reversible. (A, ii) Reducing the external Ca^{2+} concentration from 10 to 1 mM (replacement of $CaCl_2$ by $MgCl_2$) reduced reversibly the stable maximal plateau amplitude of the inward current during TG exposure. (B) Representative I/V curve obtained using a voltage ramp protocol (0.4 V/s) from -100 mV to 40 mV (difference between ramp registration before and after 2-APB application). (C) Simultaneous measurements of changes in the intrastore $[Ca^{2+}]_i$ and the membrane current following TG application. The upper red trace shows the gradual reduction of the intrastore Ca^{2+} concentration recorded by changes of Fluo-5N fluorescence. The lower black trace shows the development of the inward current. (D) GSK-7975 (10 μ M) inhibits markedly the inward current evoked by application of 2 μ M TG.

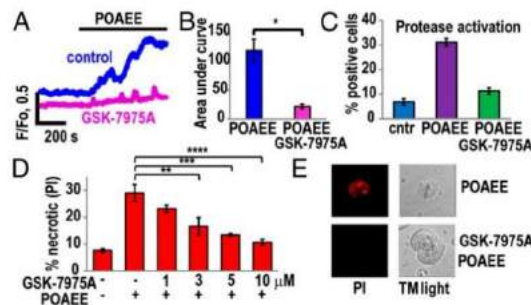


Fig. 4. GSK-7975A dramatically reduces Ca^{2+} overload and necrosis induced by the fatty acid ethyl ester POAEE. (A) Representative traces of changes in $[\text{Ca}^{2+}]_i$ in response to 100 μM POAEE in the absence ($n = 8$) and presence of GSK-7975A (10 μM) ($n = 12$). (B) Quantitative analysis of experiments of the type shown in A by comparing the integrated $[\text{Ca}^{2+}]_i$ elevation above the baseline (area under the curve) recorded during the first 10 min of POAEE application. Blue bar represents the control (without GSK-7975A), whereas the red bar represents the test results (cells pretreated with 10 μM GSK-7975A for 10 min before application of POAEE). The mean values ($\pm\text{SEM}$) are significantly different, $P < 0.0002$. (C) Pretreatment of cells with 10 μM GSK-7975A for 10 min inhibited by 64% (green bar) protease activation induced by POAEE (100 μM) (purple bar) as measured with generic protease substrate bis- α -aspartic acid amide rhodamine 110 (D2-R110). Blue bar represents the results from control (not exposed to POAEE) cells. The mean values ($\pm\text{SEM}$) in control and GSK-7975A plus POAEE treatment are not significantly different, $P = 0.05$; $n = 4$, >200 cells in each group. (D) POAEE (100 μM)-induced necrosis was dramatically reduced in cells treated with 1 μM , 3 μM , 5 μM , and 10 μM GSK-7975A for 10 min. In the control series of experiments (no POAEE treatment), the level of necrosis was low ($n = 3$ series of experiments with number of tested cells in each group >350). Inhibition of necrosis was significant for 3 μM GSK-7975A ($**P < 0.02$) and highly significant for 5 and 10 μM GSK-7975A ($***P < 0.003$ and $****P < 0.001$). (E) Necrosis was visualized by staining cells with propidium iodide (PI). All experiments were performed in the presence of 1 mM CaCl_2 .

$15 \pm 1.1\%$ in the POAEE-treated groups). Pretreatment of cells with GSK-7975A (10 μM for 10 min) before POAEE application substantially reduced trypsinogen activation ($6.9 \pm 0.7\%$ of cells, $P < 0.0009$, $n = 4$ series of experiments with number of cells >150 in each group).

Blockade of CRAC Channels Protects Against POAEE-Elicited Necrosis.

It has previously been shown that POAEE elicits Ca^{2+} -dependent necrosis of pancreatic acinar cells (37, 42). Because GSK-7975A protects against the POAEE-induced $[\text{Ca}^{2+}]_i$ rise, as well as against protease activation, we tested whether it would also protect against necrosis. As seen in Fig. 4D and E, GSK-7975A did indeed provide a concentration-dependent protection against the development of POAEE-induced necrosis. There was a protective effect already at 3 μM and at 10 μM the percentage of necrotic cells was only slightly higher than the control value (without POAEE) (Fig. 4D).

GSK-7975A Protects Against Necrosis Solely by Inhibiting Ca^{2+} Entry.

Although GSK-7975A inhibits markedly both Ca^{2+} entry and necrosis, it is theoretically possible that the protection against necrosis could be due to an effect other than on Ca^{2+} entry. To test this point, we exploited the ability of 2-APB—a well-known CRAC blocker (14) (Fig. 3)—to also elicit cytosolic Ca^{2+} signals in pancreatic acinar cells (44). At 100 μM , 2-APB induced substantial rises in $[\text{Ca}^{2+}]_i$ and also induced marked necrosis (Fig. S2), but in this situation (where the CRAC channels are already blocked by 2-APB) GSK-7975A was unable to inhibit necrosis (Fig. S2B). We also carried out an experiment in which we counteracted the inhibitory effect of GSK-7975A by increasing

$[\text{Ca}^{2+}]_o$ (Fig. S3) and tested the effect on necrosis. At $[\text{Ca}^{2+}]_o = 1$ mM, POAEE evokes a significant increase in $[\text{Ca}^{2+}]_i$ (Fig. 4A) and a substantial increase in the percentage of necrotic cells (Fig. 4D), which is markedly inhibited by GSK-7975A (Fig. 4D). Raising $[\text{Ca}^{2+}]_o$ to 10 mM in the presence of inhibitor restored the POAEE-induced $[\text{Ca}^{2+}]_i$ elevation (Fig. S3A) and increased the POAEE-induced rise in the percentage of necrotic cells to the level seen without GSK-7975A at $[\text{Ca}^{2+}]_o = 1$ mM (Fig. S3B). These experiments (Figs. S2 and S3) indicate that the protective effect of GSK-7975A against necrosis is solely due to inhibition of Ca^{2+} entry.

The Effects of Blocking CRAC Channels on $[\text{Ca}^{2+}]_i$ Changes Evoked by Acetylcholine.

We tested whether CRAC blockade would also prevent the normal cytosolic Ca^{2+} spiking, elicited by ACh or CCK. As seen in Fig. S1, a low ACh concentration (50 or 100 nM) evoked repetitive $[\text{Ca}^{2+}]_i$ spikes and this spike generation was hardly affected, at least for the first ~ 15 min, by application of 10 μM GSK-7975A (Fig. S1A, B, and D–F). Likewise, the Ca^{2+} spiking evoked by 5 pM CCK was only affected to a minor degree by CRAC blockade (Fig. S1C). A high ACh concentration (1 μM) evoked a large initial rise in $[\text{Ca}^{2+}]_i$, followed by a slow decline toward a sustained quasiplateau at a slightly elevated $[\text{Ca}^{2+}]_i$ (Fig. S1G). In this case, blockade of CRAC channels markedly reduced or even eliminated the sustained plateau phase and during continued exposure to the high (1 μM) ACh concentration, $[\text{Ca}^{2+}]_i$ returned to the prestimulation resting level (Fig. S1G and H). Because CRAC blockade markedly reduced the sustained phase of Ca^{2+} entry, during prolonged supramaximal stimulation, we tested to what an extent this would have an effect on the intracellular Ca^{2+} stores. A 1-h preincubation of the acinar cells with 10 μM GSK-7975A had very little effect on the rise in $[\text{Ca}^{2+}]_i$ in response to a supramaximal ACh stimulus (10 μM) in the presence of thapsigargin (Fig. S4A and B). To assess the potential effect of CRAC blockade on Ca^{2+} store reloading, we compared the magnitudes of the $[\text{Ca}^{2+}]_i$ response to a second stimulation with a high concentration of ACh (10 μM), after a long period of rest, under three different conditions, namely control, absence of external Ca^{2+} , and in the presence of both Ca^{2+} and the CRAC blocker (Fig. S4C). In the pancreatic acinar cells, full reloading of virtually empty ER stores is a very slow process (45, 46) and, as seen by comparing Fig. S4A with C, a second supramaximal ACh stimulus, even after a substantial interval during control conditions, only evoked a much diminished response. Even in the absence of external Ca^{2+} , there is a tiny rise in $[\text{Ca}^{2+}]_i$ following the second ACh application, most likely due to a small reuptake of Ca^{2+} into the ER before all of the released Ca^{2+} had been extruded across the cell membrane. In the presence of 10 μM GSK-7975A with external Ca^{2+} , there is a significant reduction in the amplitude of the second response to ACh compared with the control situation, but this reduced response is nevertheless significantly larger than the one seen under Ca^{2+} -free conditions (Fig. S4C and D). This is consistent with our finding that store-operated Ca^{2+} entry is not abolished by 10 μM GSK-7975A, although very markedly diminished (Fig. 1).

Effect of CRAC Blockade in Other Cell Types. We have also tested whether CRAC channel blockade in other cell types would have effects on store-operated Ca^{2+} entry. In freshly isolated mouse hepatocytes, using the classical thapsigargin protocol for examining store-operated Ca^{2+} entry, we only found a relatively modest inhibitory effect of GSK-7975A ($P < 0.042$, Fig. S5A–C) compared with what was observed in pancreatic acinar cells (Fig. 1). We also tested the pancreatic acinar cell line AR42J, which has a neuronal phenotype (47). As seen in Fig. S6, GSK-7975A had little effect on store-operated Ca^{2+} entry in these cells, in

marked contrast to what we show for the real pancreatic acinar cells (Fig. 1).

Discussion

The results presented here indicate that blockade of store-operated Ca^{2+} -selective entry channels effectively prevents an important mediator of alcohol-related pancreatitis, POAEE, from evoking sustained elevation of $[\text{Ca}^{2+}]_i$, protease activation, and pancreatic acinar cell necrosis. This indicates that pharmacological CRAC blockade has therapeutic potential as a unique rational treatment against severe acute pancreatitis, a life-threatening human disease that at the moment is untreatable. Our result, showing that a CRAC channel blocker markedly reduces the sustained $[\text{Ca}^{2+}]_i$ elevation that normally follows depletion of the Ca^{2+} store in the ER (Figs. 1 and 2), provides fresh evidence for the importance of store-operated Ca^{2+} channels in this phase of Ca^{2+} signaling, which has already been identified as crucial for the initiation of acinar cell injury (10). Although it has been known for 40 years that cytosolic Ca^{2+} signals in pancreatic acinar cells are initiated by release from internal stores (5), it has also been recognized for a long time that following the initial release from the intracellular stores there is an important Ca^{2+} entry phase that is essential for refilling the stores and indeed for stimulant-evoked enzyme secretion (48–50). Previous investigations have demonstrated that the most important mediators of acinar cell damage, namely alcohol, fatty acids, fatty acid ethyl esters, and bile acids all primarily release Ca^{2+} from various internal stores (28, 29, 37, 42, 43, 51), but that this initial phase is followed by store-operated Ca^{2+} entry, which plays a crucial role in the destruction of the cells (2, 4, 5, 10). Our electrophysiological data (Fig. 3) show that in the pancreatic acinar cells this store-operated inward current is relatively insensitive to removal of external Na^+ , but sensitive to changes in the external Ca^{2+} concentration. It is therefore not a Transient receptor potential (TRP)-type non-selective cation current, but a Ca^{2+} -selective CRAC-type current, consistent with the very marked current inhibition evoked by GSK-7975A (Fig. 3D), a relatively selective CRAC channel blocker with almost no inhibitory effect on TRP-channel currents (with the exception of those mediated by TRPV6) (33). This agent has recently been shown to block Ca^{2+} currents through CRAC channels in human lung mast cells, T cells, and platelets (31–34). The CRAC channel is emerging as a potentially important therapeutic target in a number of human diseases (52, 53) and could also be important for pancreatitis (54). We have therefore used GSK-7975A (33, 34), to inhibit store-operated Ca^{2+} entry in pancreatic acinar cells. GSK-7975A markedly inhibited Ca^{2+} and Ba^{2+} entry elicited by releasing Ca^{2+} from the ER (Figs. 1–3) as well as the late phase Ca^{2+} entry in response to stimulation with a high ACh concentration (Fig. S1). These results indicate therapeutic potential for curbing excessive Ca^{2+} entry in the early phase of pancreatitis.

We have specifically investigated one pathophysiologically relevant situation, namely the acinar cell injury initiated by POAEE, one of the known mediators of alcohol-related pancreatitis (35–37, 42). These data (Fig. 4) show not only that GSK-7975A markedly reduces the POAEE-evoked $[\text{Ca}^{2+}]_i$ elevation, but—even more importantly—also markedly inhibits the extent of the protease activation and necrosis induced by this fatty acid ethyl ester. The GSK-7975A CRAC channel blocker did not inhibit completely the unidirectional Ba^{2+} inflow evoked by arresting the ER Ca^{2+} pump (Fig. S1 I–K) and this inability to abolish store-operated Ca^{2+} entry (also reflected in Fig. 1 A–E) may be the reason that GSK-7975A has so little effect on the repetitive Ca^{2+} spiking elicited by a low ACh concentration or a physiological CCK concentration (Fig. S1). Although Ca^{2+} spikes are due to release of Ca^{2+} from intracellular stores, the cell should eventually run out of Ca^{2+} in the absence of Ca^{2+}

entry because every time $[\text{Ca}^{2+}]_i$ goes up there will be activation of the plasma membrane Ca^{2+} pump and therefore loss of Ca^{2+} to the external environment (5). However, because the loss of Ca^{2+} during short spikes of the type shown in Fig. S1 is relatively small (5), even a severely reduced level of Ca^{2+} entry may be sufficient to prevent depletion of the intracellular stores. This point is also relevant with regard to another potential concern, namely the apparent irreversibility of the effect of GSK-7975A, at least for ~10 min following start of washout (Fig. 1). Because of the incompleteness of the CRAC blockade in the acinar cells (Fig. 1 and Fig. S1 I and J), this may turn out not to be a serious problem for potential therapeutic use. Resting pancreatic acinar cells appeared to have unchanged levels of Ca^{2+} in the ER store after 1 h of incubation with GSK-7975A (Fig. S4 A and B). Although reloading of the intracellular stores after strong stimulation with ACh was reduced by the CRAC blocker, there was still a significant level of store refilling, compared with conditions when there was no Ca^{2+} entry due to absence of external Ca^{2+} (Fig. S4 C and D).

CRAC channels are widely distributed in many different cell types and effective CRAC blockade might therefore also have effects on other organ systems. However, the effects are likely to be strongest in those cell types (like the pancreatic acinar cells) in which other types of Ca^{2+} entry pathways are not quantitatively important, unlike the many types of electrically excitable cells. Mast cells and T cells, for example, will be affected by CRAC blockade (31, 34, 52, 53), but this will be advantageous in the treatment of acute pancreatitis, where the initial damage of the acinar cells leading to necrosis is followed by a strong inflammatory response, which is known to cause very significant further damage (1). CRAC blockade would have the most pronounced effect on cells with the most strongly activated Ca^{2+} entry channels, which, in cases of life-threatening severe pancreatitis, would be the pancreatic acinar cells. With regard to organ selectivity, it is interesting that CRAC channel blockade was much less effective in inhibiting store-operated Ca^{2+} entry in hepatocytes and in the neuronal-like AR42J cell line (compare Fig. 1 with Figs. S5 and S6), probably reflecting a more complex situation in these cells (47, 55).

Although CRAC channel inhibition will very effectively reduce cytosolic Ca^{2+} overload, it will not prevent the depletion of intracellular Ca^{2+} stores evoked by POAEE. It could therefore be potentially advantageous to combine CRAC blockade with inhibition of Ca^{2+} release from the internal stores using a synthetic membrane permeable calmodulin activator (29). Overall, our data provide a unique proof of principle that pharmacological CRAC channel inhibition could become an effective tool for reducing the cellular Ca^{2+} overload that is such an important feature of the changes occurring in the initial phase of acute pancreatitis. Specifically, our finding that GSK-7975A markedly inhibits not only the excessive $[\text{Ca}^{2+}]_i$ elevation evoked by POAEE, an important mediator of alcohol-related pancreatitis, but also markedly reduces the extent of the associated protease activation and necrosis—although it has little or no effect on the repetitive short-lasting Ca^{2+} spikes evoked by the physiological neurotransmitter ACh—is promising.

Materials and Methods

Full methods are provided in *SI Materials and Methods*. Details about isolation of pancreatic acinar cells were described previously (56). GSK-7975A was provided by GlaxoSmithKline (31). Fluorescent measurements were performed with Fluo-4 or Fura-2 (39), whereas necrosis was assessed with propidium iodide (39) and trypsinogen activation with trypsin fluorescent substrate (10, 29). Hepatocytes were isolated according to a protocol described previously (57). AR42J cell protocols are described in refs. 39, 47.

ACKNOWLEDGMENTS. This work was supported by Medical Research Council Programme Grant MR/J002771/1. O.H.P. is a Medical Research Council Professor (G19/22/2).

1. Pandolfi SJ, Saluja AK, Imrie CW, Banks PA (2007) Acute pancreatitis: Bench to the bedside. *Gastroenterology* 132(3):1127–1151.
2. Petersen OH, Sutton R (2006) Ca^{2+} signalling and pancreatitis: Effects of alcohol, bile and coffee. *Trends Pharmacol Sci* 27(2):113–120.
3. Hegyi P, Pandolfi S, Venglovecz V, Rakonczay Z, Jr. (2011) The acinar-ductal tango in the pathogenesis of acute pancreatitis. *Gut* 60(4):544–552.
4. Petersen OH, et al. (2009) Fatty acids, alcohol and fatty acid ethyl esters: Toxic Ca^{2+} signal generation and pancreatitis. *Cell Calcium* 45(6):634–642.
5. Petersen OH, Tepikin AV (2008) Polarized calcium signaling in exocrine gland cells. *Annu Rev Physiol* 70:273–299.
6. Tinell H, et al. (1999) Active mitochondria surrounding the pancreatic acinar granule region prevent spreading of inositol trisphosphate-evoked local cytosolic Ca^{2+} signals. *EMBO J* 18(18):4999–5008.
7. Petersen OH (2012) Specific mitochondrial functions in separate sub-cellular domains of pancreatic acinar cells. *Pflügers Arch* 464:77–87.
8. Pizzo P, Drago I, Filardi R, Pozzan T (2012) Mitochondrial Ca^{2+} homeostasis: Mechanism, role, and tissue specificities. *Pflügers Arch* 464:3–17.
9. Rizzuto R, Pozzan T (2006) Microdomains of intracellular Ca^{2+} : molecular determinants and functional consequences. *Physiol Rev* 86(1):369–408.
10. Raraty M, et al. (2000) Calcium-dependent enzyme activation and vacuole formation in the apical granular region of pancreatic acinar cells. *Proc Natl Acad Sci USA* 97(24):13126–13131.
11. Krüger R, Albrecht E, Lerch MM (2000) The role of intracellular calcium signaling in premature protease activation and the onset of pancreatitis. *Am J Pathol* 157(1):43–50.
12. Streb H, Irvine RF, Berridge MJ, Schulz I (1983) Release of Ca^{2+} from a non-mitochondrial intracellular store in pancreatic acinar cells by inositol-1,4,5-trisphosphate. *Nature* 306(5938):67–69.
13. Petersen OH (1992) Stimulus-secretion coupling: Cytoplasmic calcium signals and the control of ion channels in exocrine acinar cells. *J Physiol* 448:1–51.
14. Parekh AB, Putney JW, Jr. (2005) Store-operated calcium channels. *Physiol Rev* 85(2):757–810.
15. Feske S, et al. (2006) A mutation in Orai1 causes immune deficiency by abrogating CRAC channel function. *Nature* 441(7090):179–185.
16. Liou J, et al. (2005) STIM1 is a Ca^{2+} sensor essential for Ca^{2+} -store-depletion-triggered Ca^{2+} influx. *Curr Biol* 15(13):1235–1241.
17. Park CY, et al. (2009) STIM1 clusters and activates CRAC channels via direct binding of a cytosolic domain to Orai1. *Cell* 136(5):876–890.
18. Yuan JP, et al. (2009) SOAR and the polybasic STIM1 domains gate and regulate Orai channels. *Nat Cell Biol* 11(3):337–343.
19. Lur G, et al. (2009) Ribosome-free terminals of rough ER allow formation of STIM1 puncta and segregation of STIM1 from IP₃ receptors. *Curr Biol* 19(19):1648–1653.
20. Bahnson TD, Pandolfi SJ, Dionne VE (1993) Cyclic GMP modulates depletion-activated Ca^{2+} entry in pancreatic acinar cells. *J Biol Chem* 268(15):10808–10812.
21. Krause E, Pfeiffer F, Schmid A, Schulz I (1996) Depletion of intracellular calcium stores activates a calcium conducting nonselective cation current in mouse pancreatic acinar cells. *J Biol Chem* 271(51):32523–32528.
22. Kim MS, et al. (2009) Deletion of TRPC3 in mice reduces store-operated Ca^{2+} influx and the severity of acute pancreatitis. *Gastroenterology* 137(4):1509–1517.
23. Hoth M, Penner R (1992) Depletion of intracellular calcium stores activates a calcium current in mast cells. *Nature* 355(6358):353–356.
24. Gerasimenko JV, Tepikin AV, Petersen OH, Gerasimenko OV (1998) Calcium uptake via endocytosis with rapid release from acidifying endosomes. *Curr Biol* 8(24):1335–1338.
25. Sherwood MV, et al. (2007) Activation of trypsinogen in large endocytic vacuoles of pancreatic acinar cells. *Proc Natl Acad Sci USA* 104(13):5674–5679.
26. Gerasimenko JV, Sherwood M, Tepikin AV, Petersen OH, Gerasimenko OV (2006) NAADP, CADPR and IP₃ all release Ca^{2+} from the endoplasmic reticulum and an acidic store in the secretory granule area. *J Cell Sci* 119(Pt 2):226–238.
27. Menteyne A, Burdakov A, Charpentier G, Petersen OH, Cancela JM (2006) Generation of specific Ca^{2+} signals from Ca^{2+} stores and endocytosis by differential coupling to messengers. *Curr Biol* 16(19):1931–1937.
28. Gerasimenko JV, et al. (2009) Pancreatic protease activation by alcohol metabolite depends on Ca^{2+} release via acid store IP₃ receptors. *Proc Natl Acad Sci USA* 106(26):10758–10763.
29. Gerasimenko JV, et al. (2011) Calmodulin protects against alcohol-induced pancreatic trypsinogen activation elicited via Ca^{2+} release through IP₃ receptors. *Proc Natl Acad Sci USA* 108(14):5873–5878.
30. Ng SW, di Capite J, Singaravelu K, Parekh AB (2008) Sustained activation of the tyrosine kinase Syk by antigen in mast cells requires local Ca^{2+} influx through Ca^{2+} -release-activated Ca^{2+} channels. *J Biol Chem* 283(46):31348–31355.
31. Ashmole I, et al. (2012) CRAC/Orai ion channel expression and function in human lung mast cells. *J Allergy Clin Immunol* 129(6):1628–1635, e2.
32. van Kruchten R, et al. (2012) Antithrombotic potential of blockers of store-operated calcium channels in platelets. *Arterioscler Thromb Vasc Biol* 32(7):1717–1723.
33. Derler I, et al. (2013) The action of selective CRAC channel blockers is affected by the Orai pore geometry. *Cell Calcium* 53(2):139–151.
34. Rice LV, et al. (2013) Characterization of selective Calcium-Release Activated Calcium channel blockers in mast cells and T-cells from human, rat, mouse and guinea-pig preparations. *Eur J Pharmacol* 704(1–3):49–57.
35. Laposata EA, Lange LG (1986) Presence of nonoxidative ethanol metabolism in human organs commonly damaged by ethanol abuse. *Science* 231(4737):497–499.
36. Werner J, et al. (1997) Pancreatic injury in rats induced by fatty acid ethyl ester, a nonoxidative metabolite of alcohol. *Gastroenterology* 113(1):286–294.
37. Criddle DN, et al. (2006) Fatty acid ethyl esters cause pancreatic calcium toxicity via inositol trisphosphate receptors and loss of ATP synthesis. *Gastroenterology* 130(3):781–793.
38. Dolai S, et al. (2012) Effects of ethanol metabolites on exocytosis of pancreatic acinar cells in rats. *Gastroenterology* 143(3):832–843, e1–e7.
39. Ferdek PE, et al. (2012) A novel role for Bcl-2 in regulation of cellular calcium extrusion. *Curr Biol* 22(13):1241–1246.
40. Bakowski D, Parekh AB (2007) Voltage-dependent Ba^{2+} permeation through store-operated CRAC channels: Implications for channel selectivity. *Cell Calcium* 42(3):333–339.
41. Hofer AM, Fasolato C, Pozzan T (1998) Capacitative Ca^{2+} entry is closely linked to the filling state of internal Ca^{2+} stores: A study using simultaneous measurements of ICRCAC and intraluminal $[Ca^{2+}]$. *J Cell Biol* 140(2):325–334.
42. Criddle DN, et al. (2004) Ethanol toxicity in pancreatic acinar cells: Mediation by nonoxidative fatty acid metabolites. *Proc Natl Acad Sci USA* 101(29):10738–10743.
43. Wang Y, et al. (2009) Enhanced susceptibility to pancreatitis in severe hypertriglyceridaemic lipoprotein lipase-deficient mice and agonist-like function of pancreatic lipase in pancreatic cells. *Gut* 58(3):422–430.
44. Park M, Lee K, Uhm D-Y (2002) Slow depletion of endoplasmic reticulum Ca^{2+} stores and block of store-operated Ca^{2+} channels by 2-aminoethoxydiphenyl borate in mouse pancreatic acinar cells. *Arch Pharmacol* 365:399–405.
45. Mogami H, Tepikin AV, Petersen OH (1998) Termination of cytosolic Ca^{2+} signals: Ca^{2+} reuptake into intracellular stores is regulated by the free Ca^{2+} concentration in the store lumen. *EMBO J* 17(2):435–442.
46. Park MK, Tepikin AV, Petersen OH (1999) The relationship between acetylcholine-evoked Ca^{2+} -dependent current and the Ca^{2+} concentrations in the cytosol and the lumen of the endoplasmic reticulum in pancreatic acinar cells. *Pflügers Arch* 438(6):760–765.
47. Gallacher DV, et al. (1990) Substance P and bombesin elevate cytosolic Ca^{2+} by different molecular mechanisms in a rat pancreatic acinar cell line. *J Physiol* 426:193–207.
48. Kondo S, Schulz I (1976) Calcium ion uptake in isolated pancreas cells induced by secretagogues. *Biochim Biophys Acta* 419(1):76–92.
49. Petersen OH, Ueda N (1976) Pancreatic acinar cells: the role of calcium in stimulus-secretion coupling. *J Physiol* 254(3):583–606.
50. Mogami H, Nakano K, Tepikin AV, Petersen OH (1997) Ca^{2+} flow via tunnels in polarized cells: Recharging of apical Ca^{2+} stores by focal Ca^{2+} entry through basal membrane patch. *Cell* 88(1):49–55.
51. Gerasimenko JV, et al. (2006) Bile acids induce Ca^{2+} release from both the endoplasmic reticulum and acidic intracellular calcium stores through activation of inositol trisphosphate receptors and ryanodine receptors. *J Biol Chem* 281(52):40154–40163.
52. Parekh AB (2010) Store-operated CRAC channels: Function in health and disease. *Nat Rev Drug Discov* 9(5):399–410.
53. Di Capite JL, Bates GJ, Parekh AB (2011) Mast cell CRAC channel as a novel therapeutic target in allergy. *Curr Opin Allergy Clin Immunol* 11(1):33–38.
54. Parekh AB (2000) Calcium signaling and acute pancreatitis: Specific response to a promiscuous messenger. *Proc Natl Acad Sci USA* 97(24):12933–12934.
55. Barritt GJ, Chen J, Rychkov GY (2008) Ca^{2+} -permeable channels in the hepatocyte plasma membrane and their roles in hepatocyte physiology. *Biochim Biophys Acta* 1783(5):651–672.
56. Gerasimenko JV, et al. (2002) Menadione-induced apoptosis: Roles of cytosolic Ca^{2+} elevations and the mitochondrial permeability transition pore. *J Cell Sci* 115(Pt 3):485–497.
57. Li W-C, Ralphs KL, Tosh D (2010) Isolation and culture of adult mouse hepatocytes. *Methods Mol Biol* 633:185–196.

3.2. Кальцієва сигналізація в зірчастих клітинах підшлункової залози

Ca²⁺ signals mediated by bradykinin type 2 receptors in normal pancreatic stellate cells can be inhibited by specific Ca²⁺ channel blockade

Oleksiy Gryshchenko^{1,2}, Julia V. Gerasimenko¹, Oleg V. Gerasimenko¹ and Ole H. Petersen¹

¹Medical Research Council Group, Cardiff School of Biosciences, Cardiff University, Cardiff CF10 3AX, Wales, UK

²Bogomoletz Institute of Physiology, Kiev 01024, Ukraine

Key points

- Bradykinin may play a role in the autodigestive disease acute pancreatitis, but little is known about its pancreatic actions.
- In this study, we have investigated bradykinin-elicited Ca²⁺ signal generation in normal mouse pancreatic lobules.
- We found complete separation of Ca²⁺ signalling between pancreatic acinar (PACs) and stellate cells (PSCs). Pathophysiologically relevant bradykinin concentrations consistently evoked Ca²⁺ signals, via B2 receptors, in PSCs but never in neighbouring PACs, whereas cholecystokinin, consistently evoking Ca²⁺ signals in PACs, never elicited Ca²⁺ signals in PSCs.
- The bradykinin-elicited Ca²⁺ signals were due to initial Ca²⁺ release from inositol trisphosphate-sensitive stores followed by Ca²⁺ entry through Ca²⁺ release-activated channels (CRACs). The Ca²⁺ entry phase was effectively inhibited by a CRAC blocker.
- B2 receptor blockade reduced the extent of PAC necrosis evoked by pancreatitis-promoting agents and we therefore conclude that bradykinin plays a role in acute pancreatitis via specific actions on PSCs.

Abstract Normal pancreatic stellate cells (PSCs) are regarded as quiescent, only to become activated in chronic pancreatitis and pancreatic cancer. However, we now report that these cells in their normal microenvironment are far from quiescent, but are capable of generating substantial Ca²⁺ signals. We have compared Ca²⁺ signalling in PSCs and their better studied neighbouring acinar cells (PACs) and found complete separation of Ca²⁺ signalling in even closely neighbouring PACs and PSCs. Bradykinin (BK), at concentrations corresponding to the slightly elevated plasma BK levels that have been shown to occur in the auto-digestive disease acute pancreatitis *in vivo*, consistently elicited substantial Ca²⁺ signals in PSCs, but never in neighbouring PACs, whereas the physiological PAC stimulant cholecystokinin failed to evoke Ca²⁺ signals in PSCs. The BK-induced Ca²⁺ signals were mediated by B2 receptors and B2 receptor blockade protected against PAC necrosis evoked by agents causing acute pancreatitis. The initial Ca²⁺ rise in PSCs was due to inositol trisphosphate receptor-mediated release from internal stores, whereas the sustained phase depended on external Ca²⁺ entry through Ca²⁺ release-activated Ca²⁺ (CRAC) channels. CRAC channel inhibitors, which have been shown to protect PACs against damage caused by agents inducing pancreatitis, therefore also inhibit Ca²⁺ signal generation in PSCs and this may be helpful in treating acute pancreatitis.

O. Gryshchenko and J. V. Gerasimenko contributed equally to this work.

(Received 20 August 2015; accepted after revision 30 September 2015; first published online 7 October 2015)

Corresponding authors O. V. Gerasimenko and O. H. Petersen: Medical Research Council Group, Cardiff School of Biosciences, Cardiff University, Cardiff CF10 3AX, Wales, UK. Email: GerasimenkoOV@cardiff.ac.uk and PetersenOH@cardiff.ac.uk

Abbreviations 2-APB, 2-aminoethoxydiphenylborate; ACE, angiotensin-converting enzyme; AM, acetoxymethyl; BK, bradykinin; B2, bradykinin type 2; CCK, cholecystokinin; CCKR, cholecystokinin receptor; CFTR, cystic fibrosis transmembrane conductance regulator; CRAC, Ca^{2+} release-activated Ca^{2+} channel; DAPI, 4',6-diamidino-2 phenylindole; ER, endoplasmic reticulum; IP_3 , inositol trisphosphate; IP_3R , inositol trisphosphate receptor; PAC, pancreatic acinar cell; PI, propidium iodide; PSC, pancreatic stellate cell.

Introduction

It has been known for more than 40 years that pancreatic enzyme secretion is regulated by Ca^{2+} signals in the pancreatic acinar cells (PACs) and that the primary event is acetylcholine- (ACh) or cholecystokinin- (CCK) elicited intracellular Ca^{2+} release followed by Ca^{2+} entry (Case & Clausen, 1973; Matthews *et al.* 1973; Kondo & Schulz, 1976; Petersen & Ueda, 1976). The ACh-evoked intracellular Ca^{2+} release is mediated by inositol trisphosphate (IP_3) (Streb *et al.* 1983; Wakui *et al.* 1990), whereas the CCK-elicited Ca^{2+} release is mediated by nicotinic acid adenine dinucleotide phosphate (Cancela *et al.* 2000; Gerasimenko *et al.* 2015). As high K^+ depolarization of the PAC membrane does not evoke enzyme secretion or Ca^{2+} movement (Argent *et al.* 1971; Matthews *et al.* 1973), the Ca^{2+} entry does not occur through voltage-gated channels (Petersen, 1992), but is due to opening of Ca^{2+} release-activated Ca^{2+} (CRAC) channels (Parekh & Putney, 2005; Gerasimenko *et al.* 2013). The acinar Ca^{2+} signals also regulate acinar fluid secretion via Ca^{2+} -activated Cl^- and K^+ channels (Petersen, 1992; Park *et al.* 2001). However, the major component of pancreatic fluid secretion is contributed by the ducts and this is regulated by secretin-elicited intra-ductal cyclic AMP formation controlling cystic fibrosis transmembrane conductance regulator (CFTR) channels (Argent, 2006), whose openings are also regulated by the Cl^- concentration in the luminal fluid (Broadbent *et al.* 2015).

The often fatal human disease acute pancreatitis, in which the pancreas digests itself and its surroundings, is initiated by excessive intracellular Ca^{2+} release in the PACs followed by excessive Ca^{2+} entry, mostly elicited by combinations of alcohol and fatty acids or by bile acids (Petersen & Sutton, 2006; Gerasimenko *et al.* 2014). Pancreatitis-inducing agents also inhibit ductal fluid and bicarbonate secretion, exacerbating the disease (Pallagi *et al.* 2011; Maleth *et al.* 2015).

We have extensive knowledge of the mechanisms generating Ca^{2+} signals in the PACs, which has been built up over many decades (Petersen & Tepikin, 2008; Gerasimenko *et al.* 2014). In contrast, the more recently discovered pancreatic stellate cells (PSCs) (Watari *et al.*

1982), located in the peri-acinar space – with elongated processes around the base of the acinus – have received much less attention and it has essentially been the functional properties of cultured cells that have been investigated (Apte *et al.* 1998, 2012; Bachem *et al.* 1998; Wells & Crawford, 1998). The prevailing, and so far unchallenged, view has been that normal PSCs are quiescent and the focus in all published studies has been on the activation of PSCs and their role – in the activated state – in chronic pancreatitis and pancreatic cancer (Bachem *et al.* 1998; Wells & Crawford, 1998; Sherman *et al.* 2014). Activation of PSCs – during pancreatic injury or culturing of quiescent PSCs – induces proliferation as well as secretion of extracellular matrix components, thereby playing an important role in the fibrosis that occurs in chronic pancreatitis and pancreatic cancer (Sherman *et al.* 2014). Work on the so-called quiescent PSCs in culture has shown that they can generate substantial cytosolic Ca^{2+} signals in response to stimulation with high concentrations of the blood pressure-lowering nona-peptide bradykinin (BK) and some other substances (Won *et al.* 2011).

Because BK has long been known as an important player in inflammatory disease, including acute pancreatitis (Ryan *et al.* 1964; Hirata *et al.* 2002), we have now investigated BK-induced Ca^{2+} signal generation, and its underlying mechanism, in normal PSCs in their normal microenvironment. We find that normal PSCs are much more sensitive to BK than PSCs in culture, generating substantial Ca^{2+} signals in response to a BK concentration as low as 100 pM, with maximal effect at 1 nM, orders of magnitude lower than what has been observed in cultured cells (Won *et al.* 2011). This has important implications, as the threshold for activating normal PSCs (100 pM) is close to the normal plasma level of BK (40–70 pM) (Blais *et al.* 1999; Hirata *et al.* 2002) and any increase in the plasma or tissue BK levels, which occurs under several conditions – including acute pancreatitis and use of angiotensin-converting-enzyme (ACE) inhibitors (Liu *et al.* 1997; Blais *et al.* 1999; Tsutsumi *et al.* 1999; Hirata *et al.* 2002; Su, 2014) – would therefore elicit Ca^{2+} signals in PSCs. We have explored the Ca^{2+} signalling events and their underlying mechanisms in normal PSCs and show that BK activates bradykinin type 2 (B2)

receptors, which causes primary Ca^{2+} release from internal stores. This effect can be abolished by phospholipase C inhibition or blockade of IP_3 receptors (IP_3Rs). Following the initial intracellular Ca^{2+} release, there is opening of conventional CRAC channels (Parekh & Putney, 2005; Parekh, 2010) and we show that a recently employed CRAC channel inhibitor, which was protective against the destruction of PACs evoked by agents inducing pancreatitis (Gerasimenko *et al.* 2013, 2014), also reduces BK-induced Ca^{2+} signal generation in PSCs. We show that B2 receptor blockade protects against the necrosis evoked by pancreatitis-inducing agents and suggest that the protective effect of CRAC channel blockade against pancreatitis may in part be due to inhibition of Ca^{2+} signal generation in PSCs. Overall, our new data indicate that the so far generally accepted notion of normal PSCs being quiescent is potentially misleading as they are in fact exquisitely sensitive to relatively small changes in BK concentrations found *in vivo*.

Methods

Ethical approval

All procedures were carried out in accordance with UK Home Office regulations.

Preparation of pancreatic lobules

Pancreatic lobules and big clusters were isolated from the pancreas of adult C57Bl/6 male mice. Animals were killed according to UK Schedule 1 regulations. The pancreas was rapidly dissected, transferred to collagenase Na-Hepes-based solution (Sigma, Poole, UK) and incubated at 37°C for 5–6 min. After digestion, the tissue was kept in Na-Hepes-based extracellular media,

containing (in mM): NaCl, 140; KCl, 4.7; Hepes (KOH), 10; MgCl_2 , 1; glucose 10; CaCl_2 1; pH 7.2. Pancreatic lobules were then incubated with fluorescent dye following the manufacturer's description. All experiments were carried out with freshly prepared pancreatic lobules, attached to the coverslip of the perfusion chamber at room temperature (23°C). Penetration of various substances deep into the pancreatic lobule was highly dependent on the distance from the surface (Fig. 1A, B). It was therefore necessary, in several cases, to use relatively high concentrations (up to 5-fold higher than would have been necessary in experiments on isolated cells or very small cell clusters) and relatively long pre-incubation times.

$[\text{Ca}^{2+}]$ measurements in intact cells

Intact cells were loaded with $5\ \mu\text{M}$ Fluo-4 acetoxymethyl ester (AM), for 10 min at room temperature. Cells were transferred to a flow chamber and perfused with the Na-Hepes-based extracellular solution as described above. Cells were visualized using a Leica SP5 MP II two-photon confocal microscope, with a 63×1.2 NA objective lens. Fluo-4 was excited with a 488 nm Ar laser, at 1–4% power, and emitted light was collected at 510–580 nm. Generally, a series of images was recorded at 512×512 pixel resolution (at a speed of $0.3\ \text{frames s}^{-1}$), and analysed using Leica Confocal Software (Leica, Mannheim, Germany). Fluorescence signals were plotted as F/F_0 (F_0 is the initial level of fluorescence). Statistical analysis was performed using ANOVA or Student's *t*-test.

Measurements of necrosis level in pancreatic lobules

Pancreatic lobules were exposed to 350 mM ethanol, or 500 μM palmitoleic acid ethyl ester (POAEE) or 0.5% sodium choleate for 2 h in the presence or absence of

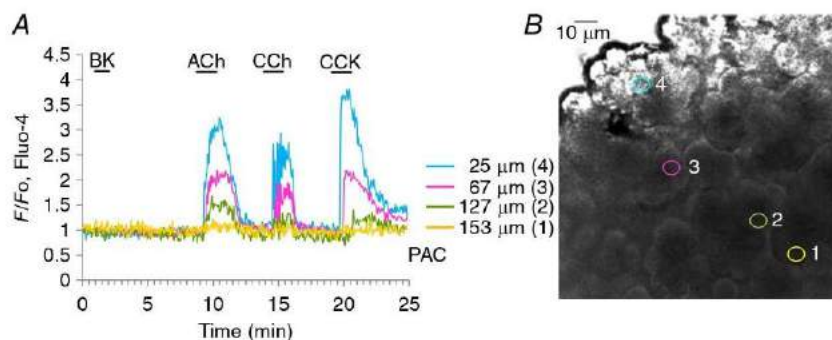


Figure 1. Pancreatic lobule preparation: penetration of applied substances into deep layers

Experiment illustrating the difficulties of attaining the full concentration level deep inside the pancreatic tissue of substances applied to the surface of a lobule. A, $[\text{Ca}^{2+}]$ traces obtained from PACs at different depths from the surface of the lobule (signposted by the colour coding shown). Responses to ACh ($10\ \mu\text{M}$), carbachol (CCh) ($10\ \mu\text{M}$) and CCK ($10\ \text{nM}$) are shown. B, transmitted light image of the lobule from which the recordings shown in A were obtained. The different recording positions are indicated using the colour coding shown in A.

0.5 μM or 10 μM WIN 64338. Ethanol- or bile-induced pancreatic necrosis was visualized by staining the lobules with propidium iodide (PI) and compared with the control necrosis level (without any treatment). Simultaneously lobules were stained with the nuclear dye Hoechst 33342 to enable cell counting. Both stainings were performed according to the manufacturer's protocols. Fluorescence of Hoechst 33342 and PI was recorded using confocal microscopy, with a 63×1.2 NA objective lens (excitations 355 and 543 nm; and emissions 390–480 and 570–650 nm, respectively).

Immunocytochemistry

Immunocytochemistry in pancreatic lobules and big clusters was performed as described by Lur *et al.* (2009) with some modifications. Following blocking with 1% BSA and 10% goat serum, the isolated pancreatic lobules were incubated for 1 h at room temperature with primary antibody (CCK-AR) in 5% goat serum in PBS. The pancreatic lobules were subsequently incubated with CruzFluor (CFL) 594-conjugated secondary antibody for 30 min at room temperature. Cells were attached to the glass coverslips covered with poly-L-lysine. For immunochemical staining with desmin antibody, pancreatic lobules were fixed with 4% paraformaldehyde followed by permeabilization with Triton X100, blocking and incubation with primary (desmin) and then with secondary (CFL) antibodies as described above.

Reagents

Chemicals, unless otherwise indicated, were obtained from Sigma or Calbiochem (Merck, UK). BK, R-715 and WIN64338 were purchased from Tocris Biosciences

(Bristol, UK). Fluo-4 AM, PI and Hoechst 33342 were purchased from Invitrogen (Life Technologies, Carlsbad, CA, USA). Antibodies against CCK-A (CCK1) receptor (sc-16172), desmin antibody (sc-7559) and donkey anti-goat IgG-CFL 594 (sc-362275) were from Santa Cruz Biotechnology (Santa Cruz, CA, USA).

Results

Separate Ca^{2+} signalling events in neighbouring PSCs and PACs

It has been shown that desmin is a good marker for PSCs (Apte *et al.* 1998) and we found that immunochemical staining with desmin antibody identified small elongated cells situated at the periphery of the dominant acinar cells (Fig. 2A–C). The presence of vitamin A in lipid droplets is another characteristic of PSCs (Bachem *et al.* 1998) and we could visualize this by intrinsic multiphoton fluorescence (Fig. 2D, E).

Cells situated in the position characteristic of desmin-containing cells (Fig. 2C) took up the Ca^{2+} -sensitive fluorescent probe Fluo-4 much more avidly than PACs (Fig. 3A–C). In large lobules stained with Fluo-4 (Fig. 3A, B), it was often possible to observe PSCs as bright 'strings', whereas in smaller cell clusters, they typically appeared as individual bright cells at the periphery of acinar units (Fig. 3Ca).

Cultured PSCs produce cytosolic Ca^{2+} signals in response to a micromolar concentration of BK (Won *et al.* 2011). In our experiments, normal PSCs in their normal micro-environment typically responded to a short-lasting exposure to a much lower BK concentration (1 nM) with a sharp transient rise in $[\text{Ca}^{2+}]_i$, quickly followed by a longer lasting (plateau) phase of elevated $[\text{Ca}^{2+}]_i$ (Figs 3Cb and 4A). Neighbouring PACs never displayed

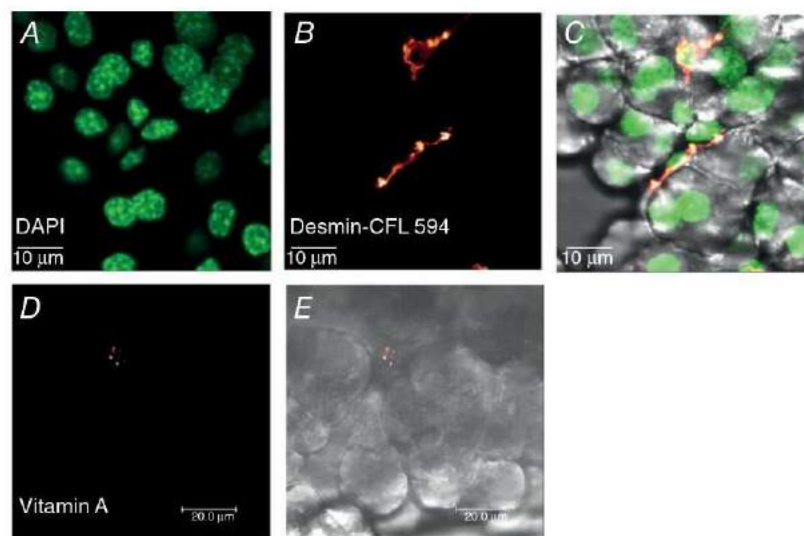


Figure 2. Identification of PSCs in lobule preparation

A, localization of nuclei is shown by staining with DAPI. B, staining with desmin antibody, visualized with conjugated secondary antibody IgG-CruzFluor 594 (CFL 594). C, overlay of transmitted light image with DAPI and desmin antibody ($n = 6$). D, visualization of lipid droplets containing vitamin A by multiphoton intrinsic fluorescence ($n = 6$). E, transmitted light image of the pancreatic lobule shown in D.

any change in $[Ca^{2+}]_i$ during the BK-induced PSC Ca^{2+} signals (>100 experiments) (Figs 3C*b* and 4A), indicating lack of functional BK receptors on PACs and lack of direct communication between neighbouring PACs and PSCs. The typical, and physiologically important, PAC stimulants ACh and CCK evoked Ca^{2+} signals in PACs (Petersen & Tepikin, 2008), which were not transmitted to the neighbouring PSCs ($n = 14$ and 17, respectively) (Figs 3C*b* and 4A). ATP ($100 \mu M$) elicited Ca^{2+} signals in a proportion of PSCs (41 of 107 cells), but failed to do so in many others (Fig. 4A). When ATP evoked a $[Ca^{2+}]_i$ rise in a PSC, it was never transmitted to the neighbouring PAC (Fig. 4A).

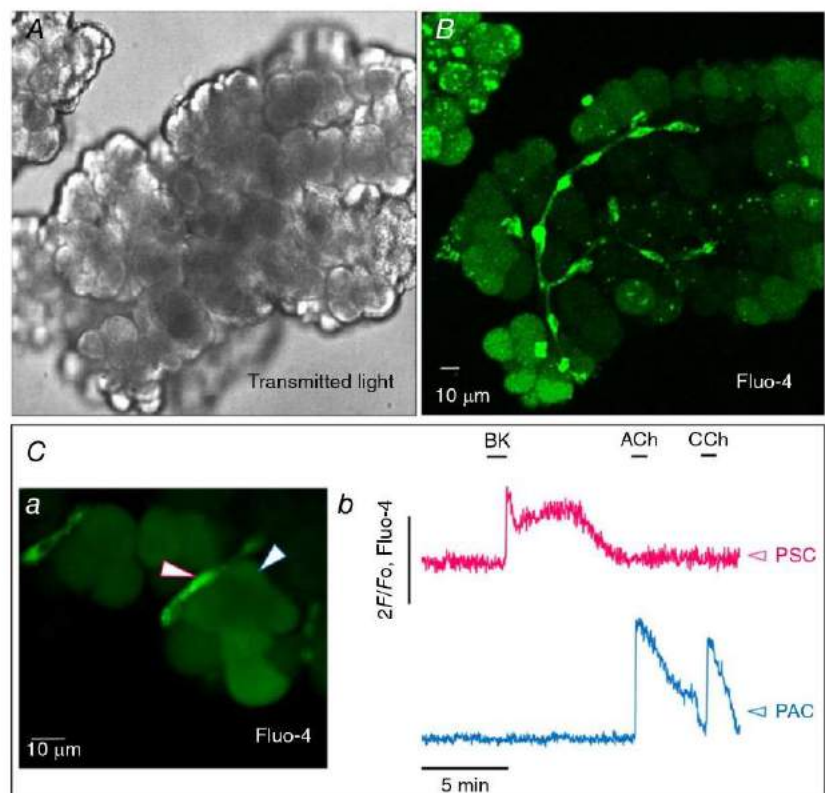
Phillips *et al.* (2010) have suggested that CCK-evoked release of ACh from PSCs could in turn activate PACs and they proposed that this could be the normal mechanism for CCK-elicited secretion from human PACs. However, we did not find any evidence for this hypothesis as CCK never evoked any Ca^{2+} signals in PSCs in our preparations ($n = 17$; at $[CCK] = 10 \text{ nM}$) and Ca^{2+} signals in PSCs consistently failed to be transmitted to neighbouring PACs (Fig. 4A). Furthermore, although a fluorescent antibody to CCK1 receptors clearly identified the presence of CCK1 receptors on PACs, it failed to do so with regard to PSCs (four experiments) (Fig. 4B).

BK evokes Ca^{2+} signals in PSCs at pico- and low nanomolar concentrations

It seemed important to explore the levels of BK needed to evoke Ca^{2+} signals (Fig. 5) in relation to what is known about BK concentrations in plasma. From measurements in humans and rats, it is known that normal plasma BK concentrations are in the range 40–70 pM (Blais *et al.* 1999; Hirata *et al.* 2002). However, in a bile duct obstruction model of acute pancreatitis induced in rats, it has been shown that the BK plasma concentration rose to $\sim 140 \text{ pM}$ (Hirata *et al.* 2002). As the BK release in acute pancreatitis primarily comes from the pancreas, the local (intra-pancreatic) BK levels could be higher (Ryan *et al.* 1964; Schachter, 1969). We found that a BK concentration as low as 100 pM ($n = 14$) could elicit PSC Ca^{2+} signals and that maximal responses were obtained at 1 nM ($n = 9$, in the series of experiments represented by Fig. 5C). Overall, in the course of this investigation, BK responses to 1 nM have been observed in >100 experiments. At the low BK concentrations we used, there was no sign of desensitization (Fig. 5A). Within the time frame of our protocols, the $[Ca^{2+}]_i$ elevation was maintained as long as the stimulus was maintained ($n = 19$) (Fig. 5A). It would therefore appear that normal PSCs are sufficiently sensitive

Figure 3. Complete separation of Ca^{2+} signalling in neighbouring PSCs and PACs

A, transmitted light image of live mouse pancreatic lobule. B, fluorescence image of the same lobule (Fluo-4). The small elongated cells with long processes (PSCs) are much better loaded with Fluo-4 than the larger PACs. C, $[Ca^{2+}]_i$ measurements in neighbouring PSCs and PACs in a small cell cluster. a, fluorescence image of the live small cell cluster from which recordings were made. A highly fluorescent PSC is signposted by the white arrow outlined in red, whereas the much less fluorescent neighbouring PAC is signposted by the white arrow with blue outline. b, $[Ca^{2+}]_i$ traces from the two cells signposted in a. Red trace from the PSC and blue trace from the PAC. BK (1 nM) evokes a typical biphasic Ca^{2+} signal in the PSC but not in the neighbouring PAC, whereas ACh ($10 \mu M$) and CCh ($10 \mu M$) evoke Ca^{2+} signals in the PAC but not in the PSC.



to BK to be able to sense relatively small increases in the surrounding BK level.

Although the PSCs in our lobule preparation were much more sensitive to BK than those previously studied in culture (Won *et al.* 2011), they do have some characteristics in common with quiescent PSCs in culture which, unlike activated PSCs, do not respond to trypsin and thrombin. As seen in Fig. 6 there was no response to thrombin ($n = 6$) (Fig. 6A) or trypsin ($n = 18$) (Fig. 6B) in cells that responded to BK with a clear Ca^{2+} signal.

The BK-elicited Ca^{2+} signals in PSCs are due to activation of B2 receptors

The BK receptor sub-type responsible for generating Ca^{2+} signals in PSCs has not previously been investigated. We employed the B2 receptor blocker WIN64338 (Hu

et al. 2004) and showed that this agent reversibly blocked BK-elicited Ca^{2+} signal generation ($n = 27$) (Fig. 7A). In contrast, the B1 receptor blocker R-715 (Abdough *et al.* 2008) failed to inhibit BK-induced Ca^{2+} signalling ($n = 8$) (Fig. 7B). Furthermore, the specific B1 agonist Sar-des-Arg-BK did not evoke any changes in $[\text{Ca}^{2+}]_i$ of PSCs ($n = 8$) (Fig. 7C). It would appear that the plateau phase of the BK-induced response to some extent depends on continued B2 receptor activation, because application of WIN64338 immediately after the initial BK-elicited Ca^{2+} spike shortened the duration of the plateau phase (Fig. 7D).

As a previous study showed that BK levels increase in acute pancreatitis and that blockade of B2 receptors attenuated the cellular changes underlying the development of acute pancreatitis evoked by obstruction of the pancreato-biliary duct in rats (Hirata *et al.* 2002), our results raise the possibility that B2 receptor-mediated

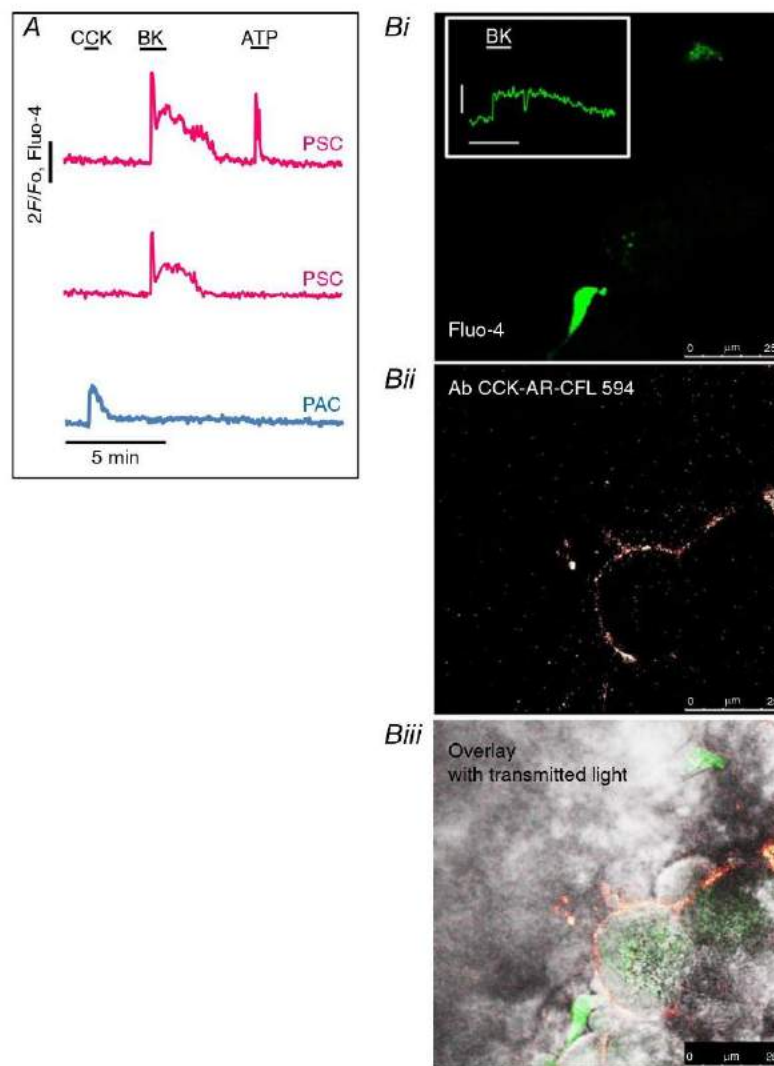


Figure 4. BK, but not CCK, evokes Ca^{2+} signal in PSCs

A, simultaneous $[\text{Ca}^{2+}]_i$ traces from two PSCs and one PAC in the same cell cluster. CCK (10 nM) only evoked a Ca^{2+} signal in the PAC but not in the two PSCs, whereas BK (1 nM) elicited Ca^{2+} signals in both PSCs but not the PAC. ATP (100 μM) evoked a response in one PSC but not in the other and not in the PAC. B, immunostaining of CCK receptors in a pancreatic lobule. *i*, a PSC identified by bright staining with Fluo-4. The response to BK (5 nM) is shown in the inset (amplitude scale bar 1 F/F₀, time scale bar 2 min). *ii*, visualization of CCK1 receptors by antibody against the CCK1 receptor with subsequent application of secondary antibody (CFL 594). *iii*, overlay of *i* and *ii* showing the localization of CCK1 receptors on the surface of PACs, but not the PSC.

Ca^{2+} signals in PSCs contribute to the negative outcome of this disease. We therefore tested whether B2 receptor blockade could protect against cellular changes relevant to the development of acute pancreatitis, which is most frequently related to alcohol abuse or biliary disease (Petersen & Sutton, 2006). In alcohol-related acute pancreatitis, the pancreas is exposed not only to alcohol, but also to fatty acid ethyl esters (non-oxidative combinations of alcohol and fatty acids), which have been shown to be particularly effective releasers of intracellular Ca^{2+} (Criddle *et al.* 2006; Gerasimenko *et al.* 2009). In biliary disease, the pancreas will be exposed to high concentrations of bile acids, which have also been shown to be effective liberators of stored Ca^{2+} (Voronina *et al.* 2002; Gerasimenko *et al.* 2006). We therefore tested the effects of B2 receptor blockade on the level of necrosis elicited by alcohol, POAEE and a bile acid mixture. As

seen in Fig. 8, B2 receptor blockade markedly reduced the extent of acinar cell necrosis induced by either a high alcohol concentration (350 mM), POAEE (500 μM) or bile acids (0.5% sodium choleate: a crude ox bile extract which contains the sodium salts of taurocholic, glycocholic, deoxycholic and cholic acids).

BK-elicited Ca^{2+} signals in PSCs are primarily due to release of Ca^{2+} from internal stores, but is followed by store-operated Ca^{2+} entry

As shown in Figs 3–5, the BK-elicited Ca^{2+} signals consist of a brief transient rise in $[\text{Ca}^{2+}]_i$, followed by a prolonged plateau phase of elevated $[\text{Ca}^{2+}]_i$. Acute removal of external Ca^{2+} did not reduce the initial phase of BK-evoked Ca^{2+} signals, but eliminated the following plateau phase (Fig. 9A, B). Re-admission of Ca^{2+} resulted in a transient increase in $[\text{Ca}^{2+}]_i$ and enabled a subsequent BK application to evoke a normal response (Fig. 9A, B). We tested the ability of PSCs to generate store-operated Ca^{2+} entry, by using the now 'classical' protocol for assessing this phenomenon (Fig. 9C), employing cyclopiazonic acid (CPA) to block the Ca^{2+} pumps in the endoplasmic reticulum (ER). As shown in Fig. 9B and C, re-admission of external Ca^{2+} after a period of external Ca^{2+} deprivation, and BK stimulation, resulted in a transient rise in $[\text{Ca}^{2+}]_i$, but, if the Ca^{2+} re-admission occurred after and during a period of continued ER Ca^{2+} pump inhibition, the $[\text{Ca}^{2+}]_i$ elevation was sustained (Fig. 9C). In this situation, Ca^{2+} entering store-operated Ca^{2+} channels cannot be taken up into the ER, but will only slowly be extruded by the plasma membrane Ca^{2+} pumps.

We tried to block the store-operated Ca^{2+} entry pharmacologically. 2-APB, a well-known, but relatively unspecific, blocker of CRAC channels (Parekh & Putney, 2005), abolished BK-induced Ca^{2+} signal generation (Fig. 9D), which may be due to blockade of IP_3Rs (Ma *et al.* 2000). We also used a more specific CRAC channel blocker, GSK-7975A, which has recently been shown to block CRAC channel currents in PACs (Gerasimenko *et al.* 2013). In these experiments, we were able to show that GSK-7975A reversibly blocked the plateau phase of the BK-induced $[\text{Ca}^{2+}]_i$ elevation, without affecting the initial spike ($n = 9$) (Fig. 9E). GSK-7975A also blocked the Ca^{2+} entry normally occurring when external Ca^{2+} was re-admitted after a period of external Ca^{2+} deprivation ($n = 14$) (Fig. 9F).

Finally, we examined the mechanism underlying the initial Ca^{2+} spike in response to BK stimulation. Having established that it is due to release of Ca^{2+} from internal stores (Fig. 9A), we tested the hypothesis that this Ca^{2+} liberation occurs through IP_3Rs . It is now well established that caffeine inhibits opening of IP_3Rs (Wakui *et al.* 1990; Ehrlich *et al.* 1994; Foskett *et al.* 2007). As seen in Fig. 9G,

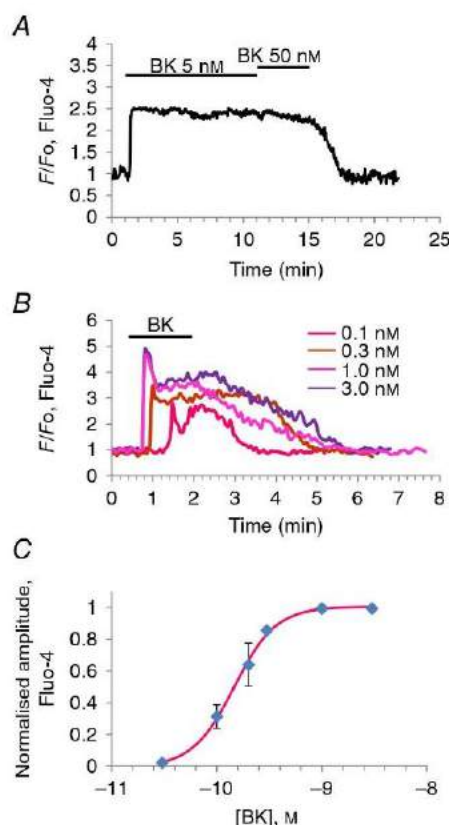


Figure 5. BK concentration–response relationship

A, $[\text{Ca}^{2+}]_i$ trace from PSC showing that 5 nM BK evokes maximal sustained response, which is not enhanced by increasing the BK concentration to 50 nM. B, family of $[\text{Ca}^{2+}]_i$ traces all obtained from the same PSC, showing responses to BK concentrations from 0.1 to 3 nM. C, BK concentration–response (amplitude of plateau phase) relationship. Half-maximal response is at a BK concentration of 200 pM. A very similar relationship was obtained for the initial peak response.

caffeine did reversibly block BK-elicited Ca^{2+} signalling ($n = 29$). BK probably activates phospholipase C, as U73122 (Bleasdale *et al.* 1990; Smith *et al.* 1990) blocked the ability of BK to evoke Ca^{2+} signals ($n = 14$) (Fig. 9H).

Discussion

Our results demonstrate for the first time that BK, in concentrations close to those measured in normal plasma (Blais *et al.* 1999; Hirata *et al.* 2002), elicits substantial

cytosolic Ca^{2+} signals in normal PSCs in their normal micro-environment and therefore cast doubt on the hitherto prevailing concept of the quiescent PSC (Apte *et al.* 1998, 2012; Sherman *et al.* 2014).

Given that an important role for BK in the development of acute pancreatitis was proposed by Ryan *et al.* (1964), that there is an increase in the plasma level of BK in acute pancreatitis (Hirata *et al.* 2002) and that a number of studies have shown that pharmacological blockade of B2 receptors is helpful in suppressing the cellular changes in several pancreatitis disease models (Griesbacher &

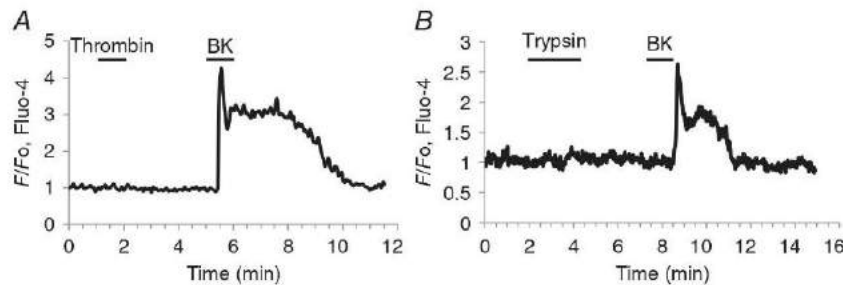


Figure 6. Thrombin and trypsin do not evoke Ca^{2+} signals in PSCs

A, thrombin (10 mU ml^{-1}) does not evoke a Ca^{2+} signal in a PSC, but a subsequent BK application (1 nM) evokes the usual response. B, trypsin ($20 \mu\text{M}$) fails to evoke a Ca^{2+} signal in a PSC, but a subsequent BK application (1 nM) does so. The apparently delayed and somewhat smaller response to BK (although still within the normal range) in B (as compared to A) is probably due to the fact that the cell cluster in this case was relatively large and the PSC deep in the tissue (see Fig. 1).

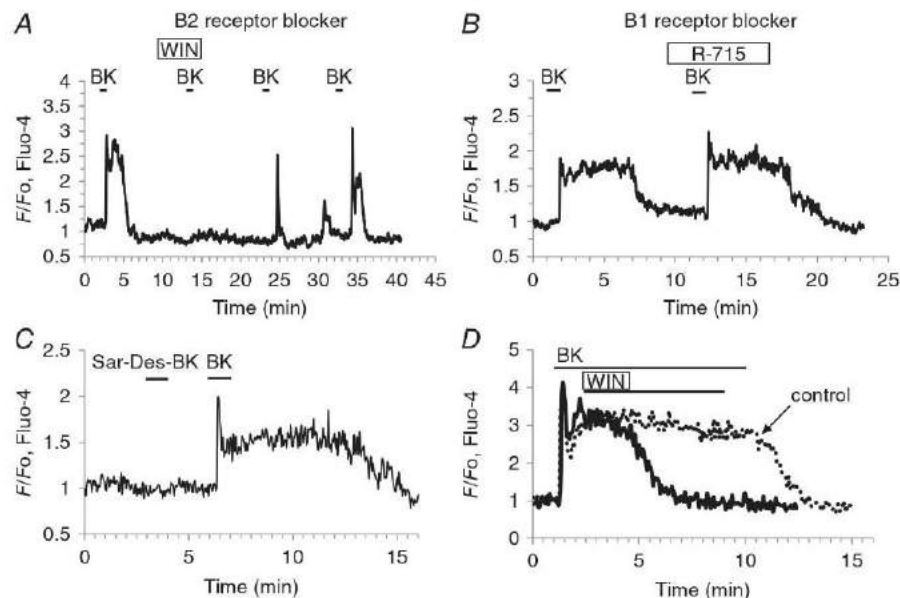


Figure 7. BK receptor pharmacology

A, the B2 receptor antagonist WIN64338 ($10 \mu\text{M}$) reversibly and completely blocked the BK- (1 nM) elicited Ca^{2+} signal, both peak ($P < 0.000003$) and plateau ($P < 0.00004$). B, the B1 receptor antagonist R-715 ($10 \mu\text{M}$) failed to block the BK- (1 nM) elicited Ca^{2+} signal. C, the B1 receptor agonist Sar-des-Arg-BK (Sar-Des-BK) ($1 \mu\text{M}$) does not evoke a Ca^{2+} signal in a PSC, whereas a subsequent application of BK (1 nM) elicits such a signal. D, the B2 receptor antagonist WIN64338 applied after the initial BK-evoked Ca^{2+} spike reduces markedly the length of the plateau phase.

Lembeck 1992; Griesbacher *et al.* 1993; Hoffmann *et al.* 1996; Bloechle *et al.* 1998; Hirata *et al.* 2002), it would seem important to identify the target for the action of BK in the pancreas and its mechanism of action.

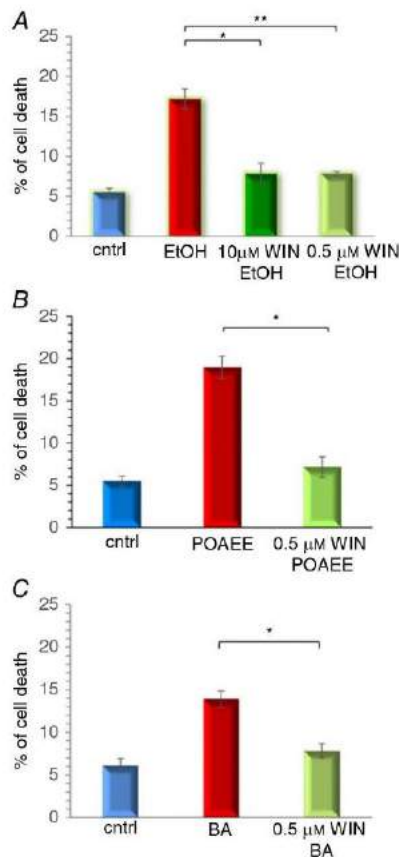


Figure 8. The extent of PAC death elicited by pancreatitis-inducing agents is markedly reduced by B2 receptor blockade

A, treatment of pancreatic lobules with ethanol (350 mM) for 2 h at room temperature increased significantly the percentage of PAC necrosis from the control level of $5.47 \pm 0.54\%$ ($n = 7$) to $17 \pm 1\%$ ($n = 7$) and this was significantly reduced to $7.85 \pm 1.3\%$ ($n = 3$) by $10 \mu\text{M}$ WIN64338 and to $7.84 \pm 0.25\%$ ($n = 4$) by $0.5 \mu\text{M}$ WIN64338 ($*P = 0.0025$ and $**P = 0.00043$, respectively, >1500 cells in each experimental group). B, treatment of pancreatic lobules with POAEE (500 μM) for 2 h at room temperature increased significantly the percentage of PAC necrosis from the control level of $5.46 \pm 1.25\%$ ($n = 3$) to $18.96 \pm 1.76\%$ ($n = 3$) and this was reduced to $7.15 \pm 0.67\%$ ($n = 3$) by $0.5 \mu\text{M}$ WIN64338 ($*P = 0.003$, >990 cells in each experimental group). C, treatment of pancreatic lobules with 0.5% sodium cholate for 2 h at room temperature also increased significantly the percentage of PAC necrosis from the control level of $6.1 \pm 0.85\%$ ($n = 3$) to $14 \pm 1\%$ ($n = 3$) and this was significantly reduced to $7.8 \pm 0.8\%$ ($n = 3$) by $0.5 \mu\text{M}$ WIN64338 ($*P = 0.0087$, >1600 cells in each experimental group). Necrosis was measured by staining of lobules with PI. Cell count was performed using nuclear staining with Hoechst 33342. Bars represent $\pm\text{SEM}$.

Won *et al.* (2011) demonstrated that BK – in high (micromolar) concentrations – evoked transient Ca^{2+} signals in quiescent and activated PSCs in culture. We focused our attention on the effect of low quasi-physiological concentrations of BK on normal PSCs in their normal micro-environment, the mechanism of action and its consequence. Our results show that whereas BK consistently evokes bi-phasic Ca^{2+} signals in PSCs, it consistently fails to do so even in closely neighbouring PACs (Figs 3 and 4). We have therefore now identified a specific cellular site for the action of BK, which may partly or fully explain its importance in pancreatitis. Furthermore, we have established that the BK-elicited Ca^{2+} signals in PSCs are due to activation of B2 receptors, providing a plausible explanation for the suppressive effect of B2 blockade on the development of acute pancreatitis (Griesbacher & Lembeck 1992; Griesbacher *et al.* 1993; Hoffmann *et al.* 1996; Bloechle *et al.* 1998; Hirata *et al.* 2002). We have also shown that PAC necrosis elicited by alcohol, POAEE or bile can be significantly reduced by B2 receptor blockade (Fig. 8).

We failed to observe any effects of CCK on PSCs, although this hormone evoked its usual effect (Petersen & Tepikin, 2008) on neighbouring PACs (Fig. 4A). Therefore, our results do not provide support for the hypothesis that CCK acting on PSCs will increase ACh secretion from these cells, which in turn would activate PACs (Phillips *et al.* 2010). We worked on normal mouse pancreatic tissue, whereas Phillips *et al.* (2010) studied ACh secretion from cultured human PSCs. Cultured PSCs clearly have different properties from normal PSCs, because in the normal mouse pancreas we have observed Ca^{2+} signal generation in PSCs in response to 0.1 nM BK (Fig. 5), whereas micromolar BK concentrations were required to obtain such responses in cultured mouse PSCs (Won *et al.* 2011). With regard to the mechanism of CCK action in the human pancreas, the simplest hypothesis remains direct action on PACs, as shown in isolated acinar cell clusters from human pancreas (Murphy *et al.* 2008).

Although the initiating event elicited by pancreatitis-inducing agents in PACs is Ca^{2+} release from intracellular stores (Gerasimenko *et al.* 2014), we have previously shown that the cellular damage only happens if there is secondary Ca^{2+} entry from the extracellular fluid (Raraty *et al.* 2000). We have recently shown that the CRAC channel blocker GSK-7975A markedly inhibits the store-operated Ca^{2+} entry that sustains the $[\text{Ca}^{2+}]_i$ elevation in PACs evoked by a pancreatitis-inducing agent (Gerasimenko *et al.* 2013, 2014), a finding recently confirmed by Voronina *et al.* (2015). We have previously shown that the CRAC channel blockade by GSK-7975A provides effective protection of the PACs from alcohol-related intracellular protease activation and necrosis (Gerasimenko *et al.* 2013) and these results have also very recently been confirmed in

a study employing three different *in vivo* mouse models of acute pancreatitis (Wen *et al.* 2015). The BK-elicited Ca^{2+} signal generation in PSCs is due to initial release of Ca^{2+} from internal stores followed by activation of Ca^{2+} entry via store-operated channels. Our new results

show that GSK-7975A is also effective in reducing the plateau phase of the BK-elicited $[\text{Ca}^{2+}]_i$ elevation in PSCs (Fig. 9E). Given that B2 receptor blockade protects against pancreatitis-like cellular changes (Fig. 8), the inhibitory effect of GSK-7975A on BK responses in PSCs

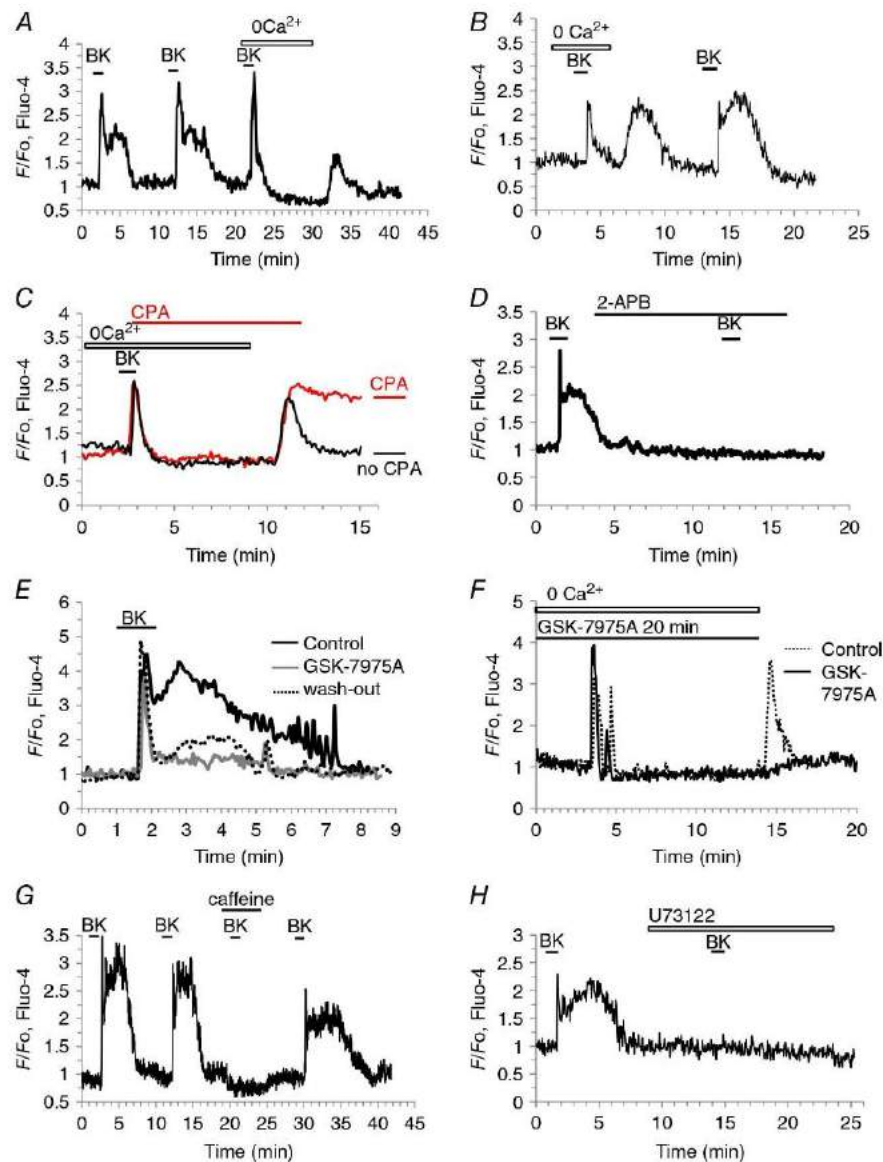


Figure 9. Mechanisms of BK-elicited Ca^{2+} signal generation in PSCs

A and B, removal of external Ca^{2+} has no effect on the initial $[\text{Ca}^{2+}]_i$ rise evoked by BK (1 nM, $P > 0.7$), but abolishes the following plateau phase ($P < 0.0003$). Readmitting external Ca^{2+} , in the absence of BK stimulation, causes a transient rise in $[\text{Ca}^{2+}]_i$. C, when the SERCA pump inhibitor CPA (20 μM) is present, the $[\text{Ca}^{2+}]_i$ rise upon readmission of external Ca^{2+} is prolonged. D, 2-APB (100 μM) (IP₃R antagonist and inhibitor of CRAC channels) blocks Ca^{2+} signalling elicited by BK (1 nM). E, the CRAC channel blocker GSK-7975A (10 μM) reduces markedly the plateau phase of the BK- (1 nM) elicited response ($P < 0.0015$). Washout of GSK-7975A partially restored the response ($P < 0.009$). F, GSK (10 μM) does not inhibit the initial BK-elicited Ca^{2+} signal occurring in the absence of external Ca^{2+} but prevents the $[\text{Ca}^{2+}]_i$ rise normally occurring upon external Ca^{2+} readmission. G, caffeine (30 mM) reversibly blocks BK- (1 nM) elicited Ca^{2+} signal. H, the phospholipase C inhibitor U73122 (30 μM) abolished Ca^{2+} signal generation elicited by BK (1 nM), both peak ($P < 0.0002$) and plateau ($P < 0.00001$).

may represent an additional potential benefit of treating cases of severe acute pancreatitis with a CRAC channel blocker. The inhibitory action of GSK-7975A on the BK-induced plateau elevation of $[Ca^{2+}]_i$ in PSCs may well have contributed to the impressive protective effects of this agent against acute pancreatitis *in vivo* (Wen *et al.* 2015).

Our new data are also relevant when considering the now widespread use of ACE inhibitors in the treatment of hypertension because ACE inhibitors inhibit the breakdown of BK, causing an increase in the tissue and plasma levels of BK (Israili & Hall, 1992; Liu *et al.* 1997; Tsutsumi *et al.* 1999; Su, 2014). Previous studies have shown that use of ACE inhibitors is associated with a significantly increased risk of developing acute pancreatitis (Tilkemeier & Thompson, 1988; Eland *et al.* 2006), but the mechanism was unknown. As we have now shown that any increase in the BK level will elicit Ca^{2+} signals in the PSCs via B2 receptors and that blockade of these receptors protects against acute pancreatitis, it is likely that Ca^{2+} signal generation in PSCs mediated by BK is at least in part responsible for the increased risk of developing acute pancreatitis during ACE inhibitor treatment.

References

- Abdoun M, Talbot S, Couture R & Hassessian HM (2008). Retinal plasma extravasation in streptozotocin-diabetic rats mediated by kinin B_1 and B_2 receptors. *Br J Pharmacol* **154**, 136–143.
- Apte MV, Haber PS, Applegate TL, Norton ID, McCaughan GW, Korsten MA, Pirola RC & Wilson JS (1998). Periacinar stellate shaped cells in rat pancreas: identification, isolation, and culture. *Gut* **43**, 128–133.
- Apte MV, Pirola RC & Wilson JS (2012). Pancreatic stellate cells: a starring role in normal and diseased pancreas. *Front Physiol* **3**, Article 344.
- Argent BE (2006). Cell physiology of pancreatic ducts. In: *Physiology of the gastrointestinal tract*, vol 2, ed. Johnson LR, pp. 1376–1396. Elsevier, San Diego.
- Argent BE, Case RM & Scratcherd T (1971). Stimulation of amylase secretion from the perfused cat pancreas by potassium and other alkali metal ions. *J Physiol* **216**, 611–624.
- Bachem MG, Schneider E, Gross H, Weidenbach H, Schmid RM, Menke A, Siech M, Beger H, Grunert A & Adler G (1998). Identification, culture, and characterization of pancreatic stellate cells in rats and humans. *Gastroenterology* **115**, 412–432.
- Blais C, Adam A, Massicotte D & Peronnet F (1999). Increase in blood bradykinin concentration after eccentric weight-training exercise in men. *J Appl Physiol* **87**, 1197–1201.
- Bleasdale JE, Thakur NR, Gremban RS, Bundy GL, Fitzpatrick FA, Smith RJ & Bunting S (1990). Selective inhibition of receptor-coupled phospholipase C-dependent processes in human platelets and polymorphonuclear neutrophils. *J Pharmacol Exp Ther* **255**, 756–768.
- Bloechle C, Kusterer K, Kuehn RM, Schneider C, Knoefel WT & Izbickei JR (1998). Inhibition of bradykinin B_2 receptor preserves microcirculation in experimental pancreatitis in rats. *Am J Physiol* **274**, G42–G51.
- Broadbent SD, Ramjeesingh M, Bear CE, Argent BE, Linsdell P & Gray MA (2015). The cystic fibrosis transmembrane conductance regulator is an extracellular chloride sensor. *Pflügers Arch* **467**, 1783–1794.
- Cancela JM, Gerasimenko OV, Gerasimenko JV, Tepikin AV & Petersen OH (2000). Two different but converging messenger pathways to intracellular Ca^{2+} release: the roles of NAADP, cADPR and IP_3 . *EMBO J* **19**, 2549–2557.
- Case RM & Clausen T (1973). The relationship between calcium exchange and enzyme secretion in the isolated rat pancreas. *J Physiol* **235**, 75–102.
- Criddle D, Murphy J, Fistetto G, Barrow S, Tepikin AV, Neoptolemos JP, Sutton R & Petersen OH (2006). Fatty acid ethyl esters cause pancreatic calcium toxicity via inositol trisphosphate receptors and loss of ATP synthesis. *Gastroenterology* **130**, 781–793.
- Eland IA, Sundstrom A, Velo GP, Andersen M, Sturkenboom MCJM, Langman MJS, Stricker BHC & Wiholm B (2006). Antihypertensive medication and the risk of acute pancreatitis: the European case-control study on drug-induced acute pancreatitis. *Scand J Gastroenterol* **41**, 1484–1490.
- Ehrlich BE, Kaftan E, Bezprozvannaya S & Bezprozvanny I (1994). The pharmacology of intracellular Ca^{2+} release channels. *Trends Pharmacol Sci* **15**, 145–149.
- Foskett JK, White C, Cheung KH & Mak DOD (2007). Inositol trisphosphate receptor Ca^{2+} release channels. *Physiol Rev* **87**, 593–658.
- Gerasimenko JV, Charlesworth RM, Sherwood MW, Ferdek PE, Mikoshiba K, Parrington J, Petersen OH & Gerasimenko OV (2015). Both RyRs and TPCs are required for NAADP-induced intracellular Ca^{2+} release. *Cell Calcium* **58**, 237–245.
- Gerasimenko JV, Flowerdew SE, Voronina SG, Sukhomlin TK, Tepikin AV, Petersen OH & Gerasimenko OV (2006). Bile acids induce Ca^{2+} release from both the endoplasmic reticulum and acidic intracellular calcium stores through activation of inositol trisphosphate receptors and ryanodine receptors. *J Biol Chem* **281**, 40154–40163.
- Gerasimenko JV, Gerasimenko OV & Petersen OH (2014). The role of Ca^{2+} in the pathophysiology of pancreatitis. *J Physiol* **592**, 269–280.
- Gerasimenko JV, Gryshchenko O, Ferdek PE, Stapleton E, Hebert TOG, Bychkova S, Peng S, Begg M, Gerasimenko OV & Petersen OH (2013). Ca^{2+} release-activated Ca^{2+} channel blockade as a potential tool in antipain pancreatitis therapy. *Proc Natl Acad Sci USA* **110**, 13186–13191.
- Gerasimenko JV, Lur G, Sherwood MW, Ebisui E, Tepikin AV, Mikoshiba K, Gerasimenko OV & Petersen OH (2009). Pancreatic protease activation by alcohol metabolite depends on Ca^{2+} release via acid store IP_3 receptors. *Proc Natl Acad Sci USA* **106**, 10758–10763.
- Griesbacher T & Lembeck F (1992). Effects of the bradykinin antagonist, HOE 140, in experimental acute pancreatitis. *Br J Pharmacol* **107**, 356–360.
- Griesbacher T, Tiran B & Lembeck F (1993). Pathological events in experimental acute pancreatitis prevented by the bradykinin antagonist Hoe140. *Br J Pharmacol* **108**, 405–411.

- Hirata M, Hayashi I, Yoshimura K, Ishi K, Soma K, Ohwada T, Kakita A & Majima M (2002). Blockade of bradykinin B2 receptor suppresses acute pancreatitis induced by obstruction of the pancreaticobiliary duct in rats. *Br J Pharmacol* **135**, 29–36.
- Hoffmann TF, Waldner H & Messmer K (1996). The bradykinin antagonist CP0597 can limit the progression of post-ischemic pancreatitis. *Immunopharmacology* **33**, 243–246.
- Hu H-Z, Gao N, Liu S, Ren J, Wang X, Xia Y & Wood JD (2004). Action of bradykinin in the submucosal plexus of guinea pig small intestine. *J Pharmacol Exp Ther* **309**, 320–327.
- Israili ZH & Hall WD (1992). Cough and angioneurotic edema associated with angiotensin-converting enzyme inhibitor therapy. A review of the literature and pathophysiology. *Ann Intern Med* **117**, 234–242.
- Kondo S & Schulz I (1976). Calcium ion uptake in isolated pancreas cells induced by secretagogues. *Biochim Biophys Acta* **419**, 76–92.
- Liu YH, Yang XP, Sharov VG, Nass O, Sabbah HN, Peterson E & Carretero OA (1997). Effects of angiotensin-converting enzyme inhibitors and angiotensin II type 1 receptor antagonists in rats with heart failure – role of kinins and angiotensin II type 2 receptors. *J Clin Invest* **99**, 1926–1935.
- Lur G, Haynes LP, Prior IA, Gerasimenko OV, Feske S, Petersen OH, Burgoyne RD & Tepikin AV (2009). Ribosome-free terminals of rough ER allow formation of STIM1 puncta and segregation of STIM1 from IP₃ receptors. *Curr Biol* **19**, 1648–1653.
- Ma H-T, Patterson RL, van Rossum DB, Birnbaumer L, Mikoshiba K & Gill DL (2000). Requirement of the inositol trisphosphate receptor for activation of store-operated Ca²⁺ channels. *Science* **287**, 1647–1651.
- Maleth J, Balazs A, Pallagi P, Balla Z, Kui B, Katona M, Judak L, Nemeth I, Kemeny LV, Lajos V, Rakonczay Z, Venglovecz V, Foldesi I, Peto Z, Somoracz A, Borka K, Perdomo D, Lukacs GL, Gray MA, Monterisi S, Zaccolo M, Sandler M, Mayerle J, Kuhn JP, Lerch MM, Sahin-Toth M & Hegyi P (2015). Alcohol disrupts levels and function of the cystic fibrosis conductance regulator to promote development of pancreatitis. *Gastroenterology* **148**, 427–439.
- Matthews EK, Petersen OH & Williams JA (1973). Pancreatic acinar cells: acetylcholine-induced membrane depolarization, calcium efflux and amylase release. *J Physiol* **234**, 689–701.
- Murphy JA, Criddle DN, Sherwood M, Chvanov M, Mukherjee R, McLaughlin E, Booth D, Gerasimenko JV, Raraty MGT, Ghaneh P, Neoptolemos JP, Gerasimenko OV, Tepikin AV, Green GM, Reeve JR Jr, Petersen OH & Sutton R (2008). Direct activation of cytosolic Ca²⁺ signaling and enzyme secretion by cholecystokinin in human pancreatic acinar cells. *Gastroenterology* **135**, 632–641.
- Pallagi P, Venglovecz V, Rakonczay Z, Borka K, Korompay A, Ozsvari B, Judak L, Sahin-Toth M, Geisz A, Schnur A, Maleth J, Takacs T, Gray MA, Argent BE, Mayerle J, Lerch MM, Wittmann T & Hegyi P (2011). Trypsin reduces pancreatic ductal bicarbonate secretion by inhibiting CFTR Cl[−] channels and luminal anion exchangers. *Gastroenterology* **141**, 2228–2239.
- Parekh AB (2010). Store-operated CRAC channels: function in health and disease. *Nat Rev Drug Disc* **9**, 399–410.
- Parekh AB & Putney JW Jr (2005). Store-operated calcium channels. *Physiol Rev* **85**, 757–810.
- Park MK, Lomax RB, Tepikin AV & Petersen OH (2001). Local uncaging of caged Ca²⁺ reveals distribution of Ca²⁺-activated Cl[−] channels in pancreatic acinar cells. *Proc Natl Acad Sci USA* **98**, 10948–10953.
- Petersen OH (1992). Stimulus-secretion coupling: cytoplasmic calcium signals and the control of ion channels in exocrine acinar cells. *J Physiol* **448**, 1–51.
- Petersen OH & Sutton R (2006). Ca²⁺ signalling and pancreatitis: effects of alcohol, bile and coffee. *Trends Pharmacol Sci* **27**, 113–120.
- Petersen OH & Tepikin AV (2008). Polarized calcium signaling in exocrine gland cells. *Annu Rev Physiol* **70**, 273–299.
- Petersen OH & Ueda N (1976). Pancreatic acinar cells: the role of calcium in stimulus-secretion coupling. *J Physiol* **254**, 583–606.
- Phillips PA, Yang L, Shulkes A, Vonlaufen A, Poljak A, Bustamante S, Warren A, Xu ZH, Guilhaus M, Pirola R, Apte & Wilson JS (2010). Pancreatic stellate cells produce acetylcholine and may play a role in pancreatic exocrine secretion. *Proc Natl Acad Sci USA* **107**, 17397–17402.
- Raraty M, Ward J, Erdemli G, Vaillant C, Neoptolemos JP, Sutton R & Petersen OH (2000). Calcium-dependent enzyme activation and vacuole formation in the apical granular region of pancreatic acinar cells. *Proc Natl Acad Sci USA* **97**, 13126–13131.
- Ryan JW, Moffat JG & Thompson AG (1964). Role of bradykinin in the development of acute pancreatitis. *Nature* **204**, 1212–1213.
- Schachter M (1969). Kallikreins and kinins. *Physiol Rev* **49**, 509–547.
- Sherman MH, Yu RT, Engle DD, Ding N, Atkins AR, Tiriach H, Collisson EA, Connor F, Van Dyke T, Kozlov S, Martin P, Tseng TW, Dawson DW, Donahue TR, Masamune A, Shimosogawa T, Apte MV, Wilson JS, Ng B, Lau SL, Gunton JE, Wahl GM, Hunter T, Drebin JA, O'Dwyer PJ, Liddle C, Tuveson DA, Downes M & Evans RM (2014). Vitamin D receptor-mediated stromal reprogramming suppresses pancreatitis and enhances pancreatic cancer therapy. *Cell* **159**, 80–93.
- Smith RJ, Sam LM, Justen JM, Bundy JL, Bala GA & Bleasdale JE (1990). Receptor-coupled signal transduction in human polymorphonuclear neutrophils – effects of a novel inhibitor of phospholipase C-dependent processes on cell responsiveness. *J Pharmacol Exp Ther* **253**, 688–697.
- Streb H, Irvine RF, Berridge MJ & Schulz I (1983). Release of Ca²⁺ from a nonmitochondrial intracellular store in pancreatic acinar cells by inositol-1,4,5-trisphosphate. *Nature* **306**, 67–69.
- Su JB (2014). Different cross-talk sites between the renin-angiotensin and the kallikrein-kinin systems. *J Renin Angiotensin Aldosterone Syst* **15**, 319–328.
- Tilkemeier P & Thompson PD (1988). Acute pancreatitis possibly related to enalapril. *N Engl J Med* **318**, 1275–1276.

- Tsutsumi Y, Matsubara H, Masaki H, Kurihara H, Murasawa S, Takai S, Miyazaki M, Nozawa Y, Ozono R, Nakagawa K, Miwa T, Kawada N, Mori Y, Shibasaki Y, Tanaka Y, Fujiyama S, Koyama Y, Fujiyama A, Takahashi H & Iwasaka T (1999). Angiotensin II type 2 receptor overexpression activates the vascular kinin system and causes vasodilation. *J Clin Invest* **104**, 925–935.
- Voronina SG, Collier D, Chvanov M, Middlehurst B, Beckett AJ, Prior IA, Criddle DN, Begg M, Mikoshiba K, Sutton R & Tepikin AV (2015). The role of Ca^{2+} influx in endocytic vacuole formation in pancreatic acinar cells. *Biochem J* **465**, 405–412.
- Voronina S, Longbottom R, Sutton R, Petersen OH & Tepikin AV (2002). Bile acids induce calcium signals in mouse pancreatic acinar cells. Implications for bile-induced pancreatic pathology. *J Physiol* **540**, 49–55.
- Wakui M, Osipchuk YV & Petersen OH (1990). Receptor-activated cytoplasmic Ca^{2+} spiking mediated by inositol trisphosphate is due to Ca^{2+} -induced Ca^{2+} release. *Cell* **63**, 1025–1032.
- Watari H, Hotta Y & Mabuchi Y (1982). Morphological studies on a vitamin A storing cell and its complex with macrophage observed in mouse pancreatic tissues following excess vitamin A administration. *Okajimas Folia Anat Jpn* **58**, 837–858.
- Wells RG & Crawford JM (1998). Pancreatic stellate cells: the new stars of chronic pancreatitis? *Gastroenterology* **115**, 491–493.
- Wen L, Voronina S, Javed MA, Awais M, Szatmary P, Latawiec D, Chvanov M, Collier D, Huang W, Barrett J, Begg M, Stauderman K, Roos J, Grigoryev S, Ramos S, Rogers E, Whitten J, Velicelebi G, Dunn M, Tepikin AV, Criddle DN & Sutton R (2015). Inhibitors of ORAI1 prevent cytosolic calcium-associated injury of human pancreatic acinar cells and acute pancreatitis in 3 mouse models. *Gastroenterology* **149**, 481–492.
- Won JH, Zhang Y, Baoan JI, Logsdon CD & Yule DI (2011). Phenotypic changes in mouse pancreatic stellate cell Ca^{2+} signaling events following activation in culture and in a disease model of pancreatitis. *Mol Biol Cell* **22**, 412–436.

Additional information

Competing interests

None declared.

Author contributions

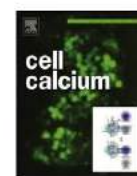
Conception and design of the experiments: O.H.P., O.V.G., O.G. and J.V.G. Collection, analysis and interpretation of data: O.G., J.V.G. and O.V.G. Drafting the article or revising it critically for important intellectual content: O.H.P., J.V.G., O.V.G. and O.G.

Funding

This work was supported by Medical Research Council Programme Grant MR/J002771/1. O.H.P. is a Medical Research Council Professor (G19/22/2).

Translational Perspective

Our work indicates that bradykinin-elicited Ca^{2+} signals in pancreatic stellate cells may influence negatively the outcome of acute pancreatitis. We tested the hypothesis that blockage of bradykinin type 2 (B2) receptors would offer protection against the pancreatic acinar cell necrosis caused by pancreatitis-inducing agents, such as alcohol, fatty acid ethyl esters or bile acids. The results showed that specific B2 receptor blockade markedly reduced the extent of necrosis observed after treatment with ethanol, POAEE or a mixture of bile acids. This suggests that B2 receptor blockade in the early stage of acute pancreatitis may be helpful in reducing the severity of the disease. We also show that the bradykinin-elicited sustained elevation of the cytosolic Ca^{2+} concentration in pancreatic stellate cells can be inhibited by a specific inhibitor of Ca^{2+} release – activated Ca^{2+} (CRAC) channels. We have recently shown that CRAC inhibition in PACs offers remarkable protection against necrosis induced by fatty acid ethyl esters. In the intact pancreas, CRAC inhibition would reduce excessive Ca^{2+} signal generation both in the acinar cells (brought about by, for example, fatty acid ethyl esters) and in the stellate cells (brought about by bradykinin). Both effects would be beneficial. Our work therefore indicates that combined treatment with a CRAC inhibitor and a B2 receptor – blocking agent should be tested *in vivo* as a potentially useful therapy against acute pancreatitis.



Review

Calcium signalling in pancreatic stellate cells: Mechanisms and potential roles



Oleksiy Gryshchenko^{a,b}, Julia V. Gerasimenko^a, Oleg V. Gerasimenko^a, Ole H. Petersen^{a,*}

^a Medical Research Council Group, Cardiff School of Biosciences, Cardiff University, Cardiff CF10 3AX, Wales, UK

^b Bogomoletz Institute of Physiology, Kiev 01024, Ukraine

ARTICLE INFO

Article history:

Received 2 February 2016

Accepted 5 February 2016

Available online 28 February 2016

Keywords:

Calcium signalling

Calcium release

Calcium entry

Bradykinin

Bradykinin receptors

Kallikrein

Kininogen

ABSTRACT

Hepatic and pancreatic stellate cells may or may not be regarded as stem cells, but they are capable of remarkable transformations. There is less information about stellate cells in the pancreas than in the liver, where they were discovered much earlier and therefore have been studied longer and more intensively than in the pancreas. Most of the work on pancreatic stellate cells has been carried out in studies on cell cultures, but in this review we focus attention on Ca^{2+} signalling in stellate cells in their real pancreatic environment. We review current knowledge on patho-physiologically relevant Ca^{2+} signalling events and their underlying mechanisms. We focus on the effects of bradykinin in the initial stages of acute pancreatitis, an often fatal disease in which the pancreas digests itself and its surroundings. Ca^{2+} signals, elicited in the stellate cells by the action of bradykinin, may have a negative effect on the outcome of the acute disease process and promote the development of chronic pancreatitis. The bradykinin-elicited Ca^{2+} signals can be inhibited by blockade of type 2 receptors and also by blockade of Ca^{2+} -release activated Ca^{2+} channels. The potential benefits of such pharmacological inhibition for the treatment of pancreatitis are reviewed.

© 2016 Elsevier Ltd. All rights reserved.

1. Introduction

Stellate cells were discovered in the liver in 1876 by Carl von Kupffer, who called them ‘Sternzellen’ (star cells) [1,2], but similar cells were only discovered in the pancreas more than 100 years later [3]. The hepatic stellate cells (HSCs) play a key role in the development of hepatic fibrosis [2] and, similarly, the pancreatic stellate cells (PSCs) are the key elements in the process of pancreatic fibrosis [4].

Molecular markers of stem cells are present in HSCs [5]. Furthermore, the space of Disse, where HSCs reside in the liver, has similarities with known stem cell niches [5]. Certainly, HSCs are characterized by considerable plasticity [2] and, given that HSCs and PSCs share many homologies—but are distinctly different from fibroblasts [4]—it is not surprising that PSCs can also undergo dramatic changes in structure and function depending on the stimuli they receive [4]. Nevertheless, it is not clear whether PSCs can

truly be regarded as stem cells, although they do possess certain progenitor cell characteristics [6].

From studies of HSCs, we know that cytosolic Ca^{2+} signals, mediated by phospholipase C-induced inositol 1,4,5-trisphosphate (IP_3) production, play a key role in the proliferation and activation of these cells [7–9]. In what follows, we shall review what is known about Ca^{2+} signalling mechanisms in PSCs and discuss the roles such signals may play.

2. Localization of stellate cells in the normal pancreas

In the normal pancreas, PSCs are seen as small elongated cells, which are situated at the periphery of acinar cells (PACs). Immunohistochemical staining with an antibody against desmin (a cytoskeletal protein that is not present in PACs) is particularly helpful in demonstrating the position of PSCs (Fig. 1A). The typical location of PSCs shown in Fig. 1A can also be seen with nonlinear optical microscopy, using two-photon excited fluorescence or second harmonic generation [11]. PSCs contain lipid droplets with vitamin A [12] and these can be visualized by intrinsic multiphoton fluorescence (Fig. 1B). The location of PSCs between acinar cells (Fig. 1B) and the peri-acinar capillaries (not visualized in Fig. 1) could be regarded as somewhat similar to the situation of HSCs in the space of Disse, where the HSCs are placed between the endothelial cells of the

* Corresponding author at: MRC Group, Cardiff School of Biosciences, Cardiff University, Sir Martin Evans Building, Museum Avenue, Cardiff CF10 3AX, Wales, UK.

E-mail address: PetersenOH@cardiff.ac.uk (O.H. Petersen).

<http://dx.doi.org/10.1016/j.ceca.2016.02.003>

0143-4160/© 2016 Elsevier Ltd. All rights reserved.

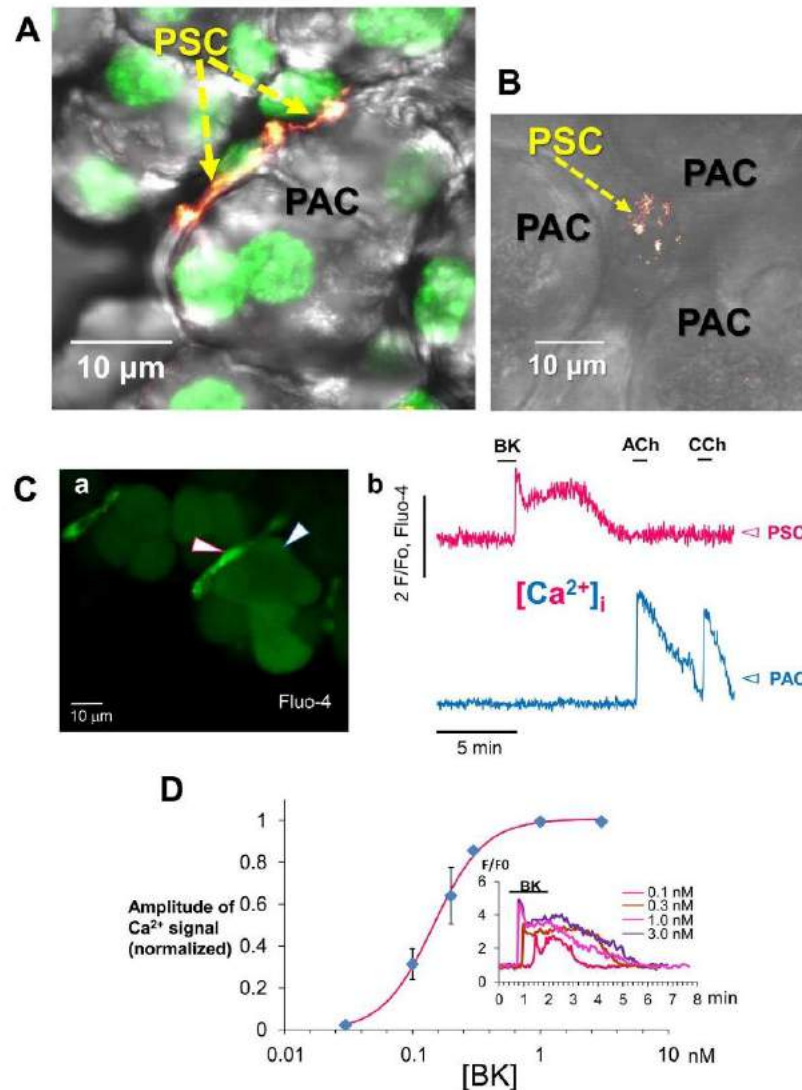


Fig. 1. Location of stellate cells in the pancreas and the effect of bradykinin (BK) on $[Ca^{2+}]_i$ in these cells (PSCs). (A) Localization of PSCs (identified by desmin antibody) at the periphery of acinar unit (pancreatic acinar cells—PACs). Nuclei are green. (B) PSC with lipid droplets containing vitamin A (identified by multiphoton intrinsic fluorescence) located in 'niche' between PACs. (C) Simultaneous recordings of $[Ca^{2+}]_i$ in neighbouring PSC and PAC. (a) Fluorescence image of small acinar cluster with two cells specifically signposted, a bright PSC (white arrow outlined in red) and a neighbouring PAC (white arrow outlined in blue), from where recordings of $[Ca^{2+}]_i$ were made. (b) Simultaneous recordings of $[Ca^{2+}]_i$ from the two cells identified in (a). BK evokes a clear Ca^{2+} signal in the PSC but not in the PAC, whereas ACh and CCh elicit Ca^{2+} signals in the PAC, but not in the PSC. (D) Concentration-response relationship for BK-elicited Ca^{2+} signals in PSCs. The inset shows the results from a single PSC. Adapted from Gryshchenko et al. [10]. (For interpretation of the references to colour in this figure legend, the reader is referred to the web version of this article.)

sinusoid capillaries and the hepatocytes [2,5]. This arrangement has been described as a stellate (stem) cell niche [5]. With regard to Ca^{2+} signalling studies on PSCs, it is advantageous that PSCs take up fluorescent probes (for example, the Ca^{2+} -sensitive Fluo-4) much more avidly than PACs. An example of this is shown in Fig. 1Ca, in which bright stellate cells are seen at the periphery of acinar units.

3. Ca^{2+} signalling in stellate cells in their normal environment

PSCs do not display Ca^{2+} signals when stimulated with acetylcholine (ACh) or cholecystokinin (CCK) [10], the physiologically important activators of acinar fluid and enzyme secretion [13].

As seen in Fig. 1C, ACh evokes a substantial increase in the cytosolic Ca^{2+} concentration ($[Ca^{2+}]_i$) of a PAC, but does not elicit such a response from the closely neighbouring PSC. Another activator of muscarinic receptors, carbachol (CCh), also fails to elicit a Ca^{2+} signal in the PSC, while causing a major rise in $[Ca^{2+}]_i$ in the neighbouring PAC (Fig. 1C). CCK also fails to elicit Ca^{2+} signals in PSCs under conditions where it evokes clear elevations of $[Ca^{2+}]_i$ in neighbouring PACs [10]. On the other hand, bradykinin (BK) consistently evoked Ca^{2+} signals in PSCs, but had no effect on $[Ca^{2+}]_i$ in closely neighbouring PACs (Fig. 1C). Pharmacological studies show that the BK-elicited Ca^{2+} signals are mediated via bradykinin type 2 receptors (B2 receptors) [10]. As seen in Fig. 1C, the BK-elicited Ca^{2+} signal consists of two components, a rapid and partially transient

$[Ca^{2+}]_i$ elevation followed by a prolonged plateau phase. The initial component is due to IP_3 -mediated Ca^{2+} release from internal stores, whereas the subsequent plateau phase is completely dependent on store-operated Ca^{2+} entry through conventional CRAC channels [10]. ATP, which very rarely evokes changes in $[Ca^{2+}]_i$ in PACs frequently, but not always, elicits Ca^{2+} signals in PSCs [10]. Thus we have complete separation of Ca^{2+} signal mechanisms in PACs and PSCs and there is no functional evidence of gap junctional communication between these two cell types [10].

4. Where is bradykinin generated and what are the physiologically relevant concentrations?

Kinin peptides (including BK) are released from kininogens, which are plasma proteins, by tissue or plasma kallikreins. In the pancreas, most of the kallikrein is present in the zymogen granules as an inactive pre-cursor—pre-kallikrein—as are many of the other pancreatic enzymes [14]. Under pathological conditions, for example acute pancreatitis, active kallikrein, like many other proteases, would be released from necrotic acinar cells resulting in enhanced BK formation [15]. The basic BK concentration in plasma is 40–70 pM [16,17], but in acute pancreatitis it increases to ~140 pM [17].

5. Are bradykinin-elicited Ca^{2+} signals in stellate cells of physiological or pathophysiological significance?

In an earlier study of Ca^{2+} signalling in PSCs, an example of a transient rise in $[Ca^{2+}]_i$ elicited by 50 nM BK was observed [18]. This BK concentration is way above the plasma values measured *in vivo* as mentioned above. In the study of Won et al. [18], concentration-response curves were not explored, so it was unclear whether BK-evoked Ca^{2+} signals could play any role in physiology or pathophysiology. However, the more recent study of Gryshchenko et al. [10] shows that PSCs are much more sensitive to BK than hitherto realized. As shown in Fig. 1D, BK at a concentration as low as 100 pM, within the range that has been measured in plasma *in vivo* in acute pancreatitis [17], elicits a clearly observable rise in $[Ca^{2+}]_i$. The BK concentration-response curve (Fig. 1D) is particularly steep in the BK concentration range 100–200 pM, which means that any rise in the plasma [BK] from the basic level (40–70 pM), to that seen in acute pancreatitis (~140 pM) would elicit a rise in $[Ca^{2+}]_i$ in PSCs. At these patho-physiologically relevant BK concentrations, there is no sign of the Ca^{2+} response becoming desensitized [10]. These data are compatible with the hypothesis that BK, via actions on PSCs, plays a role in the pathophysiology of acute pancreatitis.

6. What are the potential consequences of PSC Ca^{2+} signal generation?

Given that intracellular Ca^{2+} signals can drive numerous cellular processes [19], including gene expression [20], secretion [21], contraction [22], cell division [23,24] and cell death [25], there are many possibilities. As already mentioned, there is evidence indicating that Ca^{2+} signals in HSCs are important for proliferation and, similarly, this may also be the case for PSCs [18]. In the normal healthy pancreas, the PSCs only make up a small proportion of the pancreatic mass (Fig. 1), but in the transition from acute to chronic pancreatitis there is a marked increase in the PSC population and the PSCs also undergo dramatic changes in structure and function, allowing them respond to stimuli – for example, trypsin and thrombin – that have no effect in their normal state [4,10,18]. There is clear evidence indicating that the activated PSCs secrete excessive amounts of the extracellular matrix proteins that are responsible for pancreatic fibrosis and may be cancer promoting [4]. The transformed PSCs are commonly referred to as activated PSCs [4]. The

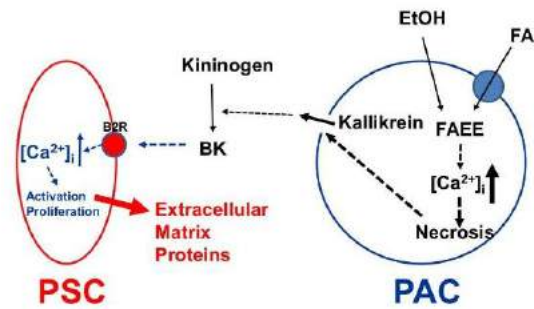


Fig. 2. Schematic diagram, illustrating potential mechanism for activating PSCs during attack of alcohol-related acute pancreatitis. EtOH, ethanol; FA, fatty acid; FAEF, fatty acid ethyl ester. For detailed explanation see text.

activation process has mostly been studied in cell cultures and a number of factors have been identified [4], but the nature of the patho-physiologically important initiation signal in the pancreas is not entirely clear.

Given that plasma [BK] increases in acute pancreatitis and that the levels attained will induce Ca^{2+} signals in normal PSCs, it does not seem unreasonable to speculate that it may be the BK-elicited Ca^{2+} signals in the PSCs that initiate the process that ultimately results in the activation of the PSCs. A possible sequence of events is illustrated in Fig. 2. Acute pancreatitis typically occurs as a consequence of excessive intake of alcohol or complications of biliary disease. In both cases the disease process is initiated by excessive release of Ca^{2+} from intracellular stores, which is primarily due to the Ca^{2+} -liberating action of a combination of alcohol and fatty acids (FAs)—fatty acid ethyl esters (FAEEs)—or bile acids [26]. This is then followed by a particularly damaging store-operated Ca^{2+} entry [26]. In severe cases of acute pancreatitis (~20%), this leads to intracellular protease activation, extensive acinar necrosis with release of many activated proteases, including trypsin and kallikrein, into the interstitial fluid. In that environment, kallikrein acts on kininogens to release BK and BK in turn elicits Ca^{2+} signals in the PSCs leading to activation and proliferation. The more numerous and activated PSCs secrete excessive amounts of extracellular matrix proteins. For the sake of diagrammatic simplicity, Fig. 2 only illustrates the case of alcohol-related pancreatitis.

It is also possible that the BK-elicited Ca^{2+} signals in PSCs could have an effect on the acinar cells. Clearly such an effect would not be the result of induction of Ca^{2+} signals in PACs, since it has been clearly shown that BK-elicited Ca^{2+} signals in PSCs do not cause any change in $[Ca^{2+}]_i$ in neighbouring PACs (Fig. 1). This, however, does not exclude other types of signal generation. It has been shown that pharmacological blockade of B2 receptors is helpful in suppressing the cellular changes in the pancreas that are characteristic for pancreatitis [17,27–30]. However, it cannot be excluded that the beneficial effect of B2 receptor blockade was mostly due to suppression of the classical effects of BK on the vasculature, namely vasodilatation and increased capillary permeability [14,31], rather than suppression of the Ca^{2+} signals in the PSCs. There is now evidence indicating that the vascular effects are not the only ones evoked by BK, since it could be shown in an *in vitro* model of isolated pancreatic lobules that B2 receptor blockade markedly reduced the extent of acinar necrosis induced by ethanol, FAEEs or bile acids [10]. This suggests that the Ca^{2+} signals in the PSCs, via a still unknown mechanism, have a negative influence on the survival of PACs during the acute phase of pancreatitis.

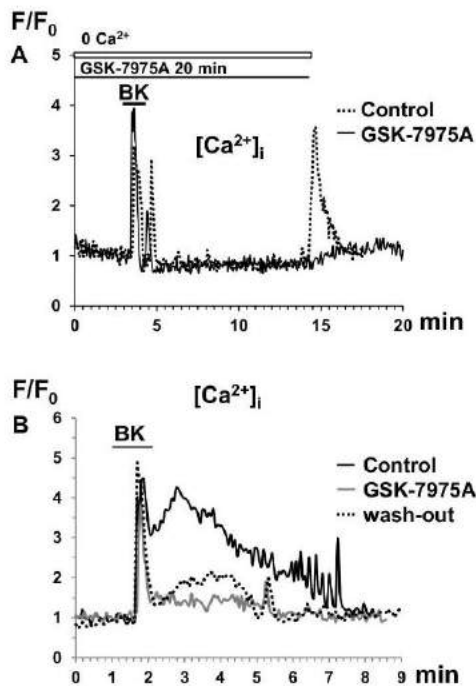


Fig. 3. Effect of CRAC channel blockade on $[Ca^{2+}]_i$ changes evoked by BK. (A) In the absence of external Ca^{2+} and irrespective of the presence or absence of the CRAC channel blocker GSK7975A, BK only evokes a short-lasting rise in $[Ca^{2+}]_i$. Admission of external Ca^{2+} causes a renewed major rise in $[Ca^{2+}]_i$, but only in the absence of the CRAC channel blocker. (B) The elevated $[Ca^{2+}]_i$ plateau phase following the initial $[Ca^{2+}]_i$ rise after BK stimulation is abolished by GSK7975A. The effect is partially reversible after wash-out of the drug. Adapted from Gryshchenko et al. [10].

7. How can we suppress the BK-elicited Ca^{2+} signals in the PSCs?

Although not investigated in the same detail as in the PACs, the available evidence from studies on PSCs strongly suggests that following BK-elicited release of Ca^{2+} from intracellular stores, there is opening of CRAC channels and that it is the inflow of Ca^{2+} through these channels that is responsible for the plateau phase of the Ca^{2+} signal [10]. There has been increasing interest in recent years in the CRAC channel as an important therapeutic target in several human diseases [32,33] and in PACs it has been shown that the sustained phase of the $[Ca^{2+}]_i$ elevation evoked by FAEs can be reduced or abolished by a CRAC channel blocker [34]. It has also been demonstrated that CRAC channel inhibition can prevent FAE-induced acinar necrosis [34].

As seen in Fig. 3A, BK only elicits a transient rise in $[Ca^{2+}]_i$ in the absence of external Ca^{2+} , but when Ca^{2+} is subsequently readmitted to the external solution there is a second $[Ca^{2+}]_i$ response due to store-operated Ca^{2+} entry. In the presence of the CRAC blocker GSK-7975A, this second phase is almost completely absent (Fig. 3A). In the presence of external Ca^{2+} , BK evokes the usual biphasic response, but when the CRAC blocker is present, the plateau phase is absent (Fig. 3B). The effect of the CRAC blockade is at least partially reversible (Fig. 3B). Thus we now have evidence demonstrating that inhibition of Ca^{2+} inflow through CRAC channels will not only reduce the deleterious effects in the PACs of all the known agents promoting acute pancreatitis [34–36], but will also reduce the plateau phase of the BK-elicited rise in $[Ca^{2+}]_i$ in the PSCs [10].

8. Conclusion

Given that B2 blockade prevents much of the necrotic damage to PACs in response to pancreatitis promoting agents [10], it is likely that the inhibition of BK-elicited Ca^{2+} signal generation caused by CRAC blockade will have contributed to its remarkable therapeutic effect against acute pancreatitis in a recent *in vivo* study [36]. Furthermore, if—as suggested in Fig. 2—it turns out that the BK-elicited Ca^{2+} signals in PSCs have a key role in the activation and proliferation of PSCs, then CRAC blockade would also be helpful in combatting the transition from acute to chronic pancreatitis and, by inhibiting the ability of PSCs to produce the cancer promoting extracellular matrix, also potentially afford some protection against the development of pancreatic cancer. On the basis of recent work on the effects of CRAC channel blockade in PACs and PSCs [10,34], Hegyi [37] has suggested that CRAC blockade may turn out to be the first pharmacological intervention that offers the potential of specific therapy in acute pancreatitis.

Acknowledgements

This original work in the authors' laboratory was supported by Medical Research Council Programme Grant MR/J002771/1. O.H.P. is a Medical Research Council Professor (G19/22/2).

References

- W.S. Haubrich, Kupffer of Kupffer cells, *Gastroenterology* 127 (2004) 16.
- S.L. Friedman, Hepatic stellate cells: protean, multifunctional, and enigmatic cells of the liver, *Physiol. Rev.* 88 (2008) 125–172.
- H. Watari, Y. Hotta, Y. Mabuchi, Morphological studies on a vitamin A storing cell and its complex with macrophage observed in mouse pancreatic tissues following excess vitamin A administration, *Okajimas Folia Anat. Jpn.* 58 (1982) 837–858.
- M. Erkan, G. Adler, M.V. Apte, M.G. Bachem, M. Buchholz, S. Detlevsen, I. Esposito, H. Friess, T.M. Gress, H.-J. Habisch, R.F. Hwang, R. Jaster, J. Kleef, G. Kloppel, C. Kordes, C.D. Logsdon, A. Masamune, C.W. Michalski, J. Oh, P.A. Phillips, M. Pinzani, C. Reiser-Erkan, H. Tsukamoto, J. Wilson, StellaTUM: current consensus and discussion on pancreatic stellate cell research, *Gut* 61 (2012) 172–178.
- I. Sawitzka, C. Kordes, S. Reister, D. Haussinger, The niche of stellate cells within rat liver, *Hepatology* 50 (2009) 1617–1624.
- E. Mato, M. Lucas, J. Petriz, R. Gomis, A. Novials, Identification of a pancreatic stellate cell population with properties of progenitor cells: new role for stellate cells in the pancreas, *Biochem. J.* 421 (2009) 181–191.
- E.M. Soliman, M.A. Rodrigues, D.A. Gomes, N. Sheung, J. Yu, M.J. Amaya, M.H. Nathanson, J.A. Dranoff, Intracellular calcium signals regulate growth of hepatic stellate cells via specific effects on cell cycle progression, *Cell Calcium* 45 (2009) 284–292.
- S.-Y. Kim, B.H. Cho, U.-H. Kim, CD38-mediated Ca^{2+} signaling contributes to angiotensin II-induced activation of hepatic stellate cells, *J. Biol. Chem.* 285 (2010) 576–582.
- K.-S. Park, P.-J. Sin, D.H. Lee, S.-K. Cha, M.-J. Kim, N.-H. Kim, S.-K. Baik, S.-W. Jeong, I.D. Kong, Switching-on of serotonergic calcium signalling in activated hepatic stellate cells, *World J. Gastroenterol.* 17 (2011) 164–173.
- O. Gryshchenko, J.V. Gerasimenko, O.V. Gerasimenko, O.H. Petersen, Ca^{2+} signals mediated by bradykinin type 2 receptors in normal pancreatic stellate cells can be inhibited by specific Ca^{2+} channel blockade, *J. Physiol.* 594 (2016) 281–293.
- W. Hu, L. Fu, Simultaneous characterization of pancreatic stellate cells and other pancreatic components within three-dimensional tissue environment during chronic pancreatitis, *J. Biomed. Optics* 18 (2013) 056002-1–056002-9.
- M.G. Bachem, E. Schneider, H. Gross, H. Weidenbach, R.M. Schmid, A. Menke, M. Siech, H. Beger, A. Grunert, G. Adler, Identification, culture, and characterization of pancreatic stellate cells in rats and humans, *Gastroenterology* 115 (1998) 412–432.
- O.H. Petersen, A.V. Tepikin, Polarized calcium signalling in exocrine gland cells, *Annu. Rev. Physiol.* 70 (2008) 273–299.
- M. Schachter, Kallikreins and kinins, *Physiol. Rev.* 49 (1969) 509–547.
- V. Orlov, N. Belyakov, Blood kallikrein, kinin system in acute pancreatitis, *Am. J. Gastroenterol.* 70 (1978) 645–648.
- C. Blais, A. Adam, D. Massicote, F. Peronnet, Increase in blood bradykinin concentration after eccentric weight-training in men, *J. Appl. Physiol.* 87 (1999) 1197–1201.
- M. Hirata, I. Hayashi, K. Yoshimura, K. Ishi, K. Soma, T. Ohwada, A. Kakita, M. Majima, Blockade of bradykinin B2 receptor suppresses acute pancreatitis

- induced by obstruction of the pancreaticobiliary duct in rats, *Br. J. Pharmacol.* 135 (2002) 29–36.
- [18] J.H. Won, Y. Zhang, J.L. Baoan, C.D. Logsdon, D.I. Yule, Phenotypic changes in pancreatic stellate cell Ca^{2+} signaling events following activation in culture and in a disease model of pancreatitis, *Mol. Biol. Cell* 22 (2011) 412–436.
 - [19] O.H. Petersen, M. Michalak, A. Verkhratsky, Calcium signalling: past, present and future, *Cell Calcium* 38 (2005) 161–169.
 - [20] P. Kar, A.B. Parekh, Distinct spatial Ca^{2+} signatures selectively activate different NFAT transcription factor isoforms, *Mol. Cell* 58 (2015) 232–243.
 - [21] O.H. Petersen, N. Ueda, Pancreatic acinar cells: the role of calcium in stimulus-secretion coupling, *J. Physiol.* 254 (1976) 583–606.
 - [22] L.V. Heilbrunn, F.J. Wiercinsky, Actions of various cations on muscle protoplasm, *J. Cell. Comp. Physiol.* 19 (1947) 15–32.
 - [23] A.R. Means, C.D. Rasmussen, Calcium, calmodulin and cell proliferation, *Cell Calcium* 9 (1988) 313–319.
 - [24] M. Whitaker, Calcium in fertilization and in early development, *Physiol. Rev.* 86 (2006) 25–88.
 - [25] D.N. Criddle, J.V. Gerasimenko, H.K. Baumgartner, M. Jaffar, S. Voronina, R. Sutton, O.H. Petersen, O.V. Gerasimenko, Calcium signalling and pancreatic cell death: apoptosis or necrosis, *Cell Death Differ.* 14 (2007) 1285–1294.
 - [26] O.H. Petersen, R. Sutton, Ca^{2+} signalling and pancreatitis: effects of alcohol, bile and coffee, *Trends Pharmacol. Sci.* 27 (2006) 113–120.
 - [27] T. Griesbacher, F. Lembeck, Effects of the bradykinin antagonist HOE 140, in experimental acute pancreatitis, *Br. J. Pharmacol.* 107 (1992) 356–360.
 - [28] T. Griesbacher, B. Tiran, F. Lembeck, Pathological events in experimental acute pancreatitis prevented by the bradykinin antagonist Hoe 140, *Br. J. Pharmacol.* 108 (1993) 405–411.
 - [29] T.F. Hoffmann, H. Waldner, K. Messmer, The bradykinin antagonist CP0597 can limit the progression of post-ischemic pancreatitis, *Immunopharmacology* 33 (1996) 243–246.
 - [30] C. Bloechle, K. Kusterer, R.M. Kuehn, C. Schneider, W.T. Knoefel, J.R. Izbicki, Inhibition of bradykinin B2 receptor preserves microcirculation in experimental pancreatitis in rats, *Am. J. Physiol.* 274 (1998) G42–G51.
 - [31] K.D. Bhoola, J.D. Calle, M. Schachter, The effect of bradykinin, serum kallikrein and other endogenous substances on capillary permeability in the guinea-pig, *J. Physiol.* 152 (1960) 75–86.
 - [32] A.B. Parekh, Store-operated CRAC channels: function in health and disease, *Nat. Rev. Drug Discov.* 9 (2010) 399–410.
 - [33] J.L. Di Capite, G.J. Bates, A.B. Parekh, Mast cell CRAC channel as a novel therapeutic target in allergy, *Curr. Opin. Allergy Clin. Immunol.* 11 (2011) 33–38.
 - [34] J.V. Gerasimenko, O. Gryshchenko, P.E. Ferdek, E. Stapleton, T.O.G. Hebert, S. Bychkova, S. Peng, M. Begg, O.V. Gerasimenko, O.H. Petersen, Ca^{2+} release-activated Ca^{2+} channel blockade as a potential tool in antip pancreatitis therapy, *PNAS* 110 (2013) 13186–13191.
 - [35] S.G. Voronina, D. Collier, M. Chvanov, B. Middlehurst, A.J. Beckett, I.A. Prior, D.N. Criddle, M. Begg, K. Mikoshiba, R. Sutton, A.V. Tepikin, The role of Ca^{2+} influx in endocytic vacuole formation in pancreatic acinar cells, *Biochem. J.* 465 (2015) 405–412.
 - [36] L. Wen, S. Voronina, M.A. Javed, M. Awais, P. Szatmary, P.D. Latawiec, M. Chvanov, D. Collier, W. Huang, J. Barrett, M. Begg, K. Stauderman, J. Roos, S. Grigoryev, S. Ramos, E. Rogers, J. Whitten, G. Velicelebi, M. Dunn, A.V. Tepikin, D.N. Criddle, R. Sutton, Inhibitors of Orai1 prevent cytosolic calcium-associated injury of human pancreatic acinar cells and acute pancreatitis in 3 mouse models, *Gastroenterology* 149 (2015) 481–492.
 - [37] P. Hegyi, Blockade of calcium entry provides a therapeutic window in acute pancreatitis, *J. Physiol.* 594 (2016) 257.

3.3. Катіонні трансмембранні струми, викликані прикладанням жовчних

КИСЛОТ

THE JOURNAL OF BIOLOGICAL CHEMISTRY
© 2005 by The American Society for Biochemistry and Molecular Biology, Inc.

Vol. 280, No. 3, Issue of January 21, pp. 1764–1770, 2005
Printed in U.S.A.

Bile Acids Induce a Cationic Current, Depolarizing Pancreatic Acinar Cells and Increasing the Intracellular Na^+ Concentration*

Received for publication, September 7, 2004, and in revised form, November 8, 2004
Published, JBC Papers in Press, November 9, 2004, DOI 10.1074/jbc.M410230200

Svetlana G. Voronina[‡], Olexyi V. Gryshchenko^{‡§}, Oleg V. Gerasimenko, Anne K. Green[¶],
Ole H. Petersen, and Alexei V. Tepikin^{||}

From the Physiological Laboratory, University of Liverpool, Liverpool L69 3BX, United Kingdom

Biliary disease is a major cause of acute pancreatitis. In this study we investigated the electrophysiological effects of bile acids on pancreatic acinar cells. In perforated patch clamp experiments we found that tauro-lithocholic acid 3-sulfate depolarized pancreatic acinar cells. At low bile acid concentrations this occurred without rise in the cytosolic calcium concentration. Measurements of the intracellular Na^+ concentration with the fluorescent probe Sodium Green revealed a substantial increase upon application of the bile acid. We found that bile acids induce Ca^{2+} -dependent and Ca^{2+} -independent components of the Na^+ concentration increase. The Ca^{2+} -independent component was resolved in conditions when the cytosolic Ca^{2+} level was buffered with a high concentration of the calcium chelator 1,2-bis(*o*-aminophenoxy)ethane-*N,N,N',N'*-tetraacetic acid (BAPTA). The Ca^{2+} -dependent component of intracellular Na^+ increase was clearly seen during stimulation with the calcium-releasing agonist acetylcholine. During acetylcholine-induced Ca^{2+} oscillations the recovery of cytosolic Na^+ was much slower than the recovery of Ca^{2+} , creating a possibility for the summation of Na^+ transients. The bile-induced Ca^{2+} -independent current was found to be carried primarily by Na^+ and K^+ , with only small Ca^{2+} and Cl^- contributions. Measurable activation of such a cationic current could be produced by a very low concentration of tauro-lithocholic acid 3-sulfate (10 μM). This bile acid induced a cationic current even when applied in sodium- and bicarbonate-free solution. Other bile acids, taurochenodeoxycholic acid, taurocholic acid, and bile itself also induced cationic currents. Bile-induced depolarization of acinar cells should have a profound effect on acinar fluid secretion and, consequently, on transport of secreted zymogens.

Bile acids can get access to pancreatic acinar cells in certain pathological conditions either as a result of bile reflux into the

pancreatic duct (due to blocked ampulla of Vater) or via interstitial leakage. Bile is considered a putative trigger of acute pancreatitis (1, 2), although issue is still debated (3–6). Bile acids have been shown to increase significantly the permeability of the ductal mucosal barrier in the pancreas (7–9), and recently two investigations demonstrated that bile acids are able to induce prolonged toxic cytosolic calcium signals in pancreatic acinar cells (1, 10).

In our previous study we found that low concentrations of tauro-lithocholic acid 3-sulfate (TLC-S)¹ produce preferentially local apical calcium signals, whereas higher concentrations of this bile acid produce sustained global calcium elevations. Other bile acids, taurochenodeoxycholic acid (TC) and taurocholic acid, also initiated cytosolic calcium responses (10). Similar results were reported by Kim *et al.* (1). Furthermore, bile acids have been shown to increase membrane permeability to ions in a number of model cell lines (11–13).

The membrane potential of pancreatic acinar cells is dependent on the activity of the Na^+/K^+ pump and is influenced by electrogenic transporters (e.g. Na^+ -amino acid co-transporters) and ionic channels (14–18). The ionic channels expressed in pancreatic acinar cells include Ca^{2+} -activated non-selective cationic channels (permeable to Na^+ and K^+) (18–20) and prominent Ca^{2+} -activated Cl^- channels (18, 20–23).

Bile acids were reported to enter into pancreatic acinar cells via an anionic HCO_3^- -dependent exchanger and a Na^+ -dependent co-transporter (1). The Na^+ /bile co-transporters have been shown to be electrogenic in hepatocytes (24) and ileal epithelial cells (25). Therefore, bile acids could potentially affect membrane voltage by activation/formation of ionic channels and by activation of electrogenic bile transporters. Activation of ionic conductances and the depolarizing effect on the transmembrane potential could be contributing factors to the pathological action of bile on pancreatic acinar cells. The electrophysiological effects of bile have not been characterized before in pancreatic acinar cells. This became a focus of our study. The largely unexpected results of this investigation are described below.

EXPERIMENTAL PROCEDURES

Cell Preparation—Pancreata were obtained from adult mice (CD1) killed by cervical dislocation in accordance with the Animal (Scientific Procedure) Act of 1986. Pancreatic acinar cells were prepared by injecting 1 ml of 200 units ml^{-1} collagenase (Worthington Lakewood, NJ) and digesting for 16–17 min at 37 °C with constant agitation. After digestion the pancreas was agitated manually to release single cells or small

* This work was supported by a Medical Research Council (MRC) program grant (to O. H. P., O. V. Gerasimenko, and A. V. T.) and an MRC Professorship (to O. H. P.). The costs of publication of this article were defrayed in part by the payment of page charges. This article must therefore be hereby marked "advertisement" in accordance with 18 U.S.C. Section 1734 solely to indicate this fact.

[‡] These authors have made equal contributions to this study.

[§] Current address: Dept. of Physiology of the Nervous System, Bogomoletz Institute of Physiology, Bogomoletz Street 4, Kiev-24, GSP 01024, Ukraine.

[¶] Current address: BioMedical Research Institute, Dept. of Biological Sciences, The University of Warwick, Gibbet Hill Road, Coventry, CV4 7AL, UK.

^{||} To whom correspondence should be addressed. Tel.: 44-151-794-53-51; Fax: 44-0-151-794-53-27; E-mail: a.tepikin@liv.ac.uk.

¹ TLC-S, tauro-lithocholic acid 3-sulfate; TCDC, taurochenodeoxycholic acid; TC, taurocholic acid; NMDG, *N*-methyl-D-glutamine; BAPTA, 1,2-bis(2-aminophenoxy)ethane-*N,N,N',N'*-tetraacetic acid; Ach, acetylcholine; DIDS, 4,4'-diisothiocyanostilbene-2,2'-disulfonic acid; 2 Na; $[\text{Ca}^{2+}]_i$, cytosolic Ca^{2+} concentration; $[\text{Na}^+]_i$, cytosolic Na^+ concentration.

clusters in solution. Cells were washed three times by centrifugation in standard Na-HEPES buffer. All experiments were performed at room temperature (22–25 °C), and cells were used within 3–4 h after isolation.

Solutions.—The standard extracellular solution (Na-HEPES buffer) used for cell preparation and for perfusion of cells during experiments contained 140 mM NaCl, 4.7 mM KCl, 1.13 mM $MgCl_2$, 1 mM $CaCl_2$, 10 mM D-glucose, 10 mM HEPES, pH 7.4. Sodium and potassium-free solutions contained 150 mM *N*-methyl-D-glucamine (NMDG⁺). In some experiments chloride was replaced by aspartate (Asp). During standard whole-cell recordings, the pipette solution contained 140 mM KCl, 1.5 mM $MgCl_2$, 2 mM MgATP, 10 mM HEPES, 0.1 mM EGTA, pH 7.2. In some experiments calcium was heavily buffered by the addition of 10 or 20 mM BAPTA and 2 mM $CaCl_2$. In K^+ -free pipette solution, K^+ was replaced by NMDG⁺; in Cl^- low pipette solution KCl was replaced by K-Asp. For perforated whole-cell recordings, the pipette solution contained 15 mM KCl, 100 mM K_2SO_4 , 10 mM NaCl, 7 mM $MgCl_2$, 10 mM HEPES, pH 7.2.

The cells were placed on a cover glass coated with poly-L-lysine (0.01%), and the cover glass was attached to an open perfusion chamber. Solutions were perfused using a gravity-fed system.

Patch Clamp Recording.—The whole cell configuration of the patch clamp technique was used to record currents from single pancreatic acinar cells. Patch pipettes were pulled from borosilicate glass capillaries (Harvard Apparatus, Edenbridge, Kent, UK) and fire-polished. The pipettes had a resistance of 3 to 5 megaohms when filled with an intracellular solution (containing 140 mM KCl). Whole cell currents were sampled at 10 KHz using an EPS-8 amplifier and Pulse software (HEKA, Lambrecht, Pfalz, Germany). In the standard protocol the membrane voltage was clamped at -30 mV, and voltage steps to $+10$ mV (test potential) were applied for 50-ms durations twice per second. The averaged currents at the holding potential and the test potential were calculated. For investigations of current-voltage relationships voltage ramps were applied from -50 to $+40$ mV (the slope was 300 or 400 mV/s). In current clamp experiments we utilized the perforated patch mode; in these experiments amphotericin B was added to the patch pipette solution at a concentration of 300 μ g ml^{-1} .

Measurements of Intracellular Sodium and Calcium Concentrations.—To monitor changes of sodium concentration in the cells we initially attempted to use the cell-permeable forms of the indicators Sodium Green (Sodium Green tetraacetate) and SBFI (SBFI, AM). The intracellular distribution of the indicators in these experiments was not uniform with patches of the indicators found in the perigranular area. With this loading we did not manage to obtain the expected responses to applications of monensin, gramicidin, and ouabain. Loading of the cell-impermeant Sodium Green, tetramethylammonium salt (40–50 μ M) through the patch pipette was much better; the distribution was uniform, and reasonable changes in fluorescence were observed. The fluorescence was monitored using the Zeiss LSM-510 confocal microscope. Sodium Green was excited by an argon laser line at 488 nm, and fluorescence was collected using a BP 505–550 emission filter. Sodium Green was calibrated in separate experiments conducted using a fluorimeter LS 50B (PerkinElmer Life Sciences). The wavelengths of excitation/emission light were similar to that used in confocal experiments. To increase the concentration of Na^+ in calibration solutions, NaCl was introduced into the solution in exchange for KCl. In our experiments the estimated dissociation constant of Sodium Green to Na^+ ($K_d = 23$ mM) was similar to that reported by Molecular Probes ($K_d = 21$ mM) for the indicator in K^+ -containing solution (www.probes.com/media/pis/mp06900.pdf).

We also attempted intracellular calibration of Sodium Green in the whole cell patch clamp configuration using gramicidin. In these experiments we recorded the expected changes of Sodium Green fluorescence but had difficulties in attaining a plateau of fluorescence for both sodium-free and high sodium solutions (possibly due to diffusion of Na^+ into the patch pipette). We, therefore, used the results of the cell-free calibration for the estimations of rates of sodium change. The intracellular calcium concentration was measured with Fluo-4 dye. 3 μ M Fluo-4 AM was loaded into the cell for 20–25 min at room temperature. The fluorescence of Fluo-4 was excited using the 488-nm laser line, and the emitted light was collected using a LP505 filter.

Chemicals.—Sodium Green tetramethylammonium salt and Fluo-4 AM were purchased from Molecular Probes, Inc. (Eugene, OR). 4,4'-diisothiocyanostilbene-2,2'-disulfonic acid, 2 Na (DIDS) was purchased from Calbiochem. TLC-S, taurochenodeoxycholic acid (TCDC), TC, sodium salt of bile acid mixture from ox bile (BA), *N*-methyl-D-glutamine (NMDG) and other chemicals were purchased from Sigma.

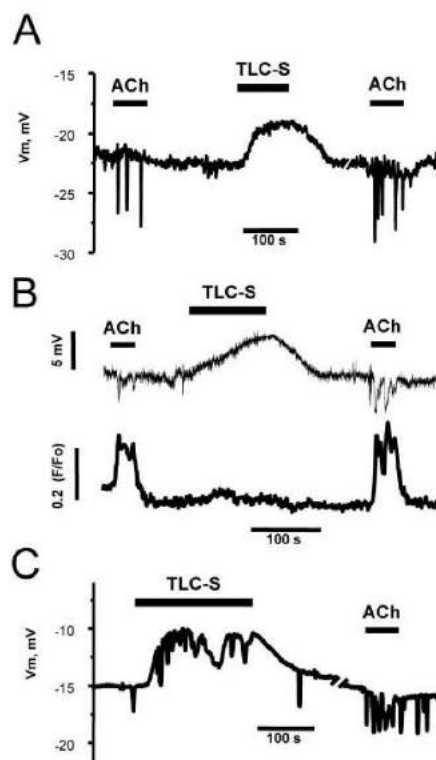


Fig. 1. Effect of the bile acid TLC-S and the neurotransmitter ACh on the membrane potential of single isolated acinar cells. The figure shows the results of perforated patch clamp experiments conducted in the current clamp mode. Agonists were applied by perfusion in the extracellular solution. **A**, application of 25 μ M TLC-S depolarizes the membrane of a single acinar cell, suggesting activation of bile-induced inward currents. ACh (50 nM) induces the opposite effect; that is, a hyperpolarization due to activation of Ca^{2+} -dependent Cl^- current. **B**, simultaneous measurements of membrane potential (upper trace) and normalized Fluo-4 fluorescence (F/F_0 , lower trace) in a single acinar cell. The depolarization induced by TLC-S (25 μ M) was accompanied by only a very small increase of Fluo-4 fluorescence. Transient hyperpolarizations triggered by ACh (50 nM) occur synchronously with substantial Ca^{2+} signals. **C**, a higher concentration of TLC-S (100 μ M) induces a response composed of transient hyperpolarizations (most probably due to calcium transients) superimposed on an elevated membrane voltage. ACh (50 nM) induced transient hyperpolarizations.

RESULTS

Voltage Changes Induced by TLC-S

Fig. 1 shows an example of perforated patch clamp experiments (current clamp mode) in which we observed voltage changes induced by the bile acid TLC-S and by the calcium-releasing secretagogue acetylcholine (ACh). Amphotericin B was used as a perforating agent; this preserves the normal composition of the cytosol of the intact cell, since only very small molecules and monovalent ions can be exchanged through amphotericin pores. The resting membrane potential recorded from isolated acinar cells in our experiments ranged from -16 to -30 mV ($n = 26$), values expected for single isolated cells, that are usually somewhat depolarized (26). The application of a low concentration of the bile acid (25 μ M) induced a slow depolarization, whereas ACh applications produced oscillatory hyperpolarizations (Fig. 1A). ACh-induced hyperpolarizations are consistent with activation of the

calcium-dependent chloride current (the reversal potential for Cl^- under the condition of these experiments was approximately -35mV). The TLC-S-induced depolarization implies activation of Na^+ or Ca^{2+} -conducting channels. In experiments with a low concentration of TLC-S ($25\text{ }\mu\text{M}$) a slow depolarization was observed in 22 of 24 cells tested. The amplitude of TLC-S-induced depolarization ranged from 4 to 23 mV and tended to be higher in cells with a more negative resting membrane potential. In one out of these 22 cells the slow depolarization was preceded by an initial fast hyperpolarization (not shown), probably reflecting a cytosolic calcium concentration rise that could be observed sometimes even at this low concentration of the bile acid (10).

An example of the combined measurements of cytosolic Ca^{2+} concentration and membrane potential in the perforated patch mode is shown in Fig. 1B (representative of four experiments). The voltage change induced by the bile acid was clearly different from that triggered by the calcium-releasing secretagogue. Although ACh produced clearly-resolved calcium responses and hyperpolarizations, a low dose of TLC-S most frequently triggered depolarization and only a very small (if any) calcium response.

We previously reported that higher doses of TLC-S induce calcium signals in the majority of pancreatic acinar cells (10). In a perforated patch clamp experiment, application of $100\text{ }\mu\text{M}$ TLC-S triggered a complex response in which fast hyperpolarizing transients were superimposed on a slow depolarization (Fig. 1C, $n = 4$).

We hypothesized that the bile-induced depolarization reflects calcium-independent activation of cationic, most probably Na^+ -permeable channels. One way to verify this hypothesis was to measure sodium changes induced by TLC-S.

Changes of $[\text{Na}^+]_i$ Induced by TLC-S— $[\text{Na}^+]_i$ was measured using the indicator Sodium Green. We loaded the indicator into the cell through a patch pipette and conducted experiments in the whole cell mode, since loading with a cell-permeant form of this probe was ineffective (see "Experimental Procedures"). In experiments where cytosolic calcium was not buffered with BAPTA, we were able to record both current and sodium changes induced by TLC-S and ACh (Fig. 2, A and B). In these experiments we used equal Cl^- concentrations in the patch pipette and in the extracellular solution; the chloride equilibrium potential should, therefore, be close to 0 mV. The calcium oscillations under this condition are reflected by transient activations of an inward chloride current (currents were recorded at -30mV).

In the experiment shown in Fig. 2A, two components of the bile-induced sodium increase can be seen. The addition of $50\text{ }\mu\text{M}$ TLC-S induced a slowly developing inward current accompanied by a slow sodium concentration increase. Increasing the bile acid concentration to $100\text{ }\mu\text{M}$ produced oscillations of the inward current (which reflects calcium oscillations) and stepwise increases of $[\text{Na}^+]_i$. Sodium changes induced by ACh seem to follow calcium transients; each spike in $[\text{Ca}^{2+}]_i$ is accompanied by a stepwise increase in sodium (Fig. 2B).

It is interesting to note that during the ACh-induced oscillations and after removal of the agonist, the recovery of $[\text{Na}^+]_i$ was much slower than the recovery of the calcium-dependent current. This provides an opportunity for the summation of sodium responses (Fig. 2B) and could result in sodium overload (if the $[\text{Ca}^{2+}]_i$ spike frequency is too high).

The kinetics of the current transients and $[\text{Na}^+]_i$ changes strongly suggest that the sodium responses induced by ACh are calcium-dependent. The two components of the TLC-S induced $[\text{Na}^+]_i$ changes could be interpreted as calcium-independent (the slow rise induced by a low dose of bile) and

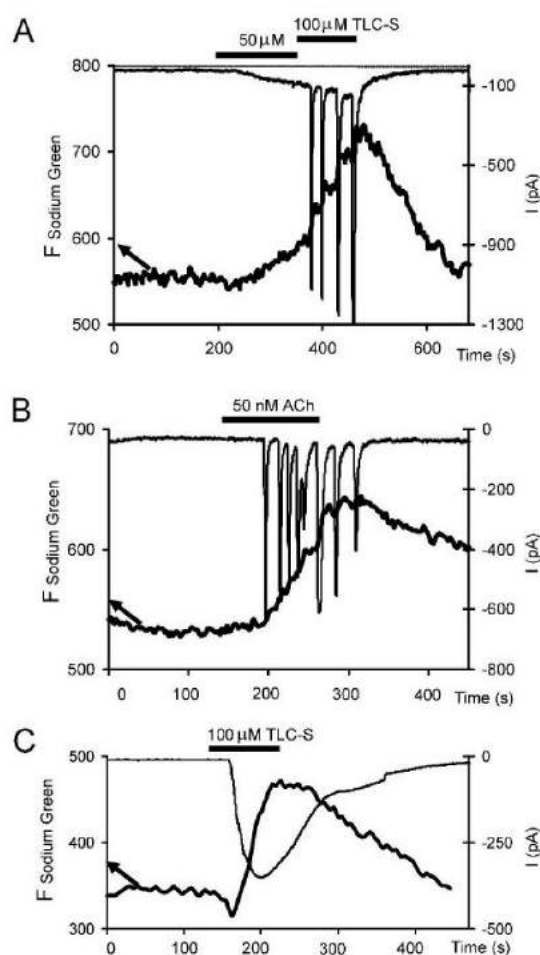


FIG. 2. Simultaneous measurements of changes in $[\text{Na}^+]_i$ and membrane currents stimulated by the bile acid TLC-S and by ACh. Ionic currents were recorded using the whole cell patch clamp configuration at a holding potential of -30mV . Sodium Green was loaded into the cells via the patch pipette ($40\text{ }\mu\text{M}$ in the experiments shown in A and B and $50\text{ }\mu\text{M}$ in the experiment shown in C). A, TLC-S ($50\text{ }\mu\text{M}$) activated an inward current (upper trace) accompanied by an elevation of the Sodium Green fluorescence (lower trace, the arrow points to the corresponding fluorescence intensity axis). Subsequent application of $100\text{ }\mu\text{M}$ TLC-S induced transients of Ca^{2+} -activated Cl^- current, superimposed on the plateau of inward current; the lower trace shows stepwise increases of sodium concentrations during the inward current transients. B, recording of Ca^{2+} -activated Cl^- current (upper trace) and changes of Sodium Green fluorescence (lower trace) induced by application of 50 nM ACh. C, in this experiment the patch pipette contained 20 mM BAPTA. The upper trace shows the development of the calcium-independent inward current upon application of $100\text{ }\mu\text{M}$ TLC-S. The lower trace shows simultaneous changes of the Sodium Green fluorescence.

calcium-dependent (stepwise increases of $[\text{Na}^+]_i$ during calcium transients). To reveal the calcium-independent component of the bile-induced sodium changes, we conducted an experiment in which $[\text{Ca}^{2+}]_i$ was effectively buffered by a calcium chelator, BAPTA, added to the patch pipette solution (and used at a very high concentration, 10 or 20 mM). In this condition application of TLC-S induce an increase in Sodium Green fluorescence accompanied by an inward current in

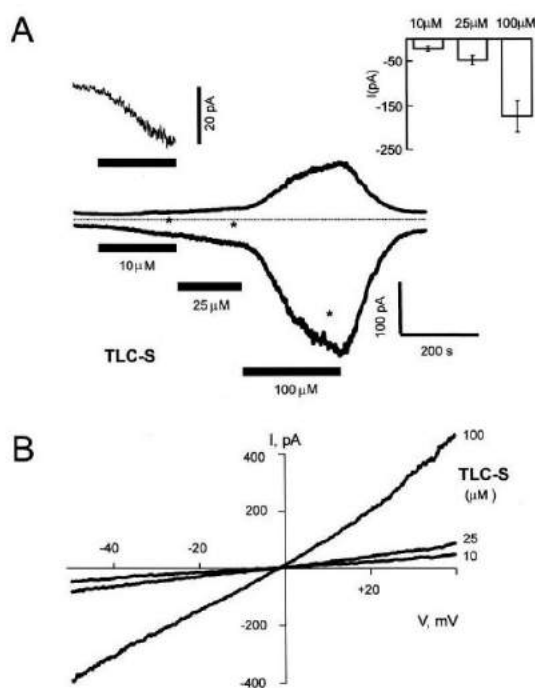


FIG. 3. Bile acid (TLC-S) induces calcium-independent cationic currents in isolated acinar cells. To eliminate the activation of Ca^{2+} -dependent channels patch clamp pipettes were filled with a solution containing 20 mM BAPTA. **A**, this part shows currents induced by increasing concentrations of TLC-S. The experiment was performed using the whole-cell patch clamp configuration in voltage clamp condition. Inward current (lower trace) was recorded at -30 mV, and outward current (upper trace) was recorded at $+10$ mV. The left inset shows the initial part of the inward current on an expanded current scale (the time scale is the same as in the main figure). The right inset shows averaged amplitudes (\pm S.E.) of currents (recorded at -30 mV, $n = 14$) induced by different concentrations of TLC-S (shown on the graph) using a voltage ramp protocol (0.4 V/s) from -50 mV to $+40$ mV. The time points of the voltage ramp experiments are indicated by asterisks in panel **A** of this figure.

cells held at -30 mV (Fig. 2C). These experiments ($n = 5$) strongly suggest the existence of calcium-independent sodium influx and a calcium-independent cationic current. The properties of this TLC-S-induced calcium-independent current were further investigated.

TLC-S-induced Currents in BAPTA-buffered Cells

Na^+/K^+ Current—In the experiments described in this section we used high concentrations of the calcium chelator BAPTA (10 or 20 mM) in the patch pipette (similarly to the experiments described above and shown in Fig. 2C) to prevent activation of calcium-dependent currents. Even a very low concentration of TLC-S (10 μM) induced a measurable current (22 ± 5 pA, $n = 14$ recorded at -30 mV, see Fig. 3 and the left inset of **A**). Subsequent increases of the bile concentration to 25 μM and then to 100 μM produced further slowly developing increases of currents (inward at -30 mV and outward at $+10$ mV). The averaged amplitude of currents induced by different concentrations of TLC-S (recorded at -30 mV) are shown in the right inset of Fig. 3A. Removal of the bile acid resulted in recovery of the currents to the prestimulated values (Fig. 3A). The recordings at -30 and $+10$ mV were interrupted by ramp

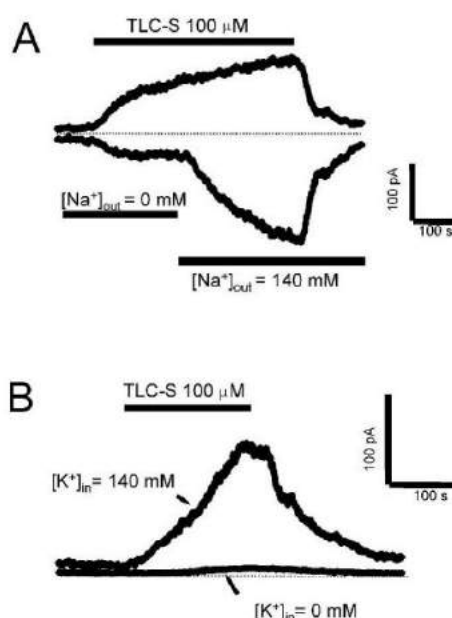


FIG. 4. Effect of substitution of small monovalent cations with NMDG^+ on bile-induced transmembrane currents. The Patch pipette solution contained 10 mM BAPTA to eliminate calcium-dependant currents. **A**, in sodium-free (NMDG^+ containing) solution, the bile acid TLC-S induced only a small inward current, probably mediated by NMDG^+ (lower trace). Substitution of bath NMDGCl with NaCl resulted in a strong rise of the inward current (lower trace) recorded at -30 mV but had only a small effect on the outward current measured at $+10$ mV (upper trace). **B**, comparison of TLC-S-induced outward currents (measured at $+10$ mV) in potassium-containing and potassium-free intracellular solution. The current traces were recorded in different cells. The upper trace shows the current recorded using standard patch pipette solution containing 140 mM K^+ . The lower trace depicts the outward current when K^+ in the patch pipette solution was replaced by NMDG^+ ; only a very small current can be recorded in these conditions.

protocols at the indicated time points. The reversal potential for bile-induced currents was close to 0 mV (Fig. 3B). The current-voltage relationship was largely linear for the range of voltages used in our experiments. The results shown in Fig. 3 suggest activation or formation of non-selective cationic channels. To verify this hypothesis we carried out substitutions of Na^+ with NMDG^+ in the extracellular solution (Fig. 4A) and K^+ with NMDG^+ in the intracellular (patch pipette) solution (Fig. 4B). In the NMDG^+ -containing extracellular solution, application of TLC-S produced only a small inward current (most probably carried by NMDG^+), and the amplitude of the inward current increased drastically when NMDG^+ was replaced by Na^+ (Fig. 4A, $n = 15$), suggesting that this current is preferentially carried by Na^+ . Substitution of K^+ by NMDG^+ in the intracellular (pipette) solution largely abolished the outward current recorded at $+10$ mV (Fig. 4B, $n = 25$), indicating that the outward current is mainly carried by K^+ .

Ca^{2+} and Cl^- Currents—The possible contribution of Ca^{2+} to the TLC-S-induced inward current was examined by comparing the inward currents (produced in NMDG^+ -based solution) in the presence and absence of calcium. In these experiments we were able to resolve a small additional inward current (Fig. 5A) when an extracellular solution with a very high calcium concentration (40 mM) was introduced ($n = 7$). In these experiments we used a very high concentration of BAPTA in the patch pipette (20 mM) to prevent any intracellular $[\text{Ca}^{2+}]$ rise

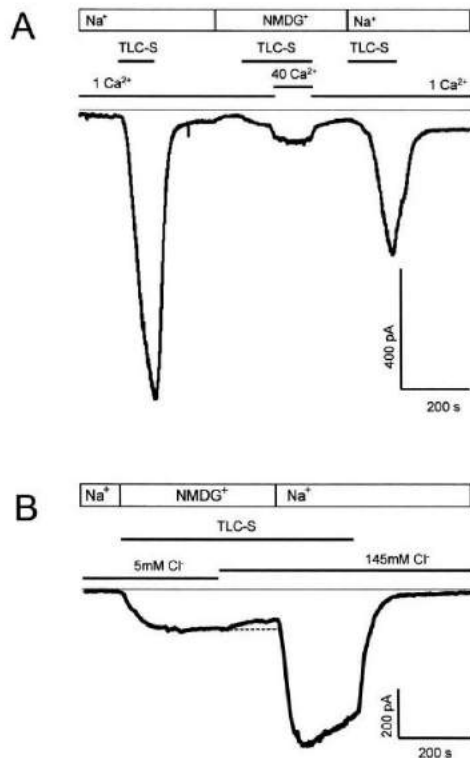


FIG. 5. Contribution of Ca^{2+} and Cl^- to the TLC-S-induced current. A, Ca^{2+} component of TLC-S-induced current. The intrapipette solution was supplemented with 20 mM BAPTA to prevent activation of Ca^{2+} -dependent currents. The bars in the upper part of the figure show periods of TLC-S (100 μM) applications, $\text{Na}^+/\text{NMDG}^+$ substitution, and changes of Ca^{2+} concentration in extracellular solution. In this experiment K^+ was replaced by NMDG⁺ in the patch pipette solution. The bar labeled NMDG indicates the period of time when all Na^+ in the extracellular solution was substituted by NMDG⁺. The figure shows the current recorded at -30 mV. The amplitude of the TLC-S-induced inward current was compared in sodium-containing extracellular solution, sodium-free extracellular solution (Na^+ substituted with NMDG⁺, $[\text{Ca}^{2+}]_o = 1 \text{ mM}$), and sodium-free extracellular solution with a high concentration of Ca^{2+} (40 mM). B, Cl^- component of total current induced by application of the bile acid TLC-S. The intrapipette solution was supplemented with 10 mM BAPTA to prevent activation of Ca^{2+} -dependent currents. A change of $[\text{Cl}^-]_o$ from 5 to 145 mM produced small changes of ionic current, recorded in Na^+ -free (NMDG⁺-containing) extracellular solution. The dashed line shows the extension of the current plateau level, attained before the change in chloride concentration. At the end of the experiment the normal sodium concentration (140 mM) in the extracellular solution was restored in the continued presence of TLC-S. This resulted in a large increase of inward current.

and activation of calcium-dependent currents. We were not able to resolve changes of the current when the extracellular calcium concentration was 10 mM ($n = 6$, not shown). TLC-S also induced a small Cl^- current. Changes of Cl^- concentration from 5 to 145 mM resulted in only a small change (Fig. 5B, representative of 14 cells) of the inward current recorded at -30 mV.

The notion that Cl^- makes only a minor contribution to the bile-induced current was challenged when we found that DIDS (usually considered an inhibitor of Cl^- currents) had a very strong inhibitory effect on both inward and outward currents triggered by TLC-S (Fig. 6A). However, TLC-S produced sub-

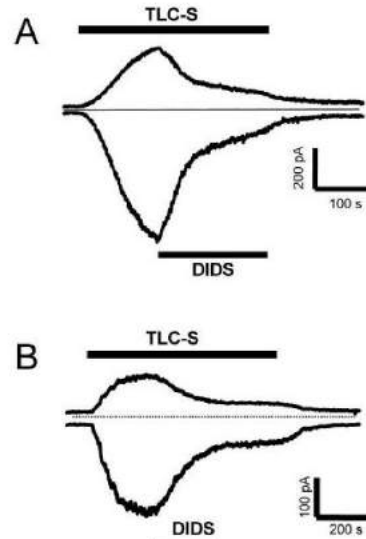


FIG. 6. Inhibition of TLC-S induced current by DIDS. A, DIDS effect in Cl^- -containing solutions. A single cell was patched with a pipette containing KCl and 10 mM BAPTA. 1 mM DIDS inhibited both inward and outward currents stimulated by 100 μM TLC-S. B, DIDS effect in low Cl^- solution. A single cell was patched with a pipette containing a low Cl^- concentration (KCl in the pipette was replaced by K-Asp and supplemented with 10 mM BAPTA). The bile acid TLC-S (100 μM) was applied in a low Cl^- extracellular solution (NaCl was substituted by Na-Asp). 200 μM DIDS inhibits inward and outward currents.

stantial currents in conditions when almost all Cl^- in the intracellular and extracellular solutions was replaced by aspartate, and DIDS strongly inhibited this Cl^- -independent bile-induced cationic current (Fig. 6B).

Calcium-independent Currents Induced by Other Bile Acids

Like TLC-S, other bile acids (TCDC and TC) induced calcium-independent currents (recorded using 10 mM BAPTA in patch pipette), although at higher concentrations than TLC-S. Fig. 7A shows currents induced by 100 μM and 250 μM TCDC. When added at a concentration of 100 μM , TCDC induced very slowly developing calcium-independent currents, and a subsequent increase of the bile acid concentration to 250 μM resulted in stronger activation of the currents ($n = 4$). TC applied at relatively high concentrations (0.5 mM followed by 1 mM) also induced calcium-independent currents (Fig. 7B, $n = 5$).

Finally, we tested the ability of bile (mixture of bile acids extracted from crude ox bile) to induce calcium-independent currents. In these experiments we sequentially tested concentrations of 0.1, 0.25, and 0.5 mg/ml. We found that bile at 0.1 mg/ml did not produce resolvable activation of currents, 0.25 mg/ml induced very small and slowly developing responses, and a higher concentration (0.5 mg/ml) induced substantial calcium-independent currents (Fig. 7C, $n = 4$).

DISCUSSION

We report that bile acids induce Ca^{2+} -independent currents mainly carried by Na^+ and K^+ . The contributions of Cl^- and Ca^{2+} to these currents are small. The activation of cationic current explains the depolarization of the cells recorded in current clamp experiments. The inward sodium current creates Na^+ influx and increase $[\text{Na}^+]_i$, resolved in our experiments with the fluorescent indicator Sodium Green. This should also

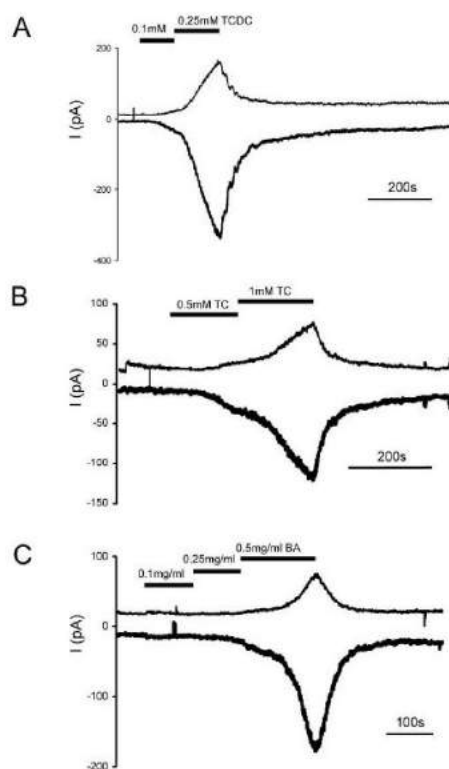


FIG. 7. Currents induced by TCDC, TC, and bile. The current were recorded at +10 mV and -30 mV. The intrapipette solution contained 10 mM BAPTA. A, inward and outward currents stimulated by application of 0.1 or 0.25 mM TCDC. B, currents stimulated by applications of 0.5 and 1 mM TC. C, currents induced by sequential application of 0.1, 0.25, and 0.5 mg/ml BA, bile acid mixture from ox bile.

be accompanied by a loss of K^+ from the cytosol of the cell.

In a study on the T84 colonic cell line, Devor *et al.* (11) characterized the electrophysiological effects of taurodeoxycholate and taurocholic acid. The authors reported activation of K^+ and Cl^- channels. These channels were Ca^{2+} -dependent; incubation of the cells with BAPTA-AM eliminated the currents through these channels (11). The pathway leading to activation of Cl^- and K^+ currents involved taurodeoxycholic acid-induced accumulation of inositol 1,4,5-trisphosphate and calcium release from internal stores. Interestingly, this study also described a taurodeoxycholic acid-induced nonselective cation current that could be blocked by replacing Na^+ in the extracellular solution with NMDG $^+$. There are, however, some differences between the nonselective cationic current characterized by Devor *et al.* (11) and the one found in our study. The nonselective current described by Devor *et al.* (11) in T84 cells was mediated by infrequent openings of very high conductance channels (channel openings were visible even in whole-cell experiments). This is clearly different from the current found in pancreatic acinar cells. There were other differences in kinetics and relative amplitude of bile-mediated cationic currents in T84 and pancreatic acinar cells (*e.g.* development of the cationic current was much slower in acinar cells, whereas the amplitude was larger). An important finding in the study of Devor *et al.* (11) that is in complete agreement with our work (Ref. 10 and this study) is that bile acids do not induce a leak of

fluorescent indicators from the cytosol of the cells. Good retention of the small molecular weight fluorescent indicator in the cytosol indicates that the detergent effect of bile acids is minimal.

It is possible that activation of Ca^{2+} -independent cationic currents also occur in other cell types exposed to elevated concentrations of bile in pathological conditions. We conducted a preliminary investigation of the effect of TLC-S on voltage-clamped and BAPTA-loaded rat hepatocytes. We resolved a calcium-independent cationic current induced by application of 100 μ M of TLC-S but had difficulties reversing this current by the removal of TLC-S ($n = 4$, not shown). The effect of TLC-S on hepatocytes and other cell types that could be exposed to this toxic bile acid deserves a separate detailed investigation.

Two types of bile acid transporters were recently described in pancreatic acinar cells; they are a Na^+ -dependent co-transporter and a HCO_3^- -dependent exchanger. It is interesting to note that the outward potassium current in BAPTA-buffered cells develops effectively in a bicarbonate-free solution and in the complete absence of extracellular Na^+ . This suggests that Na^+ -dependent and HCO_3^- -dependent transports are not essential for activation of nonselective currents by TLC-S.

In hepatocytes the amplitude of the current generated by the Na^+ /bile exchanger is only a few pA at a physiological membrane potential (24). This is much smaller than the amplitude of currents induced by TLC-S and other bile acids in pancreatic acinar cells. It is possible, therefore, that the small current of the exchanger is masked in our experiments by the much larger bile-induced cationic current. Our experiments also represent an important warning regarding measurements of the electrophysiological effects of the Na^+ /bile exchanger, since even small activation of nonselective cationic channels by bile acids could drastically affect such measurements.

The development of substantial non-selective cationic currents should result in changes of ionic concentration and would inevitably put additional stress on the energy homeostasis of the cells. The bile-induced Na^+ flux is substantial. Our estimations from experiments with Sodium Green show that the calcium-independent sodium influx results in an increase of $[Na^+]_i$ by a few mM/min (*e.g.* ~ 2 mM/min for the experiment shown in Fig. 2A and 8 mM/min for the one shown in Fig. 2C). Even more drastic sodium changes are observed during calcium oscillations. We found that during a single calcium transient $[Na^+]_i$ can increase by more than 5 mM. Both the calcium-dependent and the calcium-independent sodium influx induced by bile acids should put a very considerable pressure on ATP turnover in the acinar cell. A decrease of the transmembrane sodium gradient could also have an adverse effect on sodium dependent transporters responsible for delivery of amino acids into the cell (27) or for regulation of ionic concentrations (28–30). It is also interesting to note that for calcium-dependent sodium responses, the recovery of sodium transients is much slower than the recovery of the underlying calcium transients. This creates the possibility for summation of sodium transients and formation of a sustained elevated sodium level during calcium oscillations. This phenomenon is, however, beyond the scope of this paper and deserves a separate investigation. Another important effect of bile acids will be on fluid secretion. Bile-induced depolarization of the plasma membrane of pancreatic acinar cells, due to increased Na^+ permeability, will inevitably decrease the driving force for Cl^- efflux across the apical membrane into the luminal space. The decreased Cl^- exit (and consequently water transport) into the luminal space will suppress the initial stage of transport of secreted enzymes through the pancreatic ducts. Retention of zymogens in the vicinity of the acinar cells could increase the probability of inap-

appropriate activation of digestive enzymes within the pancreas.

It is important to emphasize that TLC-S induces activation of Ca^{2+} -independent currents even when applied at a very low concentration; 10 μM concentrations of this bile acid are sufficient to produce measurable changes in current in the majority of cells. This concentration is almost 2 orders of magnitude smaller than that found in bile (31, 32). Therefore, even minor reflux of this toxic bile component into the pancreas will most probably have deleterious effects on pancreatic functions. The low level of TLC-S, which has been found in this study to activate the Ca^{2+} -independent current, is close to the concentrations of sulfated lithocholic acid conjugates detected in serum in different pathological conditions (33, 34). The concentration of TLC-S necessary to induce cationic current is even smaller than that required to trigger cytosolic calcium responses (in our previous work we found that a higher concentration of TLC-S (25 μM) produced calcium responses in only 11% of the cells tested) and similar to the threshold concentration that has been reported to induce transient mitochondrial depolarization (35). Therefore, activation of non-selective calcium-independent conductances could be one of the primary effects of bile on pancreatic acinar cells and could conceivably occur not only due to pancreatic reflux of the concentrated bile acid but also due to the action of bile accumulated at a much lower concentration in serum. The potency of bile acids in terms of their ability to induce non-selective current in BAPTA-loaded cells, decreased with increasing number of hydroxyl groups and a decrease of hydrophobicity. TLC-S was more effective than TCDC, which in turn was more potent than TC. This suggests that the mechanism of activation of the non-selective currents requires lipid partitioning of bile acids. However, trihydroxy (such as TC) and dihydroxy (such as TCDC) bile acids are present in bile at higher concentrations than monohydroxy bile acids (e.g. TLC-S) and could, therefore, make a substantial contribution to the total non-selective currents and membrane depolarizations in the case of interstitial leakage or bile reflux.

Acknowledgments—The technical help of Mark Houghton is gratefully acknowledged. We also thank Nicholas Dolman, David Criddle, and Robert Sutton for useful suggestions and fruitful discussions.

REFERENCES

- Kim, J. Y., Kim, K. H., Lee, J. A., Namkung, W., Sun, A. Q., Ananthanarayanan, M., Suchy, F. J., Shin, D. M., Muallem, S., and Lee, M. G. (2002) *Gastroenterology* **122**, 1941–1953
- Opie, E. L. (1901) *Johns Hopkins Hosp. Bull.* **12**, 182–188
- Blackstone, M. (2003) *Gastroenterology* **124**, 863–865
- Kim, J. Y., Kim, K. H., Lee, M., Shin, D. M., Muallem, S., and Suchy, F. J. (2003) *Gastroenterology* **124**, 864–865
- Lerch, M. M., Saluja, A. K., Runzi, M., Dawra, R., Saluja, M., and Steer, M. L. (1993) *Gastroenterology* **104**, 853–861
- Moody, F. G., Senninger, N., and Runkel, N. (1993) *Gastroenterology* **104**, 927–931
- Armstrong, C. P., Taylor, T. V., and Torrence, H. B. (1987) *Dig. Dis. Sci.* **32**, 861–871
- Farmer, R. C., Tweedie, J., Maslin, S., Reber, H. A., Adler, G., and Kern, H. (1984) *Dig. Dis. Sci.* **29**, 740–751
- Reber, H. A., and Mosley, J. G. (1980) *Br. J. Surg.* **67**, 59–62
- Voronina, S., Longbottom, R., Sutton, R., Petersen, O. H., and Tepikin, A. (2002) *J. Physiol.* **540**, 49–55
- Devor, D. C., Sekar, M. C., Frizzell, R. A., and Duffey, M. E. (1993) *J. Clin. Invest.* **92**, 2173–2181
- Mauricio, A. C., and Ferreira, K. T. (1999) *Exp. Physiol.* **84**, 489–499
- Mauricio, A. C., Slawik, M., Heitzmann, D., von Hahn, T., Warth, R., Bleich, M., and Greger, R. (2000) *Pflügers Arch.* **439**, 532–540
- Kidd, J. F., and Thorn, P. (2001) *Pflügers Arch.* **441**, 489–497
- Matthews, E. K., and Petersen, O. H. (1973) *J. Physiol. (Lond.)* **231**, 283–295
- Petersen, O. H. (1973) *Proc. R. Soc. Lond. B Biol. Sci.* **184**, 115–119
- Petersen, O. H. (1992) *J. Physiol. (Lond.)* **448**, 1–51
- Thorn, P., and Petersen, O. H. (1993) *EXS (Basel)* **66**, 185–200
- Maruyama, Y., and Petersen, O. H. (1982) *Nature* **300**, 61–63
- Park, M. K., Lomax, R. B., Tepikin, A. V., and Petersen, O. H. (2001) *Proc. Natl. Acad. Sci. U. S. A.* **98**, 10948–10953
- Giovannucci, D. R., Bruce, J. I., Straub, S. V., Arreola, J., Sneyd, J., Shuttleworth, T. J., and Yule, D. I. (2002) *J. Physiol.* **540**, 469–484
- Iwatsuki, N., and Petersen, O. H. (1977) *Nature* **268**, 147–149
- Kasai, H., and Augustine, G. J. (1990) *Nature* **348**, 735–738
- Lidofsky, S. D., Fitz, J. G., Weissiger, R. A., and Scharshmidt, B. F. (1993) *Am. J. Physiol.* **264**, G478–G485
- Weinman, S. A., Carruth, M. W., and Dawson, P. A. (1998) *J. Biol. Chem.* **273**, 34691–34695
- Park, M. K., Lee, M., and Petersen, O. H. (2004) *Cell Calcium* **35**, 367–379
- Iwatsuki, N., and Petersen, O. H. (1980) *Pflügers Arch. Eur. J. Physiol.* **386**, 153–159
- Brown, D. A., Melvin, J. E., and Yule, D. I. (2003) *Am. J. Physiol. Gastrointest. Liver Physiol.* **285**, 804–812
- Muallem, S., and Loessberg, P. A. (1990) *J. Biol. Chem.* **265**, 12806–12812
- Muallem, S., and Loessberg, P. A. (1990) *J. Biol. Chem.* **265**, 12813–12819
- Cowen, A. E., Korman, M. G., Hofmann, A. F., Cass, O. W., and Coffin, S. B. (1975) *Gastroenterology* **69**, 67–76
- Hofmann, A. F. (1976) *Adv. Intern. Med.* **21**, 501–534
- Cowen, A. E., Korman, M. G., Hofmann, A. F., Turrentine, J., and Carter, J. A. (1977) *J. Lipid Res.* **18**, 698–703
- Kuipers, F., Bijleveld, C. M., Kneepkens, C. M., van Zanten, A., Fernandes, J., and Vonk, R. J. (1985) *Scand. J. Gastroenterol.* **20**, 1255–1261
- Voronina, S. G., Barrow, S. L., Gerasimenko, O. V., Petersen, O. H., and Tepikin, A. V. (2004) *J. Biol. Chem.* **279**, 27327–27338


РОЗДІЛ 4

КАЛЬЦІЄВА СИГНАЛІЗАЦІЯ В РІЗНИХ ТИПАХ КЛІТИН

4.1. Кальцієва сигналізація в клітинах екзокринної частини підшлункової залози

J Physiol 596.14 (2018) pp 2663–2678

Calcium signalling in the acinar environment of the exocrine pancreas: physiology and pathophysiology

Oleksiy Gryshchenko^{1,2}, Julia V. Gerasimenko¹, Shuang Peng^{1,3}, Oleg V. Gerasimenko¹ and Ole H. Petersen^{1,4} ¹Cardiff School of Biosciences, Cardiff University, Cardiff CF10 3AX, UK²Bogomoletz Institute of Physiology, Kyiv 01024, Ukraine³Department of Physiology, Medical College, Jinan University, Guangzhou 510632, China⁴Systems Immunity Research Institute, Cardiff University, Cardiff, CF14 4XN, UK

Edited by: Peking Fong & Kim Barrett

Key points

- Ca^{2+} signalling in different cell types in exocrine pancreatic lobules was monitored simultaneously and signalling responses to various stimuli were directly compared.
- Ca^{2+} signals evoked by K^{+} -induced depolarization were recorded from pancreatic nerve cells. Nerve cell stimulation evoked Ca^{2+} signals in acinar but not in stellate cells.
- Stellate cells are not electrically excitable as they, like acinar cells, did not generate Ca^{2+} signals in response to membrane depolarization.
- The responsiveness of the stellate cells to bradykinin was markedly reduced in experimental alcohol-related acute pancreatitis, but they became sensitive to stimulation with trypsin.
- Our results provide fresh evidence for an important role of stellate cells in acute pancreatitis. They seem to be a critical element in a vicious circle promoting necrotic acinar cell death. Initial trypsin release from a few dying acinar cells generates Ca^{2+} signals in the stellate cells, which then in turn damage more acinar cells causing further trypsin liberation.

Abstract Physiological Ca^{2+} signals in pancreatic acinar cells control fluid and enzyme secretion, whereas excessive Ca^{2+} signals induced by pathological agents induce destructive processes leading to acute pancreatitis. Ca^{2+} signals in the peri-acinar stellate cells may also play a role in the development of acute pancreatitis. In this study, we explored Ca^{2+} signalling in the different cell types in the acinar environment of the pancreatic tissue. We have, for the first time, recorded depolarization-evoked Ca^{2+} signals in pancreatic nerves and shown that whereas acinar cells receive a functional cholinergic innervation, there is no evidence for functional innervation of the

Oleksiy Gryshchenko received his PhD in biophysics in the laboratory of the late Professor Platon Kostyuk in Kyiv, working on voltage-gated ion channel function in development. He is currently an Associate Professor in the Department of Molecular Biophysics at the Bogomoletz Institute of Physiology, Kyiv, Ukraine. At present he investigates Ca^{2+} handling in the pancreatic exocrine tissue in collaboration with Professor Ole Petersen FRS and Drs Oleg and Julia Gerasimenko at Cardiff University, UK. Julia V. Gerasimenko is a Senior Lecturer at Cardiff School of Biosciences, Cardiff University, UK. She completed her PhD at the Bogomoletz Institute of Physiology in 1996. Her work has primarily been directed towards elucidating the molecular mechanisms initiating the enigmatic disease acute pancreatitis (~20 000 admissions to hospital and ~1000 deaths per year in the UK alone). There is currently no treatment for this disease, but Julia's work has opened up new possibilities for rational treatment. She has published 46 research papers on the disease mechanism in competitive peer-reviewed journals, including *Cell*, *PNAS*, *Journal of Physiology*, *Journal of Cell Science* and *Current Biology*. Julia is a Member of Faculty of 1000 (Gastro-intestinal Physiology), The Physiological Society (UK), British Society for Cell Biology and the European Calcium Society.



O. Gryshchenko and J.V. Gerasimenko contributed equally to this work

stellate cells. The stellate, like the acinar, cells are not electrically excitable as they do not generate Ca^{2+} signals in response to membrane depolarization. The principal agent evoking Ca^{2+} signals in the stellate cells is bradykinin, but in experimental alcohol-related acute pancreatitis, these cells become much less responsive to bradykinin and then acquire sensitivity to trypsin. Our new findings have implications for our understanding of the development of acute pancreatitis and we propose a scheme in which Ca^{2+} signals in stellate cells provide an amplification loop promoting acinar cell death. Initial release of the proteases kallikrein and trypsin from dying acinar cells can, via bradykinin generation and protease-activated receptors, induce Ca^{2+} signals in stellate cells which can then, possibly via nitric oxide generation, damage more acinar cells and thereby cause additional release of proteases, generating a vicious circle.

(Received 12 December 2017; accepted after revision 25 January 2018; first published online 9 February 2018)

Corresponding author O. H. Petersen: School of Biosciences, Sir Martin Evans Building, Museum Avenue, Cardiff University, Cardiff CF10 3 AX, Wales, UK. Email: PetersenOH@cardiff.ac.uk

Introduction

Ca^{2+} signalling studies on isolated pancreatic acinar cells (PACs) or small acinar cell clusters have led to a detailed understanding of the mechanisms underlying the primary intracellular Ca^{2+} release elicited by physiological and pathological agents as well as the subsequent opening of store-operated Ca^{2+} channels in the plasma membrane that accounts for the secondary Ca^{2+} entry from the extracellular solution (Petersen & Tepikin, 2008; Petersen *et al.* 2017). Physiological, short-lasting and repetitive local Ca^{2+} signals control acinar fluid and enzyme secretion (Petersen, 1992; Petersen & Tepikin, 2008), whereas sustained global elevations of the cytosolic Ca^{2+} concentration ($[\text{Ca}^{2+}]_i$), elicited by pathological agents, play a key role in the development of the acinar cell damage and death leading to acute pancreatitis (AP) (Gerasimenko *et al.* 2014). Most of the work on PAC Ca^{2+} signalling has been carried out on isolated mouse cells, but the key results have been confirmed in studies on isolated human PACs (Murphy *et al.* 2008; Liang *et al.* 2017). A limited amount of work on acinar cell Ca^{2+} signalling in pancreatic segments has confirmed that the basic character of such signals, as established in isolated cell studies, is also valid in the intact pancreas (Ashby *et al.* 2003).

PACs dominate the exocrine pancreatic tissue (Bolender, 1974), but there are other important cell types. In addition to the acinar fluid secretion, there is a ductal secretion process whereby a HCO_3^- -rich fluid is produced, which is important for neutralizing in the gut the acid secretion from the stomach (Hegyi & Petersen, 2013). Ca^{2+} signals in the pancreatic duct cells play an important role in the control of HCO_3^- secretion, and excessive Ca^{2+} signal generation, as in the acinar cells, causes Ca^{2+} overload and toxicity (Maleth & Hegyi, 2014).

More recently, Ca^{2+} signalling and ion channels have been studied in pancreatic stellate cells (PSCs) (Fels *et al.* 2016; Ferdek *et al.* 2016; Gryshchenko *et al.* 2016; Nielsen *et al.* 2017; Storck *et al.* 2017). The role of these cells in

normal physiology is unclear, but they have long been suspected of contributing to the fibrosis occurring in chronic pancreatitis as well as pancreatic cancer (Ferdek & Jakubowska, 2017; Pang *et al.* 2017). In the normal pancreas, PSCs can be observed as thin elongated structures situated at the acinar periphery, very close to the basal surface of the PACs (Gryshchenko *et al.* 2016). In spite of the close proximity of PSCs and PACs, they are not directly connected. Thus Ca^{2+} signals specifically generated in PACs are not transmitted to neighbouring PSCs and vice versa (Gryshchenko *et al.* 2016). The principal physiological agents eliciting Ca^{2+} signals in PACs are acetylcholine (ACh) and cholecystokinin (CCK), but they have no effect on PSCs (Gryshchenko *et al.* 2016). Bradykinin (BK) is the principal agent evoking Ca^{2+} signals in normal PSCs (Gryshchenko *et al.* 2016), but this peptide has no direct effect on PACs (Gryshchenko *et al.* 2016). Furthermore, PACs and PSCs possess different bile acid transporters. Whereas taurocholate and cholate elicit Ca^{2+} signals in PSCs, because they are taken up into these cells by Na^+ -dependent transporters, these bile acids hardly evoke any Ca^{2+} signals in the PACs. On the other hand, the bile acid tauro lithocholic acid sulphate (TLC-S) evokes clear Ca^{2+} signals in PACs, but has no effect on PSCs (Ferdek *et al.* 2016).

In spite of the absence of evidence for any direct connection between neighbouring PACs and PSCs, there is indirect evidence showing that Ca^{2+} signal generation in PSCs can have profound effects on PACs. Thus the level of PAC necrosis evoked by the bile acid TLC-S, which acts selectively on PACs, is markedly enhanced by stimulation with BK, which only acts on PSCs (Ferdek *et al.* 2016). Furthermore, the level of PAC necrosis elicited by a mixture of bile acids or by a fatty acid ethyl ester (FAEE), is markedly reduced by a BK type 2 receptor antagonist (Gryshchenko *et al.* 2016). Because Ca^{2+} signals in PSCs generate nitric oxide (NO), whereas this is not the case in PACs, it is possible that the effects of PSC Ca^{2+} signals on

PACs are mediated by NO diffusing from PSCs into PACs (Jakubowska *et al.* 2016).

Early studies by Scheele and Haymovits (1978, 1980) indicated that PACs are electrically excitable, as K^+ depolarization evoked Ca^{2+} -dependent enzyme secretion from guinea pig PACs, which could not be blocked by atropine. However, it turned out that the secretory response was due to the Ca^{2+} -dependent release of a non-cholinergic, non-adrenergic neurotransmitter, probably vasoactive intestinal polypeptide (VIP) and its action on the PACs (Pearson *et al.* 1981a,b). It is now well established that PACs are electrically non-excitable, as they cannot fire action potentials, and do not possess voltage-activated Ca^{2+} channels (Petersen, 1992). The functional innervation of PACs by parasympathetic nerves is physiologically important and has been studied in some detail (Petersen, 1992), but it is unknown whether PSCs are functionally innervated.

PSCs can undergo significant transformations and this occurs in pancreatitis (Ferdek & Jakubowska, 2017; Pang *et al.* 2017), but it is not known how this would affect Ca^{2+} signal generation in PSCs in response to various stimuli.

The aim of the study presented here was to provide a more complete description of cellular Ca^{2+} signalling events in and around the acinar units in the normal pancreas than has previously been available. Furthermore, we were interested in comparing PSC Ca^{2+} signalling properties in the pancreas from mice with experimental AP with those in the normal tissue, as any changes could have implications for our understanding of the mechanism underlying AP.

Our results demonstrate, that – in addition to observing Ca^{2+} signals in PACs and PSCs – it is possible to record Ca^{2+} signals from nerve cells in the peri-acinar environment. However, in contrast to the clear evidence for functional innervation of the PACs, we did not observe Ca^{2+} signals in PSCs in response to nerve stimulation. Experimental AP caused major changes in PSC Ca^{2+} signalling. In alcohol-related AP, induced by intraperitoneal injections of ethanol and fatty acids, there was a markedly reduced responsiveness to BK, but the PSCs were now able to generate substantial Ca^{2+} signals when stimulated by trypsin. These results provide fresh evidence for a significant role of PSCs in the destructive processes leading to AP.

Methods

Ethical approval

All regulated procedures carried out on animals involved in this publication were approved by Cardiff University's Animal Welfare and Ethical Review Body (AWERB), and covered by a Project Licence granted by the Home Office under the Animal (Scientific Procedures) Act, 1986. All

animals were killed humanely according to the Schedule 1 protocol by cervical dislocation. Before and throughout the experiment, mice were maintained in plastic cages with corn cob bedding; tap water and commercial pelleted diet were freely provided. The mice were killed before the removal of the pancreas according to Schedule 1 of the UK Animals Act. The investigators understand the ethical principles under which *The Journal of Physiology* operates and state that this work complies with these principles.

Induction of experimental AP

To establish AP in C57BL6/J mice (Charles River, Wilmington, MA, USA), they received two intraperitoneal injections of ethanol (1.35 g kg^{-1}) and palmitoleic acid (POA) (150 mg kg^{-1}), at 1 h intervals, preceded by injection of PBS, as previously described (Wen *et al.* 2015; Huang *et al.* 2017). Because it has been established that fatty acids and ethanol can react together inside cells to produce FAEEs (Criddle *et al.* 2006; Huang *et al.* 2014), we refer to this pancreatitis model as FAEE-AP (Wen *et al.* 2015; Huang *et al.* 2017). Control mice received injections of the PBS solution alone. Humane killing was 48 h after the last injection.

Histology

Pancreatic tissue was fixed in 4% formaldehyde and embedded in paraffin, and histological assessment was performed after haematoxylin and eosin staining of fixed pancreatic slices ($4 \mu\text{m}$ thickness). Evaluation was performed on ≥ 10 random fields (magnification: $\times 200$) by two blinded independent investigators grading (scale, 0–3) oedema, inflammatory cell infiltration and acinar necrosis as previously described (Van Laethem *et al.* 1996; Wen *et al.* 2015), calculating the means \pm SEM ($n = 3$ mice per group).

Lobule preparation

Pancreatic lobules were isolated from the pancreas of adult normal mice (Gryshchenko *et al.* 2016) or from mice in which AP had been induced as described above. The pancreas was rapidly dissected, transferred to a collagenase Na^+ -Hepes-based solution and incubated for 5–6 min at 37°C . Thereafter, the tissue was kept in a standard medium with the following composition (in mM): NaCl, 140; KCl, 4.8; Hepes (KOH), 10; MgCl_2 , 1; CaCl_2 , 1; glucose, 10; pH 7.3. In experiments where the effects of omitting extracellular Ca^{2+} were investigated, CaCl_2 was left out of the standard solution. In experiments where the effects of membrane depolarization were investigated, the medium contained 100 mM KCl and the NaCl concentration was reduced to 44.8 mM. Pancreatic lobules were then incubated with fluorescent dye following the

manufacturer's description. All experiments on normal pancreatic lobules were carried out with fresh preparations attached to the coverslip of a perfusion chamber at room temperature ($\sim 23^{\circ}\text{C}$). In experiments on lobules in which the effects of exposure to fatty acids and ethanol were investigated, the lobules were exposed to a medium containing POA ($20\ \mu\text{M}$) and ethanol ($12\ \text{mM}$) for 2.5 h before starting the experiments.

The pancreas is dominated quantitatively by exocrine cells, but also contains endocrine cells, in particular insulin-secreting β -cells. The endocrine cells are found in the islets of Langerhans and these can be identified as dense and discrete spherical or ovoid structures sharply delineated from the surrounding more translucent exocrine tissue (Dean & Matthews, 1970). We deliberately did not focus on these structures as it was our objective to specifically study Ca^{2+} signalling events in the acinar environment.

Ca^{2+} measurements

Pancreatic lobules were loaded with $5\ \mu\text{M}$ Fluo-4 acetoxy-methyl ester (AM), for 20 min at room temperature. The tissue was transferred into a flow chamber and superfused with the Na^{+} -Hepes-based extracellular solution as described above. Cells were visualized using a Leica SP5 MP11 two-photon confocal microscope, with an $\times 63$ 1.3 NA objective lens. Fluo-4 was excited with a 488 nm argon laser, at 1–4% power, and emitted light was collected at 500–580 nm. Generally, a series of images was recorded at 512×512 pixels resolution (at the speed of $1\ \text{frame s}^{-1}$), and analysed using Leica Confocal Software (Leica, Mannheim, Germany). Fluorescence signals were plotted as F/F_0 (F_0 is the initial level of fluorescence). In many experiments three-dimensional recording in time have been conducted (2–3 images per time point). Statistical analysis was performed using ANOVA or Student's *t*-test.

Results

General approach

Our general aim was to simultaneously study signalling in the various cell types to be found in the acinar environment in a live pancreatic lobule preparation. Figure 1 shows an example. As previously demonstrated (Gryshchenko *et al.* 2016), PSCs take up Ca^{2+} -sensitive fluorescent probes much more avidly than PACs, so the initial assumption – looking at the fluorescence intensity levels in the resting situation (Fig. 1Aii) – was that the bright cells represent PSCs. To check whether nerve cells were present and, if so, to test whether nerve stimulation could elicit Ca^{2+} signals in PACs or other cells, a solution with a high ($100\ \text{mM}$) K^{+} concentration was introduced. As seen in Fig. 1Aiii,

this caused a rise in $[\text{Ca}^{2+}]_i$ in several relatively large cells, which must be the always quantitatively dominant PACs. Importantly, there was no rise in $[\text{Ca}^{2+}]_i$ in the PSCs, but in one cell – partly 'hidden' by a PSC – there was a large Ca^{2+} signal. This cell is most likely a neuron (PN). The apparently unprovoked short-lasting Ca^{2+} signal in this cell occurring later in the experiment may be due to a spontaneous action potential or a short burst of action potentials. The assumption that the bright cells seen in Fig. 1Aii were PSCs was confirmed when these cells became significantly brighter, indicating rises in $[\text{Ca}^{2+}]_i$, after stimulation with BK ($1\ \text{nM}$) (Fig. 1Aiv). Finally, the lobule was stimulated by ATP ($100\ \mu\text{M}$), which caused a rise in $[\text{Ca}^{2+}]_i$ in the PACs and in a cell (green in the schematic diagram in Fig. 1Ai) that had not reacted to high K^{+} or BK exposure. The nature of this cell is unclear and it is therefore labelled X.

As mentioned in the Methods, the pancreas contains insulin-secreting β -cells, in addition to the quantitatively dominant exocrine cells. It has long been known that PACs possess insulin receptors and that insulin can affect PAC functions including Ca^{2+} signalling (Sankaran *et al.* 1981; Singh, 1985; Mankad *et al.* 2012; Samad *et al.* 2014). As described in the Methods, we did not explore Ca^{2+} signalling in or near the islets of Langerhans and it would therefore seem very unlikely that any of the cells in the acinar environment we investigated could be insulin-secreting β -cells or would be influenced by local insulin secretion. We nevertheless checked this by using the standard protocol for eliciting Ca^{2+} signals in β -cells, namely by testing the effect of elevating the external glucose concentration (Dean & Matthews, 1970) from 2 to $10\ \text{mM}$. As seen in Fig. 2, none of the peri-acinar cell types generated Ca^{2+} signals in response to glucose stimulation (see also further details in the sections below on PNs and X-cells).

Ca^{2+} signals in pancreatic nerve cells (PNs)

It is clear from experiments of the type shown in Fig. 1 that there are cells other than PACs that respond to depolarization with Ca^{2+} signals. One possibility is that they are PNs and we therefore tested this hypothesis. The fluorescent dye FluoroGold has been demonstrated to undergo retrograde axonal transport and stains nerve cells (Naumann *et al.* 2000). Figure 3A–C shows the results from an experiment ($n = 3$) in which a FluoroGold-labelled cell (Fig. 3B) responded to membrane depolarization, elicited by a high- K^{+} ($100\ \text{mM}$) solution, with an increase in $[\text{Ca}^{2+}]_i$ (Fig. 3A). A non-FluoroGold-labelled PAC also produced a rise in $[\text{Ca}^{2+}]_i$, presumably due to the action of ACh released from nerve endings (see below), whereas a PSC failed to respond (Fig. 3). We also undertook experiments in which the ultra-sensitive Ca^{2+} sensor GCaMP6 was expressed in mice by intravenous injection

of adeno-associated virus AAV9.Syn.GCaMP6s targeted to neurons (Chen *et al.* 2013). As seen in Fig. 3*Di–iii*, a short-lasting high- K^+ stimulation caused a substantial transient increase in $[Ca^{2+}]_i$ ($n = 7$).

Many of the pancreatic cells that have neuron-like properties are located close to PSCs (see Fig. 1). In several cases ($n = 14$) we could observe Ca^{2+} signal propagation in PNs along the bodies and elongated parts of PSCs as a pathway through the lobules (Fig. 4*A, B*).

The rise in $[Ca^{2+}]_i$ in PNs, elicited by K^+ -induced depolarization (Figs 1–5) could potentially be influenced by release of neurotransmitters from nerve cells not visualized in the segment under investigation and we therefore tested possible effects of various neurotransmitters (Figs 4 and 5). Figure 4*C* and *D* shows examples of Ca^{2+} signals in a PN and a PAC generated by exposure to a high- K^+ solution. The PAC signal, as expected, was clearly not mediated by depolarization of the acinar cell membrane as it was abolished by atropine ($n = 12$), in agreement with the well-established cholinergic innervation of PACs (Petersen, 1992), whereas the Ca^{2+} signal in the PN could still be observed in the presence of this muscarinic antagonist ($n = 17$). ATP

did not have any effects on PNs ($n > 100$; Fig. 4*C, D*), whereas this agent could, in several cases, produce Ca^{2+} signals in PACs and PSCs (Fig. 1), although not in the case shown in Fig. 4*C* and *D*. Ca^{2+} signals induced by the high- K^+ solution in both PACs and PNs were reversibly abolished by removal of external Ca^{2+} ($n = 4$) (Fig. 4*E, F*). Ca^{2+} signals elicited by a high- K^+ solution in PNs were not inhibited by the non-selective purinergic antagonist suramin ($n = 5$; Fig. 5*B*).

Several neurotransmitters elicited Ca^{2+} signals in PNs. Adrenaline (20 μM) evoked signals in 21 out of 35 PNs tested (Fig. 5*A*). This response was mediated by α - rather than β -receptors as the β -adrenergic agonist isoprenaline had no effect ($n = 10$) whereas the α -receptor agonists cirazoline (50 μM) and UK 14,304 (50 μM) could mimic the effect of adrenaline ($n = 8$). Ca^{2+} signals in PNs were also elicited by Substance P (10 μM) in 4 out of 7 neurons (Fig. 5*C*). Bombesin, which is known to elicit Ca^{2+} signals in PACs by interaction with receptors that are distinct from the CCK receptors (Deschodt-Lanckman *et al.* 1976; Iwatsuki & Petersen, 1978), evoked Ca^{2+} signals in 7 out of 8 PNs (Fig. 5*E*). On the other hand, PNs did not respond to BK ($n > 100$; Fig. 5*D*) or VIP ($n = 4$).

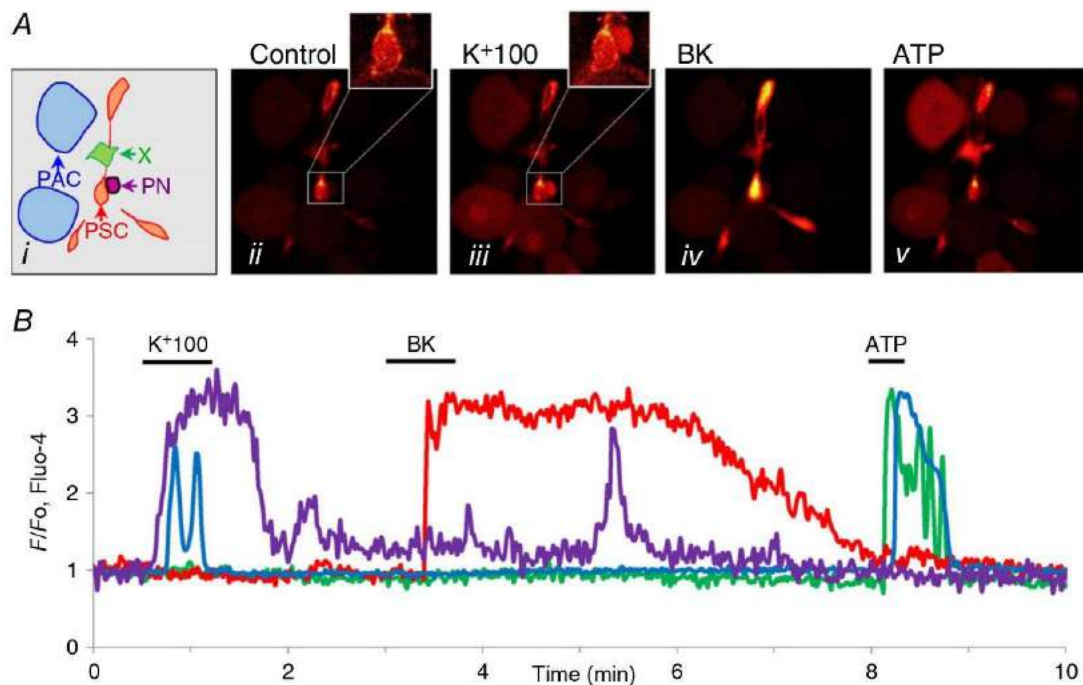


Figure 1. Simultaneous recordings of $[Ca^{2+}]_i$ changes in response to various stimuli in four different cell types in a mouse pancreatic lobule

Ai, sketch of location of different cell types in the lobule: blue, PACs; orange/red, PSCs; purple, PN; green, unknown (X). *Aii–v*, fluorescence images in control and during stimulation with high K^+ (100 mM), BK (1 nM) and ATP (100 μM). As also seen in the $[Ca^{2+}]_i$ traces shown in *B*, PN and PACs displayed rises in $[Ca^{2+}]_i$ in response to membrane depolarization. PSCs responded to BK and both PACs and X responded to ATP. The colours of the traces in *B* match the coloured arrows in *Ai*.

In the hypothalamus there are neurons responsive to glucose (Burdakov *et al.* 2005) and in the pancreas the insulin-secreting β -cells have long been known to depolarize and fire action potentials when challenged with glucose above a certain threshold concentration (Dean & Matthews, 1970; Dean *et al.* 1975; Atwater *et al.* 1978). We therefore tested whether the PNs in our preparation would be sensitive to changes in the extracellular glucose concentration. In these experiments the glucose concentration in the fluid surrounding the lobules was kept low (2 mM) for a prolonged period (15–30 min) before exposure to 10 mM glucose. As seen in Fig. 5C, a PN in which a high- K^+ solution, as well as Substance P, elicited Ca^{2+} signals failed to respond to stimulation with 10 mM glucose ($n = 13$).

PSCs are not electrically excitable but respond to some neurotransmitters

As previously described, PSCs consistently generate Ca^{2+} signals when challenged with BK (Fig. 1; Ferdek *et al.* 2016; Gryshchenko *et al.* 2016), but it is not known whether they are functionally innervated. We never observed Ca^{2+} signals in PSCs when lobules were exposed to high- K^+ solutions ($n > 100$). Figure 4E shows the result of an experiment in which a high- K^+ solution elicited Ca^{2+} signals in both a PN and a PAC without evoking a response from two PSCs, which both subsequently generated Ca^{2+} signals when stimulated by BK.

As previously shown (Gryshchenko *et al.* 2016), PSCs could (Fig. 5EF), but did not always (Fig. 1), generate Ca^{2+} signals in response to ATP (100 μM) stimulation. Bombesin (1 μM) elicited Ca^{2+} signals in some PSCs ($n = 8$

out of 21 cells tested; Fig. 5E) and VIP (100 nM) could evoke Ca^{2+} signals in 37 out of the 78 PSCs tested (Fig. 5F).

X-cells

As shown in Fig. 1 there is an unknown (X) cell type that generates a substantial Ca^{2+} signal in response to ATP stimulation ($n > 100$). In these ATP-sensitive X-cells, high- K^+ stimulation could in many, but not all, cases evoke short-lasting Ca^{2+} signals (Fig. 5D), but once these cells had been challenged with a high- K^+ pulse, they needed a long recovery time (> 30 min) before they could respond again ($n = 9$). In these cells, adrenaline (20 μM) could evoke Ca^{2+} signals (Fig. 5B, $n = 14$ out of 33 cells tested), but X-cells never responded to BK ($n > 100$) (Fig. 5D). We also tested whether the X-cells were glucose-sensitive. We used the same protocol as for the similar experiments testing glucose sensitivity in PNs (Fig. 5C) (low – 2 mM – basal glucose concentration and then a test pulse of 10 mM glucose). In five experiments, X-cells that responded to ATP stimulation with Ca^{2+} signals failed to generate any increase in $[Ca^{2+}]_i$ in response to 10 mM glucose (Fig. 2).

Alcohol-related AP changes the responsiveness of PSCs

As described in the Introduction, it is known that PSCs undergo morphological and functional changes during pancreatitis (Ferdek & Jakubowska, 2017; Pang *et al.* 2017) and we were therefore interested in exploring whether their responsiveness to BK would also change as a result of this transformation. We investigated this in two different ways. In one type of experiment, we induced changes in the pancreatic lobule preparation, similar to

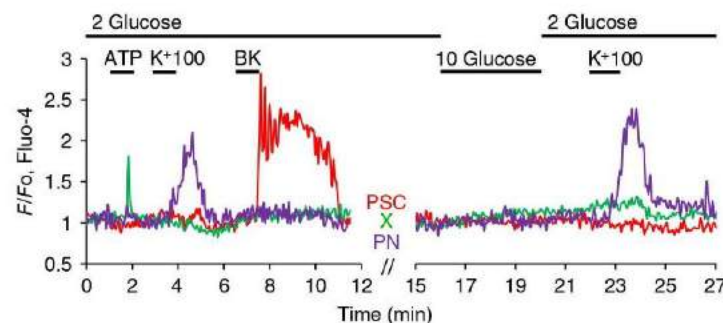


Figure 2. Elevating the extracellular glucose concentration from 2 to 10 mM has no effect on $[Ca^{2+}]_i$ in any of the peri-acinar cells

In this experiment the lobule preparation was superfused with a solution containing 2 mM glucose, which then only late in the experimental protocol was replaced by 10 mM glucose for a few minutes. As shown in the green trace, an X-cell responded to ATP (100 μM) with a rise in $[Ca^{2+}]_i$, but did not respond to subsequent challenges with high K^+ (100 mM), BK (1 nM) or 10 mM glucose. In contrast, the PSC (red trace) did not respond to ATP or high K^+ , but only to BK. The PN (purple trace) only responded, repeatedly, to the high- K^+ stimulus.

those seen in AP, by exposing the tissue to a mixture of ethanol and POA, which is known to generate palmitoleic acid ethyl ester (POAEE) inside PACs (Laposata & Lange, 1986; Criddle *et al.* 2006; Huang *et al.* 2014; 2017). In the second type of experiment, we induced AP in mice *in vivo*, by injections of ethanol and POA, and then removed the pancreas to investigate Ca^{2+} signalling properties in the lobule preparation.

Figure 6 summarizes the results from the *in vitro* series of experiments. In the control lobules (no POA/ethanol) we confirmed that PSCs respond to BK (1 nM) stimulation by

generating substantial Ca^{2+} signals and also confirmed the previously reported result that trypsin does not elicit Ca^{2+} signals (Gryshchenko *et al.* 2016). However, following exposure to POA/ethanol, the cells produced substantial Ca^{2+} signals in response to a concentration (50 nM) of trypsin that had failed to elicit signals in the control preparations (Fig. 6). As seen in Fig. 6, the effect of trypsin was acute and reversible and could therefore not be a consequence of cell death induced by digestion, but must be a receptor-mediated (protease-activated receptor) effect. Many PSCs may well have died during

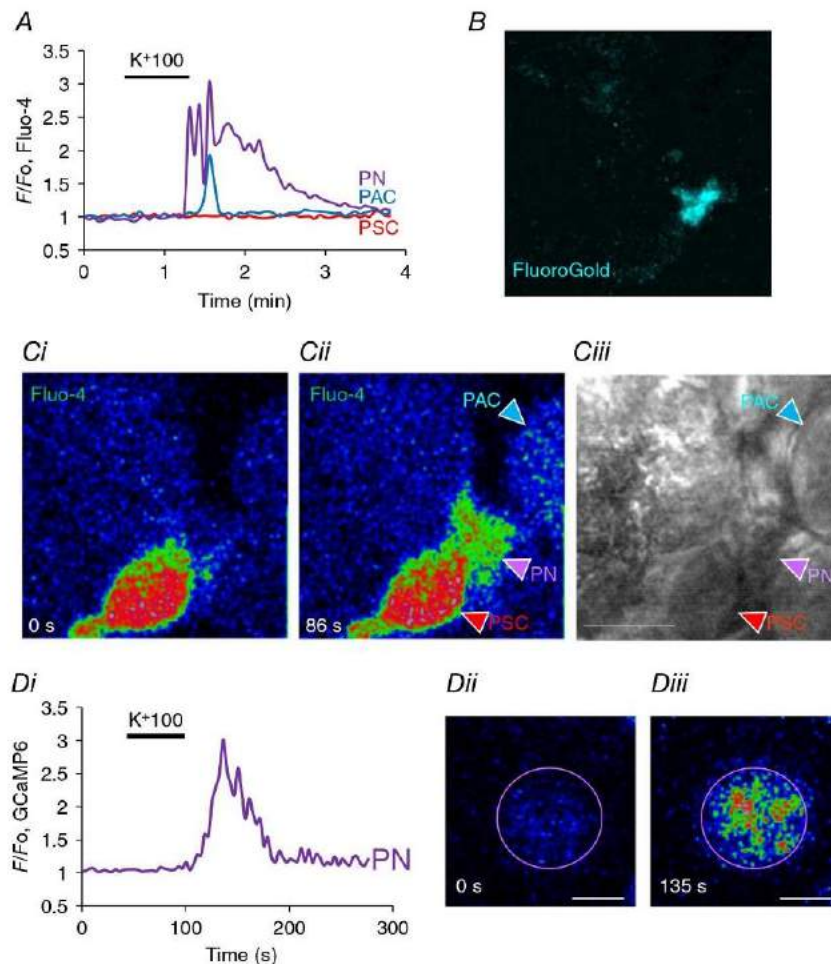


Figure 3. K^+ depolarization evokes Ca^{2+} signals in labelled pancreatic neurons

A, K^+ depolarization evoked a rise in $[\text{Ca}^{2+}]_i$ in a FluoroGold labelled PN (B) as well as in a PAC. Ci–ii, fluorescence images before (0 s) and during the high K^+ challenge (86 s) showing the evoked rise in $[\text{Ca}^{2+}]_i$ in the PN as well as the PAC, but with no change in the PSC. Ciii, transmitted light image of the field, also showing location of the different cells. Length of horizontal bar corresponds to 10 μm . D, ultrasensitive protein calcium sensor GCaMP6 was expressed in mouse pancreas by intravenous injection of adeno-associated virus AAV9.Syn.GCaMP6s (Penn Vector Core at University of Pennsylvania) targeted to neurons. K^+ depolarization evoked a significant rise in $[\text{Ca}^{2+}]_i$ (Di). As seen in Dii, at rest the PN had relatively low fluorescence (0 s) but this increased by a factor of three after depolarization with high- K^+ solution (Diii, 135 s). Length of horizontal bars in Dii and Diii corresponds to 5 μm . No other cells in the field of view displayed any changes in fluorescence intensity. In this experiment the only fluorescent probe present was GCaMP6.

the exposure to POA/ethanol, but the cells from which $[Ca^{2+}]_i$ recordings were made were still viable, as seen by their ability to bring $[Ca^{2+}]_i$ back to the control level after a short exposure to trypsin (Fig. 6B). The proportion of PSCs responding to trypsin in the AP lobules was markedly reduced by including the CRAC channel inhibitor GSK-7975A in the POA/ethanol solution used to generate AP (Fig. 6C). Because CRAC channel inhibition has been shown to reduce store-operated Ca^{2+} influx in both PACs and PSCs, this supports the idea previously proposed (Ferdek *et al.* 2016; Gryshchenko *et al.* 2016) that excessive Ca^{2+} signal generation in PACs as well as PSCs play a central role in the development of AP.

In the *in vivo* experiments, we verified that AP had been induced by evaluating pancreatic histology sections, comparing tissue from control mice with those that had been injected with POA/ethanol. Figure 7A–F summarizes these data. It can be seen that the overall histology score, the degree of oedema, the level of acinar necrosis and the extent of immune cell invasion were all markedly increased in the pancreatic tissue from the mice that had been injected with POA/ethanol as compared to the normal tissue. As seen in Fig. 7H, J and L and M, the PSCs in the AP mice, in contrast to the control mice (Fig. 7G, I, K and M), hardly responded to 1 nM BK, but in a number of PSCs Ca^{2+} signals in response to trypsin (10 nM) were observed ($n = 8$ out of 38 cells tested,

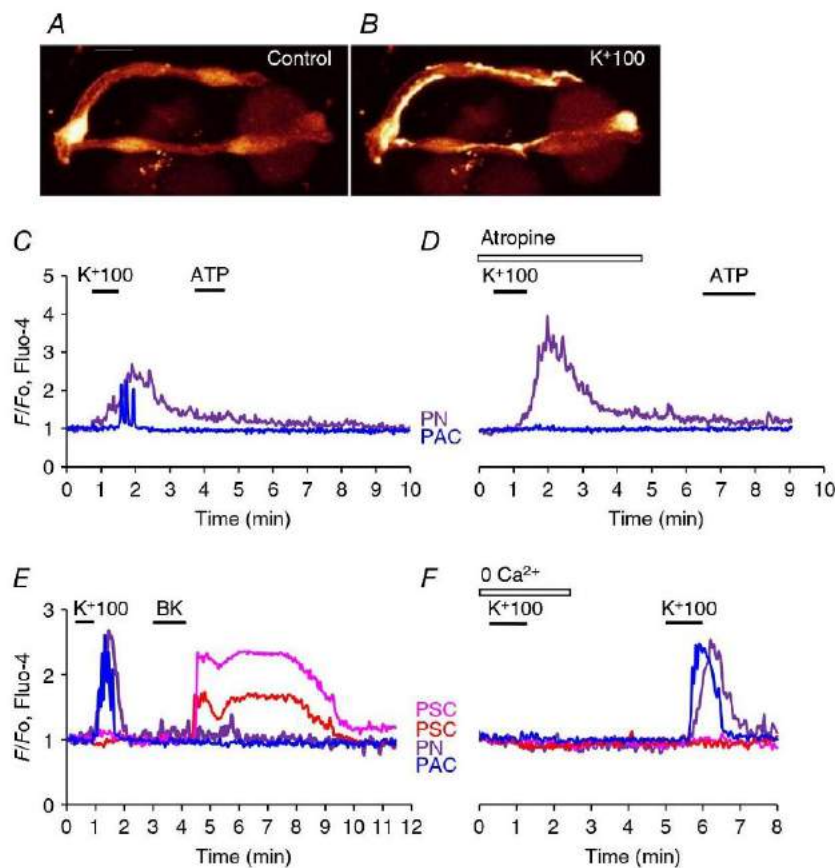


Figure 4. K^+ depolarization evokes Ca^{2+} signals in PNs that depend on extracellular Ca^{2+} but, unlike the signals in PACs, are not blocked by atropine

A and B, fluorescence images illustrating that PNs sometimes have elongated parts that seem very closely linked to PSCs. The images show Fluo-4 fluorescence before (A) and during high- K^+ stimulation (B). Length of horizontal bar in A corresponds to 10 μm . C, high- K^+ induced Ca^{2+} signals in a PN and a PAC, but subsequent stimulation with ATP did not elicit any responses. D, in the presence of atropine (10 μM), high K^+ still evoked a Ca^{2+} signal in the PN, but no longer in the PAC. E, high K^+ elicited Ca^{2+} signals in PN and PAC, but not in two PSCs in which subsequently Ca^{2+} signals were observed in response to BK stimulation. BK did not elicit Ca^{2+} signals in PN and PAC. F, in the absence of external Ca^{2+} , K^+ depolarization failed to elicit Ca^{2+} signals in PN and PAC. After reintroduction of the Ca^{2+} -containing external solution, high K^+ was again able to evoke Ca^{2+} signals in PN and PAC, but not in two PSCs.

Fig. 7H and N). Control PSCs did not respond to trypsin Fig. 7G), as also previously reported (Gryshchenko *et al.* 2016). Similar to the effects of trypsin on PSCs in lobules exposed *in vitro* to POA/ethanol mixtures (Fig. 6B), the actions of this enzyme in this series of experiments (Fig. 7H and N) were also acute and reversible, indicating

a receptor-mediated (protease-activated receptor) effect rather than a consequence of cell damage. Although many PSCs may have been destroyed by the actions of POA/ethanol *in vivo*, clearly those responding to trypsin were intact. In a few cases ($n = 3$ out of 59 cells tested), thrombin (5 mU ml^{-1}), another protease, evoked Ca^{2+}

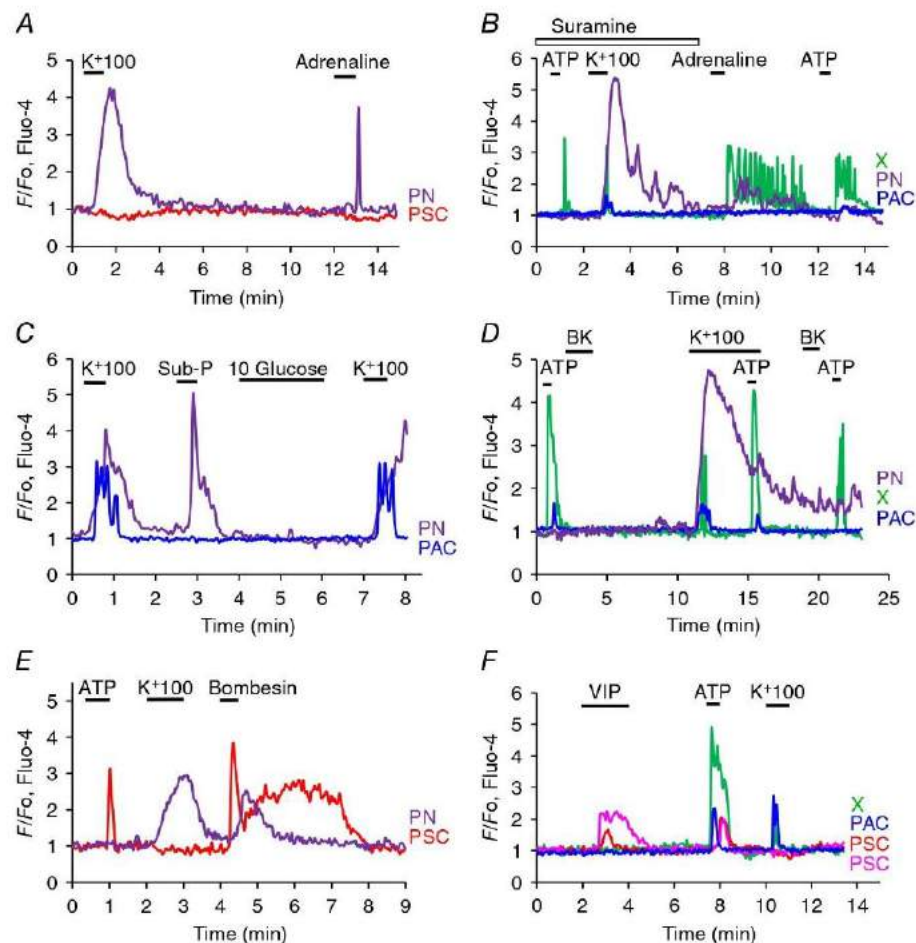


Figure 5. The effects of various neurotransmitters on $[\text{Ca}^{2+}]_i$ in the different cell types found in the lobules

A, the PN, but not the PSC, produces a Ca^{2+} signal in response to high- K^+ stimulation and subsequently generates a Ca^{2+} signal in response to stimulation with adrenaline ($20 \mu\text{M}$). B, in the presence of the purinergic receptor antagonist suramin, high- K^+ stimulation evokes a normal Ca^{2+} signal in the PN and a very short-lasting signal in the X-cell. The effect of ATP ($100 \mu\text{M}$) on the X-cell in the presence of the purinergic antagonist is very short-lasting compared to the effect of the same concentration of ATP later in the same cell after wash-out of suramin. Adrenaline ($20 \mu\text{M}$) evoked a train of Ca^{2+} spikes in the X-cell, but in this experiment only had a questionable effect on the PN. C, high K^+ elicited Ca^{2+} signals in PAC and PN. Substance P ($10 \mu\text{M}$) evoked a Ca^{2+} signal in the PN, but not in the PAC. Glucose (10 mM) failed to evoke Ca^{2+} signals in both the PN and the PAC (in these experiments the standard solution contained only 2 mM glucose). D, ATP repeatedly evoked Ca^{2+} signals in X-cell and small signals in PAC, but not in PN. High- K^+ stimulation evoked large Ca^{2+} signal in PN, but only a short-lasting signal in the X-cell. The ATP-elicited Ca^{2+} signal in the X-cell was not diminished during the period of high- K^+ depolarization. BK did not evoke any effects in these three cells. E, ATP and bombesin ($1 \mu\text{M}$) evoked Ca^{2+} signals in a PSC and bombesin also elicited a Ca^{2+} signal in a PN that responded to high- K^+ stimulation. F, VIP (100 nM) evoked Ca^{2+} signals in two PSCs, but neither in a PAC nor in a X-cell, whereas ATP produced Ca^{2+} signals in all the cells (X, PAC and PSC). High K^+ evoked Ca^{2+} signals in the X-cell and the PAC, but not in the PSCs.

signals in PSCs in lobules from FAEE-AP mice, whereas this was not observed in control tissue, as also previously reported (Gryshchenko *et al.* 2016). Because Ca^{2+} signals in normal PSCs evoked by BK is due to activation of type 2 BK receptors (Gryshchenko *et al.* 2016), the desensitization to BK seen in AP (Fig. 7K–M) would appear to represent a specific desensitization of the type 2 receptors. This is supported by the finding that although PSCs in the FAEE-AP tissue failed to respond to a BK concentration (1 nM) that elicited a maximal Ca^{2+} signal in the control tissue, some PSCs from FAEE-AP lobules could produce Ca^{2+} signals when stimulated with a high concentration (1 μM) of a BK agonist specific for type 1 BK receptors (S-BK) (Fig. 7J and N; 8 cells out of 101 tested). In contrast, S-BK only evoked a Ca^{2+} signal in one PSC out of 118 tested in lobules from control mice. Figure 7N summarizes the results of the experiments comparing the responsiveness of PSCs to S-BK, thrombin and trypsin in control and FAEE-AP.

We evaluated quantitatively the reduced responsiveness of the PSCs to BK in AP by comparing concentration–response curves for BK-elicited Ca^{2+} signal generation in control and AP (Fig. 7K–M). The results show that the concentration–response curve was shifted markedly to the right in AP, as compared to the control values. Thus a BK concentration of 1 nM, which evokes a near-maximal Ca^{2+} signal in control PSCs (Gryshchenko *et al.* 2016; Fig. 7K and M, $n = 11$), hardly evoked any change in $[\text{Ca}^{2+}]_i$ in the PSCs from the AP lobules (Fig. 7L and M, $n = 12$).

Discussion

In this study of Ca^{2+} signalling in the peri-acinar environment of the exocrine pancreas, we have for the first time been able to record Ca^{2+} signals from PNs, and demonstrated that PSCs are not electrically excitable and, in contrast to the PACs, do not appear to be functionally

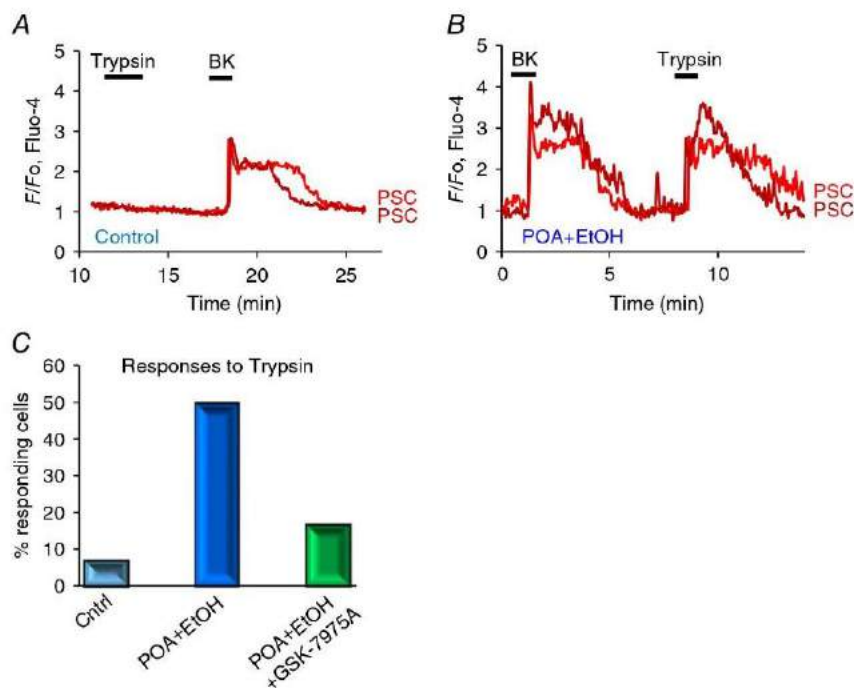


Figure 6. Exposure of pancreatic lobules to a mixture of POA and ethanol induces PSC responsiveness to trypsin

In A and B, the effects of trypsin (50 nM) and BK (1 nM) on $[\text{Ca}^{2+}]_i$ in PSCs in a control lobule are compared with those in lobules that had been exposed to a mixture of POA (20 μM) and ethanol (12 mM) for 2.5 h. In control PSCs, trypsin (50 nM) only evoked a Ca^{2+} signal in 2 cells out of 28 tested, and not in the case shown in A, whereas the same concentration of trypsin evoked a clear Ca^{2+} signal in the PSC in a lobule that had been treated with POA and ethanol ($n = 14$ out of 28 cells tested). C, summary of the results of the experiments illustrated in A and B, showing the marked increase in the percentage of PSCs responding to trypsin with Ca^{2+} signals after POA/ethanol exposure. In the presence of the CRAC channel inhibitor GSK-7975A (20 μM), the percentage of PSCs responding to trypsin in the POA/ethanol groups was markedly reduced ($n = 12$ of 71 cells tested).

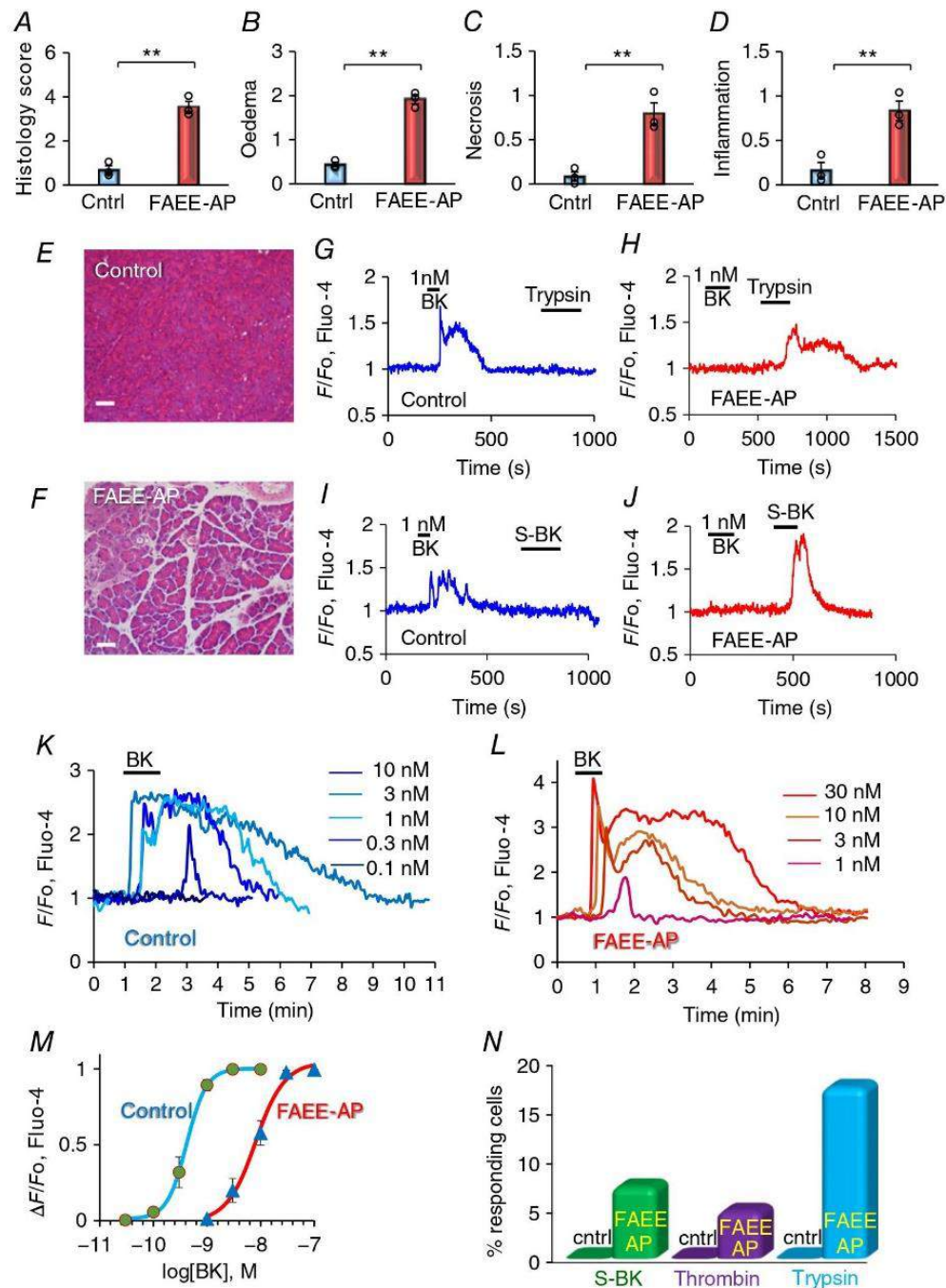


Figure 7. Functional changes in PSCs due to alcohol-induced AP (POA/ethanol *in vivo* mouse model – FAEE-AP)

A–F, the successful induction of AP was investigated by histological assessments of fixed pancreatic slices. Comparisons were made between pancreatic slices from control mice and FAEE-AP mice. Overall histology score (A), degree of oedema (B), extent of necrosis (C) and degree of inflammation (D) were recorded (** $P < 0.01$). Representative images of pancreatic histology sections from control (E) and FAEE-AP (F) mice are also shown (bars: 50 μm). In each case the number of independent experiments (from different mice) = 3 (but in each experiment >20 sections were examined; typically ~1000–2000 cells in each experimental group). G–J, representative $[\text{Ca}^{2+}]_i$ traces from PSCs in lobules from a control mouse (G, I) and a mouse with AP (H, J). In the control lobules (G, I), BK (1 nM) consistently evoked Ca^{2+} signals, whereas trypsin (10 nM) and the selective BK 1 receptor agonist Sar-[D¹Phe⁸]-des-Arg⁸-bradykinin (S-BK) (1 μM) failed to do so. In the lobules isolated from mice with FAEE-AP,

BK (1 nM) failed to elicit Ca^{2+} signals, but trypsin (10 nM) and S-BK (1 μM) were able to elicit such signals. *K–M*, quantitative evaluation of the change in PSC sensitivity to BK following induction of FAEE-AP. *K* shows traces of BK-elicited $[\text{Ca}^{2+}]_i$ changes, all from one and the same PSC, in a control lobule, whereas *L* shows the results, from one and the same PSC, in a lobule from an FAEE-AP mouse. The data from all experiments are summarized by the concentration–response curves in *M* ($n = 6–10$ for each point). *N*, comparisons of the responsiveness of PSCs to S-BK (1 μM), thrombin (5 mU mL^{-1}) and trypsin (10 nM) in control and FAEE-AP lobules.

innervated. We have also discovered a hitherto unknown cell type (X) which is very responsive to stimulation with ATP (Figs 1, 2 and 5). Further investigations will be needed to establish the character and function of this cell type.

Our new results show that experimental induction of AP causes a major change in the responsiveness of PSCs to BK. In the normal pancreas, PSCs generate small, but clear, Ca^{2+} signals in response to stimulation with 0.1 nM BK, a concentration only slightly above the resting plasma concentration of this agent (Blais *et al.* 1999; Hirata *et al.* 2002), and near-maximal Ca^{2+} signals at a BK concentration of 1 nM. In contrast, PSCs in lobules isolated from the pancreas in mice with FAEE-AP need more than 1 nM BK to produce clear signals and require a BK concentration of 30 nM to produce maximal Ca^{2+} signals. The BK concentration–response curve is thus shifted markedly to the right by induction of AP (Fig. 7M). This desensitization is probably due to BK liberation from bradykininogen, as a result of kallikrein release from PACs undergoing necrosis (Schachter 1969; Orlov & Belyakov, 1978; Griesbacher *et al.* 2003), causing a prolonged exposure of the PSCs to an elevated tissue level of BK (Griesbacher *et al.* 2003). These data in conjunction with our recent demonstration that a BK receptor antagonist markedly reduced the extent of PAC necrosis induced in lobules by exposure to FAEEs or bile acids (Gryshchenko *et al.* 2016) and our finding that bile-induced damage to PACs can be markedly enhanced by BK stimulation of PSCs (Ferdek *et al.* 2016) suggest that PSCs may be critically involved in a vicious circle promoting PAC necrosis. Figure 8 shows a schematic model in which initial damage to PACs would lead to release of activated enzymes, including kallikrein, into the interstitial fluid, causing an increase in the BK concentration, which would then generate Ca^{2+} signals in PSCs. These Ca^{2+} signals – via NO formation in PSCs and with NO diffusing into adjacent PACs (Jakubowska *et al.* 2016) – would contribute to further damage of PACs, which in turn would cause further release of kallikrein leading to a further increase in the BK level and thereby further stimulation of PSCs acting to promote PAC necrosis. We have shown that pharmacological inhibition of NO synthase provides remarkable protection against necrosis (Jakubowska *et al.* 2016), but the mechanism by which NO exerts this effect is unknown.

The BK-induced Ca^{2+} signals in PSCs are mediated by BK type 2 receptors (Gryshchenko *et al.* 2016) and in

normal PSCs an analogue of BK that selectively interacts with type 1 receptors does not elicit Ca^{2+} signals. This changes after induction of AP (Fig. 7), as PSCs can now produce Ca^{2+} signals in response to a high concentration of the BK type 1 receptor agonist S-BK (Fig. 7N). Given that the concentration of the type 1 agonist that is required to evoke a signal is very high, this may not in itself have any functional significance, but the reduced sensitivity to type 2 receptor activation and increase in sensitivity to type 1 activation is a general feature of inflammatory diseases (Petho & Reeh, 2012).

The decrease in PSC sensitivity to BK, induced by ethanol and POA, takes time to develop. Thus the exposure of pancreatic lobules to POA/ethanol for 150 min is insufficient (Fig. 6AB), whereas induction of FAEE-AP over 48 h *in vivo* produces a clear reduction in responsiveness to BK (Fig. 7). The relatively short period (150 min) of exposure of pancreatic tissue to POA/ethanol is, however, sufficient for a proportion of PSCs to become sensitive to trypsin, an enzyme that has no effect on Ca^{2+} signalling in normal PSCs (Fig. 6). In the *in vivo* FAEE-AP model there was also induction of sensitivity to trypsin (Fig. 7). These results may indicate the existence of a further necrotic amplification loop in which initial damage to PACs, induced – for example – by FAEEs or a bile acid, causes release of activated trypsin from dying PACs, which in turn activates PSCs to produce Ca^{2+} signals, generating NO that may diffuse into neighbouring PACs, thereby causing further cell death (Jakubowska *et al.* 2016) and therefore further liberation of trypsin and other proteases (Fig. 8). Thrombin may also have a role in AP (Andersson *et al.* 2010) and this enzyme sometimes induced Ca^{2+} signals in PSCs from AP lobules, but not in normal PSCs (Fig. 7). Thrombin would also act via activation of protease-activated receptors (Coughlin, 2000). The responsiveness to trypsin, and to some extent perhaps also to thrombin, highlights the importance of the protease-activated receptors in FAEE-AP. We have recently provided evidence for the importance of these receptors in drug-induced AP (Peng *et al.* 2016).

Although PSCs have not traditionally been thought to play a role in AP, our new results strengthen the case for such an involvement that began to emerge from our previous investigations of PSCs (Ferdek *et al.* 2016; Gryshchenko *et al.* 2016; Jakubowska *et al.* 2016). Specifically, our new data indicate initial roles for BK, followed by trypsin, generating Ca^{2+} signals in PSCs

(Fig. 8) and provide fresh evidence in favour of the propositions made many years ago, but largely ignored, that inhibition of BK receptors could have benefits in the treatment of AP (Griesbacher *et al.* 1993; Hirata *et al.* 2002).

We have previously shown that CRAC channel inhibition markedly reduces the prolonged $[Ca^{2+}]_i$ elevation due to the store-operated Ca^{2+} entry into the PSCs that follows the initial BK-elicited intracellular Ca^{2+} release (Gryshchenko *et al.* 2016). Since then it has been shown that PSCs possess Ca^{2+} -activated K^+ channels (Storck *et al.* 2017) and it is therefore likely that initial Ca^{2+} release from intracellular stores would activate such

channels, promoting store-operated Ca^{2+} entry due to the more favourable electrochemical gradient provided by the hyperpolarized plasma membrane. Inhibition of excessive Ca^{2+} signal generation in PACs and PSCs by partial blockade of CRAC channels is a promising therapeutic avenue in many inflammatory diseases (Parekh, 2010; Di Capite *et al.* 2011) including AP (Gerasimenko *et al.* 2013, 2014; Wen *et al.* 2015). Our new data (Fig. 6C), showing that CRAC channel inhibition largely prevents the increased responsiveness of PSCs to trypsin that occurs in AP-like conditions, provides fresh evidence in favour of CRAC channel inhibition as a potentially attractive treatment for AP.

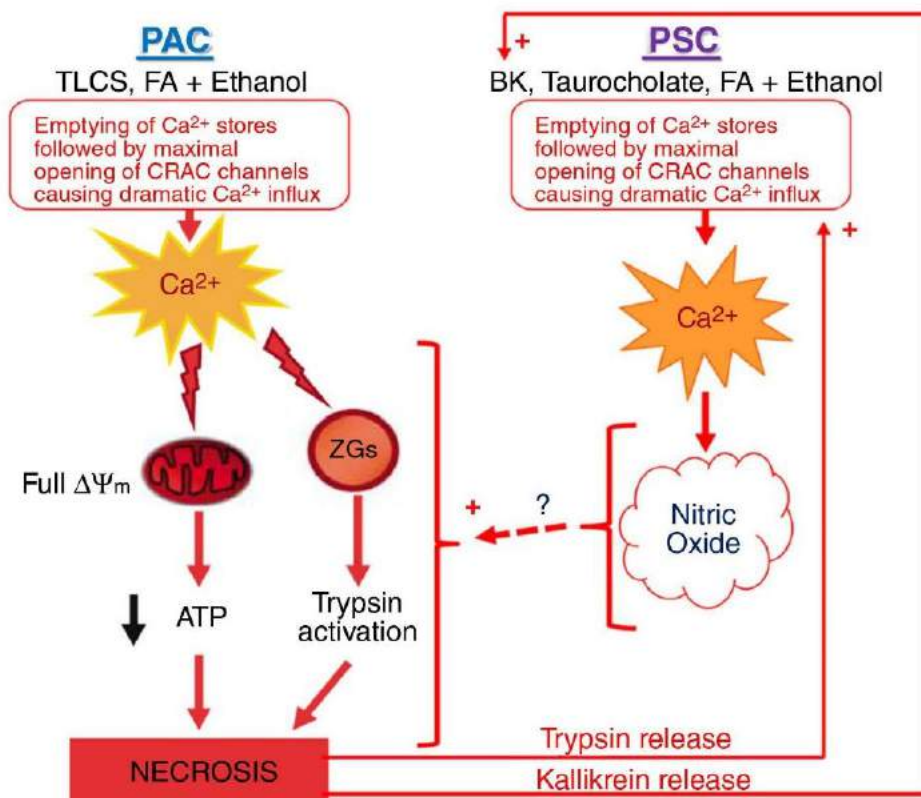


Figure 8. Schematic diagram illustrating how the PSCs may participate in a vicious circle amplifying necrotic PAC death in AP

In the PACs the initial damage leading to AP may be caused by a combination of fatty acids (FA) and ethanol or by certain bile acids (for example, TLC-S). These agents generate excessive Ca^{2+} signals in the PACs causing mitochondrial depolarization and therefore reduced mitochondrial ATP production (Gerasimenko *et al.* 2014). The excessive Ca^{2+} signals also cause intracellular trypsin activation. Necrosis in at least a proportion of PACs follows, releasing activated proteases, including trypsin and kallikrein into the interstitial fluid. Kallikrein catalyses the formation of BK from bradykininogen and BK in turn acts on PSCs to generate Ca^{2+} signals. Trypsin acts in the same way. These actions would amplify the direct actions of certain bile acids (e.g. taurocholate) and possibly fatty acids and ethanol on the PSCs. In these cells, Ca^{2+} signals activate the enzyme NO synthase, thereby producing NO and this gas may diffuse into neighbouring PACs and there, by mechanisms not yet understood, promote the necrotic process. This will then lead to additional protease release, further stimulating the PSCs, generating a vicious circle.

References

- Andersson E, Axelsson J, Eckerwall G, Ansari D & Andersson R (2010). Tissue factor in predicted severe acute pancreatitis. *World J Gastroenterol* **16**, 6128–6134.
- Ashby MC, Camello-Almaraz C, Gerasimenko OV, Petersen OH & Tepikin AV (2003). Long-distance communication between muscarinic receptors and Ca^{2+} release channels revealed by carbachol uncaging in cell-attached patch pipette. *J Biol Chem* **278**, 20860–20864.
- Atwater I, Ribalet B & Rojas E (1978). Cyclic changes in potential and resistance of the β -cell membrane induced by glucose in islets of Langerhans from mouse. *J Physiol* **278**, 117–139.
- Blais C, Adam A, Massicotte D & Peronnet F (1999). Increase in blood bradykinin concentration after eccentric weight-training in men. *J Appl Physiol* **87**, 1197–1201.
- Bolander RP (1974). Stereological analysis of the guinea pig pancreas. *J Cell Biol* **61**, 269–287.
- Burdakov D, Gerasimenko O & Verkhatsky A (2005). Physiological changes in glucose differentially modulate the excitability of hypothalamic melanin-concentrating hormone and orexin neurons in situ. *J Neurosci* **25**, 2429–2433.
- Chen T-W, Wardill TJ, Sun Y, Pulver SR, Renninger SL, Baohan A, Schreiter ER, Kerr RA, Orger MB, Jayaraman V, Looger LL, Svoboda K & Kim DS (2013). Ultra-sensitive fluorescent proteins for imaging neuronal activity. *Nature* **499**, 295–300.
- Coughlin SR (2000). Thrombin signalling and protease-activated receptors. *Nature* **407**, 258–264.
- Criddle D, Murphy J, Fisetto G, Barrow S, Tepikin AV, Neoptolemos JP, Sutton R & Petersen OH (2006). Fatty acid ethyl esters cause pancreatic calcium toxicity via inositol trisphosphate receptors and loss of ATP synthesis. *Gastroenterology* **130**, 781–793.
- Dean PM & Matthews EK (1970). Glucose-induced electrical activity in pancreatic islet cells. *J Physiol* **210**, 255–264.
- Dean PM, Matthews EK & Sakamoto Y (1975). Pancreatic islet cells: effects of monosaccharides, glycolytic intermediates and metabolic inhibitors on membrane potential and electrical activity. *J Physiol* **246**, 459–478.
- Deschodt-Lanckman M, Robberecht P, De Neef ML & Christophe J (1976). *In vitro* action of bombesin and bombesin-like peptides on amylase secretion, calcium efflux, and adenylate cyclase activity in the rat pancreas. *J Clin Invest* **58**, 891–898.
- Di Capite JL, Bates GJ & Parekh AB (2011). Mast cell CRAC channel as a novel therapeutic target in allergy. *Curr Opin Allergy Clin Immunol* **11**, 33–38.
- Fels B, Nielsen N & Schwab A (2016). Role of TRPC1 channels in pressure-mediated activation of murine pancreatic stellate cells. *Eur Biophys J* **45**, 657–670.
- Ferde PE & Jakubowska MA (2017). Biology of pancreatic stellate cells – more than just cancer. *Pflügers Arch* **469**, 1039–1050.
- Ferde PE, Jakubowska MA, Gerasimenko JV, Gerasimenko OV & Petersen OH (2016). Bile acids induce necrosis in pancreatic stellate cells dependent on calcium entry and sodium-driven bile uptake. *J Physiol* **594**, 6147–6164.
- Gerasimenko JV, Gryshchenko O, Ferdek PE, Stapleton E, Hebert TOG, Bychkova S, Peng S, Begg M, Gerasimenko OV & Petersen OH (2013). Ca^{2+} release-activated Ca^{2+} channel blockade as a potential tool in antipancreatitis therapy. *Proc Natl Acad Sci USA* **110**, 13186–13191.
- Gerasimenko JV, Gerasimenko OV & Petersen OH (2014). The role of Ca^{2+} in the pathophysiology of pancreatitis. *J Physiol* **592**, 269–280.
- Griesbacher T, Tiran B & Lembeck F (1993). Pathological events in experimental acute pancreatitis prevented by the bradykinin antagonist Hoe 140. *Br J Pharmacol* **108**, 405–411.
- Griesbacher T, Rainer I, Titan B, Fink E, Lembeck F & Peskar BA (2003). Mechanism of kinin release during experimental acute pancreatitis in rats: evidence for pro- as well as anti-inflammatory roles of oedema formation. *Br J Pharmacol* **139**, 299–308.
- Gryshchenko O, Gerasimenko JV, Gerasimenko OV & Petersen OH (2016). Ca^{2+} signals mediated by bradykinin type 2 receptors in normal pancreatic stellate cells can be inhibited by specific Ca^{2+} channel blockade. *J Physiol* **594**, 281–293.
- Hegyi P & Petersen OH (2013). The exocrine pancreas: the acinar-ductal tango in physiology and pathophysiology. *Rev Physiol Biochem Pharmacol* **165**, 1–30.
- Hirata M, Hayashi I, Yoshimura K, Ishi K, Soma K, Ohwada T, Kakita A & Majima M (2002). Blockade of bradykinin B2 receptor suppresses acute pancreatitis induced by obstruction of the pancreaticobiliary duct in rats. *Br J Pharmacol* **135**, 29–36.
- Huang W, Booth DM, Cane MC, Chvanov M, Javed MA, Elliott VL, Armstrong JA, Dingsdale H, Cash N, Li Y, Greenhalf W, Mukherjee R, Kaphalia BS, Jaffar M, Petersen OH, Tepikin AV, Sutton R & Criddle DN (2014). Fatty acid ethyl ester synthase inhibition ameliorates ethanol-induced Ca^{2+} -dependent mitochondrial dysfunction and acute pancreatitis. *Gut* **63**, 1313–1324.
- Huang W, Cane MC, Mukherjee R, Szatmary P, Zhang X, Elliott V, Ouyang Y, Chvanov M, Latawiec D, Wen L, Booth DM, Haynes AC, Petersen OH, Tepikin AV, Criddle DN & Sutton R (2017). Caffeine protects against experimental acute pancreatitis by inhibition of inositol 1,4,5-trisphosphate receptor-mediated Ca^{2+} release. *Gut* **66**, 301–313.
- Iwatsuki N & Petersen OH (1978). *In vitro* action of bombesin on amylase secretion, membrane potential and membrane resistance in rat and mouse pancreatic acinar cells. A comparison with other secretagogues. *J Clin Invest* **61**, 41–46.
- Jakubowska MA, Ferdek PE, Gerasimenko OV, Gerasimenko JV & Petersen OH (2016). Nitric oxide signals are interlinked with calcium signals in normal pancreatic stellate cells upon oxidative stress and inflammation. *Open Biol* **6**, 160149.
- Laposata EA & Lange LG (1986). Presence of nonoxidative ethanol metabolism in human organs commonly damaged by ethanol abuse. *Science* **231**, 497–499.
- Liang T, Dolai S, Xie L, Winter E, Orabi AI, Karimian N, Cosen-Binker LI, Huang Y-C, Thorn P, Cattal MS & Gaisano HY (2017). *Ex vivo* human pancreatic slice preparations offer a valuable model for studying pancreatic exocrine biology. *J Biol Chem* **292**, 5957–5969.

- Maleth J & Hegyi P (2014). Calcium signalling in pancreatic duct epithelial cells: an old friend or a nasty enemy. *Cell Calcium* **55**, 337–345.
- Mankad P, James A, Siriwardena AK, Elliott AC & Bruce JIE (2012). Insulin protects pancreatic acinar cells from cytosolic calcium overload and inhibition of plasma membrane calcium pump. *J Biol Chem* **287**, 1823–1836.
- Murphy JA, Criddle DN, Sherwood M, Chvanov M, Mukherjee R, McLaughlin E, Booth D, Gerasimenko JV, Raraty MGT, Ghaneh P, Neoptolemos JP, Gerasimenko OV, Tepikin AV, Green GM, Reeve JR Jr, Petersen OH & Sutton R (2008). Direct activation of cytosolic Ca^{2+} signaling and enzyme secretion by cholecystokinin in human pancreatic acinar cells. *Gastroenterology* **135**, 632–641.
- Naumann T, Härtig W & Frotscher M (2000). Retrograde tracing with Fluoro Gold: different methods of tracer detection at the ultrastructural level and neurodegenerative changes of back-filled neurons in long-term studies. *J Neurosci Methods* **103**, 11–21.
- Nielsen N, Kondratska K, Ruck T, Hild B, Kovalenko I, Schimmelpfennig S, Welzig J, Sargin S, Lindemann O, Christian S, Meuth SG, Prevarskaya N & Schwab A (2017). TRPC6 channels modulate the response of pancreatic stellate cells to hypoxia. *Pflügers Arch* **469**, 1567–1577.
- Orlov V & Belyakov N (1978). Blood kallikrein-kinin system in acute pancreatitis. *Am J Gastroenterol* **70**, 645–648.
- Pang TCY, Wilson JS & Apte MV (2017). Pancreatic stellate cells: what's new? *Curr Opin Gastroenterol* **33**, 366–373.
- Parekh AB (2010). Store-operated CRAC channels: function in health and disease. *Nat Rev Drug Disc* **9**, 399–410.
- Pearson GT, Davison JS, Collins RC & Petersen OH (1981a). Control of enzyme secretion by non-cholinergic, non-adrenergic nerves in guinea pig pancreas. *Nature* **290**, 259–261.
- Pearson GT, Singh J, Daoud MS, Davison JS & Petersen OH (1981b). Control of pancreatic cyclic nucleotide levels and amylase secretion by noncholinergic, nonadrenergic nerves. *J Biol Chem* **256**, 11025–11031.
- Peng S, Gerasimenko JV, Tsugorka T, Gryshchenko O, Samarasinghe S, Petersen OH & Gerasimenko OV (2016). Calcium and adenosine triphosphate control of cellular pathology: asparaginase-induced pancreatitis elicited via protease-activated receptor 2. *Phil Trans R Soc B* **371**, 20150423.
- Petersen OH (1992). Stimulus-secretion coupling: cytoplasmic calcium signals and the control of ion channels in exocrine acinar cells. *J Physiol* **448**, 1–51.
- Petersen OH & Tepikin AV (2008). Polarized calcium signaling in exocrine gland cells. *Annu Rev Physiol* **70**, 273–299.
- Petersen OH, Courjaret R & Machaca K (2017). Ca^{2+} tunneling through the ER lumen as a mechanism for delivering Ca^{2+} entering via store-operated Ca^{2+} channels to specific target sites. *J Physiol* **595**, 2999–3014.
- Petho G & Reeh PW (2012). Sensory and signalling mechanisms of bradykinin, eicosanoids, platelet-activating factor, and nitric oxide in peripheral nociceptors. *Physiol Rev* **92**, 1699–1775.
- Samad A, James A, Wong J, Mankad P, Whitehouse J, Patel W, Alves-Simoes M, Siriwardena AK & Bruce JIE (2014). Insulin protects pancreatic acinar cells from palmitoleic acid-induced cellular injury. *J Biol Chem* **289**, 23582–23595.
- Sankaran H, Iwamoto Y, Korc M, Williams JA & Goldfine ID (1981). Insulin action in pancreatic acini from streptozotocin-treated rats. 2. Binding of I-125-insulin to receptors. *Am J Physiol* **240**, G63–G68.
- Schachter M (1969). Kallikreins and kinins. *Physiol Rev* **49**, 509–547.
- Scheele GA & Haymovits A (1978). Calcium-dependent discharge of secretory proteins in guinea pig pancreatic lobules. *Ann NY Acad Sci* **307**, 648–652.
- Scheele G & Haymovits A (1980). Potassium- and ionophore A23187-induced discharge of secretory protein in guinea pig pancreatic lobules. *J Biol Chem* **255**, 4918–4927.
- Singh J (1985). Mechanism of action of insulin on acetylcholine-evoked amylase secretion in the mouse pancreas. *J Physiol* **358**, 469–482.
- Storck H, Hild B, Schimmelpfennig S, Sargin S, Nielsen N, Zaccagnino A, Budde T, Novak I, Kalthoff H & Schwab A (2017). Ion channels in control of pancreatic stellate cell migration. *Oncotarget* **8**, 769–784.
- Van Laethem J-L, Robberecht P, Resibois A & Deviere J (1996). Transforming growth factor β promotes development of fibrosis after repeated courses of acute pancreatitis in mice. *Gastroenterology* **110**, 576–582.
- Wen L, Voronina S, Javed MA, Awais M, Szatmary P, Latawiec D, Chvanov M, Collier D, Huang W, Barrett J, Begg M, Stauderman K, Roos J, Grigoryev S, Ramos S, Rogers E, Whitten J, Velicelebi G, Dunn M, Tepikin AV, Criddle DN & Sutton R (2015). Inhibitors of ORAI1 prevent cytosolic calcium-associated injury of human pancreatic acinar cells and acute pancreatitis in 3 mouse models. *Gastroenterology* **149**, 481–492.

Additional information

Competing interests

The authors declare no competing interests.

Author contributions

All experiments were carried out in the School of Biosciences at Cardiff University. All authors jointly conceived the project. OG and JVG carried out the experiments with help from SP, and these were then also analysed by OVG. JVG created the figures and OHP wrote the paper with significant intellectual input from all the other authors. All authors have approved the final version of the manuscript.

Funding

The work was supported by grants from the Medical Research Council (UK) (MR/J002771/1 and G19/22/2).

Translational perspective

Our new data indicate that the pancreatic stellate cells play an important role in acute pancreatitis. They are key amplifying elements in a process resulting in necrotic acinar cell death. Initial release of proteases—including trypsin and kallikrein—from a small proportion of dying acinar cells generates Ca^{2+} signals in the stellate cells which then, probably via formation of the diffusible gas nitric oxide in these cells, causes more acinar necrosis which, via release of proteases from the further damaged acinar cells, causes additional stellate cell stimulation, thereby generating a vicious circle. These findings have potential therapeutic implications, as they indicate that interventions that would break this vicious circle could be helpful in the treatment of acute pancreatitis, a disease for which there is currently no authorized rational therapy. The key elements in the vicious circle promoting acinar necrosis would appear to be the actions of bradykinin, generated by the action of kallikrein, and trypsin on specific stellate cell receptors. These actions cause rises in the cytosolic Ca^{2+} concentration in the stellate cells, which activate the Ca^{2+} -sensitive enzyme nitric oxide synthase, producing the very diffusible nitric oxide, which in this situation appears to be toxic for the acinar cells. There are clear pharmacological interventions that could prove effective. Bradykinin receptor antagonists, antagonists of protease-activated receptors and inhibitors of nitric oxide synthase could all be helpful. Given that excessive Ca^{2+} signal generation in both stellate and acinar cells are critical elements, our previous proposal of treating acute pancreatitis with inhibitors of store-operated Ca^{2+} entry via the so-called CRAC channels, which has received further support from our new results, remains valid. However, it may well turn out that combination therapy with Ca^{2+} channel inhibitors and, for example, bradykinin receptor antagonists, could be particularly helpful and would allow relatively low doses of these agents to be used, thereby minimizing potential side effects.

4.2. Кальцій та аденозинтрифосфат контролюють клітинну патологію

PHILOSOPHICAL
TRANSACTIONS B

rstb.royalsocietypublishing.org

Research



Cite this article: Peng S, Gerasimenko JV, Tsugorka T, Gryshchenko O, Samarasinghe S, Petersen OH, Gerasimenko OV. 2016 Calcium and adenosine triphosphate control of cellular pathology: asparaginase-induced pancreatitis elicited via protease-activated receptor 2. *Phil. Trans. R. Soc. B* **371**: 20150423. <http://dx.doi.org/10.1098/rstb.2015.0423>

Accepted: 20 April 2016

One contribution of 15 to a Theo Murphy meeting issue 'Evolution brings Ca^{2+} and ATP together to control life and death'.

Subject Areas:
physiology

Keywords:
calcium, adenosine triphosphate, asparaginase, pancreatitis, leukaemia, calcium channels

Authors for correspondence:

Ole H. Petersen

e-mail: petersenoh@cardiff.ac.uk

Oleg V. Gerasimenko

e-mail: gerasimenkoov@cardiff.ac.uk

Calcium and adenosine triphosphate control of cellular pathology: asparaginase-induced pancreatitis elicited via protease-activated receptor 2

Shuang Peng^{1,2}, Julia V. Gerasimenko¹, Tatiana Tsugorka¹,
Oleksiy Gryshchenko^{1,3}, Sujith Samarasinghe⁴, Ole H. Petersen^{1,5}
and Oleg V. Gerasimenko¹

¹Cardiff School of Biosciences, Cardiff University, Cardiff CF10 3AX, Wales, UK

²Department of Pathophysiology, Medical College, Jinan University, Guangzhou 510632, People's Republic of China

³Bogomoletz Institute of Physiology, Kiev 01024, Ukraine

⁴Great Ormond Street Hospital for Children NHS Foundation Trust, Great Ormond Street, London WC1N 3JH, UK

⁵Systems Immunity Research Institute, Cardiff University, Cardiff CF14 4XN, Wales, UK

OHP, 0000-0002-6998-0380

Exocytotic secretion of digestive enzymes from pancreatic acinar cells is elicited by physiological cytosolic Ca^{2+} signals, occurring as repetitive short-lasting spikes largely confined to the secretory granule region, that stimulate mitochondrial adenosine triphosphate (ATP) production. By contrast, sustained global cytosolic Ca^{2+} elevations decrease ATP levels and cause necrosis, leading to the disease acute pancreatitis (AP). Toxic Ca^{2+} signals can be evoked by products of alcohol and fatty acids as well as bile acids. Here, we have investigated the mechanism by which L-asparaginase evokes AP. Asparaginase is an essential element in the successful treatment of acute lymphoblastic leukaemia, the most common type of cancer affecting children, but AP is a side-effect occurring in about 5–10% of cases. Like other pancreatitis-inducing agents, asparaginase evoked intracellular Ca^{2+} release followed by Ca^{2+} entry and also substantially reduced Ca^{2+} extrusion because of decreased intracellular ATP levels. The toxic Ca^{2+} signals caused extensive necrosis. The asparaginase-induced pathology depended on protease-activated receptor 2 and its inhibition prevented the toxic Ca^{2+} signals and necrosis. We tested the effects of inhibiting the Ca^{2+} release-activated Ca^{2+} entry by the Ca^{2+} channel inhibitor GSK-7975A. This markedly reduced asparaginase-induced Ca^{2+} entry and also protected effectively against the development of necrosis.

This article is part of the themed issue 'Evolution brings Ca^{2+} and ATP together to control life and death'.

1. Background

The importance of Ca^{2+} for the control of secretion has been known for a long time [1]. However, it was only through a detailed analysis—using permeabilized adrenal chromaffin cells—that the intracellular requirements for exocytotic secretion were clarified [2]. This work established that secretion occurs when the intracellular free Ca^{2+} concentration ($[\text{Ca}^{2+}]_i$) increases from the basic level (around 100 nM) to the low μM range if, and only if, Mg-adenosine triphosphate (ATP; 0.5–5 mM) is present [2]. Under physiological conditions, the rise in $[\text{Ca}^{2+}]_i$ that initiates secretion from intact chromaffin cells, as well as nerve endings, is owing to Ca^{2+} entering the cells through voltage-gated Ca^{2+} channels [2–4]. This is, however, fundamentally different from what happens in the electrically

non-excitable exocrine gland cells [5,6], where neurotransmitter- or hormone-evoked enzyme and fluid secretion are initiated by release of Ca^{2+} from the endoplasmic reticulum (ER) [7], mediated by the intracellular messenger inositol 1,4,5-trisphosphate (IP_3) [8]. The primary intracellular Ca^{2+} release is followed by secondary Ca^{2+} entry from the extracellular solution, and this Ca^{2+} influx does not occur through voltage-gated Ca^{2+} channels, but via Ca^{2+} release-activated Ca^{2+} (CRAC) channels [9].

The physiologically relevant Ca^{2+} signals that control secretion in the pancreatic acinar cells occur as repetitive local $[\text{Ca}^{2+}]_i$ spikes in the apical secretory granule region [10,11], owing to primary Ca^{2+} release from thin strands of ER penetrating into this region [12,13], which is dominated by zymogen granules (ZG). These ER strands are fully functionally connected (ER tunnels) to the principal ER store dominating the basal region [12,13]. The IP_3 receptors (IP_3Rs) are concentrated in the apical area [11,14,15] and the functional ER tunnels effectively allow Ca^{2+} to be mobilized from the main basal store into the apical secretory granule area [12]. Plasma membrane Ca^{2+} pumps, concentrated in the apical (secretory) membrane [16], extrude Ca^{2+} from the cell during each Ca^{2+} spike, and compensatory Ca^{2+} entry and uptake into the ER are therefore necessary. This occurs through conventional [17] CRAC channels [9] localized in the baso-lateral membrane [12,18], and Ca^{2+} entering through these channels is immediately taken up into the ER by powerful Ca^{2+} pumps in the ER membrane [12]. The physiological apical Ca^{2+} release via IP_3Rs in that region results in apically confined $[\text{Ca}^{2+}]_i$ spikes owing to the mitochondrial firewall separating the ZG-containing part of the cell from the ER-dominated baso-lateral part [19]. During each apical Ca^{2+} spike, Ca^{2+} is taken up into the peri-granular mitochondria and then slowly released [13,20]. This mitochondrial Ca^{2+} uptake, activating several Ca^{2+} -sensitive dehydrogenases in the Krebs cycle [21], results in an increased cytosolic ATP level, despite the increased ATP utilization [22]. This is helpful for powering the exocytotic secretory process.

Whereas the Ca^{2+} release evoked by the neurotransmitter acetylcholine (ACh) is primarily mediated by IP_3 acting on IP_3Rs [23,24], the Ca^{2+} release elicited by physiological concentrations of the hormone cholecystokinin (CCK) is primarily mediated by the Ca^{2+} -releasing messenger nicotinic acid adenine dinucleotide phosphate (NAADP) [25–27]. The action of NAADP depends on functional ryanodine receptors (RyRs) and two-pore channels (TPCs) and also involves acid Ca^{2+} stores [27]. Physiological Ca^{2+} spiking, irrespective of whether it is evoked by ACh or CCK, depends on both functional IP_3Rs and RyRs [13,25].

Although the acinar cells in the pancreas are quantitatively dominant and perform the most crucial physiological role in the exocrine pancreas, by synthesizing and secreting the digestive (pro-) enzymes that are essential for the digestion of food in the intestine, there are other cells that need to be considered. The acinar cells secrete fluid together with the enzymes [5], but most of the fluid carrying the enzymes into the gut is produced by the duct cells, principally regulated by secretin-evoked cyclic AMP formation rather than by Ca^{2+} signals [28,29]. The acinar–ductal system is functionally integrated and regulation of one cell type has influence on the other [30]. The physiological role of the more recently discovered periacinar stellate cells has not yet been fully clarified, but they

generate substantial Ca^{2+} signals in response to concentrations of bradykinin that have been measured in plasma during exercise and pancreatitis [31,32]. They do not respond to the principal controllers of acinar cell function, namely ACh or CCK [31,32].

In the normal digestion process, the inactive acinar pancreatic pro-enzymes, which are secreted by exocytosis into the acinar lumen, are carried into the gut by acinar and ductal fluid secretion and then activated in the gut [33]. In acute pancreatitis (AP), a potentially fatal human disease, the inactive pancreatic pro-enzymes become active enzymes inside the acinar cells, digesting the pancreas and its surroundings. The main causes of AP are biliary disease (gallstone complications) and alcohol abuse [33]. More than 20 years ago, it was proposed that AP is essentially a disease brought about by excessive cytosolic Ca^{2+} signals [34] and since then a substantial amount of evidence in favour of this hypothesis has accumulated [35–38]. Pathological stimuli—for example, combinations of alcohol and fatty acids or bile acids—can evoke excessive release of Ca^{2+} from internal stores followed by excessive Ca^{2+} entry through store-operated CRAC channels, resulting in sustained global elevations of $[\text{Ca}^{2+}]_i$ [38]. This causes intracellular protease activation [38] and excessive mitochondrial Ca^{2+} uptake, leading to opening of the mitochondrial permeability transition pore (MPTP) [20,39]. The MPTP opening causes depolarization of the inner mitochondrial membrane, resulting in failure of the normal mitochondrial ATP production [20,39]. The lack of ATP prevents the acinar cells from disposing of the excess Ca^{2+} in the cytosol and, in combination with the abnormal intracellular protease activity, this leads to necrosis. It is the acinar necrosis that generates the damaging inflammatory response [39–42]. Since the primary pathological event in AP is the excessive and sustained $[\text{Ca}^{2+}]_i$ elevation and as this depends on excessive Ca^{2+} entry through CRAC channels, it would be logical, as a therapy, to target these Ca^{2+} entry channels. Gerasimenko *et al.* [9,38] demonstrated, in experiments on isolated mouse acinar cell clusters, that the intracellular protease activation and necrosis evoked by fatty acid ethyl esters—non-oxidative combinations of ethanol and fatty acids, which are important mediators of alcohol-related pancreatitis [33]—could be effectively inhibited by specific pharmacological blockade of CRAC channels. These results have recently been confirmed *in vivo*, in three different mouse models of AP [43], giving hope that CRAC channel blockade may become the first rational and effective therapy against AP [44].

As both alcohol-related and bile-induced AP are owing to toxic Ca^{2+} signal generation, it seems possible that all types of AP are Ca^{2+} toxicity diseases. We were therefore interested in exploring the mechanism underlying pancreatitis caused by a side-effect of L-asparaginase, which is used for the treatment of acute lymphoblastic leukaemia (ALL). L-asparaginase is a well-known anticancer agent effective against lymphoid malignancies. Since 1971, it has been an essential element in the successful treatment of ALL, the most common type of cancer affecting children [45,46]. However, asparaginase treatment can result in AP (asparaginase-associated pancreatitis (AAP)). This occurs in about 5–10% of cases and AAP is the most frequent cause of discontinuing the asparaginase treatment [47–50]. The mechanism underlying the development of AAP has so far not been explored [48].

The aim of the present study was to define the mechanism underlying AAP and then to identify potential steps for

therapeutic intervention. As outlined above, the history of our path to the current understanding of AP shows that studies on isolated cells or cell clusters have been enormously helpful and our approach has therefore been to study, for the first time, the effects of asparaginase on isolated mouse acinar cells or cell clusters. As *in vitro* results concerning the effects of, for example, fatty acid ethyl esters or bile acids [9,38,43] have turned out to be excellent predictors of the outcome of studies of real AP *in vivo* [39,43,51], acute studies on isolated cells are a natural starting point for investigations of the mechanism of AAP.

Our results show that asparaginase acts on protease-activated receptor 2 (PAR2) to evoke sustained elevations of $[Ca^{2+}]_i$ owing to release of Ca^{2+} from internal stores, followed by Ca^{2+} entry from the extracellular solution. The sustained $[Ca^{2+}]_i$ elevation reduces ATP formation. These effects can be markedly reduced by specific pharmacological blockade of CRAC channels, which also markedly reduces the extent of necrosis.

2. Results

(a) Asparaginase increases $[Ca^{2+}]_i$ in pancreatic acinar cells

Pancreatitis-inducing agents, combinations of ethanol and fatty acids or bile acids, are able to elevate $[Ca^{2+}]_i$ in isolated acinar cell clusters causing intracellular Ca^{2+} overload. This is owing to Ca^{2+} release from internal stores triggering excessive store-operated Ca^{2+} entry [9,38]. To identify the mechanism of action of asparaginase, we therefore started out by testing the effects of asparaginase on $[Ca^{2+}]_i$ over a wide concentration range. One of the challenges inherent in this approach is that the time course needed for a study on normal freshly isolated cells is quite different from that of the development of AAP in the clinical situation. AAP typically develops several days after several injections (over many weeks) of asparaginase [49], whereas studies on isolated cells in the laboratory require observations of the effects of asparaginase within hours. In the present study, we have worked with the lowest concentration of asparaginase that reliably evoked cellular changes that are similar to those previously found to be associated with AP initiated by alcohol metabolites or bile acids.

We found that only in some cells did a low concentration of asparaginase (20 IU ml⁻¹) induce $[Ca^{2+}]_i$ oscillations (9 out of 42 cells). Figure 1a shows a representative positive trace with repetitive Ca^{2+} spikes induced by 20 IU ml⁻¹, whereas figure 1b represents the more typical negative response (33 out of 42 cells), in which the same concentration of asparaginase failed to cause any change in $[Ca^{2+}]_i$. A higher concentration of asparaginase (200 IU ml⁻¹) elicited repetitive $[Ca^{2+}]_i$ oscillations, mostly on top of a sustained elevated $[Ca^{2+}]_i$ (43 out of 55 cells; figure 1c). The development of a sustained $[Ca^{2+}]_i$ elevation has previously been shown to be a distinctive characteristic of $[Ca^{2+}]_i$ changes induced by pathological concentrations of alcohol metabolites or bile acids [9,38], and we found that an elevated $[Ca^{2+}]_i$ plateau, although often small, was seen in the vast majority of cells (52 out of 55) stimulated by asparaginase (200 IU ml⁻¹). In some cases (12 out of 55), there were no, or very few, spikes superimposed on the elevated $[Ca^{2+}]_i$ plateau (figure 1d).

(b) The asparaginase-elicited sustained increase in $[Ca^{2+}]_i$ depends on the presence of external Ca^{2+}

Removal of external Ca^{2+} always terminated the elevated $[Ca^{2+}]_i$ plateau (figure 1c,d), but did not significantly ($p > 0.27$) change the amplitudes of the asparaginase-induced Ca^{2+} spikes ($n = 28$) within the time frame of our experiments (figure 1e). Ca^{2+} entry clearly plays an important role in the formation of the asparaginase-induced elevated $[Ca^{2+}]_i$ plateau and the role of Ca^{2+} entry was further demonstrated by increasing the external Ca^{2+} concentration to 2 mM during asparaginase stimulation, which caused a marked and sustained increase in $[Ca^{2+}]_i$ ($n = 18$; figure 1f). Subsequent removal of external Ca^{2+} and addition of the Ca^{2+} chelator EGTA (200 μ M) abolished the elevated $[Ca^{2+}]_i$ plateau, whereas the Ca^{2+} oscillations continued for some time (figure 1f).

It has previously been shown that the excessive Ca^{2+} entry into pancreatic acinar cells induced by alcohol metabolites or bile acids, as well as their pathological effects, can be markedly inhibited by the CRAC channel blockers GSK-7975A and CM-128 [9,43,52]. We have therefore tested the effect of CRAC blockade (GSK-7975A, 10 μ M) on the asparaginase-induced sustained $[Ca^{2+}]_i$ elevation and found that it was abolished in the presence of the inhibitor, although repetitive Ca^{2+} spiking was still observed within the time frame of our experiments (figure 1g, $n = 32$). Figure 1h summarizes the degree of inhibition, caused by removal of external Ca^{2+} or by GSK-7975A, of the integrated Ca^{2+} signal evoked by asparaginase.

(c) Asparaginase-elicited Ca^{2+} release involves inositol 1,4,5-trisphosphate receptors and ryanodine receptors as well as nicotinic acid adenine dinucleotide phosphate signalling

To investigate the involvement of intracellular Ca^{2+} release channels in asparaginase-induced $[Ca^{2+}]_i$ elevations, we have used caffeine, a substance known to reliably inhibit IP₃-mediated intracellular Ca^{2+} release in pancreatic acinar cells [23]. Caffeine (20 mM) substantially reduced the asparaginase-induced $[Ca^{2+}]_i$ elevations in a Ca^{2+} -free solution ($n = 8$; figure 2a; compare with figure 1e as the appropriate control). The phospholipase C (PLC) inhibitor U73122 (10 μ M) also significantly blocked the asparaginase-induced Ca^{2+} release as well as the response to 1 μ M ACh ($n = 11$; figure 2b). Ryanodine (100 μ M), inhibiting RyRs, also substantially reduced the asparaginase-induced $[Ca^{2+}]_i$ elevations ($n = 13$; figure 2c).

It has previously been shown that NAADP signalling in pancreatic acinar cells can be inactivated by the cell-permeable NAADP analogue, and selective antagonist, Ned-19 [27]. After pre-treatment of cells with 100 μ M Ned-19, the asparaginase (200 IU ml⁻¹)-induced $[Ca^{2+}]_i$ elevations were profoundly inhibited (virtually abolished; figure 2d, $n = 8$), whereas ACh (1 μ M), eliciting Ca^{2+} release via IP₃Rs independently of NAADP [25], was still able to evoke a typical $[Ca^{2+}]_i$ rise ($n = 8$; figure 2d).

(d) Protease-activated receptor 2 is involved

PAR2 is widely expressed in human and animal tissues, including the pancreas, and has previously been implicated

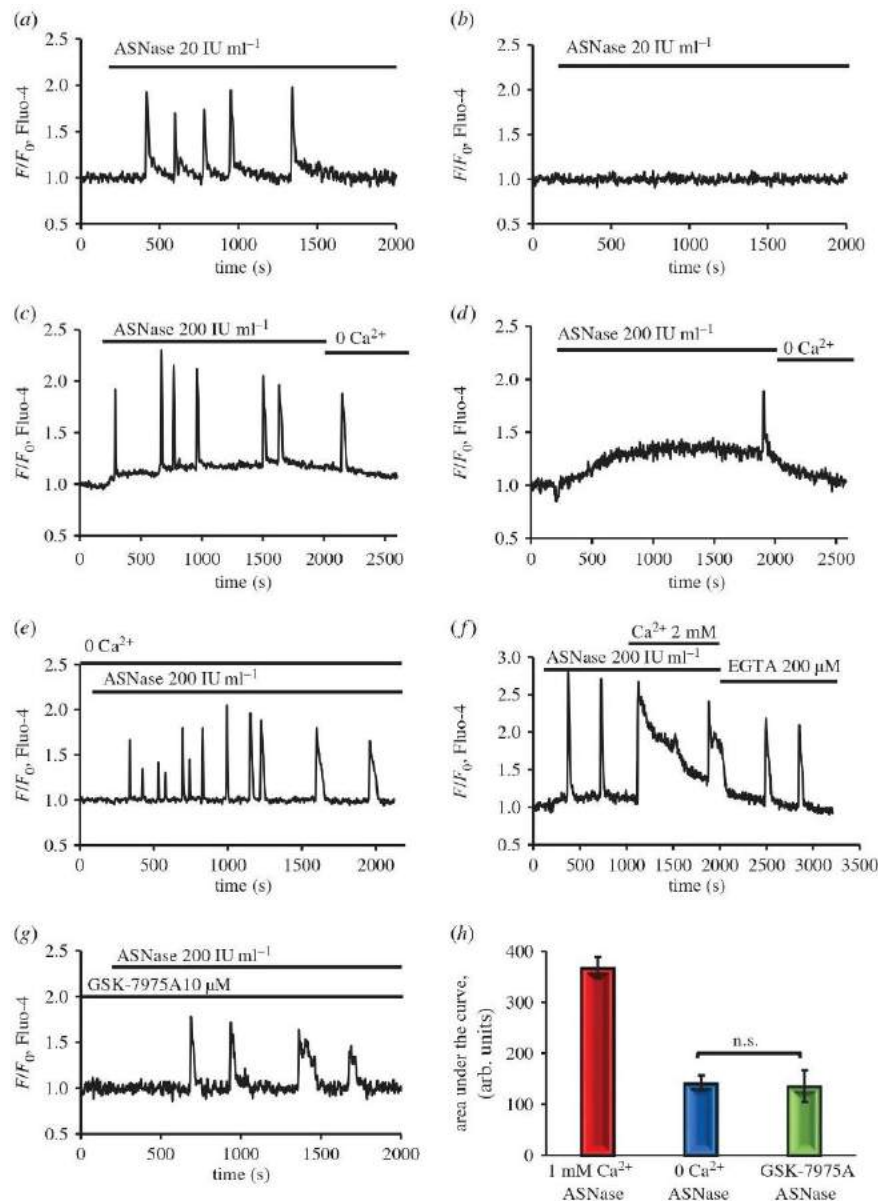


Figure 1. Asparaginase (ASNase) induces cytosolic Ca^{2+} signals in pancreatic acinar cells. A low concentration of asparaginase (20 IU ml^{-1}) induces repetitive Ca^{2+} spikes in a minority (9 out of 42) of experiments (a), but elicits no response in the majority (33 out of 42) of cases (b). A higher concentration of asparaginase (200 IU ml^{-1}) elicits an elevated $[\text{Ca}^{2+}]_i$ plateau in practically all cases (52 out of 55), often with repetitive Ca^{2+} transients on top of the plateau (43 out of 55) as shown in the representative trace (c). An elevated $[\text{Ca}^{2+}]_i$ plateau is the main type of response to asparaginase (200 IU ml^{-1} ; 52 out of 55), but in some cases (12 out of 55) with no or very few spikes (d). The sustained $[\text{Ca}^{2+}]_i$ elevation depends on the continued presence of Ca^{2+} in the external solution (c,d). In the absence of external Ca^{2+} , there is no elevated $[\text{Ca}^{2+}]_i$ plateau (e, $n = 28$). When the external Ca^{2+} concentration is increased from 1 to 2 mM, there is a marked transient $[\text{Ca}^{2+}]_i$ rise and a continuing elevated $[\text{Ca}^{2+}]_i$ plateau (f). When external Ca^{2+} is subsequently removed and a Ca^{2+} chelator (EGTA) added, the plateau gradually disappears (f; $n = 18$). In the presence of the CRAC channel blocker GSK-7975A ($10 \mu\text{M}$), asparaginase (200 IU ml^{-1}) evokes repetitive Ca^{2+} spikes without an elevated $[\text{Ca}^{2+}]_i$ plateau (g, $n = 32$). Comparison of the integrated Ca^{2+} signals ('area under the curve' from start of the Ca^{2+} signal until 1800 s later), in the presence of 1 mM external Ca^{2+} , in the absence of external Ca^{2+} and in the presence of 1 mM external Ca^{2+} with the addition of $10 \mu\text{M}$ GSK-7975A, shows that the absence of external Ca^{2+} ($n = 28$) or the addition of the CRAC blocker GSK-7975A ($n = 32$) significantly ($p < 0.0001$ in both cases) reduced the responses to asparaginase (200 IU ml^{-1} ; h). Bars represent mean \pm s.e.m. (Online version in colour.)

in the pathology of AP [53,54]. The activation of PAR family members is coupled to multiple heteromeric G proteins that lead to PLC activation and production of IP_3 and diacylglycerol [55]. Therefore, we tested the possibility that asparaginase could activate PAR2 by pre-treating the cells

with the PAR2 blocker FSLRLY-NH₂ ($10 \mu\text{M}$) before the addition of asparaginase (200 IU ml^{-1}). The PAR2 blocker reduced significantly (virtually abolished) the asparaginase-induced $[\text{Ca}^{2+}]_i$ oscillations as well as the sustained $[\text{Ca}^{2+}]_i$ elevation (figure 2e; $n = 32$).

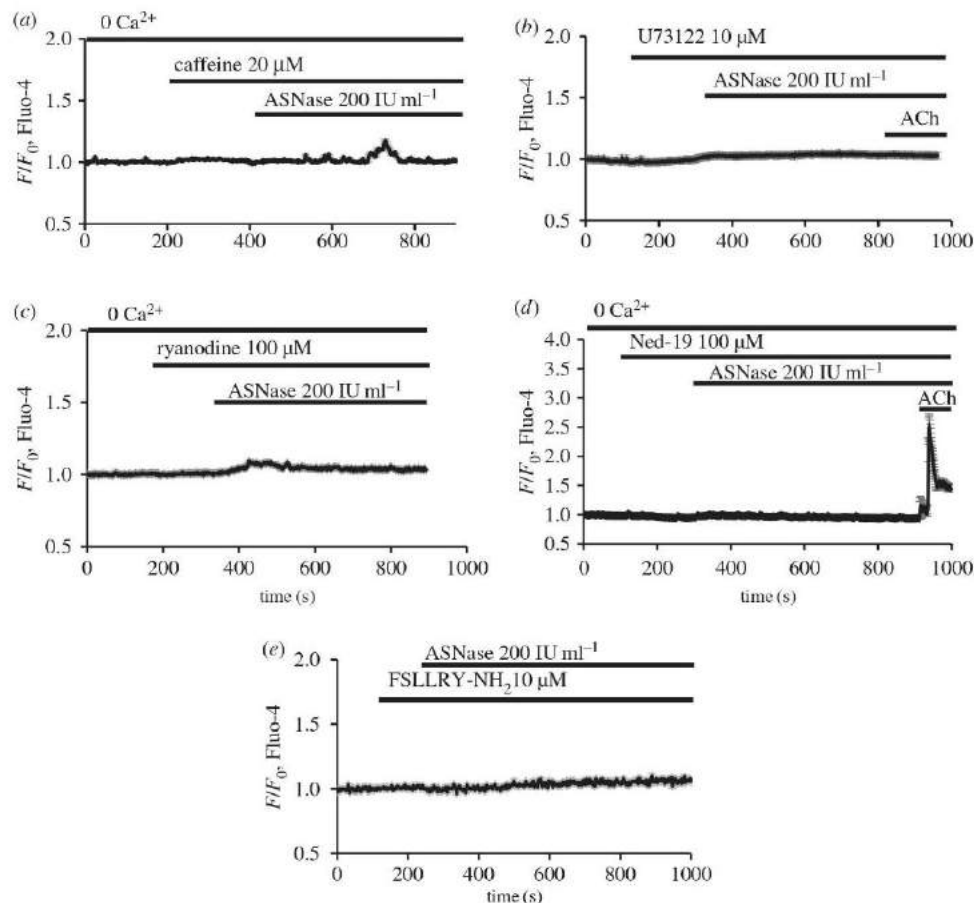


Figure 2. The primary intracellular Ca^{2+} release induced by asparaginase depends on IP_3 and NAADP signalling mechanisms. The IP_3 R blocker caffeine (20 mM) inhibited very markedly the asparaginase-induced $[\text{Ca}^{2+}]_i$ elevations in the absence of external Ca^{2+} (a, averaged trace, $n = 8$). The PLC inhibitor U73122 (10 μM) blocked the asparaginase-induced $[\text{Ca}^{2+}]_i$ elevation in the absence of external Ca^{2+} (b, averaged trace, $n = 11$). ACh (1 μM) was applied at the end of each experiment and, as expected, did not elicit any change in $[\text{Ca}^{2+}]_i$ (b) as its effect depends on IP_3 formation and IP_3 receptors [23,24]. Ryanodine (100 μM) markedly inhibited the asparaginase-induced Ca^{2+} signals in the absence of external Ca^{2+} (c, averaged trace, $n = 13$). Ned-19 (100 μM) prevented the asparaginase-induced $[\text{Ca}^{2+}]_i$ elevation in the absence of external Ca^{2+} (d, averaged trace, $n = 8$). ACh (1 μM) was applied at the end of each experiment and, as expected, caused a major $[\text{Ca}^{2+}]_i$ rise as its effect does not depend on NAADP receptors [25,27]. The asparaginase-induced Ca^{2+} signals were virtually eliminated by the PAR2 inhibitor FSLRY- NH_2 (10 μM ; e, averaged trace, $n = 32$).

(e) Ca^{2+} extrusion mechanisms are affected by asparaginase

To study Ca^{2+} movements in more detail, we have applied a specific protocol routinely used to assess Ca^{2+} entry and extrusion [9,38]. In these experiments, Ca^{2+} stores were emptied using the ER Ca^{2+} pump inhibitor cyclopiazonic acid (CPA) in a nominally Ca^{2+} -free solution. Thereafter, 2 mM of Ca^{2+} was added to the external solution for a short period and then removed (figure 3a). In the presence of asparaginase, the Ca^{2+} entry following external Ca^{2+} admission was significantly increased (figure 3a), assessed by both amplitude of the $[\text{Ca}^{2+}]_i$ change (figure 3b) and the rate of $[\text{Ca}^{2+}]_i$ increase (half-time of the increase, figure 3c). However, the quantitatively most important effect of asparaginase was to slow down the rate of Ca^{2+} extrusion after removal of external Ca^{2+} (figure 3a). The half-time of $[\text{Ca}^{2+}]_i$ recovery was more than three times longer than in the control cells (figure 3d).

(f) Asparaginase depletes intracellular adenosine triphosphate

Ca^{2+} extrusion is an energy-demanding process and has previously been found to be abnormal in pancreatic acinar cell pathologies owing to disruption of mitochondrial metabolism and, therefore, reduction of ATP levels [42]. We have conducted indirect assessments of intracellular changes in ATP concentration, using Magnesium Green (MgGreen) fluorescence measurements. As most of the intracellular ATP will be in the form of Mg-ATP, a reduction of the ATP concentration will increase the fluorescence intensity of MgGreen owing to the inevitable increase of $[\text{Mg}^{2+}]_i$ [56–58]. By this measure, asparaginase induced a substantial reduction of intracellular ATP levels (figure 4a) superseded only by the full ATP depletion caused by a mixture of the protonophore CCCP, oligomycin and iodoacetate [42].

Because the presence of external Ca^{2+} was important for the cytoplasmic and mitochondrial effects induced by

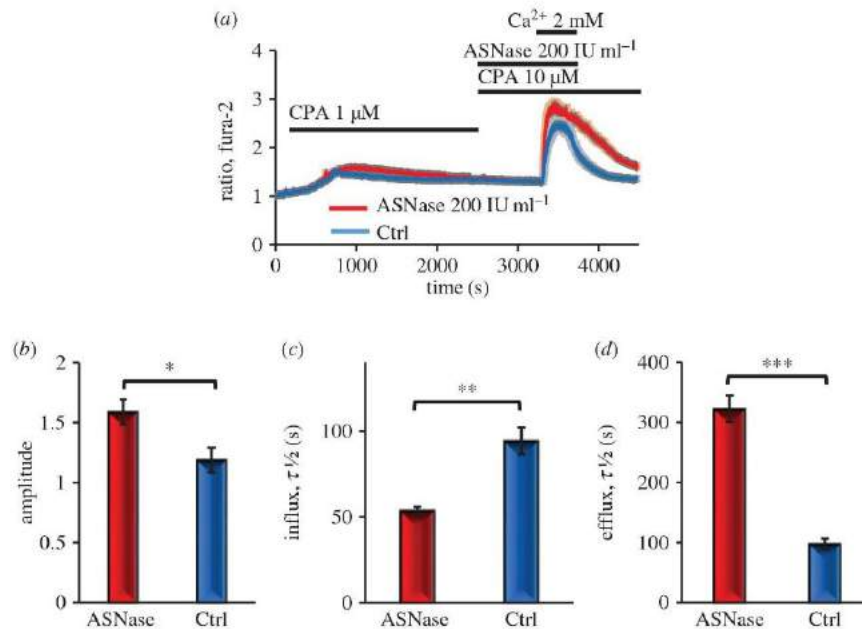


Figure 3. Asparaginase accelerates Ca^{2+} entry and substantially slows down Ca^{2+} extrusion. (a) In the absence of external Ca^{2+} , CPA, a specific inhibitor of the Ca^{2+} pump in the ER membrane, causes a modest and largely transient $[\text{Ca}^{2+}]_i$ rise. When subsequently 2 mM Ca^{2+} is added to the external solution, there is a marked rise in $[\text{Ca}^{2+}]_i$, which then declines after removal of external Ca^{2+} . In the presence of asparaginase (red averaged trace, $n = 32$), the amplitude (b) and the rate of rise of $[\text{Ca}^{2+}]_i$ (c) are somewhat increased ($p < 0.048$ and $p < 0.0001$, respectively) when compared with control (a, blue averaged trace, $n = 34$). The extrusion of Ca^{2+} by the plasma membrane Ca^{2+} pumps, observed as the decline in $[\text{Ca}^{2+}]_i$ following removal of external Ca^{2+} , is very markedly and significantly ($p < 0.0001$) reduced in the presence of asparaginase (a,d). (Online version in colour.)

asparaginase, we decided to check if inhibition of Ca^{2+} entry channels [9,43] could affect the ATP loss evoked by asparaginase. Blocking Ca^{2+} entry by GSK-7975A (10 μM) substantially reduced the ATP loss evoked by asparaginase (figure 4b).

(g) The effect of pyruvate

It has been shown previously that ethyl pyruvate (aliphatic ester derived from pyruvic acid [59]) attenuates the severe AP induced by sodium taurocholate in rats [59]. When we included 1 mM pyruvate in the external solution, we found that the asparaginase-induced ATP loss was substantially reduced compared with control experiments (figure 4c,d). The protective effect was significant and similar to what was achieved by GSK-7975A (figure 4b,d), although it did not give complete protection.

(h) Necrosis

We have previously shown that the cytosolic Ca^{2+} overload and ATP deprivation induced by fatty acid ethyl esters and bile acids lead to necrosis [38], and we have therefore now tested whether asparaginase can also induce necrosis, the hallmark of AP [33,38]. The extent of necrosis induced by asparaginase (200 IU ml⁻¹) treatment ($17.4 \pm 0.4\%$ of the cells; figure 5a) was comparable to, but somewhat smaller than, the level of necrosis induced by pamitoic acid ethyl ester (POAEE; $29 \pm 3.1\%$) or the bile acid taurocholic acid sulphate (TLC-S; $27.6 \pm 1.9\%$; figure 5a), whereas a lower concentration of asparaginase (20 IU ml⁻¹) did not increase the level of necrosis above that seen in control experiments (figure 5b). The CRAC channel

inhibitor GSK-7975A (10 μM) [9,43] reduced the asparaginase-induced necrosis to the control level ($4.5 \pm 0.7\%$; figure 5b). Pyrazole compounds have generally been thought to inhibit other types of cation channels, namely the relatively non-selective TRP (transient receptor potential) channels, which have significant Ca^{2+} permeability [60,61], but pyrazole6 (Pyr6) has been shown to have more of an effect on the very Ca^{2+} -selective CRAC channels [61], which are the ones specifically inhibited by GSK-7975A and CM-128 [9,43]. In our experiments, Pyr6 partially inhibited asparaginase-induced necrosis to $8.4 \pm 0.9\%$. Both caffeine and Ned-19 inhibited asparaginase-induced necrosis to control levels (4.2 ± 0.5 and $6.6 \pm 1.2\%$, respectively). A PAR2 inhibitor (FSLRLY-NH₂) significantly blocked asparaginase-induced necrosis (figure 5b). We also tested the effect of pyruvate on asparaginase-induced necrosis. As seen in figure 5b, this gave significant protection against necrosis. Figure 5c shows representative images of some of the cells under the treatment protocols, together with the results of staining for propidium iodide (PI). It is seen that asparaginase (200 IU ml⁻¹) elicited strong intracellular PI staining and that GSK-7975A provided protection against this.

Asparaginase kills lymphoblastic cells by depriving them of asparagine, which they—unlike normal cells—cannot produce themselves [62]. The effects of asparaginase on normal pancreatic acinar cells described in this study are therefore unlikely to be owing to asparagine deprivation. We tested whether there was any difference between the ability of asparaginase to induce necrosis in the absence or presence of asparagine. As seen in figure 5d, there was no difference in the necrosis levels evoked by asparaginase in the presence or absence of asparagine.

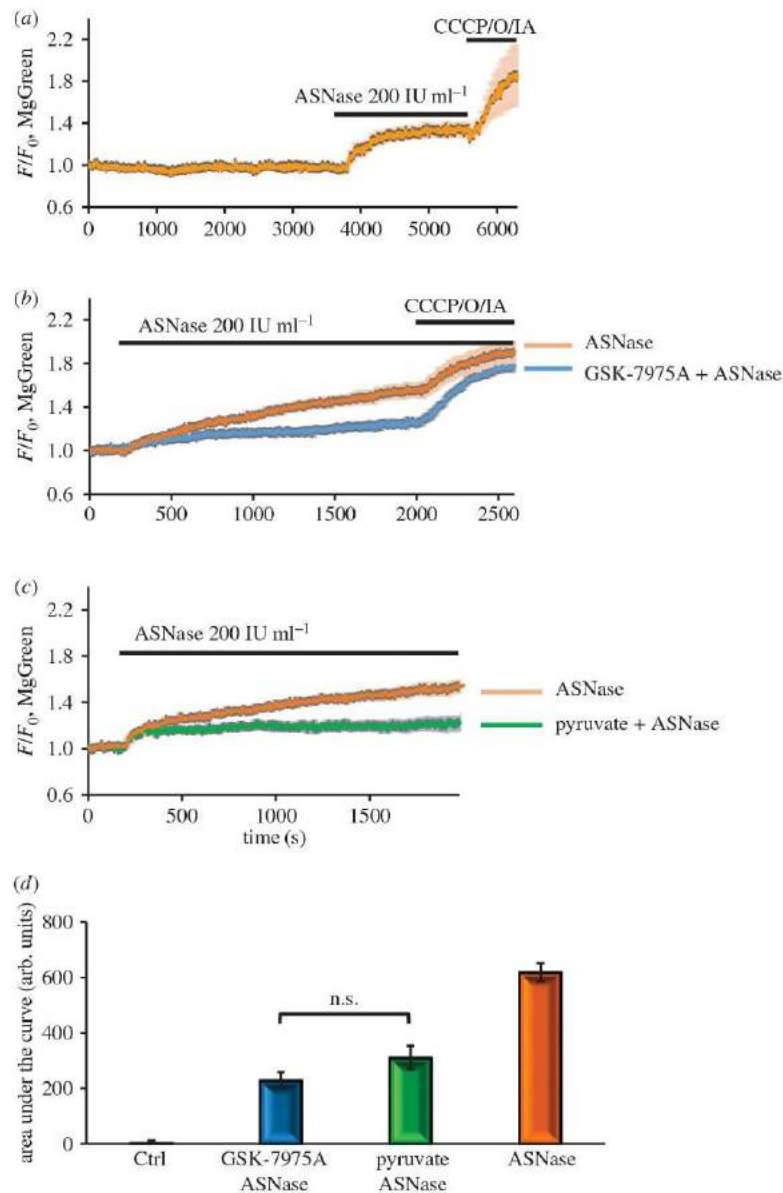


Figure 4. Asparaginase reduces intracellular ATP levels as assessed by increases in $[Mg^{2+}]_i$. In these experiments, changes in $[Mg^{2+}]_i$ were assessed by monitoring changes in MgGreen fluorescence. Most of the Mg^{2+} inside cells is bound to ATP, so when ATP declines—for example owing to interference with mitochondrial function— $[Mg^{2+}]_i$ will increase. A rise in $[Mg^{2+}]_i$ can therefore be taken to represent a reduction in the intracellular ATP level [58]. Asparaginase (200 IU ml⁻¹) markedly increased $[Mg^{2+}]_i$, and a further rise occurred after poisoning mitochondrial function with a cocktail of CCCP (5 nM), oligomycin (10 μ M) and sodium iodoacetate (2 mM; *a*, averaged trace, *n* = 39). The asparaginase effect was markedly reduced by GSK-7975A (*b*: orange averaged trace, *n* = 21; blue averaged trace, *n* = 39) and was also markedly reduced by supplementing the external medium with pyruvate (1 mM; *c*, *n* = 8). Comparisons of the integrated responses ('areas under the curve' from the start of the responses until 1800 s later) show that GSK-7975A and pyruvate significantly reduced the asparaginase-induced ATP depletion ($p < 0.0001$ for both treatments).

3. Discussion

The results presented here, on the asparaginase-elicited injury to pancreatic acinar cells, provide fresh evidence for the hypothesis that all types of AP are owing to toxic Ca^{2+} signal generation and explain how asparaginase could cause AP (figure 6). Asparaginase, like fatty acid ethyl esters and bile acids, can evoke sustained $[Ca^{2+}]_i$ elevation owing to release of Ca^{2+} from intracellular stores followed by store-operated Ca^{2+} entry through CRAC channels. Qualitatively, the effects

of asparaginase fit well with those induced by fatty acid ethyl esters and bile acids, which we have described previously [33,38]. However, the sustained $[Ca^{2+}]_i$ elevations evoked by asparaginase are somewhat smaller than those evoked by bile acids or fatty acid ethyl esters. Nevertheless asparaginase evokes significant reductions in the intracellular ATP levels and extensive necrosis. Further studies on mitochondrial Ca^{2+} handling during the action of asparaginase are warranted because the regulation of mitochondrial Ca^{2+} uptake under different conditions may be a critical issue [63,64].

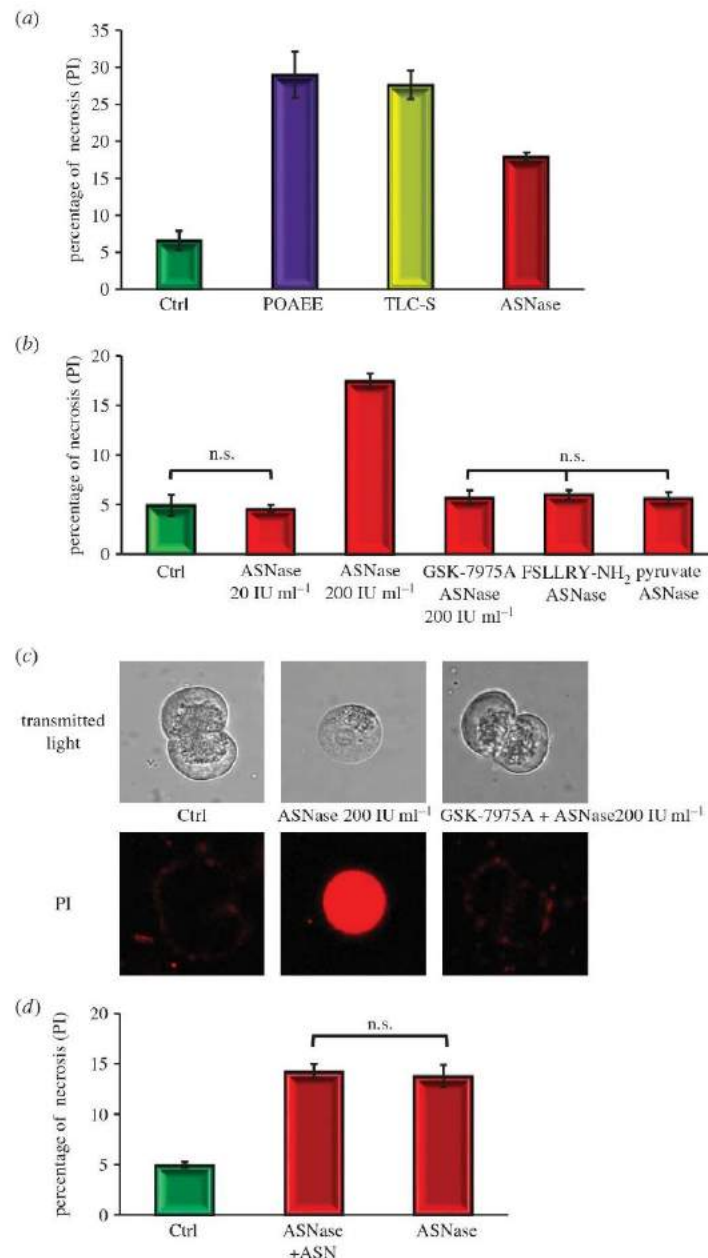


Figure 5. Asparaginase induces necrosis in pancreatic acinar cells. (a) The level of necrosis induced by 200 IU ml⁻¹ of asparaginase ($17.4 \pm 0.4\%$, eight series with $n > 250$) is comparable with, but somewhat lower than, that caused by the alcohol metabolite POAEE (100 μ M; $29 \pm 3.1\%$, three series of experiments with $n > 100$) or the bile acid TLC-S (200 μ M; $27.6 \pm 1.9\%$, three series of experiments with $n > 120$), whereas a lower concentration of asparaginase (20 IU ml⁻¹) did not induce any significant change in the level of necrosis (b) when compared with control (4.5 ± 0.4 and $4.5 \pm 0.7\%$, respectively, $p > 0.8$, each test had eight series of experiments with $n > 130$ of tested cells in each group). The CRAC channel inhibitor GSK-7975A (10 μ M) essentially abolished asparaginase-induced necrosis to a level not significantly different from control ($p > 0.24$), while significantly ($p < 0.0001$, eight series, $n > 70$) lower than that caused by 200 IU ml⁻¹ of asparaginase alone (b). The PAR2 inhibitor FSLRLRY-NH₂ (10 μ M) significantly blocked the asparaginase-induced necrosis ($p < 0.0001$; four series of experiments with $n > 150$ cells in each sample). Pyruvate (1 mM) reduced the asparaginase-induced necrosis to near the control level (b; $p < 0.0001$, three series of experiments with the number of tested cells in each group more than 130). (c) Representative images of cells from some of the experiments shown in (b). Transmitted light images (upper row) and PI-stained fluorescence images (lower row). (d) The presence or absence of asparagine (50 μ M) made no difference to the level of asparaginase-induced necrosis ($p > 0.75$, three series of experiments with more than 70 cells in each sample).

The findings presented in this study provide the first mechanistic insights into the process by which asparaginase treatment of ALL may cause AAP (figure 6). These insights also provide the first pointers to rational therapies (figure 6) that may prevent the currently necessary cessation of

asparaginase treatment of ALL in cases of severe pancreatitis. The most accessible therapeutic target is the Ca²⁺ entry route, namely the previously characterized CRAC channels [9,43,44,65]. We have now shown that the asparaginase-induced Ca²⁺ elevations depend on CRAC-mediated Ca²⁺

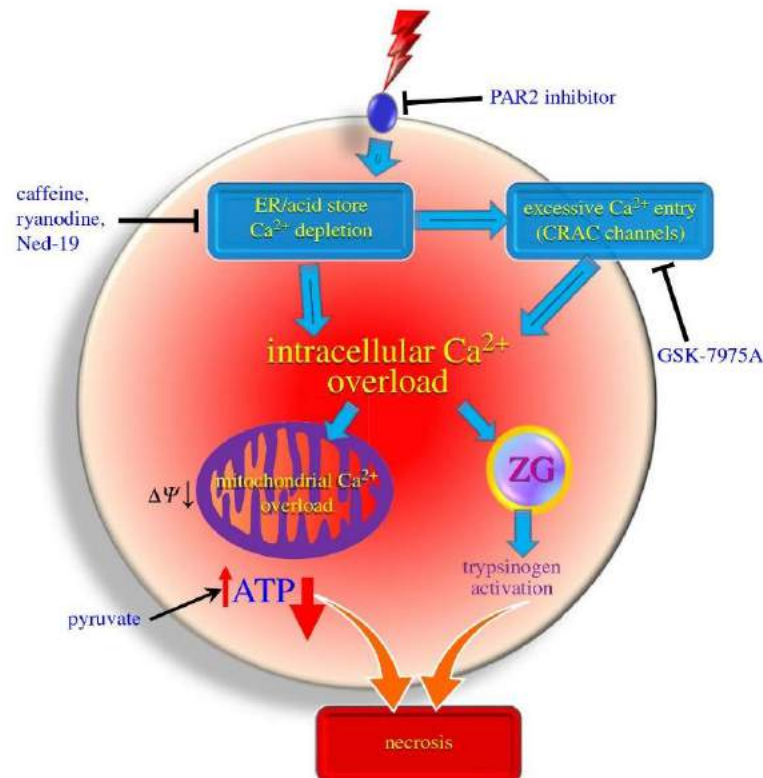


Figure 6. Schematic diagram illustrating the likely effects of asparaginase on pancreatic acinar cells, based partly on the new data shown in this study and partly on analogy with processes identified in previous studies on the mechanisms by which fatty acid ethyl esters and bile acids cause AP [38]. Potential sites for therapeutic intervention are also indicated.

entry and, therefore, are strongly inhibited by the CRAC channel inhibitor GSK-7975A and also that, consequently, asparaginase-induced necrosis is dramatically reduced to near control levels by GSK-7975A (figure 5*b*). On the basis of the previously documented protective effects of Ca^{2+} entry channel inhibition against alcohol-related pancreatic pathology in isolated cell clusters [9,38], the recent confirmation of its effectiveness *in vivo* in three different mouse pancreatitis models [43] and the very recently demonstrated inhibition of prolonged Ca^{2+} signal generation in pancreatic stellate cells [31,32], our new data indicate that this therapeutic approach is also likely to be successful against asparaginase-induced pancreatitis. Clearly, the next—but challenging—step would be to test the effectiveness of CRAC channel blockade against AAP in an *in vivo* mouse model.

The mechanism by which asparaginase induces pancreatitis is fundamentally different from its therapeutic action on the lymphoblastic cells in ALL. The asparaginase effect on cancer cells relies on depletion of asparagine, which the malignant cells cannot produce themselves, in contrast to normal cells [62], whereas the side-effect of asparaginase, inducing pancreatitis, is owing to activation of a signal transduction mechanism involving PAR2, the intracellular messengers IP_3 and NAADP, and the intracellular receptors IP_3Rs , RYRs and possibly TPCs (figure 6). The asparaginase effect on the pancreas is therefore independent of the presence or absence of asparagine (figure 5*d*). This means that there are several potential intervention points available for treating the side-effect of asparaginase (figure 6), without interfering with its primary effect on the cancer cells. The primary site of action of

asparaginase on pancreatic acinar cells seems to be PAR2. This receptor has previously been implicated in AP, although its exact role is still debated [53,54]. Blocking PAR2 in our experiments inhibited both the pathological $[\text{Ca}^{2+}]_i$ elevations (figure 2*e*) and the asparaginase-induced necrosis (figure 5*b*), suggesting that PAR2 inhibitors in addition to, or in combination with, CRAC channel inhibitors could be a useful tool to supplement asparaginase ALL treatment in AAP cases.

Both Ca^{2+} entry and extrusion are significantly affected by asparaginase, leading to formation of the pathological elevated $[\text{Ca}^{2+}]_i$ plateau, and this sustained elevation of $[\text{Ca}^{2+}]_i$ would appear to be responsible for the necrosis. The demonstrated reduction of the intensity of Ca^{2+} extrusion (figure 3*a*) is clearly a key element, and the simplest explanation for this is the reduction in the intracellular ATP level (figure 4*a*) limiting the energy supply to the Ca^{2+} ATPase in the plasma membrane. When energy supply is partially restored by the addition of pyruvate (figure 4*d*), it provides a similar degree of protection against pancreatic necrosis to PAR2 inhibition or GSK-7975A (figure 5*b*). Clearly, both Ca^{2+} and ATP play key roles in pancreatic pathology, as indeed they do in physiological regulation of secretion, and therapeutic strategies must take both into account.

4. Material and methods

(a) Materials

All fluorescent dyes were purchased from ThermoFisher Scientific (Invitrogen, UK), and CPA was from Merck Millipore (Calbiochem,

UK). Collagenase was obtained from Worthington (USA), asparaginase was from Abcam (UK), the PAR2 inhibitor FSLRY-NH2 from TOCRIS (UK) and GSK-7975A from GlaxoSmithKline (UK). All other chemicals were purchased from Sigma. C57BL/6 J mice were from Charles River UK Ltd.

(b) Isolation of pancreatic acinar cells

Pancreatic acinar cells were isolated as previously described [9]. Briefly, animals were sacrificed according to the Animal Scientific Procedures Act, 1986 and approved by the Ethical Review Committee of Cardiff University. After dissection, the pancreas was digested using collagenase-containing solution (200 U ml⁻¹, Worthington, UK) and incubated in a 37°C water bath for 14–15 min. The extracellular solution contained: 140 mM NaCl, 4.7 mM KCl, 10 mM Hepes, 1 mM MgCl₂, 10 mM glucose, pH 7.2, and CaCl₂ (0–2 mM as described in the text).

(c) Fluorescence measurements

For measurements of [Ca²⁺]_i, isolated pancreatic acinar cells were loaded with Fluo-4-AM (5 µM; excitation 488 nm) or Fura-2-AM (2.5 µM; excitation 365 and 385 nm) following the manufacturer's instruction. The cells were then washed and re-suspended in extracellular solution containing 1 mM CaCl₂.

Measurement of intracellular ATP was performed with MgGreen, which senses changes in [Mg²⁺]_i at concentrations around the resting [Mg²⁺]_i (approx. 0.9 mM). This was used as an indirect approach to detect cytosolic ATP depletion [58]. Pancreatic acinar cells were incubated with 4 µM MgGreen for 30 min at room temperature (excitation 488 nm). ATP depletion mixture (4 µM CCCP, 10 µM oligomycin and 2 mM iodoacetate) was applied for a final 10 min to induce maximum ATP depletion [42].

Necrotic cell death was assessed with PI uptake as previously described [9].

All experiments were performed at room temperature using freshly isolated cells attached to coverslips of the perfusion chamber. Fluorescence was imaged over time using an Leica TCS SPE confocal microscope.

(d) Statistical analysis

Data are presented as mean ± SEM. Statistical significance and *p*-values were calculated using *t*-test or ANOVA, with *p* < 0.05 considered significant.

Ethics. All animal-related research was run according to the Animal Scientific Procedures Act, 1986 and approved by the Ethical Review Committee of Cardiff University.

Data accessibility. Data sets for this article have been obtained and processed using Leica LAS AF software (<http://www.leica-microsystems.com/products/microscope-software/>) needed to open the original files. Supporting files will be made available in the Research section via: <https://www.cardiff.ac.uk/people/view/108900-gerasimenko-oleg>.

Authors' contributions. S.P., J.V.G., T.T., O.G., S.S., O.H.P. and O.V.G. designed the research; S.P., J.V.G., T.T. and O.G. performed the research; S.P., J.V.G., T.T., O.G. and O.V.G. analysed data; J.V.G., O.H.P. and O.V.G. wrote the study.

Competing interests. We have no competing interests.

Funding. This work was funded by a Medical Research Council Programme grant no. (MR/J002771/1) and a Children with Cancer UK grant no. (2014/167). Work was also supported by the National Institute for Health Research Biomedical Research Centre at Great Ormond Street Hospital for Children NHS Foundation Trust and University College London. S.P. is supported by China Scholarship Council (201406780021). O.H.P. is a Medical Research Council Professor (G19/22/2).

References

- Harvey AM, Madntosh FC. 1940 Calcium and synaptic transmission in a sympathetic ganglion. *J. Physiol.* **97**, 408–416. (doi:10.1113/jphysiol.1940.sp003818)
- Baker PF, Knight DE. 1981 Calcium control of exocytosis and endocytosis in bovine adrenal medullary cells. *Phil. Trans. R. Soc. Lond. B* **296**, 83–103. (doi:10.1098/rstb.1981.0174)
- Katz B, Miledi R. 1967 The timing of calcium action during neuromuscular transmission. *J. Physiol.* **189**, 535–544. (doi:10.1113/jphysiol.1967.sp008183)
- Neher E, Augustine GJ. 1992 Calcium gradients and buffers in bovine chromaffin cells. *J. Physiol.* **450**, 273–301. (doi:10.1113/jphysiol.1992.sp019127)
- Petersen OH, Maruyama Y, Graf J, Laugier R, Nishiyama A, Pearson GT. 1981 Ionic currents across pancreatic acinar cell membranes and their role in fluid secretion. *Phil. Trans. R. Soc. Lond. B* **296**, 151–166. (doi:10.1098/rstb.1981.0179)
- Schulz I, Kimura T, Wakasugi H, Haase W, Kribben A. 1981 Analysis of Ca²⁺ fluxes and pools in pancreatic acini. *Phil. Trans. R. Soc. Lond. B* **296**, 105–113. (doi:10.1098/rstb.1981.0175)
- Nielsen SP, Petersen OH. 1972 Transport of calcium in the perfused submandibular gland of the cat. *J. Physiol.* **223**, 685–697. (doi:10.1113/jphysiol.1972.sp009869)
- Streb H, Irvine RF, Berridge MJ, Schulz I. 1983 Release of Ca²⁺ from a nonmitochondrial intracellular store in pancreatic acinar cells by inositol-1,4,5-trisphosphate. *Nature* **306**, 67–69. (doi:10.1038/306067a0)
- Gerasimenko JV et al. 2013 Ca²⁺ release-activated Ca²⁺ channel blockade as a potential tool in antipain therapy. *Proc. Natl. Acad. Sci. USA* **110**, 13 186–13 191. (doi:10.1073/pnas.1300910110)
- Wakui M, Potter BVL, Petersen OH. 1989 Pulsatile intracellular calcium release does not depend on fluctuations in inositol trisphosphate concentration. *Nature* **339**, 317–320. (doi:10.1038/339317a0)
- Thorn P, Lawrie AM, Smith PM, Gallacher DV, Petersen OH. 1993 Local and global cytosolic Ca²⁺ oscillations in exocrine cells evoked by agonists and inositol trisphosphate. *Cell* **74**, 661–668. (doi:10.1016/0092-8674(93)90513-P)
- Mogami H, Nakano K, Tepikin AV, Petersen OH. 1997 Ca²⁺ flow via tunnels in polarized cells: recharging of apical Ca²⁺ stores by focal Ca²⁺ entry through basal membrane patch. *Cell* **88**, 49–55. (doi:10.1016/S0092-8674(00)81857-7)
- Petersen OH, Tepikin AV. 2008 Polarized calcium signaling in exocrine gland cells. *Annu. Rev. Physiol.* **70**, 273–299. (doi:10.1146/annurev.physiol.70.113006.100618)
- Kasai H, Li YX, Miyashita Y. 1993 Subcellular distribution of Ca²⁺ release channels underlying Ca²⁺ waves and oscillations in exocrine pancreas. *Cell* **74**, 669–677. (doi:10.1016/0092-8674(93)90514-Q)
- Nathanson MH, Fallon MB, Padfield PJ, Maranto AR. 1994 Localization of the type 3 inositol 1,4,5-trisphosphate receptor in the Ca²⁺ wave trigger zone of pancreatic acinar cells. *J. Biol. Chem.* **269**, 4693–4696.
- Belan PV, Gerasimenko OV, Tepikin AV, Petersen OH. 1996 Localization of Ca²⁺ extrusion sites in pancreatic acinar cells. *J. Biol. Chem.* **271**, 7615–7619. (doi:10.1074/jbc.271.13.7615)
- Parekh AB. 2010 Store-operated CRAC channels: function in health and disease. *Nat. Rev. Drug Discov.* **9**, 399–410. (doi:10.1038/nrd3136)
- Lur G, Haynes LP, Prior IA, Gerasimenko OV, Feske S, Petersen OH, Burgoyne RD, Tepikin AV. 2009 Ribosome-free terminals of rough ER allow formation of STIM1 puncta and segregation of STIM1 from IP₃ receptors. *Curr. Biol.* **19**, 1648–1653. (doi:10.1016/j.cub.2009.07.072)
- Tinel H, Cancela JM, Mogami H, Gerasimenko JV, Gerasimenko OV, Tepikin AV, Petersen OH. 1999

- Active mitochondria surrounding the pancreatic acinar granule region prevent spreading of inositol trisphosphate-evoked local cytosolic Ca^{2+} signals. *EMBO J.* **18**, 4999–5008. (doi:10.1093/emboj/18.18.4999)
20. Gerasimenko OV, Gerasimenko JV. 2012 Mitochondrial function and malfunction in the pathophysiology of pancreatitis. *Pflügers Arch.* **464**, 89–99. (doi:10.1007/s00424-012-1117-8)
 21. Denton RM, McCormack JG. 1986 The calcium-sensitive dehydrogenases of vertebrate mitochondria. *Cell Calcium* **7**, 377–386. (doi:10.1016/0143-4160(86)90040-0)
 22. Voronina SG, Barrow SL, Simpson AWM, Gerasimenko OV, Da Silva Xavier G, Rutter GA, Petersen OH, Tepikin AV. 2010 Dynamic changes in cytosolic and mitochondrial ATP levels in pancreatic acinar cells. *Gastroenterology* **138**, 1976–1987. (doi:10.1053/j.gastro.2010.01.037)
 23. Wakui M, Osipchuk YV, Petersen OH. 1990 Receptor-activated cytoplasmic Ca^{2+} spiking mediated by inositol trisphosphate is due to Ca^{2+} -induced Ca^{2+} release. *Cell* **63**, 1025–1032. (doi:10.1016/0092-8674(90)90505-9)
 24. Futatsugi A *et al.* 2005 IP_3 receptor types 2 and 3 mediate exocrine secretion underlying energy metabolism. *Science* **309**, 2232–2234. (doi:10.1126/science.1114110)
 25. Cancela JM, Gerasimenko OV, Gerasimenko JV, Tepikin AV, Petersen OH. 2000 Two different but converging messenger pathways to intracellular Ca^{2+} release: the roles of NAADP, cADPR and IP_3 . *EMBO J.* **19**, 2549–2557. (doi:10.1093/emboj/19.11.2549)
 26. Yamasaki M, Thomas JM, Churchill GC, Garnham C, Lewis AM, Cancela JM, Patel S, Galione A. 2005 Role of NAADP and cADPR in the induction and maintenance of agonist-evoked Ca^{2+} spiking in mouse pancreatic acinar cells. *Curr. Biol.* **9**, 874–878. (doi:10.1016/j.cub.2005.04.033)
 27. Gerasimenko JV, Charlesworth RM, Sherwood MW, Ferdek PE, Mikoshiba K, Parrington J, Petersen OH, Gerasimenko OV. 2015 Both RyRs and TPCs are required for NAADP-induced intracellular Ca^{2+} release. *Cell Calcium* **58**, 237–245. (doi:10.1016/j.ceca.2015.05.005)
 28. Scratcherd T, Hutson D, Case RM. 1981 Ionic transport mechanisms underlying fluid secretion by the pancreas. *Phil. Trans. R. Soc. Lond. B* **296**, 167–178. (doi:10.1098/rstb.1981.0180)
 29. Maléth J, Hegyi P. 2016 Ca^{2+} toxicity and mitochondrial damage in acute pancreatitis: translational overview. *Phil. Trans. R. Soc. B* **371**, 20150425. (doi:10.1098/rstb.2015.0425)
 30. Hegyi P, Petersen OH. 2013 The exocrine pancreas: the acinar-ductal tango in physiology and pathophysiology. *Rev. Physiol. Biochem. Pharmacol.* **165**, 1–30. (doi:10.1007/112_2013_14)
 31. Gryshchenko O, Gerasimenko JV, Gerasimenko OV, Petersen OH. 2016 Ca^{2+} signals mediated by bradykinin type 2 receptors in normal pancreatic stellate cells can be inhibited by specific Ca^{2+} channel blockade. *J. Physiol.* **594**, 281–293. (doi:10.1113/JP271468)
 32. Gryshchenko O, Gerasimenko JV, Gerasimenko OV, Petersen OH. 2016 Calcium signalling in pancreatic stellate cells: mechanisms and potential roles. *Cell Calcium* **59**, 140–144. (doi:10.1016/j.ceca.2016.02.003)
 33. Petersen OH, Sutton R. 2006 Ca^{2+} signalling and pancreatitis: effects of alcohol, bile and coffee. *Trends Pharmacol. Sci.* **27**, 113–120. (doi:10.1016/j.tips.2005.12.006)
 34. Ward JB, Petersen OH, Jenkins SA, Sutton R. 1995 Is an elevated concentration of acinar cytosolic free ionised calcium the trigger for acute pancreatitis? *Lancet* **346**, 1016–1019. (doi:10.1016/S0140-6736(95)91695-4)
 35. Raraty M, Ward J, Erdemli G, Vaillant C, Neoptolemos JP, Sutton R, Petersen OH. 2000 Calcium-dependent enzyme activation and vacuole formation in the apical granular region of pancreatic acinar cells. *Proc. Natl. Acad. Sci. USA* **97**, 13 126–13 131. (doi:10.1073/pnas.97.24.13126)
 36. Kruger B, Albrecht E, Lerch MM. 2000 The role of intracellular calcium signaling in premature protease activation and the onset of pancreatitis. *Am. J. Pathol.* **157**, 43–50. (doi:10.1016/S0002-9440(10)64515-4)
 37. Voronina S, Longbottom R, Sutton R, Petersen OH, Tepikin AV. 2002 Bile acids induce calcium signals in mouse pancreatic acinar cells: implications for bile-induced pancreatic pathology. *J. Physiol.* **540**, 49–55. (doi:10.1113/jphysiol.2002.017525)
 38. Gerasimenko JV, Gerasimenko OV, Petersen OH. 2014 The role of Ca^{2+} in the pathophysiology of pancreatitis. *J. Physiol.* **592**, 269–280. (doi:10.1113/jphysiol.2013.261784)
 39. Mukherjee R *et al.* 2016 Mechanism of mitochondrial permeability transition pore induction and damage in the pancreas: inhibition prevents acute pancreatitis by protecting production of ATP. *Gut*. In press. (doi:10.1136/gutjnl-2014-308553)
 40. Maléth J, Hegyi P, Rakonczay Jr, Z, Venglovecz V. 2015 Breakdown of bioenergetics evoked by mitochondrial damage in acute pancreatitis: mechanisms and consequences. *Pancreatology* **15**, S18–S22. (doi:10.1016/j.pan.2015.06.002)
 41. Criddle DN. 2015 The role of fat and alcohol in acute pancreatitis: a dangerous liaison. *Pancreatology* **15**, S6–S12. (doi:10.1016/j.pan.2015.02.009)
 42. Baggaley EM, Elliott AC, Bruce JL. 2008 Oxidant-induced inhibition of the plasma membrane Ca^{2+} -ATPase in pancreatic acinar cells: role of the mitochondria. *Am. J. Physiol. Cell Physiol.* **295**, C1247–C1260. (doi:10.1152/ajpcell.00083.2008)
 43. Wen L *et al.* 2015 Inhibitors of ORAI1 prevent cytosolic calcium-associated injury of human pancreatic acinar cells and acute pancreatitis in 3 mouse models. *Gastroenterology* **149**, 481–492. (doi:10.1053/j.gastro.2015.04.015)
 44. Hegyi P. 2016 Blockade of calcium entry provides a therapeutic window in acute pancreatitis. *J. Physiol.* **594**, 257. (doi:10.1113/JP271710)
 45. Jaffe N, Tragis D, Das L, Moloney WC, Hann HW, Kim BS, Nair R. 1971 L-asparaginase in the treatment of neoplastic diseases in children. *Cancer Res.* **31**, 942–949.
 46. Silverman LB *et al.* 2001 Improved outcome for children with acute lymphoblastic leukemia: results of Dana-Farber Consortium Protocol 91-01. *Blood* **97**, 1211–1218. (doi:10.1182/blood.V97.5.1211)
 47. Kearney SL, Dahlberg SE, Levy DE, Voss SD, Sallan SE, Silverman LB. 2009 Clinical course and outcome in children with acute lymphoblastic leukemia and asparaginase-associated pancreatitis. *Pediatr. Blood Cancer* **53**, 162–167. (doi:10.1002/pbc.22076)
 48. Raja RA, Schmiegelow K, Frandsen TL. 2012 Asparaginase-associated pancreatitis in children. *Br. J. Haematol.* **159**, 18–27. (doi:10.1111/bjh.12016)
 49. Raja RA *et al.* 2014 Asparaginase-associated pancreatitis in children with acute lymphoblastic leukaemia in the NOPHO ALL2008 protocol. *Br. J. Haematol.* **165**, 126–133. (doi:10.1111/bjh.12733)
 50. Samarasinghe S, Dhir S, Slack J, Iyer P, Wade R, Clack R, Vora A, Goulden N. 2013 Incidence and outcome of pancreatitis in children and young adults with acute lymphoblastic leukaemia treated on a contemporary protocol, UKALL 2003. *Br. J. Haematol.* **162**, 710–713. (doi:10.1111/bjh.12407)
 51. Huang W *et al.* 2014 Fatty acid ethyl ester synthase inhibition ameliorates ethanol-induced Ca^{2+} -dependent mitochondrial dysfunction and acute pancreatitis. *Gut* **63**, 1313–1324. (doi:10.1136/gutjnl-2012-304058)
 52. Voronina S *et al.* 2015 The role of Ca^{2+} influx in endocytic vacuole formation in pancreatic acinar cells. *Biochem. J.* **465**, 405–412. (doi:10.1042/BJ20140398)
 53. Namkond W, Han W, Luo X, Muallem S, Cho KH, Kim KH, Lee MG. 2004 Protease-activated receptor 2 exerts local protection and mediates some systemic complications in acute pancreatitis. *Gastroenterology* **126**, 1844–1859. (doi:10.1053/j.gastro.2004.03.019)
 54. Laukkarinen JM, Weiss ER, van Acker GJD, Steer ML, Perides G. 2008 Protease-activated receptor-2 exerts contrasting model-specific effects on acute experimental pancreatitis. *J. Biol. Chem.* **283**, 20 703–20 712. (doi:10.1074/jbc.M801779200)
 55. Soh UJ, Dore MR, Chen B, Trejo J. 2010 Signal transduction by protease-activated receptors. *Br. J. Pharmacol.* **160**, 191–203. (doi:10.1111/j.1476-5381.2010.00705.x)
 56. Leyssens A, Nowicky AV, Patterson L, Crompton M, Duchon MR. 1996 The relationship between mitochondrial state, ATP hydrolysis, $[\text{Mg}^{2+}]$, and $[\text{Ca}^{2+}]$, studied in isolated rat cardiomyocytes. *J. Physiol.* **496**, 111–128. (doi:10.1113/jphysiol.1996.sp021669)
 57. Inoue M, Fujishiro N, Imanaga I, Sakamoto Y. 2002 Role of ATP decrease in secretion induced by mitochondrial dysfunction in guinea-pig adrenal chromaffin cells. *J. Physiol.* **539**, 145–155. (doi:10.1113/jphysiol.2001.012936)
 58. Criddle D, Murphy J, Fissetto G, Barrow S, Tepikin AV, Neoptolemos JP, Sutton R, Petersen OH. 2006

- Fatty acid ethyl esters cause pancreatic calcium toxicity via inositol trisphosphate receptors and loss of ATP synthesis. *Gastroenterology* **130**, 781–793. (doi:10.1053/j.gastro.2005.12.031)
59. Luan ZG, Ma XC, Zhang H, Zhang C, Guo RX. 2013 Protective effect of ethyl pyruvate on pancreas injury in rats with severe acute pancreatitis. *J. Surg. Res.* **181**, 76–84. (doi:10.1016/j.jss.2012.05.066)
 60. Kiyonaka S *et al.* 2009 Selective and direct inhibition of TRPC3 channels underlies biological activities of a pyrazole compound. *Proc. Natl. Acad. Sci. USA* **106**, 5400–5405. (doi:10.1073/pnas.0808793106)
 61. Schleifer H *et al.* 2012 Novel pyrazole compounds for pharmacological discrimination between receptor-operated and store-operated Ca^{2+} entry pathways. *Br. J. Pharmacol.* **167**, 1712–1722. (doi:10.1111/j.1476-5381.2012.02126.x)
 62. Broome JD. 1968 Studies on the mechanism of tumor inhibition by L-asparaginase. Effects of the enzyme on asparagine levels in the blood, normal tissues, and 6C3HED lymphomas of mice: differences in asparagine formation and utilization in asparaginase-sensitive and -resistant lymphoma cells. *J. Exp. Med.* **127**, 1055–1072. (doi:10.1084/jem.127.6.1055)
 63. Spät A, Szanda G. 2012 Special features of mitochondrial Ca^{2+} signalling in adrenal glomerulosa cells. *Pflügers Arch.* **464**, 43–50. (doi:10.1007/s00424-012-1086-y)
 64. Vais H, Mallikarjuna K, Mak DO, Hoff H, Payne R, Tanis JE, Foscett JK. 2016 EMRE is a matrix Ca^{2+} sensor that governs gatekeeping of the mitochondrial Ca^{2+} uniporter. *Cell Rep.* **14**, 403–410. (doi:10.1016/j.celrep.2015.12.054)
 65. Kar P, Samanta K, Kramer H, Morris O, Bakowski D, Parekh AB. 2014 Dynamic assembly of a membrane signaling complex enables selective activation of NFAT by Orai1. *Curr. Biol.* **24**, 1361–1368. (doi:10.1016/j.cub.2014.04.046)

4.3. Галактоза захищає від пошкодження клітин при гострому панкреатиті

The Journal of Clinical Investigation

RESEARCH ARTICLE

Galactose protects against cell damage in mouse models of acute pancreatitis

Shuang Peng,^{1,2} Julia V. Gerasimenko,¹ Tetyana M. Tsugorka,¹ Oleksiy Gryshchenko,^{1,3} Sujith Samarasinghe,⁴ Ole H. Petersen,¹ and Oleg V. Gerasimenko¹

¹Cardiff School of Biosciences, Cardiff University, Cardiff, United Kingdom. ²Department of Physiology, School of Medicine, Jinan University, Guangzhou, China. ³Bogomoletz Institute of Physiology, Kiev, Ukraine. ⁴Great Ormond Street Hospital for Children, NHS Foundation Trust, London, United Kingdom.

Acute pancreatitis (AP), a human disease in which the pancreas digests itself, has substantial mortality with no specific therapy. The major causes of AP are alcohol abuse and gallstone complications, but it also occurs as an important side effect of the standard asparaginase-based therapy for childhood acute lymphoblastic leukemia. Previous investigations into the mechanisms underlying pancreatic acinar cell death induced by alcohol metabolites, bile acids, or asparaginase indicated that loss of intracellular ATP generation is an important factor. We now report that, in isolated mouse pancreatic acinar cells or cell clusters, removal of extracellular glucose had little effect on this ATP loss, suggesting that glucose metabolism was severely inhibited under these conditions. Surprisingly, we show that replacing glucose with galactose prevented or markedly reduced the loss of ATP and any subsequent necrosis. Addition of pyruvate had a similar protective effect. We also studied the effect of galactose *in vivo* in mouse models of AP induced either by a combination of fatty acids and ethanol or asparaginase. In both cases, galactose markedly reduced acinar necrosis and inflammation. Based on these data, we suggest that galactose feeding may be used to protect against AP.

Introduction

Acute pancreatitis (AP) is an inflammatory disease that originates in the exocrine pancreas, where inactive pancreatic proenzymes become prematurely activated inside the pancreatic acinar cells (PACs), digesting the pancreas and its surroundings (1, 2). The main causes of AP are excessive alcohol and fatty food intake and gallstone disease, accounting for about 80% of all cases (3). Stimulation of PACs with alcohol metabolites or bile acids (BAs) leads to aberrant calcium signaling due to excessive release from intracellular stores, followed by activation of massive Ca^{2+} entry through store-operated Ca^{2+} release-activated Ca^{2+} (CRAC) channels, causing intracellular Ca^{2+} overload (2, 4, 5).

Another cause of AP is the L-asparaginase treatment of acute lymphoblastic leukemia (ALL) (6, 7). According to Cancer Research UK, there were 832 new cases of ALL diagnosed in the United Kingdom in 2015. The incidence rates for ALL are highest in children aged 0 to 4 (2012–2014). Antileukemic drugs based on L-asparaginase are currently used in the clinic as an effective treatment for childhood ALL (8–12). However, in up to 10% of cases, the asparaginase treatment has to be truncated due to development of AP, a serious and incurable illness (6, 7, 13–17). Although asparaginase-based drugs have been used in the clinic

for many years (8), the mechanism of this side effect has not been well explored and understood.

We have recently made progress in understanding the mechanism of asparaginase-induced AP (AAP) (18). Our key findings include the activation of protease-activated receptor 2 (PAR2) as well as calcium overload and loss of ATP in PACs. We believe these findings provide the first mechanistic insight into the process by which asparaginase treatment of ALL may cause AAP. The asparaginase effect on cancer cells relies on the depletion of asparagine, which the malignant cells cannot produce by themselves, as opposed to normal cells (19, 20). However, the AP-inducing side effects of asparaginase do not depend on the presence or absence of asparagine (18). In contrast, the AP-inducing side effect of asparaginase is caused by the activation of a signal transduction mechanism involving PAR2 that, via a number of steps, causes cytosolic Ca^{2+} overloading and reduction in intracellular ATP levels. The reduction of energy supply inhibits both the plasma membrane Ca^{2+} ATPase (PMCA) and the sarco/endoplasmic reticulum Ca^{2+} ATPase (SERCA) (21–23). We have recently shown that restoration of energy supply, by the addition of pyruvate, provides an astonishingly high degree of protection against pancreatic necrosis (18).

We have now analyzed the role of glycolysis in AP in more detail, *in vivo* and *in vitro*, and specifically compared the effects of pyruvate, galactose (24), and glucose on the functional and morphological features of AP and AAP. Based on these data, we propose a simple and promising way to rescue intracellular ATP levels in AP and AAP patients.

Results

ATP loss is the common hallmark of AP. It has been established previously that ATP loss in AP is a critical part of the pathological

Authorship note: SP and JVG contributed equally to this work.

Conflict of interest: The authors have declared that no conflict of interest exists.

Submitted: April 21, 2017; **Accepted:** June 6, 2018.

License: This work is licensed under the Creative Commons Attribution 4.0 International License. To view a copy of this license, visit <http://creativecommons.org/licenses/by/4.0/>.

Reference information: *J Clin Invest.* 2018;128(9):3769–3778. <https://doi.org/10.1172/JCI94714>.

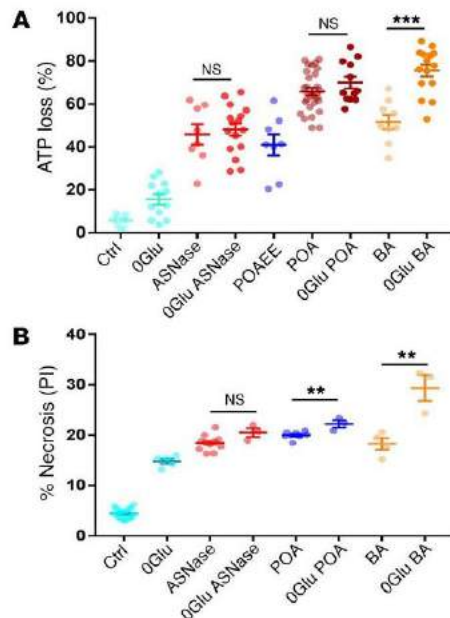


Figure 1. Asparaginase, POAEE with POA, and BAs all induce substantial ATP loss and cell necrosis. (A) Comparison of cellular ATP depletion in PACs after treatment of cells for 30 minutes with or without glucose (0Glu), or application of asparaginase (ASNase), POAEE, POA, or BA. Level of ATP loss (measured by MgGreen) is shown as a percentage of full depletion by a mixture of CCCP, oligomycin, and iodoacetate. Dots represent ATP loss (%) in each cell. Data are shown as mean \pm SEM. Ctrl, control. **(B)** Summary of cell necrosis measurements in PACs treated with asparaginase, POA, or BA for 2 hours in the presence or absence of 10 mM glucose as compared with control. Removal of glucose had little effect on asparaginase and POA, but increased BA-induced necrosis. Cells were stained with PI. Dots represent series of experiments with $n > 100$ cells in each sample. Data are shown as mean \pm SEM. ** $P < 0.01$; *** $P < 0.001$, 1-way ANOVA.

mechanism in PACs, irrespective of whether it has been initiated by alcohol metabolites or BAs (1, 22, 25). As previously described (18), we have assessed intracellular changes in ATP concentration by using Magnesium Green (MgGreen) fluorescence measurements. As most of the intracellular ATP will be in the form of Mg-ATP, a reduction of the ATP concentration will increase the fluorescence intensity of MgGreen due to the increase in free Mg^{2+} concentration. We have studied the effect of asparaginase in PACs and found that 30 minutes of exposure to this agent caused a $45.8\% \pm 4.8\%$ loss of ATP (Figure 1A).

The ATP reduction induced by asparaginase was very similar to that elicited by exposure to the nonoxidative alcohol metabolite palmitoleic acid ethyl ester (POAEE) ($40.9\% \pm 4.9\%$) and palmitoleic acid (POA) ($66.9\% \pm 4.9\%$) (26) or a BA mixture ($51.6\% \pm 3.3\%$) (Figure 1A), while removal of glucose for 30 minutes led to a substantially smaller reduction ($15.5\% \pm 0.95\%$). Interestingly, removal of glucose did not significantly increase ATP depletion induced by POA or ASNase, but partially increased ATP depletion induced by BA (Figure 1A).

Since the majority of cellular ATP is produced by glucose metabolism, we compared the effect of a glucose-free medium on necrosis to that induced by asparaginase, POAEE, POA, or BA (Figure 1B). In these experiments, lasting 2 hours, we found that removal of glucose produced a level of necrosis comparable to that of all other pathological agents ($14.8\% \pm 0.5\%$, $P < 0.0001$), but did not significantly exacerbate the effects of asparaginase ($P > 0.059$). It only marginally increased POA-elicited necrosis (from $20.0\% \pm 0.3\%$ to $22.2\% \pm 0.7\%$, $P < 0.01$) (Figure 1B) and somewhat increased BA-induced necrosis (from $18.3\% \pm 1.1\%$ to $29.4 \pm 2.5\%$, $P < 0.008$). The fact that removal of glucose did not further increase the extent of necrosis induced by asparaginase or POA may suggest that glucose metabolism is already so strongly inhibited by these 2 agents that removal of external glucose has practically no additional effect.

Pyruvate and galactose alleviate bile- and alcohol metabolite-induced pathology. In our previous study into the mechanism by which asparaginase evokes pathological changes in isolated PACs (18), we showed that inclusion of pyruvate in the bathing solution provided remarkable protection against necrosis. We further demonstrated that the reduction in the intracellular ATP level caused by asparaginase was significantly diminished when pyruvate was present (18). In addition to pyruvate, we decided to test galactose for its effectiveness in protection against alcohol- and bile-induced pancreatic pathologies. Galactose very significantly reduced the ATP loss caused by the alcohol metabolite POAEE (Figure 2, A and B) and POA (Figure 2, D and E) and also essentially prevented the necrosis induced by these agents (Figure 2, C and F). Pyruvate had a very similar effect (Figure 2F). A comparable protective effect of pyruvate was also found in the case of bile-related pathology. Pyruvate substantially reduced the ATP loss elicited by BA (Figure 2, G and H), and both pyruvate and galactose almost entirely eliminated BA-induced necrosis (Figure 2I).

Pyruvate and galactose protect against asparaginase-induced necrosis. The ability of galactose to protect against necrosis induced by POAEE, POA, or BA (Figure 2, C, F, and I) has prompted us to also test the effect of galactose on asparaginase-induced pathology (18). Both, pyruvate and galactose, at either 1 mM (Figure 3, A and B) or 10 mM (Figure 3C), had similar protective effects against asparaginase-induced necrosis in PACs. Interestingly, the presence or absence of glucose made no difference in the extent of the necrosis (Figure 1B). These data suggest that glucose metabolism is severely affected by asparaginase, but that energy supply can be replenished by galactose or pyruvate joining the glycolysis cycle.

Galactose and pyruvate, but not glucose, alleviate asparaginase-induced pathology. With regard to the primary action of asparaginase on PACs, we have previously shown that this agent evokes a sustained elevation of cytosolic Ca^{2+} concentration ($[Ca^{2+}]_i$) due to interaction with PAR2 (18). Figure 4, A and B, shows that

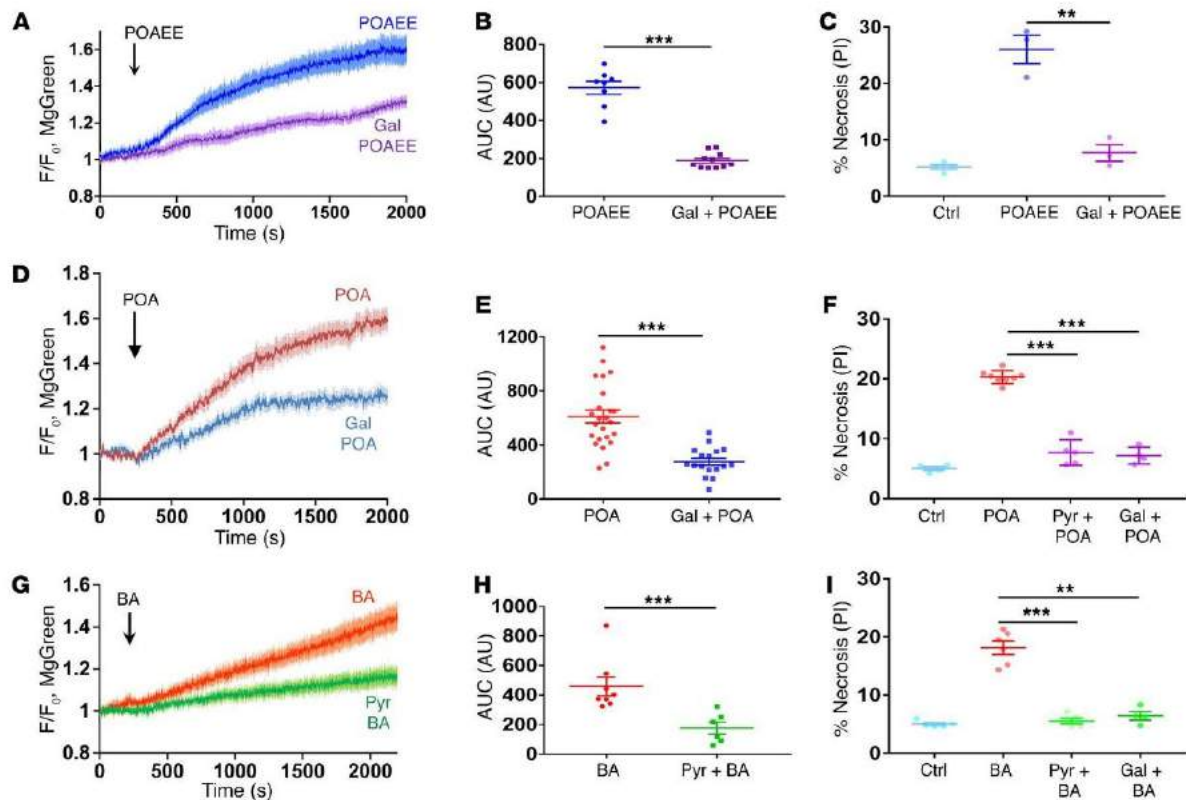


Figure 2. Pyruvate and galactose provide substantial protection against alcohol- and bile-induced ATP loss and necrosis in PACs. (A) POAEE-induced (500 μ M) ATP depletion is markedly reduced by adding 1 mM galactose (Gal). Averaged normalized (F/F_0) traces with error bars (POAEE, $n = 8$; galactose + POAEE, $n = 11$). (B) AUC comparison of traces shown in A. Galactose-reduced POAEE-induced ATP depletion ($P < 0.0001$, 2-tailed Student's t test). (C) POAEE-induced necrosis was significantly reduced by adding 1 mM galactose ($P < 0.003$, 1-way ANOVA; 3 series of experiments with more than 100 cells in each sample). (D) POA-induced (50 μ M) ATP depletion is reduced by replacing glucose with 10 mM galactose. Averaged traces with error bars (POA, $n = 24$; galactose + POA, $n = 17$). (E) AUC comparison of traces shown in D. Galactose significantly reduced POA-induced ATP depletion ($P < 0.0001$, 2-tailed Student's t test). (F) POA-induced necrosis was reduced significantly by replacing glucose with either 10 mM pyruvate (Pyr) or 10 mM galactose ($P < 0.0001$ in both series, 1-way ANOVA; dots represents a series of experiments with more than 100 cells in each sample). (G) BA mixture-induced ATP depletion is reduced by adding 1 mM pyruvate. Averaged traces with error bars (BA, $n = 8$; BA + pyruvate, $n = 6$). (H) AUC comparison of traces shown in G. Pyruvate significantly reduces BA-induced ATP depletion ($P < 0.002$, 2-tailed Student's t test). (I) BA-induced necrosis is reduced to nearly control level by replacing glucose with 10 mM pyruvate ($P < 0.00015$, 1-way ANOVA; 5 series of experiments with more than 100 cells in each sample) or 10 mM galactose ($P < 0.008$, 1-way ANOVA; 4 series of experiments with more than 100 cells in each sample). ** $P < 0.01$; *** $P < 0.001$, 2-tailed Student's t test (B, E, H); 1-way ANOVA (C, F, I).

both pyruvate and galactose very markedly reduced the increase in asparaginase-elicited $[Ca^{2+}]_i$. In control experiments, pyruvate and galactose did not change the frequency of Ca^{2+} oscillations induced by either cholecystokinin (CCK) ($P > 0.3$, $n = 11$ and $P > 0.9$, $n = 11$ respectively) or asparaginase ($P > 0.1$, $n = 33$ and $P > 0.7$, $n = 17$, respectively). There was also no significant difference with regard to the amplitude of spikes induced by CCK ($P > 0.8$, $n = 157$ and $P > 0.8$, $n = 46$, respectively). The amplitude of asparaginase-induced oscillations was reduced by 20% ($P < 0.0001$, $n = 39$) in the presence of pyruvate and by 15% ($P < 0.02$, $n = 26$) in the presence of galactose. These relatively minor effects are probably due to the increase in the cytoplasmic ATP level and, therefore, Ca^{2+} uptake after release. Previously, we have shown that asparaginase inhibits Ca^{2+} extrusion from PACs, most likely due to the reduced availability of ATP (18).

Although the asparaginase-elicited sustained elevation of $[Ca^{2+}]_i$ depends on increased Ca^{2+} entry (18), this could be com-

pensated for by an increase in the rate of active Ca^{2+} extrusion if an adequate supply of ATP were available. It would seem possible that ATP supply is enhanced in the presence of pyruvate or galactose and that this could be the mechanism by which toxic $[Ca^{2+}]_i$ increase is inhibited. We therefore tested this hypothesis by assessing changes in intracellular ATP concentration (Figure 4, C and D) as well as changes in NADH and flavin adenine dinucleotide (FAD) (Supplemental Figure 1, A and B; supplemental material available online with this article; <https://doi.org/10.1172/JCI94714DS1>).

Asparaginase induced a substantial intracellular ATP loss (Figure 4, C–E), in line with reduction of NADH (Supplemental Figure 1A). Replacement of glucose with pyruvate or galactose (both 10 mM, Figure 4, C and D) or adding 1 mM pyruvate or galactose (Figure 4E) markedly reduced asparaginase-induced ATP loss. Replacing glucose with pyruvate or galactose was very effective in protecting against ATP loss, and we therefore compared our results for the presence and absence of glucose and pyruvate (Figure 4, F–H). The

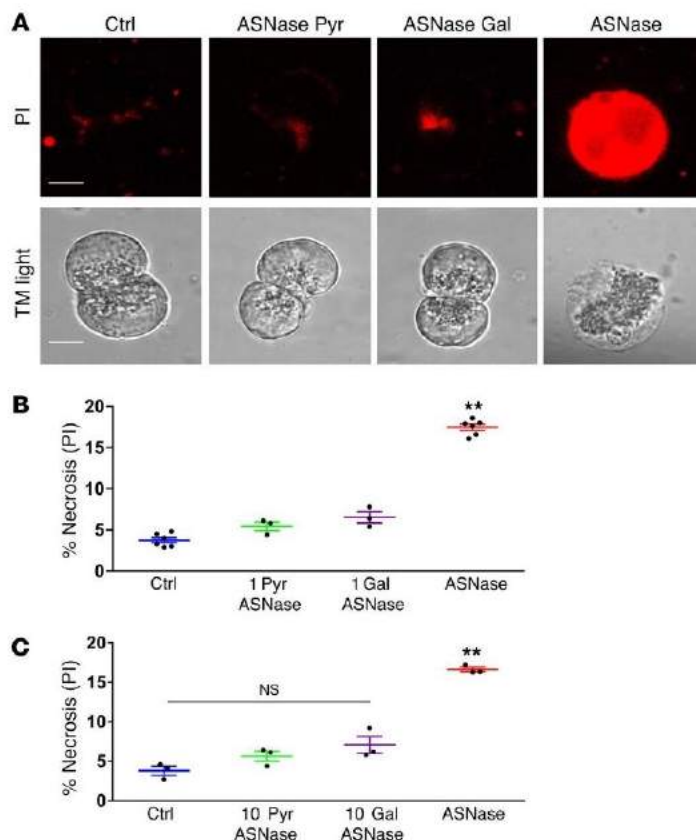


Figure 3. Pyruvate and galactose significantly reduce the level of asparaginase-induced necrosis. (A) Representative images of cells from experiments shown in B and C. Scale bars: 10 μ m. (B) In PACs, 1 mM pyruvate ($5.4\% \pm 0.5\%$, 3 series with $n > 300$, $P < 0.0002$) or 1 mM galactose ($6.5\% \pm 0.7\%$, 3 series with $n > 300$, $P < 0.0004$) reduce the asparaginase-induced necrosis level as compared with asparaginase alone ($17.5\% \pm 0.4\%$, 6 series with $n > 300$). (C) Complete replacement of extracellular glucose (10 mM) with pyruvate (10 mM) ($5.6\% \pm 0.6\%$, 3 series with $n > 300$, $P < 0.0001$) or 10 mM galactose ($7.1\% \pm 1.1\%$, 3 series with $n > 300$, $P < 0.001$) significantly reduces the asparaginase-induced necrosis level as compared with the control level ($3.8\% \pm 0.6\%$, 3 series with $n > 300$). ** $P < 0.01$, 1-way ANOVA.

ATP loss was substantially higher in the absence of pyruvate (red and orange traces) regardless of the presence or absence of glucose. Comparison of the AUC shows that 1 mM pyruvate (blue and green traces) significantly reduced ATP loss (Figure 4G), whereas the presence of 10 mM glucose did not ($P > 0.05$). Comparison of the amplitudes (Figure 4H) showed very similar results, namely that the glucose-independent ATP loss was markedly reduced by 1 mM pyruvate. Asparaginase also affected the mitochondrial potential (Supplemental Figure 2, A–F) and the mitochondrial Ca^{2+} levels (Supplemental Figure 3, A–F), but pyruvate and galactose restored these parameters to near control levels.

Pyruvate and galactose increase intracellular ATP levels. All the 3 AP-inducing factors that we tested substantially inhibited ATP production, and both asparaginase and POA severely inhibited glucose metabolism. Galactose can enter the glycolysis cycle, skipping its first step, and does not depend on hexokinase (HK) activity. Our data may therefore indicate that glucokinase/HK activity is inhibited during the induction of AP. Both galactose and pyruvate provide an additional source of ATP and increase intracellular ATP levels (Figure 5, A and B).

The glucose analogue 2-deoxy-D-glucose (2-DG) (27), which inhibits glycolysis via its indirect actions on HK, induced a substantial ATP loss (Figure 5C), necrosis (Figure 5D), and $[\text{Ca}^{2+}]$ elevation (Figure 5, E and F); these effects are very similar to those induced by asparaginase (Figure 4, A–D; Figure 3B; and Figure 5D). Pyruvate significantly reduced the 2-DG-induced sustained

$[\text{Ca}^{2+}]$ elevation (Figure 5, E and F). The protective effects of galactose were completely blocked by the glucose transport inhibitor phloretin (Supplemental Figure 1C), suggesting that only HK inhibition could explain the ATP depletion observed in AP.

HK activity is inhibited in vitro by POA and BA. To test our hypothesis that AP-inducing agents cause intracellular ATP loss by reducing HK activity, we measured the activities of the 3 major human HKs present in the pancreas in vitro (28, 29). We found that POA markedly reduced the activity of HK1 and partially reduced HK2 activity (Figure 6, A and B). Whereas POA had no effect on glucokinase (HK4), BA markedly reduced HK4 activity (Figure 6C), but had no effect on HK1 and HK2 (Figure 6, A–C). In control experiments, we found that the only other enzyme present in the cuvette (glucose-6-phosphate dehydrogenase) was not affected by either POA or BA ($P > 0.6$ and $P > 0.4$, respectively, as compared with control; $n = 5$). We also measured the activity of HK3, which has relatively low abundance in most tissues except myeloid cells, but we did not find any significant inhibition by either POA or BA as compared with control ($n = 5$). POAEE partially, but significantly, inhibited HK1 ($P < 0.004$, $n = 3$), but did not affect other HKs. Western blot (Figure 6D) showed that HK1, HK2, and HK4 were all present in mouse PACs. We conclude that pathological HK inhibition, particularly of HK1 by POA and HK4 by BA, plays a key role in the ATP depletion that is such an important feature of AP. In line with these data, a relatively high concentration of insulin (100 nM) stimulated HKs and alleviated asparaginase-, POA-,

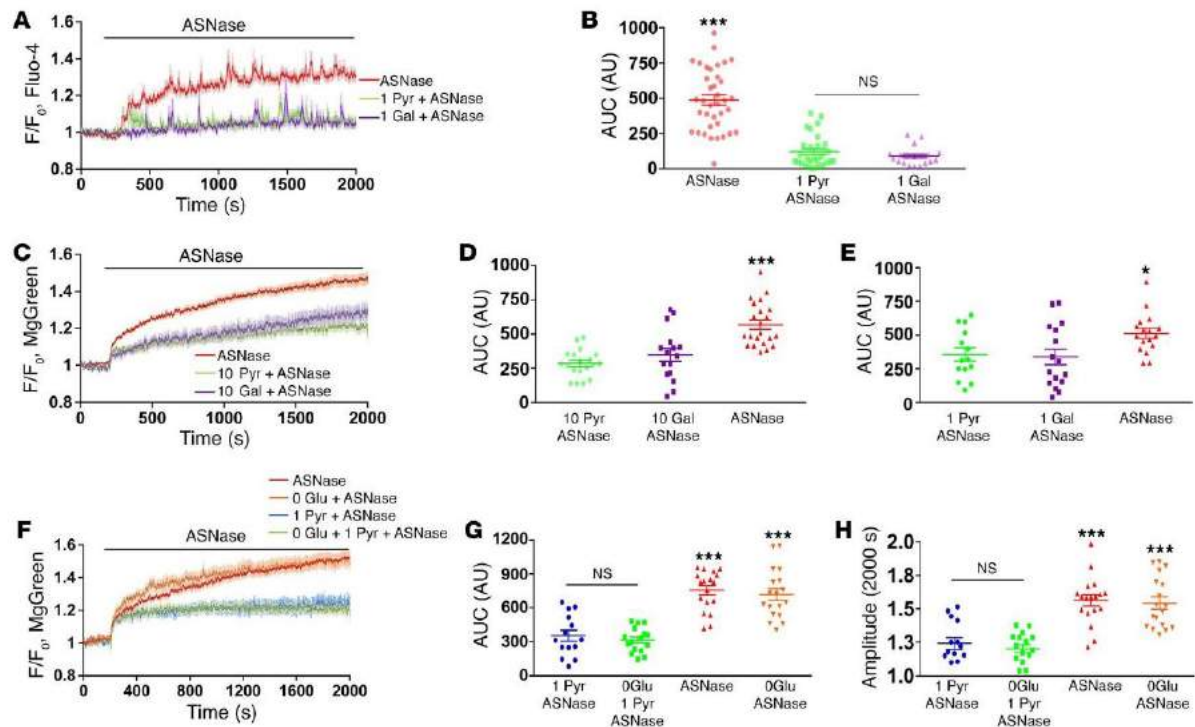


Figure 4. Asparaginase-induced Ca^{2+} overload and ATP loss were substantially reduced by galactose or pyruvate, but not glucose removal. (A) Asparaginase elicits elevated $[\text{Ca}^{2+}]$ plateau. Averaged traces with error bars shown (red, $n = 35$). Green trace shows reduced response in the presence of 1 mM pyruvate (after 5 minutes of preincubation, $n = 33$). Purple trace shows reduced response in the presence of 1 mM galactose (15 minutes of preincubation, $n = 17$). (B) Comparison of AUC shown in A during first 30 minutes of $[\text{Ca}^{2+}]$ change in the presence of pyruvate (green) and galactose (purple) or asparaginase alone (red) ($P < 0.0001$). (C) ATP loss was evaluated using MgGreen. Replacement of extracellular glucose (10 mM) with pyruvate (10 mM) (green, $n = 19$) or galactose (10 mM) (purple, $n = 16$) for 30 minutes markedly reduces $[\text{Mg}^{2+}]$ change induced by asparaginase (red, $n = 38$). (D) Quantitative analysis of experiments of type shown in C (AUC during 30 minutes; $P < 0.0005$). (E) Quantitative analysis of experiments as in C, but with 1 mM of either pyruvate (green, $n = 14$) or galactose (purple, $n = 16$). Bars show AUC recorded during 30 minutes of asparaginase application ($P < 0.015$). (F) Asparaginase induces ATP loss irrespective of glucose presence (red, $n = 21$) or absence (orange, $n = 17$). Pyruvate (1 mM) decreased ATP depletion irrespective of glucose absence (green trace, $n = 16$) or presence (10 mM) (blue trace, $n = 14$). (G) Quantitative analysis of experiments shown in F by AUC during 30 minutes of asparaginase application. Pyruvate (blue and green) was highly protected against ATP depletion ($P < 0.0001$) regardless of glucose ($P > 0.05$). (H) Amplitudes at 2,000 seconds shown in F. Pyruvate (blue and green) is protected against ATP depletion; $P < 0.0001$ regardless of presence (red) or absence of glucose (orange). * $P < 0.05$; *** $P < 0.001$, 1-way ANOVA.

and BA-induced necrosis (Supplemental Figure 1D). An increased glucose concentration (30 mM) only stimulated glucokinase and, therefore, alleviated asparaginase-induced and POA-induced, but not BA-induced, necrosis (Supplemental Figure 1D).

Galactose administration protects from alcohol-induced AP in vivo. To determine whether our findings could lead to a rational treatment of AP, we focused our attention specifically on the possibility that galactose might be helpful, as this sugar has already been included as part of human trials for the treatment of glycogen storage disease type 1b (Fabry's disease), nephrotic syndrome, and congenital disorders of glycosylation and has not been shown to have any negative effects (30–33). Galactose, an essential component of human breast milk (up to 70 mM during the first month; ref. 34), is quite stable in solution, relatively slowly metabolized compared with pyruvate, and has been administered both by i.p. injections and feeding (drink) protocols (35–37). We tested the protective effect of galactose in vivo in a realistic mouse model in which AP was induced by a mixture of POA and alcohol (FAEE-AP;

ref. 38). As shown in Figure 7, A–E, galactose significantly improved the histology score (Figure 7E) and reduced the degrees of edema (Figure 7B), inflammation (Figure 7C), and necrosis (Figure 7D). Galactose also substantially reduced the alcohol-induced increase in amylase activity (Supplemental Figure 4A), IL-6, (Supplemental Figure 4B), and intracellular trypsin (Supplemental Figure 5, A–H). Control glucose feeding did not affect amylase activity (Supplemental Figure 4A), but was able to partially restore IL-6 levels. The weight loss typically seen in AP was partially prevented by galactose, but not glucose (Supplemental Figure 4, C and D). Overall, galactose had a remarkable protective effect against experimental alcohol-related AP.

Galactose administration inhibits AAP in vivo. The experiments shown in Figure 3, B and C, indicate that it might be possible to use galactose to boost energy production in vivo to counteract the toxic effects of asparaginase. We have therefore developed a mouse model of AAP using an approach similar to that developed for studying AP induced by alcohol metabolites, bile, and caerulein (38).

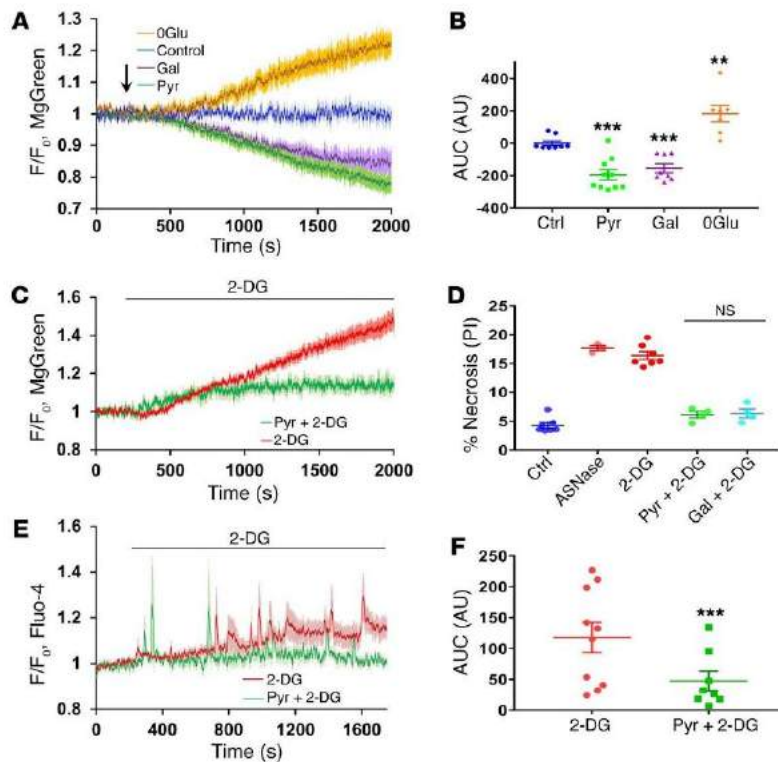


Figure 5. Pyruvate and galactose increase intracellular ATP levels and protect cells against ATP depletion induced by 2-DG. (A) Glucose removal induces substantial ATP depletion, whereas pyruvate or galactose boosts ATP production. Average traces show normalized changes of MgGreen fluorescence in PACs in the presence (blue trace, $n = 8$) or absence (orange trace, $n = 7$) of 10 mM glucose or in the presence of pyruvate (1 mM; green trace, $n = 10$) or galactose (1 mM; purple trace, $n = 8$). (B) Comparison of AUC for experiments shown in A. ** $P < 0.01$; *** $P < 0.001$, 1-way ANOVA. (C) Pyruvate markedly reduces ATP depletion induced by 10 mM 2-DG. Averaged trace (shown with error bars) represents the result of application of 2-DG in the absence (red trace, $n = 9$) or presence of 1 mM pyruvate (after 5 minutes of preincubation, green trace, $n = 7$). (D) Comparison of necrotic cell death levels induced by 2 hours of incubation of PACs with 10 mM 2-DG or asparaginase with control (nontreated cells) (PI-stained cells, $P = 0.36$, 1-way ANOVA, 3 series of experiments with $n > 100$ cells in each sample). (E) Average traces show normalized changes of Fluo-4 fluorescence in PACs induced by 10 mM 2-DG alone (red trace, $n = 10$) or after 5 minutes preincubation of cells and continuous presence of 1 mM pyruvate (green trace, $n = 8$) for 25 minutes. (F) Quantitative analysis of experiments of the type shown in E by comparing AUC for 25 minutes of the recording after application of 10 mM 2-DG. *** $P < 0.001$, 2-tailed Student's t test.

Asparaginase injections resulted in significantly increased histology scores and high degrees of edema, inflammation, and necrosis (Figure 8, A–E) that were similar to those reported for other AP models (38). As shown in Figure 8, A–E, galactose significantly reduced the histology score and the degrees of edema, inflammation, and necrosis toward much lower values in both protocols, feeding and a combination of injection and feeding, with similar efficacy. The weight loss typical for AP was also partially reduced (Supplemental Figure 4D). Therefore, we conclude that galactose could become an effective supplemental treatment for AAP.

Discussion

It is well established that the initial stages of AP are characterized by intracellular Ca^{2+} overload, causing inadequate function of the mitochondria, leading to reduction of ATP production, premature intracellular activation of digestive enzymes, and cell death, mainly by necrosis (1, 2).

Our new data reveal that AP-inducing agents, such as alcohol and fatty acids, bile, and asparaginase, markedly reduce glucose metabolism in PACs, leading to reduced ATP synthesis and, therefore, substantial ATP loss. The combination of cytosolic Ca^{2+} overload and ATP depletion leads to profound cellular necrosis that could be avoided by ATP supplementation (22).

We have now shown that the addition of pyruvate or galactose substantially reduces cell injury induced by all the principal agents inducing AP. Removal of glucose from the medium does not significantly affect the ATP loss and necrosis induced by these agents, indicating that glucose metabolism is severely inhibited. Phlor- etin, the glucose transport inhibitor (39), also completely blocked the galactose rescue effect (Supplemental Figure 1C). Glucose and

galactose are known to enter the cells by the same transporters (40), but galactose is converted to glucose-6-phosphate by several enzymes without involving HKs (41, 42). We therefore conclude that HK inhibition is likely to play an important role in the ATP depletion that is an important element in the development of AP.

Our in vitro experiments (Figure 6) suggest that both POA and BAS directly affect HK enzymes, HK1 and HK4, respectively, whereas the asparaginase effect is indirect (18). The direct inhibition of HKs reduces, but does not abolish, ATP production (Supplemental Figure 6, A–C), as there can still be some production by a number of metabolic pathways. However, cellular ATP is severely depleted, and at the same time, cells are overstimulated by pathological substances, making recovery virtually impossible. Galactose addition in vivo (as well as pyruvate in vitro) protects the cells from ATP depletion and hence necrosis.

A relatively high dose (100 nM) of insulin reduced all POA- (26), BA-, and asparaginase-induced necrosis (Supplemental Figure 1D), most likely by potentiating HKs (28, 29). An increased glucose concentration (30 mM) potentiated glucokinase, which has a low affinity for glucose (29), and also reduced both POA- and asparaginase-induced necrosis (Supplemental Figure 1D). However, such an increased glucose level failed to reduce BA-induced necrosis (Supplemental Figure 1D). This is in line with our data regarding the inhibition of glucokinase by BA (Figure 6C), whereas both POA and asparaginase have striking similarities in their pathological mechanisms, likely inhibiting HK1 (Figure 6A). Although both insulin and high glucose levels were effective in vitro, none of them could of course be employed in vivo. In contrast, galactose feeding, which appears to have no negative side effects, would be a potentially valuable therapy against AP.

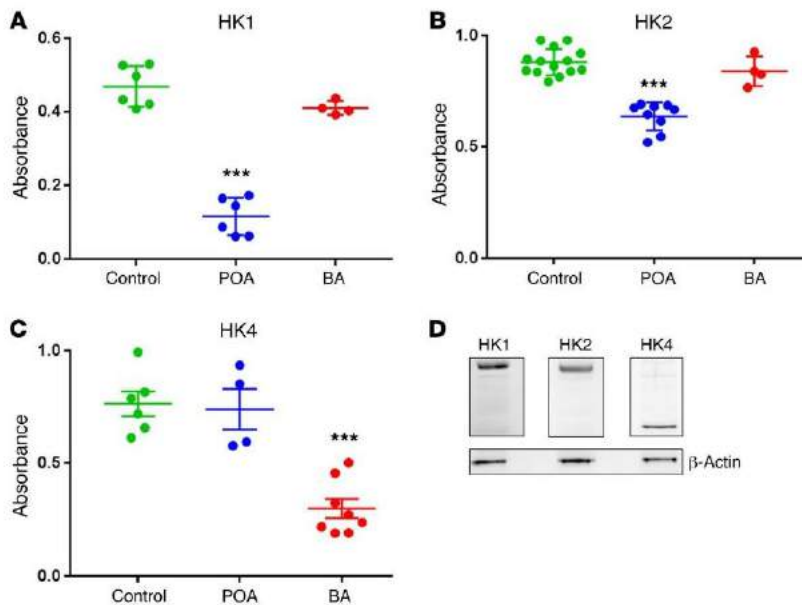


Figure 6. HK activity is significantly inhibited in vitro by POA and BA. (A) HK1 activity is reduced significantly by 0.1 mM POA ($n = 6$, $P < 0.0001$), but not changed significantly by 0.05% BA ($n = 4$, $P > 0.13$) as compared with control ($n = 6$). (B) HK2 activity is reduced significantly by 0.1 mM POA ($n = 9$, $P < 0.0001$), but not affected by 0.05% BA ($n = 4$, $P > 0.3$) as compared with control ($n = 13$). (C) HK4 activity is reduced significantly by 0.05% BA ($n = 8$, $P < 0.0001$), but not affected by 0.1 mM POA ($n = 4$, $P > 0.8$) as compared with control ($n = 6$). (D) Western blot analysis of the expression levels of HK1, HK2, and HK4 in PACs (representative case, repeated 3 times with similar results). *** $P < 0.001$, 1-way ANOVA.

Galactose could also be used preventively, which could be of particular importance in cases in which there is a significantly enhanced risk of AP (43), for example, when treating ALL with asparaginase. Our results indicate that galactose would be a valuable addition to the current asparaginase treatment protocol. Substitution of drinking water in mouse models with a 100 mM galactose solution markedly reduced all pathological scores in both asparaginase- and alcohol metabolite-induced AP. Since this approach has been successful in treating experimental AP induced by several different agents, i.e., asparaginase and POA, and relies on increasing intracellular ATP, preventing depletion of ATP, it might also become useful for treating other diseases with ATP loss and subsequent necrosis as well as counteracting similar side effects of other drugs.

With regard to the clinical treatment of patients with AP, there is currently a debate about high- versus low-energy administration in the early phase of AP (44). The protocol for a current multicenter, randomized, double-blind clinical trial only deals with the question of the potential merit of high-energy enteral tube feed versus zero-energy enteral tube feed (44). Our new results now suggest a need for clinical trials potentially using galactose instead of glucose in enteral tube feeds for patients in the early phase of AP.

Methods

Chemicals and reagents. Fluorescent dyes Fluo-4-AM, MgGreen AM, and propidium iodide (PI) were purchased from Thermo Fisher Scientific. Collagenase was obtained from Worthington, asparaginase was purchased from Abcam, and POAEE was from Cayman Chemical. All other reagents were purchased from Sigma-Aldrich. C57BL/6J mice were obtained from The Jackson Laboratory.

Antibodies. Primary antibodies were as follows: anti-HK1 mouse monoclonal antibody (clone 7A7, catalog MA5-15675, 1/500; Thermo Fisher Scientific), anti-HK2 mouse monoclonal antibody (clone 1E8-H3-F11, catalog ab131196, 1/500; Abcam); anti-HK4 (GCK) rabbit polyclonal antibody (catalog PA5-15072, 1/500; Thermo Fisher Scientific);

and anti- β -actin mouse polyclonal antibody (catalog sc-47778, 1/500; Santa Cruz Biotechnology Inc.). Secondary antibodies were as follows: Pierce goat anti-rabbit IgG, (H+L) peroxidase-conjugated antibody (catalog 31460 1/5,000; Thermo Fisher Scientific); and goat anti-mouse IgG-HRP (catalog sc-2005, 1/1000; Santa Cruz Biotechnology Inc.).

Isolation of PACs. Cells were isolated as previously described (18). After dissection, the pancreas was digested using collagenase-containing solution (200 IU/ml, Worthington) and incubated in a 37°C water bath for 14 to 15 minutes. The extracellular solution contained the following: 140 mM NaCl, 4.7 mM KCl, 10 mM HEPES, 1 mM MgCl₂, 10 mM glucose, pH 7.3, and 1 mM CaCl₂. Osmolarity was checked by Osmomat 030. All in vitro experiments were conducted using this solution unless otherwise stated.

Fluorescence measurements. For measurements of [Ca²⁺]_i, isolated PACs were loaded with Fluo-4-AM (5 μ M; excitation, 488 nm; emission, 510–560 nm) following the manufacturer's instructions. Measurement of intracellular ATP was performed with MgGreen, which senses changes in [Mg²⁺]_i at concentrations around the resting [Mg²⁺]_i (18). PACs were incubated with 4 μ M MgGreen AM for 30 minutes at room temperature (excitation, 488 nm; emission, 510–560 nm). ATP depletion mixture (4 μ M CCCP, 10 μ M oligomycin, and 2 mM iodoacetate) was applied for a final 10 minutes of each experiment to induce maximum ATP depletion (21). Asparaginase was used in a concentration of 200 IU/ml, 500 μ M POAEE (from the stock solution in ethanol, Cayman Chemical), 50 μ M POA (from 30 mM stock in ethanol), and 0.06% sodium cholate (BA) unless stated otherwise.

Necrotic cell death was assessed with PI uptake as previously described (excitation, 535 nm; emission, 617 nm) (4). The total number of cells showing PI uptake was counted in a series of 3 or more experiments for each treated group (>100 cells per each sample) to provide a percentage as the mean \pm SEM.

All experiments were performed at room temperature using freshly isolated cells attached to coverslips of the perfusion chamber. Fluorescence was imaged over time using Leica SP5 2-photon, Leica TCS SPE, and Zeiss spin-disk confocal microscopes.

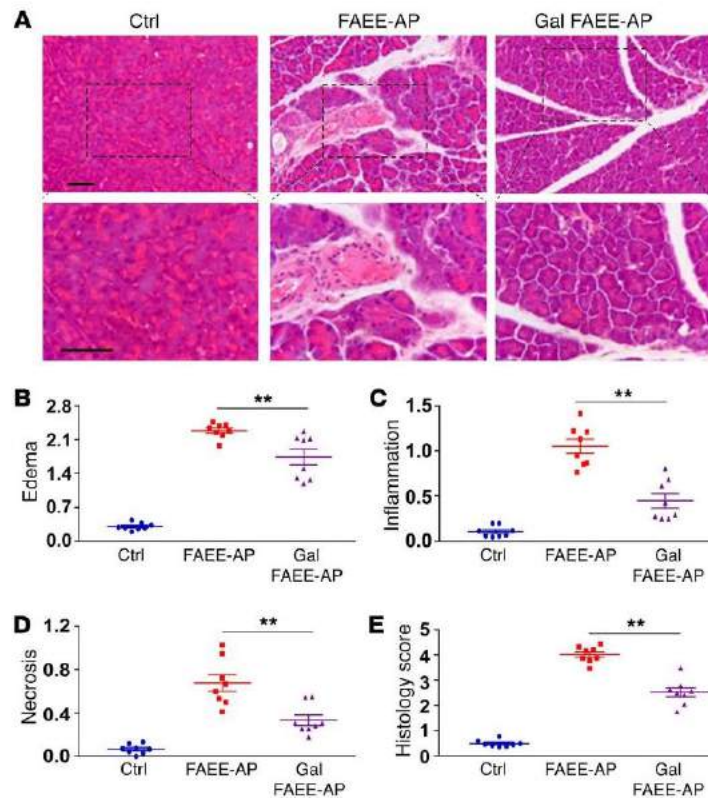


Figure 7. Galactose protects against alcohol-induced AP in vivo. (A) Galactose significantly improved the pathological scores in FAEE-AP. Representative H&E images of pancreas histology slides showing normal pancreatic histology (saline injection), and typical histopathology from FAEE-AP without or with galactose feeding (100 mM). Lower row of images shows zoomed parts of the images above. Scale bars: 50 μ m. (B–E) Overall histopathological score (E) and components: edema (B), inflammation (C), and necrosis (D). All detrimental changes induced by POA and ethanol were significantly ameliorated by galactose ($P < 0.007$). Data are shown as mean \pm SEM of 3 to 5 mice per group. ** $P < 0.01$, 1-way ANOVA.

In vivo models of asparaginase- and fatty acid ethyl ester-induced AP. Before and throughout the experiment, unless otherwise noted, mice were maintained in plastic cages with corn cob bedding; tap water and commercial pelleted diet were freely provided. To establish AAP, C57BL/6J mice received 4 daily (24 hours apart) i.p. injections of asparaginase in PBS at 20 IU/g. Control mice received PBS-only i.p. injections. Treatment groups were defined as follows: (a) galactose-fed (100 mM in drinking water 24 hours before the first i.p. asparaginase and all the following days during injections) followed by asparaginase injection (20 IU/g) or (b) galactose-fed (100 mM galactose in drinking water) with i.p. galactose (180 mg/kg/d) and asparaginase (20 IU/g) ($n = 5$ –8 mice/group). Mice were sacrificed 96 hours after first injection, and pancreas was extracted for histology or isolation of PACs. Blood was also collected for amylase and IL-6 measurements.

In the FAEE-induced AP (FAEE-AP) group, mice received 2 i.p. injections of ethanol (1.35 g/kg) and POA (150 mg/kg) at 1-hour intervals as previously described (38). The treatment group animals were fed with galactose (180 mg/kg/d) as described previously. Animals were sacrificed at 24 hours after the final injection.

Histology. Pancreatic tissue was fixed in 4% formaldehyde and embedded in paraffin. Histological assessment was performed after H&E staining of fixed pancreatic slices (4 μ m thickness). Evaluation was performed on 10 or more random fields (magnification, $\times 200$) by 2 blinded independent investigators grading (scale, 0–3) edema, inflammatory cell infiltration, and acinar necrosis as previously described (38), calculating the mean \pm SEM ($n = 3$ –5 mice/group).

HK activity. To assay inhibitory effects of POA and BA on the activity of HK1, HK2 (Novus Biological), and HK4 (Enzo Life Sci-

ences), NADH generated by glucose-6-phosphate dehydrogenase was detected at 340 nm as described in the manufacturer's protocols for the Hexokinase Assay Kit (MAK091, Sigma-Aldrich).

Western blotting. Equal amounts of proteins were resolved by sodium dodecyl sulfate-polyacrylamide gel electrophoresis (4%–12% SDS Bis Tris gels, Thermo Fisher Scientific) and blotted; membranes were probed with primary and then secondary antibodies.

Measurements of mitochondrial membrane potential. For measurements of mitochondrial membrane potential ($\Delta\psi$ m) in PACs, we used the dequench mode, as previously described (25). Freshly isolated pancreatic cells were loaded with 20 μ M tetramethylrhodamine methyl ester (TMRM) for 25 minutes at room temperature. Cells were then washed and resuspended in extracellular solution. Fluorescence was excited by a 535 nm argon laser line, and emission was collected above 560 nm. All experiments were conducted by using a Leica TCS SPE confocal microscope with a $\times 63$ oil immersion objective. The region of interest for analyzing the change of $\Delta\psi$ m was the whole cell.

Measurements of mitochondrial Ca^{2+} . For mitochondrial calcium [Ca^{2+}] measurements (45), freshly isolated PACs were loaded with 10 μ M Rhod-2-AM for 48 minutes at 30°C. After incubation, the cells were centrifuged for 1 minute and resuspended in extracellular solution. The fluorescence of Rhod-2 was excited using a 535 nm laser line, and the emitted light was collected above 560 nm.

Enzyme activity and IL-6 measurements. Serum amylase was determined by spectrophotometer measurements at 405 nm (Jenway) using the Amylase Activity Assay Kit (MAK009, Sigma-Aldrich) according to the manufacturer's instructions.

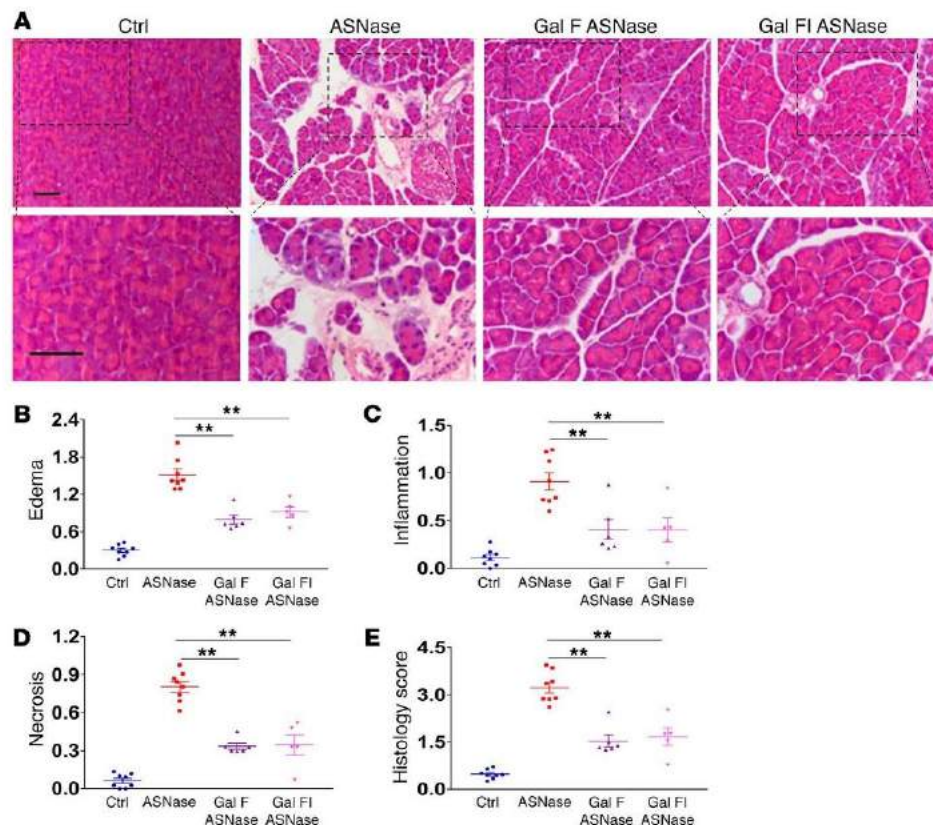


Figure 8. AAP is substantially reduced by galactose in vivo. (A) Representative H&E images of pancreas from slides showing normal pancreatic histology (saline), typical histopathology from AAP model (asparaginase 20 IU/g), and typical histopathology from treatment groups: galactose feeding (Gal F) and combination of galactose feeding and galactose injection (Gal FI). Lower row of images shows zoomed parts of the images above. Scale bars: 50 μ m. (B–E) Edema (B), inflammation (C), necrosis (D), and overall histopathological score (E) in asparaginase-induced AP and the effects of the 2 different galactose treatment protocols. All detrimental changes induced by asparaginase were significantly ameliorated by galactose ($P < 0.004$; data are shown as mean \pm SEM of 3–5 mice per group). ** $P < 0.01$, 1-way ANOVA.

For visualization of trypsin activity, PACs were incubated in extracellular solution containing 10 μ M rhodamine 110, bis-(CBZ-L-isoleucyl-L-prolyl-L-arginine amide) dihydrochloride (BZipAR) (Molecular Probes, Thermo Fisher Scientific) (4), according to the manufacturer's instructions. BZipAR was excited with a 488 nm laser line; emission was collected at 508–530 nm.

IL-6 levels were determined by enzyme-linked immunosorbent assay (Abcam).

ATP measurements. Isolated PACs were incubated for 2 hours with either POA, BA, or asparaginase with appropriate controls. Cellular ATP was determined in a homogenized cell preparation using the ATP Assay Kit (Sigma-Aldrich) according to the manufacturer's instructions.

Statistics. Data are presented as mean \pm SEM. Statistical significance and P values were calculated using Student's 2-tailed t test or ANOVA, with $P < 0.05$ and $P < 0.01$ considered statistically significant and $P < 0.001$ considered highly significant.

Study approval. All animal studies were ethically reviewed and conducted according to the United Kingdom Animal (Scientific Procedures) Act of 1986, approved by the United Kingdom Home Office. Animal procedures and experimental protocols were

approved by the Animal Care and Ethics Committees at the Cardiff School of Biosciences.

Author contributions

SP, JVG, TMT, OG, SS, OHP, and OVG designed the study. SP, JVG, TMT, OG, and OVG conducted and analyzed experiments. SP, JVG, OHP, and OVG wrote the manuscript. All authors read and approved the final draft of the manuscript.

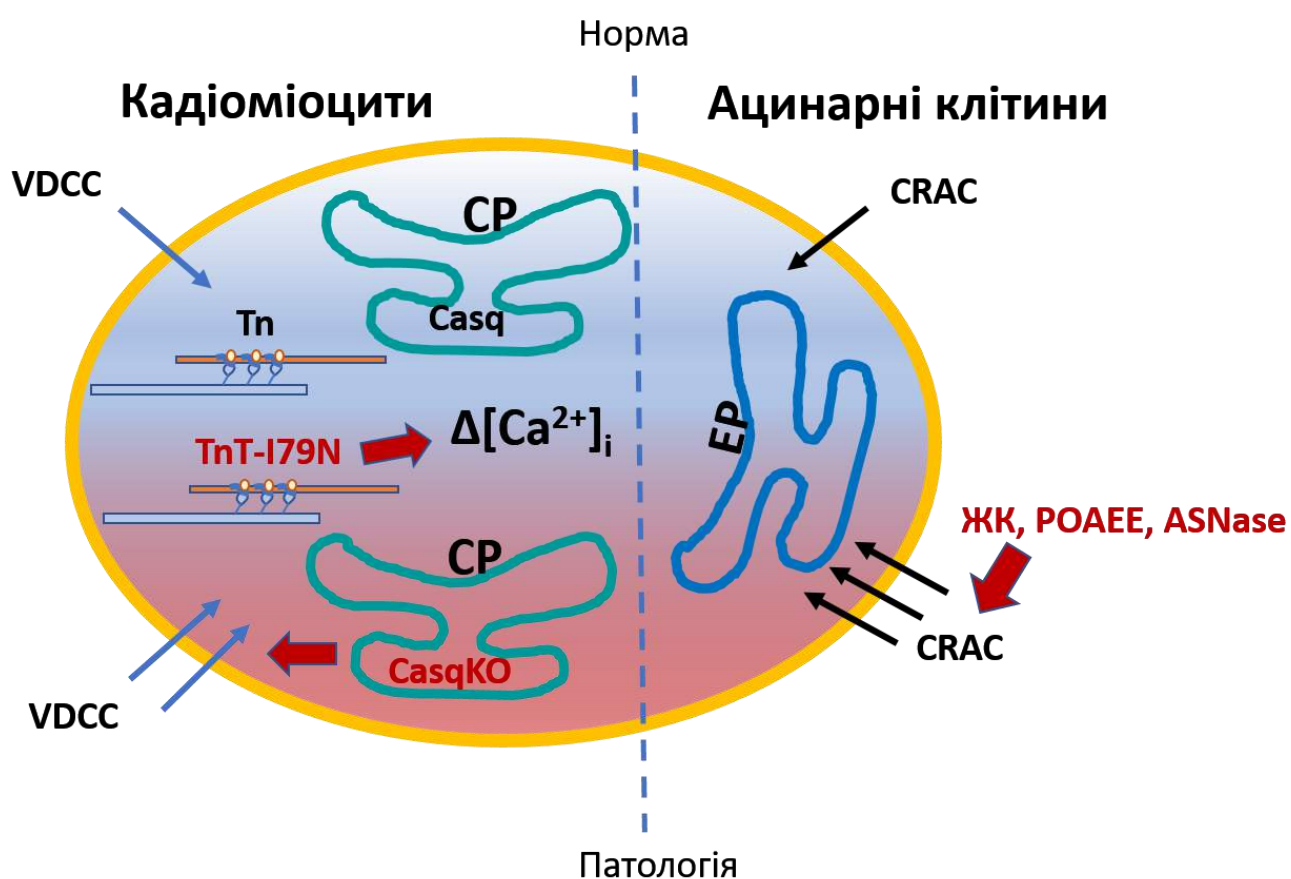
Acknowledgments

This work was funded by the Medical Research Council Programme (grant no. MR/J002771/1) and Children with Cancer UK (grant no. 2014/167). Work was also supported by the National Institute for Health Research Biomedical Research Centre at Great Ormond Street Hospital for Children, NHS Foundation Trust, and University College London. SP is supported by the China Scholarship Council (no. 201406780021).

Address correspondence to: Oleg V. Gerasimenko, Cardiff School of Biosciences, The Sir Martin Evans Building, Museum Avenue, Cardiff University, Cardiff CF10 3AX, United Kingdom. Phone: 44.29.2087.0865; Email: GerasimenkoOV@cardiff.ac.uk.

1. Petersen OH, Sutton R. Ca^{2+} signalling and pancreatitis: effects of alcohol, bile and coffee. *Trends Pharmacol Sci.* 2006;27(2):113–120.
2. Gerasimenko JV, Gerasimenko OV, Petersen OH. The role of Ca^{2+} in the pathophysiology of pancreatitis. *J Physiol.* 2014;592(2):269–280.
3. Forsmark CE, Vege SS, Wilcox CM. Acute pancreatitis. *N Engl J Med.* 2016;375(20):1972–1981.
4. Gerasimenko JV, et al. Ca^{2+} release-activated Ca^{2+} channel blockade as a potential tool in anti-pancreatitis therapy. *Proc Natl Acad Sci USA.* 2013;110(32):13186–13191.
5. Petersen OH, Tepikin AV. Polarized calcium signaling in exocrine gland cells. *Annu Rev Physiol.* 2008;70(2):273–299.
6. Wolthers BO, et al. Asparaginase-associated pancreatitis: a study on phenotype and genotype in the NOPHO ALL2008 protocol. *Leukemia.* 2017;31(2):325–332.
7. Wolthers BO, et al. Asparaginase-associated pancreatitis in childhood acute lymphoblastic leukaemia: an observational Ponte di Legno Toxicity Working Group study. *Lancet Oncol.* 2017;18(9):1238–1248.
8. Jaffe N, et al. L-asparaginase in the treatment of neoplastic diseases in children. *Cancer Res.* 1971;31(7):942–949.
9. Silverman LB, et al. Improved outcome for children with acute lymphoblastic leukemia: results of Dana-Farber Consortium Protocol 91-01. *Blood.* 2001;116(15):1211–1218.
10. Kearney SL, Dahlberg SE, Levy DE, Voss SD, Sallan SE, Silverman LB. Clinical course and outcome in children with acute lymphoblastic leukemia and asparaginase-associated pancreatitis. *Pediatr Blood Cancer.* 2009;53(2):162–167.
11. Raja RA, Schmiegelow K, Frandsen TL. Asparaginase-associated pancreatitis in children. *Br J Haematol.* 2012;159(1):18–27.
12. Samarasinghe S, et al. Incidence and outcome of pancreatitis in children and young adults with acute lymphoblastic leukaemia treated on a contemporary protocol, UKALL 2003. *Br J Haematol.* 2013;162(5):710–713.
13. Alvarez OA, Zimmerman G. Pegaspargase-induced pancreatitis. *Med Pediatr Oncol.* 2000;34(3):200–205.
14. Badalov N, Baradaran R, Iswara K, Li J, Steinberg W, Tenner S. Drug-induced acute pancreatitis: an evidence-based review. *Clin Gastroenterol Hepatol.* 2007;5(6):648–661.
15. Knoderer HM, Robarge J, Flockhart DA. Predicting asparaginase-associated pancreatitis. *Pediatr Blood Cancer.* 2007;49(5):634–639.
16. Schmiegelow K, et al. Consensus definitions of 14 severe acute toxic effects for childhood lymphoblastic leukaemia treatment: a Delphi consensus. *Lancet Oncol.* 2016;17(6):e231–e239.
17. Hijiya N, van der Sluis IM. Asparaginase-associated toxicity in children with acute lymphoblastic leukemia. *Leuk Lymphoma.* 2016;57(4):748–757.
18. Peng S, et al. Calcium and adenosine triphosphate control of cellular pathology: asparaginase-induced pancreatitis elicited via protease-activated receptor 2. *Phil Trans Royal Soc B Biol Sci.* 2016;371(1700):20150423.
19. Iwamoto S, Mihara K, Downing JR, Pui CH, Campana D. Mesenchymal cells regulate the response of acute lymphoblastic leukemia cells to asparaginase. *J Clin Invest.* 2007;117(4):1049–1057.
20. Broome JD. Studies on the mechanism of tumor inhibition by L-asparaginase. Effects of the enzyme on asparagine levels in the blood, normal tissues, and 6C3HED lymphomas of mice: differences in asparagine formation and utilization in asparaginase-sensitive and -resistant lymphoma cells. *J Exp Med.* 1968;127(6):1055–1072.
21. Baggaley E, Elliott A, Bruce J. Oxidant induced inhibition of the plasma membrane Ca^{2+} ATPase in pancreatic acinar cells: role of the mitochondria. *Am J Physiol Cell Physiol.* 2008;295(5):C1247–C1260.
22. Criddle DN, et al. Calcium signalling and pancreatic cell death: apoptosis or necrosis? *Cell Death Differ.* 2007;14(7):1285–1294.
23. Moszbacher D, et al. Restoration of energy level in the early phase of acute pediatric pancreatitis. *World J Gastroenterol.* 2017;23(6):957–963.
24. Aguer C, et al. Galactose enhances oxidative metabolism and reveals mitochondrial dysfunction in human primary muscle cells. *PLoS One.* 2011;6(12):e28536.
25. Voronina SG et al. Effects of secretagogues and bile acids on mitochondrial membrane potential of pancreatic acinar cells: comparison of different modes of evaluating ($\Delta\psi$). *J Biol Chem.* 2004;279(26):27327–27338.
26. Samad A, et al. Insulin protects pancreatic acinar cells from palmitoleic acid-induced cellular injury. *J Biol Chem.* 2014;289(34):23582–23595.
27. Barban S, Schulze HO. The effects of 2-deoxyglucose on the growth and metabolism of cultured human cells. *J Biol Chem.* 1961;236:1887–1890.
28. Roberts DJ, S Miyamoto. Hexokinase II integrates energy metabolism and cellular protection: Akt on mitochondria and TORCing to autophagy. *Cell Death Differ.* 2015;22(2):248–257.
29. Lenzen S. A fresh view of glycolysis and glucokinase regulation: history and current status. *J Biol Chem.* 2014;289(18):12189–12194.
30. Letkemann R, et al. Partial correction of neutrophil dysfunction by oral galactose therapy in glycogen storage disease type Ib. *Int Immunopharmacol.* 2017;44:216–225.
31. Frustaci A, et al. Improvement in cardiac function in the cardiac variant of Fabry's disease with galactose-infusion therapy. *N Engl J Med.* 2001;345(1):25–32.
32. Morelle W, et al. Galactose supplementation in TMEM165-CDG patients rescues the glycosylation defects. *J Clin Endocrinol Metab.* 2017;102(4):1375–1386.
33. De Smet E, Rioux JP, Ammann H, Déziel C, Quélin S. FSGS permeability factor-associated nephrotic syndrome: remission after oral galactose therapy. *Nephrol Dial Transplant.* 2009;24(9):2938–2940.
34. Grote V, et al. European Childhood Obesity Project. Breast milk composition and infant nutrient intakes during the first 12 months of life. *Eur J Clin Nutr.* 2016;70(2):250–256.
35. Berry GT, Nissim I, Lin Z, Mazur AT, Gibson JB, Segal S. Endogenous synthesis of galactose in normal men and patients with hereditary galactosaemia. *Lancet.* 1995;346(8982):1073–1074.
36. An, et al. Antioxidant effects of the orientin and vitexin in *Trollius chinensis* Bunge in D-galactose-aged mice. *Neural Regen Res.* 2012;7(33):2565–2575.
37. Sclafani A, Ackroff K. Flavor preference conditioning by different sugars in sweet agouti Trpm5 knockout mice. *Physiol Behav.* 2015;140:156–163.
38. Wen L, et al. Inhibitors of ORAI1 prevent cytosolic calcium-associated injury of human PACs and acute pancreatitis in 3 mouse models. *Gastroenterology.* 2015;149(2):481–492.
39. Shepherd PR, Kahn BB. Glucose transporters and insulin action-implications for insulin resistance and diabetes mellitus. *N Engl J Med.* 1999;341(4):248–257.
40. Gould GW, Holman GD. The glucose transporter family: structure, function and tissue-specific expression. *Biochem J.* 1993;295:329–341.
41. Holden HM, Rayment I, Thoden JB. Structure and function of enzymes of the Leloir pathway for galactose metabolism. *J Biol Chem.* 2003;278(45):43885–43888.
42. Frey PA. The Leloir pathway: a mechanistic imperative for three enzymes to change the stereochemical configuration of a single carbon in galactose. *FASEB J.* 1996;10(4):461–470.
43. Maléth J, Hegyi P. Ca^{2+} toxicity and mitochondrial damage in acute pancreatitis: translational overview. *Philos Trans R Soc Lond B Biol Sci.* 2016;371(1700):20150425.
44. Marta K, et al. High versus low energy administration in the early phase of acute pancreatitis (GOULASH trial): protocol of a multicentre randomised double-blind clinical trial. *BMJ Open.* 2017;7(9):e015874.
45. Baumgartner HK et al. Calcium elevation in mitochondria is the main Ca^{2+} requirement for mitochondrial permeability transition pore (mPTP) opening. *J Biol Chem.* 2009;284(31):20796–20803.

В роботі були дослідженні та проаналізовані різні ланки механізму кальцієвої регуляції в електрично збудливих та незбудливих клітинах, які були недостатньо висвітлені в світовій літературі. Це вхід Ca в клітину (депозалежний вхід Ca), зв'язування Ca^{2+} кальційзв'язуючими білками в цитозолі (скоротливими молекулами тропоніну) та в ретикулумі (кальсеквестрином) та їх внесок у зміни внутрішньоклітинної концентрації Ca^{2+} (кальцієву регуляцію як таку). Описано новий механізм інактивації кальцієвих каналів L-типу, що сприяє втраті рефрактерності вивільнення іонів Ca^{2+} із саркоплазматичного ретикулуму у мишей з мутацією *Casq2* (*Casq2 KO*).



Схематичне зображення основних процесів, що беруть участь у контролі концентрації Ca^{2+} в цитозолі електрично збудливих та незбудливих клітин. Верхня частина схеми (блакитний фон) ілюструє принцип кальцієвої регуляції в нормі, а нижня (червоний колір фону) під час виникнення патологій. Щоб наголосити на відмінностях між збудливими та незбудливими клітинами, зображення клітинних структур кардіоміоцита розташоване ліворуч, а

ацинарної клітини – праворуч від пунктирної вертикальної лінії. Як мутації, так і нокауту кальційзв'язуючих білків (TnT-I79N та Casq KO), а також гіперактивація CRAC-каналів під дією речовин, що призводять до виникнення панкреатиту (ЖК, POAEE, ASNase), викликають порушення клітинної кальцієвої регуляції (великі червоні стрілки), що веде до розвитку патологій.

ВИСНОВКИ

У дисертаційній роботі представлено результати комплексного дослідження механізмів кальцієвої регуляції в кардіоміоцитах та клітинах підшлункової залози за нормальних та патологічних умов. Кальцієва регуляція в електрично збудливих та незбудливих клітинах має як загальні риси, так і певну специфіку. Первинним джерелом підвищення $[Ca^{2+}]_i$ в електрозбудливих клітинах є потенціалкеровані кальцієві канали плазматичної мембрани. Ці канали здатні як запустити вивільнення іонів кальцію з ретикулуму, так і забезпечити його перезавантаження саме за рахунок входу Ca^{2+} із позаклітинного розчину. В електронезбудливих клітинах за відсутності потенціалкеруваних кальцієвих каналів основну роль постачання Ca^{2+} в клітину відіграють депокеровані кальцієві канали.

Зроблені наступні висновки:

1. Скорочення кардіоміоцитів на ранніх стадіях ембріонального розвитку не пов'язані з генерацією трансмембранних струмів, а обумовленні спонтанними коливаннями внутрішньоклітинної концентрації іонів кальцію. Ця активність не опосередковується кальцієвими каналами L-типу та взаємодією між ними та ріанодиновими кальцієвими депо, як це спостерігається у зрілих кардіоміоцитах. Показано, що електричне сполучення між клітинами через щілинні контакти забезпечує синхронізацію скорочень окремих незрілих кардіоміоцитів.
2. Ca^{2+} -сенситивізуючі мутації тропоніну T змінюють цитозольну кальцієву буферну здатність, чого достатньо для зміни глобальних цитозольних $[Ca^{2+}]_i$ транз'єнтів; такі мутації можуть лежати в основі успадкованих кардіоміопатій.
3. Відкрито новий залежний від експресії калсеквестрину механізм порушення кальмодулінзалежної інактивації кальцієвих каналів Cav1.2. Нокаут калсеквестрину призводить до зникнення рефрактерності вивільнення іонів кальцію із саркоплазматичного ретикулуму шлуночкових міоцитів миші.

4. Як показано вперше, спустошення кальцієвих депо активує кальцієвий трансмембранний струм (I_{CRAC}) в клітинах підшлункової залози миші. Активація та розвиток цього кальцієвого депозалежного струму напрядує корелює із спустошенням ендоплазматичного ретикулуму внаслідок блокування кальцієвої АТФази останнього.
5. Блокування Ca^{2+} -селективних іонних депозалежних каналів ефективно перешкоджає підвищенню внутрішньоклітинної концентрації іонів кальцію та запобігає розвиненню некрозу ацинарних клітин, що викликається ефірами жирних кислот (які, зокрема, є метаболітами етанолу).
6. Жовчні кислоти, що є одним з головних чинників розвитку гострого панкреатиту, викликають некроз ацинарних клітин в результаті активації катіонних каналів плазматичної мембрани та підвищення внутрішньоклітинних концентрацій іонів натрію та кальцію.
7. З'ясовані механізми генерації кальцієвих сигналів в зірчастих клітинах – компонентах структури панкреатичних лобул. За нормальних умов зірчасті клітини генерують двофазні кальцієві транзйєнти у відповідь на прикладання брадикініну; останній є основним фактором, що забезпечує виникнення больових відчуттів при панкреатиті. Блокування брадикінінових рецепторів типу В2 усуває кальцієві транзйєнти, спричинені БК, та запобігає розвиненню некрозу ацинарних клітин, спричиненому як етанолом і його метаболітами, так і жовчними кислотами.
8. Механізми кальцієвої сигналізації клітин в лобулах екзокринної частини підшлункової залози, зокрема в нервових та імунних клітинах мають певну специфіку. В умовах розвитку гострого панкреатиту чутливість зірчастих клітин до БК істотно зменшується. В панкреатичних лобулах нервові та імунні клітини розташовані в місцях скопичення зірчастих клітин, що вказує на вірогідність однієї досі невідомої ролі зірчастих клітин у функціюванні підшлункової залози.
9. Аспарагіназа, як і етилові ефіри жирних кислот та жовчні кислоти, може викликати стійке підвищення $[Ca^{2+}]_i$, в наслідку вивільнення цих іонів з

внутрішньоклітинних депо та їх входу через депокеровані канали. Це підвищення може призводити до розвитку некрозу ацинарних клітин.

10. Галактоза ефективно запобігає збільшенню внутрішньоклітинної концентрації іонів кальцію та зменшує некроз ацинарних клітин в моделі гострого панкреатиту, викликаного аспарагіназою.

СПИСОК ПУБЛІКАЦІЙ ЗА ТЕМОЮ ДИСЕРТАЦІЇ

1. **Gryshchenko O**, Lu ZJ, Fleischmann BK, Hescheler J. Outwards currents in embryonic stem cell-derived cardiomyocytes. *Pflugers Arch.* 2000 Apr; 439(6):798-807.
2. Igelmund P, Fleischmann BK, Fischer IR, Soest J, **Gryshchenko O**, Böhm-Pinger MM, Sauer H, Liu Q, Hescheler J. Action potential propagation failures in long-term recordings from embryonic stem cell-derived cardiomyocytes in tissue culture. *Pflugers Arch.* 1999 Apr; 437(5):669-79.
3. Viatchenko-Karpinski S, Fleischmann BK, Liu Q, Sauer H, **Gryshchenko O**, Ji GJ, Hescheler J. Intracellular Ca²⁺ oscillations drive spontaneous contractions in cardiomyocytes during early development. *Proc Natl Acad Sci U S A.* 1999 Jul 6; 96(14):8259-64.
4. **Gryshchenko O**, Fischer IR, Dittrich M, Viatchenko-Karpinski S, Soest J, Böhm-Pinger MM, Igelmund P, Fleischmann BK, Hescheler J. Role of ATP-dependent K(+) channels in the electrical excitability of early embryonic stem cell-derived cardiomyocytes. *J Cell Sci.* 1999 Sep; 112 (Pt 17):2903-12.
5. **Gryshchenko O**, Qu J, Nathan RD. Ischemia alters the electrical activity of pacemaker cells isolated from the rabbit sinoatrial node. *Am J Physiol Heart Circ Physiol.* 2002 Jun; 282(6):H2284-95.
6. Kruglikov I, **Gryshchenko O**, Shutov L, Kostyuk E, Kostyuk P, Voitenko N. Diabetes-induced abnormalities in ER calcium mobilization in primary and secondary nociceptive neurons. *Pflugers Arch.* 2004 Jul; 448(4):395-401.
7. Voronina SG, **Gryshchenko OV**, Gerasimenko OV, Green AK, Petersen OH, Tepikin AV. Bile acids induce a cationic current, depolarizing pancreatic acinar cells and increasing the intracellular Na⁺ concentration. *J Biol Chem.* 2005 Jan 21; 280(3):1764-70. Epub 2004 Nov 9.
8. Shutov L, Kruglikov I, **Gryshchenko O**, Khomula E, Viatchenko-Karpinski V, Belan P, Voitenko N. The effect of nimodipine on calcium homeostasis and pain

- sensitivity in diabetic rats. *Cell Mol Neurobiol.* 2006 Oct-Nov; 26(7-8):1541-57. Epub 2006 Jul 12. PubMed PMID: 16838100.
9. Schober T, Huke S, Venkataraman R, **Gryshchenko O**, Kryshstal D, Hwang HS, Baudenbacher FJ, Knollmann BC. Myofilament Ca sensitization increases cytosolic Ca binding affinity, alters intracellular Ca homeostasis, and causes pause-dependent Ca-triggered arrhythmia. *Circ Res.* 2012 Jul 6; 111(2):170-9.
 10. Gerasimenko JV, **Gryshchenko O**, Ferdek PE, Stapleton E, Hébert TO, Bychkova S, Peng S, Begg M, Gerasimenko OV, Petersen OH. Ca²⁺ release-activated Ca²⁺ channel blockade as a potential tool in antipancreatitis therapy. *Proc Natl Acad Sci U S A.* 2013 Aug 6; 110(32):13186-91.
 11. Kryshstal DO, **Gryshchenko O**, Gomez-Hurtado N, Knollmann BC. Impaired calcium-calmodulin-dependent inactivation of Cav1.2 contributes to loss of sarcoplasmic reticulum calcium release refractoriness in mice lacking calsequestrin 2. *J Mol Cell Cardiol.* 2015 May; 82:75-83.
 12. **Gryshchenko O**, Gerasimenko JV, Gerasimenko OV, Petersen OH. Ca(2+) signals mediated by bradykinin type 2 receptors in normal pancreatic stellate cells can be inhibited by specific Ca(2+) channel blockade. *J Physiol.* 2016 Jan 15; 594(2):281-93.
 13. **Gryshchenko O**, Gerasimenko JV, Gerasimenko OV, Petersen OH. Calcium signalling in pancreatic stellate cells: Mechanisms and potential roles. *Cell Calcium.* 2016 Mar; 59(2-3):140-4.
 14. Peng S, Gerasimenko JV, Tsugorka T, **Gryshchenko O**, Samarasinghe S, Petersen OH, Gerasimenko OV. Calcium and adenosine triphosphate control of cellular pathology: asparaginase-induced pancreatitis elicited via protease-activated receptor 2. *Philos Trans R Soc Lond B Biol Sci.* 2016 Aug 5; 371(1700). pii: 20150423.
 15. **Gryshchenko O**, Gerasimenko JV, Peng S, Gerasimenko OV, Petersen OH. Calcium signalling in the acinar environment of the exocrine pancreas: physiology and pathophysiology. *J Physiol.* 2018 Jul; 596(14):2663-2678.

16. Peng S, Gerasimenko JV, Tsugorka TM, **Gryshchenko O**, Samarasinghe S, Petersen OH, Gerasimenko OV. Galactose protects against cell damage in mouse models of acute pancreatitis. J Clin Invest. 2018 Aug 31; 128(9):3769-3778.

Апробація матеріалів дисертації:

1. P Igelmund, IR Fischer, J Soest, **O Gryshchenko**, BK Fleischmann, J Hescheler. Nimodipine induces arrhythmia in cardiomyocyte clusters in three-dimensional cell culture. PFLUGERS ARCHIV-EUROPEAN JOURNAL OF PHYSIOLOGY, 1997, 433 (6), P293-P293.
2. **O Gryshchenko**, IR Fischer, J Soest, S Viatchenko-Karpinski, P Igelmund, Fleischmann BK, Hescheler J. Bursting behavior induced by ATP-sensitive K⁺ channels in embryonal stem cell derived cardiomyocytes. PFLUGERS ARCHIV-EUROPEAN JOURNAL OF PHYSIOLOGY, 1997, 433 (6), O131-O131.
3. **O Gryshchenko**, BK Fleischmann, J Hescheler. Outward rectifier K⁺ currents in early-and late stage cardiomyocytes derived from embryonic stem cells. PFLUGERS ARCHIV-EUROPEAN JOURNAL OF PHYSIOLOGY, 1997, 433 (6), P294-P294.
4. **O Gryshchenko**, RD Nathan. Simulated ischemia alters the electrical activity of pacemaker cells isolated from the rabbit sinoatrial node: Role of pH. BIOPHYSICAL JOURNAL, 2001, 80 (1), 641A-641A.
5. **O Gryshchenko**, JH Qu, RD Nathan. Ischemia alters calcium transients in SA node pacemaker cells. BIOPHYSICAL JOURNAL, 2002, 82 (1), 99A-99A.
6. YM Du, **O Gryshchenko**, H Attaya, RD Nathan. Ionic basis of ischemia-induced bradycardia in the rabbit sinoatrial node FASEB JOURNAL, 2005, 19 (5), A1633-A1633.
7. **O Gryshchenko**, S Huke, F Baudenbacher, JD Potter, BC Knollmann. Ca²⁺ sensitizing troponin T mutations linked to hypertrophic cardiomyopathy increase apparent cytosolic Ca²⁺ binding. Biophysical Journal, 2009, 96 (3), 513a.

8. HS Hwang, **O Gryshchenko**, SS Davies, BC Knollmann. Effects of γ -Ketoaldehydes on Ca^{2+} Current Induced SR Ca^{2+} Release in Ventricular Myocytes. *Biophysical Journal*, 2010, 98 (3), 548a.
9. **O Gryshchenko**, D Kryshchal, BC Knollmann. Refractoriness of Sarcoplasmic Reticulum Calcium Release in Cardiac Muscle Due to Calsequestrin. *Biophysical Journal*, 2010, 98 (3), 547a.
10. D Kryshchal, **O Gryshchenko**, BC Knollmann. Accelerated Recovery of L-Type Ca Current Contributes to the Loss of SR Ca Release Restitution in Mice Lacking *Casq2*. *Biophysical Journal*, 2012, 102 (3), 672a.
11. **Грищенко О**, Герасименко Ю, Герасименко О, Петерсен О. Депо-залежні струми в ацинарних клітинах підшлункової залози. Тези доповіді Українського Біофізичного Товариства (Луцьк, 2015).
12. **Gryshchenko O**, Gerasimenko JV, Gerasimenko OV, Petersen OH. The blockade of BK-induced Ca^{2+} signals in pancreatic stellate cells protected against PAC necrosis evoked by agents causing acute pancreatitis. 2016, Annual Meeting of European Academy, UK.
13. **Gryshchenko O**, Gerasimenko J, Gerasimenko O, Petersen O, Stellate cells. 2017, Annual Royal Society Meeting, London, UK.
14. **Gryshchenko O**, Gerasimenko J, Gerasimenko O, Petersen O. Calcium signalling in the acinar environment of the exocrine pancreas. 2019, 8th Annual Meeting of the Ukrainian Biophysical Society, Nov. 12-15 2019, Kyiv-Lutsk (Ukraine). Публікація тез, усна доповідь.